Métabolisme et régulation des glycérolipides dans Phaeodactylum tricornutum et Nannochloropsis

Lina-Juana Dolch

THÈSE

Pour obtenir le grade de

DOCTEUR DE L'UNIVERSITÉ GRENOBLE ALPES

Spécialité : **Biologie végétale**

Arrêté ministériel : 7 août 2006

Présentée par

Lina-Juana DOLCH

Thèse dirigée par **Eric MARECHAL**

préparée au sein du **Laboratoire de Physiologie Cellulaire et Végétale**
dans **l'École Doctorale de Chimie et Sciences du Vivant**

Glycerolipid metabolism and regulation in *Phaeodactylum tricornutum* and *Nannochloropsis gaditana*

Thèse soutenue publiquement le 5 décembre 2016,
devant le jury composé de :

Dr. Giovanni FINAZZI
Président
Dr. Katrin PHILIPPAR
Rapporteur
Dr. Yonghua LI-BEISSON
Rapporteur
Dr. Olga SAYANOVA
Examinateur
Dr. Frédéric BEAUDOIN
Examinateur
Dr. Eric MARECHAL
Directeur de thèse

Wurzeln und Flügel

Johann Wolfgang von Goethe

RÉSUMÉ

Phaeodactylum et *Nannochloropsis* sont des espèces photosynthétiques modèles pour le métabolisme des glycérolipides, se distinguant par un enrichissement en acides gras polyinsaturés à très longues chaînes (VLC-PUFA) et de grandes quantités en triacylglycérol (TAG). Les proportions des différents lipides sont influencées par des facteurs environnementaux. Nous avons caractérisé le remodelage lipidique chez *Phaeodactylum* en réponse à la carence en azote et en phosphate. Ces limitations en nutriments induisent une accumulation de TAG, exploitable comme biocarburant. Nous avons identifié de nouveaux composés induisant l'accumulation de TAG et étudié le rôle potentiel du monoxyde d'azote (NO•) dans la régulation du métabolisme lipidique. Nous avons montré qu'en fonction du site de production, le NO• était un signal émis lorsque les conditions de vie étaient critiques, déclenchant l'accumulation de TAG.

Les VLC-PUFAs sont produits par des élongases et des désaturases localisées dans le RE. Nous avons identifié une nouvelle classe d'élongases d'acides gras saturés, agissant sur le 16:0, et appelées Δ0-ELO. Le *knock out* de *Δ0-ELO1* de *Nannochloropsis* réduit le niveau du monogalactosyldiacylglycérol (MGDG), principal lipide des chloroplastes. Ce phénotype met en évidence le rôle de Δ0-ELO1 dans la «voie oméga» qui contrôle le trafic des VLC-PUFAs. Nous avons débuté une dissection de la «voie oméga» par des approches de génétique et des analyses du remodelage lipidique à basse température chez *Nannochloropsis.* Le diacylglycéryl hydroxyméthyltriméthyl-β-sérine (DGTS) apparaît comme le précurseur de base pour importer des VLC-PUFAs vers le chloroplaste, suivant une voie très régulée du DGTS au MGDG. De plus nous avons montré des fonctions possibles du MGDG et des VLC-PUFAs dans la photoprotection et la régulation de la fluidité membranaire latérale.

Phaeodactylum and *Nannochloropsis* are photosynthetic model species for glycerolipid metabolism, standing out by an enrichment of very-long-chain polyunsaturated fatty acids (VLC-PUFAs) and high contents of neutral lipids such as triacylglycerol (TAG). Lipid profiles are influenced by environmental factors. We characterized the lipid remodelling occurring in *Phaeodactylum* in response to nitrogen and phosphate starvation. Nutrient limitations induce neutral lipid accumulation, which may be exploited as biofuels. We identified new triggers of TAG accumulation and investigated a potential role of nitric oxide (NO•) as second messenger in the regulation of neutral lipid levels. We conclude that in dependence of the production site, NO• serves as a signalling molecule for critical life conditions and thereby triggers TAG accumulation.

VLC-PUFAs are produced by ER-located elongases and desaturases. We identified a novel class of elongases, called Δ0-ELOs, acting on saturated fatty acids, most importantly 16:0. Knock out of *Δ0-ELO1* in *Nannochloropsis* resulted in reduced monogalactosyldiacylglycerol (MGDG) levels. MGDG is the major chloroplast lipid. This indicated a role of this initial elongase in fatty acid fate determination and thus in the elusive "omega pathway" for VLC-PUFA trafficking. We have started to investigate the "omega pathway" by reverse genetic approaches and analyses of low-temperature induced lipid remodelling in *Nannochloropsis*. Diacylglyceryl hydroxymethyltrimethyl-β-serine (DGTS) appears most likely at the base for the chloroplast import of VLC-PUFA, following a dynamically regulated DGTS-to-MGDG pathway. Additionally, we gave insights into possible functions of MGDG and VLC-PUFA in photoprotection and regulation of membrane fluidity.

ABBREVIATIONS

°C	degree Celsius
µE	microEinstein
10N10P ESAW	Enriched Seawater, Artificial Seawater with 466.7 $mg.L^{-1}$ $NaNO_3$ and 30.94 $mg.L^{-1}$ NaH_2PO_4
AAE/AAS	acyl-ACP synthetase
ABAC9	ABC class A transporter 9
ACC	acetyl-CoA carboxylase
ACP	acyl carrier protein
ACS	acyl-CoA synthetases
AF	alanine-phenylalanine dipeptide
AMP	adenosinmonophosphate
ARA	arachidonic acid
asRNA	antisense RNA
At	*Arabidopsis thaliana*
ATP	adenosintriphosphate
ATPase	adenosintriphosphate synthetase
BLAST	Basic Local Alignment Search Tool
bp	base-pair
Bq	Becquerel
BSA	bovine serum albumin
CCAP	Culture Collection of Algae and Protozoa
CCM	carbon concentration mechanism
CCMP	Pravosali-Guillard National Center for Culture of Marine Phytoplankton
CDP	cytidine diphosphate
CDP-DAG	cytidine diphosphate diacylglycerol
CE	collision energy
CEF	cyclic electron transfer
Cer	ceramide
CHAPS	3-[(3-Cholamidopropyl)dimethylammonio]-1-propanesulfonate
Chl	chlorophyll
CLSM	confocal laser scanning microscopy
CLSM	Confocal laser scanning microscopy
CoA	coenzyme A
CP26	Chloroplast protein 26
CPTIO	2-(4-Carboxyphenyl)-4,4,5,5-

	tetramethylimidazoline-1-oxyl-3-oxide
Cq	quantitation cycle
CRIBI	Interdepartmental Biotechnology Centre of the University of Padua
CRISPR	Clustered Regularly Interspaced Short Palindromic Repeats
CRYP	phytochrome
Ctp	chloroplast-like transit peptide
Cyt	cytochrome
Cytb6f	cytochrome b6f
D5	desaturase 5
Da	Dalton
DAF-FM	4-amino-5-methylamino-2',7'-difluororescein diacetate
DCMU	3-(3,4-dichlorophenyl)-1,1-dimethylurea
ddH_2O	double distilled water
DGAT	diacylglycerol acyltransferase
DGCC	diacylglyceryl-3-O-carboxyhydroxymethylcholine
DGDG	digalactosyldiacylglycerol
DGTA	diacylglyceryl hydroxymethyltrimethyl-β-alanine
DGTS	diacylglyceryl hydroxymethyltrimethyl-β-serine
DHA	docosahexaenoic acid
DMP1	disintegration per minute
DMSO	dimethyl sulfoxide
DNA	deoxyribonucleic acid
DPH	1,6-diphenyl-hexa-1,3,5-triene
dsRNA	double stranded RNA
DTT	dithiothreitol
ECR	β-hydroxylacyl-CoA eonyl reductase
EDTA	ethylenediaminetetraacetic acid
EGT	endosymbiotic gene transfer
ELO	elongase
eNOS	endothelial
EPA	eicosapentaenoic acid
ER	eonyl-reductase
ER	endoplasmic reticulum
ESAW	Enriched Seawater, Artificial Seawater
EST	estimated sequence tag
F	steady state fluorescence in light-adapted cultures
F0	steady state fluorescence in dark-adapted cultures
FAME	fatty acid methyl esters
Fat1p	fatty acid import protein 1
FATA/B	acyl-ACP thioesterases
FAX1	fatty acid export protein 1
FCP	fucoxanthin chlorophyll a/c protein

Fd	ferredoxin
FFA	free fatty acid
Fm	maximal fluorescence after a saturating light pulse on dark-adapted cultures
Fm’	maximal fluorescence after a saturating light pulse on light-adapted cultures
FNR	ferredoxin NADPH oxidoreductase
FTSH1	ATP-dependent zinc metalloprotease
Fv	difference between F0 and Fm
Fv/Fm	maximum quantum efficiency of PSII
g	gram
G3P	glycerol-3-phosphate
Gal	galactose
GC-FID	gas chromatography coupled to ion flame detection
gDNA	genomic DNA
GFP	green fluorescence protein
GLRXC2	glutaredoxin
GPAT	glycerol-sn-3-phosphate acyl-transferase
GPAT	glycerol-3-phosphate acyltransferase
GPDH	glycerol-3-phosphate dehydrogenase
h	hours
HAD	eonyl-dehydratase
HCD	β-hydroxylacyl-CoA dehydratase
HCF136	photosynthesis system II assembly factor
HGT	horizontal gene transfer
HII	hexagonal-II phase
HIS	histidine
HMM	Pfam hidden Markov models
HPLC	high performance liquid chromatography
IEM	inner envelope membrane
iNOS	inducible
k	kilo
KAR	3-ketoacyl-ACP reductase
KASIII	β-ketoacyl-ACP synthase
kb	kilobyte
KCR	β-ketoactyl-CoA reductase
kd	knock down
KO	knock out
L	litre
LACS	long acyl-CoA synthase
LDL	low-density lipoprotein
LDs	lipid droplets
LEF	linear electron flow

LEU	leucine
LHC	light harvesting complex
LHCB	light harvesting complex protein family B
LHCF	light harvesting complex protein family F
LHCII	light harvesting complex of photosystem II
LHCR	light harvesting complex protein family R
LHCX1	light harvesting complex protein family X
L-NAME	Nicotinamide adenine dinucleotide phosphate
L-NMMA	NG-monomethyl L-arginine
LPAT	lysophosphatidate acyl-transferase
LPCAT	acyl-CoA: lysophosphatidylcholine acyltransferase
LTQ	ion-trap spectrometer
LYS	lysine
m	milli
M	molar
m/z	mass/charge
Mb	megabyte
MCAT	Malonyl-CoA:acyl-carrier protein transacylase
MD	Molecular Dynamics
ME	malic enzyme
MET	methionine
MGDG	monogalactosyldiacylglycerol
min	minute
mm	millimetre
MN	meganuclease
MOPS	3-(N-morpholino)propanesulfonic acid
mRNA	messenger RNA
MS/MS	tandem mass spectrometry
NADPH	nicotinamide adenine dinucleotide phosphate
NCBI	National Center for Biotechnology Information
Ng	*Nannochloropsis gaditana*
NgWT	*Nannochloropsis gaditana* wild type
NiR	nitrite reductase
nm	nanometre
NMR	nuclear magnetic resonance spectroscopy
nNOS	neuronal
NO	nitric oxide
NOA	nitric oxide associated protein
NPQ	non-photochemical quenching
NR	nitrate reductase
nr	non-redundant
nt	nucleotide
OD	optical density
OEC	oxygen evolving complex

OEM	outer envelope membrane
$ONOO^-$	peroxinitrite
P_{680}	special chlorophyll pair in reaction center of PSII
PAGE	polyacryl amide gel electrophoresis
PAS2	β-hydroxylacyl-CoA dehydratase
PC	phosphatidylcholine
PCD	programmed cell death
PCR	polymerase chain reaction
PDAT	phospholipid:DAG acyltransferase
PDB	protein data bank
PDH	pyruvate dehydrogenase
PE	phosphatidylethanolamine
PEP	phosphoenolpyruvate
PEPCK	phosphoenolpyruvate carboxykinase
PG	phosphatidylglycerol
PGP1	phosphatidylglycerolphosphate synthase
PGPP	phosphatidylglycerol phosphatase
Phs1p	β-hydroxylacyl-CoA dehydratase
PK	pyruvate kinase
PLATE	PEG-LiAc-Tris -EDTA buffer
PLDζ	phospholipase Dζ
PPDK	plastid pyruvate orthophosphate dikinase
PPH1	protein phosphatase H1
PQ	plastoquinone
PRXQ	peroxiredoxin Q
PSB27	PSII lipoprotein 27
PSI	photosystem I
psi	Pound-force per square inch
Pt	*Phaeodactylum tricornutum*
PUFA	polyunsaturated fatty acid
qE	energy coefficient
qI	photoinhibition coefficient
qPCR	quantitative real time PCR
qT	state transition coefficient
RC	reaction center
RCII	reaction center of photosystem II
RedCAP	red linage chlorophyll a/b-binding-like protein
Rfu	relative fluorescence units
RISC	RNA-induced silencing complex
RNA	ribonucleic acid
ROS	reactive oxygen species
rpm	rounds per minute
RT	room temperature
RubisCO	ribulose-1,5-bisphosphat-carboxylase/-oxygenase

SDS	sodium dodecyl sulphate
sec	seconds
siRNA	small interference RNA
sn	stereospecific numbering
SNP	nitroprusside
Sp	signal peptide
SQD	sulfoquinovosyldiacylglycerol synthase
SQDG	sulfoquinovosyldiacylglycerol
STN7	state transition kinase 7
TAG	triacylglycerol
TAIR	The Arabidopsis information resource
TALEN	Transcription activator-like effector nuclease
TE	thioesterases
TGDG	trigalactosyldiacylglycerol
TLC	Thin Layer Chromatography
TRP	tryptophan
TRX	thioredoxins
UDP	uridine diphosphate
URA	uracil
UV	ultra violet
V	volt
VCP	violaxanthin-Chl a binding proteins
VLC-PUFA	very long-chain polyunsaturated fatty acid
W303	yeast W303-1A Mat alpha ade-ura-leu-his-trp strain
WT	wild type, *Phaeodactylum tricornutum* wild type
x g	times gravity
Y(II)	steady-state quantum yield of PSII
ZEP1	zeaxanthin epoxidase protein 1
µF	capacitance
Ω	impedance, ohm

TABLE OF CONTENTS

1 ABSTRACT

Chloroplasts play a central role in the carbon metabolism of photosynthetic organisms. Within this compartment, inorganic CO_2 is assimilated by the Calvin-Benson cycle which is fuelled with reducing energy and ATP by the light reactions taking place in the photosynthetic membranes, the thylakoids (Nelson & Ben-Shem 2004). Thylakoid membranes as well as chloroplast limiting membranes differ in primary endosymbionts such as green algae and higher plants (*Archaeplastida*) on the one hand and secondary endosymbionts such as Heterokonts including the model species *Phaeodactylum* and *Nannochloropsis* on the other hand (Moustafa et al. 2009, Tirichine & Bowler 2011).

Although thylakoid membranes contain up to 80% proteins, chloroplast lipids play an essential role in photosynthesis efficiency and regulation. Membrane or neutral lipids consisting of fatty acids and a head group bound to a glycerol backbone are called glycerolipids (in the following text also simply lipids). Glycerol is a chiral molecule and thus the esterification of fatty acids underlies stereospecific control.

According to stereospecific numbering (sn), the polar head group occupies the *sn*-3 position whereas the first fatty acid is added at *sn*-1 and the second one at the *sn*-2 position (**figure 1.1**).

The chloroplast glycerolipid profile differs from other compartments by the predominance of monogalactosyldiacylglycerol (MGDG), digalactosyldiacylglycerol (DGDG), sulfoquinovosyldiacylglycerol (SQDG) and phosphatidylglycerol (PG) (Benning 2009, Boudière & Maréchal 2014) (**figure 1.1**). Phosphatidylcholine (PC) is a minor component in the chloroplast envelope of plants and trigalactosyldiacylglycerol (TGDG) occurs under stress conditions (Benning 2009, Boudière & Maréchal 2014). The lipid quartet of MGDG, DGDG, SQDG and PG is strikingly conserved from cyanobacteria to primary and secondary endosymbionts (Boudière et al. 2013, Petroutsos et al. 2014). Fatty acid profiles of the lipid classes vary between clades, especially by the presence of very long chain polyunsaturated fatty acids (VLC-PUFAs) such as eicosapentaenoic acid (EPA, 20:5) in protists like Heterokonts, while higher plants contain maximal 18-carbon acyl chains with four double bonds (18:4) (Lemke et al. 2010, Lang et al. 2011).

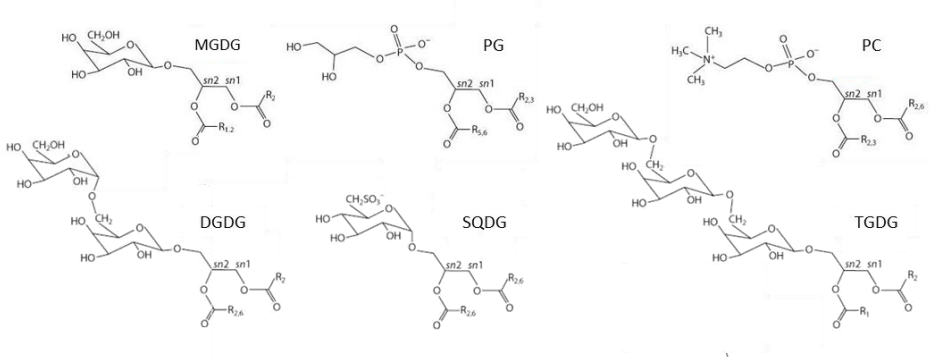

Figure 1.1. Glycerolipid classes found in chloroplast membranes. The lipid quartet MGDG, DGDG, SQDG and PG are the dominant lipid classes conserved throughout photoautotrophic species. TGDG is observed under stress conditions such as cold stress. PC is a likely precursor for chloroplast lipid synthesis and is found in the outer leaflet of the outer envelope membrane. MGDG, monogalactosyldiacylglycerol; DGDG, diagalactosyldiacylglycerol; PG, phosphatidylglycerol; SQDG, sulfoquinovosyldiacylglycerol; TGDG, trigalactosyldiacylglycerol; PC, phosphatidylcholine. The stereospecific numbering (sn) positions are indicated (modified from Benning 2009).

ABSTRACT

The glycerolipid profiles of subcellular membranes as well as the neutral lipid content stored in lipid droplets are influenced by environmental factors, a phenomenon known as lipid remodelling. One remarkable feature in higher plants is the possibility to replace endomembrane and mitochondria phospholipids by chloroplast produced DGDG when phosphate is limiting (Jouhet et al. 2004, Kelly & Dörmann 2002, Kelly et al. 2003).

Phaeodactylum and *Nannochloropsis* are model species for glycerolipid research because of their potential to be commercialized for biofuel or pharmaceutical application (Hamilton et al. 2016, Medipally et al. 2015, Vinayak et al. 2015, Wen & Chen 2003). For biofuel production, the focus lies on the production of neutral lipids, triacylglycerols (TAGs). One trigger for TAG accumulation is nutrient starvation (Du & Benning 2016). A comprehensive study on *Nannochloropsis* lipid remodelling has been carried out (Simionato et al. 2013). We performed a similar study on *Phaeodactylum* in which we investigated lipid remodelling in response to nitrogen and phosphate starvation. Furthermore, we identified *Phaeodactylum* sequences that could encode proteins involved in chloroplast lipid synthesis. We had aimed to characterize those proteins *via* reverse genetics. We have focused on *Phaeodactylum* mutant lines containing reduced levels of DGDG synthase isoforms. By comparing lipid profiles of those mutants in the presence or absence of phosphate we attempted to reveal whether the diatom was able to replace phospholipids by DGDG or betaine lipids.

Triggers of neutral lipid accumulation

The study on nutrient-driven lipid remodelling in *Phaeodactylum* has also defined our standard growth conditions, as well as reference levels for possible TAG accumulation. This was applied in further studies. One of them was a forward chemical genetics approach to identify new players in neutral lipid production. Generally, three different strategies exist to enhance neutral lipid contents by chemical or genetic engineering, which are designated as “push”, “pull” and “protect” (Van Hercke et al. 2014). “Push” means to increase the synthesis of precursor molecules, “pull” to increase the flux into neutral lipids and “protect” to prevent TAGs or lipid droplets from degradation (Van Hercke et al. 2014). We identified molecules that would act in the “pull” strategy.

Drugs that triggered lipid accumulation grouped into two categories: the inhibition of competitive pathways, and nitric oxide (NO•) signalling. While some NO• signatures are deciphered to be involved in lipid peroxidation, pathogen defence and programmed cell death (PCD) in phototrophs (Mittler 2002, Wendehenne et al. 2001), a role in signalling cascades inducing lipid accumulation was unknown. We focused on the interplay of NO• production from different sites and their possible effect in triggering neutral lipid accumulation. We conclude that in dependence of the production site, NO• serves as a second messenger for critical life conditions and thereby triggers TAG accumulation.

Production and trafficking of very long chain fatty acids

Besides the high levels of TAGs, *Nannochloropsis* and *Phaeodactylum* stand out by high levels of VLC-PUFAs, especially EPA. With the differential locations of fatty acid synthesis and desaturation in the chloroplast stroma on the one hand and fatty acid editing by elongation and desaturation events in the ER on the other hand, a controlled fatty acid trafficking system is required for the homeostasis of glycerolipids produced by the "prokaryotic", the "eukaryotic" or the "omega-pathway", respectively (Petroutsos et al. 2014). In *Arabidopsis*, the current and still incomplete model of fatty acid trafficking involves hydrolysis of stroma acyl-ACPs to free fatty acids (FFAs) by thioesterases, their passive transport over the chloroplast inner envelope, their activation to acyl-CoA on the cytosolic site of the outer envelope membrane, their import to the ER lumen, the export of the lipid precursors for chloroplast import from the ER, and the transport through the chloroplast envelope by the TGD transporter complex (Li et al. 2015b). By *in silico* analyses we did not find evidence for the existence of similar transporter systems in neither, *Phaeodactylum* or *Nannochloropsis*. Thus, how trafficking events occur through secondary plastids as found in Heterokonts is completely unknown and the present study aims to shed light into the elusive "omega pathway".

EPA synthesis relies entirely on ER located enzymes but this fatty acid specie is enriched in chloroplast lipids (Domergue et al. 2002). Therefore, the question of fatty acid fluxes in Heterokonts is intriguing. We firstly addressed the proteins involved in EPA synthesis, namely desaturases and elongases (Haslam & Kunst 2013, Arao et al. 1994).

We conducted *in silico* analyses of the enzyme equipment in *Phaeodactylum* and *Nannochloropsis* to facilitate future protein characterizations. Until now, there was evidence only for the action of PUFA elongases in EPA production in both, algae and mosses (Petrie et al. 2010, Vaezi et al. 2013, Zank et al. 2002). We have confirmed the conserved Δ6-elongase activity of a *Phaeodactylum* protein. Furthermore, our analyses identified a novel class of elongases that form a Heterokont specific phylogenetic cluster. Amino acid sequences of those putative proteins contain motifs conserved in saturated fatty acid elongases. We therefore called this new class Δ0-elongases (Δ0-ELO). We have investigated the function of the most expressed form in *Nannochloropsis* and in yeast heterologous system. Knock out mutants have reduced MGDG levels and altered photosynthesis and photoprotection properties. Based on our results we assume Δ0-elongases to play in the "omega pathway" of fatty acid translocations.

With the aim to elucidate the "omega pathway", we started to investigate the potential EPA-carrying precursor molecule which would be imported into the chloroplast *via* reverse genetics in *Phaeodactylum*. Furthermore, in all studies on *Nannochloropsis* we could observe a tight balance of the MGDG and DGTS proportions. We therefore speculate the betaine lipid to be at the base for VLC-PUFA import into the chloroplast.

The interplay of chloroplast lipids and photosynthesis

Not only the "omega pathway" is unknown but also the function of VLC-PUFAs in a redox poise environment as the thylakoid membrane remains elusive. We were able to provide knowledge on the role of EPA-rich MGDG in photosynthesis and photoprotection in *Nannochloropsis*. These light-responsive processes occur in the thylakoids of all photosynthetic organisms. Distinct thylakoid membrane structures in secondary endosymbionts compared to primary plastids come along with differences in light reactions (Kuczynska et al. 2015, Lepetit et al. 2012). Light quality and quantity influence the balance between photochemistry and photoprotection in dependency of time, speed and the interaction with other stresses. This complicated interplay is far from being understood. Photoreceptor proteins, chlorophylls, xanthophylls, carotenoids, photosynthesis related retrograde signals,

reactive oxygen species (ROS), and redox and pH regulated proteins respond directly or indirectly to light and function in short or long term light acclimation (Eberhard et al. 2008, Rolland et al. 2012). Non-photochemical quenching (NPQ) is the most important short term high light response (Eberhard et al. 2008, Rolland et al. 2012). Diatoms compared to higher plants have higher NPQ capacities although they rely mostly on one of the three quenching parameters, *i.e.* the energy-dependent qE (Derks et al. 2015, Goss & Lepetit 2015). Diatoms possess a specific qE-related xanthophyll cycle with pigments that are more soluble in the lipid phase and thus more accessible to deepoxidase, which itself has higher activities compared to the plant analog (Goss & Lepetit 2015, Grouneva et al. 2011, Lepetit et al. 2012, Nymark et al. 2009). The hexagonal phase II (HII) building galactolipid MGDG is supposed to be required for the induction of NPQ by facilitating solubilisation processes (Demé et al. 2014, Goss & Jakob 2010). In the Δ0-elongase mutant possessing lower MGDG levels, NPQ is increased. Based on our data and comparison with MGDG regulations reported in literature we pointed a possible role of this EPA-rich lipid class in high light signalling.

The role of chloroplast lipids in the regulation of membrane viscosity

MGDG and EPA are discussed to regulate lateral membrane fluidity with opposing effects (Garab et al. 2016, Los & Murata 2004). During cold stress, membranes become more rigid and cells of poikilothermic organisms therefore induce fatty acid desaturation to counteract reduced mobility (Sinensky 1974). As expected, the amount of VLC-PUFAs increased in cold-stressed *Nannochloropsis*. By comparing the cold stress response of *Nannochloropsis* wild type and the Δ0-elongase mutant having reduced MGDG levels under optimal conditions, we observed a head start in the temperature acclimation response in the mutant, thereby confirming the assumption of a negative impact of MGDG on membrane viscosity.

Taken together this study advances the understanding of the “omega pathway” and the role of EPA in the thylakoid membranes in Heterokont species. We provide the first comprehensive study on homeoviscous adaptation in a VLC-PUFA-rich organism. New players in neutral lipid accumulation were revealed including a regulatory function of the ubiquitous second messenger NO•.

2 LITERATURE REVIEW

2.1 Heterokonts are secondary endosymbionts and important model organisms for glycerolipid research

2.1.1 *Endosymbiosis*

Most eukaryotic photosynthetic organisms are monophyletic since they share one common ancestor, which is a cyanobacterium engulfed by a heterotrophic cell (Tirichine & Bowler 2011). This first endosymbiosis event occurred 1.8 billion years ago (Tirichine & Bowler 2011). From this primary endosymbiont the superphylum *Archaeplastida* or *Plantae* descends which are monophyletic in both host and plastid (Qiu et al. 2013). A noticeable exception concerns a distinct primary endosymbiosis which has given rise to euglyphid amoebae (McFadden 2014). *Archaeplastida* comprise

the green lineage (*Viridiplantae*) possessing the photosynthetic pigments chlorophyll (Chl) *a* and *b*, *Rhodophyta* possessing Chl *a* and *c*, and *Glaucophyta* possessing only Chl *a*, that have diverged more than 550 million years ago (Cavalier-Smith 2003, Moreira & Deschamps 2014).

Multiple secondary endosymbiosis events occurred during which a primary endosymbiont was integrated into another host cell. This includes two green algae engulfment and an unknown number of red algae captures (Moreira & Deschamps 2014). The red lineage comprises the large kingdom of *Chromalveolata* that covers the phyla *Cryptophyta*, *Haptophyta*, *Dinoflagellata*, *Apicomplexan* and *Heterokonta* (Heterokonts) (Moustafa et al. 2009, Tirichine & Bowler 2011). This event is discussed to date 300 million years ago (Scala et al. 2002). Heterokonts comprise diatoms including *Phaeodactylum* and Eustigmatophyceae including *Nannochloropsis* that will be in the focus of this work. The first fossil record of diatoms dates 146 years ago (Vardi et al. 2008b), the one of a pennate diatom 90 million years ago (Bowler et al. 2008). Whether the red lineage has diverged from a secondary endosymbiosis or a tertiary endosymbiosis is under debate. In the theory of a tertiary endosymbiosis, the uptake of a *Prasinophyceae* (green algae) occurred prior to the engulfment of a red alga (Moustafa et al. 2009). This is based on phylogenetic assessments of nuclear endosymbiotic gene transfer (EGT)-derived genes in diatoms. According to their automated method, “green” genes are four times more abundant than “red” genes (Moustafa et al. 2009). However, this idea is challenged by more recent analyses by Moreira and Deschamps who pointed methodical limitations of the earlier study (Moreira & Deschamps 2014). Besides mathematical obstacles, one problem is the low number of sequenced organisms from the red lineage and thus divergence of a given sequence from the reference pool could be due to incomplete sampling. Indeed, the ratio of protein references from the red:green lineage were 1:17. Manual sequence analyses revealed 90% of the EGT genes attributed to the green lineage as false positive and only 30 diatom genes have a clear green origin. Therefore these authors deny the existence of tertiary endosymbiosis (Moreira and Deschamps 2014). On the other hand, among the algae derived genes in the green algae *Bigelowiella natans,* 22% have a red algal origin that could indicate a cryptic red alga

endosymbiont and thus supports the hypothesis of tertiary endosymbiosis (Curtis et al. 2012, Qiu et al. 2013). Evidence in favour or against the existence of tertiary endosymbiosis is besides technical restrictions complicated by potentially long evolutionary distances and high selection pressure (Qiu et al 2013).

The endosymbiont loses autonomy by reduction or loss of its organelles. A co-infection with parasitic *Chlamydia* during primary endosymbiosis is discussed to have facilitated the establishment of a chloroplast in the host cell due to the secretion of proteins that allowed carbon and energy transfer between the host and the endosymbiont (reviewed in Qiu et al 2013). Accordingly, 55 genes with a putative chlamydial origin are present in photosynthetic eukaryotes, 37 of which potentially targeted to the chloroplast. However, *Chlamydia* infections are never observed in endosymbionts and this phylum groups closer to non-photosynthetic single celled organisms (Moreira and Deschamps). Great extents of EGT from the engulfed genome to the host nucleus occur while other genes might be lost. A typical chloroplast does thus possess less than 250 genes (Qiu et al 2013). Due to the new environment, the evolutionary pressure is high on endosymbionts and EGT sequences evolve rapidly complicating their identification (Moreira and Deschamps 2014). EGT accounts for 6-20% in photosynthetic eukaryotes and 7.5% of estimated sequence tags (EST)s in *Phaeodactylum* derive from horizontal gene transfer from other unicellular eukaryotes or bacteria (Qiu et al. 2013, Vardi et al. 2008b). Furthermore, a high number of transposable elements contribute to Heterokont genomes. Large scale gene duplication events do not appear to be important for diatom evolution. Notably, 95% of the *Phaeodactylum* genome is non-coding (Vardi et al 2008). For further information on the evolution of *Chromalveolata* the reader is referred to (Petroutsos et al 2014, McFadden 2014, Qiu et al. 2013, Keeling 2010).

The “mosaic genome” of *Chromalveolata* including *Phaeodactylum* and *Nannochloropsis* might have contributed to the success of the versatile red lineage in marine habitats. One outstanding feature is the high biomass productivity that is caused by very efficient photosynthesis taking place in the chloroplasts. Chloroplasts in secondary endosymbionts are also called “secondary plastids”, “complex plastids” or “phaeoplast” in diatoms but in the present work the term *chloroplast* will be used for

simplicity reasons. They differ from primary plastids in the organization of the membranes limiting the organelle or embedding the photosynthetic machinery, as well as in photosynthetic pigments and proteins.

2.1.2 *Structure and composition of chloroplast membranes*

2.1.2.1 Chloroplast limiting membranes

While the chloroplast in the green lineage possesses two limiting membranes, *i. e.* the inner and outer envelope membrane, secondary endosymbiont chloroplasts are surrounded by three or four membranes (Flori et al. 2016), McFadden 2014, Petroutsos et al 2014) (**figure 2.1**). The two inner membranes derive from the cyanobacteria, the third from the primary endosymbiont, and the outermost membrane from the host cell upon phagocytosis of the alga (Petroutsos et al 2014, Chevalier-Smith 2003). The third membrane, also referred to as the periplastidial membrane, enclose a tiny compartment that represents reduced cytoplasm and might in some species even contain a reduced nucleus from the engulfed eukaryote (Flori et al. 2016, Grosche et al. 2014). In some *Chromalveolata* species including Heterokonts, the outermost secondary chloroplast limiting membrane, the chloroplast-endoplasmic reticulum membrane, is still contiguous with the host ER and nucleus whereas other species have lost this connection (Flori et al. 2016, Keeling 2010, Ma et al. 2016). Given the three origins of the four membranes, different lipid compositions can be assumed. Since the two outer Heterokont chloroplast membranes derive from a heterotroph cell, a phospholipid constitution is likely (Petroutsos et al 2014). In the green lineage and probably in the inner membranes of Heterokont chloroplasts, four glycerolipid classes are conserved, *i.e.* MGDG, DGDG, SQDG and PG. The same lipid quartet is found in thylakoid membranes (**figure 1.1**) (Boudière et al 2014).

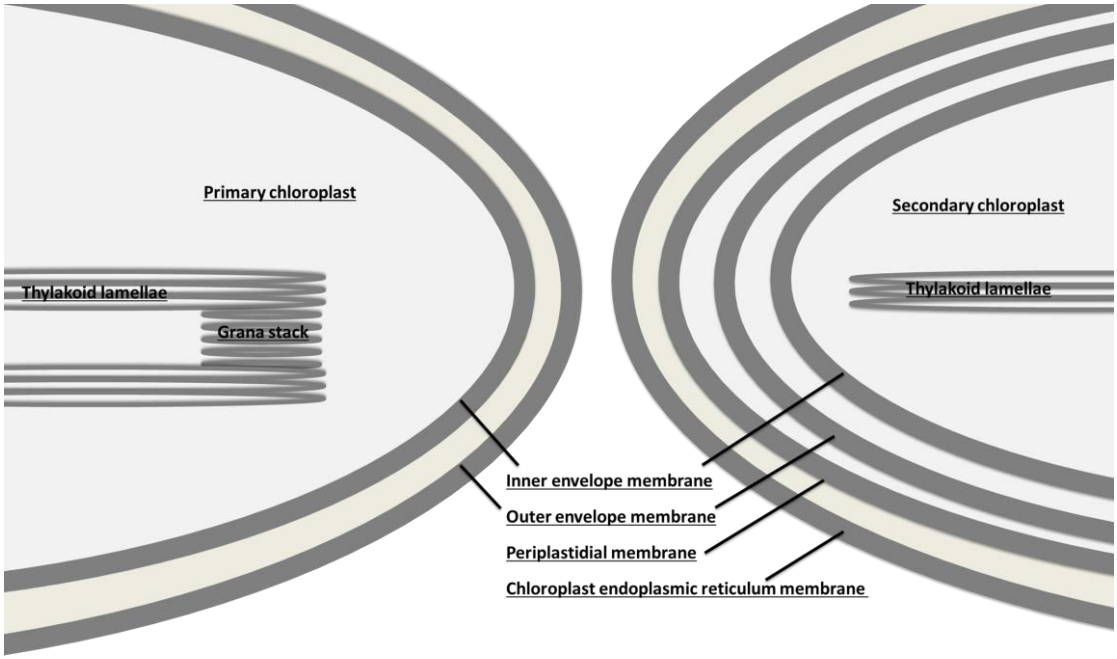

Figure 2.1: Scheme of the chloroplast structure in primary endosymbionts (primary chloroplast) and secondary endosymbionts (secondary chloroplast). Thylakoid membranes are present in the stoma of the chloroplast and have a bipartite macrostructure in primary chloroplasts. In primary endosymbionts, the photosynthetic organelle is limited by an envelope consisting of an inner and outer envelope membrane. Secondary plastids contain one or two additional membranes surrounding the envelope.

2.1.2.2 Organization of glycerolipids in thylakoid membranes

The dense protein loading of thylakoid membranes requires a controlled and dynamic lipid matrix. One feature of thylakoids is the high abundance of polyunsaturated fatty acids that fill the grooves of membrane spanning proteins (Garab et al. 2016). While in plants the highest desaturation degree is found at 18:4, Heterokont chloroplast lipids are rich in 20:4 and 20:5 (Abida et al. 2015, Dolch & Maréchal 2015, Simionato et al. 2013) (**figure 2.2**).

An open question is whether the specific enrichment in VLC-PUFAs in thylakoid lipids have contributed to the success of the red lineage in marine systems that have higher photosynthetic and photoprotection capacities compared to the most green algae allowing higher biomass production (Kuczynska et al. 2015, Goss and Lepetit 2014, Chevalier-

Smith 2003). Desaturation levels are dynamically changed in response to environmental factors as growth phase (Meï et al. 2015), temperature (**see 2.7.3**) and light quality. Blue light causes the absence of 20:0 and an increase in 20:5 in *Nannochloropsis* (Chen et al. 2013, Teo et al. 2014). This finding is especially interesting considering the opposing effects of blue and red light on photosynthesis, which indicates that a higher desaturation level is maintained when photoprotection is induced. The Heterokont fatty acid profiles of the four chloroplast lipids vary with the highest desaturation levels in MGDG, followed by DGDG based on the predominance of 20:5 in these lipids (Abida et al. 2015, Simionato et al. 2013).

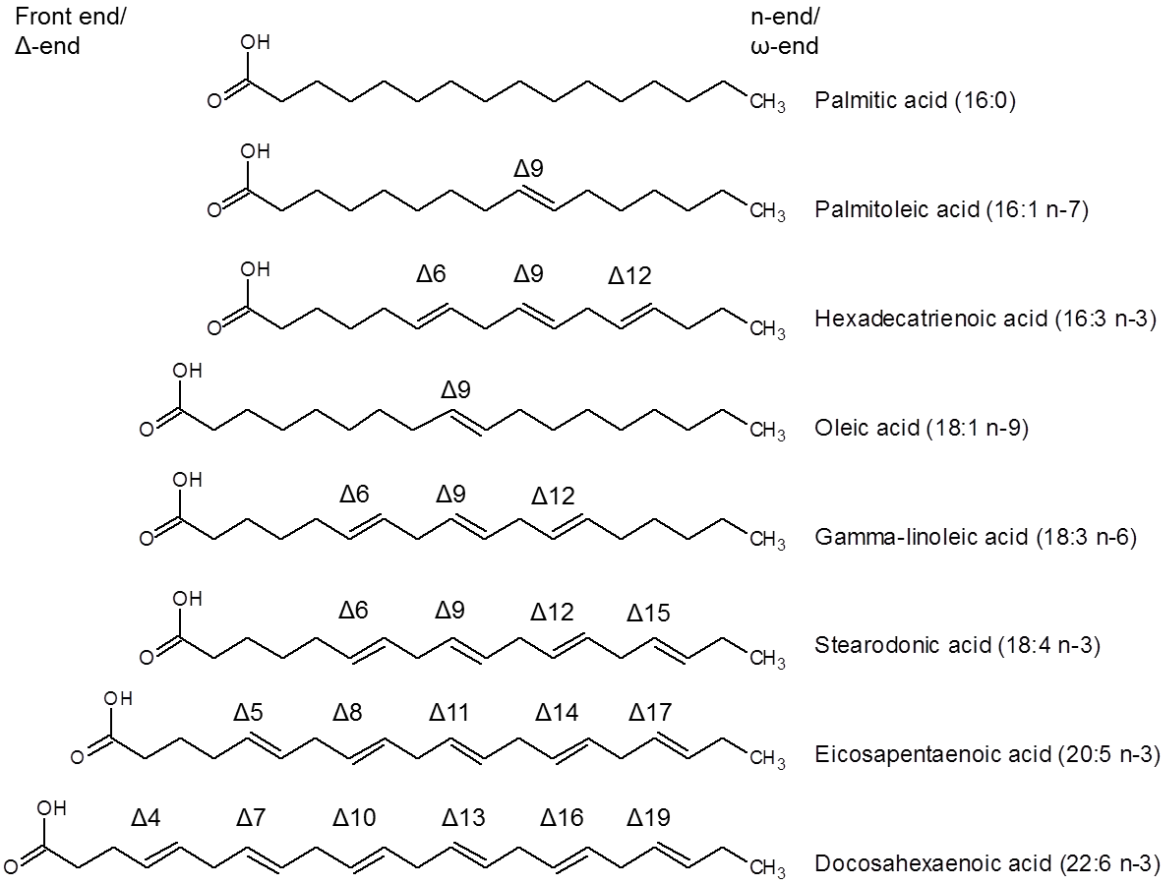

Figure 2.2. Overview of the most important fatty acid species in *Phaeodactylum* and *Nannochloropsis*. The carboxyl-end, also called front end is designated as Δ-end and the methyl-end is designated as n-end or ω-end. Positions of double bonds are indicated. Molecular structures were drawn using SketchChem software.

The importance of the lipid head group paired with a specific fatty acid profile is yet to be investigated but it is obvious that both play a role in the lipids' function, and that distributions are not random. Molecular Dynamic Simulations (MD) on cyanobacteria *Thermosynechococcus vulcanus* or spinach thylakoids indicate heterogeneous lipid distribution on the nanoscale (van Eerden et al. 2015). While according to the computer modelling distribution of PG is random, SQDG is seldom a neighbour molecule. This is likely caused by repulsion of the two negative charges. The small head group of PG could serve as a counterion bridge to neutralize charges in the membrane. All-atom simulations indicate low abundances of DGDG-DGDG binding probably due to steric hindrance. Simulations on spinach thylakoids point the presence of PG-MGDG clusters as well as PG-rich nanodomains. On the fatty acid level, saturated and trans-unsaturated fatty acids interact more with each other than with unsaturated. PUFA containing lipids cluster together compared to the same classes with other acyl groups such as 18:3/18:3 MGDG and 18:3/18:3 DGDG. Calculations of lateral fluidity indicate a similar diffusion speed for all lipids and slightly higher velocities for PUFA-containing lipids and PG. On the other hand, bulky head groups as in DGDG have a lower diffusion constant (van Eerden et al. 2015). Lateral fluidity is an important regulator of photosynthesis under different growth conditions and is supposed to involve high desaturation levels and MGDG (see also photoprotection and homeoviscous adaptation). This is however poorly understood.

The nature and role of MGDG is probably the most ambiguous and results on membrane phases at MGDG rich regions are controversial (Garab et al. 2016). Pleiotropic phenotypes of mutants with reduced MGDG levels complicate functional interpretations. Those lines display growth and photosynthesis reduction, lower chlorophyll contents, impaired chloroplast and thylakoid biogenesis, lower PSII core protein repair and thus higher susceptibility to photoinhibition (Boudière et al. 2014). MGDG comprises an uncharged, bulky galactose head that gives the lipid a cone shape that causes inverted hexagonal phase structures (**figure 2.3**). This is important for membrane curvature and might facilitate membrane fusions and stacking. Notably, the presence of a hexagonal II phase

in the thylakoid lumen is discussed that could facilitate the xanthophyll cycle (**see section 2.3**) (Garab et al. 2016).

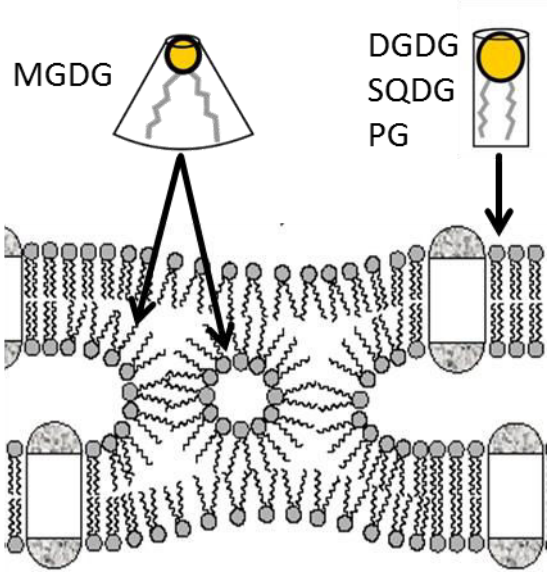

Figure 2.3: Scheme of the hypothetical thylakoid membrane curvature. DGDG, SQDG and PG are bilayer forming lipids. Hexagonal II phase MGDG might facilitate membrane curvature and is discussed to fill the luminal space. Modified from (Garab et al. 2016).

While PG, SQDG and DGDG are bilayer forming lipids by inert properties, MGDG is a hexagonal II phase building lipid and does not spontaneously form bilayers (**figure 2.3**) (Deme et al. 2014). However, other studies indicate that MGDG fatty acid composition determines its aggregation. When both fatty acids are saturated and have a chain length of C10-20, or 16:0/16:1, or even 64% 18:3, MGDG built lamellar phases at temperatures below 80°C (Baczynski et al. 2015). Concomitantly, PUFA-rich MGDG facilitate transition from bilayer to non-bilayer phase (Van Eerden et al. 2015). MD studies of the structural properties of hydrated bilayer with 18:3/18:3 MGDG reveal that the cone shaped lipid is able to form stable bilayer structures on a sub-microsecond scale. MGDG could thus globally make bilayers and locally inverted hexagonal phases (Baczynski et al. 2015). Coexistence of lamellar and non-bilayer phases are indicated experimentally by NMR following radiolabeled PG to monitor lipid phases in spinach thylakoids and by

neutron diffraction (Demé et al. 2014, Krumova et al. 2008). Data indicate that between 14°C and 28°C PG is found in both lamellar and less organized structures accounting for the presence of both bilayer and inverted hexagonal phases, which are interconnected. With elevated temperatures, the bilayer proportion decreases (Garab et al. 2016, Krumova et al. 2008).

The two negatively charged lipids PG and SQDG are dynamically regulated in response to phosphate availabilities. In addition, PG might completely substitute SQDG since *Arabidopsis* SQDG-null mutants are not only viable but do not have a fitness phenotype under optimal growth conditions. On the other hand, abolishing PG is lethal and reduced levels cause severe photosynthesis and growth retardations (Boudière et al. 2014). The dependency on SQDG or PG for the cells fitness is strongly species dependent (Sato 2004).

In species from the green lineage, thylakoid membranes are organized in stroma lamellar regions enriched in PSI and grana stacks enriched in PSII (**figure 2.1 and figure 2.4**) (Pribil et al. 2014). PSII and LHCII have flat stromal surfaces that allow stacking whereas ATPsynthase and PSI are bulky (Kirchhoff 2013). Heterokonts lack the bipartite structure and possess only lamella stacks consisting of three thylakoid membranes that span throughout the chloroplast (**figure 2.1 and figure 2.4**) (Lepetit et al. 2012). Distribution of the components of the photosynthetic machinery and lipids are not random. According to the current understanding, in the stacks consisting of three double membranes, stroma exposed regions are enriched in PSI, PSI-specific FCPs and probably the bulky ATP synthase. These “outer” membranes enclose "inner” membranes in which PSII and major FCPs are more abundant. Cytb6f is equally distributed. On the lipid level, MGDG is thought to be predominant in inner membranes and SQDG in outer membranes. The negatively charged lipid is supposed to inhibit NPQ whereas the HII lipid is beneficial and thus, diatom thylakoids are partitioned in both, linear electron flow and photoprotection sites. PSI however is protected from oxidative damage by the presence of FCPs. Further microdomain organization is likely since SQDG inhibits the Cytb6f complex which might be protected by an MGDG shield (Lepetit et al. 2012). This model is currently re-examined in our laboratory.

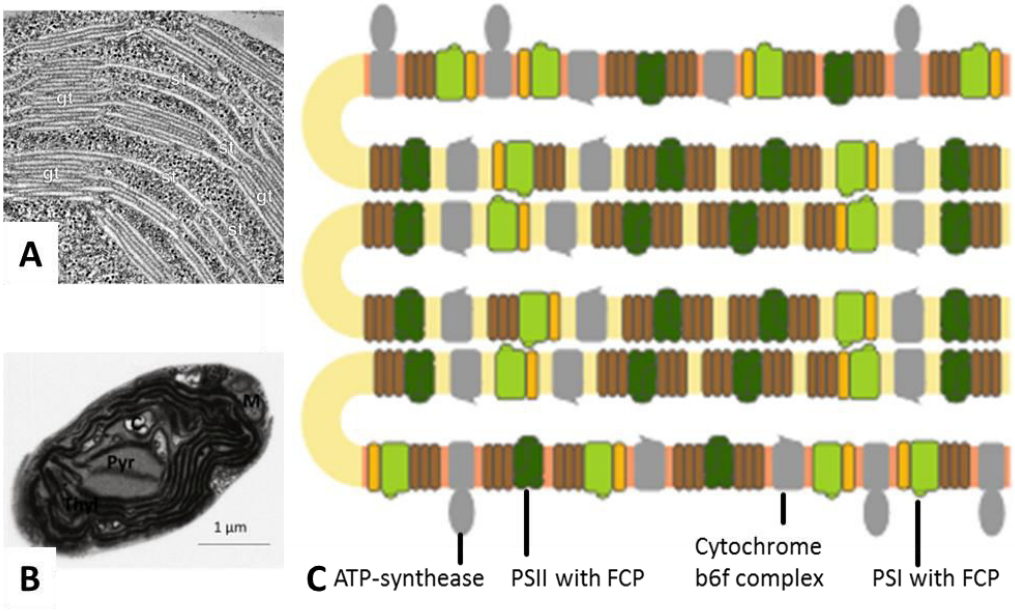

Figure 2.4. Thylakoid membrane structures in higher plants (A), *N. gaditana* (B) and *P. tricornutum*. A. Thylakoids of higher plants form stacks that are connected by lamellae (Austin & Staehelin 2011). B. In the chloroplast of P. tricornutum (c) typically possesses seven thylakoid (Thyl) lamellae consisting of three membranes. Thyl surround a specific suborganelle, the pyrenoid (Pyr) (Flori et al. 2016). C. Schematic view on P. tricornutum thylakoids. The lamella setup is similar to Nannochloropsis. Due to steric properties, PSI and ATP-synthase are discussed to be enriched in stroma-exposed membranes and PSII in inner membranes of the stack of three thylakoid double membranes (Lepetit et al. 2012).

2.1.3 *The model organisms Phaeodactylum tricornutum and Nannochloropsis gaditana*

More than 23,000 Heterokont species are described (Chapman 2009, (Riisberg et al. 2009). They make the major part of marine phytoplankton and are estimated to contribute to 20% of the worlds' primary production (Falkowski et al. 1998, Vardi et al. 2008b). Indeed, per year around 45 gigatons of organic carbon are produced by the oceans (Falkowski et al. 1998).

Heterokonts include both photoautotroph and heterotroph species. Photosynthetic Heterokonts group into the *Phaeista* including the *Eustigmatophyceae* class and *Khakista* including *Bacillariophyceae* (diatoms) that are differentiated based on sequence comparisons and morphologies (Riisberg et al. 2009). Diatoms possess

frustules, which are silica-containing cell walls. This is a unique feature of this phylogenetic group and the use in defence of desiccation are discussed (Sims 2006). While *Bacillariophyceae* forms the largest group with 4,256 accepted species, only 35 *Eustigmatophyceae* are known (Chapman 2009). The group of diatoms is furthermore split into centric and pennate species that have diverged 90 million years ago, but their genomes have strongly evolved so that less than 60% of the genes are shared (Bowler et al. 2008).

Morphological characteristics of pennate diatoms are presented in **figure 2.5** (Falciatore & Bowler 2002). The cell contains a single photosynthetic plastid, the phaeoplast (called chloroplast in the following), and all common eukaryotic organs including lipid droplets. A silica containing frustule encloses the cell and consists of two engaged halves, the larger epitheka and the smaller hypotheca. The larger outer surface is called valve and is engraved by circular silica bands, the girdle. The raph slit allows secretion of mucus for motility purposes (Falciatore & Bowler 2002).

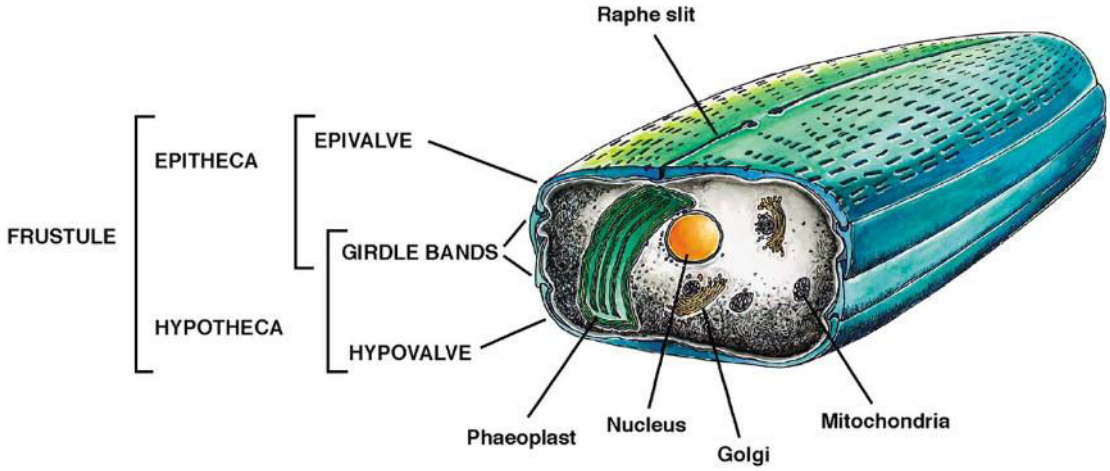

Figure 2.5. Scheme of a pennate diatom cell such as *Phaeodactylum*. The cell contains all typical organs including a vacuole (not shown). The symplast is enclosed by a silica-containing frustule that is built like a box (hypotheca) with a lid (epitheca). Both theceae possess a valve and girdle bands. The Epitheca contains the raphe slit for mucus secretion (Falciatore & Bowler 2002).

Four different morphotypes of pennate diatom *Phaeodactylum tricornutum* are known, *i. e*. the cruciform, triradiate, fusiform and oval cells. Depending on the strain, the one or the other is dominant but proportions can vary in response to culture conditions as temperature and age by transformation of the different cell shapes (**figure 2.6 A**) (He et al. 2014). Indeed, a cell can diverge from one morphotype into another (He et al. 2014 24710200, Lewin et al. 1958). Division of a more oval shaped cell gives rise to one fusiform and one oval shape daughter cell. Oval cells are observed to be motile and are enriched in silica (Lewin et al. 1958).

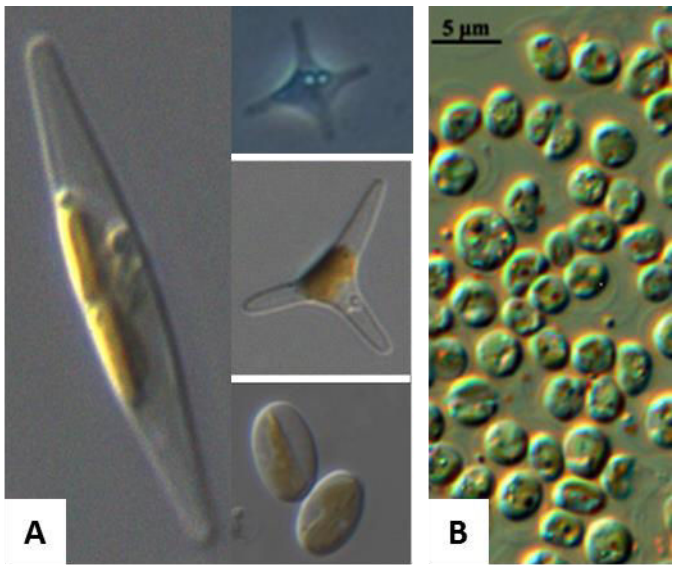

Figure 2.6. Microscope images of *P. tricornutum* and *N. gaditana* cells. **A. Four different morphotypes** of *P. tricornutum* (Vardi et al. 2008b, He et al. 2014). In Pt_1, the fusiform is dominant. **B. *N. gaditana* cells** vary in size and shape (Hibberd 1981, https://ncma.bigelow.org/ccmp527 06.08.2016).

Species of the *Nannochloropsis* genus are round and reach a cell diameter of maximal 5 µm and are not motile. They are euryhaline and primarily found in marine habitats (Hibberd 1981). Today, the genus comprises six species: *N. gaditana*, (**figure 2.6 B**) *N. oceanica, N. granulata, N. limnetica, N. oculata and N. salina* (Ma et al. 2016).

Both *Nannochloropsis* and *Phaeodactylum* are able to grow under photoautotroph or mixotroph conditions (Ma et al. 2016, Liu et al. 2009). *Phaeodactylum* reaches the

highest growth rates when fed with glycerol or acetate, whereas glucose and autotroph have similar effects. However, various strains and even ecotypes display differences in in ther use of carbohydrates (Liu et al. 2009).

Given the aquatic habitat, nutrients are often limited and provided upon turbulences. Heterokonts have adapted to this fluctuating environment by a rapid nutrient uptake that might be stored in a vacuole or as triacylglycerol (TAG) for later utilization (Vardi et al. 2008b). In the last decades *N. gaditana* and *N. oceanica* as well as *P. tricornutum* have been most intensively studied with a focus on the optimization of one or several strains for the production of either long chain monounsaturated fatty acids (MUFA) bound to triacylglycerols (TAG) for biodiesel application or of valuable pigments and VLC-PUFA (Garay et al. 2014, Liu et al. 2013a, Mühlroth et al. 2013) being beneficial for human health (Gil & Gil 2015). Properties of *Nannochloropsis* TAGs already fulfil the requirements for biodiesel application (Ma et al. 2016). The great capacity of TAG synthesis together with high biomass production in various scales has qualified these three species as model organisms (Lebeau & Robert 2003, Ma et al. 2016, Radakovits et al. 2012). An economic and environmental advantage is the possible cultivation in waste water on non-arable land (Ma et al. 2016). Additionally, Heterokonts have a broad tolerance towards culture medium pH, salt and temperature (Radakovits et al. 2013).

Lipid and biomass productivity and lipid quality are highly sensitive to environmental factors and important efforts have been put in optimizing those factors in the last five years: fatty acid profiles and the resulting biofuel qualities or EPA/DHA quantities (Ma et al. 2016, Chen et al. 2013), oil stability (Ryckebosch et al. 2013), biomass production in response to different gas and light intensities and qualities (Chen et al. 2013, Chiu et al. 2009, Work et al. 2012), culture media (Chen et al. 2013, Meng et al. 2015), photobioreactor types and seasonal changes in outdoor facilities (Camacho-Rodríguez et al. 2014, Rodolfi et al. 2003). Nonetheless, a consensus model *Nannochloropsis* strain is not yet defined since they all have favourable characteristics. *N. oceanica* IMET1 stands out with the highest lipid productivity, *N. oculata* and *N. granulata* have the highest monounsaturated fatty acid (MUFA) contents important for biofuel applications, *N. salina* is used in waste water treatment, and *N. gaditana* is well studied for EPA

production and a molecular toolbox for genetic engineering of this species is available (Ma et al. 2016). The present study will focus on the pennate diatom *Phaeodactylum tricornutum* and the *Eustigmatophyceae Nannochloropsis gaditana*.

2.1.3.1 The interest in very long chain polyunsaturated fatty acids (VLC-PUFAs)

Lipids in the *Chromalveolata* kingdom are enriched in VLC-PUFAs with four or more desaturations, whereas in the green lineage linoleic acid (18:2 n-6, LA) and α-linolenic acid (18:3 n-3, ALA) are the most dominant VLC-PUFA species (Lang et al. 2011). EPA is enriched in *Chlorophyceae*, *Chrysophyceae*, *Prasinophyceae*, *Eustigmatophyceae* and *Bacillariophyceae* (Wen & Chen 2003). Fatty acid profiles reflect phylogenetic relations (Lang et al. 2011). VLC-PUFAs are differentiated into the ω-3 and ω-6 series according to the position of the first double bond counted from the carboxyl-end of the fatty acid (**figure 2.2**). These are in the ω-3 series ALA, stearidonic acid 18:4 n-3, eicosatetraenoic acid 20:4 n-3, eicosapentaenoic acid 20:5 n-3 (EPA) and docosahexaenoic acid 22:6 n-3 (DHA). Marine ω-6 VLC-PUFAs are LA, γ-linolenic acid 18:3 n-6 (GLA) and arachidonic acid 20:4 n-6 (ARA). While C18-PUFAs are widely spread among the kingdoms, species that produce EPA and DHA except for microalgae are rare. Some bacteria and *Mucorales* fungi have the capacities of VLC-PUFA production (Bajpai & Bajpai 1993). Marine *Shewanella* and similar bacteria may contain up to 40% EPA (Yazawa 1996). Those species are found in the intestines of several fishes (Dailey et al. 2015). A lower plant, the liverwort *Marchantia polymorpha* contains up to 6% EPA and 3% ARA (Kajikawa et al. 2008). While most eukaryotic heterotrophs obtain ω-3 VLC-PUFAs via diet, scallop has the ability to synthesize EPA (Hall et al. 2002). For mammals, VLC-PUFAs are essential but production of EPA and DHA can be achieved in transgenic lines (Lee et al. 2016).

The interest in VLC-PUFAs for human nutrition is high. Mammals lack the Δ12FAD and are unable to synthesize the ω-6 fatty acid LA ($18:2^{\Delta 9,12}$) and the ω-3 fatty acid ALA ($18:3^{\Delta 9,12,15}$) (Lee et al. 2016, Sayanova & Napier 2004). The dietary intake of these essential fatty acids determines the ratio of synthesized PUFAs of the ω-3 and ω-6

series. LA is being elongated and desaturated by substrate unspecific enzymes into ARA ($20:4^{\Delta5,8,11,14}$) and ALA into EPA ($20:5^{\Delta5,8,11,14,17}$) and DHA ($22:5^{\Delta4,7,10,13,16,19}$) (Dolch & Maréchal 2015, Sayanova & Napier 2004). However, the human capacity of elongation and desaturation of C18 species into EPA and DHA is only 8% and 0-4%, respectively, and thus a dietary intake is required to meet the demand of ω-3 VLC-PUFA (Ruiz-Lopez et al. 2015, Sayanova & Napier 2004). It is believed that human physiology has adapted to an ω-6:ω-3-intake ratio of about 1 but in todays' Western diet the ratio is 15-17:1, thus enriched in pro-inflammatory fatty acids that may have a negative health impact (Ruiz-Lopez et al. 2015). VLC-PUFAs serve as substrates for hormone-like regulatory molecules, eicosanoids, namely prostaglandins, thromboxanes and leukotrienes, which depending on their ω-3 or ω-6 structure act as antagonists in different processes. They regulate inflammation, immune-reactivity, blood pressure, and platelet aggregation; and function in the prevention of atherosclerosis, arthritis, arrhythmia, heart attack, and thrombosis, TAG, metabolic disorders, diabetes, some cancer, multiple sclerosis, Alzheimer's disease and asthma (Funk 2001, Ji et al. 2015, Lee et al. 2016, Ruiz-Lopez et al. 2015, Wen & Chen 2003). Docosanoids including resolvins and protectins are all anti-inflammatory and involved in brain development and neurodegeneration and eye function (Lee et al. 2016). Furthermore, DHA is present in structural lipids in human membranes, where it is involved in lipid raft formation (Ruiz-Lopez et al. 2015).

The worlds' annual demand of EPA for medical applications alone is about 300 tons and the fatty acid must be refined from fish oil (Wen & Chen 2003). Herring, mackerel, sardine and salmon are the greatest dietary VLC-PUFA sources (Ruiz-Lopez et al. 2015). However, consumption of high quantities of fish may have negative health impacts due to the pollution of the oceans with cadmium, lead, mercury, dioxins, furans, polychlorinated biphenyls and polybrominated diphenyl ethers that accumulate in fish (Domingo et al. 2007). To reduce toxin indigestion, purified oils could serve as an alternative. Today, the major industrial source for EPA is oil from cod, menhaden, herring and krill (Robles Medina et al. 1998). Commercialized fish oil EPA pills contain 9-26% EPA and 9-17% DHA. Microalgae may contain twice as much of these fatty acid

species (Robles Medina et al. 1998). Furthermore, cultivation of algae does not interfere with the marine ecosystem that suffers from man-made loss of equilibrium and biodiversity (Worm et al. 2006). The conclusion on a need for industrialization of microalgae for EPA and DHA production is thus obvious.

Although *Phaeodactylum* wild type does not have the highest VLC-PUFA proportions, early studies on microalgae revealed the highest EPA productivity with up to 47.8 $mg.L^{-1}.d^{-1}$ (Robles Medina et al. 1998). Application of Heterokonts for food and feed does not necessarily involve TAG purification since the biochemical composition of *Nannochloropsis spp*. fulfils human nutrition demands. Protein, fibre, nucleotide, ash, nitrate and toxic heavy metal contents are low, but antioxidant, calcium, magnesium and zinc levels are high. Lipid and carbohydrate make more than 50% of biomass (Rebolloso-Fuentes et al. 2001). Microalgae and especially diatoms are already used in wastewater treatment, and the production of biofuel, fertilizers and secondary metabolites for medical compounds and pharmaceutics, as well as for food and feed for example in commercial aquaculture (Levitan et al. 2014, Vinayak et al. 2015). However, it is likely that gene engineered strains will be commercialized. In order to avoid having gene modified organisms in the food chain, EPA-rich oils could be extracted and used as feedstock for fish (Sayanova & Napier 2004).

For now, the only commercialized biotechnological resource providing an alternatively to fish are the yeast *Yarrowia lipolytica* and *Thraustochytrids* species that are related to Heterokonts (Gupta et al. 2012a, Ji et al. 2015, Lewis et al. 1999). A recent study compared an engineered *Phaeodactylum* strain that accumulates DHA (Pt_Elo5, overexpressing the Δ5-ELO from *Ostreococcus tauri*) to the wild type in which DHA is barely detected in different culture systems with volumes up to 1250 L. By modelling various growth factors (UV irradiation, light intensity, light phase duration, CO_2 availability and mixotroph growth), the transgenic line yielded 6.4 $\mu g.mg^{-1}$ dry weight DHA during mid-log growth, a value that would allow commercialization (Hamilton et al. 2015). Notably, these authors found mixotroph growth to not only to enhance the biomass yield in each growth system tested but to uncouple biomass production from the culture volume (Hamilton et al. 2015). Expression of the *O. tauri* Δ5-ELO in a

trophically converted *P. tricornutum* strain cultivated on glucose in the light increased biomass production by about 20% compared to photoautotroph Pt_Elo5. Allowing mixotroph growth, EPA and DHA accumulated best. On the other hand, fatty acid profiles changed in the heterotroph strain when grown in darkness with reduced EPA and DHA accumulation (Hamilton et al. 2016). This case study indicates a high potential of the diatom for VLC-PUFA production. VLC-PUFA are dominant in membrane lipids, while medium fatty acid chains with low desaturation degrees allocate in neutral lipids and may be used as biofuels.

2.1.3.2 The interest in biofuels produced by microalgae

Worldwide, 96% of transportations rely on fossil fuels and cause 36% of the rise in atmospheric CO_2 (Levitan et al. 2014). With the background of global warming and fossil resource exhaustion, the need for stronger implementation of alternative diesel is striking. In 2010, 18.2 billion liters of biodiesel have been produced (Liang & Jiang 2013). However in the same year, the petroleum consumption was about 3,830 billion liters, numbers still rising in spite of the Kyoto protocol (www.eia.gov/cfapps/ipdbproject/iedindex3.cfm?tid=5&pid=54&aid=2; 18.06.2016). Thus biodiesel compensated only about 0.5% of total fuel consumption. The yearly exploitation of fossil petroleum is worth about one million years of algal oil accumulation (Levitan et al. 2014).

Those species that stand at the base of fossil petroleum are now of interest for third generation biofuel production. High biomass producing oleaginous microorganisms in which 20-50% of dry weight is lipids have the highest potential to entirely replace fossil energy (Liang & Jiang 2013). Importantly, microalgae cultivation does not compete with agriculture. Indeed, since 22% of soy beans cultivated in the USA are used for biodiesel production the soybean oil price has increased by 100% (Durrett et al. 2008). In addition to using neutral lipids that accumulate in lipid droplets for diesel production, the algal biomass may also be used for the production of other energy carriers as hydrogen, ethanol, gas and oil (Paul Abishek et al. 2014). Notably, although environmental

advantages of biodiesel are obvious, negative health impacts are likely to be similar to fossil fuels (Madden 2016).

Methods to enhance TAG production on this purpose can involve biochemical and genetic engineering. In the biochemical approach, cells are stressed to remodel fluxes into lipid synthesis (Courchesne et al. 2009). Most studies on *Nannochloropsis* or *Phaeodactylum* use this strategy but the rising availability of tools for genetic engineering might shift the research focus towards targeted gene or transcription factor modelling (Li et al. 2014).

2.1.3.3 Genetic engineering possibilities of *Nannochloropsis* and *Phaeodactylum*

The genomes of three model species have been sequenced (Bowler et al. 2008, Corteggiani Carpinelli et al. 2014, Radakovits et al. 2012, Vieler et al. 2012). The genome of *N. oceanica* contains 28.7 Mb encoding about 12,000 genes (Vieler et al. 2012). The *N. gaditana* genome is of similar size but comprises only 9,052 gene models. Despite a low total gene number compared to other microalgae, the *N. gaditana* genome is enriched in lipid metabolism associated genes that represent almost 50% of all ESTs (Radakovits et al. 2012). *P. tricornutum* has a genome size of 27.4 Mb containing 10,402 predicted genes (Bowler et al. 2008).

Targeted gene insertion to remove or substitute an endogene, silencing of protein translation of a specific mRNA, or the overexpression of a desired sequence provide powerful tools to study protein functions. Breeding could also contribute to the establishment of heterozygous mutants in case null-mutation of the desired gene is lethal. This requires sexual reproduction which for now is not reported to occur under lab conditions in *Phaeodactylum* or *Nannochloropsis* although the required genes might be encoded in the genome (Patil et al. 2015, Hibberd 1981). Nonetheless, several methods are described for genetic engineering of both *Phaeodactylum* and *Nannochloropsis*, but only a few studies using these techniques are published (Weeks 2011). A summary of gene engineered *Phaeodactylum* strains is given in **table 2.1**.

Table 2.1. Studies using genetic engineering for increased lipid production in *P. tricornutum*. Antisense (as) or overexpression (OE) lines of different targets genes leading to higher total fatty acid (FA), triacylglycerol (TAG) or eicosapentanoic acid (EPA) contents.

Target gene	Regulation	Total FA increase	TAG increase	EPA increase	Reference
CGI58	as		yes		Leterrier et al. 2015
DGAT2	OE		35%	76%	Niu et al. 2013
D5	OE		65%	58%	Peng et al. 2014
GPAT	OE				Niu et al. 2013
GPDH	OE			60%	Yao et al. 2014
ME	OE	250%			Xue et al. 2015
NR	as	50%			Levitan et al. 2015
PDH	as		82%		Ma et al. 2014
PEPCK	as			15%	Yang et al. 2016
Pt_Elo5 (heterotroph)	OE			450% DHA	Hamilton et al. 2016
TE	OE	72%			Gong et al. 2011
TE from *Cinnamomum camphora*	OE	medium chain increase			Radakovits et al. 2011
TE from *Umbellularia californica*	OE	medium chain increase			Radakovits et al. 2011

Classic gene knock out relies on sequence substitution by homologous recombination. This mechanism is functional in haploid *Nannochloropsis* (Kilian et al. 2011). In the pioneer study, *Nannochloropsis spp*. endogenous nitrate reductase (NR) and nitrite reductase (NiR) entire gene sequences are replaced by a gene mediating resistance to the antibiotic zeocin (*sh ble*). To this end, cells were transformed with a knock out cassette comprising the *sh ble* sequence and 1 kb sequences homologous to the flanking regions of the targeted genes (Kilian et al. 2011). In this way, the machinery to repair DNA damages by substitution of homologous sequences is induced (Liu & Huang 2016). To our knowledge, no other study using gene knock in *Nannochloropsis* is published. The classic method of gene substitution *via* homologous recombination is not successful in *P. tricornutum*. In diatoms, vegetative cells are diploid and homologous recombination

is inefficient (Vardi et al. 2008b). However, the homologous recombination machinery exists in the diatom and co-transformation of an enzyme sequence enhancing this mechanism in mammals has the potential to increase targeted gene insertion efficiency in *Phaeodactylum* (Daboussi et al. 2014).

In the last three years, new targeted knock out methods were developed for *P. tricornutum*. Different types of nucleases that cut genomic DNA at defined sequences can be engineered to induce double strand ruptures at desired loci. In *Phaeodactylum*, meganucleases (MN), transcription-activator-like effector nucleases (TALEN) and clustered regulatory interspaced short palindromic repeats (CRISPR/Cas9) are successfully applied in a proof of principle study (Daboussi et al. 2014). In contrast to homologous recombination where colonies are homogenous because only cells expressing the antibiotic resistance gene survive, nuclease mediated techniques do not involve antibiotic selection. The nucleases permanently induce a double strand break when constitutively expressed but the activity is counteracted by the endogenous DNA repair mechanisms (Li & Xu 2016, Tsutakawa et al. 2014). Thus, the time point when a mutation is successfully induced and not repaired may differ between single cells in the same colony. The subset of TALEN transformed cells within a colony may vary tremendously, from 7-56% with 6-100% targeted mutagenesis efficiency in the first published study (Daboussi et al. 2014). Consequentially, identification by sequencing and isolation of mutant lines is time intensive.

Gene silencing *via* small interfering RNA (siRNA/RNAi) is a long known alternative, when targeted gene knock out is impossible or lethal. In the RNAi approach, small constructs carrying an antibiotic resistance cassette and a short sequence homologous to a part of the target gene is expressed in the host cell. After transcription, the inserted sequence and the endogenous mRNA hybridize. This induces the defence mechanisms against double stranded RNA that in turn reduces translation of the endogenous mRNA (**figure 2.7**) (Cerutti et al. 2011, De Riso et al. 2009). Evaluation of residual expression levels requires quantitative real time PCR or protein blot analyses. Antisense lines of *Phaeodactylum* endogens as well as transgenes are successfully generated (De Riso et al. 2009). However, endogene silencing efficiency is low since only 10% of transformants

display altered target protein levels with reductions ranging from 10-50% (De Riso et al 2009). Furthermore, silencing strains are not necessarily stable over time (personal communication Angela Falciatore).

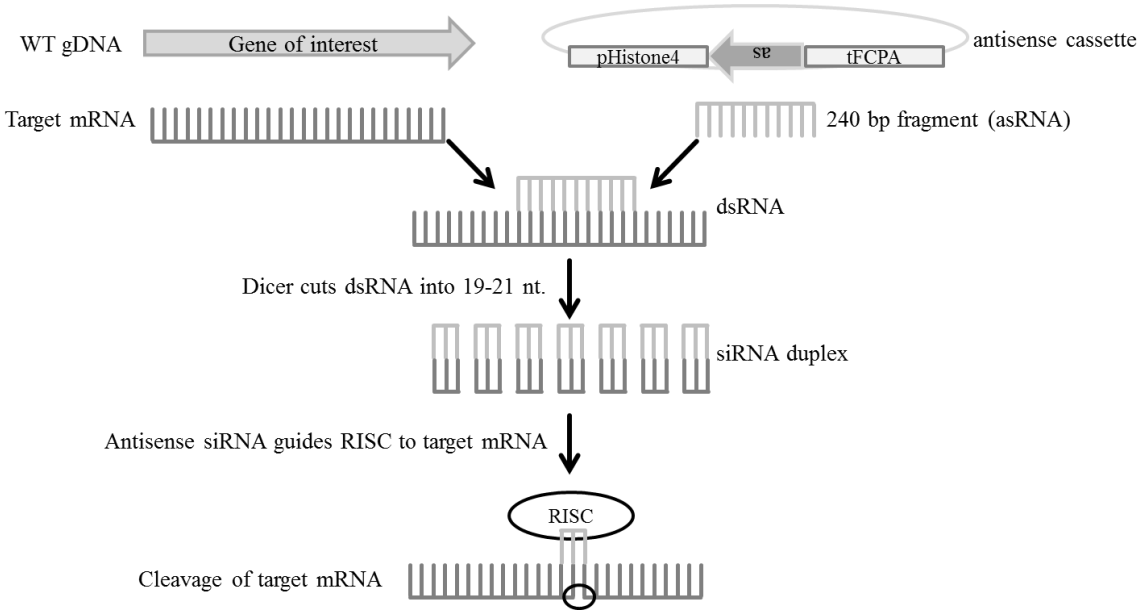

Figure 2.7. Schematic view on antisense gene silencing method in *Phaeodactylum* as applied in the present work. From the wild type genomic DNA (WT gDNA), the target mRNA is transcribed for protein expression. The silencing vector comprises a constitutive promotor, pHistone4 and the FCP protein terminator, tFCPA, which enclose the antisense sequence. This 240 bp sequence is homologous to a part in the middle of the coding sequence of the gene of interest. After transcription, mRNA and antisense RNA (asRNA) hybridize to form double stranded RNA (dsRNA). This activates an RNase III-like endonuclease (Dicer) that cuts the long dsRNA into fragments of 19-21 nucleotides, so called small interfering RNA (siRNA). After unwinding of the dsRNA, 5'-phosphorylated asRNA guides the RNA-induced silencing complex (RISC) to the target mRNA which is then cleaved (Cerutti et al. 2011).

2.2 Photochemistry

2.2.1 *Light perception and pigments*

In aquatic habitats light intensities are at least two orders of magnitude lower compared to terrestrial environments. The deeper the lower the total irradiance and the higher relative proportions of high energy wavelength, *i. e*. UV, blue and green light. The position of water organisms is not stable but depends on active movements or different degrees of turbulences (Depauw et al. 2012). Phototaxis is observed for diatoms that control their lateral position by filling or emptying their vacuole (Falciatore & Bowler 2002). Light quality and quantity therefore vary not only upon shading and seasonal changes but depend on water depth and dissolved particles (Depauw et al. 2012). As a consequence, aquatic photosynthetic organisms are exposed to fluctuating light conditions and light intensity change velocities differ with its cause (Giovagnetti et al. 2014). It is thus obvious, that Heterokonts like diatoms and *Eustigmatophyceae* constantly have to adapt to light intensities to maximize utilization but avoid photodamage. This is achieved by a broad usage of the light spectrum for photosynthesis and the rapid switch to or from photoprotection (**figure 2.8**) (Mann & Myers 1968). Indeed, the efficiency indicated by growth rates in *N. gaditana* is similar when cells are irradiated with a broad illumination range of 15-450 $\mu E.m^{-2}.s^{-1}$. At 5 $\mu E.m^{-2}.s^{-1}$ light energy is limiting but cultures reach the same stationary phase; at intensities of 1200 $\mu E.m^{-2}.s^{-1}$ and above (high light), exponential growth is similar but the stationary phase is lower (Simionato et al. 2011).

Chlorophylls and carotenoids including carotenes and xanthophylls absorb light (**figure 2.9**). Their capacity of collecting and transferring excitation energy until the release of a valent electron is the basis of photosynthesis. Photosynthetic pigments have different light absorption properties that depend on the molecular structure and the way they are bound by proteins (Kuczynska et al. 2015).

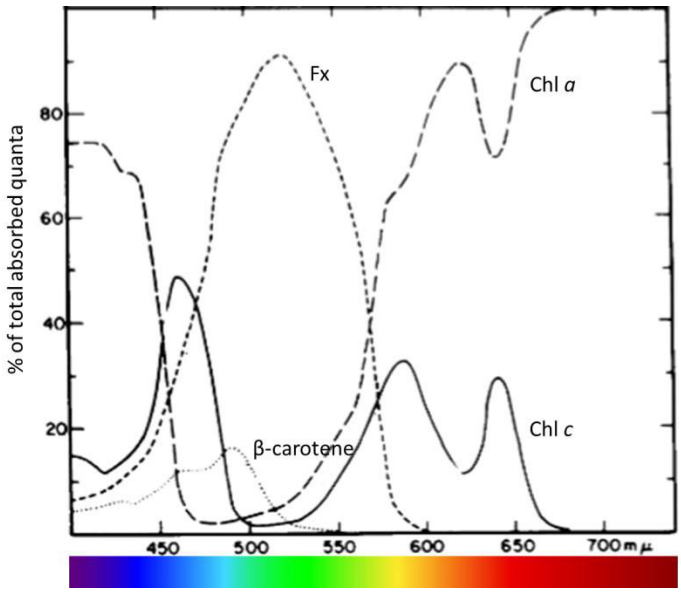

Figure 2.8: *Phaeodactylum* pigment fractional absorptions per wavelength. Indicated are the proportions of light absorption by the different pigment classes at a given wavelength. Modified from (Mann & Myers 1968).

Starting from glutamate, chlorophylls are synthesized in a complex pathway (Brzezowski et al. 2015) that in *Phaeodactylum* involves nuclear encoded proteins and one chloroplast subunit (Nymark et al. 2009). Chlorophylls consist of cyclic tetrapyrroles that are complexed by a magnesium ion, and a long-chain isoprenoid alcohol group (phytyl) (**figure 2.9**). The poryphyrin ring contains four nitrogen atoms. Species of chlorophyll *c* (Chl *c*) lack the phytyl chain and differ in one residue on a tetrapyrrol ring that determines their light absorption properties (Kuczynska et al. 2015). Heterokonts lack Chl *b* and *Nannochloropsis* also lacks chlorophyll *c*. Chl *c* has strong absorption at blue and a weaker at red wavelengths when compared to Chl *a* that absorbs in red and far red regions (**figure 2.8**) (Kuczynska et al. 2015, Mann and Myers 1968). Chl *a* absorption in the red light region is the so called Qy band. Chl *b* and *c* have shorter wavelength Qy bands and can therefore transfer absorbed energy to Chl *a*. Due to the structural differences of Chl *b* that possesses like Chl *a* a chlorin ring and Chl *c* that comprise an unsaturated porphyrin system, energy transfer capacities are lower for Chl *c* (Akimoto et al. 2014). While chlorophylls serve as light harvester, carotenoids

have additional functions as in energy dissipation molecules and as antioxidants preventing lipids from peroxidation (Goss & Jakob 2010).

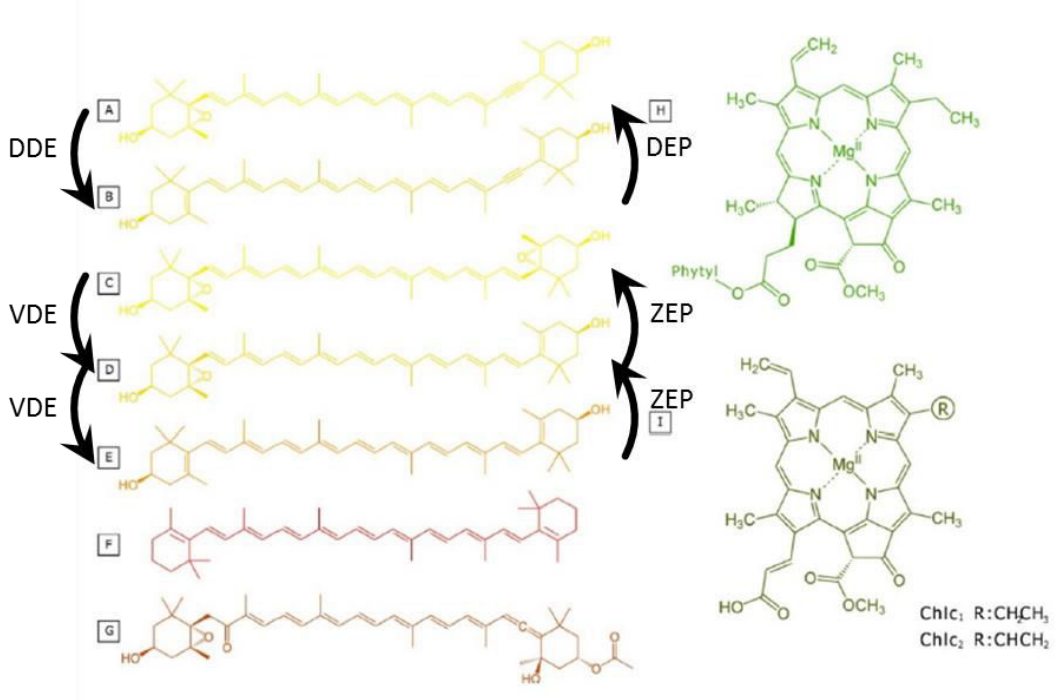

Figure 2.9. Chemical structure of photosynthetic pigments. (A) diadinoxanthin (Ddx); (B) diatoxanthin (Dtx). Diadinoxanthin deepoxidase (DDE) converts Ddx into Dtx, diadinoxanthin epoxidase Dtx into Ddx. (C) violaxanthin (Vx); (D) antheraxanthin (Ax); (E) zeaxanthin (Zx). Violaxanthin deepoxidase (VDE) converts Vx into Ax and Zx, zeaxanthin epoxidase Zx into Ax and Zx. (F) β-carotene; (G) fucoxanthin (Fx); (H) chlorophyll (Chl) *a*;(I) Chl *c* (modified from Kuczynska).

Diatoms contain seven out of 700 identified carotenoids of an all-*trans* polyene chain that is terminated by ring structures possessing oxygen (xanthophylls, i.e. Fx, Dtx, Ddx, Zx, Ax, Vx) (**figure 2.9**) or not (carotenes, lutein) (Kuczynska et al. 2015). Fx, Dtx and Ddx are absent from *Nannochloropsis*. The *Eustigmatophyceae* contain additional secondary ketocarotenoids, *i.e.* astaxanthin, canthaxanthin and vaucheriaxanthin (Lemoine & Schoefs 2010). Carotenoids (**figure 2.9**) derive from the isoprenoid pathway. Lycopene is the substrate for both α-carotenoids including α-carotene and lutein and β-carotenoids, including β-carotene and xanthophylls. Lycopene cyclases (Lcy) are conserved among carotenoid containing species, namely fungi, microalgae and

plants, and catalyse the ring formation of ψ-carotene. Depending on the position of the double bond in the hexagonal structure, α- or β-pigments are formed. Lcy-β-cyclases give rise to both structures, whereas Lcy-ε-cyclase is specific for the α-branch that contains α-carotene and lutein (Koc et al. 2015, Sedkova et al. 2005). A β-carotene hydroxylase (BCH) hydroxylates β-carotene in a two-step reaction first into β-cryptoxanthin and then into zeaxanthin. However, the *Phaeodactylum* genome lacks a typical BCH sequence and thus the conversion of carotenes to xanthophylls is elusive in diatoms. Violaxanthin deepoxidases (VDE) and its antagonist zeaxanthin epoxidase (ZEP) are required for the interconversion of zeaxanthin (Zx), antheraxanthin (Ax) and violaxanthin (Vx) (**figure 2.9**) (detailed in section **2.3**). Neoxanthin synthase (NXS) is using Vx for the synthesis of neoxanthin which is then supposed to be converted into diadinoxanthin (Ddx, see section **2.3**) and Fx in an unknown pathway. Again, no NXS is found in diatoms (Mikami & Hosokawa 2013).

The ionone ring of carotenoids determines the absorption spectrum of carotenoids, typically ranging from 400-500 nm (Kuczynska et al. 2015). The diatom specific Fx covers most of the green light region by absorbing between 460 and 570 nm (Mann and Myers 1968). Those wavelengths are enriched under water (Akimoto et al. 2014). **Figure 2.8** indicates the proportions to which each of the four major *Phaeodactylum* light harvesting pigments contribute to absorption at a given wavelength (Mann and Myers 1968). It is obvious, that the diatom has the equipment to use all wavelengths of the visible light. This contributes to the finding that diatoms have higher light harvesting efficiencies and biomass productivity than green and red algae. Indeed, there is a dynamic balance of the chlorophyll:Fx ratio that adapts to different light qualities occurring in different water depth (Kuczynska et al. 2015). Fx is absent from *Nannochloropsis*. Otherwise, wavelength dependent chlorophyll fluorescence analysis of *N. oculata* results in similar spectra than of *P. tricornutum*. Maximal absorption is observed at 440 nm, 540 nm describes the minimum and absorption increases with higher wavelength until 625 nm (Szabó et al. 2014).

Except for Fx and Vx, the xanthophylls Dtx, Ddx, Zx and Ax are more involved in photoprotection mechanisms than in photosynthesis (see section **2.3**). The all-*trans*

configuration of carotenoid hydrocarbon chain determines their susceptibility to oxidation as well as to heat, light and chemicals that induce *cis*-isomerization. This conversion changes their orientation in the thylakoid membrane thereby altering the permeability of small molecules such as oxygen, protecting the membrane from oxidative damage (Kuczynska et al. 2015).

Since the light spectrum is covered by different pigments, it is not surprising that on an equal photon dose basis, different light qualities induce distinct changes in the photosynthetic machinery (Valle et al. 2014). Overall, the action spectra of *N. oculata* reflect a trend towards higher photosynthetic quantum yields with increasing wavelength from the blue to the red region (Tamburic et al. 2014). This trend seems to be conserved in Heterokonts. At low light, light quality has no effect on electron flow from photosystem II (PSII) to photosystem I (PSI) and cell growth in *P. tricornutum* (Schellenberger Costa et al. 2013). Green and red light induce the expression of light harvesting and electron transfer genes faster than blue and white light but long-term irradiation lead to similar expression levels independent of the light quality (Valle et al. 2014). Blue and white light raise maximum photosynthetic capacity and cell growth at medium light intensities, whereas red light does not (Schellenberger Costa et al. 2013). Red light is unable to trigger photoprotection and therefore, long term irradiation leads to PSII inactivation caused by oxidative damage (Valle et al. 2014). In *Phaeodactylum*, the of light harvest complex protein F15 (LHCF15) is specifically expressed under red light illumination and downregulated in blue light (Schellenberger Costa et al. 2013). Furthermore, red light irradiation leads to the accumulation of PSI complexes, strong reduction in Chl *c* and alterations in thylakoid stacking (Bína et al. 2016). Blue light triggers photoprotection and the blue absorption band is increased during high light. Accordingly, lower doses of blue light are required for the onset of non-photochemical quenching (NPQ) compared to white light (Szabó et al. 2014). The blue light response is independent of photochemistry but possibly involves the activity of the phytochrome CRYP (Valle et al. 2014). Similarly, some PSII associated genes are responsive to green light but the signal transduction is insensitive to the PSII inhibitor 3-(3,4-dichlorophenyl)-1,1-dimethylurea (DCMU), despite the absence of a known green light

receptor. By contrast, some of the responses to red, blue and green light involves some linear electron flow dependent retrograde signals because the effect is reduced when cells are treated with the inhibitor. Notably, DCMU treatment causes higher singlet oxygen levels that could play an inhibitory role in the retrograde regulation of photosynthesis gene expression (Valle et al. 2014).

Photosynthetic organisms are also influenced by light outside the visible range. Very low dose UV irradiation increases growth and maximal cell concentrations in stationary phase of *Nannochloropsis*. Similar to high light, chlorophyll and Zx levels decrease whereas β-carotene, canthaxanthin and Zx increase. C16:0 and C14:0 levels increase on the cost of VLC-PUFAs (Forján et al. 2011). Research on molecular mechanisms and signalling pathways in response to different wavelengths is on-going in our laboratory.

2.2.2 *Photochemistry*

Photosynthesis is well studied in *Viridiplantae*. In linear electron flow, light energy is harvested by antenna complexes containing light harvesting complex proteins (LHCs), chlorophylls and accessory pigments. Light energy is transferred to the reaction center (RC) of PSII (RCII). Upon excitation, a valent electron is released. Oxidized RCII catalyse the lysis of water by the luminal oxygen evolving complex (OEC) for its re-reduction. PSII generated electrons are accepted by plastoquinone (PQ) and transported through cytochrome b6f complex (Cytb6f) to PSI. Here, light energy is captured for the transport through the PSI complex from the luminal to the stromal side where electrons are accepted by ferredoxin (Fd). Ferredoxin-$NADP^+$-oxidoreductase (FNR) mediates the reduction of $NADP^+$ with electrons donated by Fd, resulting in the electron carrier NADPH. The electron transport promotes translocation of protons, building up the proton motive force that drives the F-ATP-synthase (ATPase). NADPH and ATP are injected in the Calvin cycle to assimilate carbon to generate cellular building blocks (Nelson & Ben-Shem 2004). During linear electron flow, eight photons are consumed for the release of one molecule oxygen (O_2) and two protons (H^+). Two additional protons are transported to the luminal side of the thylakoid membrane by the net transportation of an electron. Thereby, four reducing equivalents are regenerated that

promote the assimilation of one CO_2 molecule (Kanervo et al. 2005). The general mechanisms of photosynthetic reactions are conserved in all eukaryotic photosynthetic organisms but some details vary between the phyla.

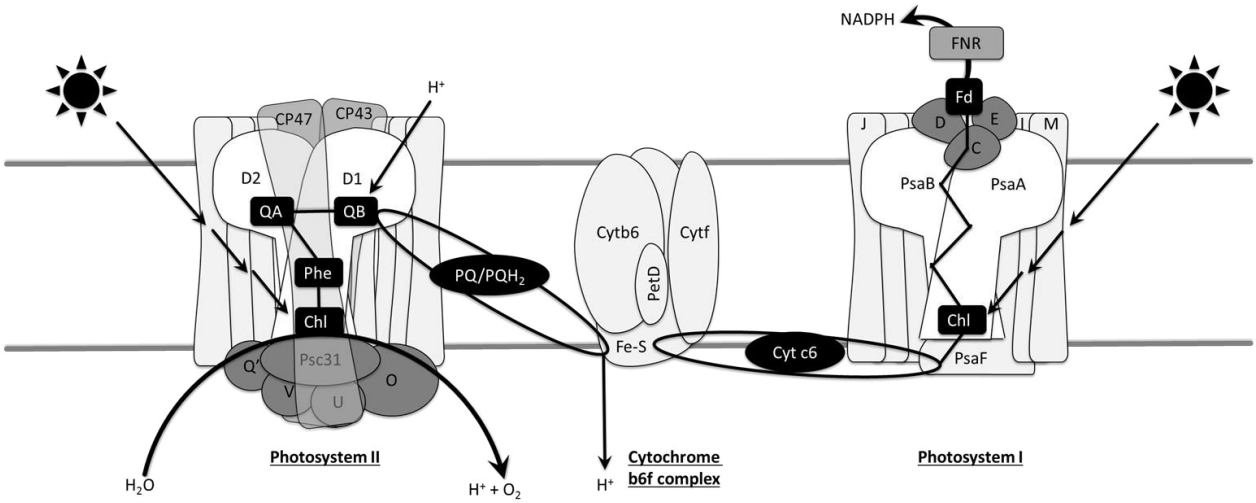

Figure 2.10: Schematic view of the protein complexes forming the photosynthetic machinery and linear electron flow in *Phaeodactylum tricornutum*. Using two-dimensional protein gels, proteins from extracted thylakoids were separated and identified via MS (Grouneva et al. 2011). White shapes display the major proteins of photosystem (PS) II and PSI core, *i.e*. DA and D2, and PsaA and PsaB. Other protein subunits are indicated in grey shades. The major linear electron flow route is indicated in black (Roach & Krieger-Liszkay 2014). Light-driven water oxidation released electrons that are directed through the special chlorophyll pair (Chl), pheophytins (Phe), the quinone pockets of D1 and D2 (QA and QB). Plastoquinone (PQ) accepts electrons from QB and protons from the stromal side, and migrates to the cytochrome b6f complex to reduce the iron-sulphur cluster (Fe-S) and releases protons to the luminal side. Cytochrome c6 (Cyt c6) transports electrons to PSI. Harvested light energy fuels the transport of electrons from the luminal side to the stromal side of PSI, where they are accepted by ferredoxin (Fd). Ferredoxin-NADPH oxidoreductase (FNR) generates NAPDH. The proton gradient fuels an ATPsynthetase (not shown) (Derks et al. 2015, Nelson & Ben-Shem 2004).

The protein equipment of *P. tricornutum* photosynthetic membranes is revealed by mass spectrometric (MS) analyses of two-dimensional protein gels from isolated thylakoid membranes and allows the reconstitution presented in **figure 2.10** (Grouneva et al. 2011). A similar detailed study has not been conducted on *Nannochloropsis* species but

due to the similarities presented below we assume a conserved setup in both Heterokonts.

Major differences in Heterokont and plant photosynthetic apparatus are the absence of Chl *b* and plastocyanin, and a differential regulation of RubisCO. Interestingly, those proteins are in plants great sinks for iron, copper and nitrogen, respectively (Losh et al. 2013, Peers & Price 2006). One reason for these changes could thus be the lower nutrient availability in aquatic habitats (Depauw et al. 2012). In diatoms and potentially all Heterokonts, photoprotection differ from the green lineage by higher capacities of NPQ although the state transition component (qT) is absent and photoinhibition (qI) is less important (Goss & Lepetit 2015, Lavaud & Lepetit 2013).

2.2.2.1 Light harvesting at the photosystems

Antenna complexes that consist of LHC proteins and bound pigments associate with the photosystems. Light energy is absorbed and transferred to the RC of the photosystems. Pigment nature but also position and orientation controlled by LHCs are important to maintain a certain excitation state that allows directed energy transfer. On the other hand, LHC function changes towards photoprotection when light intensities exceed the redox capacities of electron transfer (high light). PSII in vascular plants is surrounded by light LHC proteins consist of the LHCB protein family (LHCII). The majority forms trimers that harbour Chl *a* and Chl *b* and accessory pigments. One PSI core binds four LHCA proteins (Nelson & Ben-Shem 2004). Analogs to plant LHC proteins are Fx-Chl *a*/*c* binding proteins (FCPs) in diatoms and violaxanthin-Chl *a* binding proteins (VCPs) in *Nannochloropsis.* These LHC proteins are present in the antennae surrounding both PSII and PSI (Goss & Lepetit 2014). Similar to LHCII, FCPs and VCPs appear in trimers but may also form hexamers in the outer antennae (Carbonera et al. 2014, Lepetit et al. 2012). It is likely that *Phaeodactylum* FCP-PSII binding is weaker than LHCII-PSII binding since attempts to isolate a diatom PSII supercomplex failed thus far (Lepetit et al. 2012). Similarly, *N. gaditana* PSII-VCP bonds are very weak compared to other species (Basso et al. 2013).

Heterokonts possess four different kinds of LHC proteins: LHCF that build the FCP complexes in peripheral antennae of PSI and PSII, PSI-specific LHCR proteins, red lineage chlorophyll *a*/*b*-binding-like proteins (RedCAP) of unknown function, and LHCX proteins present in both FCP antenna complexes and PSI (Goss & Lepetit 2014). *P. tricornutum* genome encodes 15 LHCF and 14 LHCR, 12 and respectively 7 of which are located in the FCP together with LHCX1, and the RedCAP protein of unknown function Lhl1. According to sequence homology with diatom proteins, *N. oceanica* genome encodes at least three LHCF-like, 14 LHCR-like-, and two LHCSR/LHCX-like proteins (Vieler et al. 2012). *N. gaditana* expresses eight isoforms of both LHCF and LHCR, as well as five LHCX (Alboresi et al. 2016). A RedCAP protein is associated with PSI in *Nannochloropsis* (Litvín et al. 2016).

RedCAPs form a monophyletic group preserved in and restricted to red algae and species with a red algal origin as Heterokonts, *Cryptophyta* and *Haptophyta*. Amino acid comparisons indicate that these LHC-related proteins are less efficient in Chl binding. However, expression patterns of RedCAPs are similar to light harvesting LHCF2 in *Phaeodactylum*, with the strongest expression during low light and strong downregulation upon high light. RedCAPs might thus be involved in light harvesting but not in photoprotection (Sturm et al. 2013).

VCP and FCP proteins in the antenna contribute to light harvesting. Not much is known about the precise energy transfer mechanism from pigments in LHCs to the cores of the photosystems. Time resolved fluorescence spectra measurements using cells of *Chaetoceros gracilis* reveal energy transfer from Fx to Chl *a* in FCP proteins surrounding PSII. However, two different energy states of Fx occur with absorption maxima at 580 nm and 550 nm, respectively. Only the lower energy Fx contributes entirely to Chl *a* excitation. Excited Chl *c* does not transfer all absorbed energy to Chl *a* in the same FCP but probably also to neighbouring FCP or PSII complexes (Akimoto et al. 2014). Whatever the precise mechanism, excitation energy is directed from the antenna to the reaction center.

2.2.2.2 PSII core

From the peripheral antenna, excitation energy is transferred to the core of PSII. One plant PSII supercomplex is composed of a PSII core dimer, two strongly bound CP26, CP29 and LHCIIs. It might form megacomplexes with two moderately bound CP24 and LHCII and a dynamic number of weakly bound LHCIIs (Derks et al. 2015). By contrast, diatom PSII does not form stable supercomplexes or megacomplexes (Grouneva et al. 2011). Extracted supercomplexes from *N. gaditana* indicate presence of PSII monomers and oligomers with conserved absorption spectra (Basso et al. 2013). The diatom PSII core complex consists of D1, D2, CP43, CP47, plus OEC and around 10 small polypeptides (Grouneva et al. 2011**)** (**figure 2.10**). CP43 and CP47 bind Chl *a* molecules in the proximal PSII antenna that directly transfer the energy to the RC. RCII contains six pigments, different Chl *a* and two pheophytins (Phe) which are magnesium-free chlorophylls. These pigments have different energy states allowing directed energy transfer. D1 and D2 form the energy conversion site. Energy is collected by a special Chl *a* pair, P_{680}, which releases a valent electron upon excitation. Two photons are required to reduce PQ that resides in the Q_B pocket of PSII. PQH_2 then enters the electron transfer chain (**figure 2.10**). Reduced P_{680} provides an electron sink for the oxygen evolving complex (OEC) that resides on the luminal side of PSII. Within this complex, the Mn_4Ca cluster plus the energy of four photons splits two water molecules into O_2 and protons (Derks et al. 2015).

2.2.2.3 Electron transfer from PSII to PSI

Reduced PQ migrates through the membrane and donates the electron to the Cyt b6f complex (**figure 2.10**). Electron transport through these proteins supports the endergonic transport of protons across the thylakoid membrane from the stromal to the luminal side. Consequentially, a pH gradient is built up and this proton motive force powers the F-ATP-synthase, relocating protons back to the stroma. Molecular oxygen is the proton acceptor on the stromal side of the thylakoid membrane. This proton flux along the

chemical-osmotic gradients provides energy for the generation of ATP from ADP and inorganic phosphate (Nelson & Ben-Shem 2004). The setup of the Cyt b6f complex in *Phaeodactylum* is illustrated in **figure 2.10** but to our knowledge not functionally characterized in Heterokonts.

The mobile electron carrier between the Cyt b6f complex and PSI is plastocyanin in higher plants, but this luminal protein is absent from the red lineage. Instead, cytochrome (Cyt) c6 is present in the luminal fraction of extracted thylakoids and acts as mobile electron carrier to reduce PSI (Grouneva et al. 2011). Electron transfer to PSI is realized after an electrostatic complex is established and redox partners are brought in vicinity. This mechanism is studied in Cyt and PSI proteins isolated from *Phaeodactylum* by laser-flash absorption spectroscopy. Complex assembly and PSI reduction in *Phaeodactylum* is much lower than what is typically observed in species of the green lineage that possess plastocyanin. Besides the properties of the heme protein donating the electron, the luminal loop domain of PsaF that contributes to complex formation is different in the diatom. It contains less positively charged residues that are required for electrostatic and hydrophobic interactions. Accordingly, Cyt c6 contains less negative charges compared to protein homologs from the green lineage. Thus in *Phaeodactylum*, electron donor and acceptor display weaker affinities, causing lower PSI reduction efficiencies but facilitate complex disassembly (Bernal-Bayard et al. 2013).

2.2.2.4 Energy flows at PSI

The reaction center of PSI is reduced by electrons from the cyt b6f complex. RCI also receives light energy captured in its antenna. Electrons transported through the PSI complex are used for the reduction of $NADP^+$ (Nelson & Ben-Shem 2004). PSI appears as a monomer in both diatoms and higher plants. Besides a similar structure, two diatom-specific proteins of unknown function, Phatr2|42506 and Phatr2|33844, appear in the PSI fraction, the latter only at high light conditions. Some of the PSI subunits found in higher plants are absent from diatoms*, i. e.* PsaG, PsaH, PsaN involved in

plastocyanin binding, and PsaO putatively involved in state transitions (Grouneva et al. 2011). PSI structure in *Nannochloropsis* seems to have unique features. The relative proportion of total Chl *a* associated with PSI is about 35% in higher plants but only 10% in *N. salina*. One *Eustigmatophyte* PSI is larger than the barley counterpart and harbours about 4 times more chlorophyll per reaction center (Brown 1987). Accordingly, the PSI-LHC supercomplex is larger in *N. gaditana* compared to that in the moss *Physcomitrella* or the vascular plant *Arabidopsis* (Basso et al. 2013). Preparations of *N. salina* PSI complexes result in high amounts of free pigments that indicate loose bindings (Brown 1987). Whether this distinct supramolecular organization is correlated to the function of PSI-specific LHCR proteins is unknown.

Linear and cyclic electron flows

The photosynthetic flow that generates electrons at PSII which are finally accepted by $NADP^+$ and introduced into the Calvin cycle is designated as linear electron flow (LEF). There are several alternative routes that contribute to the production of ATP without NADPH generation. This is required because in the Calvin cycle, two molecules of ATP and one molecule of NADPH are consumed per turn, and ATP is also required for other cellular processes (Kanervo et al. 2005). In the Mehler-ascorbate pathway, electron flow from PSII to the acceptor site of PSI follows LEF, but then molecular oxygen is the electron acceptor. Produced superoxide is detoxified by superoxide dismutase and catalase, in the chloroplast and peroxisome, respectively. A second water-to-water cycle involves plastoquinone terminal oxidase that accepts electrons donated from PQ. Cyclic electron flow around PSII as well as photorespiration might as well contribute to balance ATP and NADPH (Cardol et al. 2011). PSI electrons may be reintroduced into the electron transfer chain at the level of PQ. This route is designated as cyclic electron flow around PSI (CEF) (Allen 2003). Besides the additional ATP production, CEF might be required for the generation of a large pH gradient inducing NPQ when LEF is saturated (Johnson 2005). CEF is induced with the onset of illumination after dark adaptation or under high light conditions when the onset of the Calvin cycle is rate limiting (Johnson 2005, Reiland et al. 2011).

In most species of the green lineage, two CEF pathways are conserved: the proton gradient regulating protein 5 (PGR5)-dependent and the NADPH dehydrogenase (NDH)-dependent re-integration of Fd-derived electrons into the electron transport chain (Joliot & Johnson 2011). A number of photosynthetic species have lost NDH genes that derive from the cyanobacteria ancestor. They are absent from all red algae and descendants, including Heterokonts (Grouneva et al. 2013). Notably, a centric diatom-specific protein, gi|223995405 displays some sequence similarity with a NDH (Grouneva et al. 2011). NDH mediates the reduction of PQ with electrons donated by NADPH, whereas in the Fd-depended pathway a heterodimer of PGR5 and PGR5-like protein 1 (PGRL1) oxidize Fd with subsequent reduction of PQ (Kanervo et al. 2005, Allen 2003,Hertle et al. 2013). Iwai and coworkers identified a protein supercomplex which is crucial for the induction of CEF in state 2 (see state transition) in *C. reinhardtii* and thus controls the energy balance between the photosystems. This super-complex contains PSI, LHCI, LHCII, Cyt b6f, FNR and PGRL1 in *C. reinhardtii* and additionally PRG5 in *A. thaliana* (DalCorso et al. 2008, Iwai et al. 2010). The PGRL1-PGR5 mediated redox-dependent PQ reduction indicates that this dimer functions as the long sought Fd-PQ-reductase (Iwai et al. 2010, Hertle et al. 2013). The presence of FNR in the *C. reinhardtii* CEF-supercomplex found by Iwai and colleagues contradicts the study of Hertle and coworkers that found Fd to be able to reintroduce electrons directly into the electron transfer chain (Iwai et al. 2010, Hertle et al. 2013). Furthermore it is unclear, which components undergo the relocation from PSI to the PQ site of the cyt b6f complex. Homologs of PGR5 and PGRL1 are present in diatom thylakoids but may have species-dependent adaptations. *P. tricornutum* PGRL sequence exhibits two transmembrane domains whereas the respective *T. pseudonana* sequence indicates only one (Grouneva et al. 2011). In *Phaeodactylum*, CEF may play a minor role under optimal conditions since flux balance modelling points towards an involvement in channelling NADPH to the mitochondria to balance the ATP/NADPH ratio. If ATP demands are increased, CEF may be induced (Cardol et al. 2011, Kim et al. 2015). Similarly, CEF contributed to 10% of all thylakoid electron fluxes in high light treated *N. gaditana* cells (Meneghesso et al. 2016).

Beside alternative electron fluxes, the transport of energy carriers between different organelles was found to be important for the regulation of photosynthesis in microalgae (Cardol et al. 2011). Furthermore, photoprotection is induced when light energy cannot be quenched by photochemistry.

2.3 Photoprotection

High light is defined as a light intensity that induces photoprotection because absorption of the full irradiation would cause photooxidative damage. When absorbed energy exceeds either P_{680}^{+} re-reduction by water or oxidized PQ is limiting, redox stress could not only inactivate PSII but harm the entire cell (Derks et al. 2015). Lack of radical P_{680}^{+} quenching can lead to oxidation of surrounding molecules including lipids. Furthermore ROS are generated by incomplete water oxidation, chlorophyll triplets or radical chlorophyll pairs. A first level of protection from radical chlorophyll pairs is permitted by the close localization to carotenoids that serve as antioxidants and emit the excessive energy as heat (Derks et al. 2015).

What light quantity is considered as high light depends on light quality as well as on the physiological state of the cell, especially the thylakoid components. It is the light intensity that induces short- and long term changes to avoid photooxidative damage by either scavenging ROS or preventing its formation. *Long term* is considered as starting after several minutes thus not involving sudden changes (Eberhard et al. 2008). However, the distinction in short and long term is not strict and time and extent of photoprotection induction depends also on light quantity, quality and velocity of the change (Derks et al. 2015, Giovagnetti et al. 2014). Long term changes involve differential enzyme regulation and degradation, transcriptional changes and protein *de novo* synthesis. Thus, among the three non-photochemical quenching parameters, photoinhibition (qI) and state transition (qT) fall under the definition of long term response, whereas energy-dependent quenching (qE) is a short term response together with ROS production and changes in electron flow (Eberhard et al. 2008). In higher

plants, about 75 % of the photons absorbed can be eliminated in this protection mechanisms reducing electron transfer (Kanervo et al. 2005).

During long term changes as upon diurnal or seasonal changes in plants, antenna sizes and PSI:PSII stoichiometry are altered (Eberhard et al 2008). This might not be the case in Heterokonts. In *Phaeodactylum*, light harvest adaptations occur mainly by changing the area covered by thylakoids and thereby total pigment and photosystem contents. Relative to the ATP synthase, both proteins and light harvesting pigments decrease proportionally during high light adaptations and the FCP:photosystem ratio declines by only 10% in response to high light with a conservation of the PSI-specific FCP. Thus, stoichiometric differences are less pronounced when the high light response of diatoms is compared to higher plants (Lepetit et al. 2012). Data on light dependent antenna size-modulation in *N. gaditana* are controversial. The same laboratory first stated that *N. gaditana* PSII antenna sizes are not responsive to light (Simionato et al. 2011), but in a later study they concluded on a high light induced reduction of both the antenna:RC ratio and the PSII:PSI ratio (Alboresi et al. 2016). The parallel decrease of chlorophyll, carotenoid, 20:4 and 20:5 levels in *N. sp*. shifted to high light is consistent with the observation in diatoms that total thylakoids are reduced rather than antenna sizes (Sukenik et al. 1989). By contrast, in the recent study, the chlorophyll to carotenoid ratio decreased in high light treated *N. gaditana* (Alboresi et al. 2016).

Antennae that surround the photosystems are changed in the composition of both proteins and pigments in response to high light. The light harvesting protein isoforms differ in Vx affinities and even within a given LHC, Vx binding properties differ depending on which of the three binding pockets is occupied (Jahns et al. 2009). Among *Phaeodactylum* FCP proteins, transcript levels of LHCF and most LHCR proteins are downregulated except for photoprotection associated LHCR6, LHCR8, LHCX2 and LHCX3 that were strongly upregulated in microarray analyses of high light irradiated cells. LHCSR6, LHCSR8 and LHCX3 levels declined during the photoacclimation period whereas LHCX2 remained at high levels (Nymark et al. 2009). LHCX1 protein levels increase (Lepetit et al. 2012). In *N. gaditana*, only one of the five LHCX isoforms was responsive to high light, Naga_101036g3 (Alboresi et al. 2016). The upregulated

LHC proteins are readily induced in response to blue and white light but only marginally or not at all responsive to green or red light irradiation in *Phaeodactylum*. LHCX induction relies not only on blue light reception but can also be controlled by the redox state of PQ, ROS levels and eventually unknown photosynthesis derived signalling (Derks et al. 2015).

Upon high light, a sudden reduction of nucleus encoded Chl *a* synthesis genes occurs whereas the only chloroplast encoded subunit (CHL1) is not affected. With prolonged high light irradiation, Chl *a* synthesis gene expressions recovers to low light levels (Nymark et al. 2009). Carotenoid synthesis gene expressions are not altered in response to high light except for ZEP isoforms (see **section 2.3.2**). ZEP1 is initially downregulated but ZEP3 upregulated, both recover after 48 hours (Nymark et al. 2009). The expression level of most ROS scavenging proteins remained unaltered upon HL irradiation except for a strong induction of the plastid peroxiredoxin Q (PRXQ), different isoforms of thioredoxins (TRX) and a glutaredoxin GLRXC2 potentially required for the thiol-dependent regeneration of the antioxidant (Nymark et al. 2009).

Together with these changes in gene expression of pigment binding proteins, chlorophyll and carotenoid levels are adjusted during high light irradiation. Generally, the carotenoid:chlorophyll ratio is higher in diatoms FCPs compared to LHCII proteins higher plants (Kuczynska et al. 2015). Light harvesting Fx and Ddx drop immediately while chlorophyll levels decline progressively in *Phaeodactylum* (Nymark et al. 2009). The Fx:Chl *a* ratio decreases up to 30% in diatoms (Lepetit et al. 2012). Dtx levels increase with the onset of qE. Notably, Ddx is discussed to be a precursor for Fx, an idea that is strengthened by simultaneous decrease under high light conditions (Nymark et al. 2009). In response to high light, xanthophylls are readily interconverted and contribute to qE. On the other hand, under prolonged light changes, Dtx increases without triggering NPQ. Similarly, under long term light stress, *Nannochloropsis* induces *de novo* xanthophyll synthesis (Gentile & Blanch 2001). The interplay of *de novo* xanthophyll synthesis induction and NPQ activation in response to slow light changes *versus* fast changes as caused by shading are addressed in the diatom *Pseudo-nitzschia multistriata* by shifting cells from darkness to light intensities between 100-650 $\mu E.m^{-2}s^{-}$

[1] with different velocities. As a general rule, the slower the irradiation increase and the lower the final light intensity, the higher the contribution of xanthophyll synthesis relative to NPQ to photoacclimation. This is indicated by higher proportions of *de novo* synthesized Vx, Zx and Ddx that fuel the increasing Dtx pool, whereas qE induction is weaker when progressive high light acclimation is slow. Notably, when light intensities are gradually increased, no drop in chlorophyll content is observed as occurs upon sudden high light irradiation. Thus, the dynamic regulation of NPQ and *de novo* carotenoid synthesis allows diatoms to readily acclimate to short and long term changes in the light regime (Giovanetti et al. 2014).

Beside the possible increase of Dtx without NPQ induction, Ddx cycle pigment abundances are not correlated to maximum NPQ levels. Drastically, *Phaeodactylum* is able to induce NPQ in absence of Dtx in a mechanism involving oxygen (Lepetit et al. 2012). This is in stark contrast to higher plants, where the major part of NPQ depends on the xanthophyll cycle, which in turn is activated upon luminal acidification. Therefore, plant qE is commonly correlated with higher ETR that enhances the proton motive force (Eberhard et al. 2008). By contrast, even with PSII inactivation, *P. tricornutum* can still induce NPQ (Grouneva et al. 2011) and the proton motive force alone is unable to regulate the Dtx cycle (Kuczynska et al. 2015).

2.3.1 *The role of the proton gradient for NPQ*

In higher plants, onset of qE depends on the proton motive force, driven by ETR (Goss & Lepetit 2015). Upon the shift to high light, *Phaeodactylum* PSII quantum yield decreases whereas the ETR remains stable during the first 12 hours of photoacclimation and increases when NPQ relaxes. Hence, there is no direct antiproportional correlation between NPQ onset and the trans-thylakoid proton gradient in diatoms (Nymark et al. 2009).

Stress related luminal LHC-like proteins differ between the species with PsbS in higher plants, LI818/LHCSR in green algae and LHCX in Heterokonts. PsbS is the luminal sensor protein that upon protonation induces the xanthophyll cycle probably acting in the regulation of structural reorganizations such as LHCII aggregation. It is proposed to

function in the organization of the quenching site since the protein is mobile in the thylakoid membrane (Goss & Lepetit 2015). PsbS is dispensable for plant NPQ when the luminal pH is very low (Goss & Lepetit 2015). In agreement with a less important role of the trans-thylakoid pH gradient for diatom NPQ, *P. tricornutum* LHCX genes are not conserved in pH-sensing domains (Lepetit et al. 2012).

In contrast to plants, the proton gradient is important for NPQ relaxation in diatoms. When measuring NPQ via fast fluorescence kinetics, values decline when high light is shut off and the PSII quantum yield increases progressively. NH_4Cl is a proton uncoupler that abolishes the trans-thylakoid pH gradient but also affects PSII function. When cells are treated with this dissipator, NPQ relaxation is strongly impaired. Inhibition of the stromal Dtx epoxidase (DDE) has a similar effect leading to the conclusion, that diatom epoxidation activity is pH regulated (Roháček et al. 2014). Based on the data, the role of the proton gradient appears to be the opposite in the green and diatoms with a role in the onset and offset of qE, respectively.

Nannochloropsis pH-dependent NPQ regulation differs from both green algae and diatoms. Induction of qE is sensitive to proton gradient uncoupler nigericin and NH_4Cl and completely abolished in response to the VDE inhibitor DTT (Cao et al. 2013). However, a strong correlation of ETR and NPQ is not observed. When *N. gaditana* is grown at high light conditions, ETR is higher but NPQ induction lower compared to medium light (Alboresi et al. 2016). In contrast to diatoms, *Nannochloropsis* NPQ offset is independent of the trans-thylakoid gradient. The xanthophyll cycle is indispensable for NPQ in the *Eustigmatophyte* (Cao et al. 2013).

2.3.2 *Function and regulation of the xanthophyll cycle*

In higher plants, green and brown algae, the xanthophyll cycle is conserved whereas the Ddx cycle is restricted to species of *Bacillariophyceae*, *Xanthiphyceae*, *Haptophyceae* and *Dinophyceae*. This photoprotection mechanism is induced upon high light or blue light irradiation and contributes to qE (Derks et al. 2015). In this pathway, a light harvesting xanthophyll is converted into a heat emitting pigment by a luminal protein and the reaction is reversed by a stromal protein. Pigments of the xanthophyll cycle are

Vx, Ax and Zx while the Ddx cycle involves Ddx and Dtx (**figure 2.9**). Vx is de-epoxidized twice, to the di-epoxyxanthophyll Ax and to epoxy-free Zx (Goss & Jakob 2010). While in plants under low light the xanthophyll:chlorophyll ratio is about 1:25, high light increases it by 2-3 times due to LHC reductions and xanthophyll cycle induction (Jahns et al. 2009). This reaction occurs even in diatoms where those carotenoid species are detected only under prolonged high light irradiation and in which qE relies on mainly on the epoxidation of Ddx to Dtx (Goss & Jakob 2010, Kuczynska et al. 2015). Some plants also perform lutein epoxidation, for review see Jahns et al (Jahns et al. 2009). In *Nannochloropsis*, secondary ketocarotenoids such as astaxanthin, canthaxanthin and vaucheriaxanthin serve as antioxidants and accordingly, synthesis is induced under oxidative stress as high light, UV irradiation or nutrient depletion (Lemoine & Schoefs 2010, Meneghesso et al. 2016). Singlet oxygen quenching efficiencies of astaxanthin and canthaxanthin are higher than other xanthophylls or carotenes occurring in Heterokonts (Di Mascio et al. 1990). Briefly, the two Heterokont species have evolved different mechanisms for efficient light detoxification with the Dtx cycle in *Phaeodactylum* and the Vx cycle, plus the increase of secondary ketocarotenoids in *Nannochloropsis*.

Three Ddx/Dtx pools exist in the thylakoids of diatoms. The largest pool is bound to FCP antenna and LHCX proteins and forms the greatest source for qE. A second pool is located in a MGDG shield around FCP and supposed have an antioxidant function. Both pools are light-responsive. The third pool resides with LHCR proteins at PSI and act in light harvesting (Goss & Lepetit 2015). Changes in light intensities cause shifts in the distribution of Dtx between the different pools. Diatom species differ in relative and total pool sizes as well as the contribution of *de novo* synthesized xanthophylls, features that are correlated to NPQ inducibility (Lavaud & Lepetit 2013). Furthermore, Dtx quenching capacities vary among different *Phaeodactylum* species that indicates that not only different pool sizes but probably also FCP-Dtx binding strength and expression levels of photoprotective proteins play in the regulation NPQ capacities (Lepetit et al. 2012). Ddx epoxidation in *Phaeodactylum* starts after 30 seconds of high light irradiation and NPQ and Dtx production are linear during high light. If the luminal pH is

low, Dtx synthesis is induced without NPQ (Lavaud et al. 2012). Taken together, regulation of diatom-specific Dtx cycle regulation differs from the Vx cycle. This is probably related to different characteristics of the key proteins, *i. e.* Vx deepoxidase (VDE) and Zx epoxidase in plants, and Ddx deepoxidase (DDE) and Dtx epoxidase (DEP) in diatoms as well as LHC proteins.

2.3.2.1 The deepoxidases

In the xanthophyll cycle Vx is deepoxidized into Ax and Zx by the lipocalin protein family member VDE, while the diatom specific DDE uses Ddx as substrate to convert it into Dtx. In plants Zx is the major product but in *Nannochloropsis* the conversion of Vx results in 76 % Ax and 24 % Zx (Gentile & Blanch 2001). This is explained by a higher VDE affinity towards Vx than to Ax (Goss & Jakob 2010). VDE and DDE share common features. The soluble lumen proteins possess a binding pocket for all epoxy xanthophylls, a catalytic domain and a cysteine rich domain (DTT sensitive), and require ascorbate and a certain luminal pH (Goss & Jakob 2010, Goss & Lepetit 2015, Jahns et al. 2009). The unspecific binding pocket allows *Phaeodactylum* DDE to also act on Vx however with lower activity. It is not clear whether DDE also de-epoxidizes Vx *in vivo* during long term high light exposure (Kuczynska et al. 2015). *P. tricornutum* encodes one DDE, two VDE-like proteins and one VDE-related protein. The VDE sequences lack residues potentially required for membrane binding and is proposed to act in the synthesis of xanthophylls and Fx (Goss & Lepetit 2015).

Ascorbate in its acid form donates electrons and protons for the epoxidase reaction and is regenerated in an unknown mechanism (Jahns et al. 2009). A luminal pH below 5 is required to induce VDE activity upon which the deepoxidase undergoes dimerization and binds to the thylakoid membrane (Goss & Lepetit 2015). VDE sensing of luminal pH involves a highly charged glutamic acid enriched region that is not conserved in DDE (Goss & Jakob 2010). As a consequence, DDE compared to VDE is active at higher pH and has a broader optimum between pH 5 and 6. Activity can be maintained even in darkness at a pH of 7.2 that is caused by chlororespiration (Goss & Jakob 2010,

Goss & Lepetit 2015). Also, the demand for ascorbate is lower in the Dtx cycle (Goss & Lepetit 2015). Downregulation of *P. tricornutum* DDE does not interfere with cellular chlorophyll, Fx, carotene, or Ddx contents. Accordingly, no photosynthetic phenotype occurred under low light conditions. In moderate high light, DDE knock down lines have a similar phenotype than DTT (VDE inhibitor) treated cells resulting in lower Dtx generation. Ddx deepoxidation starts after 30 sec of high light irradiation. DDE knock down lines display a lag phase in low light Dtx generation and overall lower de-epoxidation efficiency (Lavaud et al. 2012). The distinct DDE characteristics may contribute to the observed higher NPQ capacity in diatoms compared to the green lineage (Goss et al. 2005).

The *Nannochloropsis* xanthophyll cycle is supposed to be similar to the plant one. *N. gaditana* VDE has however distinct affinities since the first deepoxidation is much more efficient due to reduced Ax affinity (Goss & Jakob 2010, Gentile & Blanch 2011). As in diatoms, in response to longer high light exposure times, pigments derive not only from Vx conversion but also from *de novo* synthesis in *Nannochloropsis* (Gentile and Blanch 2011). Similarly, a high ETR does not correlate to high NPQ (Alboresi et al. 2016). One may therefore assume that *Nannochloropsis* qE is more distinct from the green lineage than currently known.

2.3.2.2 The epoxidase

The lipocalin proteins that invert the epoxidation reactions are Zx epoxidase (ZEP) in Zx cycle containing species and the diatom Dtx epoxidase (DEP) that require FAD and NADPH as cofactors (Goss & Lepetit 2015). ZEP is located on the stromal side and probably intercalated into the thylakoid membrane in the vicinity of PSII-LHCII complexes. This is supposed to facilitate the reintegration of Vx into light harvesting complexes (Goss & Jakob 2010). DEP localization on either site of the membrane is unclear but due to the presence of a membrane spanning domain, the protein could be located at the stromal side and detect protons on the luminal site that would lead to its inactivation (Goss & Lepetit 2015).

In plants, ZEP is active at all light regimes including darkness in neutral or basic pH with oxygen but its' *in vivo* reaction kinetics is about 10 times lower compared to VDE (Goss & Lepetit 2015, Goss & Jakob 2010). Thus, the plant xanthophyll cycle relies on the regulation of VDE kinetics and constitutive but slow ZEP activity. On the other hand, diatom DEP is strongly regulated by light and pH. Enzymatic activity is higher under low light or dark conditions and inactivated by the generation of a trans-thylakoid proton gradient (Kuczynska et al. 2015). *P. tricornutum* VDE and DEP are responsive to blue light and this finding together with an observed increase in the xanthophyll pool indicates an upregulation of *de novo* carotenoid synthesis (Schellenberger Costa et al. 2013). Albeit the differential regulations, the deepoxidase/epoxidase couple controls the xanthophyll pool in both the green and the red lineage. They form the switch from photosynthesis to photoprotection according to energy transfer or NPQ properties of the respective pigment. In order to provide a quenching site, pigments must be solubilized in the thylakoid membrane.

2.3.2.3 Xanthophyll solubilisation and interaction with MGDG

Solubilisation of xanthophylls is beneficial for NPQ induction as indicated by higher VDE activities in *in vitro* preparations of thylakoid membranes that are devoid of LHCs (Jahns et al. 2009). Accordingly, *N. gaditana* VDE activity can be enhanced by the addition of iodoacetamide. Iodoacetamide induces an increase in membrane viscosity while Zx is assumed to rigidify membranes in order to counteract high light or heat induced enhanced molecular movements. Without treatment, VDE converts 33% of present Vx within 1 hour. After treatment, 50% of the Vx pool was converted within 30 min, with Ax making 10% and Zx 90% (Gentile & Blanch 2011). On the other hand, mutants with increased free Vx pool do not exhibit stronger VDE activity (reviewed in Jahns et al. 2009). *In vitro* de-epoxidation activity measurements of *C. meneghiniana* DDE or wheat VDE on isolated Vx and Ddx incubated with different concentrations of MGDG or PE reveal that MGDG can solubilize more pigments than PE and more Ddx than Vx (Goss et al 2005). DDE activity is saturated at a lipid:pigment ratio of 5. Excess of MGDG inhibits deepoxidation probably due to lipid aggregation (Goss et al 2005).

This allows a higher Ddx or Dtx concentration in the MGDG shield around FCP (**figure 2.11**) (Goss & Lepetit 2015).

Having Vx solubilized in a lipid phase, it is likely that the VDE enzyme binds to the thylakoid membrane in order to synthesize Ax and Zx. This is supposed to be facilitated by protonation of a C-terminal charged domain. Indeed, lipid affinity precipitation indicate that VDE binds best to MGDG with 4-38 higher affinities depending on the fatty acid structure (Jahns et al. 2009). It thus seems that MGDG is required for the formation of a qE platform to allow VDE-pigment contacts (Garab et al. 2016). Once a NPQ platform is established, energy quenching can occur.

2.3.3 *Chlorophyll and xanthophyll quenching mechanism*

Molecules possess a certain energy state. Upon excitation with light energy, chlorophylls and carotenoids internal energy gets higher. Energy conversion by transfer to a neighbouring molecule with a lower energy state, or internal dissipation as heat and fluorescence allows the pigment to go back to the energetic ground state (Alia et al. 2013).

By changing the epoxidation state of the Vx/Zx couple, light harvest and heat emission proportions in antenna are rapidly altered. In theory, the energy state of Vx should be similar or higher than that of Chl *a* whereas the one of Zx should be lower to direct the energy transfer. However, there are opposing results for the energy states obtained from different methods, either confirming the theory or demonstrating a lower energy state in both xanthophylls compared to the chlorophyll (Derks et al. 2015). The mechanism of chlorophyll energy quenching by Dtx is unknown and both Ddx and Dtx have a lower excitation state compared to Chl *a*. Hence, a direct Chl *a* energy transfer from Ddx and respectively to Dtx could be achieved only if the respective pigment binding proteins provoke a conformation with different energy levels (Goss & Lepetit 2015). Indeed, Chl *a* quenching by Zx in LHCII requires protein aggregation induced by Zx (Lepetit et al. 2011, Valle et al. 2014). Alternatively, a Dtx-Chl a radical intermediate can be formed that upon relaxation would dissipate the energy as heat (Goss & Lepetit 2015). Chlorophyll quenching by a xanthophyll can also involve electronic interactions in

which one pigment becomes an anion and the other one a cation. Upon spontaneous recombination of charges, energy is emitted as heat. This process is rather attributed to minor antenna complexes than LHCII and is believed to involve PsbS activity (Valle et al. 2014). The different possible mechanisms suggest therefore the occurrence of multiple potential NPQ sites.

2.3.3.1.1 Possible non-photochemical quenching sites

Not only the nature of the pigment is important for the switch from light harvest to photoprotection but also the protein binding (Kuczynska et al. 2015). The xanthophyll cycle takes place at PSII and is therefore localized to grana stacks of higher plants thylakoid membranes. When the grana structure is unstacked in *in vitro* experiments by depletion of magnesium and sorbitol, NPQ is barely induced. Both, the presence of Mg^{2+} as cofactor and the structure of a macrodomain spanning adjacent membranes are supposed to be important for qE (Goss & Lepetit 2015). Experiments on *Arabidopsis* protoplasts however indicate grana unstacking in response to high light. Grana shrink in the lateral diameter and grana-grana contacts are reduced. Thereby, PSII and LHCII become more exposed to the stroma (Herbstová et al. 2012). This remodelling is assumed to facilitate D1 repair by increasing protein intrusion of the grana stacks and depends on phosphorylation events (see section **2.3.4**). Thus, the actual quenching site and localization of PSII and LHCII are unknown in plants.

NPQ is correlated to PSII-LHCII disconnection (Herbstova et al. 2012). LHCII aggregation is induced by high proton concentrations and Zx, as occurring at high light. Mutants in LHCII or minor antenna proteins have reduced NPQ capacities but the nature of the precise qE platform is not revealed (Goss & Lepetit 2015). *Phaeodactylum* FCP form trimers and their light harvesting complex protein (LHCF) composition differs in respect to the light conditions, with LHCF5 allowing a higher Fx:Chl *c* ratio to be predominant under low light and LHCF4 causing a low Fx:Chl *c* under high light irradiation (Kuczynska et al. 2015). Active Dtx alters the conformation of antenna proteins towards aggregation to build a quenching platform. This can be quantified by ambient temperature absorption spectra changes at 522 nm, measurements that can be

used as a fingerprint for the involvement of Dtx in diatom species. For *Phaeodactylum*, compared to centric diatom species, the vast part of NPQ relies on Dtx mediated FCPII aggregation (**figure 2.11**) (Lavaud & Lepetit 2013).

Chl *a* quenching at PSI is currently hypothesized to be involved in diatom NPQ. This idea is based on pigment analysis *via* fluorescence measurements at 77 K which revealed one diatom Chl *a* pool abundance to be positively correlated with Ddx/Dtx levels and accordingly NPQ capacities. This Chl *a* pool emits between 710 nm and 717 nm (Chl a_{711}). High light induced Chl a_{711} quenching is less pronounced than PSII associated Chl a_{687} quenching. In another study, the 710 nm emission band was attributed to FCP complexes that disconnect from the reaction center upon high light irradiation (Lavaud & Lepetit 2013). Chl a_{710} fluorescence is found in PSI-bound FCPs that due to their lower energy state serve as quencher for PSI (P_{700}) energy (Yamagishi et al. 2010). Thus, Chl $a_{710/711}$ emission serves as fingerprint for FCP complexes in which NPQ takes place (Lavaud & Lepetit 2013). Despite the importance of antenna protein aggregation for qE there might be a second quenching site in the PSII.

The model of Holzwarth and coworkers describes two distinct quenching sites Q1 and Q2 (Holzwarth et al. 2009) (**figure 2.11**). Q1 in plants involves the action of PsbS that regulates LHCII detachment from PSII and protein aggregation. Q1 does not require the xanthophyll cycle and relaxes rapidly within 1-5 min (Goss & Lepetit 2015). The strong antioxidant capacities of Fx may contribute to Dtx-independent energy quenching (Mikami & Hosokawa 2013). Furthermore, the MGDG shield around FCP might function in redox poise scavenging (Goss & Lepetit 2015, Kuczynska et al. 2015). Q2 composes of CP24, CP26 and CP29 that are enriched in xanthophylls and whose quenching activity relies on Zx/Dtx formation. Q2 NPQ offset time is long taking 10-15 min. Notably, Q2 does not involve MGDG. Evidence for the existence of these two quenching sites proposed by Holzwath is obtained from ultrafast fluorescence measurements on diatoms under high light conditions. Aggregation of *Phaeodactylum* FCPs is similar to LHCII oligomerization in higher plants and involves magnesium and protonation of luminal loops of LHCF and LHCX proteins. This aggregation is supposed to form the Q1 site of NPQ. Quenching at detached FCP complexes is independent of

Dtx. Alternative energy quenching mechanisms are proposed, involving possible interactions between two Chl *a* molecules or Chl *a* with Fx. However, Dtx must be somehow involved in Q1 quenching since cells devoid of this xanthophyll are unable to induce NPQ. In the current model of diatom NPQ, the Q2 site at the PSII reaction center is composed of FCP trimers including LHCX that bind to Ddx. In response to a high light signal, the xanthophyll cycle would be active and convert Ddx to Dtx, which in turn induces higher oligomerizations of peripheral FCPs that detach from the core and form the Q1 site (Goss & Lepetit 2015).

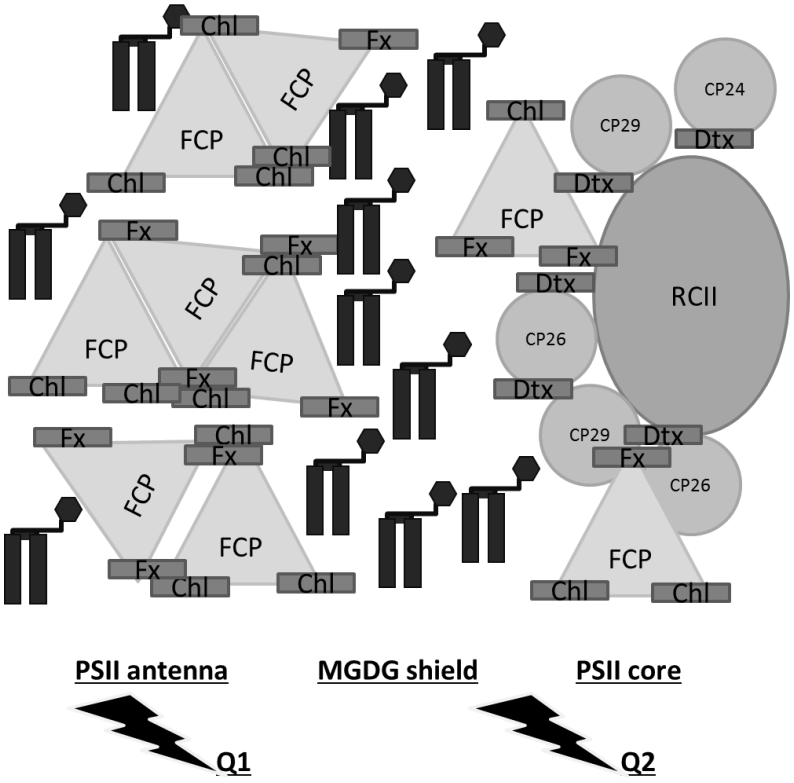

Figure 2.11. Possible non-photochemical quenching sites in *Phaeodactylum* according to the Holzwarth model. Fucoxanthin binding proteins (FCP) appear in trimers (indicated as triangle) or higher oligomeric states upon protein aggregation after detachment from PSII. This provides the Q1 platform for NPQ, probably in the PSII antenna regions. MGDG surrounds FCPs in an MGDG "shield" and might serve in energetic isolation. Energy quenching occurs possibly via chlorophyll (Chl) and Fucoxanthin (Fx) interactions. Q2 at the PSII core involves the xanthophyll cycle dependent quenching property of Dtx and is located in vicinity of the reaction center of PSII (RCII) together with chloroplast proteins (CP) 24, 26 and 29. The sites may be conserved throughout autotrophs (Goss & Lepetit 2015, Holzwarth et al. 2009).

An alternative model of NPQ in higher plants is proposed by Horton and colleagues. It involves four different quenching states of LHCII that are controlled by the xanthophyll cycle and the proton gradient. In state 1, LHCIIs bind Vx and are not aggregated. This occurs during darkness or low light irradiation, during which the cell is in light harvesting mode. Upon the onset of illumination, state 3 is induced in which LHCII proteins become protonated and begin to aggregate, while they still bind Vx. High light irradiation then induces the xanthophyll cycle and LHCII appears in state 4,, during which they bind Zx, and protein aggregation and NPQ levels are at their maximum. State 2 describes LHCII that bind Zx which is slowly removed by ZEP activity as it occurs upon transition from high light to darkness or low light, during which a certain level of NPQ persists (Goss & Lepetit 2015).

2.3.4 *Photoinhibition*

The qI component of NPQ is the least well understood and defined by its long persistence when the high light source is shut off. The major part of qI is attributed to a prolonged energy quenching in LHCII and is poorly investigated (Ruban et al. 2012). The term photoinhibition traditionally refers to the D1 repair cycle.

The D1 repair cycle

When energy quenching is insufficient, light conversion in PSII is accompanied by oxidative damage. The RCII protein D1 is most susceptible to photooxidative damage that increases under high light. Induction of the D1 repair cycle leads to photoinhibition that reduces PSII capacities. Photoinhibition is defined as the balance between the rate of photodamage to PSII and the rate of D1 repair (Takahashi & Murata 2008). It defines a part of qI and is the latest part of NPQ (Szabó et al. 2005). Under high light both, the expression level of D1 as well as D1 turnover are increased (Li et al. 2009, Pesaresi et al. 2011).

Upon light damage in higher plants, D1 becomes phosphorylated and the respective PSII complex moves from grana regions to the stromal lamellae where the damaged D1 is

substituted by a newly synthesized protein. D1 turnover correlates with the degree of its phosphorylation but this modification is not crucial (Pesaresi et al. 2011). Light induced phosphorylations are absent from diatom thylakoids (Grouneva et al. 2013). Furthermore, due to the absence of grana stacking, the D1 repair mechanism is probably different in Heterokonts. Luminal osmotic swelling is discussed to contribute to D1 migration by reducing steric hindrances, but it is not known if this phenomenon occurs in Heterokonts (Kirchhoff 2013).

The role of photoinhibition in NPQ

Possibly also due to the structural differences, D1 repair is less important in diatom NPQ and as demonstrated in *Thalassiosira*, not necessarily associated with PSII inactivation. The centric diatom is able to maintain D1-free PSII complexes (Grouneva et al. 2013). Most of PSII core proteins are constitutively expressed in *Phaeodactylum*, including D1 (Nymark et al. 2009). Indeed, in plants and Heterokonts D1 regulation is posttranslational (Domingues et al. 2012). In agreement with high light induced PSII inactivation, putative genes coding for the oxygen evolving complex and some PSII reaction center proteins were downregulated under high light conditions. In contrast, D1 degrading metalloproteases FTSH1 and FTSH2 and two proteins assumed to act in PSII assembly and repair, *i.e. PSB27* and *HCF136,* were initially upregulated and then gradually declined in *Phaeodactylum* (Nymark et al. 2009). Accordingly, D1 levels decrease under high light conditions and are abolished when chloroplast protein synthesis is inhibited (Domingues et al. 2012). During NPQ relaxation, offset of qI is very slow and photochemistry may not have fully recovered after one hour in darkness. However, as indicated by fast NPQ offset kinetics that are sensitive to VDE inhibition but only marginally to inhibition of chloroplast protein translation, qI is less important in diatoms compared to plants (Domingues et al 2012, (Lavaud et al. 2012). Knowledge on *Nannochloropsis* is missing but according to a similar thylakoid structure in Heterokonts, one could assume conservation between diatoms and the *Eustigmatophyceae*. The last component of NPQ, qT, is absent from diatoms.

2.3.5 *State transitions*

Light harvest capacities between the two photosystems are balanced in response to different light qualities or quantities by reversible migration of mobile LHCII trimers and association with either PSII or PSI. In state 1, LHCII trimers are located at PSII. During transition to state 2, LHCII trimers migrate away from PSII and re-associate with PSI (Lemeille & Rochaix 2010). *A. thaliana* mutants which are disturbed in state transitions do not have strong phenotypes in development and fitness so its role in vascular plants is not clear (Pesaresi et al. 2011). It is discussed that *A. thaliana* state transitions are induced to maintain LEF under a given light regime (Pesaresi et al. 2011). About 80% *Chlamydomonas* but only 25% *Arabidopsis* LHCII proteins associate with the PSI-LHCI complexes (Minagawa 2011, Samol et al. 2012). Interestingly, enhanced light harvesting activity in state 2 is only observed in the green algae where, in contrast to plants, state transitions are accompanied by CEF (Kanervo et al. 2005, Lemeille & Rochaix 2010). Regulation of state transitions involves phosphorylation of LHCII proteins by state transition 7 (STN7) protein for the induction of state 2 and dephosphorylation by PPH1 (Lemeille & Rochaix 2010, (Pribil et al. 2010).

State transitions are believed to not occur in diatoms (Grouneva et al. 2013). Accordingly, they lack the PSI subunit PsaO putatively involved in state transitions (Grouneva et al. 2011) and light dependent phosphorylations are absent from thylakoids of diatoms (Grouneva et al. 2013).

2.3.6 *Light reactions in Heterokonts differ from vascular plants*

Light is the primary energy source driving carbon assimilation in all photoautotroph organisms. Electron flows are globally conserved between Heterokonts and higher plants in spite of the absence of plastocyanin, the NDH-dependent CEF, and some PS core proteins (**figure 2.12**) (Grouneva et al. 2011). Some of those missing core subunits are associated with energy balance mechanisms that are conserved in the green lineage but absent from Heterokonts, *i. e.* plastocyanin binding, phosphorylations, and state transitions. Accordingly, photoprotection mechanisms are different in Heterokonts. A distinct thylakoid structure accounts for a part of these differences and the mechanism of

D1 repair in photoinhibition is not resolved in the red lineage (Goss & Lepetit 2015, Lavaud & Lepetit 2013). Albeit the lack of qI and qT, NPQ capacities are higher in diatoms compared to the green lineage (Goss et al. 2005). The major component of NPQ is qE, in which absorbed light energy is emitted as heat and fluorescence. This involves the xanthophyll cycle as well as antenna protein aggregation and chlorophyll quenching (**figure 2.12**) (Goss & Lepetit 2015).

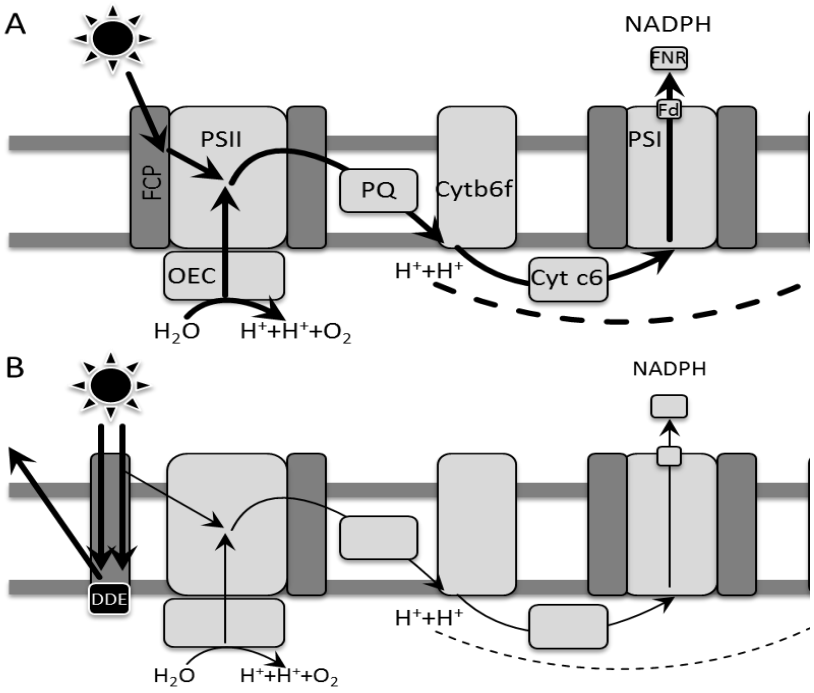

Figure 2.12. Schematic view on energy balance in diatoms under low light (A) and high light (B) conditions. A. During linear electron flow, light energy is captured by fucoxanthin binding proteins (FCPs) and transferred to photosystem II (PSII). PSII reduces plastoquinone (PQ) and is oxidized by the oxygen evolving complex (OEC) upon photolysis of water. PQ transports electrons to the cytochrome b6f complex (Cytb6f) that reduces photosystem I (PSI). PSI harvests light energy to reduce ferredoxin (Fd) for the generation of NAPDH by Fd-NAPD-oxidoreductase. The electron transfer system also transports protons (H^+) to the luminal side that drive the ATPsynthase (Derks et al. 2015, Nelson & Ben-Shem 2004). **B. Upon high light**, FCP disconnects from PSII and the diadinoxanthin deepoxidase (DDE) induces the xanthophyll cycle. Thereby, electron generation at PSII is reduced (Kuczynska et al. 2015, Goss & Lepetit 2015, Lavaud & Lepetit 2013).

While in higher plants, the xanthophyll cycle is induced by luminal acidification and thus correlates to higher ETR, diatom qE induction is independent of a trans-thylakoid gradient (**figure 2.12**). Protein aggregation appears to play a more important role in diatom NPQ and might provide a quenching platform (Goss & Lepetit 2015), Kuczynska et al. 2015).

The MGDG shield around FCP might facilitate pigment solubilisation for the xanthophyll cycle (Demé et al. 2014, Goss & Jakob 2010, Jahns et al. 2009). However, the precise role of MGDG and other thylakoid lipids in photoprotection is not understood and data from *in vivo* experiments are scarce.

Some of the differences between land plants and Heterokonts might be caused by the lower nutrient availability in aquatic habitats (Depauw et al. 2012). The efficient adaptation of the photosynthetic apparatus to the light conditions observed in Heterokonts might have contributed to their success as most abundant phytoplankter (Goss & Lepetit 2015, Chevalier-Smith 2003). Some important differences occur also on the level of carbon fixation and metabolism that rely on the supply of ATP and NADPH from the light reactions.

2.4 Carbon metabolism

2.4.1 *Carbon concentration mechanism*

In contrast to higher plants that are exposed to the atmosphere, CO_2 availability in aquatic habitats is often limited due to inefficient solubilisation. In water, CO_2 is in equilibrium with CO_3^{2-}, HCO_3^- and H_2CO_3. To enhance the availability of inorganic carbon, Heterokonts have developed efficient carbon concentration mechanisms (CCM) (Hopkinson 2013). This mechanism shares features with C4 photosynthesis and hence there is a debate on the existence C4 metabolism in *Phaeodactylum* (Haimovich-Dayan et al. 2013).

In diatoms, the intracellular carbon status is sensed in a pathway involving cyclic-AMP and leads to the expression of CCM genes (Hopkinson 2013). HCO_3^- and high medium pH induce carbon transporters and C4 photosynthesis proteins, while RubisCO abundances are lowered (Mus et al. 2013). CO_2 is incorporated into the cell by diffusion but HCO_3^- import is active. The "chloroplast pump" model proposed by Hopkinson proposes that inorganic carbon could be concentrated in the vicinity of RubisCO. Indeed, concentrations in the pyrenoid of *Phaeodactylum* can be 15 times higher than in the culture media. By the action of HCO_3^- transporters and carbonic anhydrases (CAs), a CO_2 gradient is established over the cell. CAs dehydrate HCO_3^- and provide CO_2. Pyrenoid CA activity is four times higher than in the cytosol and provides a sink for the carbon moieties. Relatively low concentrations in the cytoplasm trigger the constant influx of CO_2 from the exterior. CO_2 is then dissolved to HCO_3^-, catalysed by chloroplast membrane bound CA. HCO_3^- is actively transported into the chloroplast. *P. tricornutum* encodes homologs of the human bicarbonate transporters SLC4 and SLC6. Within the chloroplast, the specific localization of CA causes a suborganelle CO_2 gradient, one third of which is directly consumed by RubisCO, whereas the rest diffuses back to the cytosol. In agreement with the model, seven CAs have been identified in *P. tricornutum* chloroplast membranes, the pyrenoid (**figure 2.4**), and mitochondria (Hopkinson 2013, (Kroth et al. 2008). The *Phaeodactylum* thylakoid located CA is induced under low CO_2 concentrations whereas the isoenzymes at the ER and the periplasmic space are constitutively expressed (Kroth et al. 2008).

Data on *Nannochloropsis* CCM are less conclusive. In *N. oculata*, cell division is induced when cultures are bubbled with up to 8% CO_2 instead of air. Higher CO_2 concentrations cause chlorosis and growth arrest likely due to a severe medium acidification (Hsueh et al. 2009). On the contrary, inhibition of photosynthesis by UV radiation leads to a decrease in carbon uptake in *N. gaditana* that relies on HCO_3^- and is not affected by CO_2 concentrations (Sobrino et al. 2005). CO_2 fluxes are followed in *N. gaditana* by mass spectrometry analysis. In light, cells take up HCO_3^- whereas in darkness CO_2 is released. This equilibrium is regulated by light-dependent inorganic carbon consumption by the Calvin cycle and intracellular CAs. The CAs do not function

in active HCO_3^- uptake which remains elusive (Huertas et al. 2000). These studies could allow concluding on a less controlled inorganic carbon homeostasis in the *Eustigmatophyceae* compared to diatoms.

2.4.2 *Carbon fixation*

The Calvin-Benson-Bassham cycle (in the following only Calvin cycle) is the only eukaryotic carbon fixation pathway and has probably evolved in cyanobacteria. It fixes inorganic CO_2 and generates 3-phosphoglycerate (Hügler & Sievert 2011). The reaction is fuelled by ATP and NADPH generated by the light reactions. In the first step of the Calvin cycle, CO_2 is fixed via the carboxylation of ribulose 1,5-bisphosphate. This gives rise to an unstable product which decays into two molecules of 3-phosphoglycerate. The product is integrated in sugar metabolism or used for the regeneration of ribulose 1,5-bisphosphate. To this end, 3-phosphoglycerate kinase generates 1,3-bisphosphoglycerate and glyceraldehyde-3-phosphate dehydrogenase glyceraldehyde-3-phosphate. The C3-moieties may be withdrawn for glycogenesis or glycolysis to pyruvate (Berg et al. 2002).

The energy-dependent generation of three molecules of ribulose 1,5-bisphosphate requires five 3-phosphoglycerate. Ribulose 1,5-bisphosphate carboxylase/oxygenase (RubisCO) and phosphoribulokinase are the key enzymes of the Calvin cycle. In plants, RubisCO has low affinities for CO_2 and has a four-times lower activity on oxygen. Oxygenase activity of RubisCO is called photorespiration during which one 3-phosphoglycerate and one phosphoglycolate are produced. The latter can enter sugar anabolism circuitously with a lower net energy gain (Berg et al. 2002). The affinity for CO_2 *versus* O_2 is much higher in diatom RubisCO compared to the isoenzyme in the green lineage and thus photorespiration is reduced (Kroth et al. 2008). Proteins of the glycolate pathway are present in diatoms that allow the recycling as serine or the introduction into glycolytic pathways (Kroth et al. 2008). Furthermore, in *Phaeodactylum* glycolate may be excreted (Singh et al. 2015).

To compensate low efficiencies, RubisCO is the most abundant protein in plant species thus presenting a great nitrogen sink (Berg et al. 2002). By contrast, phytoplankton samples from the Californian coast typically contain less than 6% RubisCO (Losh et al.

2013). Plant RubisCO locates in the stroma, whereas in diatoms the Calvin cycle takes place in the pyrenoid (**figure 2.4**) (Haimovich-Dayan et al. 2013). Also in contrast to higher plants, *Phaeodactylum* RubisCO levels are negatively regulated by CO_2 availability and the growth state. RubisCO accounts for 3.5% of total protein extracts when cells are in exponential growth, and less than 2% in stationary phase (Losh et al. 2013). Similarly, in *N. gaditana* RubisCO expression is not constitutive but increases with light intensities (Simionato et al. 2011). In the diatom however, Calvin cycle protein gene expression was unaffected by high light (Nymark et al. 2009) but regulation on the protein level cannot be excluded. RubisCO regulation and carbon concentration mechanisms (CCM) appear to be versatile in different diatoms species (Young et al. 2016). The efficient CO_2 accumulation allows regulated RubisCO protein abundances in phytoplankton species. Therefore, RubisCO reflects a much smaller nitrogen sink in Heterokonts compared to higher plants.

The concentration of inorganic carbon in the vicinity of RubisCO observed in Heterokonts is similar to C4-plants. All diatoms encode C4-specific proteins but activity of the pathway seems to be species dependent. Radiolabeling experiments in two centric diatoms indicate the presence of C4 metabolites, mainly malate, in *Thalassiosira weissflogii* but not *T. pseudonana*, where hexose-phosphates make the bulk of carbohydrate moieties (Roberts et al. 2007). We would rather speculate that these proteins are involved in balancing carbon moieties between the different organelles and molecular sinks.

2.4.3 *The role of pyruvate in the production of carbon precursors for glycerolipid synthesis*

After CO_2 fixation, carbon blocks are built up to store the energy and to serve as a supply for metabolic building blocks. Glycerol-3-phosphate, the backbone of glycerolipids is produced during glycolysis by the activity of glycerol-3-phosphate dehydrogenase (GPDH) on dihydroxyacetone phosphate, a reaction that is conserved in Heterokonts (Yao and Yao 2014). Alternative glycolytic pathways are present in *Phaeodactylum* that contribute to glycerol-3-phosphate, namely the oxidative pentose

phosphate pathway and the Enter-Doudoroff pathway (Kim et al. 2016, Kroth et al. 2008).

Pyruvate is an important carbon intermediate and is involved in protein, sugar and fatty acid synthesis as well as energy production. In the tricarbonic acid (TCA) cycle taking place in mitochondria, acetyl-CoA generated by pyruvate decarboxylase (PDC) is consumed for energy production (**figure 2.13**). Alternatively, acetyl-CoA can be channelled into the chloroplast to be used for fatty acid synthesis (**figure 2.14**). Similarly, chloroplast pyruvate can be converted into acetyl-CoA by pyruvate dehydrogenase which is then transformed to malonyl-ACP, the substrate for fatty acid synthesis (Kim et al. 2016, Kroth et al. 2008, Singh et al. 2015). The C4-like pathway in *Phaeodactylum* might be involved in balancing pyruvate between the different sinks.

In C4 plants, the first reaction of the Calvin cycle is performed in mesophyll cells, whereas the product is reduced in bundle-sheath cells, to increase CO_2 concentrations in the vicinity of poor affinity RubisCO. *P. tricornutum* encodes all genes required for this pathway that is described to occur in some unicellular species. However, target peptides of the respective proteins do not predict colocalization. Plastid pyruvate orthophosphate dikinase (PPDK) is required for the phosphorylation of pyruvate to phosphoenolpyruvate (PEP) in C4 metabolism (Kroth et al. 2008, Haimovich-Dayan et al. 2013). PPDK activity in *P. tricornutum* is low but knock down of this sequence further redirects the carbon flux from amino acid synthesis to carbohydrate and glycerolipid synthesis (Haimovich-Dayan et al. 2013). This is because the PPDK reaction is in equilibrium with the carboxylation of PEP by phosphoenolpyruvate carboxykinase (PEPCK) that gives rise to oxaloacetate. The C4-moiety might be directly converted into aspartate and thus serves in protein synthesis (Haimovich-Dayan et al 2013). Knock down of PEPCK in *Phaeodactylum* slightly increases neutral lipid contents (Yang et al.2016).

In diatoms, oxaloacetate may be transported into the chloroplast, where malate dehydrogenase (MDH) and malic enzyme (ME) converts it into pyruvate at the base of fatty acid synthesis (**figure 2.13**) (An et al. 2015, Doubnerová Hýsková et al. 2014).

Consistently, overexpression of ME in *Phaeodactylum* increases the production of fatty acids, which are then channelled into TAGs (Xue et al. 2015). Similarly, ME transcripts increase under nitrogen starvation, a condition known to trigger TAG accumulation (Xue et al. 2015). Whether malate produced in the mitochondria may be transported into chloroplasts in *Phaeodactylum* is unknown and respective transporters are not identified (Kroth et al. 2008). Accordingly, a carbon flux through plastid ME is not predicted to occur in *Phaeodactylum* (Kim et al. 2016). Oxaloacetate might be transformed to malate by malate dehydrogenase or be converted back to PEP by PEP carboxykinase. Both, PEP and malate can be converted to the C3 moiety pyruvate (Kroth et al. 2008).

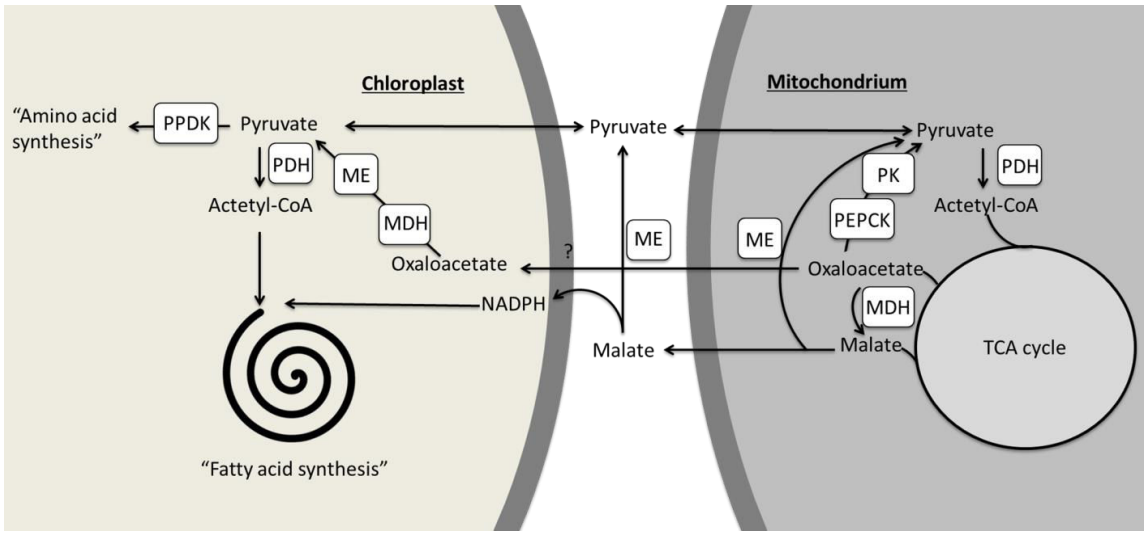

Figure 2.13. Pyruvate, malate and oxaloacetate shuffling between mitochondria and chloroplasts. Pyruvate derived from glycolytic pathways can be converted into acetyl-CoA by pyruvate dehydrogenase complex (PDH). Acetyl-CoA in the chloroplast is incorporated into fatty acid synthesis, and in the mitochondria into the TCA cycle. Oxaloacetate can be converted back into pyruvate by phosphoenolpyruvate carboxykinase (PEPCK) and pyruvate kinase (PK). Oxaloacetate can be converted into malate by malate dehydrogenase (MDH). Malate can be converted into pyruvate by malic enzyme (ME) generating NADPH. Plastid pyruvate orthophosphate dikinase (PPDK) converts pyruvate into phosphoenolpyruvate (PEP). PEP and oxaloacetate might be consumed in amino acid synthesis.

Oxaloacetate is also the intermediate metabolite that condenses with acetyl-CoA in the first step of the TCA cycle resulting in citrate production. Citrate exits the mitochondria

when high concentrations are reached. A citrate-pyruvate shuttle exists in *Phaeodactylum* to regulate the balance of the two carbon sources (Liang & Jiang 2013). Thus, protein, sugar and fatty acid synthesis compete for pyruvate and repression of the flux into proteins is one attempt to increase TAG productivity in oleaginous species (Liang & Jiang 2013).

2.5 Fatty acid synthesis

In chloroplast lacking heterotrophs, fatty acid synthesis takes place in the cytosol and mitochondria (Tehlivets et al. 2007). In all photoautotroph organisms studied, proteins involved in this process are located in the chloroplast (**figure 2.14**) and in mitochondria for the specific production of lipoic acid (Chen & Smith 2012, Gueguen et al. 2000). *N. gaditana* and some cyanobacteria furthermore encode a cytosolic fatty acid synthase that is similar to fungal polyketide synthase that might contribute to fatty acid synthesis under high light condition (Alboresi et al. 2016).

The production of acetyl-CoA in the chloroplast or its import from the cytosol is the first step in fatty acid synthesis (**figure 2.14**). Plastidial pyruvate dehydrogenase (PDH) complex catalyses its decarboxylation and condensing of acetate with CoA. This provides the major acetyl-CoA source in seeds of higher plants (Ke et al. 2000). PDH complex is conserved but in green algae it displays species dependent kinetics that correlate with acetyl-CoA availability, fatty acid productivity and TAG levels (Avidan et al. 2015). *N. gaditana* encodes two PDH, one of them likely to be located in the chloroplast (Jinkerson et al. 2013). In *Phaeodactylum*, knock down of the PDH kinase that deactivates PDH drastically increases fatty acid production and TAG contents (Ma et al. 2014).

Acetyl-CoA carboxylase (ACC) adds a carboxyl group onto acetyl-CoA thereby generating malonyl-CoA (**figure 2.14**). In all living organisms, a homomeric ACC is located in the cytosol. Secondary endosymbionts possess a second homomeric

chloroplast targeted form (Huerlimann et al. 2015). In plants, plastidial ACC is heteromeric, consisting of four subunits, namely a carboxyltransferase, a biotin carboxyl carrier protein, a biotin carboxylase and a β-subunit of a carboxyltransferase (Gu et al. 2011). Overexpression of an ACC and a thioesterase in *E. coli* increases fatty acid synthesis. This indicates that the conversion of acetyl-CoA to malonyl-CoA is inhibited by acyl-ACP (Davis & Cronan 2001). Similarly, yeast ACC transformants exhibit an increased fatty acid production (Wang et al. 2016). ACC overexpression in a non-oleaginous plant like potato increases fatty acid and TAG contents (Klaus et al. 2004, Xian et al. 2013). In tobacco leaves and seeds it leads to higher biomass production (Madoka et al. 2002). The regulation of ACCs does not seem to be conserved among *Chromalveolata* species. Nitrogen limitation leads to the upregulation of the plastidial ACC in *Chromera velia* but in *Isochrysis aff. galbana* ACC expression is lowered in TAG accumulating conditions. *C. velia* cytosolic ACC expression is lowered upon nitrogen stress and correlates with an increase in medium chain fatty acids (Huerlimann et al. 2014).

Malonyl-CoA:acyl-carrier protein transacylase (MCAT, encoded by *fabD*) catalyse the condension of malonyl-CoA with holo-acyl carrier protein to malonyl-ACP (**figure 2.14**). The protein is involved in chloroplast type II fatty acid synthesis and thus absent from heterotrophic eukaryotes (Liu et al. 2015, Natarajan et al. 2012). *N. gaditana MCAT* is induced under nitrogen limitation and cold stress. The sequence resembles diatom MCAT, indeed the phylogenetic branch differentiating the two Heterokont groups is not well supported by bootstrap values (Tian et al. 2013). One could therefore speculate on a conserved protein function and regulation. Expression of *Schizochytrium* and *Streptomyces* MCAT in yeast and *E. coli*, respectively, increases fatty acid synthesis and allows higher biomass production (Cheng et al. 2013, Zhang et al. 2012). Functional characterization of Heterokont MCAT is however missing to that date.

The fatty acid synthesis cycle is initiated by a β-ketoacyl-ACP synthase III (KASIII) (**figure 2.14**). The protein is conserved from bacteria, including cyanobacteria, to higher plants (Dehesh et al. 2001, González-Mellado et al. 2010, Gu et al. 2016, Misra et al. 2013). KASIII catalyses the condensation of malonyl-CoA with acetyl-CoA or acyl-.

CoA. It accepts straight and branched acyl-CoA moieties as substrate, with species-dependent specificity. Genetic engineering towards the accumulation of medium chain fatty acids by heterologous gene expression is thus possible, as already performed by several groups (Abbadi et al. 2000, Gu et al. 2016, Li et al. 2005, Matsumoto et al. 2009, Smirnova & Reynolds 2001). Obviously, to be effective in photoautotroph organisms, KASIII needs to be chloroplast targeted (Verwoert et al. 1995). KASIII function is critical in the fatty acid synthesis cycle as indicated by a *Arabidopsis* mutant with lower KASIII activity. In this mutant, fatty acid contents are decreased, chlorophyll levels and photosynthetic efficiency are reduced, and plants become sensitive to cold induced PSII photoinhibition (Takami et al. 2010). Although KASIII endogenous and heterologous expression have been widely studied, to our knowledge Heterokont orthologs were never tested.

The 3-ketoacyl-ACP product from KASIII is reduced into 3-hydroxyacyl-ACP by a 3-ketoacyl-ACP reductase (KAR) (**figure 2.14**). This intermediate serves as a substrate for an eonyl-dehydratase (HAD). The product, 2,3-transeonyl-ACP, is reduced by an eonyl-reductase (ER) into an acyl-ACP that contains two additional carbons compared to the initial substrate. The new acyl-ACP is recognized by a β-ketoacyl-ACP synthase I (KASI) for further chain elongation. The conversion of 16:0 to 18:0 is carried out by a β-ketoacyl-ACP synthase II (KASII). Substrate specificities of the proteins and the presence of thioesterases (TE, see below) that cut the ACP bond determine the exit of an acyl-chain from the FA synthesis cycle (Li-Beisson et al. 2010). Modulation of KASII activity alters the C16:C18 ratio (Aslan et al. 2015, Gupta et al. 2012b, Teh & Ramli 2011). Knock out of KASII is lethal but knock down lines display a shift towards C16 accumulation in tobacco (Aslan et al. 2015). This might indicate that plants do not have the ability to compensate loss of plastid 16:0 to 18:0 elongation by a ER located elongase. In *Phaeodactylum*, all fatty acid synthesis proteins are annotated, but none of these proteins have been functionally studied in Heterokonts.

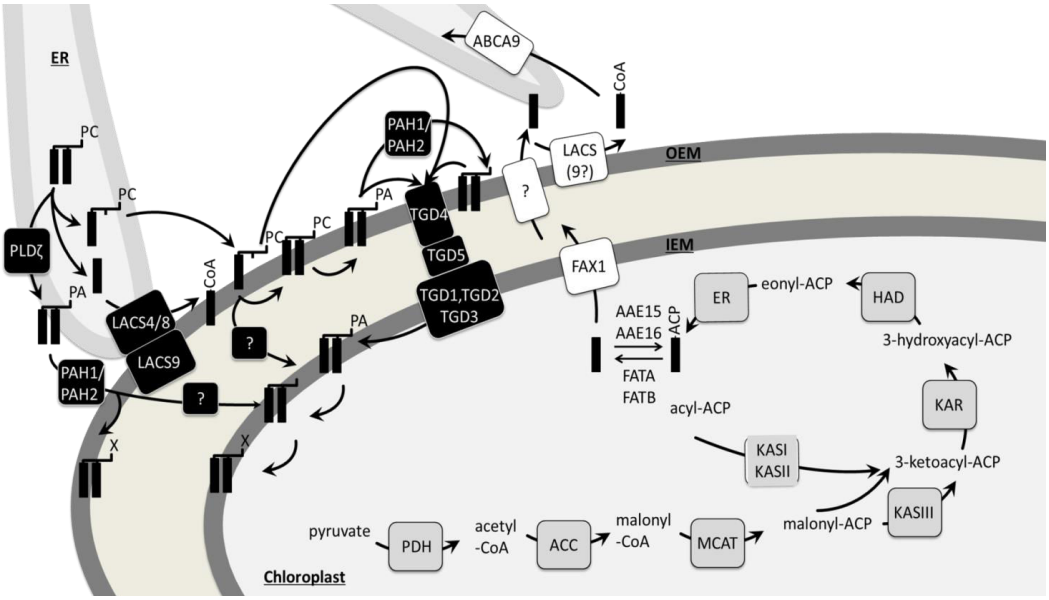

Figure 2.14: Hypothetical model of the eukaryotic fatty acid (FA) synthesis and trafficking pathway in *Arabidopsis thaliana*. FAs are represented as black bars. FA synthesis proteins are highlighted in grey. FA synthesis starts with 3-carbon pyruvate that is decarboxylated into acetyl-CoA by a pyruvate dehydrogenase (PDH) complex. Acetyl-CoA is carboxylated to malonyl-CoA by an ACC and the protein ligand is exchanged by a malonyl-CoA:acyl-carrier protein transacylase (MCAT). Malonyl-ACP condenses with acetyl-CoA by a β-ketoacyl-ACP synthase (KAS) III or an acyl-CoA by KASI and KASII. The product is reduced and dehydrated into acyl-ACP by a 3-ketoacyl-ACP reductase (KAR), an eonyl-dehydratase (HAD) and an eonyl-reductase (ER). FAs are either bound to acyl-carrier protein (ACP) by acyl-ACP synthetases (AAE15 and AAE16) or released as free fatty acids (FFA) by thioesterases (FATA and FATB). FFA translocation involves proteins represented as white boxes, *i. e*. fatty acid export protein 1 (FAX1) in the inner envelope membrane (IEM), an unknown transport over the outer envelope membrane (OEM), an activation on the cytosolic site into acyl-CoA, probably by a long acyl-CoA synthase (LACS), and an import into the ER by a transporter that was identified in developing seeds as ABC class A transporter 9 (ABAC9). Proteins involved in the reimport of FA-moieties are presented as black boxes. One hypothesis involves the disassembly and reassembly of PC in the ER and OEM, respectively. According to this idea, ER-produced PC is deacylated into lyso-PC and a FFA by a phospholipase. By the interaction of ER-located LACS4 and or LACS8 with OEM-located LACS9, the FFA is activated to acyl-CoA and together with lyso-PA translocated to the OEM, where PC is reassembled and possibly converted into PA. PA is believed to be transported over the chloroplast envelope with the help of a five component ABC transporter (TGD). In the IEM, PA could be dephosphorylated into DAG which serves as the precursor for eukaryotic chloroplast lipid synthesis. Alternatively to PA, DAG could be imported into chloroplast membranes. Cytosolic PA-phosphatases (PAH1 and PAH2) produce DAG from PA possibly located at the ER or the OEM. DAG could be used for glycerolipid synthesis in the OEM or transported into the IEM by either an unknown transport or via the TGD complex. A third possible pathway involves an unknown import of lyso-PC.

2.6 Fatty acid trafficking between the chloroplast and the ER

2.6.1 *Preparation for the export*

Produced fatty acids are bound to acyl carrier proteins (ACPs) in the chloroplast stroma. From here, acyl-ACPs have two possible fates: the incorporation into chloroplast glycerolipids by the "prokaryotic pathway", or an export for ER-located pathways, *i.e.* the production of endomembrane glycerolipids or acyl modification by elongation and desaturation prior to a reimport to the chloroplast by the "eukaryotic pathway" in vascular plants. Because in Heterokonts the precursor molecule of ER synthesized VLC-PUFAs that is crossing the four membranes limiting secondary plastids is unknown, this pathway is designated as the "omega pathway" (Petroutsos et al. 2014). The model organism *Arabidopsis thaliana* is grouped among the 16:3-plants which are characterized by having exclusively C16 FAs at the *sn*-2 position of chloroplast lipids (**figure 1.1**). This is because of the high proportion of fatty acids retained in the plastid for the "prokaryotic pathway" while only 62% of stroma produced fatty acids are exported (Browse et al. 1986). 18:3-plants, such as rice, possess chloroplast lipids that mainly derive from the "eukaryotic pathway" (Petroutsos et al. 2014). The amount of fatty acids retained in the chloroplast or exported is determined by the activity of acyl-acyl carrier protein (ACP) synthases (AAS) and counteracting thioesterases that release free fatty acids (FFAs). The activation of fatty acids by the introduction of a thioester bond can involve a CoA as ligand in the cytosol and ACP in the chloroplast (Shockey et al. 2003). AASs belong to the adenylate-forming enzyme class 1 that bind fatty acids with a chain length of C14-C18 onto the 4'- phosphopantetheine arm of holo-ACP via ATP hydrolysis (Jiang et al. 2006). Two candidate genes for AAS proteins are identified in *Arabidopsis*, *AAE15* (At4g14070) and *AAE16* (At3g23790). Mutants have reduced capability to elongate radiolabeled C8-C14 substrates that are not recognized by ER elongases (Koo et al. 2005). Expression of *AAE15* in a *Synechocystis* AAS mutant can complement the phenotype of missing medium chain fatty acid elongation (Kaczmarzyk et al. 2016). Based on amino acid sequence similarity to *AAE15,* and on the presence of amp-dependent synthetase and ligase domains, and on chloroplast localization predictions, poorly conserved gene candidates for AAS were identified in *N. gaditana,*

(Naga_100047g8 with 32% sequence identity), and *P. tricornutum*, (Phatr2_12420 with 43% sequence identity), conservation between both Heterokont sequences was 42%. Up to now, these gene candidates are not functionally studied.

While AAS is responsible for the synthesis of acyl-ACPs that serve as precursors for chloroplast acyl-transferases, free fatty acids are released from the ACP ligand by the acyl-ACP thioesterases FatA and FatB that act on 16:0-ACP, 18:0-ACP and 18:1-ACP with different specificities (Tjellström et al. 2013). Three loci have been annotated to encode proteins with an acyl-ACP hydrolase activity in *Arabidopsis*, At3g25110 (FatA), At1g08510 (FatB) and At4g13050 (retrieved from www.arabidopsis org. 13.04.2016). In vitro assays using recombinant proteins revealed an AtFATA preference for 18:1-ACP whereas AtFatB preferred 16:0-ACP but accepted also 14:0-ACP, coinciding with a major export of 18:1 and 16:0 from *Arabidopsis* chloroplasts (Salas & Ohlrogge 2002). Consistently in *AtFatB* mutant plants, biomass production is lower due to a reduced wax load, and endomembrane lipids contained less 16:0 and 18:0 (Bonaventure et al. 2003).

Substrate specificities vary between FAT proteins from different species (Salas & Ohlrogge 2002). This is important to note because it complicates knowledge transfer from vascular plants to Heterokonts in which the fatty acid specie(s) introduced into ER editing systems are unknown. AtFatA and AtFatB are not conserved in Heterokonts with the closest hits being Naga_100005g67 and Naga_100140g5, sharing 23% and 35% amino acid identity, respectively, and Phatr2_48828 and Phatr2_39389 with 27% sequence identity. These four Heterokont proteins contain predicted transmembrane domains and domains similar to cation channels (SMART EMBL) but lacked the acyl-ACP thioesterase domain. Indeed, domain BLAST searches using the Pfam domain PF01643 as query reveal that acyl-ACP thioesterase domains were absent from the proteomes of both, *N. gaditana* and *P. tricornutum* . However, *in silico* analysis supported chloroplast localization. The AMP-binding domain (PF00501) for putative AAS proteins was conserved in the Heterokont sequences, further supporting a conservation of acyl-ACP production in the stroma.

One thioesterase has been identified in *P. tricornutum* (PtTE) that does not share any similarity with bacterial or plant proteins. Expression of PtTE is induced under nitrogen starvation. Heterologous expression in *E. coli* revealed al PtTE activity with a substrate preference for 18:1 followed by 18:0 and lower activity towards 16:0 (Gong et al. 2011). This study indicates that the fatty acid species exported from the chloroplast of diatoms and plants are the same. In *N. gaditana*, one gene (Naga_100095g12) is annotated as acyl-coenzyme a thioesterase 13, but no TE is described in literature. Thus, among Heterokonts, differential fatty acid export systems in *Eustigmatophyceae* and diatoms cannot be excluded.

2.6.2 *Export across the chloroplast limiting membranes to the cytosol*

Only one fatty acid carrier protein required for the export of free fatty acids from the chloroplast has been identified in *Arabidopsis*. Fatty acid export 1 (FAX1) is located in the chloroplast envelope, most likely to the inner membrane. Based on its protein sequence, FAX1 is speculated to facilitate membrane flipping of free fatty acids in a passive mode by inserting a hydrophobic α-helix into the lipid bilayer of the inner envelope membrane. Complementation of a yeast mutant deficient in the fatty acid import protein (Fat1p), transporter activity was observed after heterologous expression of *Arabidopsis* FAX1, with a preference for C16 species over C18 species, but accepting differentially unsaturated acyl-chains. *In planta*, 18:1 is the major product of fatty acid synthesis and export. FAX1 is thus believed to act passively in response to substrate concentrations. Knock out lines of FAX1 produced less biomass due to a 50% reduced C29-ketone wax load of stem epidermis cells and had a male-sterile phenotype caused by retarded pollen cell wall assembly. Globally, about 50% of all lipid species are affected in *Arabidopsis fax1* lines. A shift towards lipids and free fatty acids derived from the prokaryotic pathway is observed as well as an overall increase of PG and a decrease of PC and PE in the mutant. Altered endomembrane lipid profiles pointed towards a FAX1 function in FA export, not import, from the chloroplast. The *Arabidopsis* genome encodes seven FAX isoforms, four of which have chloroplast signal peptides (Li et al. 2015a). Therefore, loss of FAX1 function could be partially

rescued by other isoforms, but one cannot exclude the existence of other fatty acid export mechanisms through the inner chloroplast membrane. FAX1 orthologs were only found in the green lineage so again indicating distinct membrane trafficking pathways in *Archaeplastida* and Heterokonts.

To our knowledge, fatty acid transfer from the inner chloroplast envelope membrane to the outer leaflet of the outer membrane is unknown. A receptor for chloroplast protein import located in contact sites of the inner and outer envelope membrane was identified in electron micrographs of isolated pea chloroplasts by immunogold (Pain et al. 1988). Such domains could potentially facilitate membrane-to-membrane fatty acid transport by membrane flipping, as proposed for chloroplast-ER contact sites (Block & Jouhet 2015), but remains to be investigated. It was long assumed that after passing the chloroplast envelope, fatty acids are activated into acyl-CoA but recently the only plastid located fatty acyl-CoA synthase (ACS) was found to be exclusively required for chloroplast import, not export (see below). Thus, fatty acid trafficking from the inner chloroplast limiting membrane to the ER remains elusive in any species.

2.6.3 *Traffic into the ER and back to the cytosol*

An *Arabidopsis* protein is identified to be associated with ER fatty acid uptake. ER-located ABC class A transporter 9 (ABCA9) (**figure 2.14**) is only expressed in siliques and induced at such stages of seed development during which TAG accumulation is accelerated. Mutants accumulate 35% less TAGs compared to the wild type and overexpression lines accumulate more TAGs, both without changes in the fatty acid profiles of the lipid classes. Therefore, ABCA9 is postulated to increase the sink for cytotoxic FFA and acyl-CoAs during times of high demands (Kim et al. 2013). However, the absence of this transporter from vegetative tissues leaves the question of fatty acid import into the ER open.

To cross the cytosol in a water-soluble form, fatty acids are supposed to become activated into acyl-CoA by ACS in a similar mechanism as the activation into acyl-ACPs. ACS are involved in several anabolic and catabolic steps of fatty acid metabolism and reside in different organelles (Schnurr et al. 2002). One out of nine *Arabidopsis*

ACS specific for long chain fatty acids (LACS), LACS9, locates at the outer chloroplast membrane. *In vivo*, LACS9 gene expression is induced in young leaves and siliques, thus in TAG producing tissues. Mutant plants expressing a truncated LACS9 protein that lack both AMP-binding domain and putative substrate binding domains, have no growth or lipid phenotype under normal conditions. However, when chloroplasts isolated from *Arabidopsis* wild type and *lacs9* leaves are incubated with radiolabeled 18:1 and 16:1, acyl-CoA formation is inhibited by 90% in the mutant (Schnurr et al. 2002). Thus, the absence of a *lacs9* phenotype in intact cells compared to compromised activity in isolated chloroplasts could indicate an *in vivo* compensation by (proteins in) other cell compartments, an idea that again points organelle contact sites.

While the early publication of Schnurr and coworkers concluded on a LACS9 function in fatty acid export from the chloroplast, a recent mutant study reveals a function of ER-located LACS4 and envelope-located LACS9 in fatty acid trafficking from the ER to the chloroplast, probably within a membrane contact site. LACS4 is located at the ER and, similar to *lacs9*, a *lacs4* single mutant does not display growth or lipid-related phenotypes. Three different radioactive experiments on *lacs4_lacs9* double mutants give evidence for a role in retrograde trafficking rather than chloroplast export. Radiolabelled acetate is incorporated into chloroplast fatty acid synthesis before long chain fatty acids are exported for PC assembly in the ER. Since PC labelling is marginally affected in *lacs4_lacs9* double mutants, a role in fatty acid export is unlikely. Pulse chase experiments with radiolabelled acetate results in two peaks for MGDG: an early strong incorporation *via* the prokaryotic pathway with subsequent dilution, and a later that relies on the eukaryotic fatty acid supply. This later peak is absent from *lacs4_lacs9* double mutants. In a different pulse chase experiment using detached leaves, labelled 18:1 substrate is almost exclusively channelled into the eukaryotic pathway. Again, using this approach, MGDG labelling is impaired in *lacs4_lacs9* double mutants. A function in the regulation of the acyl-CoA pool is indicated by 20% lower acyl-CoA contents and 67% higher FFA levels in *lacs4_lacs9.* Lipid class abundances are unchanged in double mutants but higher 18:1 and 18:2 levels with reduced 18:3 are observed in PC, PE and PG, and galactolipids with prokaryotic FA profiles increased.

While 18:3 levels are reduced in membrane lipids, they allocate more into TAGs in *lacs4_lacs9* double mutants. Based on these data, the LACS4-LACS8/9 couple is proposed to be responsible for the generation of an 18:2-CoA pool for chloroplast fatty acid import at ER-chloroplast contact sites. LACS8 and LACS9 have the highest sequence similarity among the nine LACS isoforms and might have overlapping functions since a triple mutant of *lacs4_lacs8_lacs9* is embryo-lethal (Jessen et al. 2014).

2.6.4 *Import across the chloroplast limiting membranes into the stroma*

After ER editing, fatty acids from the "eukaryotic pathway" or the "omega pathway" are reimported into chloroplasts. Radiolabeling experiments indicate PC to be at the origin of the "eukaryotic pathway" (Roughan et al. 1980) and the recently established model of Jessen and coworkers suggest a parallel transport of lyso-PC and 18:2-CoA from the ER to the chloroplast (Jessen et al. 2015). How the putative PC-derived precursor molecule would be channelled into DAG is not experimentally established and the current model involves a reassembly of 18:2 containing PC by an acyl-CoA-lyso-PC acyltransferase with subsequent conversion to PA in the outer envelope membrane (Jessen et al. 2015). Concomitantly, in isolated ER-chloroplast membranes, peptides of the PC synthase are detected (Andersson et al. 2007a).

Up from the outer chloroplast membrane, the transport concerns no longer unesterified fatty acids but glycerolipid molecules. Glycerolipids cannot spontaneously flip flop between the membranes but require the action of flippases such as ATP binding cassette (ABC) transporters and P-type ATPases (Li-Beisson et al. 2010). For the transport of the glycerolipid precursor from the outer over the inner chloroplast membrane, an ABC transporter complex possessing three core subunits and at least two associated subunits is required. Since they are identified based on the accumulation of the stress related galactolipid trigalactosyldiacylglycerol (TGDG), these components are therefore designated as TGD1-5 (Xu et al. 2003). Single mutants of each of these proteins have similar phenotypes of stunted growth, male sterility and reduced thylakoid membranes

and grana stacks (Fan et al. 2015). On the molecular level, galactolipids proportions are lower in *tgd* mutants and prokaryotic structures are enriched (Xu et al. 2008).

The transporter subunit TGD4 is located at the outer chloroplast membrane. Knock out of *tgd4* does not alter the numbers of ER-chloroplast contact sites as indicated by similar frequencies after GFP staining of the ER. A combination of *act1* mutation, which abolishes the prokaryotic pathway, with *tgd4* is lethal in the absence of sucrose, indicating a directed transport function from the ER (Xu et al. 2008). A unidirectional transport of glycerolipid intermediates into the chloroplast is proposed based on comparative analyses of *tgd1* and *tgd4* single mutants or double mutants deficient in the respective TGD protein and either the plastid (FAD6) or the ER-located (FAD2) desaturase introducing the second double bond into 18:1. Because 18:2 can be translocated between organelles, *fad6* and *fad2* mutants are viable. The combination with a *tgd* mutation abolished photoautotroph growth only in *fad6* due to the loss of plastid 18:2 and subsequent chloroplast malformations and chlorosis. On the other hand, *tgd_fad2* double mutants are similar to *tgd* single mutants. Phosphate starvation induced DGDG export from the chloroplast is unaffected in *tgd*. These evidences suggest a TGD1-5 complex function in chloroplast import, not export (Xu et al. 2010).

The small protein TGD5 as well as the ABC transporter complex TGD1-3 are located in the inner chloroplast envelope membrane as indicated by thermolysin treatments on isolated chloroplasts. TGD5 is supposed to serve as a bridge to establish a trafficking platform from TGD4 to the inner envelope transporter based on protein interaction with TGD1-4 revealed coimmunoprecipitation analyses (Fan et al. 2015). The ABC transporter possesses the permease TGD1, the ATPase TGD3, and the substrate binding protein TGD2 (Awai et al. 2006, Lu & Benning 2009). Importantly, knock out of different combinations of the TGD1-5 proteins as *tgd5* with *tgd1*or *tgd2* are embryo-lethal (Fan et al. 2015). By the synergistic action of TGD1-3 the lipid precursor is imported into the chloroplast and incorporated into chloroplast lipid synthesis (Fan et al. 2015). Again, TGD orthologs are only found in the green lineage and are not conserved in Heterokonts.

The fatty acyl-containing molecule that is transported over the chloroplast limiting membranes remains elusive. Proposed candidate molecules are PA, lyso-PC and DAG (**figure 2.14**) (Mongrand et al. 2000, Nakamura et al. 2014, Wang et al. 2013). The TGD4 sequence contains PA binding domains in a motif that is predicted to face the cytosol and to accept PA after protein homodimerization (Wang et al. 2013). In addition, TGD2 binds PA in the C-terminus facing the intermembrane space (Awai et al. 2006, Lu and Benning et al. 2009). PA binding does not necessarily involve this lipid intermediate to be the actual substrate. PA as well as PG binding to the *Arabidopsis* MGDG synthase 1 (MGD1) is required for its activation although neither phospholipid is used for MGDG synthesis (Dubots et al. 2010). Additionally, lipids can be involved in mediating protein-protein interactions (de Meyer et al. 2010, Nilsson et al. 2016).

If PA would be the transported molecule, it would need to be converted into DAG by a PA-phosphatase (PAP) in order to serve as a substrate for chloroplast lipid synthesis. While the TGD transporter system is present in both 18:3 and 16:3 plants, no PAP enzyme or PAP activity is found in the chloroplast membranes of 18:3 plants (Gardiner et al. 1984, Maréchal & Bastien 2014). In chloroplast preparations of 18:3 species compared to 16:3 species, radiolabelled acetate is poorly incorporated into DAG and very little channelling from this DAG into galactolipids occurs. Radiolabelled PA accumulates in the intact chloroplasts from 18:3 plants but not from 16:3 plants (Gardiner et al. 1984). These experiments suggest that 18:3-plants depend on the "eukaryotic pathway" due to their inability of producing DAG in the chloroplast membrane. As a consequence, DAG rather than PA should be the imported lipid moiety, at least in 18:3-plants. Concomitantly, *in silico* flux modelisations deny an important import of PA into the chloroplast to allow PG synthesis exclusively via the "prokaryotic pathway" (Gardiner et al. 1984, Maréchal & Bastien 2014). Cytosolic PAP proteins are discussed to be at the base of the potential DAG import into the chloroplast (Nakamura et al. 2009). *Arabidopsis* PAH1 and PAH2 are suggested to use PA either in the OEM or in the ER for the production of DAG (**figure 2.14**). Authors conclude on such a pathway based on the sensitivity of *pah* mutant lines to phosphate starvation, a condition during

which DGDG synthesis is induced to replace endomembrane phospholipids (Nakamura et al. 2009).

Lyso-PC is the third proposed import molecule (Mongrand et al. 2000) (**figure 2.14**). This idea is based on pulse-chase experiments using intact leek cells with subsequent chloroplast isolation for glycerolipid extraction. In endomembrane PC, the radiolabel is higher at *sn*-2 compared to *sn*-1 in this 18:3-plant, but in chloroplast lipids, the label is exclusively found at the *sn*-1 position (Mongrand et al. 2000). In conclusion, at least in 18:3 plants, PA is unlikely to serve as chloroplast import molecule. It remains to be investigated if lyso-PC and DAG could be transported by the TGD transporter complex. This question being unresolved in plants, it is not surprising that the fatty acyl molecule that is transported over the four chloroplast limiting membranes in Heterokonts is elusive.

2.6.5 *Interaction of the chloroplast outer envelope membrane with the ER membrane*

Contact sites between the ER and the chloroplasts might be important for fatty acid or glycerolipid trafficking. Those contact sites are identified in *A. thaliana via* confocal laser scanning microscopy (CLSM) using an ER lumen GFP-marker. From those protoplasts, isolated chloroplasts retain GFP staining after the extraction procedure indicating a strong chemical connection. Indeed, when protoplasts are disrupted using a laser scalpel and the chloroplast captured and stretched with optical tweezers, the ER-chloroplast connection remains intact under a pressure that usually breaks protein-protein interactions (Andersson et al. 2007b). Fluorescence protein marked ER and chloroplast derived stromules display strong spatial connections in CLSM imaging of tobacco leaves suggesting a role in increasing ER-chloroplast contact surfaces (Schattat et al. 2011). Stromules are conserved in plants but absent from Heterokonts in which membrane interconnections are different. In some *Chromalveolata* species belonging to the classes of *Cryptophyceae* and *Chrysophyceae* (Heterokonts) (Gibbs 1962), the outer chloroplast limiting membrane is in continuum with the nuclear envelope membrane and the ER (Falciatore & Bowler 2002, Watson 1955). In Heterokonts compared to higher

plants, membranes are directly interconnected and given that none of the candidate proteins involved in the "eukaryotic pathway" are conserved, this highlights that the "omega pathway" must operate in a very distinct way (Petroutsos et al. 2014). This unknown "omega pathway" must however be of great importance in Heterokonts, where the supply of the major chloroplast fatty acid relies on the production in the ER by elongases and desaturases.

2.7 Fatty acid elongation and desaturation

EPA is the most abundant fatty acid species in Heterokonts under certain growth conditions. Given the great interest in this VLC-PUFA, many studies have focused on the optimization of culture conditions. Generally, VLC-PUFAs compared to medium chain saturated fatty acids have an inverse regulation due to their predominance in membrane or neutral lipids, respectively. Low light, cold temperatures and high growth conditions increase the proportions of VLC-PUFAs in Heterokonts (Li et al. 2014).

The production of EPA is very efficient in *Phaeodactylum* and *Nannochloropsis* since intermediates are barely detected *in vivo*. Nonetheless, the synthesis pathways including elongase and desaturase activities in the ER are revealed by feeding experiments with radiolabelled C18 or C20 substrates (Domergue et al. 2002, Arao & Yamada 1994). Indeed, although EPA is found mainly in chloroplast lipids, its synthesis relies only on ER located enzymes (Domergue et al. 2002). Thus, EPA must be reimported into the chloroplast by the unknown "omega-pathway" where it pairs frequently with prokaryotic 16:x on galactolipids (**figure 2.15**) (Petroutsos et al. 2014, Domergue et al. 2002, Abida et al. 2015 Yongmanitchai & Ward 1993). In eight out of eleven *Phaeodactylum* MGDG species, EPA is bound at the *sn*-1 position and 16:3, 16:4, or 16:1 at *sn*-2 (Yongmanitchai & Ward 1993). The most abundant FA couple among the eight DGDG species is 20:5/16:1 followed by 16:1/16:1, 20:5/16:0 and 20:5/16:3 (Yongmanitchai & Ward 1993). Figure 2.15 describes the compartmentalization of *Phaeodactylum* EPA synthesis main route with the identified desaturases and the Δ6-elongase (Domergue et

al. 2002). Notably, the fatty acid species being exported from the chloroplast are not known in Heterokonts.

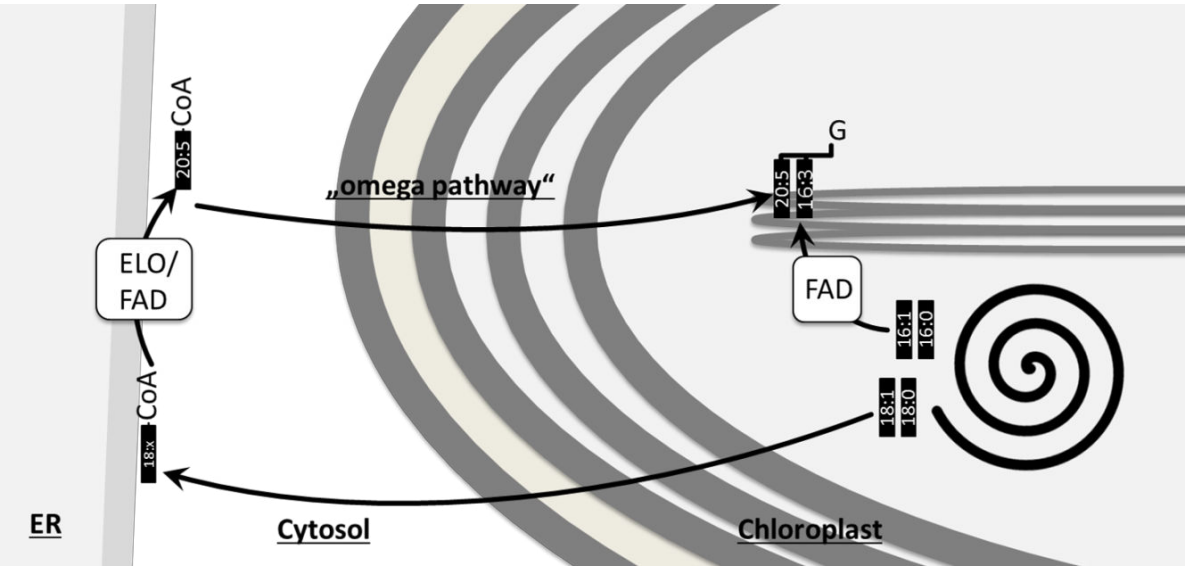

Figure 2.15. Compartmentalization of 20:5/16:3-MGDG synthesis in *Phaeodactylum*. Fatty acids are synthesized in the chloroplast stroma. Chloroplast desaturases desaturate 16:0, mainly to 16:3, which is added at the *sn*-2 position of the MGDG precursor. A C16 or C18-fatty acid enters the ER elongation and desaturation pathway. Produced 20:5 is imported into the chloroplast *via* the "omega pathway" and bound to MGDG at the *sn*-1 position (Petroutsos et al. 2014, Domergue et al. 2002).

2.7.1 *Fatty acid elongation*

Fatty acid feeding experiments in presence or absence of the fatty acid synthesis inhibitor cerulenin in *Arabidopsis* leaves indicate that acyl-chains shorter than C14 are necessarily transported into the chloroplast to increase their chain length before they can undergo ER elongation events. On the other hand, acyl-chains longer than C14 are readily edited in the ER (Koo et al. 2005). Thus the diversity of fatty acid species relies on chloroplast and ER modifications. The general mechanism of fatty acid synthesis and elongation is the same: in four reactions a C2 moiety is added to a substrate. These are carried out in the ER by multiple heterotetrameric elongase complexes that are conserved throughout the phyla. The first step of fatty acid elongation is the condensation of malonyl-CoA with an activated acyl chain to a β-ketoactyl-CoA

catalysed by the β-ketoactyl-CoA synthase (KCS). The fatty acid elongation pathway has been first described in yeast where the characterization of elongation defective mutants leads to the identification of elongase proteins. In yeast, Elo1p elongates C14 to C16, Elo2p from C16 to C24 and Elo3p from C16 to C26. Yeast Elop proteins are homologous to human ELOVL condensing enzymes and to four ELO proteins in *Arabidopsis* but not to plant fatty acid elongation 1 (FAE1)-type KCS (Haslam & Kunst 2013). KCS differ in their substrate binding properties, tissue specificity, transcriptional and maybe translational regulation and do thereby allow a vast diversity of VLCFAs (Joubès et al. 2008). In the production of EPA in Heterokonts, the Δ6-elongase uses 18:3n-6 and 18:4n-3. The presence of an alternative Δ9-elongase using 18:3n-3 remains elusive (Arao & Yamada 1994, Domergue et al. 2002).

The other proteins in the elongation cycle are not specific for a fatty acyl chain and are functionally conserved throughout the phyla including Heterokonts. They typically appear in low copy numbers. Mutations typically have a severe effect on the cells or are lethal (Haslam & Kunst 2013). *Saccharomyces cerevisae* is a tool for the identification and characterization of elongation and desaturation proteins due to its simple fatty acid profile and the availability of mutants that are viable when respective substrates are added to the media or complementing sequences are transformed. Ybr159p is identified as a β-ketoactyl-CoA reductase (KCR) protein that catalyses the second step in fatty acid elongation (Beaudoin et al. 2002). *Arabidopsis* encodes two KCR isoforms and while knock out of AtKCR1 is lethal, AtKCR2 is dispensable. Similarly, only AtKCR1 can complement the *ybr159p* mutant (Beaudoin et al. 2009). The yeast β-hydroxylacyl-CoA dehydratase (HCD) Phs1p is an ortholog of *Arabidopsis* PASTICCINO2 and expression of the one gene in the mutant background of the other rescues the phenotype in both the plant and the budding yeast (Bach et al. 2008). Yeast β-hydroxylacyl-CoA eonyl reductase (ECR) Tsc13p is essential, whereas four *Arabidopsis* genes share the required steroid-5-reductase motif (Kohlwein et al. 2001, Zheng et al. 2005). Accordingly, mutation of an *Arabidopsis* ECR isoform, AtCER10, has severe fitness impairments but is not lethal (Zheng et al. 2005). These data indicates that the protein complex involved

in fatty acid elongation is highly conserved between the phyla. Similarly, desaturases are conserved.

2.7.2 *Fatty acid desaturation*

For an introduction on fatty acid desaturation the reader is referred to Dolch and Marechal 2015 and Dolch et al 2016. Here, current knowledge on desaturation processes in response to cold stress is reported, the so called homeoviscous adaptation.

2.7.3 *Homeoviscous adaptation*

Membrane fluidity is defined as the extent of membrane lipid disorder and molecular motion and determines horizontal and lateral permeability (Mikami & Murata 2003). Maintenance of membrane integrity is essential to prevent from (electrolyte) leakage and loss of compartmentalization. When temperature decreases, fatty acids go into a higher ordered state and build a viscous gel phase, whereas higher temperature renders the membranes to a more fluid liquid-crystalline state. To facilitate membrane lateral dynamics at low temperatures and to avoid bilayer disintegration at high temperatures, fatty acids and lipid classes are modulated (Los & Murata 2004, Mikami & Murata 2003). The higher the desaturation degree of a given fatty acid chain, the lower is its transition temperature from liquid-crystalline to gel phase (Huang & Li 1999). Evidence for the role of proportional unsaturated fatty acid increase in response to decreasing temperature was first given by electron spin resonance (ESR) experiments that reveal a reduced membrane viscosity in *E. coli* under cold stress (Sinensky 1974). Here, the term of homeoviscous adaptation is introduced that describes the adjustment of the fatty acid profile to counteract temperature-dependent membrane trafficking immobilization (Sinensky 1974).

In prokaryotes, environmental signal perception like temperature is realized by sensor-transducer systems that commonly comprise a histidine kinase (Hik) and a cognate response regulator (Rre) (Los et al. 2010). The induction mechanism of desaturases upon membrane rigidification rather than cold temperature itself is studied intensively in *Bacillus megaterium*. This prokaryote encodes a single FAD introducing a Δ5 double

bound in unsaturated fatty acid species. The *des* gene is closely located to a two-gene operon consisting of the histidine kinase/phosphatase *DesK* and its response regulator *DesR* which are controlling *des* expression. The sunken-buoy motif in the transmembrane DesK protein comprises two hydrophilic amino acids located at the transmembrane-water-interphase of the plasma membrane. When the temperature decreases, the higher order of fatty acids leads to thickening of the membrane and thus a shift of the environment of the sunken-buoy motif. There is evidence that this transition regulates DesK auto-phosphorylation which inhibits the transmembrane proteins phosphatase activity on DesR, thereby inducing *des* expression. Δ5-FAD activity in turn reduces the membrane order and by that inhibiting DesK-autophosphorylation (de Mendoza 2014). Whereas this regulatory loop is restricted to one gene, the cyanobacterium *Synechocystis* sensor proteins Hik33 and Hik19 regulate about 30 cold-inducible genes including Δ6 and ω3-FAD (de Mendoza 2014). *Synechocystis* encodes 47 putative Hiks and 45 putative Rres that are not organized in operons. One Hik may interact with several Rres in response to one or several abiotic changes, but the Hik33-Rre16 couple is found to be specific for cold-stress responses (Los et al. 2010). Besides the plasma membrane, there are temperature perception pathways at the thylakoid membranes that are studied in *Synechococcus sp*. The small heat shock protein (HSP17) resides in thylakoids and is transiently transported to the cytoplasm upon heat shock to induce heat signalling processes. It mediates the heat adaptation of PSII light harvesting and electron transport processes by stabilizing the membrane lipid phase and protecting cyanobacterial light harvesting structures from degradation (Vigh et al. 2007).

A positive correlation of membrane lipid fatty acid unsaturation and increased membrane fluidity is found in all studied cold-treated poikilotherm organisms ranging from bacteria including cyanobacteria, over algae and plants and eukaryotic heterotrophs as *Tetrahymena*, yeast or scallop (Mikami & Murata 2003; Nozawa 2011; Rodríguez-Vargas et al. 2007; Upchurch 2008; Hall et al. 2002; Los & Murata 2004). Not every organism is able to adapt to chilling to the same extent. Among vascular plants, cold susceptibilities vary a lot between the species from sensitive species as tomato and potato to tolerant species as *Arabidopsis* or even insensitive species as pea and spinach

(Kaniuga 2008). Some features of the plant physiology are different between the more tolerant compared to more susceptible plants, such as a higher content of betaine and higher basal but lower cold-induced chloroplast lipid degradation by the action of unspecific lipolytic acid anhydrases. These enzymes generate free fatty acids that might be oxidized by lipoxygenase or ROS-dependent pathways. Oxidation products are consequentially elevated. ROS detoxification mechanisms are more active in cold-tolerant plants preventing the cell from oxidative damage (Kaniuga 2008). Indicators for cold tolerance are globally more unsaturated membrane fatty acids and especially cis-unsaturated phosphatidylglycerol (PG) species (Kaniuga 2008, Somerville 1995). Genetic modification in tolerant plants towards lower desaturation degrees of PG enhances cold sensitivity and strikingly, freezing damage as chlorosis and necrosis occur after long term incubation. Late freezing damage indicate that the role of fatty acids in freezing tolerance is rather during membrane biogenesis or repair under cold conditions than in preventing from membrane disintegration upon the temperature shift (Somerville 1995).

For cold acclimation processes bacteria and cyanobacteria are most studied. Many species are marine and experience great temperature changes in different depth. Several studies pointed out two major metabolic changes in response to cold. In order to overcome cold-induced inhibition of translation and the renewal of photosynthesis genes, mRNA- ribosome stabilizing proteins are induced. Secondly, different degrees on regulation of desaturases cause cold tolerance or sensitivity (Los et al. 2010). Cyanobacteria possess only three different desaturases and serve thus as model organisms for homeoviscous adaptation: a Δ9FAD encoded by *desC* that introduces the first double bound on C18:0 at the Δ9 position, Δ12FAD encoded by *desA* and converting $18:1^{\Delta 9}$ to $18:2^{\Delta 9,12}$, and Δ6FAD encoded by *desD* desaturating the dienoic substrate to $18:3^{\Delta 6,9,12}$ (Hongsthong et al. 2003). *Nostoc sp.* is a cold tolerant species that expresses the well conserved FAD genes *desA* and *desB* constitutively at low temperatures and has a higher C18/C16 ratio compared to mesophylic species like *Synechococcus*, which is unable to grow at 10°C (Chintalapati et al. 2007). In 18:3-rich *Spirulina platensis* on the other hand, only *desD* expression is induced upon cold-shift

but the half-life of *desA*, *desC* and *desD* are increased to different extents, allowing the accumulation of 18:3 to the expense of 18:2 (Deshnium et al. 2000). A more precise study on *S. platensis* desaturases addresses the correlation of protein levels and localizations in response to prolonged cold stress and reveals differential regulations at the plasma membrane, compared to thylakoid membranes. Δ9FAD is located in both membranes and not responsive to cold stress. Increase of 18:1 after the shift is rather caused by reduced Δ12FAD activities and thus less substrate consumption. Interestingly, *Spirulina* expresses two splicing isoforms of Δ12FAD, one being located at both membranes and degraded in response to cold stress, and the other one exclusively in the chloroplast and stable. Δ6FAD is 2.5-fold induced in thylakoids after one day and then restored, whereas it is not regulated at the plasma membrane. This is not directly reflected in an 18:3 increase that occurs stronger and earlier in the plasma membrane compared to thylakoids (Hongsthong et al. 2003). Eukaryotic microalgae from the green lineage live in similar habitats as cyanobacteria and are their evolutionary descendant. But surprisingly, the accumulation of trienoic fatty acids upon cold stress is not conserved in the fresh water species *Chlamydomonas*. When the green algae is shifted from 25°C to 5°C, organelles become disorganized and disrupted, photosynthesis and cell growth are strongly retarded and the carbon metabolism shifts from lipids to starch, although ACC and ACP-thioesterase, acyl-CoA-thioesterase and acyl-CoA-transferase are upregulated. Fatty acid unsaturation increases only on the level of 16:2 and 18:2 upon a three-fold induction of chloroplast Δ9FAD (SAD) and a 2.5-fold induction of Δ5FAD, whereas ERΔ12FAD and ERΔ9FAD remain unaltered (Valledor et al. 2013). *Chlamydomonas* is unable to recover from incubation at 0°C but recovers from 42°C (Hema et al. 2007). Thus, dienoic fatty acids appear to have a lower potential to mediate cold tolerance than trienoic fatty acids.

The interplay of desaturases during homeoviscous adaptation is more complex than in cyanobacteria, since more desaturase proteins exist with differential subcellular localizations (Dolch and Maréchal 2015). Vascular plants can be differentiated according to a predominant supply route of fatty acids at the *sn*-2 position of chloroplast lipids by the “prokaryotic pathway”, 16:3 plants, or the “eukaryotic pathway”, 18:3

plants (Petroutsos et al. 2014). Interestingly, the induction of the prokaryotic pathway is induced in both plant types when shifted to chilling temperatures and thus an overall increase of C16/C18 species can be considered as a general plant cold stress response (Li et al. 2015c). The model plant *Arabidopsis* is designated as cold resistant since despite growth retardations it can perform a full life cycle at 5°C (Chen & Thelen 2013). As in cyanobacteria, cold adaptation in *Arabidopsis* involves a global increase of polyunsaturated fatty acids with a strong increase of 18:3 accompanied by 18:2 reduction, and an induction of 18:1 (Li et al. 2015c). This phenotype relies predominantly on the activity of the ERΔ12FAD catalysing the bottleneck reaction of $18{:}1^{\Delta 9}$ to $18{:}^{2\Delta 9,12}$. Indeed, among the different *Arabidopsis* desaturases, only the knockout of FAD2 is lethal when grown at 6°C (Miquel & Browse 1992). A mutant of the chloroplast counterpart cis-ω-6FAD (AtFAD6) using lipid-linked 18:1 and 16:1 as substrate survives at 5°C, albeit growth retardations and chlorosis (Chen & Thelen 2013, Hugly & Somerville 1992). Desaturase candidates introducing the third double bound into 18:2 and 16:2 are ERΔ15FAD AtFAD3 using phospholipid-linked substrates, and two chloroplast ω3-desaturase isoforms AtFAD7 and AtFAD8 acting on C16 or C18 bound to a glycolipid (Dolch and Marechal 2015). *FAD7* is constitutively expressed but *FAD8* is strongly induced under cold stress and mutation in *FAD8* does not result in a fitness loss under control conditions (Gibson et al. 1994). Indeed, the C-terminus of FAD8 mediates the proteins auto-destabilization under high temperatures (Matsuda et al. 2005).

Overexpression of the plastid AtFAD7 in *Nicotiana abacus* causes higher cold resistance (Kodama et al. 1994). In *Arabidopsis*, most lipid-linked fatty acids have a chain length of 16 or 18 carbon atoms and the first double bound is inserted by a Δ7-desaturase acting on 16:0-*sn*-2-MGDG (AtFAD5/ADS3), a Δ3-*trans* desaturase specific for 16:0-*sn*-2-PG (AtFAD4), seven isoforms of SADs introducing a Δ9 desaturation in 18:0-ACP or 16:0-ACP in the chloroplast stroma, or by nine ADS using unsaturated CoA-bound FA substrates consisting of 18 or more carbon atoms (Dolch & Maréchal. 2015, Chen & Thelen, 2013). Although ADS are predicted to be in the endomembrane system, localization studies on the cold-induced ADS2 isoform reveals multiple protein

locations, namely in the ER, the Golgi and the chloroplast (Chen & Thelen, 2013). Mutations in this Δ9FAD point an important function in homeoviscous adaptation since no growth phenotype or strong alterations in the FA or lipid profiles are observed at control conditions but become obvious under cold stress. Leaky *ads2* mutant lines display 27-35% lower 16:2 and 16:3 levels with greater 16:0 accumulation and 87-110% 18:1 reduction, indicating that ADS2 would also accept 16:0 as a substrate and has a great activity on 18:0 at 6°C. Exclusively endomembrane PG and chloroplast MGDG C34 species are affected by the mutation but C34 and C36 DGDG species are reduced at cold stress (Chen & Thelen, 2013). The cold stress phenotype of *ads2* is more severe than the one of *fad5* and double mutation reveal additive effects on 16:0 and 18:0 accumulations (Chen & Thelen, 2013). Thus, in response to cold stress in plants, the desaturation degree is enhanced at the level of C16 and C18.

While in cyanobacteria and plants the maximal desaturation degree is three on fatty acids with a chain length of 16 or 18 carbon atoms, there is evidence that the accumulation very long chain polyunsaturated fatty acids as 20:5 and 22:6 is beneficial for growth in cold habitats. In scallop, cold adapted gill membranes contain higher levels of 20:5 and are less ordered according to electron spin resonance measurements compared to 20:5-poor membranes (Hall et al. 2002). Accordingly, an emerging number of gram-negative bacteria containing 20:5 or 22:6 are found in deep and shallow seas. One candidate is *Shewanella* that possesses five genes required for 20:5 synthesis. These genes are silent under optimal conditions but induced at 3°C leading to the accumulation of 10-15% 20:5. When these genes are expressed *in E. coli*, the temperature margin allowing optimal cell growth shifts to 12-22°C and requires higher $NaCl_2$ concentrations, but cells are more prone to photo-oxidation (Valentine & Valentine 2004).

Evidence of an increase of PUFAs in response to chilling temperatures is convincing throughout poikilothermic organisms. The role of the distinct PUFA containing lipid classes during homeoviscous adaptation however is less clear. A role for cis-desaturated PG species in lowering the phase transition temperature of thylakoid membranes is indicated from comparative studies. PG in cold tolerant plants typically consists of less

than 20% saturated fatty acids, whereas more than 40% are saturated in sensitive species (Somerville 1995). By comparing different rice cultivars a correlation between the PG desaturation status and the maintenance of photosynthesis for cellular energy production during cold stress is observed (Zhu et al. 2008), but shifts in total PG or other lipid class contents in response to temperature are not established. In *Arabidopsis* for example, temperature shift from 23°C to 6°C causes a reduction of the relative abundance of MGDG and an increase in PE and LPE (Chen & Thelen, 2013). In a different study using the same *Arabidopsis* ecotype, upon the shift from 23°C to 4°C the relative amount of MGDG remains unchanged but DGDG and PE and PA increase while PI, PG and PC decrease (data in table 3 converted to mol% (Welti et al. 2002). The shift from 22°C to 10°C in a third study on *A. thaliana* Col-0 indicate an increase of MGDG concomitant with an 1.6 x induction of MGD1 gene expression whereas DGDG and PG remained unchanged albeit an 1.9 x induction of DGD1 expression, and other phospholipid classes are reduced (Li et al. 2015c). In thermotolerant *Synechococcus sp.* PCC 7002, a temperature shift from 38°C to 22°C induces the overall desaturation levels but leads to a decrease of SQDG and DGDG whereas MGDG remains unchanged (Sakamoto et al. 1997). These inconsistencies complicate concluding on a role of a specific lipid class during homeoviscous adaptation of photoautotroph organisms.

Despite contradicting studies, the DGDG/MGDG balance is assumed to be important for lateral membrane fluidity with higher DGDG levels favouring higher lipid levels to increase fluidity on the one hand and MGDG accumulation inducing protein incorporation into membranes and thus higher rigidity (Garab et al. 2000). Cone shaped MGDG is a hexagonal II phase building lipid whereas DGDG self organizes into a lamellar structure. In reconstituted thylakoid membranes, only DGDG but not SQDG nor PG is responsible for the phase organization with a minimal requirement of DGDG/MGDG ratio of 0.6 to allow lamellar formation at normal hydration levels (Deme et al. 2014). Also proteins act in forcing hexagonal II lipids into the bilayer structure (Garab et al. 2000). Upon water removal as it occurs in nature during drought or freezing, artificial membranes with a given DGDG/MGDG ratio undergo a shift towards hexagonal II phase, a phenomenon that is discussed to be involved in freeze

damaging (Steponkus et al. 1994, Deme et al. 2014, Welti et al. 2002). Reduction of relative MGDG abundances during cold acclimation may thus allow higher cold temperature tolerances by maintaining lateral membrane fluidity upon increased lipid incorporation and prevent from freeze-thawing membrane damage. Consistently, in the heterotroph species *Tetrahymena*, the hexagonal II phase lipid class PE is reduced under cold stress (Nozawa 2011).

One could rule out an increase in fatty acid desaturation and a reduction of relative MGDG abundances as general cold stress responses in photosynthetic organisms. But due to its predominance in chloroplast membranes and the specific fatty acid profile, MGDG is the greatest sink for VLC-PUFAs fatty acids in photoautotrophs. The relevance of these contradicting aspects has not yet been addressed.

2.8 Lipid synthesis

2.8.1 *Membrane lipid synthesis*

Different lipid species contain controlled proportions of “eukaryotic”, “prokaryotic” or “omega pathway” derived fatty acid species (Petroutsos et al. 2014). Chloroplast lipid and especially galactolipid synthesis has been intensively studied and reviewed in our lab (Bastien et al. 2016, Boudière et al. 2014, Dubots et al. 2012, Petroutsos et al. 2014). An overview is given in **figure 2.16**. The synthesis of phospholipids in the ER is beyond the scope of this thesis and the reader is referred to (Li-Beisson et al. 2010).

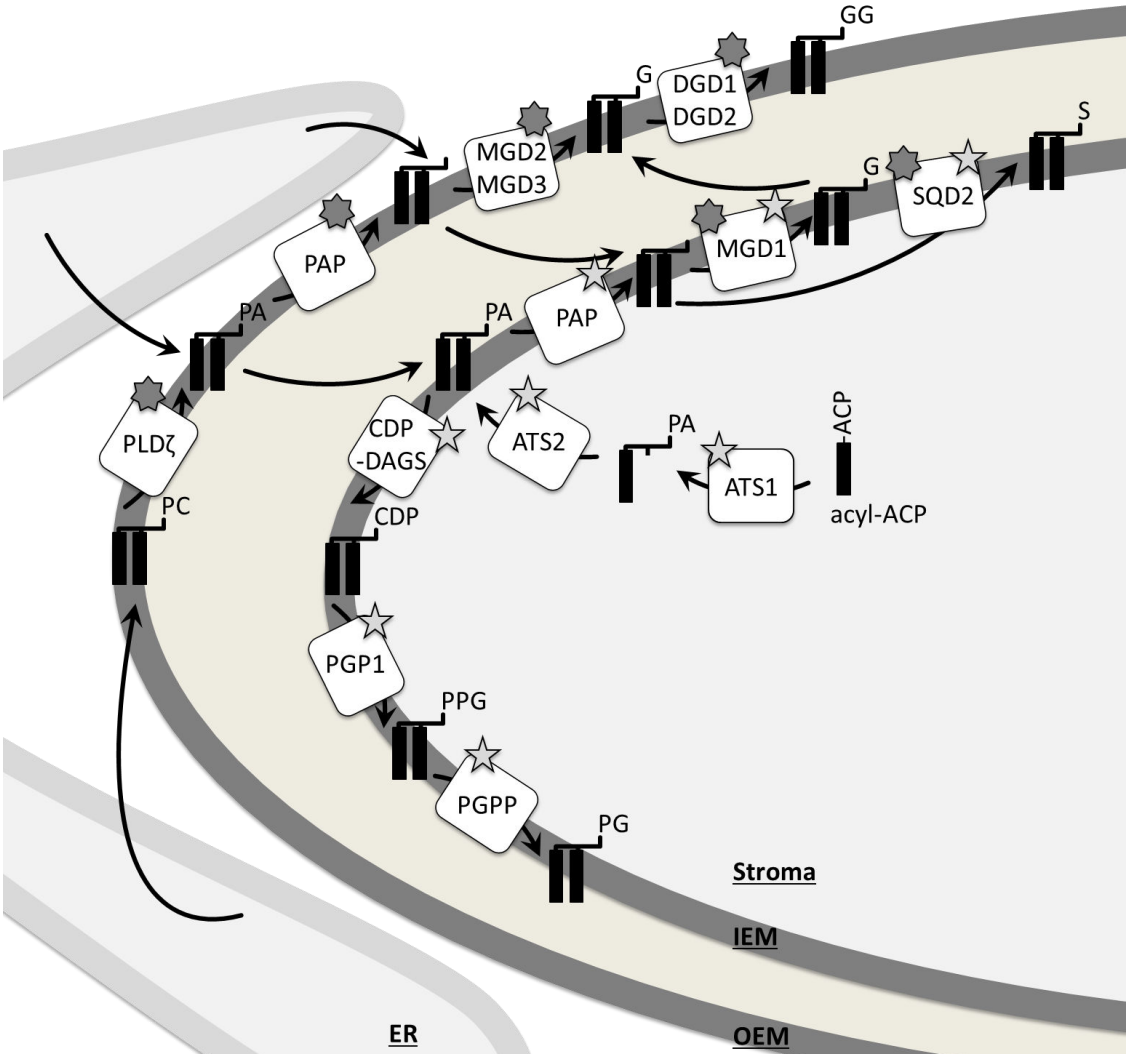

Figure 2.16. Chloroplast lipid synthesis. MGDG (G), DGDG (GG), SQDG (S) and PG are produced in the envelope of plants. Enzymes acting in the "prokaryotic pathway" are marked with a star, those acting in the "eukaryotic pathway" with a sun. Proteins carrying both labels have species dependent substrate specificities. Acyl-ACPs are bound onto a glycerol phosphate backbone via acyltransferase 1 (ATS1) and ATS2. The produced PA is used for PG synthesis by cytidine diphosphate diacylglycerol synthase (CDP-DAG), phosphatidylglycerolphosphate synthase (PGP1) and phosphatidylglycerol phosphatase (PGPP). MGDG and SQDG are synthesised from a DAG precursor in the inner envelope membrane (IEM) by MGDG synthase 1 (MGD1) and SQDG synthases SQD1 (not shown) and SQD2. In 16:3-plants, this DAG probably derives from PA *via* PA-phosphatase activity (PAP). In 18:3-plants, this DAG possibly derives from the outer envelope membrane (OEM) or imported PA. In the OEM, PC, PA or DAG is imported from the ER. PC might be converted into PA by phospholipase D-zeta (PLDζ), PA into DAG by PAP. DAG in the OEM serves as precursor for MGD2 and MGD3, and for DGDG synthases DGD1 and DGD2.

Among *Arabidopsis* chloroplast lipids, MGDG and SQDG are present in a "prokaryotic" and "eukaryotic" structure, DGDG mainly "eukaryotic" and PG exclusively "prokaryotic" (Boudière et al. 2014, Fritz et al. 2007). In Heterokonts, overall levels of C18 fatty acids are very low (Abida et al. 2015, Simionato et al. 2013). *Phaeodactylum* C20 fatty acids are exclusively found in the *sn*-1 position of chloroplast lipids whereas C16 is predominant in *sn*-2 (Abida et al. 2015). In respect of the *sn*-2 position, most Heterokont chloroplast lipids should be designated as "prokaryotic" in spite of the ER origin of at least the C20 moiety (Arao and Yamada 1994, Domergue et al., 2002). It is thus not clear in which compartment an EPA containing lipid precursors is synthesized in Heterokonts and in which form this VLC-PUFA is imported by the "omega pathway". At some point, EPA should be bound to PA in either chloroplast membrane.

The "prokaryotic" or "eukaryotic" chloroplast lipid structure is determined by the origin of phosphatidic acid (PA) (**figure 2.16**). At the beginning of "prokaryotic" chloroplast lipid synthesis is the production of PA from acyl-ACP and glycerol-3-phosphate. The first acyl chain is added onto the glycerol backbone by acyltransferase 1 (ATS1) forming lyso-PA. A second acyl-ACP chain is esterified at the *sn*-2 position by ATS2 that resides in the inner envelope membrane of vascular plants. ATS1 has specificity for 18:1 and ATS2 for 16:0 that give rise to lipids with the prokaryotic signature (Dubots et al. 2012, Petroutsos et al. 2014). In 16:3-plants, PA at the inner envelope membrane might also be imported from the outer envelope membrane where it derives from PC, lyso-PC or PA that contains ER-modified fatty acid species. These "eukaryotic" fatty acid species contain 18:x, mostly 18:3, at the *sn*-2 position (Petroutsos et al. 2014). The inner envelope of 18:3-plants lacks a PAP enzyme and lipid synthesis in this membrane relies most likely on DAG (Gardiner et al. 1984). From one of the two possible lipid precursors, MGDG and SQDG are synthesised. The preference of the MGDG synthase 1 (MGD1) and the SQDG synthase 2 (SQDG2) for "prokaryotic" or "eukaryotic" fatty acid signatures is species dependent. SQDG1 provides the sugar head for the assembly of this glycolipid (Boudière et al. 2014, Petroutsos et al. 2014). PG is exclusively synthesised by the "prokaryotic pathway" (Xu et al. 2002, 2006). For PG synthesis, the head group of PA is replaced by cytidine diphosphate (CDP) by the action a CDP-

diacylglycerol synthase (CDP-DAG). Afterwards, this CDP-activated DAG molecule is converted into phosphatidylglycerolphosphate by phosphatidylglycerolphosphate synthase (PGP1) and finally into PG by phosphatidylglycerol phosphatase (PGPP) (Dubots et al. 2012). Similarly to the situation in chloroplast membranes of 16:3-plants ER-located PA is the key intermediate in endomembrane lipid and neutral lipid synthesis.

2.8.2 *TAG synthesis*

TAGs store twice more energy per weight unit than starch. These neutral lipids accumulate in lipid droplets (LDs) when growth is arrested (**figure 2.17**) (Goold et al. 2014, Levitan et al. 2014). Except for *Chlamydomonas* where lipid droplets possibly derive from chloroplasts, the synthesis of TAG occurs in the ER from where lipid droplets emerge (Chen & Smith 2012). Multiple routes are known for TAG production, either *via* a *de novo* pathway or *via* recycling of phospholipids, mainly PC.

TAGs are produced *de novo* via the sequential addition of fatty acids onto the glycerol-3-phosphate (G3P) backbone at the ER in the Kennedy-pathway (**figure 2.17**) (Chapman & Ohlrogge 2012, Chen & Smith 2012, Liang & Jiang 2013). This pathway starts with condensing a G3P with an acyl-CoA by a glycerol-*sn*-3-phosphate acyl-transferase (GPAT) (Liang & Jiang 2013, Ma et al. 2016). The formed product is the substrate for lysophosphatidate acyl-transferase (LPAT) adding a second acyl chain with a preference to CoA bound thioester resulting in PA (Arroyo-Caro et al. 2013). PAP controls the flux between TAG and phospholipid synthesis. In yeast and mammals, PAP mutants have higher PC levels but lower neutral lipid contents (reviewed in Chapman & Ohlrogge 2012). Yeast PAP (PAH1p) mutants have lower LD numbers of various sizes. LDs and membranes of those mutants contain less proportions of TAG but more sterol esters (Adeyo et al. 2011). Upon dephosphorylation of PA, diacylglycerol (DAG) is formed and serves as substrate for a TAG-synthase as diacylglycerol acyltransferase (DGAT) that esterifies the third fatty acid onto the backbone, generating TAG (Ma et al. 2016, Liang & Jiang 2013).

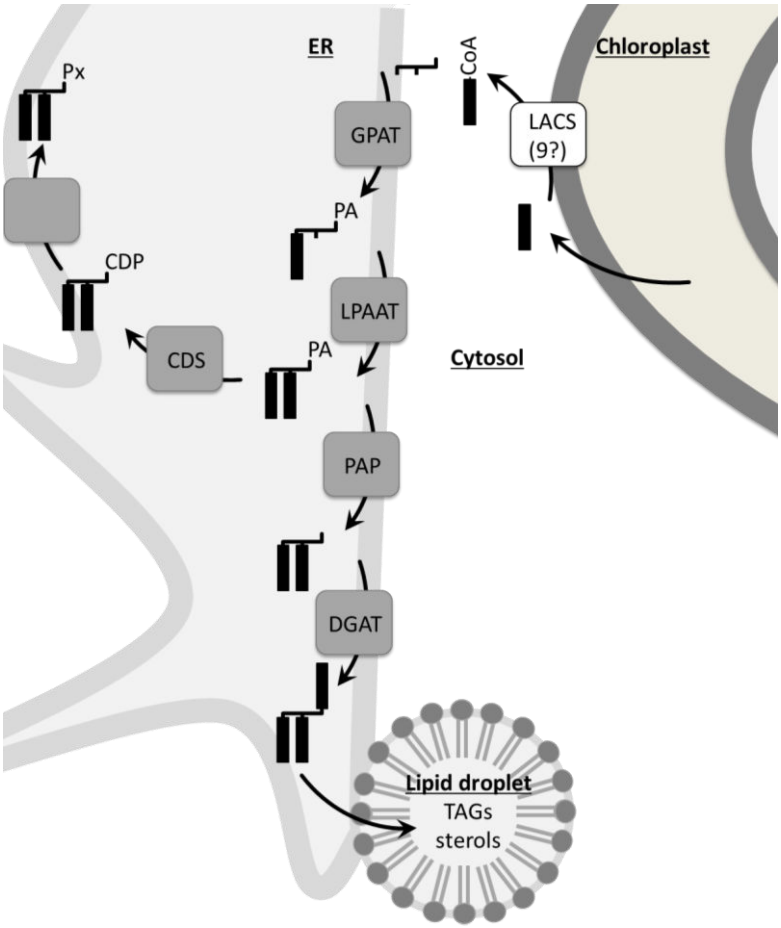

Figure 2.17. *De novo* neutral lipid synthesis in the ER membranes. Triacylglycerol (TAG) is produced by the sequential addition of acyl-CoAs onto a glycerol-3-phosphate backbone by the action of a glycerol-*sn*-3-phosphate acyl-transferase (GPAT), lysophosphatidate acyl-transferase (LPAT), PAP, and diacylglycerol acyltransferase (DGAT). TAGs are then directed into lipid droplets that emerge from the ER membrane. PA alternatively serves in phospholipid synthesis starting with cytidine diphosphate synthase (CDS) activity.

The Kennedy-pathway proteins are targets for genetic engineering of oleaginous species for applied purposes. GPAT is the least active enzyme in the Kennedy pathway (Liang & Jiang). Its overexpression in *P. tricornutum* increases TAG contents and proportions of unsaturated fatty acids (Niu et al. 2016). Two different forms of LPATs exist with LPAT1 being conserved among the phyla and LPAT2 specific for the green lineage (Misra et al. 2014). Heterologous expression of LPAT2 from several plants in *Arabidopsis* increases TAG contents (Chen et al. 2015, Maisonneuve et al. 2010).

The addition of the third fatty acid onto DAG is attributed to TAG synthase enzymes. Several protein families possessing TAG-synthase activities are described in different phyla (for review Chen & Smith 2012). The major TAG-synthases are either DGAT1 or DGAT2 that do not share sequence or structure similarity (Chen & Smith 2012). These proteins are intensively studied in a variety of phototrophs. *Phaeodactylum* genome encodes one DGAT1 and five DGAT2 isoforms. Multiple *DGAT2* but a single *DGAT1* gene is a common feature among microalgae but not in higher plants or heterotrophs (Chen & Smith 2012). Only PtDGAT2B can restore a TAG deficient yeast phenotype (Gong et al. 2013). PtDGAT2B overexpression in *P. tricornutum* increases not only lipid droplet formation but enhances PUFA production, especially EPA (Gong et al. 2013, Niu et al. 2013). Similarly, *Thalassiosira* DGAT2 expression in yeast increases TAGs and the flux of PUFAs into the neutral lipid (Xu et al. 2013). This is surprising because yeast expression of *P. tricornutum* DGAT2B reveal the preferred substrates to be 16:1 and 18:1 whereas saturated FAs and PUFAs are less used (Gong et al. 2013). Interestingly, *Phaeodactylum* DGAT2B expression levels *in vivo* do not match high TAG production phases (Gong et al. 2013). This is in agreement with the observation that in *Nannochloropsis* the Kennedy-pathway accounts for only 7% of TAG synthesis whereas the bulk derives from phospholipid remodelling (Ma et al. 2016).

Indeed, a second general pathway for TAG production exists that includes phospholipid remodelling. The key enzyme is a phospholipid:DAG acyltransferase (PDAT) or DAG:DAG acyltransferase generating one TAG and one lyso-lipid (Chapman & Ohlrogge 2012). PDAT is conserved in every phylum. The fatty acid specificity of PDAT varies among the species but PC occurs to be the preferred lipid substrate (Dahlqvist et al. 2000). From the produced lyso-PC, PC can be reconstituted by the Lands' cycle. In this process, an acyl-chain is added onto lyso-PC by the action of a lysophosphatidylcholine acyltransferase (LPCAT). In plants, fatty acid editing occurs on the acyl-chain bound to PC at the *sn*-2 position. PC is thus an intermediate molecule for PUFAs, before these acyl-chains can be channelled into other lipid classes including TAGs by lyses of PC. With the action of LPCAT, PC containing $18:1^{\Delta 9}$ at *sn*-2 can be restored, but the same enzyme also catalyses the back reaction thus determining PC

turnover (Bates 2016). A similar mechanism might occur in Heterokonts since some elongases heterologously expressed in yeast act on PC-linked substrates. By contrast, desaturation can occur on acyl-CoAs (Domergue et al. 2005, Hoffmann et al. 2008, Sayanova et al. 2012, Vaezi et al. 2013).

A mechanism similar to the Lands' cycle contributes to TAG production in PC-lacking *Chlamydomonas* (Li et al. 2012). Plastid galactoglycerolipid degradation (PGD1) is a *sn*-1 lipase. It acts preferentially on newly synthesized MGDG that in contrast to mature, more desaturated MGDG, is enriched in $18:1^{\Delta 9}$. Liberated fatty acids are then channelled into ER synthesized lipids, mainly into TAGs and to a lower extent into PE and DGTS (Li et al. 2012). The PGD1-mediated MGDG turnover and concomitant TAG accumulation is required to scavenge reducing power generated by photosynthesis during nitrogen starvation (Li et al. 2012). Accordingly, putative orthologs of PGD1 are upregulated during nitrogen starvation in *Chlorella* and *N. oceanica* (Mansfeldt et al. 2016, Li et al. 2014b).

No matter the fatty acid source, TAGs are stored in lipid droplets (LDs). Besides "push" and "pull" approaches to increase neutral lipid contents, ways to "protect" this TAG storage organs are investigated (Liang & Jiang 2013).

2.8.2.1 TAGs are stored in lipid droplets

In single celled organisms as well as in vegetative tissues of macrocellular species, TAGs are stored in LD (**figure 2.17**). These dynamic organelles are conserved among the phyla. In plants LDs function in carbon storage, stress response, pathogen resistance, hormone metabolism, anther development and pollen coat barrier formation (Chapman et al. 2012). LDs contain neutral lipid esters or lipid based polymers and (Murphy 2012, Yang et al. 2012). Lipids make 90% of the LDs weight whereas proteins account for only 1-5%. Pigments and free fatty acids may be present (Goold et al. 2015). A lipid monolayer with a unique lipid composition limits the organelle (Goold et al. 2015). LDs vary in size and number between organisms, tissues and culture conditions. In microalgae, small LDs occur as intermediates of membrane synthesis while under

nutrient stress, bigger but fewer structures occur (Goold et al. 2015, Murphy 2012). In *Phaeodactylum*, lipid droplet sizes range from 0.1-53 μm^3 (Wong & Franz 2013). A typical wild type cell contains one to six LDs that increase in size during the transition to stationary phase or nutrient stress. In order to increase size, pre-existing LDs take up newly derived TAG (**figure 2.17**) (Wong & Franz 2013). This phenomenon supports a maintained ER-LD association in the diatom. Alternatively, small LDs can fuse (Sun et al. 2013).

LDs emerge from the ER. The assembly starts between the two leaflets of the ER-limiting membrane with subsequent expansion towards the cytosol (Chapman et al. 2012). This mechanism is thermodynamically exhaustive since lateral dispersion of TAGs need to be prevented and the required curvature is energetically unfavourable. This might be facilitated by the local formation of LD genesis subdomains enriched in proteins and cone shaped or highly charged lipids (Murphy 2012). Accordingly, ultrastructure imaging on plant seeds reveal the presence of defined LD generation sites (Chapman et al. 2012). In yeast, in those loci Nem1-Spo7 membrane protein complexes are enriched possessing catalytic PAP activity in which DAG production takes places (Adeyo et al. 2011). LDs remain in the ER membrane, reside in the cytosol or at least in yeast enter the vacuole (Wang et al. 2014). In mammals, LDs are mobile and might randomly move short distances or undergo microtubule-dependent directional long distance translocations (Fujimoto & Parton 2011, Suzuki et al. 2011). Whether algal LDs are disconnected and mobile or stay in continuum with the ER is unknown.

Although more than 200 proteins are found to associate with LDs in *Chlamydomonas* with a high similarity to mammal LD proteins, only a few are functionally characterized (Goold et al. 2015). They include proteins involved in lipid metabolism such as the Kennedy-pathway proteins, as well as lipases, trafficking and redox regulation (Goold et al. 2015). Hydrophobic LD proteins in plants are ER membrane located caleosins, oleosins, perpilin adipophilin and 47-kDa tail interacting proteins (PAT), steroleosins, proteases, lipases, lipoxygenases and unknown proteins. They modulate LD stability and metabolism of the components (Chapman et al. 2012). The proteome of *P. tricornutum* LDs is studied but only the five most abundant proteins are published. Stramenopile-

type lipid droplet protein (StLDP) is the most abundant *Phaeodactylum* LD protein and has sequence similarities to lipid droplet surface protein (LDSP) in *Nannochloropsis* and plant oleosins. It possesses a hydrophobic central region which is enriched in proline residues (Yoneda et al. 2016). Plant oleosins are involved in the prevention of LD coalescence, thus regulating LD biogenesis, size and stability (Chapman et al. 2012). Green algae like *Dunaliella* contain a major lipid droplet protein that displays no structural or sequential similarities with characterized LD proteins but possesses also a 4-proline motif (Davidi et al. 2012). *Nannochloropsis sp*. LDSP cannot entirely functionally replace oleosin1 in *Arabidopsis* (Vieler et al. 2012). Thus, functions of the most abundant LD protein might be species dependent. The other four published *Phaeodactylum* LD lipids are an acyl-CoA binding protein, a heat shock protein 70 (Hsp70), a thioredoxin-like hypothetical protein and a oxygenase superfamily hypothetical protein (Yoneda et al. 2016).

LD stabilization is part of genetic engineering attempts to increase neutral lipid yields. In *Phaeodactylum* a homolog of the mammal comparative gene identification 58 (CGI58) is located at the LD surface and possibly facilitates peroxisomal lipid degradation. This protein is conserved in photosynthetic species as well as yeast and human and has both lipase and LPAT activity (Trentacoste et al. 2013). Downregulation of *PtCGI58* is associated with an increase in cellular TAG contents (Leterrier et al. 2015). This protein is not published to be found in the LD extractions performed by Yoneda and coworkers (Yoneda et al. 2016) and thus further studies on Heterokont LD proteins are awaited.

2.8.2.2 Abiotic stresses induce membrane glycerolipid remodelling and TAG accumulation

TAG accumulation is induced by a variety of stresses. While nutrient deprivation is a commonly method, air drying that cause dehydration and low salt stress is as effective as nitrogen starvation in green algae (Shiratake et al. 2013). On the other hand, low pH or high salinity stress are unable to induce TAG synthesis in *Phaeodactylum* (Mus et al.

2013). Phosphate limitation is able to induce TAG accumulation but the response is slower compared to nitrogen (Valenzuela et al. 2012). This is due to an effective phospholipid recycling that lowers the cellular phosphate demand by 50% and allows cells to maintain growth. The phosphate liberated from membrane lipids and cell surface phosphate monoesters is used for nucleotide or ATP production (Feng et al. 2015). In brief, PG can be replaced by SQDG in the chloroplast and in the endomembranes betaine lipids compensate for the reduction of PC (Van Mooy et al. 2009). At least in higher plants, DGDG is exported to replace endomembrane phospholipids when phosphate is limiting (Härtel et al. 2000, Jouhet et al. 2004, Kelly et al. 2003). If the DGDG export is conserved in betaine lipid containing microalgae is not known. Alternatively, betaine lipids may functionally replace PC (Riekhof et al. 2005, 2014).

Nitrogen deficiency is commonly used to trigger TAG accumulation. Under this condition, *Phaeodactylum* fatty acid levels increase four fold and 75-89% of fatty acids are bound as TAG (Alipanah et al. 2015, Guihéneuf et al. 2011, Tonon et al. 2002). Although a general reduction of VLC-PUFA during TAG accumulation is consistent, studies vary in their report on EPA proportions in TAG in both *Phaeodactylum* and *Nannochloropsis* species (Alipanah et al. 2015, Chen et al. 2013, Ge et al. 2014, Gong et al. 2013, Guihéneuf et al. 2011, Hu et al. 2015, Liu et al. 2013a, Meng et al. 2015, Simionato et al. 2013, Tonon et al. 2002, Van Vooren et al. 2012). Furthermore, reduced proportions of VLC-PUFAs are at least partially accounted to growth reductions and thus decreased demand of membrane lipids under stress conditions (Alipanah et al. 2015).

A variety of "omics" studies point out the remodelling of metabolic pathways in *P. tricornutum* when nitrogen or phosphate are limited. Pyrimidine and purine as well as protein and ribosome biosynthesis is reduced and amino acid recycling is induced (Alipanah et al. 2015, Feng et al. 2015). Catabolism of branched chain amino acids plays a dual role in recycling cellular nitrogen and feeding the mitochondrial carbon metabolism (Ge et al. 2014). Most affected by nitrogen starvation are photosynthesis proteins and pigments as well as carbon concentration and fixation proteins (Alipanah et al. 2015). This is in contrast to phosphate starvation in *Phaeodactylum*, in which light

reactions also decline but carbon fixation is induced (Feng et al. 2015). In response to both stresses, the C:N ratio increases. This is because glycolysis, TCA and pyruvate metabolism are strongly induced, providing acetyl-CoA, the building block for fatty acid synthesis. A shift from sugar to fatty acid production occurs (Alipanah et al. 2015, Feng et al. 2015, Ge et al. 2014, Valenzuela et al. 2012, Yang et al. 2014). Given this controlled dynamics of carbon and nitrogen responses, understanding the cellular nitrogen metabolism is beneficial for lipid research.

2.9 Nitrogen metabolism and NO• signalling

The most studied context triggering TAG accumulation in microorganisms including Heterokonts is that of a nitrogen shortage. In this section, a brief overview on both documented and possible relationships between nitrogen nutrients and other inorganic forms are given with a focus on correlations of nitrogen and carbon metabolism.

2.9.1 *Nitrogen fixation in Heterokonts*

In the marine nitrogen cycle (**figure 2.18**), fixed nitrogen in form of amino acids, urea or other nitrogen compounds in dead organic material from phytoplankton and grazers are degraded by bacterioplankton. Nitrite (NO_2^-), nitrate (NO_3^-) and ammonium (NH_4^+) are the products of bacterial nitrification. These three inorganic nitrogen moieties are the most available for marine primary producers (Zehr et al. 2002). Concentrations depend on the depth with 7-31 µM nitrate, 0.01-0.3 µM nitrite and 0.006-0.1 µM ammonium (Sanz-Luque et al. 2015). *Nannochloropsis* prefers ammonium over the oxygenated nitrogen moieties (Hii et al. 2011). Nitrate reductases (NR) use nitrate for the production of nitrite but have also affinity for nitrite resulting in NO• production. Nitrite is scavenged by nitrite reductases (NiR) that catalyse the reduction of $NO_2^- \rightarrow NH_4^+$ (Schreiber et al. 2012). Chloroplast located NiR requires Fd as a cofactor and variation of photochemistry is the only known regulatory mechanism for this enzyme (Kuznetsova et al. 2004). High levels of nitrite are cytotoxic and are therefore excreted (Sanz-Luque et al. 2015). Some bacteria may excrete organic carbon moieties as urea (Zehr et al.

2002). Lysine and arginine are also readily taken up and utilized by *Phaeodactylum* (Flynn et al. 1986). In this way, Heterokonts have multiple strategies to acquire nitrogen to maintain growth.

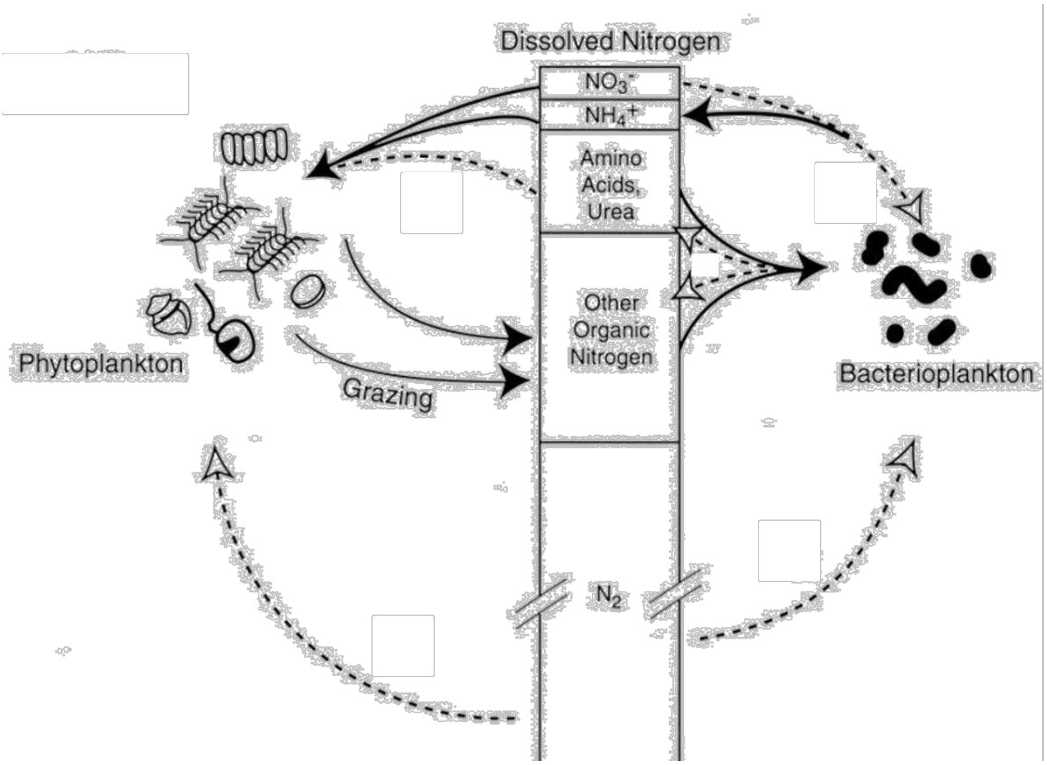

Figure 2.18. The marine nitrogen cycle. Atmospheric nitrogen (N_2) is fixed by specific plankton species. Additionally, bacterioplankton takes up dead organic material to recycle nitrogen. The release inorganic nitrogen compounds, *i. e.* nitrate (NO_3^-), nitrite (NO_2^-) or ammonium (NH_4^+) and eventually organic compounds. Phytoplankter assimilate those nitrogen molecules and release organic compounds after cell death (Zehr & Ward 2002)

Nitrogen assimilation and neutral lipid production are tightly correlated. When nitrogen is limited, growth is arrested and internal organic sources are recycled. *Phaeodactylum* dry mass contains about 40% proteins that provide the greatest sink for nitrogen and are thus reduced in times of limitations. The released carbon moieties are channelled into TAGs (Mus et al. 2013). Heterokonts contain the urea (CH_4N_2O) cycle for amino acid production starting from the condensing of ammonium and bicarbonate. They are not only able to take it up but urea is also the more efficient nitrogen source promoting high

biomass production in *Phaeodactylum* (Yongmanitchai & Ward 1993). Furthermore, among the mentioned nitrogen sources, urea allows the highest fatty acid production in diatoms (Fidalgo et al. 1998). One intermediate in the urea cycle is argininosuccinate that can be converted to fumarate which is a substrate in the TCA cycle which is converted into malate (www.genome.jp/kegg-bin/show_pathway?map00020+C00122, 30.06.2016). Malate can serve for acetyl-CoA and thus fatty acid synthesis (see carbon metabolism). This interconnection of fatty acid and amino acid synthesis is currently considered as the major driving force for the shift towards lipid production under nitrogen deficiency.

2.9.2 *Nitric oxide production and possible function in lipid metabolism*

One identified signalling molecule in nitrogen deficiency response is nitric oxide (NO•). This gaseous transmitter increases in *Chlamydomonas* cells after the shift to nitrogen starvation and correlates with decreasing photosynthesis in the green algae (Wei et al. 2014). NO• has a half-life of 0.1-2 ms and concentrations range between 100 pmol and 5 nmol, dependent on organism and tissue (Hall & Garthwaite 2009). NO• dependent S-nitrosylation of cysteine residues may have activating or inhibiting function on some target proteins and may influence their function, stability, and location (Gould et al. 2013). Furthermore, NO• regulates directly or indirectly the expression of responsive genes (Wendehenne et al. 2001). In accordance with the importance of the spatio-temporal patterns of signalling molecules, several NO• production sites exist (Batistič & Kudla 2012).

In human, three different nitric oxide synthases (NOS) have been identified. They use arginine as a substrate for NO production and are designated as neuronal (nNOS), endothelial (eNOS) and inducible (iNOS). NOS catalyse the production of NO• from arginine. The nNOS and eNOS produce NO• at pM or nM levels whereas iNOS NO• production reaches a pathological level in µM amounts, promoting the oxidation of low-density lipoprotein (LDL). LDL uptake into macrophages leads to the generation of foam cells and iNOS derived NO• enhances oxidised LDL-dependent cholesterol

accumulation that contributes to atherosclerosis (Zhao et al. 2014). Low concentrated NO• produced by eNOS has however an anti-atherosclerosis effect and mediates smooth muscle relaxation (Zhao et al. 2013, O'Donnell & Freeman 2001). The regulation of iNOS-dependent NO• production is controlled by eicosanoids and NO•. One of the beneficial properties of eicosanoids produced by oxidation of VLC-PUFAs from the ω-3 series is indeed the inhibition of NOS activity (O'Donnell & Freeman 2001). Algae derived EPA-rich MGDG or DGDG reduces iNOS levels and inhibit NO• production in macrophages (Branskota et al. 2013). The control gets more complicated by the finding that NO• inhibits cytochrome P450 involved in lipid oxidation thus acting in as a feed-forward signal (O'Donnell & Freeman 2001). On the contrary, NO• directly terminates lipid peroxidation via the interaction with radical intermediates. Reactive nitrogen derivates like peroxynitrite ($ONOO^-$) can again promote radical lipid oxidation (O'Donnell & Freeman 2001). Fatty acid β-oxidation in mice liver is also regulated by S-nitrosylation of VLC-acyl-CoA dehydrogenase protein that renders the structure towards higher mobility thereby facilitating substrate binding for fatty acid degradation (Doulias et al. 2013).

Thus, NO• can have an enhancing or reducing effect on lipid accumulation in human by either regulating gene expression or protein turnover, or to interfere with lipid oxidation. A role of NO• in the regulation of fatty acid peroxidation may be important in thylakoid membranes of photoautotrophs where redox poise and VLC-PUFA contents are high. This was however never studied. In photosynthetic organisms, the best studied NO• function is in redox signalling during abiotic stress and defence (Durner & Klessig 1999). NO• responsive genes in plants include metabolism and development genes as well as stress and defence related genes, acting in oxidative stress regulation and hormone interplay (Moreau et al. 2010). Although NO• signalling is investigated in phototrophs, the production in those organisms remains unclear. Based on the stimulatory effect of arginine on NO• production and the sensitivity to NO• inhibitors of plants but not all algae, the presence of an enzyme possessing NOS activity without structural analogy to human NOS is discussed (Moreau et al. 2010, Sakihama et al. 2002, Wendehenne et al. 2001). Structural analogs of NOS enzymes are present in the

green algae *Ostreococcus tauri, O. lucimarinus* and the diatom *Pseudo-nitzschia multistriata* but sequences are not conserved among other algae (Di Dato et al. 2015, Foresi et al. 2016). However, since in *O. tauri* NOS activity does not directly correlate to NO• levels, alternative sources must exist even in those phototrophs possessing NOS-like enzymes (Foresi et al. 2016).

Different possible alternatives for NO• production exist. Hydroxylamineoxidoreductase converts NH_2OH to NO• in annamox bacteria. In photoautotrophs, light mediated conversion of carotenoids may lead to NO• production (Durner & Klessig 1999). Low pH favours chemical NO• generation as well as hypoxia (Hockin et al. 2012, Moreau et al. 2010). Several enzymatic pathways are proposed in plants involving a plasma membrane bound nitrite:NO• reductase, an electron transfer chain dependent reductase as well as redox mediated NO• generations such as xanthine oxidoreductase, and NR activity on nitrite (Hockin et al. 2012, Moreau et al. 2010, Sanz-Luque et al. 2015).

NR is a ubiquitous protein that uses nitrite for NO• production when NO_2^- out-competes NO_3^- (Sakihama et al. 2002, Schreiber et al. 2012). This process provides the greatest NO• source in *Arabidopsis* (Moreau et al. 2010). About 1-10% of plant NR activity results in NO• production (Moreau et al. 2010, Sanz-Luque et al. 2015). Accordingly, in the red macroalga *Gracilaria chilensis* as well as in *Chlamydomonas* high nitrite concentrations stimulate NO• production (Wei et al. 2014, Chow et al. 2013). NR itself is regulated by NO• in a species-dependent manner. Addition of the chemical NO donor molecule sodium nitroprusside (SNP) as well as the NO• scavenger 2-(4-Carboxyphenyl)-4,4,5,5-tetramethylimidazoline-1-oxyl-3-oxide (CPTIO) to *G. chilensis* or *O. tauri* cultures reduce NR activity (Foresi et al. 2015, Chow et al. 2013). Arginine analogs that repress NOS also reduce NR activity in *Ostreococcus* (Foresi et al. 2015). In *Chlamydomonas*, NO• inhibits NR *in vivo* by an unknown mechanism that does not involve cyclic nucleotides, peroxynitrite, or a direct interaction since the enzyme activity was not inhibited by a NO• donor molecule *in vitro* (Sanz-Luque et al. 2013). Furthermore, ammonium, a building block for arginine represses NR function *via* feedback regulation in *Chlamydomonas* (Sanz-Luque et al. 2015). On the other hand, arginine is having an inhibitory effect on NiR in cyanobacteria (Sing & Bisen 1994). As

a consequence, arginine would increase nitrite levels for NR reaction. Mammal eNOS also possesses nitrite reductase activity for NO• production and this reaction is inhibited by Nω-Nitro-L-arginine methyl ester hydrochloride (L-NAME), NG-monomethyl L-arginine (L-NMMA) and L-arginine (Milsom et al. 2010, Webb et al. 2008). Due to these versatile modes of regulation, conclusions on a regulatory function of NO• on NR must be handled with care. Furthermore, the importance of concentration and location of a second messenger strongly influences its response (Batistič & Kudla 2012). A more detailed study on tomato roots reveals a dual function of NO• on NR activity. In the presence of low nitrate concentrations NO• stimulates NR in a dose-dependent manner, whereas it inhibits the enzyme when nitrate levels are high (Jin et al. 2009). Therefore it is likely, that NO• also plays a role in nitrogen deficiency induced lipid accumulation in photosynthetic organisms. Accordingly, NR, as well as nitrite reductases (NIA/NiR), ureases and nitrogen transporter genes are differentially regulated under nitrogen deficiency (Allen et al. 2006, Hockin et al. 2012). In *Phaeodactylum*, NR levels increase when nitrogen becomes limited (Levitan et al. 2015). The same condition leads to induction of both, NR and NIR in *Chlamydomonas* (Miller et al. 2010).

As NR is a NO• source in a diversity of organisms, *Arabidopsis nia1_nia2* lack the NO• increase in response to developmental or physiological processes. By contrast, these double mutants maintain the NO• signalling under pathogen stress as infection, salicylic acid treatment or mechanical stress. The screen for an alternative source led to the identification of *Arabidopsis* nitric oxide associated protein 1 (NOA) (Gas et al. 2009). Mutation of this protein leads to reduced NO• generation under certain stress conditions (Moreau et al. 2010). Together with one of the AtNIA proteins, AtNOA is involved in NO• generation during salicylic acid treatment in *Arabidopsis* (Mandal et al. 2012). AtNOA dependent NO• production occurs in the chloroplast and does not involve NR activity (Tewari et al. 2013). NOA is a GTPase and possesses an YqeH domain that is required for ribosome assembly and stability in *Bacillus subtilis* (Gas et al. 2009). The protein contains a fatty acid binding domain and is inhibited and destabilized upon 18:1 binding in chloroplast nucleoids (Mandal et al. 2012). NOA is conserved in *P. tricornutum* where Phatr2_56150 is one out of two encoded YqeH protein subfamily

proteins (Vardi et al. 2008a). Overexpression of the endogenous NOA sequence in *Phaeodactylum* results in higher NO• production as well as photosynthesis and growth reductions. The negative effect of NOA overexpression is reported to be restored by the addition of CPTIO (Vardi et al. 2008a). A similar observation is made in nitrogen starved *Chlamydomonas* where SNP treatment increases PSII inactivation while CPTIO slows down this process when the treatment is repeated over time (Wei et al. 2014). This could be explained by the interplay of NO• and O_2^- that is frequently generated by PSII. NO• and O_2^- form $ONOO^-$ that nitrates substrate proteins leading to their inhibition or downregulation. Among peroxynitrite targets in higher plant cells are FNR, CA and NADPH-dependent isocitrate dehydrogenase (TCA cycle) (Corpas & Barroso 2013). On the other hand, linear electron flow should reduce NR activity on nitrite since NiR uses electrons derived from Fd for the production of ammonium. Accordingly, blocking PSII with DCMU increases NO• concentrations (Sakihama et al. 2002). A negative effect of NO• on photochemistry does not seem to be conserved among the species. It is not observed in G. chilensis when treated with SNP (Chow et al. 2013). In *Chlamydomonas*, nitrogen starvation reduces Cytb6f abundances and this degradation correlates with nitrite dependent NO• production (Wei et al. 2014).

Taken together these data indicate a complicated interplay of nitrogen and carbon metabolism that might not be conserved among the species. Although some signalling functions of NO• and the regulation of the nitrogen deficiency marker NR are revealed, a correlation between NO• and lipid metabolism is unknown in Heterokonts. The finding of NO• signalling during nitrogen deficiency raises the question whether this second messenger may play a role in TAG accumulation in oleaginous Heterokonts. This question was addressed in the present study.

3 LIPID AND FATTY ACID PROFILES IN *PHAEODACTYLUM TRICORNUTUM* UNDER DIFFERENT GROWTH REGIMES

3.1 Introduction and overview

Membrane lipid profiles are dynamically changing in response to both abiotic and biotic stress conditions (Okazaki & Saito 2014). This phenomenon is conserved from actinobacteria to human (Turkish & Sturley 2009). In microalgae, nutrient deprivation is a widespread method applied to induce TAG accumulation accompanied by the transition to stationary growth (Hu et al. 2008). Studies on lipid remodelling events are mainly focused on neutral lipid accumulation for therapeutic or biofuel applications (Masoodi et al. 2014, Merchant et al. 2012). On the other hand, chloroplast galactolipids appear to be prone to nutrient deprivation (reviewed in (Moellering & Benning 2011, Okazaki & Saito 2014, Upchurch 2008) but a conductive comparison in diatoms was missing. In this chapter we explore the *P. tricornutum* lipid remodelling events in response to nitrogen or phosphate limitations after having determined control conditions.

In response to phosphate starvation, we found an increase of both DGDG and DGTA in *Phaeodactylum*. In plants that do not possess betaine lipids, DGDG is able to replace phospholipids outside the chloroplast (Jouhet et al. 2004, Kelly & Dörmann 2002, Kelly et al. 2003). Whether such a function is operational in diatoms or obsolete due to the possible substitution by DGTA is unknown.

We aimed to elucidate this question by the characterization of proteins involved in lipid synthesis in *Phaeodactylum*. The cornerstones to verify the function of putative lipid synthesis proteins were laid in this study by the construction of antisense lines. This method has the great disadvantage that expression levels are often unstable. Due to knock down levels in cells transformed with antisense constructs, we were able to provide only preliminary data on the effect of downregulation of three DGDG synthase isoforms in *Phaeodactylum*. Cells appeared to be highly sensitive even to mild changes in the expression level as they displayed strongly altered cell morphologies and impaired growth. Future work should re-address the sequences identified here by targeted gene knock out methods that have been established recently (Nymark et al. 2016).

3.2 Determination of culture conditions for comparative studies using *P. tricornutum*

3.2.1 *Long term cultivation of P. tricornutum*

At the moment, *P. tricornutum* does not yet fulfil the required efficiencies of TAG accumulation for broad fuel commercialization. We believe that fundamental understanding of the lipid remodelling networks is required to engineer this organism for green energy production. Towards this goal, we conducted a comprehensive study on lipid remodelling in response to nitrogen and phosphate deprivation, compared to optimal growth conditions. Firstly, this reference condition had to be defined. The growth media of choice was enriched seawater/artificial water (ESAW), classically containing 0.55 mM of $NaNO_3$ and 0.022 mM of NaH_2PO_4 (1N1P) (Berges et al. 2001). However, the nitrogen resource in 1N1P ESAW media was consumed quicker than phosphate and thus did not allow differentiating the two stress conditions in older cultures. We compared cell growth as a general fitness parameter and Nile red fluorescence indicating cellular TAG contents that reflect nutrient limitations in cell cultures grown in classic ESAW media (1N1P ESAW) and in 10-fold enriched nitrogen and phosphate conditions (10N10P ESAW) over a period of 17 days, by sampling from 50 mL cultures (**figure 3.1**). After inoculation at a concentration of 10^6 cells.mL^{-1} and a 24 hour lag phase, a steady increase in the cell concentration during the first week of culturing was observed under both conditions. In 1N1P ESAW cultures, growth was arrested between day 7 and day 8 with a concentration of $1.4 \times 10^7 \pm 9.55 \times 10^5$ cells.mL^{-1} whereas the average growth rate of 1.49 ± 0.5 persisted in 10N10P ESAW cultures throughout the 17 days of experiment (**figure 3.1.A**). Growth arrest in 1N1P ESAW cultures was accompanied by a 4-5 fold increase in Nile red fluorescence compared to earlier time points (**figure 3.1.B**) and the appearance of the two characteristic lipid droplets flanking the chloroplast when observed in epifluorescence microscopy (**figure 3.1.C**).

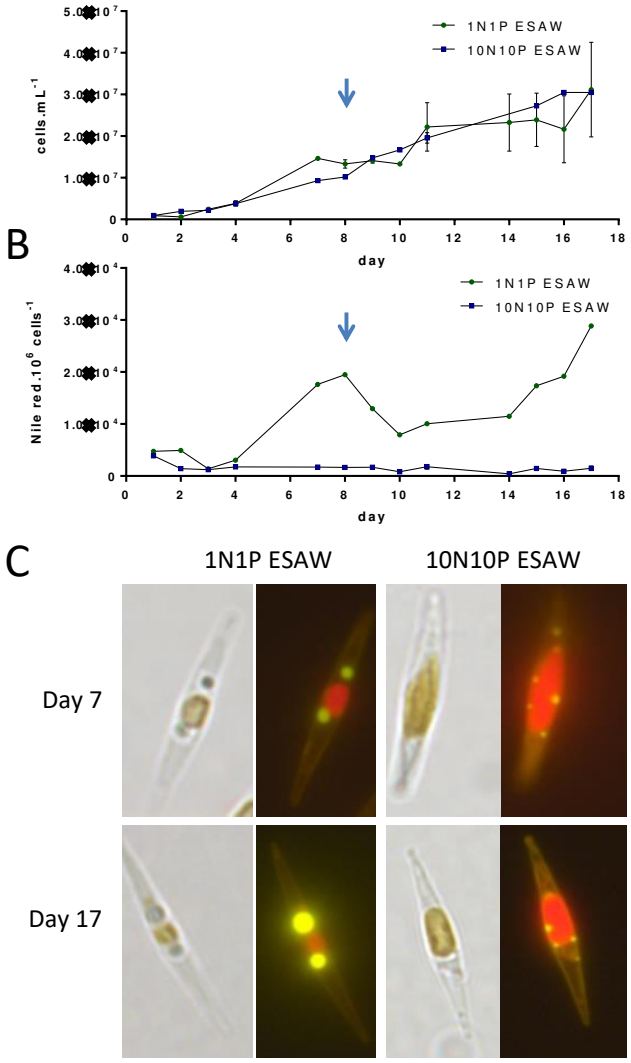

Figure 3.1. Time course of *Phaeodactylum* cell growth and lipid accumulation in 1N1P ESAW and 10N10P ESAW. From a 3 day old mother culture, 50 mL cultures were inoculated at a density of 10^6 cells.mL^{-1} into the indicated media and 200 µl aliquots were taken for daily analyses, n = 1-3. **A. Cell concentrations** were calculated using a Malassez counting chamber and plotted as cells.mL^{-1}. **B. Nile red fluorescence was quantified** using a TECAN plate reader and **C. qualified in epifluorescence microscopy** (Zeiss) with constant FITC filter gain of 200. At day 8, nitrogen and phosphate levels were restored by addition of $NaNO_3$ and NH_2PO_4 into the 1N1P ESAW culture (blue arrow).

To further promote growth in 1N1P ESAW cultures, 0.55 mM of $NaNO_3$ and 0.022 mM of NaH_2PO_4 were added on day 8. After a lag phase of one day, cells started dividing again and quantitative Nile red fluorescence decreased by 50% in the following two days

of cultivation. This stress relaxation indicated that indeed the lack of one of the macroelements was the cause for the stationary phase. Afterwards, Nile red values increased progressively due to the onset of a new stationary phase at $2.44 \times 10^7 \pm 3.86 \times 10^6$ cells.mL^{-1} in 1N1P ESAW cultures reaching 50% higher fluorescence values at day 17 compared to day 7, probably due to bigger and denser lipid droplets, reflected by increased fluorescence intensities. By contrast, cultures grown in enriched media grew constantly without supplementation of nutrients. Nile red fluorescence values did not increase over the time and intracellular lipid droplets were small and numerous. We concluded that cells grown in 10N10P ESAW media did not suffer from nutrient limitation and we defined this condition as the control to study lipid remodelling in response to nitrogen and phosphate deprivation.

3.2.2 *Short term cultivation of P. tricornutum*

The frequent observation of a correlation between TAG accumulation and a lag phase after inoculation of a new *P. tricornutum* batch culture or after nutrient supplementation of a pre-existing culture led us to address this question, with a more detailed study of this phenomenon. This analysis was also required in order to define conditions for short term experiments with the aim of investigating lipid phenotypes in different strains.

As observed in cell cultures of any unicellular organism, *P. tricornutum* growth consists of distinct phases: an initial lag phase during which no cell division occurs followed by an exponential phase before a stationary phase is formed (Peleg & Corradini 2011). Duration of the different phases depends on a variety of factors as nutrient availability and abiotic conditions (Rolfe et al. 2012). The early *Phaeodactylum* growth curve after dilution clearly divided into two phases (**figure 3.2 A**). When the linear regressions of the natural logarithm (LN) were compared, exponential growth was not mathematically supported when all time points of the experiment were considered (green line, R^2 = 0.8499). A confidence interval of >95% was given for time points up from 24 h (light blue, R^2 = 0.9935) but not during earlier time points (dark blue, R^2 = 0.03842) (**figure 3.2 B**). Thus, when an inoculum size of one fifth of the mother culture was transferred to fresh 10 mL 1N1P ESAW or 10N10P ESAW media, a clear growth restriction was

observed in the new cultures during the first 24 hours after dilution while the mother culture maintained growth during the same period.

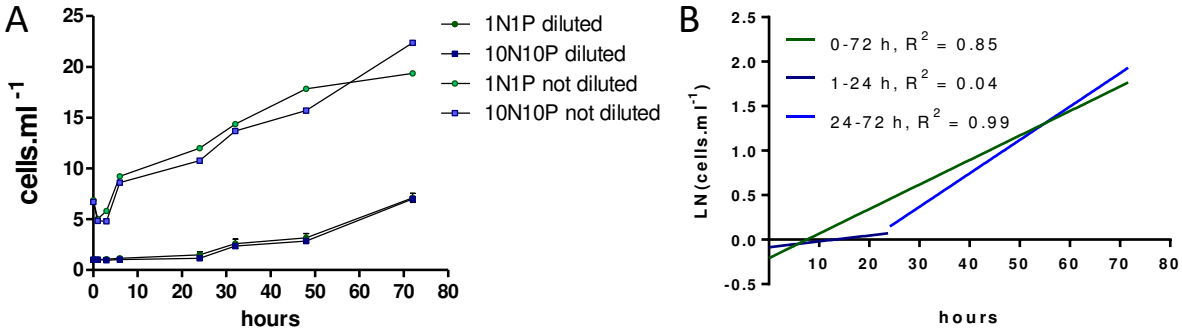

Figure 3.2. Time course of cell growth in 1N1P ESAW and 10N10P ESAW grown *Phaeodactylum* liquid cultures. From a 3 day old mother culture, 10 mL cultures were inoculated at a density of 10^6 cells.mL^{-1} into the indicated media or left unchanged. Aliquots of 300 µL were collected and cell concentrations were estimated by the absorption at 750 nm using a TECAN plate reader. **A. Values were plotted as 10^6 cells.mL^{-1}**. **B. The natural logarithm of diluted growth curves** was calculated and the linear regressions plotted. Splitting the values indicated the onset of the exponential growth phase after 24 h after lag phase as supported by the confidence intervals of the linear regressions (blue lines). If all data points were taken into account, exponential growth was not supported (green line).While during long term cultivation of *Phaeodactylum*, cultures in 10N10P ESAW compared to 1N1P ESAW maintained low neutral lipid levels, the dilution effect on a transient Nile red increase was independent of the growth media used (**figure 3.3**). Upon dilution of a three day old mother culture, neutral lipid fluorescence increased by 30% after six hours and decreased progressively (**figure 3.3 A**). After 24-48 hours, control levels were reached, during which neutral lipid contents increase in the undiluted 1N1P ESAW control (having a culture age of five days), as expected from long term experiments. In epifluorescence microscopy, small lipid droplets appeared in the diluted samples (**figure 3.3. B**). Thus, the lag phase induced neutral lipid formation.

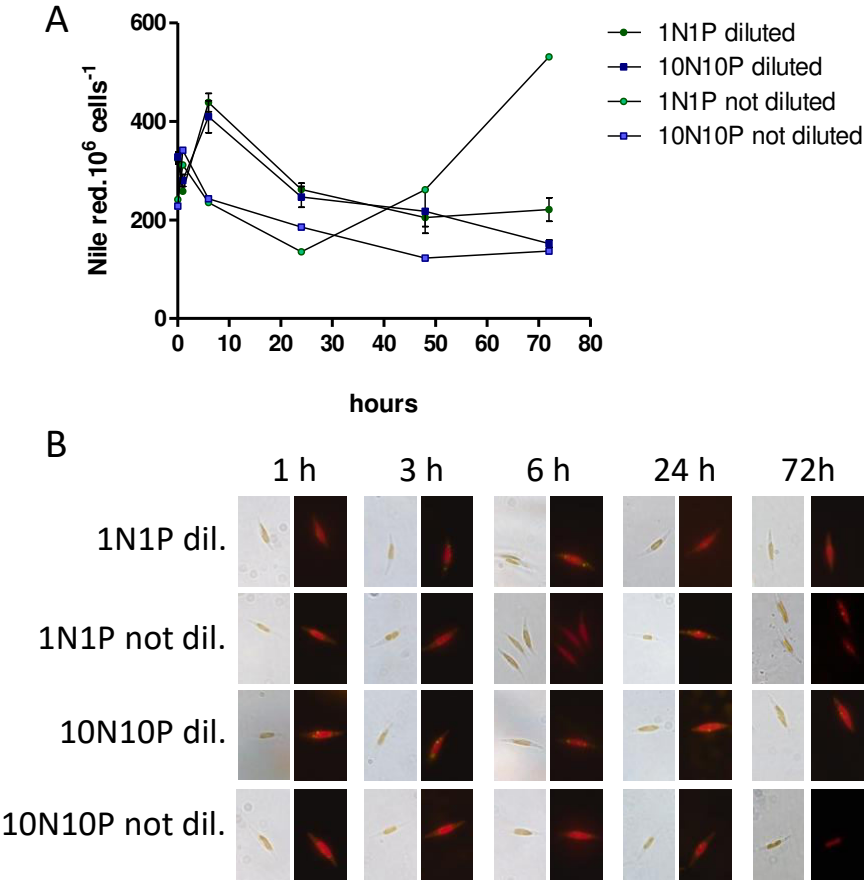

Figure 3.3. Time course of Nile red fluorescence in 1N1P ESAW and 10N10P ESAW grown *Phaeodactylum* liquid cultures. From a 3 day old mother culture, 10 mL cultures were inoculated at a density of 10^6 cells.mL^{-1} into the indicated media or left unchanged. Aliquots of 300 µL were collected for Nile red staining. **A. Relative Nile red fluorescence** was measured using a TECAN plate reader and normalized to the cell concentration. **B. Nile red fluorescence qualified in epifluorescence microscopy** (Zeiss) with constant FITC filter gain of 200.

The lag phase is the least well understood growth phase. Transcriptome analysis of *Salmonella enterica* cultures revealed a differential regulation of more than half of the encoded genes when comparing stationary phase grown cells to different time points during a standardized lag phase. Differentially expressed genes pointed out a recovery of the cells from stressful conditions experienced during stationary phase as well as a preparation for cell growth (Rolfe et al. 2012). Authors confirm earlier evidence that the inoculum size and the growth state of cells were correlated to the length of the lag phase (Fogg & Thake 1987). Furthermore, if stationary phase grown diatom cells were

transferred into fresh media, the lag phase correlated with the duration of nutrient starvation (Collos 1986). It is considered, that nutrient uptake and metabolization is required prior to the onset of cell division. Consistently, upon transfer of *Salmonella* cells from the stationary phase into fresh media, cell sizes increase by 41% during lag phase (Rolfe et al. 2012). We also observe a progressive increase in cell size, evaluated by the optical measurement of the cell length, during the lag phase of fusiform *Phaeodactylum*, but to a lower extent. The average cell length of *Phaeodactylum* was 7.87 µm ± 0.37. Upon dilution, cell length increased transiently reaching 12% larger cells after 3 h (p-value 0.001) and 6 h (p-value 0.025) (**figure 3.4**). The maximum cell size correlated with the peak in Nile red fluorescence. Cell size decreased with the onset of mitosis and reached control levels after 24 .

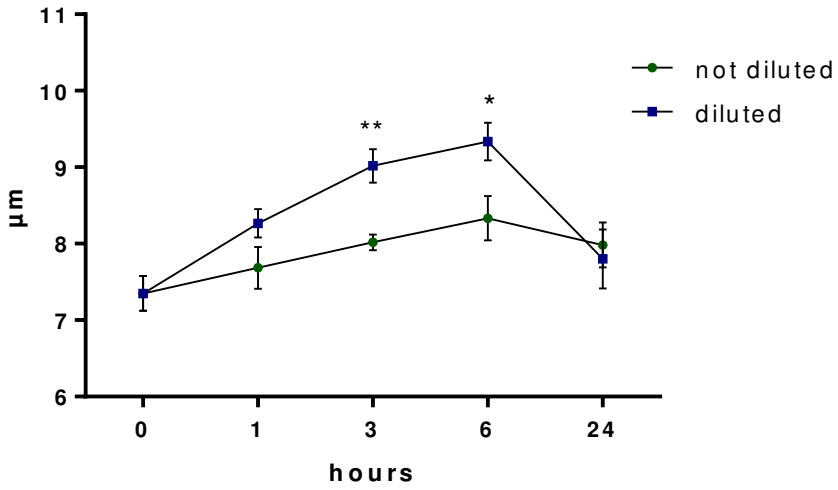

Figure 3.4. Time course of cell length and 10N10P ESAW grown *Phaeodactylum* liquid cultures after dilution. From a 3 day old mother culture, 10 mL cultures were inoculated at a density of 10^6 cells.mL^{-1} or left unchanged. Aliquots of 13 µL were taken to measure the average cell size using a Luna Cell counter.

There are two different causes for lag phases, one occurring after nutrient addition as observed in the long term cultivation experiment (**figure 3.1**) and the other one when cells experience a new environment. The second case becomes evident when cells are inoculated into the “old” media with nutrient re-enrichment compared to fresh media.

The first treatment was observed to shorten the lag phase in some Heterokonts. This is discussed to be caused by signalling molecules that would either inhibit growth and would not be present in the "old" media or on the opposite, a positive regulator of cell division with which it would be pre-requisited (Fogg & Thake 1987). Here, 1N1P ESAW and enriched 10N10P ESAW were compared to exclude the influence of nutrient limitations which could occur in simple ESAW media. At the same time, this comparison allowed to estimate an influence of the pH. Fresh 10N10P ESAW media had a pH of 7.6 which then increased to 9.0 after 3 days while the pH of 10N10P ESAW remained stable at 8.1. Given the similar lag phase in both growth media, neither pH nor nutrient availability was responsible for the lag phase.

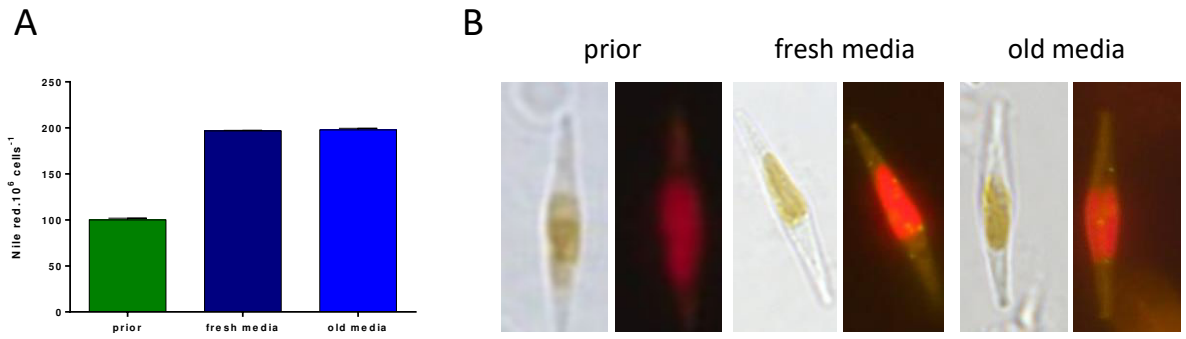

Figure 3.5. Nile red fluorescence in 10N10P ESAW grown *Phaeodactylum* liquid cultures 3 hours after dilution. From a 3 day old mother culture, 50 mL cultures were inoculated at a density of 10^6 cells.mL^{-1} into the indicated media or left unchanged. Either fresh media or media being harvested from a cell culture of the same age (old) was used for subculturing. Aliquots of 160 µL were collected for Nile red staining. **A. Relative Nile red fluorescence** was measured using a TECAN plate reader and normalized to the cell concentration counted using a Malassez counting chamber. **B. Nile red fluorescence qualified in epifluorescence** microscopy (Zeiss) with constant FITC filter gain of 200.

A potential impact of putative signalling molecules as suggested by Fogg and coworkers was investigated by comparing the effect of resuspension of a 3 day old 10N10P ESAW culture into fresh media or into the supernatant of the initial (old) culture after centrifugation (Fogg & Thake 1987). In both cases, dilution dependent TAG accumulation was similar in quantity (**figure 3.5 A**) and quality (**figure 3.5 B**) so the

presence or absence of signalling molecules did not appear to play a role in lag phase formation.

Although nutrient dependent lag phases were studied in a variety of diatom species and the induction of fatty acid synthesis during this phase was indicated in *Salmonella* (Fogg et al. 1987, Rolfe et al. 2012), to our knowledge no one has reported TAG accumulation in diatoms during the lag phase of growth. Indeed, an increase in neutral lipids was never investigated during lag phase although a variety of eukaryotic and some prokaryotic unicellular organisms produce TAG when growth is arrested upon nutrient limitation when transition to stationary phase is induced (Alvarez 2015, Liu et al. 2013b). Therefore, this simple study could give rise to new ideas of batch culturing for industrial applications if we imagine a bioreactor to which an additional volume of media would be added to trigger lag phase induced TAG accumulation before a part of the culture would be harvested. This could allow a considerable rise in cellular TAG contents given the up to two-fold induction observed here with cells that derived from a relatively healthy mother culture.

Our purpose on performing these comparisons was however to define standard conditions for future experiments. The diatom *P. tricornutum* accumulated lipid droplets not only during stationary phase growth but also during the lag phase, thus in two very different physiological states that feature repression of cell division. As reported earlier, the inoculum size and the nutrient status of the mother culture had a strong influence of the lag phase. With our dilution routine of inoculating a fresh culture with 1.10^6 cells.mL^{-1} every three to four days, we observed maximal lag phases of two days and the onset of stationary phase in 1N1P ESAW grown cultures after five to six days. Also, the short culturing intervals facilitated the maintenance of a healthy culture since in *Salmonella,* stationary phase caused cell damages were repaired during lag phase as indicated by an upregulation of reactive oxygen responsive and protein repair genes (Rolfe et al. 2012). On the negative side, this culture regime left a very short time span of comparative studies to investigate triggers of TAG accumulation when the simple media was used, whereas Nile red fluorescence values remained stable over a 17-day period in enriched media (see above). We therefore suggest the choice of 10N10P

ESAW over 1N1P ESAW and minimal experimental time span of two, rather three days for comparative lipodomics on *P. tricornutum*.

3.3 Membrane glycerolipid remodelling triggered by nitrogen and phosphorus starvation in *Phaeodactylum tricornutum*

3.3.1 *Identification of phosphorous starvation-responsive genes in Phaeodactylum tricornutum by comparative analyses of lipid profiles and transcriptomic data from Thalassiosira pseudonana*

In order to reveal a conservation of diatom responses to phosphorous limitations, we compared our lipid profiles from *P. tricornutum* to transcriptomic and lipodomic data from phosphate deprived *Thalassiosira* cells provided in the study of Dyhrman and coworkers (Dyhrman et al. 2012). To this end, we screened the data for the presence of lipid related keywords in their GO name, KOG or EC definition. Glycerolipid related *Thalassiosira* protein sequences were extracted and blasted against the *P. tricornutum* database in NCBI for the identification of possible homologs for the selection of putative target genes to study phosphate-dependent lipid remodelling in the future (**table 3.1**).

We retrieved 13 *Thalassiosira* sequences of proteins potentially involved in galactolipids synthesis sharing 35-69% sequence identity with *P. tricornutum* hits. Seven of these sequences were slightly downregulated in response to phosphate starvation and two candidate genes were 1.77-fold (Protein ID 264013) and 6.53-fold (Protein ID 261140) upregulated. The respective *P. tricornutum* hits shared 53% and 40% sequence homology and are thus interesting candidates which might regulate the observed accumulation of DGDG with stable MGDG levels under phosphate deprived conditions (Abida et al. 2015). The third glycolipid, SQDG, was also induced under phosphate stress conditions in both diatoms. Among six SQDG synthases in *T. pseudonana*, the expression of two isoforms were marginally reduced but two were more than 2-fold induced (Protein ID 29728 and 26939) and had homologs in *P. tricornutum*

with 69% and 70% sequence identity. Phospholipids are largely reduced during phosphate limitations and according to *Thalassiosira* transcriptomic data, PG synthesis genes should be most downregulated. On the other hand, enzymes involved in phosphoinositol (PI) synthesis were induced under phosphate stress in *Thalassiosira* while we could not detect PI in *P. tricornutum*. This might be due to a channelling of PI into sphingolipids which we do not extract. Ten sequences putatively involved in neutral lipid metabolism were retrieved from the *Thalassiosira* transcriptomic data and a massive TAG accumulation was observed in both species upon phosphate deprivation. Four proteins annotated as DGATs that are required for *de novo* TAG synthesis were only marginally induced. This indicated that fatty acids provided for storage lipid production were more likely to derive from lipid remodelling rather than *de novo* synthesis.

Table 3.1. Extract of the transcriptome of phosphate starved *Thalassosira*. From transcriptomic data provided by (Dyhrman et al. 2012), lipid-related proteins were retrieved and grouped according to the respective glycerolipid class and their regulation in phosphate starved and repleted conditions. *Phaeodactylum* homologs of differentially regulated *Thalassiosira* protein sequences were retrieved after NCBI BLASTp and the closest hits are shown.

Thalassiosira					*Phaeodactylum*							
Lipid class	Protein ID	gene ID	fold change -P/+P	KOG definition	Accession number	Evalue	Identity	Accession number	Evalue	Identity	Accession number	Evalue	Identity
MGDG/DGDG	269819	7444304	0,79	Glycosyltransferase	XP_002185822.1	2,00E-132	47%	XP_002183068.1	1,00E-08	25%			
MGDG/DGDG	269773	7452698	0,85	Galactosyltransferases	XP_002185211.1	6,00E-104	46%	XP_002184812.1	5,00E-79	41%	XP_002184801.1	6,00E-68	38%
MGDG/DGDG	263534	7448859	0,88	Glucosyltransferase - Alg8p	XP_002178810.1	3,00E-75	39%	XP_002186451.1	1,00E-20	26%			
MGDG/DGDG	269121	7442394	0,89	GPI-alpha-mannosyltransferase III (GPI10/PIG-B) involved in glycosylphosphatidylinositol anchor biosynthesis	XP_002178736.1	7,00E-93	34%						
MGDG/DGDG	268486	7448774	0,91	Mannosyltransferase	XP_002178609.1	5,00E-118	40%						
MGDG/DGDG	262287	7451956	0,94	Galactosyltransferases	XP_002185211.1	5,00E-115	60%	XP_002184812.1	7,00E-69	42%	XP_002184801.1	1,00E-68	42%
MGDG/DGDG	264314	7443935	0,98	NA	XP_002176800.1	0.0	65%	XP_002186355.1	4,00E-133	47%	XP_002181685.1	5,00E-61	37%
MGDG/DGDG	263200	7447073	1,17	NA	XP_002181685.1	1,00E-164	62%	XP_002176800.1	2,00E-69	38%	XP_002186355.1	6,00E-59	33%
MGDG/DGDG	5034	7448465	1,2	Galactosyltransferases	XP_002177722.1	4,00E-57	46%	XP_002183293.1	0.001	21%	XP_002184033.1	0.019	25%
MGDG/DGDG	25320	7442170	1,26	Galactosyltransferases									
MGDG/DGDG	262632	7442272	1,4	UDP-Gal:glucosylceramide beta-1,4-galactosyltransferase	XP_002180427.1	1,00E-79	69%						
MGDG/DGDG	264013	7445775	1,71	NA	XP_002186355.1	1,00E-164	53%	XP_002176800.1	2,00E-154	55%	XP_002181685.1	3,00E-74	39%
MGDG/DGDG	261140	7452531	6,53	Galactosyltransferases	XP_002185211.1	1,00E-56	40%	XP_002184032.1	3,00E-49	39%	XP_002184034.1	3,00E-47	39%
SQDG	35532	7447193	0,84	UDP-glucose 4-epimerase/UDP-sulfoquinovose synthase	XP_002185705.1	0.0	75%	XP_002179903.1	4,00E-122	51%			
SQDG	23033	7451178	0,85	UDP-glucose 4-epimerase/UDP-sulfoquinovose synthase	XP_002185679.1	2,00E-41	25%	XP_002185705.1	0.001	21%	XP_002179589.1	0.002	23%
SQDG	35046	7448594	1,18	UDP-glucose 4-epimerase/UDP-sulfoquinovose synthase	XP_002179157.1	3,00E-29	26%	XP_002179147.1	2,00E-25	28%	XP_002185968.1	0.001	28%
SQDG	40675	7451777	1,61	UDP-glucose 4-epimerase/UDP-sulfoquinovose synthase	XP_002179903.1	9,00E-151	59%	XP_002185705.1	1,00E-126	51%			
SQDG	29728	7445840	2,27	UDP-glucose 4-epimerase/UDP-sulfoquinovose synthase	XP_002179485.1	0.0	69%	XP_002179157.1	0.0	74%	XP_002179147.1	2,00E-165	66%
SQDG	269393	7452379	2,43	UDP-glucose 4-epimerase/UDP-sulfoquinovose synthase	XP_002185968.1	0.0	78%						
betaine lipids	29008	7450716	0,48	Homoserine dehydrogenase	XP_002182284.1	4,00E-133	33%						
betaine lipids	24587	7450556	0,87	Homoserine dehydrogenase	XP_002183131.1	3,00E-11	26%						
betaine lipids	29144	7450163	0,89	Homoserine dehydrogenase	XP_002183131.1	2,00E-154	56%	XP_002179435.1	7,00E-111	50%			
betaine lipids	40655	7449696	1,02	Homoserine dehydrogenase	XP_002179435.1	0.0	69%	XP_002183131.1	4,00E-111	45%			
betaine lipids	35420	7449212	1,3	Betaine aldehyde dehydrogenase	XP_002180386.1	0.0	59%						
betaine lipids	28592	7448609	1,42	Homoserine kinase	XP_002181002.1	0.0	76%						
phospholipid	260941	7449788	=0.07445049	CDP-alcohol phosphatidyltransferase/Phosphatidylglycerol-phosphate synthase	AEZ63317.1	6,00E-51	48%						
PE/PC	6716	7446185	0,76	sn-1,2-diacylglycerol ethanolamine- and cholinephosphotranferases	XP_002178244.1	2,00E-121	46%						
PI	181	7446841	0,81	N-acetylglucosaminyltransferase complex, subunit PIG-A/SPT14, required for phosphatidylinositol biosynthesis/Sulfolipid synthase	XP_002176995.1	0.0	63%	XP_002185276.1	1,00E-04	22%			
PE/PC	6504	7446325	0,93	sn-1,2-diacylglycerol ethanolamine- and cholinephosphotranferases	XP_002181307.1	1,00E-53	46%	XP_002178244.1	1,00E-18	30%			
PI	261271	7446473	1,55	Phosphatidylinositol synthase	XP_002177371.1	5,00E-42	39%						
PI	38775	7448886	1,98	N-acetylglucosaminyltransferase complex, subunit PIG-A/SPT14, required for phosphatidylinositol biosynthesis/Sulfolipid synthase	XP_002185276.1	0.0	74%	XP_002177026.1	5,00E-41	32%	XP_002176995.1	2,00E-04	21%
PI	35830	7452880	3,08	Phosphatidylinositol synthase	XP_002177371.1	1,00E-11	37%						
DAG	30747	7448866	0,79	CDP-diacylglycerol synthase	XP_002181477.1	8,00E-131	62%						
TAG	928	7445057	0,93	Acyl-CoA:diacylglycerol acyltransferase (DGAT)	XP_002184162.1	8,00E-23	32%	AFQ23660.1	6,00E-17	29%	XP_002177131.1	6,00E-17	29%
DAG	263499	7443495	0,98	CDP-diacylglycerol synthase	XP_002181988.1	2,00E-19	35%	XP_002181477.1	9,00E-07	35%			
DAG	25085	7443992	1,04	beta-1,6-N-acetylglucosaminyltransferase, contains WSC domain	XP_002178439.1	1,00E-08	27%						
TAG	38490	7443332	1,08	Acyl-CoA:diacylglycerol acyltransferase (DGAT)	XP_002184162.1	2,00E-22	35%	AFQ23661.1	3,00E-18	32%			
TAG	20846	7445142	1,08	Acyl-CoA:diacylglycerol acyltransferase (DGAT)	XP_002184226.1	1,00E-97	48%	AFQ23659.1	3,00E-97	48%	XP_002177131.1	5,00E-23	29%
TAG	37867	7444209	1,1	Acyl-CoA:diacylglycerol acyltransferase (DGAT)	AFQ23661.1	6,00E-26	31%	XP_002177637.1	6,00E-26	31%			
DAG	260816	7453442	2,1	Predicted diacylglycerol kinase	XP_002182098.1	3,00E-39	32%						
DAG/sterol	261279	7446478	2,49	Sterol O-acyltransferase/Diacylglycerol O-acyltransferase	ADY76581.1	3,00E-171	56%	AEG79729.1	2,00E-170	55%	XP_002177753.1	2,00E-160	55%
DAG	15977	7444581	2,8	Diacylglycerol kinase	XP_002182098.1	5,00E-156	67%						

Taken together, the phosphate deprivation response of both diatom species *T. pseudonana* and *P. tricornutum* shared trends in lipid remodelling with an induction of DGDG, SQDG and TAG while phospholipids were reduced. Based on sequence

comparisons from *Thalassiosira* transcriptomic data, *Phaeodactylum* gene homologs were identified that could play in phosphate dependent lipid homeostasis.

3.3.2 *Membrane Glycerolipid Remodeling Triggered by Nitrogen and Phosphorus Starvation in Phaeodactylum tricornutum* (***published article***)

Membrane Glycerolipid Remodeling Triggered by Nitrogen and Phosphorus Starvation in *Phaeodactylum tricornutum*[1]

Heni Abida[2], Lina-Juana Dolch[2], Coline Meï[2], Valeria Villanova, Melissa Conte, Maryse A. Block, Giovanni Finazzi, Olivier Bastien, Leïla Tirichine, Chris Bowler, Fabrice Rébeillé, Dimitris Petroutsos*, Juliette Jouhet*, and Eric Maréchal*

Environmental and Evolutionary Genomics Section, Institut de Biologie de l'École Normale Supérieure, Centre National de la Recherche Scientifique Unité Mixte de Recherche 8197, Institut National de la Santé et de la Recherche Médicale, U1024, 75005 Paris, France (H.A., L.T., C.B.); Laboratoire de Physiologie Cellulaire et Végétale, Unité Mixte de Recherche 5168 Centre National de la Recherche Scientifique-Commissariat à l'Energie Atomique-Université Grenoble Alpes, Institut de Recherche en Sciences et Technologies pour le Vivant, Commissariat à l'Energie Atomique Grenoble, 38054 Grenoble cedex 9, France (L.-J.D., C.M., M.C., M.A.B., G.F., O.B., F.R., D.P., J.J., E.M.); and Fermentalg SA, F–33500 Libourne, France (V.V.)

Diatoms constitute a major phylum of phytoplankton biodiversity in ocean water and freshwater ecosystems. They are known to respond to some chemical variations of the environment by the accumulation of triacylglycerol, but the relative changes occurring in membrane glycerolipids have not yet been studied. Our goal was first to define a reference for the glycerolipidome of the marine model diatom *Phaeodactylum tricornutum*, a necessary prerequisite to characterize and dissect the lipid metabolic routes that are orchestrated and regulated to build up each subcellular membrane compartment. By combining multiple analytical techniques, we determined the glycerolipid profile of *P. tricornutum* grown with various levels of nitrogen or phosphorus supplies. In different *P. tricornutum* accessions collected worldwide, a deprivation of either nutrient triggered an accumulation of triacylglycerol, but with different time scales and magnitudes. We investigated in depth the effect of nutrient starvation on the Pt1 strain (Culture Collection of Algae and Protozoa no. 1055/3). Nitrogen deprivation was the more severe stress, triggering thylakoid senescence and growth arrest. By contrast, phosphorus deprivation induced a stepwise adaptive response. The time scale of the glycerolipidome changes and the comparison with large-scale transcriptome studies were consistent with an exhaustion of unknown primary phosphorus-storage molecules (possibly polyphosphate) and a transcriptional control of some genes coding for specific lipid synthesis enzymes. We propose that phospholipids are secondary phosphorus-storage molecules broken down upon phosphorus deprivation, while nonphosphorus lipids are synthesized consistently with a phosphatidylglycerol-to-sulfolipid and a phosphatidycholine-to-betaine lipid replacement followed by a late accumulation of triacylglycerol.

Diatoms are a major component of phytoplankton communities, believed to be responsible for up to one-fourth of global primary productivity (Scala and Bowler, 2001). They live in an environment where light, temperature, pH, oxygen, carbon dioxide, nutrients, and all kinds of physicochemical parameters can vary dramatically. Nitrogen (N), phosphorus (P), and iron are the most often limiting or colimiting nutrients (Mills et al., 2004; Moore et al., 2013), and N is more often limiting than P in marine systems, with the reverse in freshwaters (Hecky and Kilham, 1988). As a selection pressure, the relative fluctuations of N and P have been proposed to be responsible for the differences of size distributions of diatoms, freshwater species being smaller than marine ones due to the ambient scarcity of P (Litchman et al., 2009). Nutrient scarcity is a criterion to define oligotrophic areas in oceans. A study by Van Mooy et al. (2009) on phytoplanktonic communities in an oligotrophic marine region, where P is scarce (less than 10 nM), observed that diatoms reduced their P requirements by synthesizing less phosphoglycerolipids, in particular phosphatidylcholine (PC) and phosphatidylglycerol (PG), and more

[1] This work was supported by the Agence Nationale de la Recherche (grant no. ANR–12–BIME–0005 [DiaDomOil] to C.B., G.F., D.P., and E.M.), the Commissariat à l'Energie Atomique Life Science Division (bioenergy grant EliciTAG to M.C. and E.M.), a European Research Council Advanced Grant (Diatomite; to C.B.), the Centre National de la Recherche Scientifique (Défi Transition Energétique grant to L.T. and G.F.), the OCEANOMICS program from the French Ministry of Research (to E.M.), and the Institut Carnot Lipides pour la Santé et l'Industrie (to E.M.).

[2] These authors contributed equally to the article.

* Address correspondence to dimitris.petroutsos@cea.fr, juliette.jouhet@cea.fr, and eric.marechal@cea.fr.

The author responsible for distribution of materials integral to the findings presented in this article in accordance with the policy described in the Instructions for Authors (www.plantphysiol.org) is: Eric Maréchal (eric.marechal@cea.fr).

H.A., L.-J.D., C.M., V.V., M.C., F.R., D.P., and J.J. performed the experiments; O.B. achieved the bioinformatic analyses; M.A.B., G.F., L.T., and C.B. contributed to the design and analyses of experiments; D.P., J.J., and E.M. designed, supervised, and analyzed the experiments. All authors contributed to the writing of the article.

www.plantphysiol.org/cgi/doi/10.1104/pp.114.252395

nonphosphorus lipids, such as sulfoquinovosyldiacylglycerol (SQDG) and betaine lipids (BL), as compared with communities growing in a P-rich region (more than 100 nM). However, that study did not consider the levels of two other nonphosphorus lipid classes (i.e. the chloroplast galactoglycerolipids, in particular monogalactosyldiacylglycerol [MGDG]) and digalactosyldiacylglycerol (DGDG), and triacylglycerol (TAG). When Van Mooy et al. (2009) examined planktonic membrane lipids at the two locations, their observations were consistent with a PG-to-SQDG and a PC-to-BL replacement triggered by P shortage. In a complementary set of experiments, they cultivated the diatom *Thalassiosira pseudonana* in a P-depleted or P-replete artificial medium and found variations of the SQDG-PG and BL-PC ratios in line with their on-site observations (Van Mooy et al., 2009), supporting that lipid remodeling could be one of the most essential mechanisms allowing a given species to acclimate and populate oligotrophic areas.

Phospholipid-to-nonphosphorus lipid replacement has been studied in depth in the plant Arabidopsis (*Arabidopsis thaliana*; Benning and Ohta, 2005; Shimojima and Ohta, 2011; Boudière et al., 2012; Dubots et al., 2012; Nakamura, 2013; Petroutsos et al., 2014). In Arabidopsis, PC and PG contents decrease upon P starvation, and the synthesis of plastid glycolipids (i.e. MGDG, DGDG, and SQDG) increases coincidentally. Based on the acyl profiles of glycerolipids, it is possible to identify the metabolic routes that are mobilized in this remodeling. In Arabidopsis, MGDG can be synthesized using diacylglycerol (DAG) generated locally inside the plastid, via the so-called prokaryotic pathway, or using diacyl precursors diverted from nonplastid phospholipids, via the so-called eukaryotic pathway (Browse et al., 1986). The prokaryotic structure is characterized by a 16-carbon (C16) fatty acid (FA) at position *sn*-2 of the glycerol backbone, like cyanobacterial lipids, whereas the eukaryotic structure contains an 18-carbon (C18) FA at position *sn*-2. Thus, in Arabidopsis, (1) 18:3/16:3-MGDG originates from the stepwise galactosylation of prokaryotic 18:1/16:0-DAG followed by a rapid desaturation into the trienoic form; and (2) 18:3/18:3-MGDG relies on the import and galactosylation of eukaryotic precursors derived from phospholipids, most notably having 18:2/18:2 structures (Maréchal et al., 1994), also followed by a desaturation into the trienoic form. Upon P shortage, the eukaryotic pathway is activated; PC hydrolysis releases a diacyl intermediate, which is then transferred to the plastid to synthesize MGDG and DGDG (Jouhet et al., 2003), creating a virtuous recycling of lipid intermediates between phospholipid breakdown and galactolipid increase. The Arabidopsis response to low P combines a rapid metabolic regulation, coupling MGDG synthesis to the phospholipid status (Dubots et al., 2010, 2012), with a longer term genomic reprogramming (Misson et al., 2005; Morcuende et al., 2007) characterized by the up-regulation of phospholipases C and D (hydrolyzing phospholipids) and of monogalactosyldiacyl and digalactosyldiacyl isoforms (the galactosyltransferases synthesizing MGDG and DGDG, respectively). In P-starved conditions, a PG-to-SQDG replacement is observed and is considered to be a ubiquitous phenomenon in photosynthetic organisms, enabling the preservation of an anionic lipid environment to the photosystems in the thylakoids (Boudière et al., 2014). No intense trafficking is required for this replacement, as SQDG and PG are both chloroplast lipids. The most spectacular feature of Arabidopsis lipid remodeling consists in the replacement of PC in a variety of subcellular locations, such as the plasma membrane, the tonoplast, and the mitochondria (but not observed in the endoplasmic reticulum [ER]), by DGDG synthesized in the chloroplast, using still uncharacterized lipid export systems (Andersson et al., 2003, 2005; Jouhet et al., 2003, 2004, 2007, 2010; Sandelius et al., 2007; Tjellström et al., 2008).

Lipid modifications triggered in Arabidopsis by a deprivation of N have not been studied as extensively. Upon N shortage, the quantity of N-containing lipids, in particular PC and phosphatidylethanolamine (PE), seems to be unaffected (Gaude et al., 2007). On the other hand, the main response includes a relative decrease of MGDG and an increase of DGDG, concomitant with an up-regulation of the genes encoding both digalactosyldiacyl isoforms, and a small increase of TAG synthesis (Gaude et al., 2007). It is not known whether any lipid trafficking can be triggered by N shortage, nor whether there are any changes in the lipid composition of cell compartments, like those documented in cells exposed to P shortage.

No such comprehensive study has been made in a diatom model. Acyl profiles of all glycerolipid classes and quantifications still have to be determined. The existence of redundant metabolic routes, similar to the prokaryotic and eukaryotic pathways dissected in Arabidopsis, also requires assessment. The conservation of some processes occurring in plants, such as a decrease of MGDG and an increase of DGDG in N-depleted conditions or an increase of MGDG and DGDG and a putative PC-to-DGDG replacement in P-depleted conditions, also should be investigated.

Studies in diatoms have benefited from developments in two model species, the centric diatom *T. pseudonana* (Coscinodiscophyceae) and the pennate diatom *Phaeodactylum tricornutum* (Bacillariophyceae), for which intense efforts have resulted in fully sequenced genomes (Armbrust et al., 2004; Bowler et al., 2008) and provided reference data for transcriptomic (Maheswari et al., 2005, 2009; Allen et al., 2008; Sapriel et al., 2009; Shrestha et al., 2012; Chauton et al., 2013) and whole-cell proteomic (Montsant et al., 2005; Nunn et al., 2009) analyses. *P. tricornutum* is pleiomorphic, with three major morphotypes (fusiform, triradiate, and oval). A series of axenic strains have been collected in various marine environments worldwide, denoted Pt1 to Pt10 (De Martino et al., 2007), allowing analyses of phenotypic variations and the adaptation to various habitats.

In photosynthetic organisms, it is usually considered that, in standard conditions, phospholipids are mostly present in the endomembrane system, whereas nonphosphorus glycolipids are in the plastid. However, this distinction might be more complex in diatoms due to the physical connection between some membranes limiting the plastid with the endomembrane system and/or

mitochondria. Briefly, like all eukaryotes, diatoms contain a conventional endomembrane system comprising the ER, nuclear envelope, Golgi, trans-Golgi network, plasma membrane, etc., which are connected to each other by vesicular shuttles or tubular structures (Brighouse et al., 2010). In addition, two semiautonomous organelles of endosymbiotic origins are present, a mitochondrion limited by two membranes and a plastid bounded by four membranes, which originate from a secondary endosymbiosis (Dorrell and Smith, 2011; Petroutsos et al., 2014). A continuum occurs between the ER and the outermost membrane of the plastid (Kroth et al., 2008). The glycerolipid composition of each of the four membranes that surround the plastid is simply unknown. Therefore, it is difficult to speculate on the location of MGDG and DGDG synthesis and whether any export of DGDG to other locations of the cell could be plausible, like that observed in plants. Given the current state of membrane fractionation techniques, only global analyses can be performed. By contrast with other omics data, and although previous targeted studies have allowed the structural determination of some isolated glycerolipid classes (Arao et al., 1987; Yongmanitchai and Ward, 1993; Naumann et al., 2011), the complete membrane glycerolipidome of *P. tricornutum* has not been fully characterized. The analyses of membrane glycerolipid remodeling in diatoms should also consider the accumulation of TAG triggered by nutrient shortage, which has been scrutinized in much more detail due to the potential applications for biofuels and green chemistry (Alonso et al., 2000; Rezanka et al., 2011; Zendejas et al., 2012; Levitan et al., 2014).

In this article, by combining multiple analytical techniques, we sought to characterize comprehensively the major membrane glycerolipid classes in *P. tricornutum*, together with TAG. FA profiles of each class have been determined, providing acyl signatures that can be used as markers for diacyl moiety origins and fluxes. With a fully characterized glycerolipidome in hand, we then analyzed changes triggered by N and/or P depletion and deduced from lipid class and acyl signature variations the dynamic processes driving the observed lipid remodeling.

RESULTS

Comparison of *P. tricornutum* Ecotypes in Nutrient-Replete and Nutrient-Limiting Batch Cultivation

We examined the responses of all available *P. tricornutum* accessions, collected originally in various geographical regions and covering all known morphotypes (i.e. the fusiform shape commonly observed in laboratory conditions, the triradiate shape thought to be more abundant in nature, and the oval shape, indicative of a temperature or salinity stress; De Martino et al., 2007; Fig. 1A). In our growth conditions, most accessions were fusiform except Pt8, which is mainly triradiate, and Pt3 and Pt9, which are oval. Cells grown in nutrient-replete conditions (0.55 mM N and 0.0224 mM P, called here 1N1P) were shifted to −N (0N1P) or −P (1N0P) medium.

Nonpolar lipid accumulation (mainly TAG), known to be triggered by nutrient shortage in phytoplankton, was monitored using Nile Red fluorescence staining. N depletion triggered a faster TAG accumulation as compared with P depletion; therefore, the comparison of the response of the different ecotypes to −N or −P was made 3 d after N depletion (Fig. 1B) and 8 d after P depletion (Fig. 1C). All accessions showed a marked accumulation of TAG shortly after N depletion, except Pt4, which exhibited a relatively modest increase (a representative experiment is shown in Figure 1B). The detection of nonpolar lipid accumulation in response to low P required a much longer cultivation time in P-depleted medium, and no significant TAG accumulation could be detected after 3 to 5 d. After 8 d of growth in a P-limited medium, a contrasting phenotype in the series of Pt accessions could be observed (a representative experiment is shown in Figure 1C), with a substantial accumulation of nonpolar lipid in all accessions except Pt4, Pt10, and PtHK, in which the Nile Red staining was lower than a 2-fold increase, as compared with cells grown in a replete medium.

We did not observe any correlation between the magnitude of response to N or P depletion and the corresponding morphotypes. Phenotypic variations might be related, rather, to the efficiency of N or P storage systems in the different accessions and/or to the signaling and metabolic processes activated by the lack of nutrients. In all cases, an increase of Nile Red fluorescence, even moderate, was always detected, thus demonstrating that TAG accumulation is a marker of nutrient shortage. We decided to pursue our experiments on Pt1, the most commonly used strain in laboratories, which responded significantly to both N and P deprivations.

Effects of N and P Depletion on the Growth and Photosynthesis of *P. tricornutum*

Since P depletion exerted an effect after a longer time period than N depletion, we had to be sure, when studying the effect of P shortage, that no exhaustion of N occurred during the time of observation and that control conditions were indeed kept replete. To avoid such issues, we adjusted the initial nutrient-replete conditions to concentrations 10 times higher than that applied in our comparative study of ecotypes (i.e. 5.5 mM N and 0.22 mM P [a medium called 10N10P]). We checked that the 10N10P medium supported the growth of *P. tricornutum* Pt1 at higher cell densities compared with the 1N1P medium (Supplemental Fig. S1A). Most importantly, the photosynthetic capacity of cells, probed as photosynthetic capacity (F_v/F_m), remained unaltered for 10 d in the 10N10P medium, in stark contrast with cells grown in 1N1P medium, where F_v/F_m dropped quickly during the growth period (Supplemental Fig. S1B). After 5 d of cultivation in 1N1P medium, a decrease of F_v/F_m and an increase of nonpolar lipid content were measured

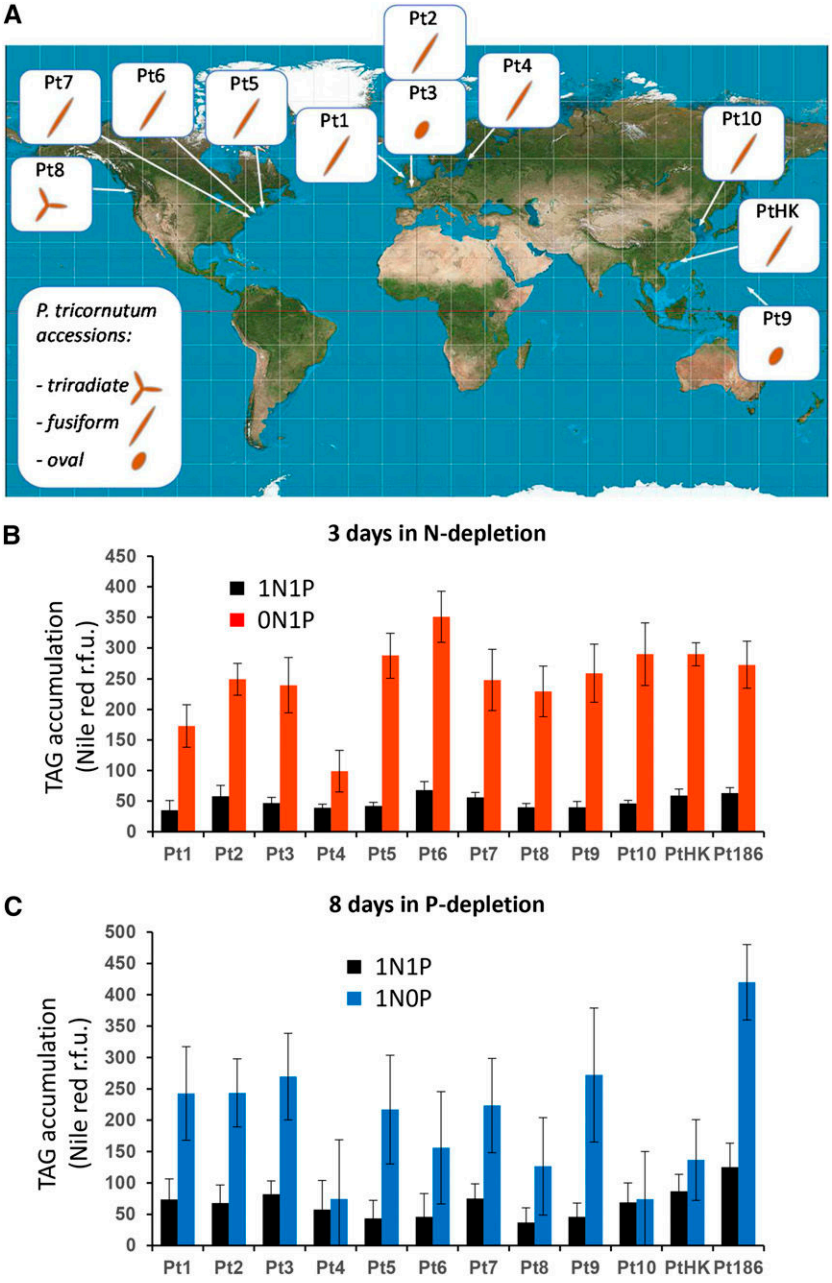

Figure 1. Preliminary comparison of accessions of *P. tricornutum* grown in artificial medium depleted in N or P. A, Geographical origin and major morphotypes of Pt accessions. The origin areas of sampling of Pt accessions are shown: Pt1 off Blackpool, United Kingdom; Pt2 and Pt3 off Plymouth, United Kingdom; Pt4 near the island of Segelskå; Pt5 in the Gulf of Maine; Pt6 off Woods Hole, Massachusetts; Pt7 off Long Island, New York; Pt8 near Vancouver, Canada; Pt9, Territory of Guam, Micronesia; PtHK, near Hong Kong; and Pt10, in the Yellow Sea. The genomic strain Pt1 8.6 derives from the Pt1 accession. Pt3 is a stress form deriving from Pt2. Major morphotypes observed for each accession in artificial seawater are indicated (i.e. the triradiate, fusiform, and oval morphotypes; from De Martino et al. [2007]). B, Accumulation of nonpolar lipids in N-limiting conditions. Cells in the exponential phase of growth were harvested by centrifugation and transferred to a fresh replete (1N1P; black bars) or N-depleted (0N1P; red bars) ESAW medium. Nonpolar lipid accumulation was measured after 3 d by Nile Red staining and expressed as fluorescence intensity normalized by cell number. C, Accumulation of nonpolar lipids in P-limiting conditions. Cells in the exponential phase of growth were harvested by centrifugation and transferred to a fresh replete (1N1P; black bars) or P-depleted (1N0P; blue bars) ESAW medium. Nonpolar lipid accumulation was measured after 8 d by Nile Red staining and expressed as fluorescence intensity normalized by cell number. r.f.u., Relative fluorescence units.

(Supplemental Fig. S1C), reflecting a nutrient limitation in the 1N1P medium that did not occur in the 10N10P condition.

We then evaluated the time scale of the Pt1 response after transfer to nutrient-limiting conditions. For this, the diatoms were grown in 10N10P medium until they reached a cell density of 6 to 7 million cells mL^{-1}. Cells were centrifuged, washed with 0N0P medium, and resuspended in 10N10P, 0N10P, and 10N0P media at a starting cell density of 3 to 3.5 million cells mL^{-1}. N depletion resulted in growth arrest after 1 d (Supplemental Fig. S2A) and led to an accumulation of nonpolar lipids after 4 d (based on Nile Red fluorescence; Supplemental Fig. S2B). P depletion affected neither growth nor lipid accumulation between days 0 and 4 (Supplemental Fig. S2, A and B), consistent with the delay observed for the different accessions grown in 0N1P or 1N0P medium, before any visible effect could be measured (Fig. 1, B and C).

We then cultivated Pt1 cells in sufficient amounts to analyze in parallel their cell phenotypes, photosynthetic properties, and lipidomic profiles. Based on previous experiments (Supplemental Fig. S2B), F_v/F_m was selected as an indicator of nutrient limitation (Fig. 2A). At day 5, cells grown in 10N10P and 0N10P were harvested, whereas cells grown in 10N0P were kept in the culture medium until day 13. We should note that at days 5, 8, and 10, 30% of the 10N0P culture volume was replaced by fresh 10N0P medium to ensure that no other

nutrient limitation besides P would occur. In parallel, a 10N10P culture was similarly complemented with fresh 10N10P medium and kept as a control condition during the same period. After 13 d of P limitation, the cells were clearly impacted in their photosynthetic activity (Fig. 2A) and showed a high nonpolar lipid content (Fig. 2B). At the same time point, the control cultures also showed a slightly diminished F_v/F_m, which was not attributed to N or P deprivation, since we did not observe any TAG accumulation (Fig. 2B). Since we did not detect any significant change in the TAG content and membrane glycerolipid profile of cells grown in 10N10P medium collected after 5 or 13 d of culture, we used cells collected after 5 d in 10N10P as a control to compare nutrient-starved and nutrient-replete cells.

Comprehensive Characterization of the Glycerolipid Content of *P. tricornutum* Pt1 Grown in Nutrient-Replete Medium

We extracted the lipids from *P. tricornutum* cells with great caution to avoid lipid degradation. For this purpose, samples were freeze dried rapidly after harvest and lipids were extracted following a treatment in boiling ethanol to inactivate lipase activities. An aliquot fraction of the total extract of glycerolipids was transesterified in the presence of methanol, thus producing fatty acid methyl esters (FAMEs) that were separated by gas chromatography and quantified by flame ionization detection (GC-FID), as described in "Materials and Methods." We used thin-layer chromatography (TLC) to separate the different classes of glycerolipids, combining robust one-dimensional and two dimensional TLC systems to separate, on the one hand, nonpolar glycerolipids and free FA, and on the other hand, polar glycerolipids (phosphoglycerolipids and nonphosphorus glycerolipids; Fig. 3; Supplemental Fig. S3). We analyzed the structure of lipids in each spot revealed on the TLC plate (see "Materials and Methods") by mass spectrometry (MS; Tables I–III) and determined the corresponding FAME profiles by GC-FID.

The total glycerolipid extract from *P. tricornutum* grown in a 10N10P medium had a FA composition similar to those already reported in the literature for diatoms (Guschina and Harwood, 2006; Liang et al., 2014) and eustigmatophytes such as *Nannochloropsis graditana* (Simionato et al., 2013): that is, strikingly enriched in C16 molecular species (16:0, 16:1, 16:2, and 16:3) and eicosapentaenoic acid (20:5) and poor in C18 FAs (Fig. 4A).

We analyzed the different classes of glycerolipids in the extract (Fig. 4B), providing, to our knowledge, the first reference for a complete glycerolipidome of *P. tricornutum* in unstressed conditions. The profile is dominated by MGDG, SQDG, and PC, which together represent more than 75% of the total content. We also confirmed the presence of 20:5 acyl-SQDG, as reported previously (Naumann et al., 2011; Supplemental Fig. S4). We identified a spot corresponding to diacylglyceryl-hydroxymethyl-*N*,*N*,*N*-trimethyl-β-alanine (DGTA; Figs. 3 and 4B; Supplemental Fig. S3), a betaine glycerolipid that had not yet been reported for *P. tricornutum* but has been reported for other algae such as *Phaeocystis* sp. (Haptophycea), *Ochromonas danica* (Chrysophyceae),

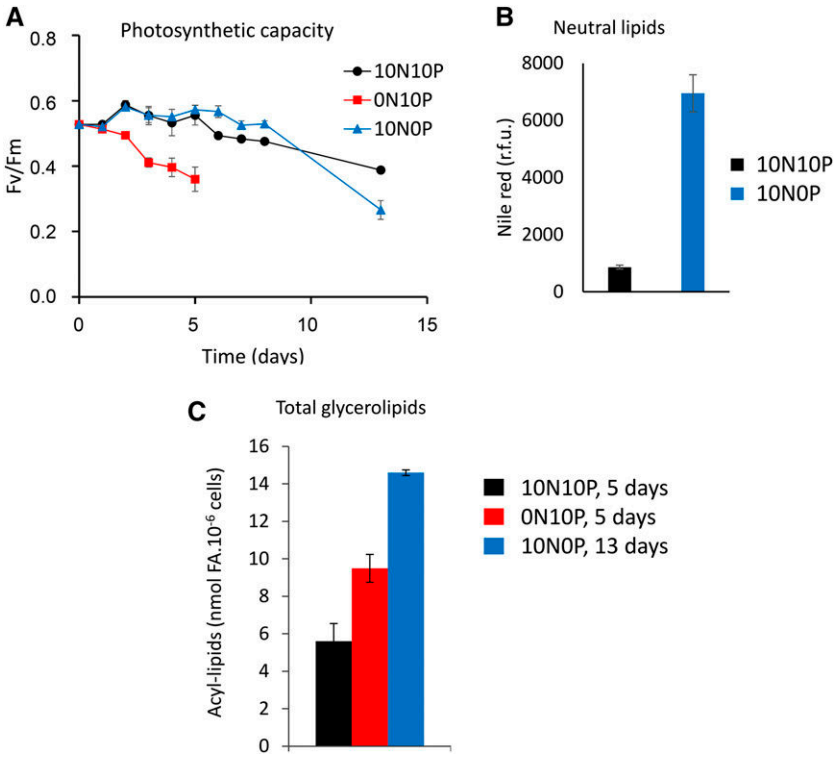

Figure 2. Photosynthetic activity and lipid accumulation in the Pt1 ecotype of *P. tricornutum* cultivated in replete or N- or P-depleted conditions. A, Time-course evolution of photosynthetic efficiency. The F_v/F_m ratio, representative of the photosynthetic efficiency of the diatom, was measured for Pt1 cells grown either in a replete medium (10N10P; black) or in medium deprived of N (0N10P; blue) or P (10N0P; red). B, Nonpolar lipid accumulation measured at day 13. Nonpolar lipid accumulation was estimated by Nile Red fluorescence normalized to cell number. In 10N10P, the fluorescence signal remained at background level, indicating that the F_v/F_m decrease was not due to N or P starvation. r.f.u., Relative fluorescence units. C, Total glycerolipid accumulation. The total level of glycerolipids (membrane lipids + TAG) was estimated by the total FA content after 5 d of cultivation in the replete condition (black bar) or following N starvation (red bar) or 13 d of P starvation (blue bar). To avoid any N deficiency in 10N10P or 10N0P culture, the media were replaced by fresh ESAW 10N10P medium every 3 d.

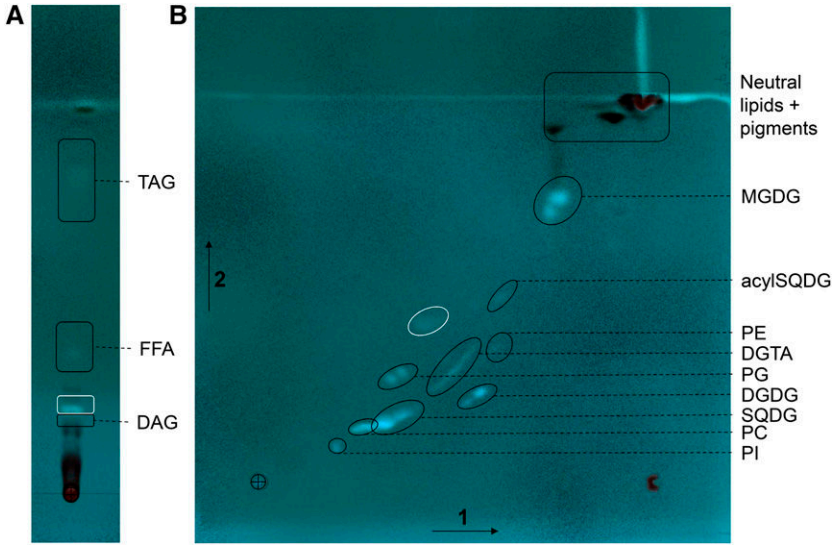

Figure 3. Separation by TLC of the glycerolipids from *P. tricornutum*. Lipids from Pt1 cells grown in a replete medium (10N10P) were extracted and resolved following the procedures described in "Materials and Methods." The cross indicates the initial deposit. A, One-dimensional separation of nonpolar lipids (DAG and TAG) and free FA (FFA). Migration was performed in hexane:diethylether:acetic acid (70:30:1, v/v). B, Two-dimensional separation of polar (membrane) lipids. Migration was performed in chloroform:methanol:water (65:25:4, v/v) for the first dimension (arrow 1) and chloroform:acetone:methanol:acetic acid:water (50:20:10:10:5, v/v) for the second migration (arrow 2). Lipids were visualized under UV light, after spraying with 2% 8-anilino-1-naphthalenesulfonic acid in methanol, and scraped off the plate for analyses. Identification of the lipid in each spot was performed by MS2 analyses. The spot circled in white is an unknown compound with a structure that differs from a glycerolipid.

and some brown algae such as *Fucus vesiculus* (Phaeophyceae; Dembitsky, 1996). DGTA has the same mass as diacylglyceryl-*N*,*N*,*N*-trimethylhomoserine (DGTS) but could be discriminated by a different migration position on two-dimensional TLC (Vogel and Eichenberger, 1992) and, following tandem mass spectrometry (MS2) fragmentation, by the absence of a fragment corresponding to a loss of mass-to-charge ratio (*m/z* 87; Armada et al., 2013). We did not detect the presence of DGTS in *P. tricornutum*.

Nonpolar lipids, DAG and TAG, are also present but in minor amounts (e.g. TAG represented only 1%–3% of the total glycerolipids when cells were grown in the 10N10P medium; Fig. 4B). We were not able to identify in our TLC system any spot corresponding to phosphatidic acid, diphosphatidylglycerol, and phosphatidyl-Ser. This does not mean that these phospholipids are absent in *P. tricornutum* but indicates that they each represent less than 1% of the total glycerolipid content. Overall, the main lipids are the four chloroplast lipids present in every photosynthetic membrane (i.e. MGDG, SQDG, DGDG, and PG) together with PC, which is usually the main glycerolipid in nonplastid membranes, although in diatoms its abundance in the four membranes surrounding the chloroplast cannot be excluded.

The positioning of FAs on each glycerolipid (summarized in Table III) was determined using MS and MS2 analyses, as described in Table II. The FA molar profiles (percentage) of the three main membrane lipids and the nonpolar glycerolipids are shown in Figure 5.

Several general features can be deduced from Table III. First, we confirmed previous analyses (Arao et al., 1987; Yongmanitchai and Ward, 1993) reporting that 16:3 is always located at the *sn*-2 position and 20:5 at the *sn*-1 position, except when two 20:5s are present. Almost all glycoglycerolipids have a C16 FA at the *sn*-2 position, suggesting that the plastid lysophosphatidic acid acyltransferase (LPAAT), an enzyme called Arabidopsis seed gene2 (ATS2) in plants, has a very high selectivity for a C16-acyl carrier protein (C16-ACP), as in higher plants (Frentzen et al., 1983), and that the plastid pathway (also known as the prokaryotic pathway) for the synthesis of the diacylglycerol backbone of glycoglycerolipids is largely dominant in diatoms (Mongrand et al., 1998). Considering MGDG, for example, the most abundant species is 20:5/16:3, in agreement with our gas chromatography analyses (Fig. 5). Generally speaking, 16:3 and 16:4 are restricted to MGDG and only found at the *sn*-2 position. Considering DGDG, synthesized from MGDG, the *sn*-2 position is also esterified exclusively to a C16-FA, suggesting that these molecular species could originate from the same plastidic pathway. FAs in the *sn*-2 position are more saturated than those in MGDG (no 16:3 and 16:4 could be detected), suggesting that the desaturation of MGDG in 16:3 and 16:4 could be a way to lock an MGDG diacylglycerol backbone, preventing its utilization as a substrate for the synthesis of other glycerolipids, as shown previously in plants (Boudière et al., 2012; Petroutsos et al., 2014) and in *Chlamydomonas reinhardtii* (Li et al., 2012). By contrast with plants, the *sn*-1 position of MGDG contains a very low proportion of C18 molecular species, with only about 8% of 18:0/16:3. The acyl profile of the different lipid classes, therefore,

Table I. *Identification of glycerolipids from P. tricornutum*

Characteristic fragments generated by fragmentation of the parent ion (MS2) are shown, together with the associated references.

Analyzed Lipids	Polarity	Ion Analyzed	Specific Fragments in MS2 Scan	References
Phospholipids				
PC	+	$[M + H]^+$	Neutral loss of *m/z* 59	Domingues et al. (1998)
PE	+	$[M + H]^+$	Neutral loss of 141	Brügger et al. (1997)
Phosphatidylserine	+	$[M + H]^+$	Neutral loss of 185	Brügger et al. (1997)
PG	+	$[M + NH_4]^+$	Neutral loss of 189	Taguchi et al. (2005)
PI	+	$[M - H]^-$	Precursors of *m/z* 241	Hsu and Turk (2000b)
Phosphatidic acid	+	$[M + NH_4]^+$	Neutral loss of 115	Li-Beisson et al. (2010)
Nonphosphorus glycerolipids				
SQDG	–	$[M - H]^-$	Precursors of *m/z* 225	Gage et al. (1992); Welti et al. (2003)
ASQ	–	$[M - H]^-$	Precursors of *m/z* 509	Naumann et al. (2011)
MGDG	+	$[M + NH_4]^+$	Neutral loss of 179	Li-Beisson et al. (2010)
DGDG	+	$[M + NH_4]^+$	Neutral loss of 341	Moreau et al. (2008)
DGTA	+	$[M + H]^+$	Precursors of *m/z* 236; neutral loss of 59; no neutral loss of 87 as found for DGTS	Armada et al. (2013)
Neutral glycerolipids				
Free FA	–	$[M - H]^-$		
DAG	+	$[M + NH_4]^+$	Scan of $[M+NH_4\text{-}RCOONH_4]^+$	Camera et al. (2010)
TAG	+	$[M + NH_4]^+$	Scan of $[M+NH_4\text{-}RCOONH_4]^+$	Hsu and Turk (2010)

indicates (1) that the FA synthases of the chloroplast produce 14:0, 16:0, and 18:0 species, (2) that the acyl-ACP Δ9-desaturase is mainly active on 16:0 rather than on 18:0, and (3) that the plastid glycerol-3-phosphate acyltransferase (an enzyme called ATS1 in plants) may have a lower affinity for C18 substrates than plant ATS1. The relative availability of acyl-ACP substrates (C16, C18, and C20 molecular species) also might be an important determinant, as it was recently reported that the level of C18 FA increased in MGDG when shifting the growth temperature from 20°C to 30°C, a condition known to lower 20:5 biosynthesis (Dodson et al., 2014).

PE, PC, and DGTA, which are likely synthesized in extraplastidic membranes, also contain C16 species at the *sn*-2 position, together with C18 and C20 FAs. The occurrence of a C16 FA at the *sn*-2 position in this lipid is consistent with two hypotheses: either an export of a prokaryotic diacylglycerol backbone or the fact that the microsomal LPAAT has no selectivity for FA molecular species, by contrast with the plastid LPAAT. Thus, in *P. tricornutum*, no specific signature could be determined for a potential eukaryotic pathway providing diacyl precursors to plastid lipids, as defined, respectively, in Arabidopsis and other microalgae such as *C. reinhardtii* (Fan et al., 2011). A similar unbiased chain-length incorporation at the *sn*-2 position in *P. tricornutum* has also been observed in some chlorophytes such as *Dunaliella bardawil* (Davidi et al., 2014), despite their distant lineages. In addition, PE, PC, and DGTA retained most of the C18 present in the cells. It is also noteworthy that we

Table II. *Conditions for the regiochemical assignment of FAs at sn-1, sn-2, and sn-3 positions in glycerolipids from P. tricornutum*

Analyzed Lipids	Polarity	Ion Analyzed	MS2 Fragment Properties	References
Phospholipids				
PC	+	$[M + H]^+$	$[M+H\text{-}R_2CH = C = O]^+ > [M+H\text{-}R_1CH = C = O]^+$	Hsu and Turk (2003)
PE	–	$[M - H]^-$	$[R_2COO]^- > [R_1COO]^-$	Hsu and Turk (2000a)
PG	–	$[M - H]^-$	$[M\text{-}H\text{-}R_2COOH]^- > [M\text{-}H\text{-}R_1COOH]^-$	Hsu and Turk (2001)
PI	–	$[M - H]^-$	$M\text{-}H\text{-}R_2COOH]^- > [M\text{-}H\text{-}R_1COOH]^-$	Hsu and Turk (2000b)
Nonphosphorus glycerolipids				
SQDG	–	$[M - H]^-$	$[M\text{-}H\text{-}R_1COOH]^- > [M\text{-}H\text{-}R_2COOH]^-$	Zianni et al. (2013)
ASQ	–	$[M - H]^-$	$[M\text{-}H\text{-}R_1COOH]^- > [M\text{-}H\text{-}R_2COOH]^-$	Naumann et al. (2011)
MGDG	+	$[M + Na]^+$	$[M+Na\text{-}R_1COO^-]^+ > [M+Na\text{-}R_2COO^-]^+$	Guella et al. (2003)
DGDG	+	$[M + Na]^+$	$[M+Na\text{-}R_1COO^-]^+ > [M+Na\text{-}R_2COO^-]^+$	Guella et al. (2003))
DGTA	+	$[M + H]^+$	$[M+H\text{-}R_2COOH]^+ > [M+H\text{-}R_1COOH]^+$	By analogy with phospholipid diacylglycerol moiety
Nonpolar glycerolipids				
DAG	+	$[M + NH_4]^+$	$[M+NH_4\text{-}R_1COONH_4]^+ > [M+NH_4\text{-}R_1COONH_4]^+$	Camera et al. (2010)
TAG	+	$[M + NH_4]^+$	$[M+NH_4\text{-}R_{1/3}COO^-]^+ > [M+ NH_4\text{-}R_2COO^-]^+$	Hsu and Turk (2010)

Table III. *Positional distribution of FAs, and molecular species found in each glycerolipid class*

Only molecules that represent more than 5% of all the species present in the class are indicated. The asterisk indicates where the *sn*-1 and *sn*-2 positions could not be discriminated. Major molecular species of a given lipid class are shown in bold characters.

sn-1/*sn*-2	MGDG	DGDG	SQDG	ASQ	PG	PC	DGTA	PE	PI	DAG	TAG
14:0/16:0			6.9	6							
14:0/16:1			16.5	13.2						14.5	
16:0/16:0			4.6								
16:1/16:0	5.2	8.7	**23.9**	8.2	**31.7**				**100**	**54.8***	
16:1/16:1	6.6	14.1			4.9	5.2	5.1			**30.8**	
16:1/16:2		5.4									
16:1/16:3	7.9										
16:1/18:1	5.4										
16:1/24:0			9.7								
16:2/16:0			9.6								
16:2/16:3	10.5										
18:0/16:3	7.7										
18:2/18:2						5.2					
20:5/14:0				12.7							
20:5/16:0		6.6	9.4	**53.5**	11.2	6.9					
20:5/16:1		16.1			**48.5**	12.1	**13**	11.3			
20:5/16:2	5.1	**34.3**				5	5.2	6.4			
20:5/16:3	**19.1**	7.3									
20:5/16:4	7.4										
20:5/18:2							7	7.8			
20:5/18:3						7	4.9	5.6			
20:5/18:4							5.7	6.2			
20:5/20:4						7.2		9.2			
20:5/20:5						**20.1**	**11.1**	**24**			
sn-1/*sn*-2/*sn*-3											
14:0/16:1/16:1											6.5
14:0/16:1/16:0											9.3
16:1/16:1/16:1											11
16:1/16:1/16:0											**23.5**
16:1/16:0/16:0											**16**
16:1/16:0/20:5											5

found only one species of phosphatidylinositide (PI), with a 16:1/16:0 scaffold, suggesting a peculiar role for this phospholipid. PG showed two major species, 20:5/16:1 and 16:1/16:0, always with a C16 at position *sn*-2. It was reported previously that 16:1 at the *sn*-1 position was 16:1 (*ω*-7) (cis-desaturation in *ω*-7 or Δ-9 position) and 16:1 at the *sn*-2 position was 16:1(*ω*-13)t (trans-desaturation at position *ω*-13; Arao et al., 1987). Because the C16 trans-isomer is found only in chloroplast PG, it is likely that the 20:5/16:1 PG is located in plastids and that the 16:1/16:0 PG, similar to PI, is an extraplastidic PG species.

We also found that acyl-SQDG always harbors a 20:5 linked to its polar head, with the same diacylglycerol backbones as those found in SQDG species but with a highly dissimilar distribution. The main species of 20:5 acyl-SQDG was 20:5/16:0, and the corresponding SQDG substrate represented only 10% of its own class of lipid. Assuming that acylation occurs on SQDG (Riekhof et al., 2003), this observation suggests that it should be quite specific for the molecular species 20:5/16:0.

Concerning nonpolar lipids, the DAG pool is mainly constituted of three different molecular species, dominated by 16:1/16:0 and 16:1/16:1, with a lower amount of 14:0/16:1. Although minor amounts of C18 and C20 were detected in DAG by gas chromatography analysis (Fig. 5), these FAs were not detected by MS analyses, indicating that DAG species having a C18 or C20 were minor and could not be discriminated from the background. The DAG acyl composition (Table III) does not reflect the composition found in the main membrane lipids, in support of a de novo synthesis rather than a recycling of the diacylglycerol backbone from membrane lipids. These DAG molecular species are clearly at the origin of the TAG pool, also dominated by 16:0 and 16:1, with lower amounts of 14:0 and some 20:5 at position *sn*-3 (or *sn*-1). The proportion of TAG among other glycerolipids was low, reflecting the absence of any nutrient limitation.

Based on our structural determination of glycerolipid classes, we thus generated a reference profile for glycerolipids in *P. tricornutum* grown in nutrient-replete conditions. Based on this, we then assessed the variation of the glycerolipidome in nutrient-limited cells.

Impact of N and P Shortage on the Glycerolipid Content of *P. tricornutum* Pt1

We analyzed the glycerolipid profile in *P. tricornutum* Pt1 cells after 5 d of N starvation and 13 d of P starvation:

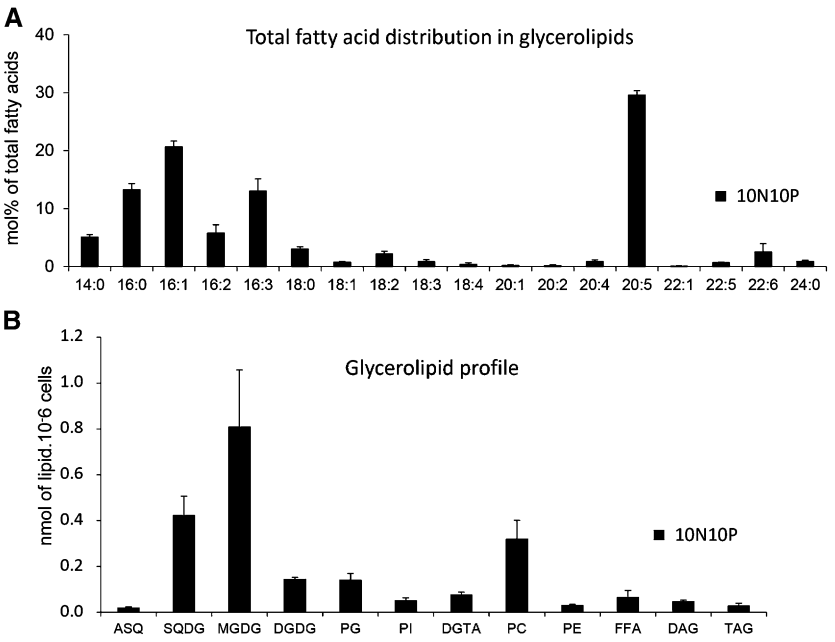

Figure 4. Quantitative analysis of *P. tricornutum* glycerolipids. Lipids from Pt1 cells grown in a replete medium (10N10P) were extracted, separated by TLC, and analyzed as described in "Materials and Methods." A, Global FA profile in a total lipid extract. FA proportions are given in percentages. B, Quantitative analysis of the various glycerolipids identified after TLC separation. Glycerolipids are expressed in nmol 10^{-6} cells and not as the summed FA content in each class. Each result is the average of three biological replicates ± SD. ASQ, 20:5-Acyl-SQDG; FFA, free FAs.

that is, when strong impacts on both the photosynthetic capacity (based on the F_v/F_m ratio) and the nonpolar lipid content (based on Nile Red staining) could be observed (Figs. 1 and 2). Figure 6A shows the glycerolipid profile in the three contexts: control (10N10P), N oligotrophic (0N10P), and P oligotrophic (10N0P). We observed the following trends. (1) A considerable increase of TAG content, on a per cell basis, was observed in both N- and P-limiting conditions, reaching 40 and 60%, respectively, of the total glycerolipid content (i.e. a 45-fold and a 100-fold increase when compared with control conditions). (2) The MGDG content decreased in both conditions. This decrease was more pronounced in the case of N shortage, whereas the levels of the other membrane lipids remained almost unchanged, except for PG, which also decreased by a factor of 2. (3) A total disappearance of the phospholipids was observed in the P-starved condition, including the major phospholipids PC and PG, coinciding with a strong increase of DGTA and slight increases of DGDG and SQDG.

The nature and amounts of FA, measured as a whole (Fig. 6B), were also affected by nutrient limitation, with marked increases of 16:0 and 16:1 and a smaller albeit significant increase of 14:0, in support of an induced FA neosynthesis. Interestingly, the total amount of 20:5, the dominant FA in the control condition, remained almost unchanged. Thus, in the nutrient-limiting conditions, the dominant FA is no longer 20:5 but 16:1. Generally speaking, with the notable exception of TAG, the FA composition remained unchanged in the different glycerolipids (data not shown). A specific focus on TAG (Fig. 6C) indicated that not only 14:0, 16:0, and 16:1 but also 20:5 increased. In fact, the proportion of 20:5 in this class of lipids increased from about 1% in the control conditions to 8% in the N-starved and 6% in the P-starved conditions, suggesting a specific enrichment of 20:5 in TAG. MS analysis indicated that 20:5, as observed in control cells, was esterified at the *sn*-3 (or *sn*-1) position, indicating that this FA had been incorporated during the latter phases of TAG biosynthesis.

In order to better understand the origin of these FAs accumulating in TAGs, we measured the amount of 16:1 and 20:5 in each glycerolipid (Fig. 7A). The level of 16:1 remained approximately constant in all glycerolipids except in TAG, indicating that the observed increase of 16:1 (Fig. 6B) was mainly, if not only, correlated to the increase of TAG synthesis and reflected FA neosynthesis. In the N-starved condition, the level of 20:5 increased in TAG and decreased in MGDG by about the same amount (Fig. 7B). Because it almost remained constant in the other glycerolipids, this result suggests a 20:5 transfer from MGDG to TAG, as observed previously in *N. graditana* (Simionato et al., 2013) and *C. reinhardtii* (Fan et al., 2011).

In the P-limiting conditions, the situation was more complex. A stronger increase of 20:5 was observed in the TAG pool, together with a smaller decrease in the MGDG pool than was observed in N-starved cells. No phospholipid, containing initially a high proportion of 20:5, could be detected. Recycling of phospholipid FAs, therefore, also could contribute to the 20:5 enrichment of TAG. Furthermore, an increase of SQDG and DGTA was observed (Fig. 6A), consistent with (1) a PG replacement by SQDG in the plastid and (2) a possible recycling of the PC diacylglycerol moiety into DGTA, taking place in an extraplastidic membrane. This hypothesis is based on the strong increase of 20:5 in DGTA, likely reflecting the quantitative increase of the DGTA pool (Fig. 6A) rather than a specific 20:5 enrichment, because the global FA composition remained largely unaffected.

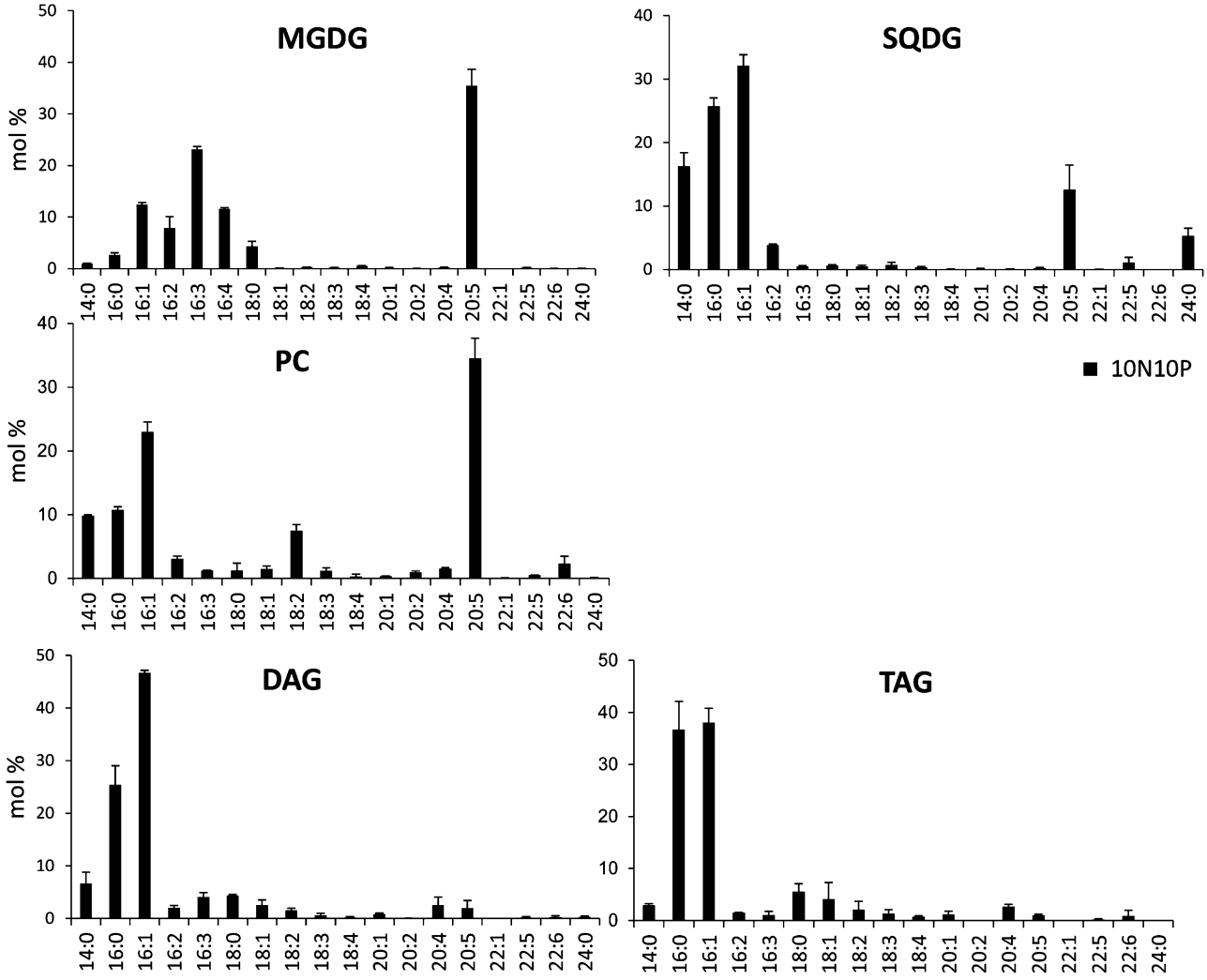

Figure 5. Molar profiles of FAs in PC, DAG, TAG, MGDG, and SQDG. Lipids from Pt1 cells grown in a replete medium (10N10P) were extracted, separated by TLC, and analyzed for their FAs as described in "Materials and Methods." Note that a cross contamination is possible between SQDG and PC due to the proximity of the TLC spots, leading to moderate enrichment of 20:5 in SQDG and 14:0 in PC. Each result is the average of three biological replicates ± SD.

DISCUSSION

A Reference Glycerolipid Profile for *P. tricornutum*

The glycerolipid composition of *P. tricornutum* presents a strong similarity with those reported for other photosynthetic unicellular eukaryotes (Dembitsky, 1996) but also specific differences. Besides the major lipids conserved in photosynthetic membranes (i.e. MGDG, DGDG, SQDG, and PG), we confirmed the presence of 2′-*O*-acylsulfoquinovosyldiacylglycerides (20:5-acyl-SQDG [ASQ]), largely dominated by the molecular species *sn*-1:20:5/*sn*-2:16:0/2′:20:5 (Naumann et al., 2011). The presence of ASQ has also been reported for *C. reinhardtii*, although 18:3 or 18:4 acyl groups were the FAs involved in the 2′-acylation of the sulfoquinovose moiety (Riekhof et al., 2003). To date, there is no evidence for a physiological or biochemical role of ASQ. The large proportion of SQDG also suggests that this lipid might not be restricted to chloroplast membranes; therefore, the subcellular localization of SQDG and ASQ should be assessed in the future.

Notwithstanding, an *SQD1 C. reinhardtii* mutant, lacking SQDG and ASQ, was clearly impaired in its photosynthetic capacities and in its response to inorganic phosphate deficiency, indicating altered membrane properties and an inability to adjust its membrane composition to adapt to environmental change (Riekhof et al., 2003). These experiments did not reveal any specific role of ASQ versus SQDG, but the results presented here indicate that, if SQDG is the precursor of ASQ, as postulated previously (Riekhof et al., 2003), this acylation process is quite specific for one minor SQDG species, *sn*-1:20:5/*sn*-2:16:0, representing less than 10% of the total SQDG. Such specificity in the acylation process suggests the existence of a specific role for ASQ.

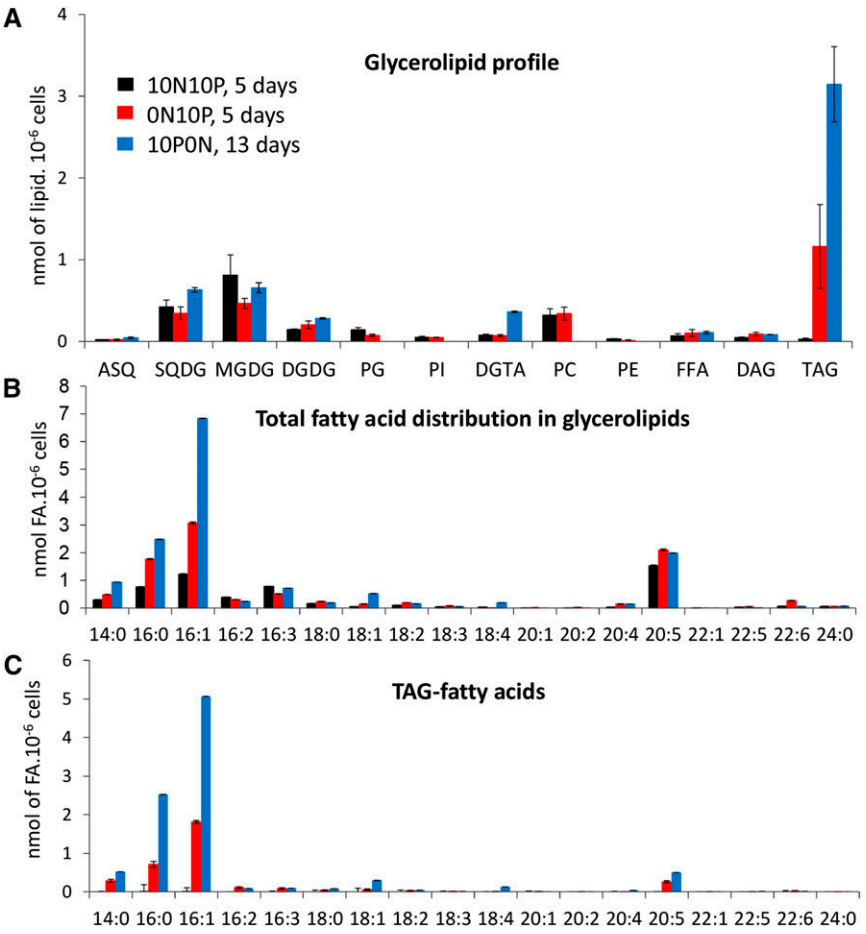

Figure 6. Quantitative analysis of FAs and glycerolipids in *P. tricornutum* grown in nutrient-replete conditions or in medium devoid of either N or P. Lipids from Pt1 cells grown either in a replete medium (10N10P; black) or in medium deprived of N (0N10P; blue) or P (10N0P; red) were extracted, separated by TLC, and quantified as described in "Materials and Methods." To avoid any N deficiency in 10N10P or 10N0P culture, media were replaced by fresh ESAW 10N10P or 10N0P medium every 3 d. Lipids were analyzed after 5 d of cultivation in replete conditions (black bars), N starvation (red bars), or after 13 d for P starvation (blue bars). A, Changes in glycerolipid content. Note that in the P-depleted condition, phospholipids were not detectable. B, Changes in FA content. C, FA profile in TAG. Each result is the average of three biological replicates ± SD. ASQ, Acyl-SQDG; FFA, free FAs.

Based on sequence similarity, we identified gene candidates for a plastid-localized synthesis of glycerolipids: a putative chloroplast glycerol-3-phosphate acyltransferase (ATS1 homolog; Phatr_3262), a chloroplast 1-acyl-*sn*-glycerol-3-phosphate acyltransferase (ATS2 homolog; Phat_43099), three MGDG synthase isoforms (three monogalactosyldiacyl homologs; Phatr_14125, Phatr_54168, and Phatr_9619), three DGDG synthase isoforms (three digalactosyldiacyl homologs; Phatr_12884, Phatr_11390, and Phatr_43116), a UDP-sulfoquinovose synthase (SQD1; Phatr_21201), and two SQDG synthase isoforms (two SQD2 homologs; Phatr_50356 and Phatr_42467). One or both of these SQD2 homologs also could be involved in the synthesis of ASQ.

The results obtained in this study indicate that FAs are synthesized in the stroma of chloroplasts by type II FA synthases, mainly as 14:0-, 16:0-, and 18:0-ACP. The presence of the saturated form of C18 in plastid lipids (i.e. 18:0) and the position of desaturation of $16:3^{\Delta 6,9,12}$ in MGDG (Domergue et al., 2003) suggest that the plastid Δ9-acyl-ACP desaturation might operate only on 16:0-ACP, releasing 16:1(ω-7)-ACP.

In plants, there are two pools of PG: one localized in the plastid, with a prokaryotic diacylglycerol backbone and a specific FA at the *sn*-2 position, 16:1(ω-13)t; and one in microsomal membranes and mitochondria, with a so-called eukaryotic diacylglycerol backbone assembled in the ER. In Arabidopsis, two enzymes are thus responsible for PG synthesis: Phosphatidylglycerophosphate synthase1 (PGP1), localized in both chloroplast and mitochondria (Babiychuk et al., 2003), and PGP2, localized in the ER (Müller and Frentzen, 2001). By studying *pgp* mutants, it was established that the PGP1-dependent pathway was responsible for 70% of PG synthesis in leaves and was required for the development of green leaves and chloroplasts with well-developed thylakoid membranes (Hagio et al., 2002; Xu et al., 2002), whereas the *pgp*2 mutant showed a small decrease in PG content compensated by a slight increase in PI content (Tanoue et al., 2014). Based on the facts that PG and PI biosynthesis pathways share their precursors (i.e. phosphatidic acid and cytidine diphosphate-diacylglycerol [CDP-DAG]) and that PGP2, the PI synthase, and the extraplastidic CDP-DAG synthases are all localized in the ER (Löfke et al., 2008; Zhou et al., 2013), the accumulation of PI in the Arabidopsis *pgp*2 mutant is consistent with an accumulation of CDP-DAG. In *P. tricornutum*, we found only two species of PG, the 20:5/16:1 form, which is probably plastidic with 16:1(ω-13)t at the *sn*-2 position, and the 16:1/16:0 form, which we expect to be extraplastidic, having exactly the same composition as PI. Together, these results suggest that the extraplastidic CDP-DAG synthase

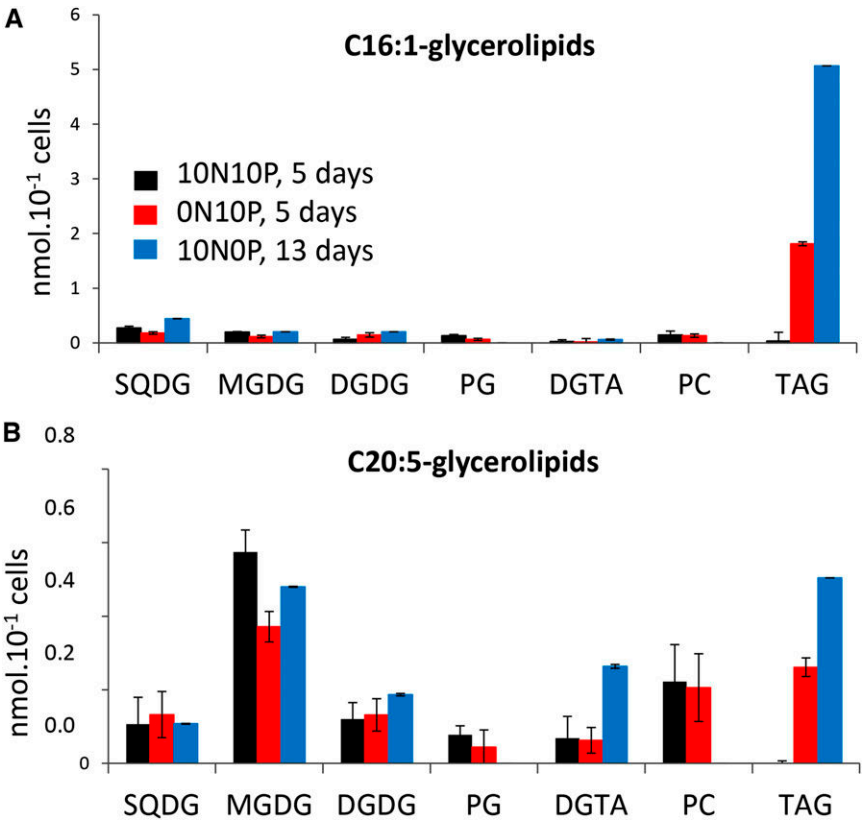

Figure 7. Distribution of 16:1 and 25:0 FAs in the glycerolipid classes of *P. tricornutum* grown in nutrient-replete conditions or in medium devoid of either N or P. Lipids from Pt1 cells grown in a replete medium (10N10P) were extracted, separated by TLC, and quantified as described in "Materials and Methods." Lipids were analyzed after 5 d of cultivation in replete condition (black bars), N starvation (red bars), or after 13 d of P starvation (blue bars). A, Quantitative distribution of 16:1 in the major glycerolipid classes. B, Quantitative distribution of 25:0 in the major glycerolipid classes. Each result is the average of three biological repeats ± SD.

is highly specific for a 16:1/16:0 substrate. Furthermore, the conservation of 16:0 at the *sn*-2 position in extraplastidic PG and PI in different algae species (Araki et al., 1987; Giroud et al., 1988; Liang et al., 2014) differs strikingly from the eukaryotic route observed in plants.

The preservation of the medium-chain FA in PI and extraplastidic PG might be important for their biological function. This result further supports either the absence of any FA selectivity of the extraplastidic LPAAT as being the basis of the plant eukaryotic signature or an export of the prokaryotic diacylglycerol backbone, as suggested in *C. reinhardtii* (Fan et al., 2011). In the *P. tricornutum* genome, two putative CDP-DAG synthases can be predicted (Phatr_559 and Phatr_7678), and future functional studies should help to ascertain whether one is specific for the production of PG/PI precursors.

In addition to the classical phospholipids that make up the bulk of nonphotosynthetic membranes, we report the presence of DGTA, a betaine glycerolipid never observed previously in *P. tricornutum*. BL have been detected in numerous algae (comprehensively reviewed by Dembitsky [1996]). Both DGTA and DGTS are usually associated with nonplastid membrane compartments (Künzler et al., 1997) and have structural similarities to PC (Sato and Murata, 1991). Therefore, we can speculate that DGTA might be more abundant in the endomembrane system and may be present in the outermost of the four membranes of the chloroplast, connected to the nuclear envelope. We identified a candidate gene that might be involved in BL synthesis, Phatr_42872, whose role should be assessed in the future based on functional genomics approaches.

Concerning FAs, eicopentaenoic acid (20:5) is the major molecular species, found in all membrane lipids of *P. tricornutum*. It is also a major FA in numerous microalgae, such as *Porphyridium cruentum* (Khozin et al., 1997), *N. gaditana* (Simionato et al., 2013), *Monodus subterraneus* (Khozin-Goldberg et al., 2002), and *Chromera velia* (Botté et al., 2011). This polyunsaturated very-long-chain FA is usually synthesized in the ER (Khozin et al., 1997) following complex desaturation and elongation processes (for review, see Petroutsos et al., 2014). The synthesis of 20:5 in the ER has not been unambiguously demonstrated in *P. tricornutum*. Nevertheless, the two front-end desaturases involved in this pathway, the Δ6 and Δ5 desaturases (Phatr_2948 and Phatr_46830, respectively), do not contain any predicted signal peptide and plastid-like transit sequence that could be involved in a targeting to the chloroplast. The synthesis of 20:5, therefore, is very likely to occur outside chloroplasts in *P. tricornutum* as well. The dominant species of MGDG in *M. subterraneus* (Khozin-Goldberg et al., 2002) and *P. cruentum* (Khozin et al., 1997) are 20:5/20:5. In these organisms, it was proposed that PE and PC were, respectively, donors for the DAG moiety responsible for these eukaryotic-like MGDG species. In *P. tricornutum*, however, all MGDG species having a 20:5 FA at the *sn*-1 position have a C16 at the *sn*-2 position, displaying a prokaryotic signature. Therefore, the acyl position in *P. tricornutum* MGDG supports a different

scenario from that documented for Arabidopsis eukaryotic MGDG: once synthesized in cytosolic membranes, 20:5 has to be released from a phospholipid into the cytosolic acyl-CoA pool and then transported into the chloroplasts to be attached to the glycerol-3-phosphate at the *sn*-1 position by the first acyltransferase, ATS1. We denoted this unique route, misleadingly thought to correspond to the plant eukaryotic pathway, the omega pathway (Petroutsos et al., 2014). The precise details and the enzymes and transporters involved in these events remain to be characterized.

The question of the putative existence of a eukaryotic pathway with a recycling of an intact diacylglycerol backbone coming from phospholipid for galactolipid synthesis, as described in higher plants, remains unsolved. Indeed, there is no visible signature for the eukaryotic pathway to follow, the typical eukaryotic 20:5/20:5 backbone found in extraplastidic glycerolipids (i.e. PC, PE, and DGTA) and described in other algae (Khozin et al., 1997; Khozin-Goldberg et al., 2002) being absent in plastid glycoglycerolipids. Since PC harbors a high proportion of C16 at the *sn*-2 position, we cannot exclude that some MGDG species could result from the galactosylation of a diacylglycerol backbone with this signature. However, considering that C18 is almost absent from galactoglycerolipids, this pathway should operate a sorting of diacyl molecular species, excluding PC with a C18 at position *sn*-2.

Remodeling of Membrane Glycerolipids in N- and P-Limiting Conditions

Based on our reference glycerolipid profile in a replete medium, we could compare the variations of the membrane lipid distribution occurring upon N or P starvation and attempt to deduce some likely remodeling scenarios. N shortage induces visible effects over a shorter time scale (3–4 d) compared with P shortage (8–13 d, depending on the initial level of this nutrient). This feature has been observed for all the Pt accessions examined here. Based on our observations, N limitation seems to trigger a serious and rapid stress response, presumably related to the need for protein synthesis, whereas more sophisticated lipid-remodeling systems seem to be operative during P limitation, perhaps as an adaptive response. This difference is also reflected at the level of photosynthesis; based on the F_v/F_m ratio, photosynthesis was apparently affected more rapidly in low-N than in low-P conditions.

Considering membrane glycerolipids, N deprivation has no effect on the level of N-containing lipids such as PC, PE, and DGTA. As in Arabidopsis, N-containing lipids are not a form of N storage (Gaude et al., 2007), in contrast with phospholipids, which are clearly a biochemical parameter tuned by photosynthetic organisms. The only significant changes we observed were a relative decrease of the proportion of MGDG and an increase in DGDG, leading to a diminished MGDG-DGDG ratio, a lipid change that also has been observed in Arabidopsis upon N shortage (Gaude et al., 2007). The physiological significance of this phenomenon is unknown, but a reduced MGDG-DGDG ratio is often observed in chloroplasts with impaired photosynthesis (Boudière et al., 2014). We could also detect a slight decrease in the proportion of PG, possibly reflecting senescence of the thylakoid membranes.

Following P deprivation, all phospholipids, including PC and PG, were completely undetectable, compensated by an increase of nonphosphorus lipids synthesized in endomembranes (indicated by a 5-fold-increase of DGTA) and in the plastid (indicated by a 2-fold increase of DGDG and a 1.5-fold increase of SQDG). The proportion of MGDG decreased by a factor of 1.5, but the overall proportion of galactoglycerolipids (MGDG and DGDG) increased. Similar observations have been made in higher plant cells (Jouhet et al., 2003), although the impact on phospholipids was not as dramatic as that recorded here. The best documented form of BL in the literature is DGTS, and, because it sometimes has an inverse concentration relationship with PC, it is thought to replace PC in extraplastidic membranes (Moore et al., 2001), as suggested for *C. reinhardtii*, which lacks PC (Riekhof et al., 2005, 2014), and further supported by the comparison of phytoplankton communities collected in P-rich and P-oligotrophic regions (Van Mooy et al., 2009). Consistent with this postulate, the increase of DGTA in the P-starved conditions reached a value that was about identical to that measured for PC in control cells, thus supporting that a PC-to-DGTA replacement occurred in extraplastidic membranes. In terms of lipid trafficking, no specific machinery would be required, since both DGTA and PC are likely synthesized in the same membrane system (i.e. the ER). It is also known that an increase of SQDG could compensate the absence of PG in plastids (Jouhet et al., 2010). Similarly, this remodeling would not require any massive lipid transport, since PG and SQDG are localized in the same membranes (i.e. thylakoids).

In plants, P deprivation induces an increase of galactolipid production, using a eukaryotic diacylglycerol moiety diverted from hydrolyzed phospholipids, and an export of DGDG from plastids to extraplastidic membranes, such as the plasma membrane, the tonoplast, and/or mitochondrial membranes (Andersson et al., 2003, 2005; Jouhet et al., 2004). First, based on our results, there is no evidence for a eukaryotic pathway in *P. tricornutum* as described in plants, but rather an omega pathway, which might participate in the recycling of the phospholipid hydrophobic moiety, possibly by free FA transfers. Second, in *P. tricornutum*, the plastid envelope contains four membranes, with the two outermost ones being derived from the ER. DGDG has never been found in the ER of higher plants, and this lipid is transferred toward mitochondria via contact sites, indicating that the ER is not involved in DGDG trafficking, at least for this interorganellar transfer (Jouhet et al., 2004). Similar physical links between the secondary plastid and the mitochondria might occur in *P. tricornutum*, since both organelles are very close (Prihoda et al., 2012). Third, the increase of

SQDG and DGTA could quantitatively compensate for the decrease of PG and PC, respectively. There is no obvious necessity for an export of DGDG toward extraplastidic membranes in the cells of *P. tricornutum* exposed to P limitation. It is possible, therefore, that an increase of DGDG, observed during both N and P limitation, might counteract the decrease of MGDG and contribute to the protection of photosynthetic membrane integrity.

In a recent report on the transcriptome changes occurring in *P. tricornutum* upon P shortage, transcripts for the ATS1 homolog (Phatr_3262), one of the MGDG synthase homologs (Phatr_54168), the two SQDG synthase isoforms (Phatr_50356 and Phatr_42467), and the putative gene involved in DGTA synthesis (Phatr_42872) were significantly up-regulated (Yang et al., 2014). Likewise, in the centric diatom *T. pseudonana*, genes coding two putative SQD1 homologs (gene identifiers 7445840 and 7452379) and two putative monogalactosyldiacyl homologs (gene identifiers 7447073 and 7445775) were found to be up-regulated in response to P limitation (Dyhrman et al., 2012). Therefore, the remodeling of lipids in diatoms seems to be transcriptionally controlled following, at least in part, the model dissected previously in plants, in which some of the genes encoding MGD, digalactosyldiacyl, and SQD2 isoforms (in Arabidopsis, MGD2, MGD3, DGD2, and SQD2; Misson et al., 2005) were shown to be specific to the P starvation response and activated by signaling cascades responding to low P. An in-depth study of the transcriptome of *P. tricornutum* cultivated in identical conditions to those used here will help identify all genes that are likely to be transcriptionally coordinated upstream of the observed remodeling and search for the corresponding cis-elements and transcriptional systems.

Accumulation of TAG in Conditions of N and P Starvation

All accessions of *P. tricornutum*, collected in various oceanic locations, showed an increase of TAG, albeit with some variations in the time scale and magnitude of accumulation of this class of nonpolar lipids. There was no apparent correlation between TAG accumulation and morphotype (triradiate, fusiform, or oval) or the initial geographic location. Pt10 and PtHK, which were both less sensitive to P shortage, were collected on the eastern coast of China, albeit at very distant sites, which could suggest an environmental impact on the physiology of these strains, perhaps with a higher capacity to store P. Interestingly, Pt4 was not able to accumulate large amounts of TAG in either N- or P-limiting conditions, which could suggest that it is affected in its ability to synthesize or store TAG. Pt4 was collected in the Baltic Sea, a relatively closed sea, but the long-term influence of this particular area on the physiological and metabolic behavior of these algae remains to be determined. Clearly, a genomic analysis of these strains is required to draw further conclusions.

P and N limitation affect both the lipid content and the photosynthetic capacities of Pt1 cells. Although N deprivation has a strong and almost immediate effect on cell division, it is important to note that P deprivation requires a much longer period to induce any visible effect. Diatoms, therefore, might struggle more with a lack of N than with a lack of P, possibly because of the existence of powerful P-storage systems within the cell, such as polyphosphate, a ubiquitous P polymer (Martin et al., 2014). N and P limitation will impact both the biosynthesis of proteins and the level of phosphorylated metabolites, which, in turn, will affect numerous metabolic functions, including growth and photosynthesis. However, oil accumulation depends on the availability of a carbon source (Fan et al., 2011), and this is in apparent contradiction with an increase of TAG concomitant with a decline of photosynthesis. In this study, this source of carbon possibly arises from the remaining photosynthetic activity and/or from stored carbohydrates (Li et al., 2011). Thus, it is likely that, in the case of a growth arrest linked to a mineral deficiency, the available carbon and energy unused for cell division and membrane expansion are diverted toward lipid biosynthesis and storage. This could be part of a cellular strategy to allow a better and quicker restart when environmental conditions become favorable again. Whether the arrest of cell division is an absolute requirement to trigger TAG accumulation is thus an important open question.

During both N and P shortages, we observed a significant increase in the neosynthesis of 16:0 and 16:1, which was mainly if not uniquely associated with the accumulation of TAG, whereas we observed only little change in the FA composition of the various glycerolipids, besides a 16:1 and 20:5 enrichment in TAG. This confirms previously published reports, in a variety of photosynthetic eukaryotes, showing that the accumulation of TAG triggered by a shortage of N originated mainly from FA neosynthesis (Simionato et al., 2013). Whatever the growth conditions, the small pool of DAG is constituted of three main species comprising only 14:0, 16:0, and 16:1 acyl groups, with 14:0 being less abundant than the others and always esterified at the *sn*-1 position, when present. Interestingly, the *sn*-1 and *sn*-2 positions in TAG completely mirror the DAG pool, and the *sn*-3 position is occupied by a 16:0 or 16:1 FA in 80% to 90% of the molecular species. These two FAs are also the main ones overproduced in nutrient-limiting growth conditions. Clearly, these data do not support any substantial recycling of DAG moieties deriving from membrane glycerolipids, by contrast with higher plants (Bates and Browse, 2012). Therefore, it is likely that TAGs are mostly synthesized via a route involving a diacylglycerol acyltransferase and de novo DAG and acyl-CoA synthesis (Kennedy pathway).

During both N and P limitation, TAGs were enriched in 20:5 at the *sn*-3 or *sn*-1 position, whereas the global level of 20:5 inside the cell was not affected. Since 20:5 is produced at the level of phospholipids in nonplastid membranes, it has to be transferred to TAG, most likely via the acyl-CoA pool or via a phosphatidyl diacylglycerol acyltransferase. In the N-deprived condition, it was striking to observe that the increase of 20:5 in TAG,

on a per cell basis, roughly corresponds to the decrease of 20:5 in MGDG, suggesting that MGDG also could contribute to TAG synthesis, as described in *N. graditana* (Simionato et al., 2013) and *C. reinhardtii* (Fan et al., 2011; Li et al., 2012). Based on this mechanism, the eicopentaenoic acid released in the acyl-CoA pool following the degradation of MGDG (or other membrane lipids such as phospholipids) should be recycled mainly into other glycerolipids such as TAG, rather than oxidized through the β-oxidation pathway.

CONCLUSION

The overall goal of this work was first to define a reference for the glycerolipidome of *P. tricornutum*, with MGDG, DGDG, SQDG, and PG as conserved lipids in photosynthetic membranes and PC and DGTA as major lipids in extraplastidic membranes. We also detected the presence of ASQ. Based on this reference, we could deduce that the FAs were most likely synthesized de novo in the stroma of chloroplasts as 14:0-, 16:0-, and 18:0-ACP species. We identified only one gene candidate coding for a putative palmitoyl-ACP Δ9-desaturase (Phatr_9316). When exported to the cytosol, FAs can be elongated and desaturated to generate 20:5. Acyl-ACP can be used in the plastid for the production of MGDG, DGDG, SQDG, and part of PG via a canonical prokaryotic pathway, and acyl-CoA can be used in the cytosol and endomembranes to generate PC, DGTA, or TAG. We could identify gene candidates coding for putative enzymes involved in these pathways. Extraplastidic PG and PI seem to share a common CDP-DAG precursor with a 16:1/16:0 signature. We could not detect any specific signature for an extraplastidic eukaryotic pathway as in plants and could not assess the possibility of the import of eukaryotic precursors inside the chloroplast. Rather, the plastid lipid profiles we obtained would be consistent with an import of 20:5 FAs, hydrolyzed from extraplastidic phospholipids, to serve as precursors for plastid acyltransferases, eventually producing MGDG, DGDG, and SQDG. We called this pathway the omega pathway, and future challenges include the deciphering of the machinery importing 20:5 FA into the chloroplast.

We compared the remodeling triggered by the deprivation of two major nutrients fluctuating in the oceans, N and P. On the one hand, N oligotrophy is apparently a severe stress for *P. tricornutum*, triggering a rapid senescence of chloroplast membranes, an arrest of cell division, and an accumulation of TAG. By contrast, a complex adaptation to P deprivation is observed, with a first phase of consumption of specific P-storage forms, most likely polyphosphate, followed by a breakdown of phospholipids, behaving like a secondary form of P storage, and their replacement by nonphosphorous lipids, most likely following PG-to-SQDG and PC-to-DGTA replacements. A phospholipid-to-DGDG replacement cannot be ruled out in some of the membranes limiting the chloroplast, but this has to be confirmed.

Future work should entail the characterization of the enzyme isoforms and the machineries for lipid synthesis, lipid breakdown, and lipid trafficking involved in the lipid changes described here and the systems controlling them. A survey of transcriptome variations occurring in *P. tricornutum* or *T. pseudonana* supports a transcriptional control, which should be studied further in the future. The task is as complex as that in plants, since some pathways, like the omega pathway, are apparently specific to chromalveolates, and their components cannot be deduced from previous studies. Nevertheless, the possibility to perform large-scale omics studies and to characterize the function of gene products is among the advantages of the *P. tricornutum* model. Future work starting with the gene candidates listed here will hopefully help to unravel the adaptive system of this diatom to cope with a fluctuating environment.

MATERIALS AND METHODS

Strains and Culture Conditions

Phaeodactylum tricornutum strains were obtained from the culture collections of the Pravosali-Guillard National Center for Culture of Marine Phytoplankton (CCMP) and the Culture Collection of Algae and Protozoa (CCAP), using axenic accessions characterized by De Martino et al. (2007): Pt1, CCAP 1055/3; Pt2, CCMP2558; Pt3, CCMP2559; Pt4, CCAP 1055/2; Pt5, CCMP630, Pt6 (fusiform), CCAP 1054/4; Pt7, CCAP 1055/6; Pt8, CCAP 1055/7; Pt9, CCAP 1055/5; Pt10, CCAP 1055/8. We completed this series of accessions with the fully sequenced reference strain for *P. tricornutum*, derived from Pt1, Pt1.8.6 (Bowler et al., 2008; CCAP1055/1), and with an axenic strain isolated in Hong Kong, PtHK. Cells were maintained and grown in enriched seawater, artificial water (ESAW) medium, as described by Falciatore et al. (2000). The different cell shapes described here are those of algae grown and maintained in artificial medium. In the preliminary comparative study of Pt1 to Pt10 ecotypes by microscopic imaging, cells were grown either in the presence of 0.55 mM N and 0.0224 mM P or in the absence of one or both of these nutrients. Cultures were grown in exponential phase in 50-mL single-use flasks with 100 rpm shaking, an irradiance of 100 μmol photons m^{-2} s^{-1}, and a 12-h-light/12-h-dark photoperiod at 19°C.

For the Nile Red measurements, 50-mL cultures were grown in exponential phase before being centrifuged at 1,500*g* for 30 min and suspended in 10 mL of replete or deficient medium. Initial cell densities for P-deficient and N-deficient experiments were 10^4 and 10^5 cells mL^{-1}, respectively. In the in-depth analysis performed on the Pt1 strain, cells were grown in batch conditions in 250-mL flasks containing 50 mL of ESAW medium with or without N or P. Replete conditions consisted of 5.5 mM N and 0.22 mM P, in order to avoid nutrient exhaustion in the batch culture over the observation period and to increase the contrast in the analyzed lipid profiles between nutrient-rich and -depleted conditions. Cells were cultivated in an artificial climate incubator, with 100 rpm shaking, under an irradiance of 40 μmol photons m^{-2} s^{-1} and with a 12-h-light/12-h-dark photoperiod at 19°C. The initial inoculum was 0.5 to 1.1^6 cells mL^{-1}. Cells were collected after 5 or 13 d and counted with a Malassez chamber using an aliquot fraction before any further manipulations.

Chlorophyll Fluorescence Measurements

The parameter F_v/F_m was used as an indicator of PSII activity in a dark-adapted state. For this, in vivo chlorophyll fluorescence was determined using a Speedzen MX fluorescence imaging setup (JBeamBio). Excitation was done in the blue range (λ = 450 nm) using short pulses (10 μs). Emission was measured in the near far red. Saturating pulses (duration of 250 ms) were provided by a green (λ = 520 nm) light-emitting diode array. Measurements were done 15 min after dark adaptation of the samples.

The variable fluorescence (F_v) was calculated as $F_v = F_m - F_o$, where F_m is the maximum fluorescence in the dark-adapted state and F_o is the minimal fluorescence in the dark-adapted state (Genty et al., 1990).

Nile Red Staining of Nonpolar Lipids

Accumulation of nonpolar lipids and oil droplets was monitored by Nile Red (Sigma-Aldrich) fluorescent staining (excitation wavelength at 532 nm and emission at 565 nm), as described previously (Cooksey et al., 1987). In brief, 200 μL of culture was stained with 50 μL of a Nile Red stock solution (2.5 μg mL^{-1} in dimethyl sulfoxide), and fluorescence was measured by flow cytometry using a Partec Cube8 device equipped with a 532-nm green laser. When the number of cells was estimated, specific fluorescence was determined by dividing Nile Red fluorescence intensity by the number of cells.

Glycerolipid Extraction, Separation by TLC, and Analyses by GC-FID and MS

Glycerolipids were extracted from freeze-dried *P. tricornutum* cells grown in 50 mL of ESAW medium with variable initial supplies of P and/or N. First, cells were harvested by centrifugation and then immediately frozen in liquid N. Once freeze dried, the pellet was suspended in 4 mL of boiling ethanol for 5 min to prevent lipid degradation, and lipids were extracted according to Simionato et al. (2013) by the addition of 2 mL of methanol and 8 mL of chloroform at room temperature. The mixture was then saturated with argon and stirred for 1 h at room temperature. After filtration through glass wool, cell debris was rinsed with 3 mL of chloroform:methanol (2:1, v/v), and 5 mL of 1% (w/v) NaCl was then added to the filtrate to initiate biphase formation. The chloroform phase was dried under argon before solubilizing the lipid extract in pure chloroform.

Total glycerolipids were quantified from their FAs: in an aliquot fraction, a known quantity of 15:0 was added and the FAs present were transformed as FAMEs by a 1-h incubation in 3 mL of 2.5% (v/v) H_2SO_4 in pure methanol at 100°C (Jouhet et al., 2003). The reaction was stopped by the addition of 3 mL of water and 3 mL of hexane. The hexane phase was analyzed by a GC-FID (Perkin-Elmer) on a BPX70 (SGE) column. FAMEs were identified by comparison of their retention times with those of standards (Sigma-Aldrich) and quantified by the surface peak method using 15:0 for calibration. Extraction and quantification were performed at least three times.

To quantify the various classes of nonpolar and polar glycerolipids, lipids were separated by TLC onto glass-backed silica gel plates (Merck) using two distinct resolving systems (Simionato et al., 2013). To isolate nonpolar lipids including TAG and free FA, lipids were resolved by TLC run in one dimension with hexane:diethylether:acetic acid (70:30:1, v/v). To isolate membrane glycerolipids, lipids were resolved by two-dimensional TLC. The first solvent was chloroform:methanol:water (65:25:4, v/v) and the second was chloroform:acetone:methanol:acetic acid:water (50:20:10:10:5, v/v). Lipids were then visualized under UV light, after spraying with 2% (v/v) 8-anilino-1-naphthalenesulfonic acid in methanol, and scraped off the plate. No phosphatidylethanol could be detected after TLC or following MS analyses, indicating that the boiling ethanol treatment did not give rise to this category of glycerolipid derivative by nonspecific chemical reactions. Lipids were recovered from the silica powder after the addition of 1.35 mL of chloroform:methanol (1:2, v/v) thorough mixing, the addition of 0.45 mL of chloroform and 0.8 mL of water, and collection of the chloroform phase (Bligh and Dyer, 1959). Lipids were then dried under argon and either quantified by methanolysis and GC-FID as described above or analyzed by MS.

For MS analyses, purified lipid classes were dissolved in 10 mM ammonium acetate in pure methanol. They were introduced by direct infusion (electrospray ionization-MS) into a trap-type mass spectrometer (LTQ-XL; Thermo Scientific) and identified by comparison with standards. In these conditions, the produced ions were mainly present as H^-, H^+, NH_4^+, or Na^+ adducts. Lipids were identified by MS2 analysis with their precursor ion or by neutral loss analyses as indicated in Table I. All experiments were performed in triplicate.

Positional Distribution of FAs Esterified to Glycerolipids

The positions of FA molecular species esterified to the glycerol backbone of the various glycerolipids were determined based on MS2 analyses. Glycerol carbons were numbered following the stereospecific number (*sn*) nomenclature. Depending on the nature of the glycerolipid and the type of adduct, the substituents at the *sn*-1 (or *sn*-3) and *sn*-2 positions are differently cleaved when subjected to low-energy collision-induced dissociation. This is reflected in MS2 analyses by the preferential loss of one of the two FAs, leading to a dissymmetrical abundance of the collision fragments. The patterns of MS2 fragments for all glycerolipids have been described in previous studies (Table II), except for DGTA. In this study, we hypothesized that the loss of FAs in DGTA following low-energy collision-induced dissociation is similar to that observed for other polar lipids, such as PC.

Supplemental Data

The following supplemental materials are available.

Supplemental Figure S1. Growth, photosynthetic activity, and intracellular triacylglycerol content of Pt1 cells in 1N1P and 10N10P conditions.

Supplemental Figure S2. Growth, photosynthetic activity, and intracellular triacylglycerol content of Pt1 cells in 10N10P, 0N10P, and 10N0P conditions.

Supplemental Figure S3. General structure of glycerolipids.

Supplemental Figure S4. Structural analysis of ASQ.

ACKNOWLEDGMENTS

We thank Yahui Gao (Xiamen University), who kindly provided the PtHK strain isolated in Hong Kong Harbor in October 2010, and Catherine Cantrel (Institut de Biologie de l'École Normale Supérieure), Mathilde Cussac, Valérie Gros, and Guillaume Tourcier (Laboratoire de Physiologie Cellulaire et Végétale) for helpful technical support.

Received October 23, 2014; accepted December 5, 2014; published December 8, 2014.

LITERATURE CITED

Allen AE, Laroche J, Maheswari U, Lommer M, Schauer N, Lopez PJ, Finazzi G, Fernie AR, Bowler C (2008) Whole-cell response of the pennate diatom Phaeodactylum tricornutum to iron starvation. Proc Natl Acad Sci USA **105:** 10438–10443

Alonso DL, Belarbi EH, Fernández-Sevilla JM, Rodríguez-Ruiz J, Molina Grima E (2000) Acyl lipid composition variation related to culture age and nitrogen concentration in continuous culture of the microalga Phaeodactylum tricornutum. Phytochemistry **54:** 461–471

Andersson MX, Larsson KE, Tjellström H, Liljenberg C, Sandelius AS (2005) Phosphate-limited oat: the plasma membrane and the tonoplast as major targets for phospholipid-to-glycolipid replacement and stimulation of phospholipases in the plasma membrane. J Biol Chem **280:** 27578–27586

Andersson MX, Stridh MH, Larsson KE, Liljenberg C, Sandelius AS (2003) Phosphate-deficient oat replaces a major portion of the plasma membrane phospholipids with the galactolipid digalactosyldiacylglycerol. FEBS Lett **537:** 128–132

Araki S, Sakurai T, Kawaguchi A, Murata N (1987) Positional distribution of fatty acids in glycerolipids of the marine red alga, Porphyra yezoensis. Plant Cell Physiol **28:** 761–766

Arao T, Kawaguchi A, Yamada M (1987) Positional distribution of fatty acids in lipids of the marine diatom Phaeodactylum tricornutum. Phytochemistry **26:** 2573–2576

Armada I, Hachero-Cruzado I, Mazuelos N, Ríos JL, Manchado M, Cañavate JP (2013) Differences in betaine lipids and fatty acids between Pseudoisochrysis paradoxa VLP and Diacronema vlkianum VLP isolates (Haptophyta). Phytochemistry **95:** 224–233

Armbrust EV, Berges JA, Bowler C, Green BR, Martinez D, Putnam NH, Zhou S, Allen AE, Apt KE, Bechner M, et al (2004) The genome of the diatom Thalassiosira pseudonana: ecology, evolution, and metabolism. Science **306:** 79–86

Babiychuk E, Müller F, Eubel H, Braun HP, Frentzen M, Kushnir S (2003) Arabidopsis phosphatidylglycerophosphate synthase 1 is essential for chloroplast differentiation, but is dispensable for mitochondrial function. Plant J **33:** 899–909

Bates PD, Browse J (2012) The significance of different diacylgycerol synthesis pathways on plant oil composition and bioengineering. Front Plant Sci **3:** 147

Benning C, Ohta H (2005) Three enzyme systems for galactoglycerolipid biosynthesis are coordinately regulated in plants. J Biol Chem **280:** 2397–2400

Bligh EG, Dyer WJ (1959) A rapid method of total lipid extraction and purification. Can J Biochem Physiol **37:** 911–917

Botté CY, Yamaryo-Botté Y, Janouskovec J, Rupasinghe T, Keeling PJ, Crellin P, Coppel RL, Maréchal E, McConville MJ, McFadden GI (2011) Identification of plant-like galactolipids in Chromera velia, a photosynthetic relative of malaria parasites. J Biol Chem **286:** 29893–29903

Boudière L, Botté CY, Saidani N, Lajoie M, Marion J, Bréhélin L, Yamaryo-Botté Y, Satiat-Jeunemaître B, Breton C, Girard-Egrot A, et al (2012) Galvestine-1, a novel chemical probe for the study of the glycerolipid homeostasis system in plant cells. Mol Biosyst **8:** 2023–2035

Boudière L, Michaud M, Petroutsos D, Rébeillé F, Falconet D, Bastien O, Roy S, Finazzi G, Rolland N, Jouhet J, et al (2014) Glycerolipids in photosynthesis: composition, synthesis and trafficking. Biochim Biophys Acta **1837:** 470–480

Bowler C, Allen AE, Badger JH, Grimwood J, Jabbari K, Kuo A, Maheswari U, Martens C, Maumus F, Otillar RP, et al (2008) The Phaeodactylum genome reveals the evolutionary history of diatom genomes. Nature **456:** 239–244

Brighouse A, Dacks JB, Field MC (2010) Rab protein evolution and the history of the eukaryotic endomembrane system. Cell Mol Life Sci **67:** 3449–3465

Browse J, Warwick N, Somerville CR, Slack CR (1986) Fluxes through the prokaryotic and eukaryotic pathways of lipid synthesis in the '16:3' plant Arabidopsis thaliana. Biochem J **235:** 25–31

Brügger B, Erben G, Sandhoff R, Wieland FT, Lehmann WD (1997) Quantitative analysis of biological membrane lipids at the low picomole level by nano-electrospray ionization tandem mass spectrometry. Proc Natl Acad Sci USA **94:** 2339–2344

Camera E, Ludovici M, Galante M, Sinagra JL, Picardo M (2010) Comprehensive analysis of the major lipid classes in sebum by rapid resolution high-performance liquid chromatography and electrospray mass spectrometry. J Lipid Res **51:** 3377–3388

Chauton MS, Winge P, Brembu T, Vadstein O, Bones AM (2013) Gene regulation of carbon fixation, storage, and utilization in the diatom *Phaeodactylum tricornutum* acclimated to light/dark cycles. Plant Physiol **161:** 1034–1048

Cooksey KE, Guckert B, Williams SA, Callis PR (1987) Fluorometric determination of the neutral lipid content of microalgal cells using Nile Red. J Microbiol Methods **6:** 333–345

Davidi L, Shimoni E, Khozin-Goldberg I, Zamir A, Pick U (2014) Origin of β-carotene-rich plastoglobuli in *Dunaliella bardawil*. Plant Physiol **164:** 2139–2156

De Martino A, Meichenin A, Shi J, Pan K, Bowler C (2007) Genetic and phenotypic characterization of Phaeodactylum tricornutum (Bacillariophyceae) accessions. J Phycol **43:** 992–1009

Dembitsky VM (1996) Betaine ether-linked glycerolipids: chemistry and biology. Prog Lipid Res **35:** 1–51

Dodson VJ, Mouget JL, Dahmen JL, Leblond JD (2014) The long and short of it: temperature-dependent modifications of fatty acid chain length and unsaturation in the galactolipid profiles of the diatoms Haslea ostrearia and Phaeodactylum tricornutum. Hydrobiologia **727:** 95–107

Domergue F, Spiekermann P, Lerchl J, Beckmann C, Kilian O, Kroth PG, Boland W, Zähringer U, Heinz E (2003) New insight into *Phaeodactylum tricornutum* fatty acid metabolism: cloning and functional characterization of plastidial and microsomal Δ12-fatty acid desaturases. Plant Physiol **131:** 1648–1660

Domingues P, Amado FML, Santana-Marques MGO, Ferrer-Correia AJ (1998) Constant neutral loss scanning for the characterization of glycerol phosphatidylcholine phospholipids. J Am Soc Mass Spectrom **9:** 1189–1195

Dorrell RG, Smith AG (2011) Do red and green make brown? Perspectives on plastid acquisitions within chromalveolates. Eukaryot Cell **10:** 856–868

Dubots E, Audry M, Yamaryo Y, Bastien O, Ohta H, Breton C, Maréchal E, Block MA (2010) Activation of the chloroplast monogalactosyldiacylglycerol synthase MGD1 by phosphatidic acid and phosphatidylglycerol. J Biol Chem **285:** 6003–6011

Dubots E, Botté C, Boudière L, Yamaryo-Botté Y, Jouhet J, Maréchal E, Block MA (2012) Role of phosphatidic acid in plant galactolipid synthesis. Biochimie **94:** 86–93

Dyhrman ST, Jenkins BD, Rynearson TA, Saito MA, Mercier ML, Alexander H, Whitney LP, Drzewianowski A, Bulygin VV, Bertrand EM, et al (2012) The transcriptome and proteome of the diatom Thalassiosira pseudonana reveal a diverse phosphorus stress response. PLoS ONE **7:** e33768

Falciatore A, d'Alcalà MR, Croot P, Bowler C (2000) Perception of environmental signals by a marine diatom. Science **288:** 2363–2366

Fan J, Andre C, Xu C (2011) A chloroplast pathway for the de novo biosynthesis of triacylglycerol in Chlamydomonas reinhardtii. FEBS Lett **585:** 1985–1991

Frentzen M, Heinz E, McKeon TA, Stumpf PK (1983) Specificities and selectivities of glycerol-3-phosphate acyltransferase and monoacylglycerol-3-phosphate acyltransferase from pea and spinach chloroplasts. Eur J Biochem **129:** 629–636

Gage DA, Huang ZH, Benning C (1992) Comparison of sulfoquinovosyl diacylglycerol from spinach and the purple bacterium Rhodobacter spaeroides by fast atom bombardment tandem mass spectrometry. Lipids **27:** 632–636

Gaude N, Bréhélin C, Tischendorf G, Kessler F, Dörmann P (2007) Nitrogen deficiency in Arabidopsis affects galactolipid composition and gene expression and results in accumulation of fatty acid phytyl esters. Plant J **49:** 729–739

Genty B, Harbinson J, Briantais JM, Baker NR (1990) The relationship between non-photochemical quenching of chlorophyll fluorescence and the rate of photosystem 2 photochemistry in leaves. Photosynth Res **25:** 249–257

Giroud C, Gerber A, Eichenberger W (1988) Lipids of Chlamydomonas reinhardtii: analysis of molecular species and intracellular site(s) of biosynthesis. Plant Cell Physiol **29:** 587–595

Guella G, Frassanito R, Mancini I (2003) A new solution for an old problem: the regiochemical distribution of the acyl chains in galactolipids can be established by electrospray ionization tandem mass spectrometry. Rapid Commun Mass Spectrom **17:** 1982–1994

Guschina IA, Harwood JL (2006) Lipids and lipid metabolism in eukaryotic algae. Prog Lipid Res **45:** 160–186

Hagio M, Sakurai I, Sato S, Kato T, Tabata S, Wada H (2002) Phosphatidylglycerol is essential for the development of thylakoid membranes in Arabidopsis thaliana. Plant Cell Physiol **43:** 1456–1464

Hecky RE, Kilham P (1988) Nutrient limitation of phytoplankton in freshwater and marine environments. Limnol Oceanogr **33:** 786–822

Hsu FF, Turk J (2000a) Characterization of phosphatidylethanolamine as a lithiated adduct by triple quadrupole tandem mass spectrometry with electrospray ionization. J Mass Spectrom **35:** 595–606

Hsu FF, Turk J (2000b) Characterization of phosphatidylinositol, phosphatidylinositol-4-phosphate, and phosphatidylinositol-4,5-bisphosphate by electrospray ionization tandem mass spectrometry: a mechanistic study. J Am Soc Mass Spectrom **11:** 986–999

Hsu FF, Turk J (2001) Studies on phosphatidylglycerol with triple quadrupole tandem mass spectrometry with electrospray ionization: fragmentation processes and structural characterization. J Am Soc Mass Spectrom **12:** 1036–1043

Hsu FF, Turk J (2003) Electrospray ionization/tandem quadrupole mass spectrometric studies on phosphatidylcholines: the fragmentation processes. J Am Soc Mass Spectrom **14:** 352–363

Hsu FF, Turk J (2010) Electrospray ionization multiple-stage linear ion-trap mass spectrometry for structural elucidation of triacylglycerols: assignment of fatty acyl groups on the glycerol backbone and location of double bonds. J Am Soc Mass Spectrom **21:** 657–669

Jouhet J, Dubots E, Maréchal E, Block MA (2010) Lipid trafficking in plant photosynthetic cells. *In* **H Wada, N Murata**, eds, Lipids in Photosynthesis, **Vol 30**. Springer, Dordrecht, The Netherlands, pp 349–372

Jouhet J, Maréchal E, Baldan B, Bligny R, Joyard J, Block MA (2004) Phosphate deprivation induces transfer of DGDG galactolipid from chloroplast to mitochondria. J Cell Biol **167:** 863–874

Jouhet J, Maréchal E, Bligny R, Joyard J, Block MA (2003) Transient increase of phosphatidylcholine in plant cells in response to phosphate deprivation. FEBS Lett **544:** 63–68

Jouhet J, Maréchal E, Block MA (2007) Glycerolipid transfer for the building of membranes in plant cells. Prog Lipid Res **46:** 37–55

Khozin I, Adlerstein D, Bigongo C, Heimer YM, Cohen Z (1997) Elucidation of the biosynthesis of eicosapentaenoic acid in the microalga *Porphyridium cruentum*: II. Studies with radiolabeled precursors. Plant Physiol **114:** 223–230

Khozin-Goldberg I, Didi-Cohen S, Shayakhmetova I, Cohen Z (2002) Biosynthesis of eicopentaenoic acid (EPA) in the fresh water eustigmatophyte Monodus subterraneaus (Eustigmatophyceae). J Phycol **38:** 745–756

Kroth PG, Chiovitti A, Gruber A, Martin-Jezequel V, Mock T, Parker MS, Stanley MS, Kaplan A, Caron L, Weber T, et al (2008) A model for

carbohydrate metabolism in the diatom Phaeodactylum tricornutum deduced from comparative whole genome analysis. PLoS ONE **3:** e1426

Künzler K, Eichenberger W, Radunz A (1997) Intracellular localization of two betaine lipids by cell fractionation and immunomicroscopy. Z Naturforsch C **52:** 487–495

Levitan O, Dinamarca J, Hochman G, Falkowski PG (2014) Diatoms: a fossil fuel of the future. Trends Biotechnol **32:** 117–124

Li X, Moellering ER, Liu B, Johnny C, Fedewa M, Sears BB, Kuo MH, Benning C (2012) A galactoglycerolipid lipase is required for triacylglycerol accumulation and survival following nitrogen deprivation in *Chlamydomonas reinhardtii*. Plant Cell **24:** 4670–4686

Li Y, Han D, Sommerfeld M, Hu Q (2011) Photosynthetic carbon partitioning and lipid production in the oleaginous microalga Pseudochlorococcum sp. (Chlorophyceae) under nitrogen-limited conditions. Bioresour Technol **102:** 123–129

Liang Y, Maeda Y, Yoshino T, Matsumoto M, Tanaka T (2014) Profiling of polar lipids in marine oleaginous diatom Fistulifera solaris JPCC DA0580: prediction of the potential mechanism for eicosapentaenoic acid-incorporation into triacylglycerol. Mar Drugs **12:** 3218–3230

Li-Beisson Y, Shorrosh B, Beisson F, Andersson MX, Arondel V, Bates PD, Baud S, Bird D, Debono A, Durrett TP, et al (2010) Acyl-lipid metabolism. The Arabidopsis Book **8:** e0133, doi/10.1199/tab.0161

Litchman E, Klausmeier CA, Yoshiyama K (2009) Contrasting size evolution in marine and freshwater diatoms. Proc Natl Acad Sci USA **106:** 2665–2670

Löfke C, Ischebeck T, König S, Freitag S, Heilmann I (2008) Alternative metabolic fates of phosphatidylinositol produced by phosphatidylinositol synthase isoforms in Arabidopsis thaliana. Biochem J **413:** 115–124

Maheswari U, Mock T, Armbrust EV, Bowler C (2009) Update of the Diatom EST Database: a new tool for digital transcriptomics. Nucleic Acids Res **37:** D1001–D1005

Maheswari U, Montsant A, Goll J, Krishnasamy S, Rajyashri KR, Patell VM, Bowler C (2005) The Diatom EST Database. Nucleic Acids Res **33:** D344–D347

Maréchal E, Block MA, Joyard J, Douce R (1994) Kinetic properties of monogalactosyldiacylglycerol synthase from spinach chloroplast envelope membranes. J Biol Chem **269:** 5788–5798

Martin P, Dyhrman ST, Lomas MW, Poulton NJ, Van Mooy BAS (2014) Accumulation and enhanced cycling of polyphosphate by Sargasso Sea plankton in response to low phosphorus. Proc Natl Acad Sci USA **111:** 8089–8094

Mills MM, Ridame C, Davey M, La Roche J, Geider RJ (2004) Iron and phosphorus co-limit nitrogen fixation in the eastern tropical North Atlantic. Nature **429:** 292–294

Misson J, Raghothama KG, Jain A, Jouhet J, Block MA, Bligny R, Ortet P, Creff A, Somerville S, Rolland N, et al (2005) A genome-wide transcriptional analysis using Arabidopsis thaliana Affymetrix gene chips determined plant responses to phosphate deprivation. Proc Natl Acad Sci USA **102:** 11934–11939

Mongrand S, Bessoule JJ, Cabantous F, Cassagne C (1998) The C16:3/C18:3 fatty acid balance in photosynthetic tissues from 468 plant species. Phytochemistry **49:** 1049–1064

Montsant A, Maheswari U, Bowler C, Lopez PJ (2005) Diatomics: toward diatom functional genomics. J Nanosci Nanotechnol **5:** 5–14

Moore C, Mills M, Arrigo K, Berman-Frank I, Bopp L, Boyd P, Galbraith E, Geider R, Guieu C, Jaccard S, et al (2013) Processes and patterns of oceanic nutrient limitation. Nat Geosci **6:** 701–710

Moore TS, Du Z, Chen Z (2001) Membrane lipid biosynthesis in *Chlamydomonas reinhardtii*: in vitro biosynthesis of diacylglyceryltrimethylhomoserine. Plant Physiol **125:** 423–429

Morcuende R, Bari R, Gibon Y, Zheng W, Pant BD, Bläsing O, Usadel B, Czechowski T, Udvardi MK, Stitt M, et al (2007) Genome-wide reprogramming of metabolism and regulatory networks of Arabidopsis in response to phosphorus. Plant Cell Environ **30:** 85–112

Moreau RA, Doehlert DC, Welti R, Isaac G, Roth M, Tamura P, Nuñez A (2008) The identification of mono-, di-, tri-, and tetragalactosyl-diacylglycerols and their natural estolides in oat kernels. Lipids **43:** 533–548

Müller F, Frentzen M (2001) Phosphatidylglycerophosphate synthases from Arabidopsis thaliana. FEBS Lett **509:** 298–302

Nakamura Y (2013) Phosphate starvation and membrane lipid remodeling in seed plants. Prog Lipid Res **52:** 43–50

Naumann I, Klein BC, Bartel SJ, Darsow KH, Buchholz R, Lange HA (2011) Identification of sulfoquinovosyldiacyglycerides from Phaeodactylum tricornutum by matrix-assisted laser desorption/ionization QTrap time-of-flight hybrid mass spectrometry. Rapid Commun Mass Spectrom **25:** 2517–2523

Nunn BL, Aker JR, Shaffer SA, Tsai S, Strzepek RF, Boyd PW, Freeman TL, Brittnacher M, Malmström L, Goodlett DR (2009) Deciphering diatom biochemical pathways via whole-cell proteomics. Aquat Microb Ecol **55:** 241–253

Petroutsos D, Amiar S, Abida H, Dolch LJ, Bastien O, Rébeillé F, Jouhet J, Falconet D, Block MA, McFadden GI, et al (2014) Evolution of galactoglycerolipid biosynthetic pathways: from cyanobacteria to primary plastids and from primary to secondary plastids. Prog Lipid Res **54:** 68–85

Prihoda J, Tanaka A, de Paula WBM, Allen JF, Tirichine L, Bowler C (2012) Chloroplast-mitochondria cross-talk in diatoms. J Exp Bot **63:** 1543–1557

Rezanka T, Lukavský J, Nedbalová L, Sigler K (2011) Effect of nitrogen and phosphorus starvation on the polyunsaturated triacylglycerol composition, including positional isomer distribution, in the alga Trachydiscus minutus. Phytochemistry **72:** 2342–2351

Riekhof WR, Naik S, Bertrand H, Benning C, Voelker DR (2014) Phosphate starvation in fungi induces the replacement of phosphatidylcholine with the phosphorus-free betaine lipid diacylglyceryl-N,N,N-trimethylhomoserine. Eukaryot Cell **13:** 749–757

Riekhof WR, Ruckle ME, Lydic TA, Sears BB, Benning C (2003) The sulfolipids 2′-*O*-acyl-sulfoquinovosyldiacylglycerol and sulfoquinovosyldiacylglycerol are absent from a *Chlamydomonas reinhardtii* mutant deleted in *SQD1*. Plant Physiol **133:** 864–874

Riekhof WR, Sears BB, Benning C (2005) Annotation of genes involved in glycerolipid biosynthesis in Chlamydomonas reinhardtii: discovery of the betaine lipid synthase BTA1Cr. Eukaryot Cell **4:** 242–252

Sandelius AS, Andersson MX, Goksor M, Tjellstrom H, Wellander R (2007) Membrane contact sites: physical attachment between chloroplasts and endoplasmic reticulum revealed by optical manipulation. Chem Phys Lipids **149:** S42–S43

Sapriel G, Quinet M, Heijde M, Jourdren L, Tanty V, Luo G, Le Crom S, Lopez PJ (2009) Genome-wide transcriptome analyses of silicon metabolism in Phaeodactylum tricornutum reveal the multilevel regulation of silicic acid transporters. PLoS ONE **4:** e7458

Sato N, Murata N (1991) Transition of lipid phase in aqueous dispersions of diacylglyceryltrimethylhomoserine. Biochim Biophys Acta **1082:** 108–111

Scala S, Bowler C (2001) Molecular insights into the novel aspects of diatom biology. Cell Mol Life Sci **58:** 1666–1673

Shimojima M, Ohta H (2011) Critical regulation of galactolipid synthesis controls membrane differentiation and remodeling in distinct plant organs and following environmental changes. Prog Lipid Res **50:** 258–266

Shrestha RP, Tesson B, Norden-Krichmar T, Federowicz S, Hildebrand M, Allen AE (2012) Whole transcriptome analysis of the silicon response of the diatom Thalassiosira pseudonana. BMC Genomics **13:** 499

Simionato D, Block MA, La Rocca N, Jouhet J, Maréchal E, Finazzi G, Morosinotto T (2013) The response of Nannochloropsis gaditana to nitrogen starvation includes de novo biosynthesis of triacylglycerols, a decrease of chloroplast galactolipids, and reorganization of the photosynthetic apparatus. Eukaryot Cell **12:** 665–676

Taguchi R, Houjou T, Nakanishi H, Yamazaki T, Ishida M, Imagawa M, Shimizu T (2005) Focused lipidomics by tandem mass spectrometry. J Chromatogr B Analyt Technol Biomed Life Sci **823:** 26–36

Tanoue R, Kobayashi M, Katayama K, Nagata N, Wada H (2014) Phosphatidylglycerol biosynthesis is required for the development of embryos and normal membrane structures of chloroplasts and mitochondria in Arabidopsis. FEBS Lett **588:** 1680–1685

Tjellström H, Andersson MX, Larsson KE, Sandelius AS (2008) Membrane phospholipids as a phosphate reserve: the dynamic nature of phospholipid-to-digalactosyl diacylglycerol exchange in higher plants. Plant Cell Environ **31:** 1388–1398

Van Mooy BAS, Fredricks HF, Pedler BE, Dyhrman ST, Karl DM, Koblízek M, Lomas MW, Mincer TJ, Moore LR, Moutin T, et al (2009) Phytoplankton in the ocean use non-phosphorus lipids in response to phosphorus scarcity. Nature **458:** 69–72

Vogel G, Eichenberger W (1992) Betaine lipids in lower plants: biosynthesis of DGTS and DGTA in Ochromonas danica (Chrysophyceae) and the possible role of DGTS in lipid metabolism. Plant Cell Physiol **33:** 427–436

Welti R, Wang X, Williams TD (2003) Electrospray ionization tandem mass spectrometry scan modes for plant chloroplast lipids. Anal Biochem **314:** 149–152

Xu C, Härtel H, Wada H, Hagio M, Yu B, Eakin C, Benning C (2002) The *pgp1* mutant locus of Arabidopsis encodes a phosphatidylglycerolphosphate synthase with impaired activity. Plant Physiol **129:** 594–604

Yang ZK, Zheng JW, Niu YF, Yang WD, Liu JS, Li HY (2014) Systems-level analysis of the metabolic responses of the diatom Phaeodactylum tricornutum to phosphorus stress. Environ Microbiol **16:** 1793–1807

Yongmanitchai W, Ward OP (1993) Positional distribution of fatty acids, and molecular species of polar lipids, in the diatom Phaeodactylum tricornutum. J Gen Microbiol **139:** 465–472

Zendejas FJ, Benke PI, Lane PD, Simmons BA, Lane TW (2012) Characterization of the acylglycerols and resulting biodiesel derived from vegetable oil and microalgae (Thalassiosira pseudonana and Phaeodactylum tricornutum). Biotechnol Bioeng **109:** 1146–1154

Zhou Y, Peisker H, Weth A, Baumgartner W, Dörmann P, Frentzen M (2013) Extraplastidial cytidinediphosphate diacylglycerol synthase activity is required for vegetative development in Arabidopsis thaliana. Plant J **75:** 867–879

Zianni R, Bianco G, Lelario F, Losito I, Palmisano F, Cataldi TR (2013) Fatty acid neutral losses observed in tandem mass spectrometry with collision-induced dissociation allows regiochemical assignment of sulfoquinovosyldiacylglycerols. J Mass Spectrom **48:** 205–215

3.3.3 *Characterization of DGDG synthases in Phaeodactylum*

3.3.3.1 Sequence analysis of *Phaeodactylum* DGDG synthases

Higher plants encode two DGDG synthases (DGD) that are located in the outer envelope membrane of primary chloroplasts (OEM) (Boudière et al. 2014). We used the *Arabidopsis* sequences for the identification of homolog genes in *Phaeodactylum* (**figure 3.6**). AtDGD1 is the major isoform of DGDs and stands out by a 337 amino acid long N-terminal extension compared to AtDGD2 (Kelly et al. 2003). Both *Arabidopsis* DGDs share 54% sequence identity (**appendix 8.2.1**). We identified three putative *Phaeodactylum* DGD isoforms, which share 39-41% amino acids between each other and 34-38% identity with AtDGD1. They are closer related to the stress-responsive AtDGD2 with 37-43% protein sequence identity, but with a substantially longer N-terminus. DGD proteins displayed a more conserved C-terminus than N-terminus (**figure 3.6**) with the greatest conservation in a part of the glycosyl-transferases group 1 Pfam domain (PF13692), namely KVFxNxSxxxVxCTxxAEALAMGKxVxxxxHxSNxEFxxFPNC. Upstream of PF13692, a proline-rich hydrophobic Src homology 3 domain (SH3) was located. This poorly characterized domain is associated with functions as increases in local protein concentration, complex assembly or alterations in subcellular localizations (Morton & Campbell 1994). Notably, neither domain was predicted in the most distinct isoform, DGD3.

Protein homologs of *Arabidopsis* DGDG synthases in *Phaeodactylum* displayed slightly higher sequence identities to those isoforms which are induced under phosphate starvation compared to the constitutively expressed form in higher plants (Misson et al. 2005). Localization, expression and substrate specificities of *Phaeodactylum* DGD isoforms are unknown. In order to characterize the protein functions, antisense lines against the six galactolipid synthases were constructed and the WT transformed.

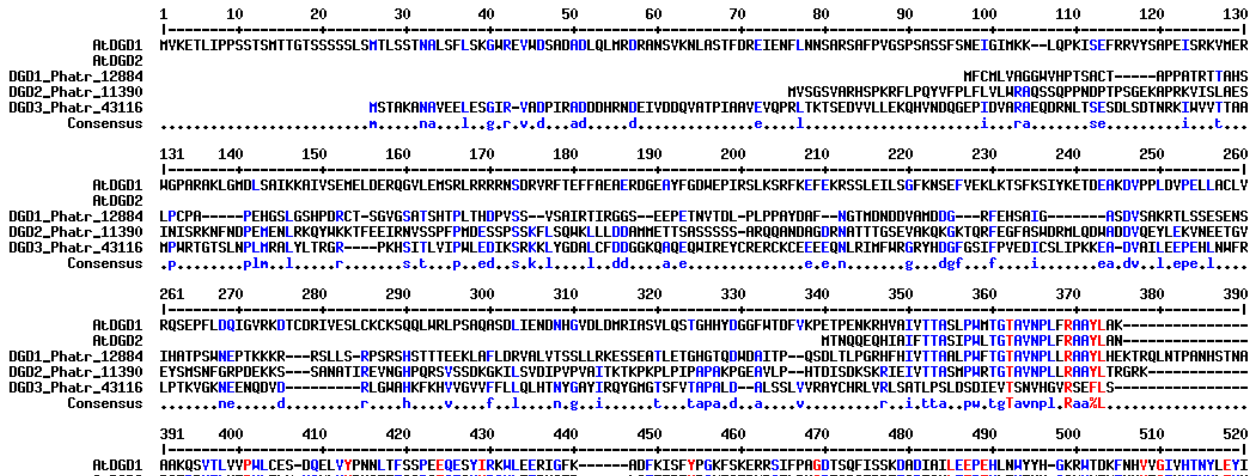

Figure 3.6. Amino acid alignment of the two *Arabidopsis* DGDG synthase (DGD) isoforms and gene candidates from *P. tricornutum*. *Arabidopsis* sequences (At) were retrieved from arabidopisis.org and used for the identification of *Phaeodactylum* homologs using BLAST analysis on the jgi database. *Phaeodactylum* hits were numbered (DGD1-3) and the protein ID (Phatr) is indicated. An alignment was created using a blocks substitution matrix (Blosum 62-12-2). Identical amino acids are displayed in red, similar ones in blue (http://multalin.toulouse.inra.fr/multalin/).

3.3.3.2 Identification of DGD antisense lines in *P. tricornutum*

We have addressed the function of the three DGD isoforms in *Phaeodactylum via* reverse genetics. To this end we have cloned antisense constructs into the pH4 vector backbone. After transformation of *Phaeodactylum* WT cells with antisense constructs

against the three DGD isoforms or with the empty vector (pH4), eight colonies of different sizes were selected per construct and inoculated into 2 mL cultures. From those, three lines with the strongest growth retardation were selected. The expression level of the respective gene that we attempted to silence was verified in qPCR and the two lines with the strongest downregulation were selected for phenotyping (**figure 7.3**).

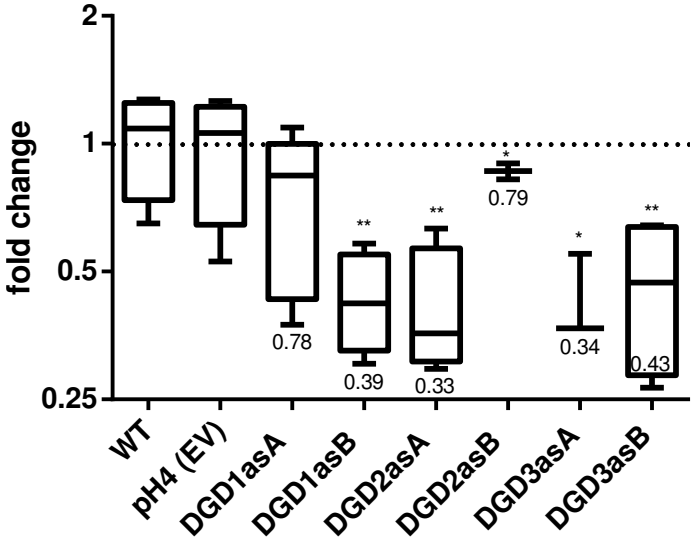

Figure 3.7. Relative mRNA levels of the respective DGD synthase isoforms in knock down lines compared to the expression variance in *Phaeodactylum* wild type (WT). RNA was extracted from cell pellets and reversely transcribed. Quantitative real time PCR was performed and curves were evaluated using the∆∆Cq method provided with the BioRad CFX software. Relative gene expression levels were normalized to the mRNA level in the WT, both corrected to the Cq of the housekeeping genes *RPS* and *TUB*. Antisense lines (as) of DGD1 (DGD1as) were tested on *DGD1* expression, DGD2as lines against *DGD2* and DGD3as lines against *DGD3*. Data is shown as boxplots with the line at the median, representing the fold change of gene expression in three biological replicates. To indicate natural variance of expression, WT and empty vector fold changes of the three DGDG synthases expressions are also plotted. Statistically significant were the changes in DGD1asB (p-value 0.007), DGD2asA (p-value 0.008), DGD3as A (p-value 0.0173) and DGD3asB (p-value 0.004).

The remaining expression of the respective DGD isoforms in the antisense lines were as follows: DGD1asA 78% (p-value 0.188), DGD1asB 39% (p-value 0.007), DGD2asA 0.33% (p-value 0.008), DGD2asB 79% (p-value 0.369), DGD3as A (p-value 0.0173) and DGD3asB 43% (p-value 0.0040) (**figure 3.7**). These reductions were similar to what

was observed in earlier silencing studies in which around 10% of all antibiotic-resistant transformants had typically about 50-75% lower expression levels (De Riso et al. 2009). The time point for the extraction was chosen randomly, in the middle of the light phase. Since we do not know the diurnal pattern of DGD expression and differential regulations in response to the antisense transformation, we cannot exclude stronger or weaker effects at other time points. Therefore, lipids were extracted from cells harvested at the same time as for RNA extractions.

3.3.3.3 Lipid profiles of DGDas lines grown at standard conditions

Lipid profiles were addressed in the six DGDas lines, the WT, and empty vector transformed cells, pH4. First, lipodomic analyses were performed on cells grown under standard conditions in 10N10P ESAW media. Although in some mutant lines the expression of the respective DGDG synthase was downregulated by more than 50%, cellular DGDG proportions were not significantly altered when compared to the control lines (**figure 3.8**). By contrast, MGDG levels were higher with a 1.21 induction in DGD1asB (p-value 0.001), 1.15 in DGD2asA (p-value 0.018), 1.7 in DGD3asA (p-value 0.077) and DGD3asB (p-value 0.075). It hence seems that the WT-like DGDG levels were maintained by increasing substrate availability. Furthermore, DGD1, DGD2 and DGD3 could have overlapping functions and might at least partially compensate for the downregulation of one. We could not detect a co-regulation of the other DGD isoforms in a given DGDas line via qPCR (not shown).

The induction of MGDG correlated to the strength of the downregulation of the respective DGD. No effect was observed for DGD1asA and DGD2asB, the two lines with the highest variation in expression among the biological replicates, in which the average reduction of about 20% is not significant in t-test (**figure 3.7**). We were therefore confident that the observed phenotype was indeed a consequence of lowered DGD expression.

In plants, 16:3-containing MGDG species are locked as MGDG whereas the 16:0-MGDG can be used as a substrate for DGDG synthases (Boudière et al. 2012). Similarly, 20-5_16-3 is the most common fatty acid couple in MGDG in *Phaeodactylum* whereas 20-5_16-2 and 20-5_16-1 are dominant in DGDG (Abida et al. 2015, **section 3.3.2**). If a plant-like 16:3-lock would exist in the diatom, we would expect altered MGDG fatty acid compositions in the DGDas lines and we thus deciphered the galactolipid fatty acid profiles in more detail (**figure 3.9**). *Phaeodactylum* DGDG contained about 5% 20-5_16:3, indicating that a potential 16-3 lock was not strict in diatoms –**figure 3.9A**).

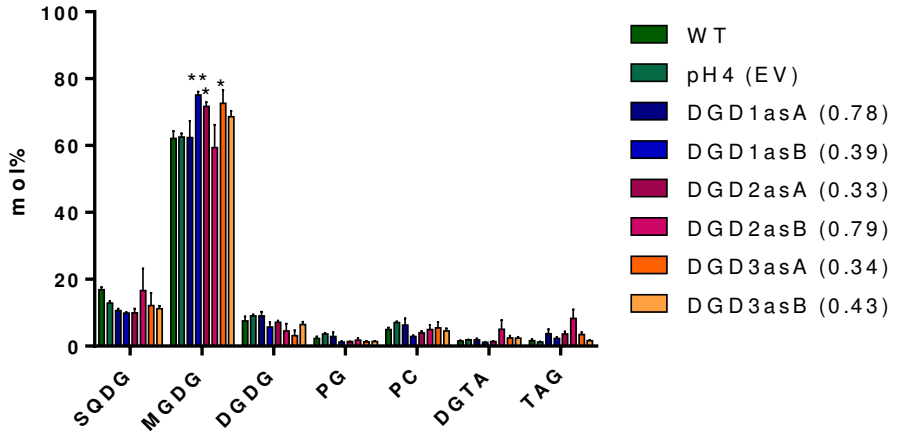

Figure 3.8 Analysis of glycerolipid classes from *Phaeodactylum* wild type (WT), empty vector (EV) transformants (pH4) and cells transformed with antisense (as) constructs against DGDG synthase (DGD) isoforms 1, 2 and 3. Two transformant lines were characterized per DGD isoform, A and B, with fold changes of gene expression as indicated in parenthesis. Glycerolipids were extracted, and their cellular contents determined based on gas chromatography coupled to ion flame detection after fatty acid methyl ester separation. Lipid classes were analysed using high performance liquid chromatography coupled to tandem mass spectrometry (HPLC-MS/MS), as described in the Method section. The proportion of each lipid class is indicated. Error bars correspond to standard error of the mean (SEM, n = 3). Stars indicate significant changes at the level of MGDG for DGD1asB (p-value 0.001), DGD2asA (p-value 0.018), and DGD3asA (p-value 0.07).

The MGDG fatty acid profile appeared surprisingly stable in the DGDas lines (**figure 3.9A**) and trends of increased proportions of 20-5_16-3 in DGD2as and DGD3as were not statistically relevant. We also observed a conservation of MGDG under nutrient deprivation in *P. tricornutum* WT (Abida et al. 2015, **section 6**). Chloroplast lipids rely on the import of VLC-PUFAs from the ER. In plants, PC is the precursor molecule in the "eukaryotic pathway" but the EPA-carrying precursor in Heterokonts is unknown. We considered PC and the betaine lipid DGTA (and respectively DGTS in *Nannochloropsis*, **section 6**) to be possible precursors of the "omega pathway" (Petroutsos et al. 2014). Given the conserved MGDG profile we checked whether fatty acids compositions were altered in either potential precursor (**figure 3.10**).

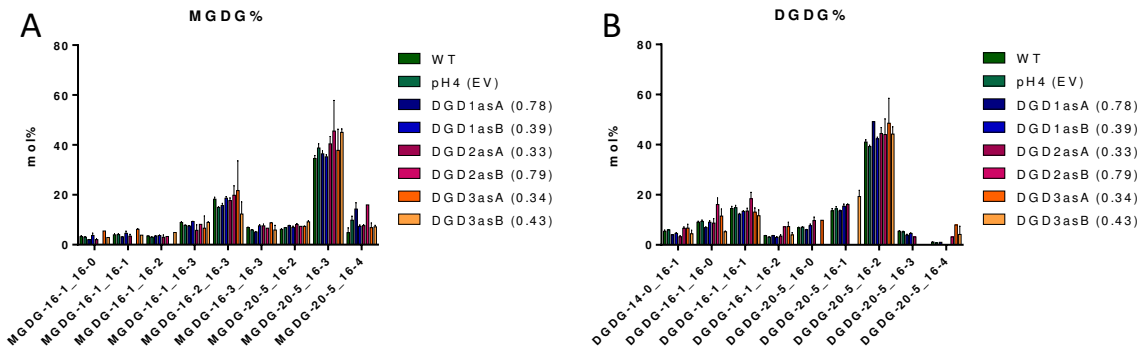

Figure 3.9. Analysis of glycerolipid fatty acid profiles from *Phaeodactylum* wild type (WT), empty vector (EV) transformands (pH4) and cells transformed with antisense (as) constructs against DGDG synthase (DGD) isoforms 1, 2 and 3. Two transformant lines were characterized per DGD isoform, A and B, with fold changes of gene expression as indicated in parenthesis. Glycerolipids were extracted, and their cellular contents determined based on gas chromatography coupled to ion flame detection after fatty acid methyl ester separation. Lipid classes were analysed using high performance liquid chromatography coupled to tandem mass spectrometry (HPLC-MS/MS), as described in the Method section. The proportion of fatty acid couples in **(A) monogalactosyldiacylglycerol (MGDG) and (B) digalactosyldiacylglycerol (DGDG)** are indicated. Error bars correspond to standard error of the mean (SEM, n = 3).

In those lines with trends of increased DGTA contents, also the fatty acid profile of the betaine lipid was altered (**figure 3.10A**). DGD2as and DGD3as lines but not DGD1as had reduced DGTA-16-0_16-1, DGTA-16-1_16-1 proportions, while PUFA containing

DGTA species were enriched. Most important, a drastic DGTA-22-6_22-6 increase was observed. This is usually a minor DGTA species, making about 1% in the control lines but 6.4% in DGD2asA, 26% in DGD2asB (p-value 0.007), 20% in DGD3asA (p-value < 0.0001) and 11% in DGD3asB (p-value 0.004). Similarly, 20-5_16-3 being the dominant fatty acid couple in MGDG accumulated in DGTA in DGDas lines, it is minor compound in control lines. This is especially interesting because based on profile comparisons we have assumed PC to stand at the base for VLC-PUFA import in *Phaeodactylum*, similar to what is observed in higher plants (Abida et al. 2015). With the accumulation of MGDG-like DGTA in mutant lines displaying lower galactolipid contents, these data indicate DGTA to be involved in the ”omega pathway”. Furthermore, the reduction of C16-containing DGTA together with increased cellular TAG contents in which 16:0 and 16:1 are the dominant fatty acids, it seems that DGTA could be a branch point between chloroplast lipid and neutral lipids (**see section 6**). This idea is further strengthened by the absence of a PC fatty acid profile phenotype in DGDas mutants (**figure 3.10B**).

Based on these analyses, each of the DGDas isoforms could indeed act in DGDG synthesis. Future experiments shall involve *in vitro* experiments in order to reveal the substrate specificities and kinetics. Given the stronger alterations of the DGTA fatty acid profile in DGD3as lines together with the strongest growth impairment (**figure 3.11**) we propose a dominant function of DGD3 in the synthesis of DGDG. The three diatom DGD isoform sequences displayed higher similarity to AtDGD2 than to AtDGD1. These plants homologs are differentially regulated under stress situations, especially phosphate deprivation (Kelly et al. 2003). We were therefore interested in deciphering the response to phosphate starvation in *Phaeodactylum* cells with reduced DGDG synthases expression.

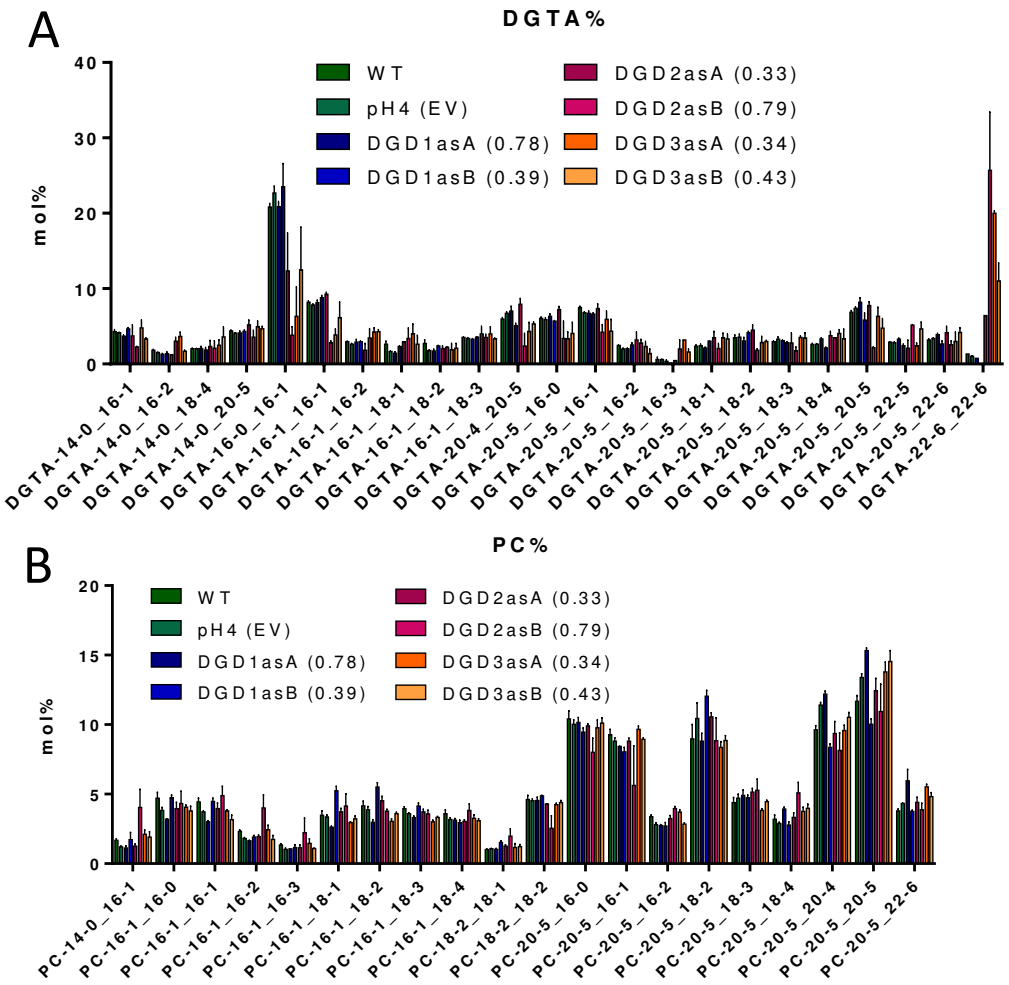

Figure 3.10. Analysis of glycerolipid fatty acid profiles from *Phaeodactylum* wild type (WT), empty vector (EV) transformands (pH4) and cells transformed with antisense (as) constructs against DGDG synthase (DGD) isoforms 1, 2 and 3. Two transformant lines were characterized per DGD isoform, A and B, with fold changes of gene expression as indicated in parenthesis. Glycerolipids were extracted, and their cellular contents determined based on gas chromatography coupled to ion flame detection after fatty acid methyl ester separation. Lipid classes were analysed using high performance liquid chromatography coupled to tandem mass spectrometry (HPLC-MS/MS), as described in the Method section. The proportion of fatty acid couples in **(A) diacylglycerylhydroxymethyltrimethylalanine (DGTA)** and **(B) phosphatidylcholine (PC)** are indicated. Error bars correspond to standard error of the mean (SEM, n = 3).

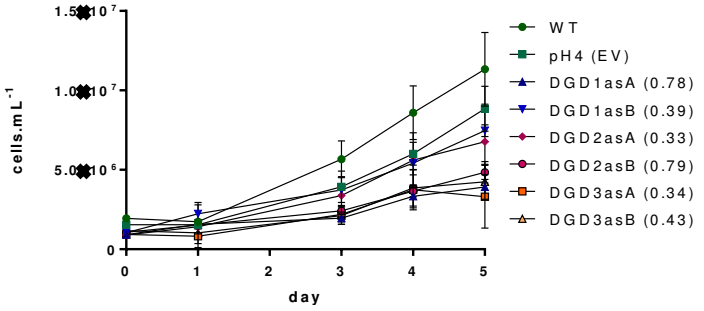

Figure 3.11. Cell growth in 10N10P ESAW grown *Phaeodactylum* wild type (WT), empty vector (EV) transformands (pH4) and cells transformed with antisense (as) constructs against DGDG synthase (DGD) isoforms 1, 2 and 3. Two transformant lines were characterized per DGD isoform, A and B, with fold changes of gene expression as indicated in parenthesis. From triplicates of 2 mL cultures, 300 µL were taken for the calculation of cell concentrations were *via* the absorption at 730 nm using a TECAN plate reader.

3.3.3.4 Lipid profiles of DGDas lines grown under phosphate starvation

DGTA might replace phospholipids in the endomembranes

DGDG in higher plants can replace phospholipids inside and outside the chloroplast (Kelly et al. 2003, Jouhet et al. 2004). Alternatively, SQDG might compensate for a partial loss of chloroplast PG (Sato 2004, Boudière et al. 2013, **section 2.1.2**). In the endomembranes DGTA might have the potential to replace PC when phosphate becomes limited (Riekhof et al. 2005, 2014). Phytoplankton species as *Phaeodactylum* have an efficient phosphate metabolism and can endure 50% lower cellular phosphate levels compared to depleted levels without fitness impairment (Feng et al. 2015). *Phaeodactylum* contains both PC and DGTA and it is unknown if DGDG may cross the four membranes limiting the chloroplast.

Cells were harvested at day 9 of cultivation in phosphate depleted conditions and lipids were extracted. As expected from our reference study, TAG contents were drastically increased making about 60% of all lipid classes (not shown). For easier interpretation of

changes in membrane lipids, neutral lipids were excluded from the representation. As observed in our earlier study, PG and PC were reduced and DGDG and DGTA induced in the WT upon shortage in phosphate (**figure 3.12**) but to a lower extent than what we observed after 13 days of stress (Abida et al. 2015, **section 3.3.2**). Importantly, when compared to the reference study reporting lipid profiles during prolonged phosphate limitation, induction of DGTA was an earlier response than the increase in DGDG or SQDG after 13 days. This could be either due to the predominance of phospholipids in the endomembrane system which would be then replaced by the betaine lipid. Alternatively, DGTA as a potential precursor for chloroplast VLC-PUFA import would be induced to serve as a substrate donor for galactolipid synthesis.

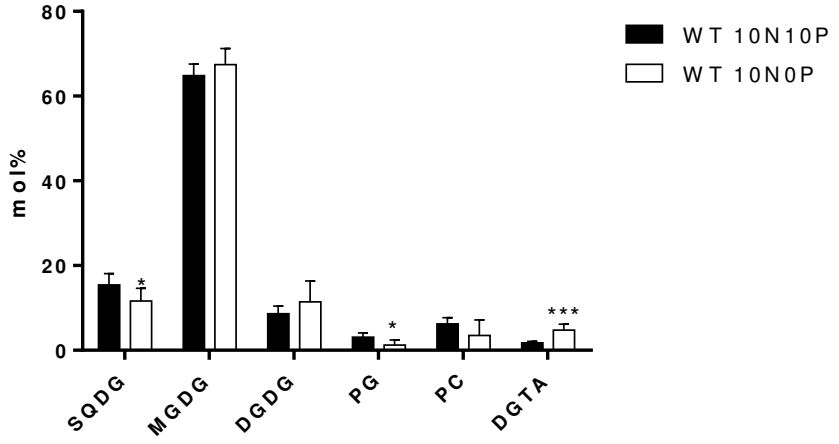

Figure 3.12 Analysis of glycerolipid classes from *Phaeodactylum* wild type (WT) grown in enriched ESAW medium (10N10P) and phosphate depletion (10N0P) for nine days. Glycerolipids were extracted, and their cellular contents determined based on gas chromatography coupled to ion flame detection after fatty acid methyl ester separation. Lipid classes were analysed using high performance liquid chromatography coupled to tandem mass spectrometry (HPLC-MS/MS), as described in the Method section. The proportion of each lipid class is indicated. Error bars correspond to standard error of the mean (SEM, n = 3). Stars indicate significant changes at the level of SQDG (p-value 0.0408), PG (p-value 0.0178) and DGTA (p-value 0.0004).

Upon the shift to phosphate starvation the fatty acid profile of the glycerolipid classes changed (**figure 3.13**). EPA is most likely produced on non-lipid-linked acyl-chain precursors (**section 2.8.2**). If we assume that in galactolipids only EPA derives from the "omega pathway" while the second fatty acid being a C16:x would be provided by the "prokaryotic pathway", changes in DGTAs containing C18 upon phosphate starvation should represent a function of the betaine lipid in the substitution of endomembrane phospholipids. Indeed, in phosphate limiting conditions DGTA-14-0_18-4, DGTA-16-1_18-3 and DGTA-16-1_18-3 underwent the greatest increase, while DGTA-16-0_16-1 was largely repressed (**figure 3.13**).

The decrease in membrane lipids would also indicate a reinforcement of the Kennedy pathway to allocate saturated and monounsaturated C16 species into TAGs. Lipid remodelling contributed to TAG production during phosphate limitation as indicated by increased EPA-carrying TAGs (**figure 3.13**). When comparing TAG and PC profiles, one could consider the phospholipid as the major source for EPA allocated into neutral lipids (**figure 3.13**).

Relative EPA contents in DGTA decreased under phosphate limitation. We interpreted that to be caused by an increased pull from the chloroplast due to induced DGDG and hence MGDG synthesis being the substrate. This assumption is strengthened by increased MGDG-20-5_16-3 proportions which are less efficiently converted into DGDG. This increase was the dominant MGDG response to phosphate stress while in DGDG the 20-5_16-0 and 20-5_16-1 couples accumulated (**figure 3.14**). Introduction of desaturations are a time consuming (Mei et al. 2016) and thus the lower unsaturation grade of DGDG would indicate increased *de novo* synthesis as it would be expected from the observed DGDG induction under prolonged phosphate starvation (Abida et al. 2015).

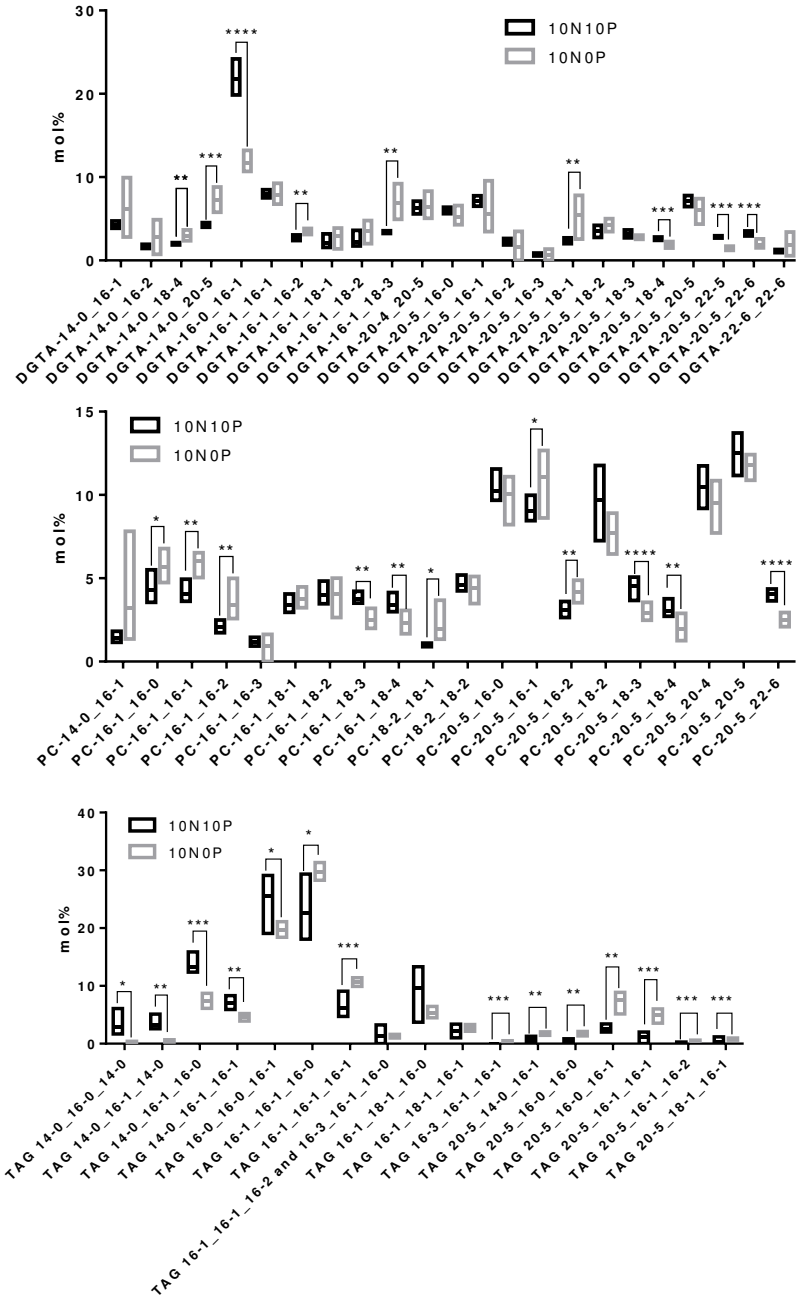

Figure 3.13 Analysis of glycerolipid classes from *Phaeodactylum* grown in enriched ESAW medium (10N10P) and phosphate depletion (10N0P) for nine days. Glycerolipids were extracted, and their cellular contents determined based on gas chromatography coupled to ion flame detection after fatty acid methyl ester separation. Lipid classes were analysed using high performance liquid chromatography coupled to tandem mass spectrometry (HPLC-MS/MS), as described in the Method section. The proportion of each lipid class is indicated. Error bars correspond to standard error of the mean (SEM, n = 6, a pool of WT and empty vector transformants). Stars indicate significant changes with **** having a p-value <0.0001, *** < 0.001, ** < 0.01, * < 0.05.

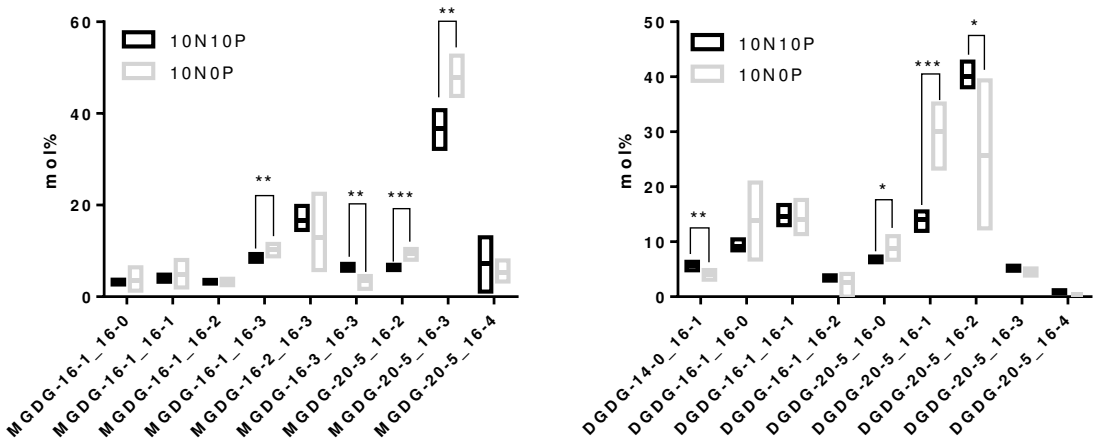

Figure 3.14. Analysis of galactolipid classes from *Phaeodactylum* grown in enriched ESAW medium (10N10P) and phosphate depletion (10N0P) for nine days. Glycerolipids were extracted, and their cellular contents determined based on gas chromatography coupled to ion flame detection after fatty acid methyl ester separation. Lipid classes were analysed using high performance liquid chromatography coupled to tandem mass spectrometry (HPLC-MS/MS), as described in the Method section. The proportion of each lipid class is indicated. Error bars correspond to standard error of the mean (SEM, n = 6, a pool of WT and empty vector transformants). Stars indicate significant changes with **** having a p-value <0.0001, *** < 0.001, ** < 0.01, * < 0.05.

As a conclusion we propose the betaine lipid to play a key role in the homeostasis of galactolipids, phospholipids and maybe neutral lipids. DGTA was likely to serve in recycling of phosphate when the macroelement was limiting. Furthermore it could be considered as the most likely EPA-donor for chloroplast lipid synthesis thus playing in the "omega pathway" (see also **section 6**).

DGD3 seems to be involved in the adaptation to phosphate limitation

In order to challenge the DGDas mutants in their response to phosphate deprivations, cells were shifted into 10N0P media and the growth was followed (**figure 3.15A**). While growth in the first four days of cultivation was similar in 10N10P and 10N0P ESAW, phosphate depletion led to the onset of the stationary phase after five days. At day 5 in control lines, cell concentrations were 1.5 times greater when grown in 10N10P

compared to 10N0P ESAW (p-value 0.05) (**figure 3.15B**). A similar observation was made for the stronger DGD1 mutant line DGD1asB, but no other mutant. This indicated that in DGD2as and DGD3as growth was already strongly arrested in repleted conditions and not further affected by the nutrient stress.

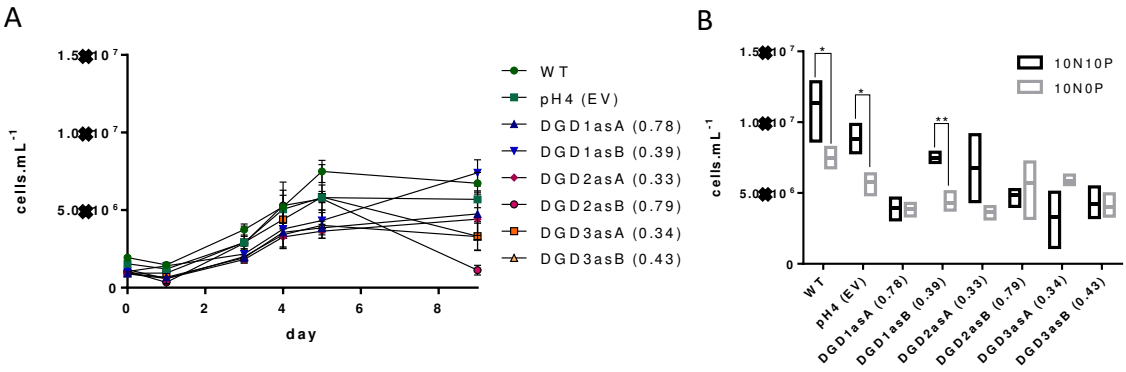

Figure 3.15. Cell growth of grown *Phaeodactylum* wild type (WT), empty vector (EV) transformands (pH4) and cells transformed with antisense (as) constructs against DGDG synthase (DGD) isoforms 1, 2 and 3. Two transformant lines were characterized per DGD isoform, A and B, with fold changes of gene expression as indicated in parenthesis. From triplicates of 2 mL cultures, 300 µL were taken for the calculation of cell concentrations were *via* the absorption at 730 nm using a TECAN plate reader. A. Time course of cell growth in 10N0P ESAW. B. Comparison of cell concentrations at day five in 10N10P and 10N0P. Stars indicate significant changes in response to phosphate deprivation in WT (p-value 0.05), pH4 (p-value 0.05) and DGD1asB (p-value 0.002).

The glycerolipid profile was analysed after nine days of phosphate deprivation (**figure 3.16**). DGD1as lines again displayed only marginal changes in the glycerolipid profile recorded under phosphate starved conditions (**figure 3.16A**). While DGDG levels remained WT-like, the reduction of PC and PG was more pronounced in DGD2as and DGD3as compared to control lines (**figure 3.16A**). In all mutants, neutral lipids accumulated stronger under phosphate starvation than in control lines (**figure 3.16B**). Similarly to the phenotype in control conditions, MGDG quantities were increased in DGD3as compared to the WT and empty vector transformants. DGD3as lines were also strongly impaired in cell growth under both phosphate repleted and depleted conditions, and DGTA levels were higher than in the WT when grown in 10N10P ESAW. By

contrast, the DGTA induction observed in the WT upon phosphate starvation was less pronounced in DGD3 as lines (**figure 3.16A**). This result was inconsistent with the other phenotypes and so we sought whether the strong pressure given by the nutrient stress would have altered the knock down level.

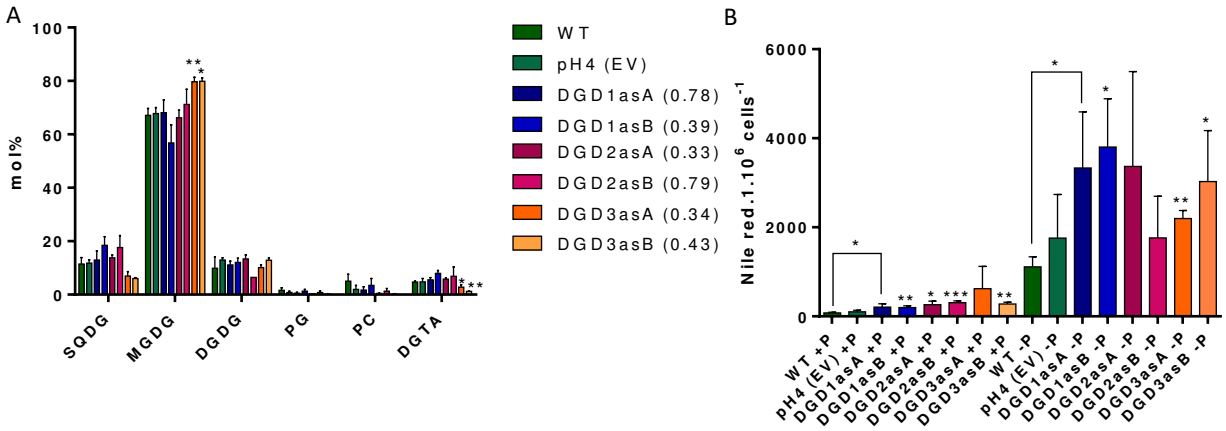

Figure 3.16 Analysis of glycerolipid classes from *Phaeodactylum* wild type (WT), empty vector (EV) transformands (pH4) and cells transformed with antisense (as) constructs against DGDG synthase (DGD) isoforms 1, 2 and 3 after 9 days of growth in phosphate deprived medium. Two transformant lines were characterized per DGD isoform, A and B, with fold changes of gene expression as indicated in parenthesis. Glycerolipids were extracted, and their cellular contents determined based on gas chromatography coupled to ion flame detection after fatty acid methyl ester separation. Lipid classes were analysed using high performance liquid chromatography coupled to tandem mass spectrometry (HPLC-MS/MS), as described in the Method section. The proportion of each lipid class is indicated. Error bars correspond to standard error of the mean (SEM, n = 3). Stars indicate significant changes with **** having a p-value <0.0001, *** < 0.001, ** < 0.01, * < 0.05.

Based on the lipodomic data we assume all three DGD isoforms to be involved in *Phaeodactylum* DGDG synthesis. Among the mutant lines, reduction of DGD3 led to the strongest phenotype under phosphate starvation, namely a low stationary phase, TAG accumulation and lower phospholipid contents. The reduced DGTA levels together with the increase in MGDG and neutral lipids indicated that mutant cells counteract reduced DGD3 activity by increasing the substrate MGDG which in turn promoted a strong pull on the potential EPA-donor DGTA. We would therefore suspect DGD3 to be the dominant DGDG synthase isoform under phosphate deprivation. DGD2as and

DGD1as lipid profiles were not significantly different from control lines and did seem to be involved in DGDG synthesis under optimal conditions.

The question of distinct roles of the three DGDG synthases shall be subject of future studies. Protein levels of the different isoforms should be revealed, if possible after fractionation of the different membranes. However, isolation of single chloroplast membranes from a secondary endosymbiont was unsuccessful to date. Furthermore, the balance of the three DGDs in response to stress should be addressed in qPCR or immunoblotting.

In order to give first insights into consequences on phosphate starvation on the DGDas lines, the cells morphologies were recorded by epifluorescence microscopy after Nile red staining (**figure 3.17**). In line with the strongest fitness phenotype observed for DGD3as, also the cell morphologies were strongly altered when grown in 10N10P ESAW. DGDas cells did not display the typical fusiform cell form observed for the WT. Cells were less elongated and had less defined shapes compared to control lines. In DGD1asB, about half of the cells were impaired in cell morphology. This already indicated that during the time course, some cells had silenced the antisense construct and the regained fitness advantage hence being able to overgrow the mutants. With increased selection pressure upon the shift to phosphate starvation, the odd-shaped cells were strongly diminished in all DGDas lines (**figure 3.17**). Most mutant cells appeared WT-like under phosphate starvation but displayed larger lipid droplets compared to control lines. Thus, one has to assume that the expression level of the respective DGD isoforms changed in the mutant lines during phosphate starvation. The use of targeted gene knock outs may overcome this problem in the future.

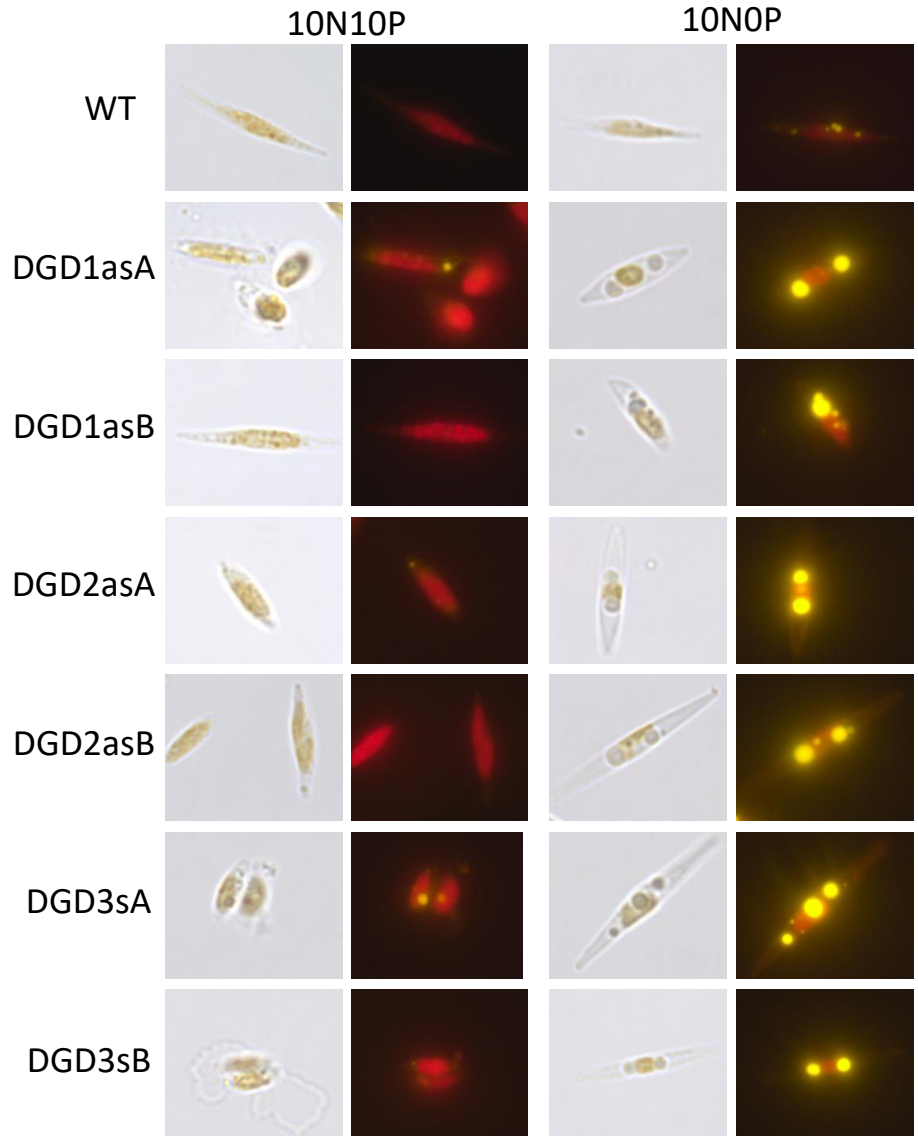

Figure 3.17. Morphotypes of *Phaeodactylum* wild type (WT) and cells transformed with antisense (as) constructs against DGDG synthase (DGD) isoforms 1, 2 and 3 after six days of growth in phosphate deprived medium. From a 2 mL culture, a 300 µL aliquot was collected. Nile red staining was performed as described in the Method section. Cells were imaged in epifluorescence microscopy (Zeiss) and lipid droplets were visualized with constant FITC filter gain of 200.

4 NITRIC OXIDE SIGNALLING IN LIPID ACCUMULATION

4.1 Introduction and overview

The gas NO• is a ubiquitous second messenger in plants and animals (Wendehenne et al. 2001). Its signalling function has already been addressed in *Phaeodactylum* but its implementation in the regulation of cellular lipid contents was unknown. We have addressed this question based on the results of a forward chemogenomics approach (Conte et al. 2015) that pointed several molecules interfering with NO• signalling to trigger TAG accumulation. We firstly tried to confirm earlier observations that *Phaeodactylum* compared to other diatoms is less sensitive to a specific oxylipin that induces cell death (DD) (Ribalet et al. 2007, Vardi et al. 2006, 2008a). Since this was

not successful we readdressed putative NO• synthesis pathways and revealed the dominance of NR-dependent NO• production by a substrate feeding assay. Additionally, the *Phaeodactylum* NOA operates in chloroplast NO• production (Tewari et al. 2013) and might involve arginine as a substrate or regulator. NR is cytosolic (Cookson et al. 2005) and inducing it's NO• production activity in *Phaeodactylum* did not alter neutral lipid contents, as measured in substrate feeding assays. However, neutral lipids accumulated when the NO• signal derived from chloroplast as *via* PtNOA or from outside the cell, as indicated by the treatment of water-diluted SNAP but not from the cytosol as indicated by the overexpression of *N. gaditana* NOA in *Phaeodactylum* cells (Pt::OE-NgNOA). Based on the results presented below we hypothesize that chloroplast and extracellular NO• signatures indicate stress situations that induce TAG synthesis in *Phaeodactylum*, similar to nutrient deprivations. The signalling cascade could involve regulation of NR.

Experiments presented in this chapter were part of collaboration with TOTAL Energies. The use of NO• or NOA for TAG accumulation purposes has been protected (Dolch & Marechal 2016a, Dolch & Marechal 2016b).

4.2 Small molecule screen

In order to identify new chemicals that are able to trigger TAG accumulation in *Phaeodactylum*, Melissa Conte carried out a forward chemogenomics approach using small inorganic molecules. A strain expressing eYFP was used to facilitate biomass estimation via YFP fluorescence. To 450 µL cultures inoculated at 1.10^6 cells.mL^{-1}, 50 µL of a tested chemical diluted in 5% DMSO or the detergent solution alone was added. After two days of incubation, fluorescence measurements were performed. According to values in nitrogen repleted and depleted controls, relative chlorophyll and YFP levels were expressed as percentage of nitrogen repleted conditions and Nile red relative to nitrogen starved conditions. Out of 43 Prestwick Chemical Library molecules

tested, 36 triggered neutral lipid accumulation in at least two out of three screens (**table 4.1**).

Table 4.1. List of Prestwick Library molecules found to trigger neutral lipid accumulation in *Phaeodactylum*. Drugs were screened for their ability to increase Nile red fluorescence in small scale cultures after two days of incubation. Positive hits were sorted according to their general site of action and gave rise to two groups: inhibitors of competitive pathways (blue shades) and NO• signalling (red shades). Chemical names are not shown for intellectual property reasons, but the therapeutic group, the pathway and possible mode of action are indicated.

	Drug interfers in	Therapeutic group	Pathway involved	Possible mechanism of action	Screening results
Inhibition of competetive pathways	sterol	estrogen	contraception	estrogen receptor activator	NILE RED PERCENT OF AVG >120% & NON TOXIC
	sterol	Antihyperlipidemic	lowers LDL cholesterol content	HMG-CoA reductase inhibitor	NILE RED PERCENT OF AVG >120% & TOXIC
	sterol	Antifungal	ergosterol sunthesis	Cytochrome P450c17 inhibitor	HIGH NR IN 2/3 TESTS
	sterol	antifungal	reduces sterols	ergosterol synthesis inhibition	HIGH NR IN 2/3 TESTS
	sterol	anticholesteremic agent, antibiotic	lowers ergosterol content	3-hydroxy-3-methylglutaryl-coenzyme A reductase (HMG-CoA) reductase inhibitors	NILE RED PERCENT OF AVG >120% & NON TOXIC
	sterol	Estrogen		Estrogen receptor agonist	HIGH NR IN 2/3 TESTS
	phosphoinositol	Nasal decongestant Vasoconstrictor	adrenalin response	Adrenergic alpha-agonists	NILE RED PERCENT OF AVG >120% & TOXIC
	phosphoinositol	Antihypertensor	reduction of blood pressure	Beta1 antagonist	HIGH NR IN 2/3 TESTS
	phosphatidylcholine	Antispasmodic	acetylcholine competior	Cholinergic	HIGH NR IN 2/3 TESTS
	nucleotide	antiurolithic	lowers uric acid and purin content	Xanthine oxidase inhibitor	NILE RED PERCENT OF AVG >120% & NON TOXIC
	nucleotide	AntifungalAntibacterial	ROS, e- TP, apoptosis, mit. DNA	bitor of mitochondrial electron transj	NILE RED PERCENT OF AVG >120% & NON TOXIC
	nucleotide	antiviral	RNA synthesis inhibitor	Nucleic Acid Synthesis Inhibitors	NILE RED PERCENT OF AVG >120% & TOXIC
	nucleotide	nti-metaboliteanti-cancer drug	blocking thymidylic acid synthesis	Thymidylate Synthase inibitor	NILE RED PERCENT OF AVG >120% & TOXIC
	nucleotide	Antibacterial		Ribosomal protein synthesis inhibitor	HIGH NR IN 2/3 TESTS
	nucleotide	Antiparasitic	inhibtion of DNA, RNA, phospholipids and proteins synthesis	-	HIGH NR IN 2/3 TESTS
	nucleotide	Antineoplastic	Alkylation of DNA		HIGH NR IN 2/3 TESTS
	nucleotide	antibacterial	inhibiting bacterial ribonucleic acid (RNA) synthesis		HIGH NR IN 2/3 TESTS
	sugar	Contrasting product	may inhibit glucose metabolism	-	HIGH NR IN 2/3 TESTS
	sugar	antidiabetic	inhibits carbohydrate breakdown into glucose	inhibits alpha-glucosidases	HIGH NR IN 2/3 TESTS
	amino acid	Ankylostomiasis Antihelmintic			HIGH NR IN 2/3 TESTS
	amino acid	Antiparasitic		GABAergic Agonist	HIGH NR IN 2/3 TESTS
Nitric oxide signaling	relaxant	Spasmolytic Vasodilatator	muscle relaxion	Anticholinergic Phosphodiesterase inhibitor	NILE RED PERCENT OF AVG >120% & TOXIC
	relaxant	Antianginal	lowering heart and blood pressure	Beta1 antagonist	HIGH NR IN 2/3 TESTS
	relaxant	Tranquilizer	Seretonin antagonist	5-HT2 antagonist	HIGH NR IN 2/3 TESTS
	relaxant	Spasmolytic	?	Nicotinic receptor antagonist	HIGH NR IN 2/3 TESTS
	relaxant	Antihypertensor	inhibition of Na/Cl cotransporter and Ca2+ activated K+channel	Na+ Cl- transport inhibitor	HIGH NR IN 2/3 TESTS
	relaxant	Bronchodilator	inhibit inflammation, increase heart muscle contraction	Phosphodiesterase III inhibitor Phosphodiesterase IV inhibitor	HIGH NR IN 2/3 TESTS
	relaxant	Vasodilator	non-selective phosphodiesterase inhibitor, inhibition of thrombozyte aggregation	PDGF antagonist	HIGH NR IN 2/3 TESTS
	relaxant	Antihypertensive	acetylcholine competitor, ganglionic blocker in treating hypertension	Cholinergic receptor antagonist	HIGH NR IN 2/3 TESTS
	histamine	Antiemetic	anticholinergic, central nervous system depressant, and local anesthetic effects	Histamine antagonist	HIGH NR IN 2/3 TESTS
	histamine	Neurotransmitter		5-HT agonist	HIGH NR IN 2/3 TESTS
	histamine		NO synthase inhibiton and H2	Histamine H2 receptor agonist	HIGH NR IN 2/3 TESTS
	prostaglandin	Antineoplastic	lowers prostaglandin and trombocytes	Microtubule poison	NILE RED PERCENT OF AVG >120% & NON TOXIC
	prostaglandin	Anti-inflammatory	prostaglandin synthesis	Cyclooxygenase inhibitor	HIGH NR IN 2/3 TESTS
	prostaglandin	Anti-inflammatory Analgesic	inhibition of prostanoids synthesis	Cyclooxygenase inhibitor	HIGH NR IN 2/3 TESTS
	prostaglandin	antiulcerative	indirect inhibition of adenylate cyclase	prostaglandin E1 analog that inhibits gastric acid secretion	HIGH NR IN 2/3 TESTS

Most chemicals appeared to be cytotoxic. We have grouped the positive hits into different classes according to available information on the drugs' effects. We were able to differentiate molecules that could inhibit competitive pathways and thus facilitate carbon channelling into TAGs (blue shades). Among those, drugs interfering in sterol metabolism were enriched (Conte et al. 2015). Similarly, chemicals inhibiting the synthesis of other carbon rich moieties as nucleotides, amino acids and sugars were

found to trigger TAG in *Phaeodactylum*. The second group of drugs found to induce neutral lipid contents is attributed to nitric oxide associated processes (red shade). Those 15 molecules were subgrouped according to their function as muscle relaxants, or to be involved in histamine or prostaglandin functions. Smooth muscle tone is regulated by NO• in mammals (Bennett 1997, Serio et al. 2003). Histamines, prostaglandins and serotonin act as modulators of inflammation, a process well known to involve NO signals (Kular et al. 2011, Mokhtari-Zaer et al. 2015). Histamines derive from the amino acid histidine and prostaglandins derive from VLC-PUFAs (Lee et al. 2016, Ruiz-Lopez et al. 2015). Thus, there is a chance that drugs interfering with those modulator molecules would as well allow the redirection of carbon precursors into neutral lipids by inhibition of competitive pathways. The enrichment of those drugs together with the numerous muscle tone regulating agents as vasodilators suggested a possible role of NO• in neutral lipid accumulation in *Phaeodactylum* and motivated a more detailed study.

4.3 Oxylipin induced cell death does not trigger TAG accumulation in *Phaeodactylum*

In plants, the best studied roles of NO• signalling are in lipid peroxidation, pathogen defence and programmed cell death (PCD) (Mittler 2002, Wendehenne et al. 2001). Also in *Phaeodactylum*, NO• was indicated to play a role in the cells defence by modulating the susceptibility to the diatom-derived aldehyde 2E,4E/Z-decadienal (DD) (Vardi et al. 2006, 2008a). DD belongs to the molecule class of oxygenated fatty acyl chains, oxylipins. They are not only toxic to grazers such as copepods and having negative effects on their reproduction, they might also act in phytoplankton cell-to-cell communication to induce PCD (Ianora & Miralto 2010, Pohnert 2005, Romano et al. 2003). PCD involves a metacaspase cascade in photosynthetic organisms including diatoms (Bidle & Falkowski 2004, Choi & Berges 2013). NO• regulation of PCD also takes the metacaspase route which is also responsive to DD (Ruocco et al. 2016, Wang et al. 2010). *Phaeodactylum* encodes seven putative metacaspases (Vardi et al. 2008a). Phytoplankton PCD was observed to occur in response to both, biotic stress and nutrient

deprivation (Bidle & Falkowski 2004). Because nutrient limitation as well as small molecules that interfere with NO• signalling pathways were shown to trigger neutral lipid accumulation in *Phaeodactylum*, we aimed to investigate a correlation of TAG synthesis and PCD. One may assume that under stressful life conditions, the cells could either to undergo PCD to liberate nutrients for the community or to store carbon in lipid droplets to be prepared for better conditions. This assumption is based on the observation that early steps of PCD are reversible (van Doorn & Woltering 2005). Since the cell cycle is arrested during PCD, one could assume that neutral lipids could serve as an alternative sink for carbon building blocks in oleaginous microalgae. If environmental conditions would ameliorate before the point of no return in PCD, cells would be pre-equipped for the resumption of growth. To test this idea, we first tried to reproduce the DD treatment on *Phaeodactylum* as performed in Vardi (Vardi et al. 2008a). However, in contrast to the earlier study we found DD to be highly cytotoxic even in low concentrations (**section 4.4**, Dolch et al.).

To test whether the aldehyde triggered PCD, we treated 500 µL *Phaeodactylum* cultures with both DD and the caspase inhibitor carbobenzoxy-valyl-alanyl-aspartyl-[O-methyl]-fluoromethylketone (Z-VAD-FKM) (**figure 4.1**). After two days of incubation in the respective chemicals or DMSO treated controls, fitness parameters were measured. As observed after two days of 3.3 µM DD treatment (section 4.4, Dolch et al.), cell concentrations in samples treated with both DD and Z-VAD-FKM were 20-30% lower compared to non-treated controls (**figure 4.1 A**).

Relative chlorophyll fluorescence was similar in Z-VAD-FKM and solvent treated control samples. By contrast, fluorescence was abolished in samples containing DD independent on the presence or absence of the caspase inhibitor (**figure 4.1 B**). Similarly, Z-VAD-FKM did not alter the *Fv/Fm* of control or DD treated samples (**figure 4.1 B**). In conclusion, Z-VAD-FKM was inefficient to prevent cells from death induced by 3.3 µM DD. This is contradicting the study of Vardi and coworkers that state but does not show that Z-VAD-FKM treatment rescued the growth reduction triggered by DD by 25% (Vardi et al. 2008a). By contrast, 20 µM Z-VAD prevented nutrient

deficiency induced PCD in the diatom *Thalassiosira pseudonana* (Bidle & Bender 2008).

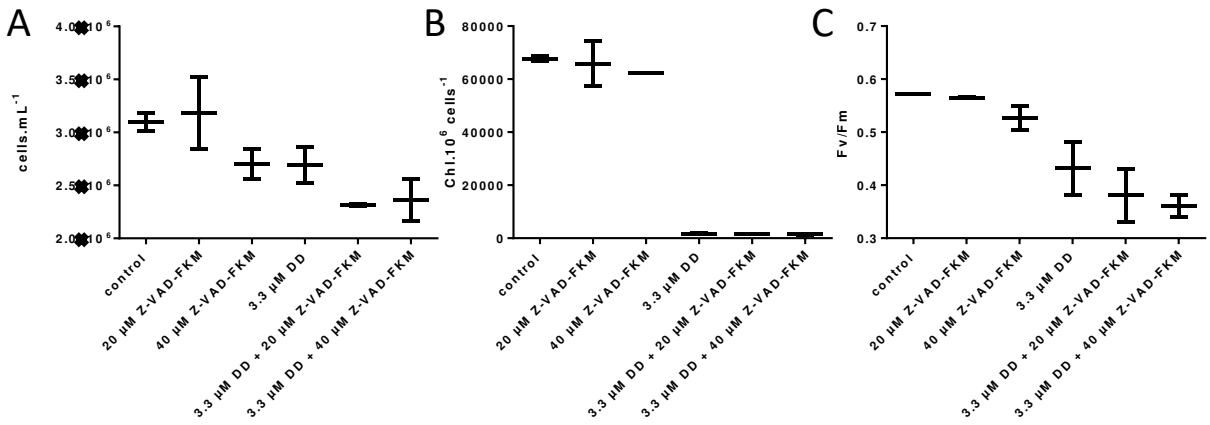

Figure 4.1. The caspase inhibitor Z-VAD-FKM is unable to rescue DD-treated cells from cell death. To 500 µL cultures inoculated at 1.10^6 cells.mL^{-1} with different concentrations of Z-VAD-FKM, 3.3 µM DD were added and incuvated for 48 hours. **A. Cell concentrations** were estimated with the help of a Malassez counting chamber **B. Relative chlorophyll fluorescence** at 680 nm was measured using a TECAN plate reader and values normalized to the cell concentration. **C.** *Fv/Fm* was measured via room temperature chlorophyll fluorescence kinetics using a Speedzen MX fluorescence imaging system.

Vardi and coworkers found a higher DD susceptibility in overexpression lines of NOA (Vardi et al. 2008a). To investigate if SNAP would also boost the negative impact of DD, cells were treated with 5 µM of the aldehyde and the NO donor molecule in concentrations ranging from 0.3-5 mM (**figure 4.2**). As observed with the caspase inhibitor, the presence or absence of SNAP did not alter the effect of DD causing a drop of chlorophyll fluorescence (**figure 4.2 A**) and *Fv/Fm* (**figure 4.2 B**). It therefore seems that the cytotoxic effect of 3.3 or 10 µM DD in *Phaeodactylum* did not rely on PCD processes. Accordingly, cell poisoning was rapid (Dolch et al. in preparation) but PCD is commonly a slow process taking hours or even month, depending on the species (Cao et al. 2003, Lim et al. 2007, Ribalet et al. 2007, Tarallo & Sordino 2004). In phytoplankton including diatoms, PCD markers such as altered nucleus shape and DNA degradation as

well as an enrichment of vesicles were observed to occur 48 hours after the death signal (Ribalet et al. 2007).

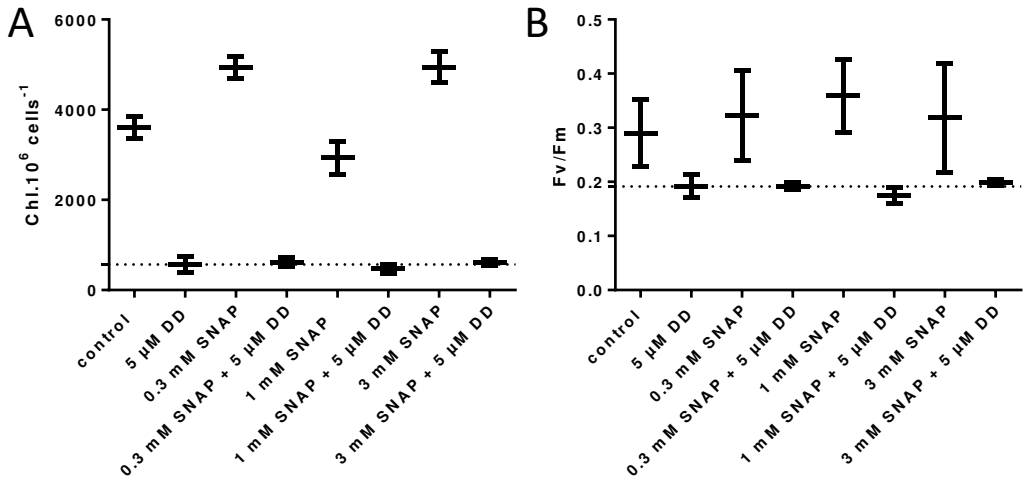

Figure 4.2. The addition of SNAP does not alter the effect of DD in *Phaeodactylum*. After the inoculation of 500 µL cultures at 1.10^6 cells.ml^{-1} with different concentrations of SNAP, 5 µM DD were added. After three hours of incubation, fluorescence was measured. **A. Relative chlorophyll fluorescence** at 680 nm was measured using a TECAN plate reader and values normalized to the cell concentration estimated with the help of a Malassez counting chamber. **B. *Fv/Fm*** was measured via room temperature chlorophyll fluorescence kinetics using a Speedzen MX fluorescence imaging system.

The half maximal effective concentration (EC_{50}) of DD in different phytoplankton species gave rise to PCD markers (Ribalet et al. 2007). Cell death staining values increased with the time. The EC_{50} after 24 hours of incubation ranged between 0.1 and 2.2 µM DD in *Thalassiosira weissflogii*, *Isochrysis galbana, Micromonas pusilla, Amphidinium carterae, Dunaliella tertiolecta, Tetraselmis suecica* and *Skeletonema marinoi* (Ribalet et al. 2007). Diatoms appeared more sensitive when compared to other phytoplankton species. At 10 µM DD, growth was abolished in each of the seven phytoplankter (Ribalet et al. 2007). In about 50 diatoms species tested, upon cell disruption, 0.01 to 9.8 fmol of oxylipins per cell were released (Wichard et al. 2005).

These levels are much lower than what was reported for *Phaeodactylum* (Vardi et al. 2006).

Imaging of cells treated with 3.3 µM DD revealed degradation of the chloroplast (Dolch et al. in preparation). Similarly, Sytox Green measurements of plasma membrane leakage in response to DD (unfortunately the concentration is not mentioned) occurred in 90% of Phaeodactylum cells (Vardi et al. 2006). Rapid loss of membrane integrity is a parameter of necrotic cell death in phytoplankton (Franklin et al. 2006). Notably, the chloroplast phenotype of DD treated cells was not based on elevated oxidative damage. ROS levels were measured by addition of 2',7'-dichlorodihydrofluorescein diacetate (**figure 4.3**). Incorporated into the cell, the reaction with ROS releases 2,7-dichlorofluorescein (DCF) that is fluorescent. While the positive control treatment with 100 µM H_2O_2 quickly raised DCF fluorescence compared to the solvent control, DD treatment did not (**figure 4.3**). This was in agreement with earlier observations using the ROS indicator dihydrorhodamine 123 (Vardi et al. 2006). The oxidative burst is a common feature of plant PCD (Lim et al. 2007). In diatoms, it might be involved in pathogen or grazer defence, mechanisms in which DD is playing as well (Babior 1978, Caldwell 2009, Ianora & Miralto 2010). Similar to the massive ROS production occurring upon pathogen invasion (Lim et al. 2007), diatom cells induce the production of oxylipins including DD within seconds after cell wounding (Ianora & Miralto 2010, Pohnert 2005). Thus, the burst of oxylipins in diatoms might have similar functions in defence from biotic attacks than the ROS release in plants.

In summary, we were unable to confirm the high DD tolerance of *Phaeodactylum*. The speed of the destructive effect and the inability of the caspase inhibitor to partially restore growth, *Fv/Fm* or fluorescence at 680 nm in cells treated with 3.3 µM DD led us to conclude on a sudden cell death such as necrosis rather than PCD. We assume that the DD concentrations chosen are too high to allow PCD in the Pt_1 CCAP 1055/3 *Phaeodactylum* accession. Controversially, in Pt_1 CCMP 632 treatment with 6.6 µM DD did not induce cell death, and had no negative effect on the *Fv/Fm* or cell growth measured over a period of seven days (Vardi et al. 2008a). In an earlier study from the same authors however, the EC_{50} of DD was reported to be 7.06 µM ± 2.44 after 24 hours

of cultivation (Vardi et al. 2006). Our data would indicate an even higher susceptibility as observed for other diatoms (Ribalet et al. 2007). Besides the use of a different strain, an important difference is their method to calculate DD concentrations by measuring absorption at 274 nm while we calculated it via the molecular mass and density. Thus, there could be differences is the real DD concentration applied to the cells. Furthermore, Vardi and coworkers used methanol while we used DMSO as a solvent (Vardi et al. 2008a).

Due to the spontaneous death in response to 3.3 µM DD we were unable to detect any neutral lipid accumulation in response to the treatment (not shown). We therefore concentrated on NO signalling in neutral lipid production. This we have explored in Dolch et al. (**section 4.4**).

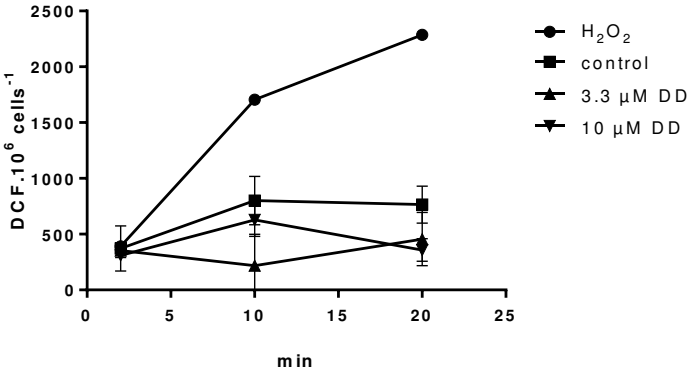

Figure 4.3. The DD response in *Phaeodactylum* does not involve ROS production. A 3 day old culture was treated with DCF and aliquoted to 500 µL cultures at a concentration of 1.10^6 cells.mL^{-1}. To these cultures, 100 µM H_2O_2 was added as a positive control, DMSO as negative control and 3.3 µM and 10 µM DD, respectively. DCF fluorescence was measured at indicated time points using a TECAN plate reader and normalized to the cell concentration estimated using a Malassez counting chamber.

4.4 NOA-dependent nitric oxide activates the transcription of nitrogen assimilation genes and triggers a glycerolipid remodelling in *Phaeodactylum tricornutum* (**article in preparation**)

Authors:

Lina-Juana Dolch[1], Guillaume Tourcier[1], Mariette Bedhomme[1], Séverine Collin[2], Leonardo Magneschi[1], Melissa Conte[1], Khawla Seddiki[1], Laurent Fourage[2], Giovanni Finazzi[1], Erwan Corre[3], Fabrice Rébeillé[1], Juliette Jouhet[1], Patrick McGuinn[3], Eric Maréchal[1,*]

Affiliations:

[1]Laboratoire de Physiologie Cellulaire et Végétale, Unité mixte de recherche 5168 CNRS - CEA - INRA - Université Grenoble Alpes, Institut de Biosciences Biotechnologies de Grenoble, CEA Grenoble, 17 rue des Martyrs, 38054, Grenoble Cedex 9, France.

[2]Total Refining Chemicals, Brussels, Belgium

[3]Station Biologique de Roscoff, Analyses and Bioinformatics for Marine Science, Roscoff, France

[4]National Research Council of Canada, Aquatic and Crop Resource Development, 1411 Oxford Street, Halifax, NS, Canada

* Correspondence: eric.marechal@cea.fr

Keywords:

Diatoms, *Phaedoactylum*, nitric oxide, nitrogen cycle, NOA, triacylglycerol

Abstract

Nitric oxide (NO) is a reactive intermediate of the nitrogen cycle, which level increases globally following anthropogenic activities. NO is an important pollutant in industrial wastes (flue gases and waste waters) and a marker of climate change. In eukaryotes, NO is known to act as a gaseous signal transmitter in a variety of cellular processes including defense and stress signaling in mammals as well as in photosynthetic organisms. Diatoms are dominant phytoplankton species in oceans and may be used for biotechnological purposes following cultivation in waste water; hence the understanding of the impact of increased NO levels on diatom cellular processes needs to be addressed. NO was reported to act in the programmed cell death (PCD) signaling pathway in the model diatom *Phaeodactylum*, in response to the diatom-derived aldehyde 2E,4E/Z-decadienal (DD). Using the Pt1 *Phaeodactylum* strain, a much higher susceptibility to DD was observed compared to previous studies. DD triggered unspecific cellular membrane disruptions and necrosis. Production of NO in *Phaeodactylum* in response to DD exposure could not be observed. We did not confirm any involvement of neither DD nor NO in PCD. Increased NO levels as indicated by DAF-FM fluorescence had mild inhibitory effects on cell growth when NO was applied as gas, in form of the SNAP NO donor molecule, or *via* the over expression of the *Phaeodactylum* NO associated protein, NOA. In *Phaeodactylum*, NO was not enzymatically produced by a NO synthase activity using arginine as substrate, but rather *via* the conversion of nitrite by a nitrate reductase. Transcriptional analyses of wild type cells treated with NO or of NOA-overexpressing lines indicate a control of genes involved in nitrogen assimilation. We observed a correlation between increased NO levels and neutral lipid contents. Triacylglycerols serve as a carbon storage when growth is arrested but its accumulation is not a known feature of PCD. Our data indicate that environmental NO signals could transmit the information of stressful growth conditions and could act upstream the redirection of assimilated carbon from cellular building blocks into neutral lipids

.

Introduction

Nitric oxide ($NO^{\bullet}$) is an intermediate of the nitrogen (N) cycle (Fowler et al., 2013). This cycle is a complex network of reactions interconverting dinitrogen (N_2), the most abundant gas in the atmosphere, into gaseous nitrogen oxides or 'NOx' ($NO^{\bullet}$; nitrogen dioxide, NO_2 and nitrous gas, N_2O), water soluble ions (ammonium, NH_4^+; nitrite, NO_2^- and nitrate, NO_3^-), organic molecules (from small soluble compounds like urea to proteins, lipids and nucleic acids) and mineral forms (Holloway and Dahlgren, 2002; Fowler et al., 2013). $NO^{\bullet}$ is an important pollutant in industrial flue gases (Vunjak-Novakovic et al., 2005; Zhu et al., 2015) and in wastewaters following both nitrification and denitrification treatments (Kampschreur et al., 2009; Pan et al., 2015). All gases in the N cycle, including $NO^{\bullet}$, are also present in oceans (Zehr and Ward, 2002; Nicholls et al., 2007), either because of gas exchanges at the air-water interface (Nicholls et al., 2007) or because they are generated within oceans. $NO^{\bullet}$ is generated in sea water by non-biological photochemical reactions (Olasehinde et al., 2010), large scale electrical discharges (Gallardo and Rhodes, 1997) and enzymatic activities in organisms living in the aerobic photic zone (Zhang et al., 2006; Olasehinde et al., 2010; Kumar et al., 2015; Eroglu et al., 2016) or in oxygen minimum zones (Naqvi et al., 1998; Nicholls et al., 2007; Martens-Habbena et al., 2015). Among the key biogeochemical cycles, on which ecosystems depend for their sustainability, the N cycle is clearly the most perturbed by human activities (Fowler et al., 2013), marked by massive anthropogenic leakage of nitrate and ammonia from fertilized soils (Nicholls et al., 2007; Fowler et al., 2013) and emissions of NOx acting as greenhouse gases (Nicholls et al., 2007; IPCC, 2014; Michalski et al., 2014).

There is no reliable report on $NO^{\bullet}$ concentration in aquatic ecosystems, because this reactive molecule has a lifetime of only a few seconds (Naqvi et al., 1998; Zehr and Ward, 2002; Zhang et al., 2006; Olasehinde et al., 2010). In natural seawater, $NO^{\bullet}$ concentration has been estimated between 0.01-10 nM (Zhang et al., 2006). In industrial microalga cultivation systems supplied with industrial CO_2-rich flue gas (Vunjak-Novakovic et al., 2005), we estimate that NOx/$NO^{\bullet}$ concentrations could reach the

micro- to millimolar range, *i.e.* one thousand to one million folds the natural level. $NO^{\bullet}$ diffuses freely and even minor and transient variations could have high impacts on living organisms, in which $NO^{\bullet}$ is also known to act as a signaling molecule.

$NO^{\bullet}$ has been reported to act as a gasotransmitter in a plethora of biological functions in prokaryotes and eukaryotes, in non-photosynthetic and photosynthetic cells and in terrestrial or aquatic ecosystems (Wendehenne et al., 2001; Moreau et al., 2010; Kumar et al., 2015; Eroglu et al., 2016). Two major enzymatic pathways are known to produce $NO^{\bullet}$, either *via* a nitric oxide synthase (NOS) using arginine as a substrate (Wilson et al., 2008), or *via* a nitrate reductase (NR) using nitrite as a substrate (Yamasaki and Sakihama, 2000; Stohr et al., 2001; Rockel et al., 2002). The role of $NO^{\bullet}$ in phytoplankton has been recently reviewed based on the available published data, showing that it could be synthesized in photosynthetic eukaryotes containing primary plastids (chlorophyta, rhodophyta) or secondary plastids (e.g. diatoms, haptophytes, etc.) (Kumar et al., 2015).

In the green alga *Chlamydomonas*, nitrite is assumed to be the only $NO^{\bullet}$ source since the addition of arginine or the analogue Nω-Nitro-L-arginine (L-NNA) had no effect on its production (Sakihama et al., 2002). $NO^{\bullet}$ was shown to act on nitrogen assimilation, by repressing nitrate assimilation at two levels. Firstly, $NO^{\bullet}$ represses the expression of the NR and the nitrate and ammonium transporters (de Montaigu et al., 2010). Secondly, it directly regulates the activities of NR and nitrate and ammonium transporters in *Chlamydomonas* (Sanz-Luque et al., 2013). Following a starvation of the medium in nitrogen, $NO^{\bullet}$ was also shown to be produced from intracellular nitrite and to act in the specific cytochrome b6f degradation pathway (Wei et al., 2014). In *Chlamydomonas*, $NO^{\bullet}$ appears therefore to have a dual role, repressing nitrogen assimilation and acting in response to nitrogen starvation. In other photosynthetic eukaryotes, $NO^{\bullet}$ may have opposing effects depending on the nitrogen status (Jin et al., 2009).

In the marine diatom *Phaeodactylum* $NO^{\bullet}$ has been proposed to act in population size control, being involved in a “stress surveillance system” upon exposure to high

concentrations of the diatom derived aldehyde 2E,4E/Z-decadienal (DD) (Vardi et al., 2006; Vardi et al., 2008). DD is enzymatically synthesized from diatoms' fatty acids and is released upon biotic stress, such as in the presence of grazing copepods (Ianora and Miralto, 2010; Lauritano et al., 2011; Lauritano et al., 2012) or abiotic stress, when diatoms grow in nutrient-limiting conditions (Ribalet et al., 2007). The treatment of *Phaeodactylum* with DD was reported (1) to induce the synthesis of $NO^{\bullet}$ *via* an arginine-dependent pathway, (2) to trigger the expression of nitric oxide associated protein (*NOA*), coding for a homologue of a plant chloroplast protein involved in $NO^{\bullet}$ production, and eventually (3) to promote the entry into programmed cell death (PCD) (Vardi et al., 2006; Vardi et al., 2008). The reduction of $NO^{\bullet}$ produced by *Phaeodactylum* in presence of a NOS-inhibitor (*NG*-monomethyl-L-arginine or NMMA) and DD led to the conclusion that $NO^{\bullet}$ was produced by a NOS enzyme (Vardi et al., 2006), in spite of the absence of any *NOS* gene in the *Phaeodactylum* genome (Di Dato et al., 2015). $NO^{\bullet}$ was proposed to act on the diatom itself, triggering PCD, and to diffuse outside the plasma membrane, spread rapidly through diatom population as a cell-to-cell signal, triggering death in surrounding cells, eventually acting in the control of the population size (Vardi et al., 2008; Bidle, 2015).

Climate change being marked by an increase in $NO^{\bullet}$ emissions, the impact on phytoplankton has to be evaluated. *Phaeodactylum* appears as an appropriate model for this evaluation, firstly because the biosynthesis and physiological roles of $NO^{\bullet}$ have been previously investigated (Vardi et al., 2006; Vardi et al., 2008) and secondly because some diatom strains have been considered for biotechnological applications, based on their neutral lipid contents (Levitan et al., 2014). Following nitrogen starvation, *Phaeodactylum* was shown to remodel its glycerolipids, accumulating triacylglycerol (Abida et al., 2015), but it is still unknown whether $NO^{\bullet}$ could play a role in the diatom response to low nitrogen. In the present article, we analyzed therefore the response of *Phaeodactylum* at various doses of $NO^{\bullet}$ and found unsuspected results that led us to re-examine the pathway of $NO^{\bullet}$-production by this diatom and the physiological responses this gasotransmitter could trigger.

Materials and methods

Chemicals

The chemicals used in the composition of growth media, the solvents as well as 3-[(3-cholamidopropyl)dimethylammonio]-1-propanesulfonate (CHAPS), 1,2-dioleoyl-sn-glycerol (DAG), 3-(N-morpholino)propanesulfonic acid (MOPS), nitroso acetyl penicillamine (NAP), S-nitroso-N-acetylpenicillamine (SNAP), phosphatidylglycerol (PG) and unlabeled uridine di-phosphogalactose (UDP-Gal) were obtained from Sigma-Aldrich. The fluorophore 4-amino-5-methylamino-2',7'-difluorescein diacetate (DAF-FM) was purchased from Thermofisher Scientific. The diatom derived aldehyde 2E,4E/Z-decadienal (DD) was obtained from Acros organics. [^{14}C]-labeled (11.0 GBq.mmol-1) UDP-Gal was obtained from New England Nuclear.

Cultivation of Phaeodactylum tricornutum

Phaeodactylum tricornutum (Pt1) Bohlin Strain 8.6 CCMP2561 (Culture Collection of Marine Phytoplankton, now known as NCMA: National Center for Marine Algae and Microbiota) was used in all experiments. Pt1 cells were maintained and grown in 20 mL or 50 mL at 20°C, in 250 mL flasks, in a modified ESAW (Enriched Seawater, Artificial Water) medium (NaCl 362.7 mM; Na_2SO_4 25 mM; KCl 8.03 mM; $NaHCO_3$ 2.067 mM; KBr 0.725 mM; H_3BO_3 0.372 mM; NaF 0.0657 mM; $MgCl_2$ 47.18 mM; $CaCl_2$ 9.134 mM; $SrCl_2$ 0.082 mM; Na_2-glycerophosphate 21.8 µM; Na_2SiO_3 105.6 µM; Na_2EDTA 14.86 µM; $Fe(NH_4)_2(SO_4)_2$ 5.97 µM; $FeCl_3$ 0.592 µM; $MnSO_4$ 2.42 µM; $ZnSO_4$ 0.254 µM; $CoSO_4$ 0.0569 µM; Na_2MoO_4 0.52 µM; H_3BO_3 61.46 µM; Na_2SeO_3 10 nM; biotin (vitamin H) 8.18 nM; cobalamin (vitamin B12) 2.94 nM; thiamine (vitamin B1) 0.594 µM) (Falciatore et al., 2000), using either ten times enriched nitrogen and phosphate sources ("10 x ESAW", containing 5.5 mM $NaNO_3$ and 0.22 mM NaH_3PO_4) (Abida et al., 2015) or the same medium without nitrogen. Cells were grown on a 12:12 light (30 µE $m^{-2}.sec^{-1}$) / dark cycle. Cells were sub-cultured twice a week by inoculating 1.10^6 cells.mL^{-1} with fresh media. Growth was evaluated by cell counting using a Malassez counting chamber or by the absorption at 750 nm using a TECAN plate reader. For

experiments in photo-bioreactors, cells were pre-cultured in a 50 mL volume of medium, in 250 mL Erlenmeyer flasks, until they reached a density of 2-4.10^6 cells.mL^{-1}. Cells were then centrifuged at 3,500 g for 5 min and re-suspended in either 10 x ESAW or medium F (HEPES 100 mM, pH 7.5; NaCl 420 mM; $MgSO_4$ 5 mM; Na_2SO_4 3.5 mM; $CaCl_2$ 2.5 mM; $NaNO_3$ 70 mM; KH_2PO_4 0.88 mM; K_2HPO_4 2.3 mM; $NaHCO_3$ 10 mM; EDTA-Fe(III)-Na 0.11 mM; Na_2EDTA 0.18 mM; $ZnSO_4$ 4 µM; $CoCl_2$ 1.2 µM; $MnCl_2$ 15.5 µM; $CuSO_4$ 1.3 µM; biotin (vitamin H) 0.1 µM; cobalamin (Vitamin B12) 0.1 µM; thiamine (vitamin B1) 3.7 µM) (Benvenuti et al., 2015) to a final concentration of 2.10^6 cells.mL^{-1}. Cells were grown under a constant light regime at 20°C in small scale bioreactors (Multi-Cultivator MC 1000, Photon Systems Instruments, Czech Republic). Culture mixing throughout cultivation time was provided by gas sparging as in air-lift photobioreactors. Precise CO_2 supplies to bioreactor tubes was controlled by a gas mixing system GMS 150 (Photon Systems Instruments, Czech Republic) following manufacturer's instructions.

Incubation of **Phaeodactylum** *with $NO^{\bullet}$-saturated solutions or $NO^{\bullet}$-donors*

Incubation of *P. tricornutum* with gaseous $NO^{\bullet}$ was performed by using $NO^{\bullet}$-saturated aqueous solutions. In this approach, a tank of pure $NO^{\bullet}$ was bubbled into a small quantity of distilled water until the saturation point was reached, confirmed by mass spectrometric analysis of the solution. The concentration of $NO^{\bullet}$ in a saturated solution is 1.9 mM (Gerrard, 1980). $NO^{\bullet}$ saturates were then typically diluted 20-200 fold for use with live *Phaeodactylum* suspensions. Alternatively, a $NO^{\bullet}$-donor agent, S-Nitroso-N-acetylpenicillamine (SNAP) was used. This compound releases $NO^{\bullet}$ when dissolved (Miller and Megson, 2007) and was therefore prepared freshly immediately before use. Nitroso-acetylpenicillamine (NAP) was used as a non-active compound for control experiments.

Incubation of **Phaeodactylum** *with the diatom derived aldehyde DD*

DD being a highly toxic and volatile compound, all experiments were performed under a fume hood safety cabinet and only freshly prepared DD solutions were used. A 500 µL

volume of a *Phaeodactylum* culture was inoculated with a cell density of 2.10^6 cell.mL^{-1} and after a 24 hour-preincubation under gentle agitation, cells were treated with different concentrations of DD or the solvent (DMSO). Untreated and treated cells were then observed by confocal microscopy, using the 680 nm fluorescent filter allowing chlorophyll detection. Relative fluorescence at 680 nm was quantified using a TECAN infinite M1000Pro plate reader.

Measure of nitric oxide using DAF-FM, a fluorescent reporter

The fluorophore 4-amino-5-methylamino-2',7'-difluororescein diacetate (DAF-FM) allows the sensitive detection of low levels of nitric peroxide ($ONOO^-$), which is in equilibrium with $NO^\bullet$ and thus indicates $NO^\bullet$ levels (St Laurent et al., 2015). DAF-FM was previously used to detect $NO^\bullet$ levels in *P. tricornutum* cells (Vardi et al., 2008). Cultures were diluted to obtain 10^6 cells.mL^{-1} in 10 mL and cells were incubated under gentle shaking with 20 µL DAF-FM 5 mM (in 100% DMSO) for 1.5 hours, at room temperature and in the dark. Cells were washed and resuspended in 10 mL of fresh 10 x ESAW medium. Aliquot fractions (500 µL) were transferred to a 48 well culture plate, to which SNAP was added as indicated. For the examination of DAF-FM-dependent detection of nitric peroxide, 150 µL of samples were transferred into a 96 well plate and fluorescence was measured with a TECAN infinite M1000Pro plate reader (excitation wavelength at 488 nm, emission at 529 nm).

Fast chlorophyll fluorescence kinetics measurements

To determine photosynthesis parameters in cell cultures, room temperature fast chlorophyll fluorescence kinetics were measured using a Speedzen MX fluorescence imaging system (JBeamBio) with settings previously described (Allorent et al., 2013). To this end, a 150 µL volume of *P. tricornutum* culture was transferred to a transparent 96 well-plate and dark-incubated for 15-30 min before measurements. Excitation was performed in the blue range (λ = 450 nm, *F0*) and actinic light pulses were given with a photosynthetic active wavelength of 520 nm. *F0* is the steady state fluorescence in dark-adapted cultures, *F* in light-adapted cultures; *Fm* is the maximal fluorescence after a

saturating light pulse of dark-adapted cultures, *Fm'* the same in light adapted cultures, *Fv* is the difference between *F0* and *Fm*. With these parameters, the maximum efficiency of energy conversion at photosystem II (PSII) can be calculated as *Fv/Fm* (Misra et al., 2012).

Measure of triacylglycerol accumulation by Nile Red staining

Accumulation of triacylglycerol droplets was monitored by Nile Red (Sigma Aldrich) fluorescent staining (Excitation wavelength at 485 nm; emission at 525 nm) as previously described (Cooksey et al., 1987; Abida et al., 2015). In brief, cells were diluted and adjusted to a cell density that was linearly correlated with Nile Red fluorescence. Nile Red solution (40 µL of a 2.5 µg.mL^{-1} stock solution in 100% DMSO) was added to 160 µL cell suspensions. Oil bodies stained with Nile Red were then visualized using a Zeiss AxioScope.A1 microscope (FITC filter; Excitation wavelength at 488 nm; emission at 519 nm). The productivity, corresponding to the accumulation of TAG per volume and per time unit was calculated based on the staining by Nile Red, and expressed in relative fluorescence unit (Rfu) of Nile Red per mL and per day of incubation. Alternatively, Nile red fluorescence values were normalized to the cell concentration.

Genetic construction for NOA overexpression.

Genomic DNA was extracted from *Phaeodactylum tricornutum* Pt1 cells using the following procedure. Firstly, 10^8 cells were harvested and frozen in liquid nitrogen. A volume of 20 µL of Edward-Buffer (Tris-HCl 200 mM, pH 7.5; NaCl 250 mM; EDTA 25 mM; SDS 0.5%, w/v) was added, then samples were homogenized and debris removed by centrifugation. The supernatant was transferred to the same volume of isopropanol to precipitate DNA. After an additional 15 minute centrifugation at 10,000 x g, the pellet was washed with ethanol 70%, dried and solubilized in TE buffer (10 mM Tris-HCL pH7, 1 mM EDTA). DNA concentration was measured using a Nanodrop 2000 spectrophotometer (Thermo Scientific). Using genomic DNA as matrix, a 2,352-bp sequence was amplified by polymerase chain reaction (PCR) with the following

oligonucleotides designed from Phatr2_56150 (Vardi et al., 2008) and carrying respectively *Xba*I and *EcoR*I restriction sites (underlined sequence): NOA-Fw *Xba*I 5'-TTTATCTAGAATGGTCCCCACTGGTTGTATG-3', NOA-Rev *EcoR*I 5'-TTTAGAATTCCTAATTACGCCCTACACCTTTTCTTC-3'. PCR was performed using Phusion High Fidelity polymerase (Thermo Scientific) according to the manufacturer's instructions. The PCR product was digested by *EcoR*I and *Xba*I, purified and cloned in the linearized expression vector. The expression vector used for overexpression corresponds to the pH4-GUS vector (De Riso et al., 2009). The vector contains a gene coding for resistance to zeocin (Shble), allowing selection of transformed cells. Expression of the NOA gene is controlled by the constitutive histone 4 promoter.

Transformation of **Phaeodactylum** *and selection of strain overexpressing NOA.*

Wild type *Phaeodactylum tricornutum* cells were transformed *via* particle-bombardement under aseptic conditions (Kikkert, 1993), following a diatom protocol (Falciatore et al., 1999) modified as follows. A three to four day-old Pt1 culture was concentrated to 4.10^7 cells in 500 µL and spread onto a 1% agar-plate containing 1 x ESAW medium. While shaking vigorously, 2-3 µg of non-linearized plasmid were added to 25 µL ethanol-sterilized tungsten particles (Sigma), together with 25 µL of 2.5 M $CaCl_2$ and 10 µL of 0.1 M spermidine. After mixing for three minutes using a vortex, the pellet was washed two times (1,500 g; 5 sec; room temperature) with 700 µL precooled 100% ethanol. DNA-coated tungsten particles were then resuspended in 25 µL 100% ethanol. A 12 µL fraction of the mix was transferred onto a macrocarrier and bombardment was carried out using 1,550 psi rupture disks (BioRad). After two to three days of incubation under continuous illumination, cells were transferred to similar agar-plates containing 100 $\mu g \cdot mL^{-1}$ zeocin (Promega) for the selection of resistant transformed cells. Colonies appearing after 4 to 6 weeks were transferred to a new plate for one week, prior to inoculation of 20 mL-liquid cultures.

Measure of NOA gene expression in Phaeodactylum tricornutum *cells.*

To quantify the *NOA* mRNA level in overexpressing lines, quantitative polymerase chain reaction (qPCR) was performed after reverse transcription (RT) of extracted RNA. RNA was extracted from 10^7 cells that were previously pelleted, frozen in liquid nitrogen and stored at -80 °C until processing. A volume of 1 mL TriReagent (Sigma) was added to the frozen pellet and transferred to a new Eppendorf tube. After mixing for 30 sec using a vortex, samples were incubated for 5 min at room temperature. Chloroform (200 µL) was added and tubes, inverted and incubated for 15 min at room temperature. Phase separation was achieved by centrifugation (1,500 g; 30 min; 4°C). The upper phase was transferred to a new tube and RNA was precipitated using 1 volume isopropanol (1,500 g; 30 min; 4°C), washed with 75 % ice cold ethanol (1,500 g; 5 min; 4°C) and the pellet was dried in a Speed Vac system (Eppendorf Concentrator 5301) prior to suspension in 30 µL diethyl dicarbonate (DECP) treated water (Sigma) at 65 °C for 10 min. RNA was purified following a second ethanol precipitation using 1 volume of 5 M NH_4^+, acetate (2.5 M final concentration) and 1 volume isopropanol. Samples were incubated for 10 min on ice and centrifuged, washed, dried and re-suspended as above. Concentration was determined using a NanoDrop device (Life Inc.). Obtained RNA (1 µg) was used for reverse transcription after DNAse treatment (Qiagen) following manufacturer's instructions so as to yield 1 µg cDNA, which were diluted to 10 $ng.\mu L^{-1}$. For quantitative real time PCR, housekeeping gene oligonucleotides previously described (Siaut et al., 2007), namely *RPS* (5′-CGAAGTCAACCAGGAAACCAA-3′ and 5′-GTGCAAGAGACCGGACATACC-3′) and *TUBA* (5′-CTGGGAGCTTTACTGCTTGGA-3′ and 5′-ATGGCTCGAGATCGACGTAAA-3′), were used as internal controls. *NOA*-specific oligonucleotides were 5'-CCTGAAAAGTTCGCTACGCA-3' and 5'-CGGATCCTTTTTGCCCTGAG-3'. The total qPCR reaction volume was 10 µL (120 nM per oligonucleotide, 20 ng cDNA, 5 µL 2X SYBR Green Sso Advanced (BioRad)). A two-step thermo-profile in 40 cycles was applied after 3 min at 95 °C initial denaturation (95°C for 10 sec; 58°C for 30 sec) and a melt curve was detected (from 65°C to 95 °C with a 0.5 °C increment) (BioRad CFX Connect Real-Time System).

Evaluation of gene expression was carried out in 3 biological replicates, each one with technical triplicates, using the CFX Connect Real-Time System software, with *TUBA* and *RPS* as internal controls.

Lipidomic profiling by liquid chromatography – tandem mass spectrometry

Glycerolipids were extracted from freeze-dried *P. tricornutum* cells grown in 50 mL of medium. About 50.10^6 to 100.10^6 cells are required for a triplicate analysis. First, cells were harvested by centrifugation then immediately frozen in liquid nitrogen. Once freeze-dried, the pellet was suspended in 4 mL of boiling ethanol for 5 minutes to prevent lipid degradation, and lipids were extracted as described previously (Simionato et al., 2013) by addition of 2 mL methanol and 8 mL chloroform at room temperature. The mixture was then saturated with argon and stirred for 1 hour at room temperature. After filtration through glass wool, cell debris were rinsed with 3 mL chloroform/methanol 2:1, v/v, and 5 mL of NaCl 1% were then added to the filtrate to initiate phase separation. The chloroform phase was dried under argon before solubilizing the lipid extract in 1 mL of chloroform. Total glycerolipids were quantified from their fatty acids (FAs): in a 10 µL aliquot fraction a known quantity of saturated 15-carbon FA (15:0) was added and all FAs were methanolyzed into methyl esters (FAME) by a 1 hour incubation in 3 mL 2.5% H_2SO_4 in pure methanol at 100°C (Jouhet et al., 2003). The reaction was stopped by addition of 3 mL water, and 3 mL hexane were added for phase separation. After 20 min of incubation, the hexane phase was transferred to a new tube. FAMEs were extracted a second time via the addition, incubation and extraction of another 3 ml hexane. The combined collected hexane fractions (6 ml) were argon-dried and FAMEs were suspended in 30 µL hexane for analysis by gas chromatography coupled with flame ionization detection (GC-FID) (Perkin Elmer), using a BPX70 (SGE) column. FAMEs were identified by comparison of their retention times with those of standards (Sigma) and quantified by the surface peak method using 15:0 for calibration. Extraction and quantification were performed with at least three biological replicates. Glycerolipids were then analyzed and quantified by high pressure liquid chromatography-tandem mass spectrometry (HPLC-MS/MS), with appropriate standard lipids. For a technical triplicate analysis of TAG, an aliquot of

the lipid extract containing 25 nmol of total FAs was dried under argon and dissolved in 100 µL of a methanol/chloroform solution (1:2) containing 125 pmol of 18:0/18:0/18:0 TAG as internal standard. For each replicate, 20 µL were injected in the HPLC-MS/MS system. The analytic device comprised a LC system with binary pumps (Agilent 1260 Infinity) coupled to a QQQ MS (Agilent 6460) equipped with a JetStream electrospray vane of injection. TAGs were separated by HPLC from other lipids using a diol column (Macherey-Nagel, EC 150/2 Nucleosil 100-5 OH) maintained at 40°C. Chromatography was performed using two solvents, i.e. solvent A (isopropanol/water/ammonium acetate 1 M pH 5.3 (850:125:1, v/v) and solvent B (hexane/isopropanol/water/ammonium acetate 1 M pH 5.3 (625:350:24:1, v/v) and the following gradient: from 0 to 5 min, 100% B; from 5 to 30 min, a linear increase of A to 100%; from 30 to 45 min, 100% A; from 45 to 50 min, a linear increase of B to 100%, and from 50 to 70 min, 100% B. The various glycerolipid species were detected from their *m/z* ratio by MS/MS using the Multiple Reaction Monitoring (MRM) mode. The various transition reactions used to identify the different glycerolipid species are those previously established with *Phaeodactylum tricornutum* (Abida et al., 2015). Quantification was made using the Agilent Mass Hunter software furnished by the MS supplier.

MGDG synthase enzymatic assay

A culture of *Phaeodactylum tricornutum* (50 mL in 10 x ESAW medium) was arrested in exponential phase and protein concentration determined using the Lowry method (Lowry et al., 1951). Cells were harvested by a centrifugation for 10 min at 1,500 x g at 4°C. The pellet was completed with 1 volume of CHAPS 12 mM and MOPS-KOH 20 mM pH 7.8 and incubated during 20 minutes at 4°C to solubilize membrane proteins. Detergent solubilized proteins (10 µg) were then incubated during 1 hour with variable concentrations of SNAP (from 0 to 2 mM, as indicated) at room temperature an in the dark in a final volume of 66.5 µL. After incubation with SNAP, galactosyltransferase enzyme activity was assayed in mixed micelles at 25°C, as described previously (Marechal et al., 1994, 1994). Phosphatidylglycerol (1.3 mM) and 1,2-dioleoyl-sn-glycerol (160 µM) dissolved in chloroform were first introduced into clean glass tubes. After evaporation of chloroform under a stream of argon, 300 µL of incubation medium

adjusted to contain 10 µg proteins, 6 mM CHAPS, 250 mM KCl, 250 mM KH_2PO_4/K_2HPO_4 and 10 mM MOPS-KOH pH 7.8 were added. The mixture was mixed vigorously and kept 1 hour at 25°C for equilibration of mixed micelles. Reaction was then started by addition of 1 mM UDP-[^{14}C]Gal (37 Bq.µmol^{-1}) and stopped after 20 min by addition of chloroform/methanol (1:2, v/v). The lipids were subsequently extracted (Bligh and Dyer, 1959) and the radioactivity of the [^{14}C]-labeled MGDG produced, determined by liquid scintillation counting. Activity is expressed in nmol incorporated galactose.h^{-1}.mg protein^{-1}.

RNAseq analyses.

Two sets of RNAseq analyses have been performed. A first set corresponds to *Phaeodactylum* cells exposed to increasing concentrations of NO$^{\bullet}$, provided at 0, 30 and 60 µM using a calibrated NO$^{\bullet}$ saturated aqueous solutions. A second set of experiments corresponds to the comparison of *Phaeodactylum* WT and *NOA*-overexpressing lines. In the first experiments, RNA extraction was performed prior sample transfer for RNAseq analyses. In brief, cell aliquots were processed individually by grinding in liquid nitrogen in a mortar and pestle followed by extraction in RNA Pro lysis solution (MP Biomedicals) using a FastPrep homogenizer (Two 40-sec cycles, with power set at level 6, following manufacturer instructions). After centrifugation the supernatant was recovered and extracted with chloroform; RNA was precipitated by addition of an equal volume of cold absolute ethanol and incubation at -20°C overnight. Precipitated RNA was recovered by centrifugation, washed in 75% ethanol and air dried. The pellet was dissolved in RNase-free water and further purified using the clean-up protocol for the Qiagen RNeasy Mini Kit. RNA samples were quantified with a NanoDrop spectrophotometer and analyzed on an Agilent BioAnalyzer using the Plant RNA Nano program. 2.5 µg of each RNA was sent for RNA-Seq analysis at the McGill University and Genome Quebec Innovation Centre. Libraries for each sample were prepared for stranded 100 bp paired end sequencing and samples were combined and analyzed in a single Illumina Hiseq 2000 lane. In the second experiment, frozen cells (2.10^8 cells) were sent to BGI (Hongkong, China) for RNA extraction using the TRIzol reagent (Chomczynski and Sacchi, 1987) allowing the collection of 10-20 µg RNA per sample,

which quality was assessed based on 28S/18S and RNA Integrity Number (RIN) tests, using an Agilent 2100 Bioanalyzer. Libraries for each sample were prepared for stranded 100 bp paired end sequencing and samples were analyzed independently using an Illumina Hiseq 4000 system (20 M reads). Reads were mapped on the most recent genome version of *Phaeodactylum tricornutum* (http://protists.ensembl.org/Phaeodactylum_tricornutum) using the Star (Spliced Transcripts Alignment to a Reference) method (Dobin et al., 2013; Engstrom et al., 2013). Data were filtered based on the detection of 1 read in at least one sample per treatment or genomic mutation and then normalized using the DESseq2 method (Varet et al., 2016). Clustering was achieved based on expression profiles.

Results and Discussion

Re-evaluation of the previously reported production of NO• by *P. tricornutum* upon exposure to DD (2E,4E/Z-decadienal).

We initiated our study by setting up an experimental protocol previously reported to allow measuring the production of NO• by *P. tricornutum* in response to compounds released from other disrupted diatoms cells (Vardi et al., 2006; Vardi et al., 2008). Following wounding or exposure to nutrient stresses, fatty acids deriving from diatom's phosphoglycerolipids and chloroplast-glycoglycerolipids are oxidized enzymatically and generate volatile polyunsaturated aldehydes (PUAs), *i.e.* 2E,4Z,7E-decatrienal and 2E,4E-decadienal (DD) (Miralto et al., 1999), which were shown to impair grazer's reproduction (Ianora and Miralto, 2010). PUAs have been considered as potent interspecific and intraspecific signaling compounds (Casotti et al., 2005; Vardi et al., 2006). By treating *P. tricornutum* and *Thalassiosira weissflogii* with increasing doses of DD (33-66 µM), a burst of NO• was observed using DAF-FM as a reporter. The signal appeared as early as 5 minutes following treatment and intensity was proportional to DD concentration (Vardi et al., 2006). This production of NO• was inhibited by NMMA, supporting a possible production by an arginine-dependent NOS enzyme. Both DD and externally provided NO• were then reported to trigger programmed cell death (PCD) (Vardi et al., 2006).

First, we sought to detect the endogenous biosynthesis of NO• in *Phaeodactylum* WT cells, following treatment with supposedly non-lethal doses of DD, set at 3.3 µM and 10 µM. However, such DD treatments led to a rapid reduction of chlorophyll fluorescence in *Phaeodactylum* cultures (Figure 1). After 30 min of incubation, relative fluorescence at 680 nm normalized to the cell concentration was reduced by 50 % and further decreased with prolonging time compared to the untreated or solvent treated control (Figure 1A).

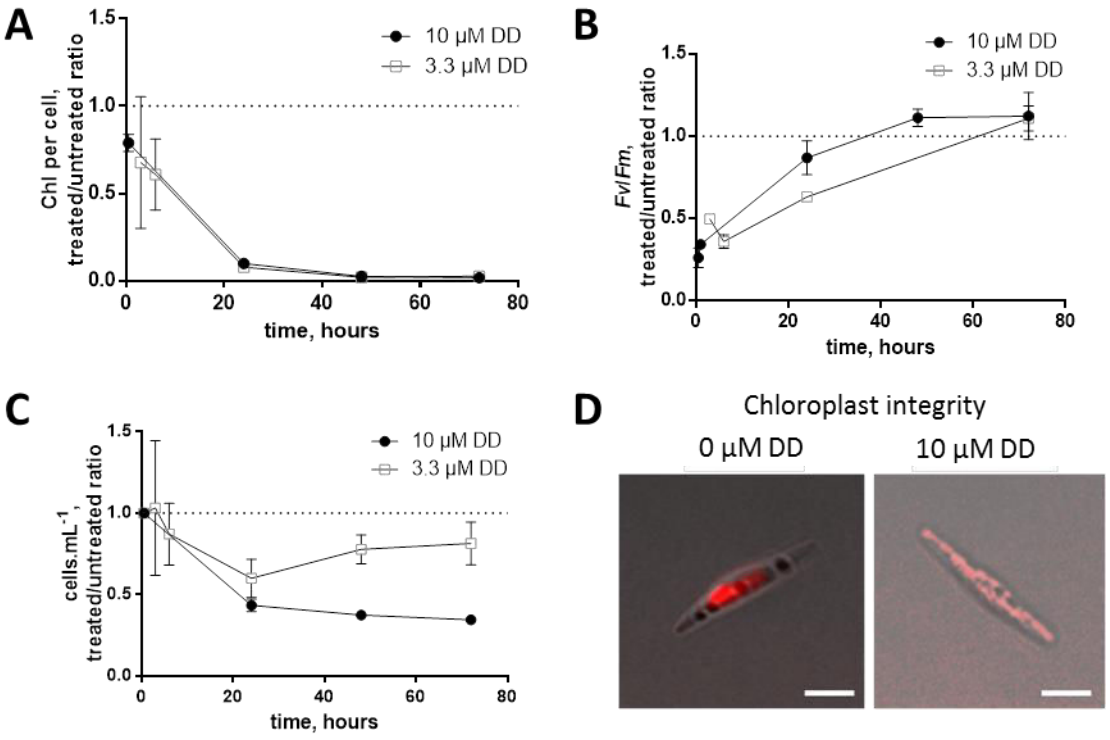

Figure 1. Toxicity of 2E,4/ZE-decadienal (DD) on *Phaeodactylum tricornutum* cells. *Phaeodactylum* cultures were inoculated with a cell density of 2.10^6 and after a 24 hour-preincubation, 3.3 or 10 µM DD were added or cells were left untreated (0 µM DD). **A. Relative chlorophyll content.** Spectrophotometric measurement of fluorescence was performed at 680 nm at room temperature using a 160 µL culture aliquot. **B. Photosynthesis efficiency.** *Fv*/*Fm* was measured *via* fast fluorescence chlorophyll kinetics. **C. Cell concentrations**. Cell concentrations were estimated using a Malassez counting chamber. Values were expressed compared to untreated control at the same time point. **D. Chloroplast integrity.** Cells treated with DD for 2 h or left untreated were observed using a confocal laser scanning microscope. Whereas for untreated samples a gain of 521 HV for the 650 nm to 750 nm waveband was used to visualize chlorophyll autofluorescence, this was insufficient to detect fluorescence in cultures treated with 10 µM DD for 2 h. Increased gains led to a low signal-to-noise ratio without the detection of chloroplast structures in DD treated samples but a saturation of chlorophyll fluorescence in control cells. A 2-h incubation with 10 µM DD led therefore to a loss of chloroplast integrity in treated cells.

Accordingly, the *Fv*/*Fm* ratio dropped immediately after addition of DD, with a strong reduction of fluorescence in dark-adapted cultures (*F0*) that correlates to chlorophyll

concentrations. The *Fv/Fm* ratio relaxed over the time (Figure 1B). Concomitantly, cell growth was arrested in DD treated cells (Figure 1C). The discrepancy of chlorophyll decrease but artifact *Fv*/*Fm* recovery was possibly due to chloroplast degradation. This was confirmed by confocal imaging showing a disintegration of *Phaeodactylum* chloroplasts in response to DD (Figure 1D), consistent with the known unspecific effect of PUAs on membrane integrity (Ribalet et al., 2007). We repeated these experiments and noticed that the destructive effect of DD was similar if the PUA was directly added to the culture or from a stock solutions prepared in 100% DMSO (final concentration 0.5%).

The sensitivity of *Phaeodactylum* cells to DD was therefore much higher than previously published (Vardi et al., 2006; Vardi et al., 2008). We addressed the response of cells to lower DD doses and found a similar response at concentrations ranging from 0.1 µM to 3.3 µM DD with a prominent decline in chlorophyll contents and photosynthetic quantum yield (Figure 2). Indeed even at concentrations as low as 100 nM, the *Fv/Fm* measures were already half of that of untreated cells (Figure 2). In our experimental design, it was therefore not possible to test whether PCD could be triggered by $NO^{\bullet}$. Instead, our results indicate an immediate non-specific death of *Phaeodactylum* cells in presence of DD, which toxicity is already high at 100 nM.

Based on our previous analyses of *Phaeodactylum tricornutum* glycerolipids, the cellular level of polyunsaturated fatty acids (mainly eicosapentaenoic acid, EPA) is rather stable, regardless of the growth medium, *i.e.* about 2 nmol per 10^6 cells in nutrient replete, or nitrogen- or phosphorus-deprived media (Abida et al., 2015). Supposing that all EPA could be converted into PUAs, one should consider that 5.10^6 *Phaeodactylum* cells should be lysed per mL to reach a level of 10 µM PUAs, the level of DD used here, and at least $1.65.10^7$ to $3.3.10^7$ lysed cells per mL to reach 33 and 66 µM PUAs, the levels of DD used in previous studies (Vardi et al., 2006). Such concentrations of diatom cells are far above those recorded *in situ*, by at least three orders of magnitude, and indeed the most recent survey of PUA levels in oceans shows that the highest concentration was in the nanomolar range (Ribalet et al., 2014). Based on the results presented here, we could not confirm that DD could act as a cell-to-cell specific signal in a micromolar

concentration range, but was rather a cell membrane disrupting molecule inducing non-specific death.

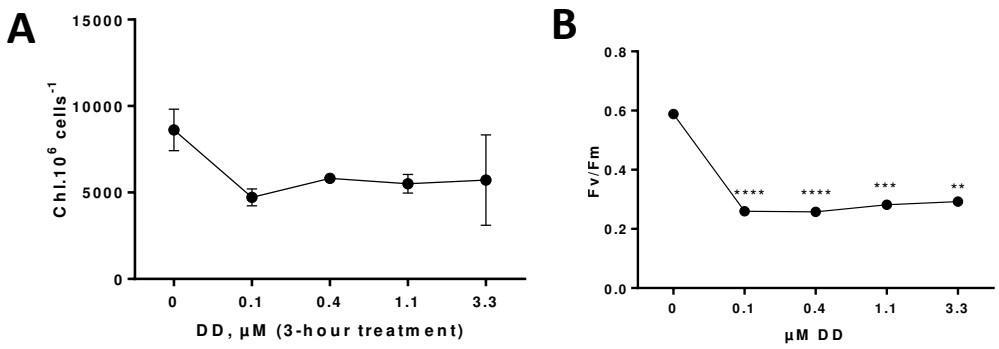

Figure 2. Impairment of *Phaeodactylum* photosynthesis following treatment with 2E,4/ZE-decadienal (DD). Cells were incubated with 0, 0.1, 0.4, 1.1, 3.3, 10 µM DD for 3 h. **A. Chlorophyll content.** Spectrophotometric measurement of fluorescence was performed at 680 nm at room temperature using 10^6 cells. **B. Photosynthesis efficiency.** *Fv*/*Fm* was measured *via* fast fluorescence chlorophyll kinetics. Decreases in *Fv/Fm* in response to DD were significant in t-test (p-value 0.0002, < 0,0001, 0,0004 and 0,001 for 0.1, 0.4, 1.1, 3.3 µM DD, respectively).

The cPTIO reagent (carboxy-2-phenyl-4,4,5,5-tetramethyl-imidazoline-1-oxyl-3-oxide) donates an oxygen atom to $NO^{\bullet}$ to generate NO_2 and is often used to scavenge $NO^{\bullet}$ and act as an antidote (Keszler et al., 2010). We sought whether DD-treated cells could be rescued by cPTIO treatment, as previously reported (Vardi et al., 2008). Unexpectedly, *Phaeodactylum* cells proved to be sensitive to cPTIO, with a one third decrease of chlorophyll and a 20% decline in *Fv/Fm* after incubation with 100 µM cPTIO (dissolved in ESAW) (Figure 3). Cytotoxic effect of PTIO was also observed (not shown). In addition, whereas a caspase inhibitor, carbobenzoxy-valyl-alanyl-aspartyl-[O-methyl]-fluoromethylketone (Z-VAD-FKM) had been stated to partly rescue *Phaeodactylum* cells treated with DD (Vardi et al., 2008), we could not detect any effect of Z-VAD-FKM supplied at 20 to 40 µM on cells treated with 3.3 µM DD (not shown).

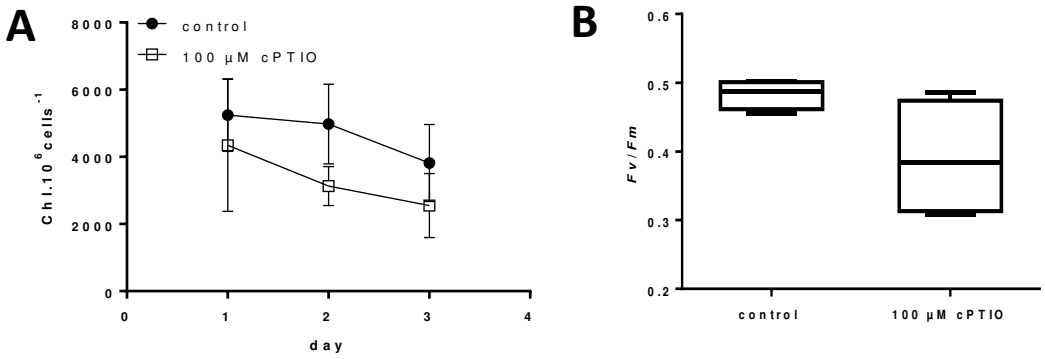

Figure 3. Impairment of *Phaeodactylum* photosynthesis following treatment with cPTIO. A culture volume of 500 µL was inoculated at 50^5 cells.mL^{-1} and medium-dissolved cPTIO was added or cells were left untreated. At indicated time points, a 160 µL culture aliquot was taken for measurements. **A. Chlorophyll content.** Spectrophotometric measurement of fluorescence was performed at 680 nm at room temperature at time points indicated. **B. Photosynthesis efficiency.** *Fv*/*Fm* was measured via fast fluorescence chlorophyll kinetics.

Taken together, we could not obtain results consistent with previously published studies showing a specific DD → NO• → PCD cascade. We therefore reconsidered the question of the physiological role of NO•. In the following experiments, neither cPTIO nor PTIO could be used to revert the effects observed after NO• treatments.

External supply of NO• impairs the growth of *P. tricornutum*

We used two systems for supplying nitric oxide to *P. tricornutum* cells, either by providing NO• directly as a gas, mitigated to saturation in the growth medium (1.9 mM saturated concentration) or by adding a NO•-donor agent, S-Nitroso-N-acetylpenicillamine (SNAP). Nitroso-acetylpenicillamine (NAP) was used as a non-active compound for control experiments. We verified the production of NO• following SNAP dissolution by two methods. Firstly, using Membrane Inlet Mass Spectrometry (MIMS, NRC Halifax analytical platform), we observed an increase of the NO• signal (*m/z* = 30) with increasing doses of SNAP, up to a concentration of 600 µM

(Supplementary Figure 1). Secondly, using the DAF-FM probe, we detected a signal in less than 30 minutes following dilution (Supplementary Figure 2), showing the efficiency of this $NO^{\bullet}$-donor in our experimental design.

Both $NO^{\bullet}$ supplied directly as a gas (Supplementary Figure 3) and donated by SNAP (Figure 4) impaired the growth of *Phaeodactylum* in a dose dependent manner, as previously reported (Vardi et al., 2006; Vardi et al., 2008). While concentrations at 1 mM SNAP and below reduce growth by only 20%, a decrease of about 60% was observed for higher concentrations. Therefore, a concentration of 1 mM SNAP was selected for further experiments. In contrast to DD, SNAP treatment did not affect chlorophyll levels (Figure 3).

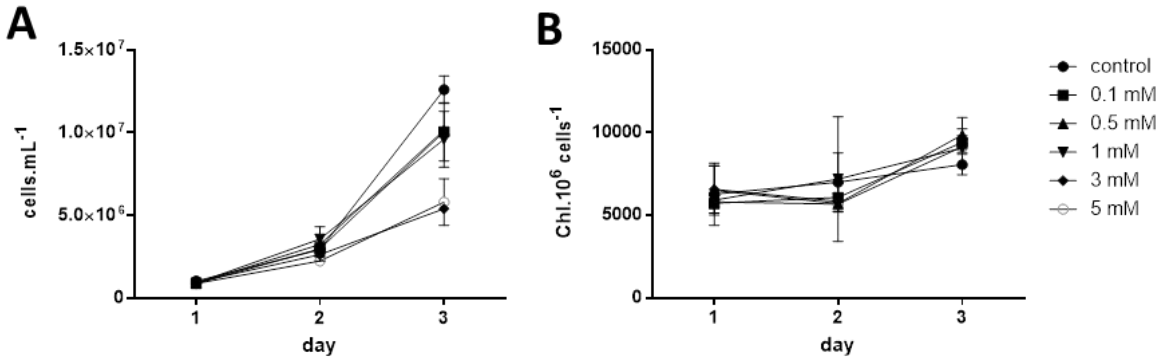

Figure 4: Effect of $NO^{\bullet}$ supplied by SNAP on the growth of *Phaedoactylum*. The incubation was performed in a volume of 500 µL, inoculated at 10^6 cells.mL^{-1}, with immediate addition of SNAP. **A. Cell concentrations.** Cell concentrations were estimated using a Malassez counting chamber. **B. Chlorophyll content.** Spectrophotometric measurement of fluorescence was performed at 680 nm at room temperature using 10^6 cells.

External supply of $NO^{\bullet}$ triggers the accumulation of triacylglycerol (TAG) within *P. tricornutum* cells

$NO^{\bullet}$ is known to act as a signaling molecule, in particular in *Chlamydomonas* grown in N-starved conditions, a condition also known to trigger the accumulation of triacylglycerol (TAG) in microalgae. We analyzed the accumulation of TAG droplets in

Phaedoactylum by Nile Red fluorescent staining. We observed that a 2-day incubation with 1 mM SNAP in a 500 µL culture volume triggered a 2.2 fold increase of TAG per cell (Figure 5A) and a >2 fold increase of TAG productivity, corresponding to the level of TAG per volume of culture and per day (Figure 5B). Interestingly, while upon nitrogen starvation two large lipid droplets are visible, flanking the chloroplast (Abida et al., 2015), in SNAP treated cells numerous lipid droplets of variable sizes can be observed (Figure 5C).

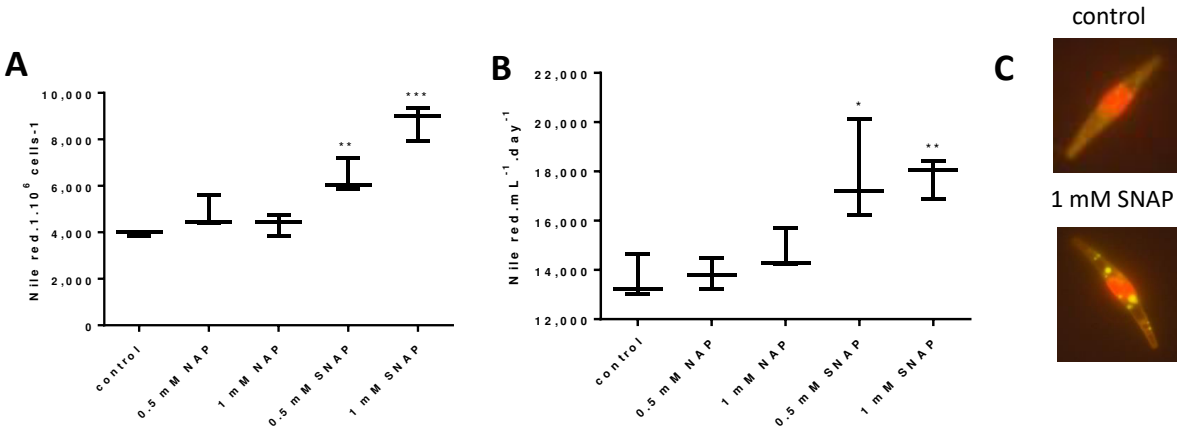

Figure 5. Effect of increasing concentrations of SNAP on the production of TAG in *Phaedocatylum tricornutum*. The incubation was performed in a volume of 500 µL, inoculated at 10^6 cells.mL^{-1}, with immediate addition of chemicals. Measurements were performed after 2 days of incubation. **A. Effect of increasing concentrations of SNAP on TAG level per cell.** TAG level per cell were measured using Nile Red fluorescent staining and is given in relative fluorescence units per 10^6 cells. Stars indicate statistical relevant treated compared to untreated samples, with p-value 0.005 and 0.0004 for 0.5 mM SNAP and 1 mM SNAP, respectively. **B. Effect of increasing concentrations of SNAP on TAG productivity.** TAG productivity is given in relative fluorescence unit (Rfu) corresponding to the fluorescence of Nile Red per mL and per day. **(C) Epifluorescence images** on Nile red stained treated and untreated cells. Statistically relevant were the responses to 0.5 mM SNAP (p-value 0.03) and 1 mM SNAP (p-value 0.004).

TAG accumulation in *Phaeodactylum* being a classical response to multiple stresses (Abida et al., 2015), we sought therefore whether this effect could be attributed to $NO^{\bullet}$ as an external stressor or as an internal signal, enzymatically produced by the diatom

itself. To that purpose, we re-examined the question of the endogenous production of $NO^{\bullet}$.

Arginine-independent and nitrite-dependent biosynthesis of $NO^{\bullet}$ in *Phaeodactylum*

Data from previous studies on $NO^{\bullet}$ production by diatoms are confusing. On the one hand, it was shown that $NO^{\bullet}$ production was blocked by NMMA (Vardi et al., 2006) and authors concluded on the action of a NOS using arginine as a substrate. Intriguingly, it was not possible to detect any NOS-like sequence in the genome of *P. tricornutum* (Di Dato et al., 2015), so the biochemical evidence for an arginine-dependent NOS could not be supported at the molecular level. On the other hand, an orthologous sequence of the plant chloroplast NO-associated (NOA) protein sequence was identified (Vardi et al., 2008). NOA-overexpression led to a $NO^{\bullet}$ increase, a reduction of growth and a decrease of *Fv/Fm*. NOA overexpressors were also reported to be hypersensitive to DD, with a growth arrest at 3.3 µM or 6.6 µM DD, compared to WT cells being unaffected by such a treatment (Vardi et al., 2008), conditions that were shown here to trigger unspecific cell death in the WT. The *Arabidopsis* homolog AtNOA acts in $NO^{\bullet}$ production but the protein does not possess any NOS function *in vitro* (Moreau et al., 2008). AtNOA1 together with nitrate reductase (NR) are responsible for the majority of $NO^{\bullet}$ releases (Gas et al., 2009; Moreau et al., 2010). The direct mode of action of AtNOA1 remains elusive although it might be involved in the regulation of NR activity (Jin et al., 2009; Mandal et al., 2012). In the NR-dependent pathway, $NO^{\bullet}$ is produced by reduction of nitrite (NO_2^-) by a NR (Supplementary Figure 4). Nitrite is mostly reduced to ammonium (NH_3) by the nitrite reductase (NiR), and ammonium is a substrate for the biosynthesis of arginine. Therefore, addition of arginine could have a negative feedback regulation on NiR thereby providing high nitrite levels for NR-dependent $NO^{\bullet}$ production (Supplementary Figure 4). This could explain a positive action of arginine supply on $NO^{\bullet}$ production, *via* NR and in the absence of any NOS. A way to make the distinction between $NO^{\bullet}$ produced from arginine *via* a NOS or *via* a NR is to detect an

inhibition of the NOS-pathway by NMMA or by L-NAME (Nω-nitro-L-arginine methyl ester).

We analyzed therefore the endogenous level of $NO^{\bullet}$ in *Phaeodactylum* culture in presence of the two potential substrates, arginine and NO_2^-. The detection of $NO^{\bullet}$ in *Phaeodactylum* was much higher when the diatoms were cultured in presence of NO_2^-, should it be in the presence or absence of NO_3^- (Figure 6), supporting a production *via* the action of NR. By contrast, addition of arginine did not impact significantly on the production of $NO^{\bullet}$. Similarly, addition of L-NAME did not lead to any significant change when cells were co-fed with NO_3^- or arginine (Figure 6).

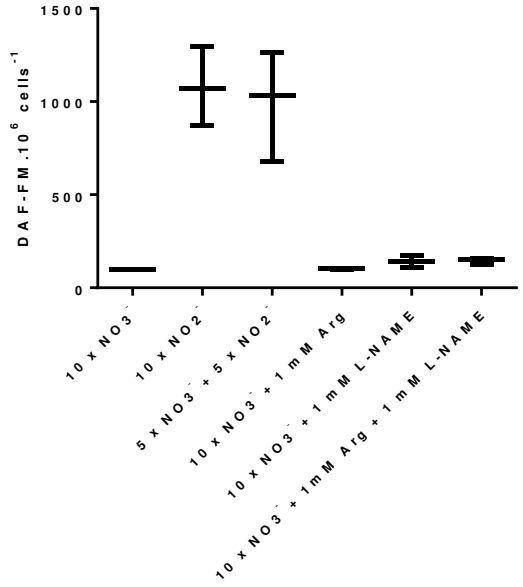

Figure 6. Detection of NO in *Phaedocatylum* based on nitrogen sources. Cells were harvested from complete media and inoculated in nitrogen-free media at 20^6 cells.mL^{-1}. DAF-FM (100% DMSO, Sigma) was added at a concentration of 10 µM. After dark incubation and washing, cells were aliquoted into 500 µL cultures supplemented with the indicated nitrogen sources: nitrate (NO_3^-, standard medium), nitrite (NO_2^-), 1 mM arginine (Arg) and the NOS-blocking agent L-NAME. DAF-FM fluorescence was recorded after three hours of incubation.

Taken together, these results support an arginine-independent (NOS-independent) and nitrite-dependent (NR-dependent) production of $NO^{\bullet}$ in *Phaeodactylum* WT under standard conditions. Our data confirm that NR is an efficient source for $NO^{\bullet}$ as observed in other photosynthetic eukaryotes from distant clades, such as *Arabidopsis* (Moreau et al., 2010; Sanz-Luque et al., 2015), the red macroalga *Gracilaria chilensis* (Chow et al., 2013) and the green alga *Chlamydomonas* (Wei et al., 2014). We do not confirm the previously reported NOS activity for $NO^{\bullet}$ production in *Phaeodactylum* (Vardi et al., 2006; Vardi et al., 2008). Authors had concluded on a NOS activity based on increased $NO^{\bullet}$ production in response to DD measured with the help of a citrulline/arginine feeding methods on whole cell protein extracts (Vardi et al., 2006). Given the destructive effect of DD, one cannot exclude an interference with the method. In our study, feeding arginine to *Phaeodactylum* cultures without additional DD treatment did not support the presence of a NOS activity. In the present work, we used the *Phaeodactylum* accession Pt1 CCAP 1055 whereas the previously study used CCMP 632, thus we cannot exclude strain dependent differences.

Evaluation of the role of NOA in $NO^{\bullet}$ production by *Phaeodactylum*

We sought whether the NOA protein could be involved in the endogenous production of $NO^{\bullet}$ *via* a NOS-independent pathway. We designed genetic constructions for *NOA* overexpression. Genomic DNA was extracted from *P. tricornutum* Pt1 strain. Using gDNA as matrix, a 2352 bp sequence was amplified by PCR using oligonucleotides designed from Phatr2_56150 (Vardi et al., 2008) and carrying cloning restriction sites. The PCR product cloned into the pH4 vector (De Riso et al., 2009), transformed *P. tricornutum* WT cells and obtained overexpressing lines after zeocin selection, including NOAOE4 and NOAOEf generated by two independent series of transformation experiments (Figure 7).

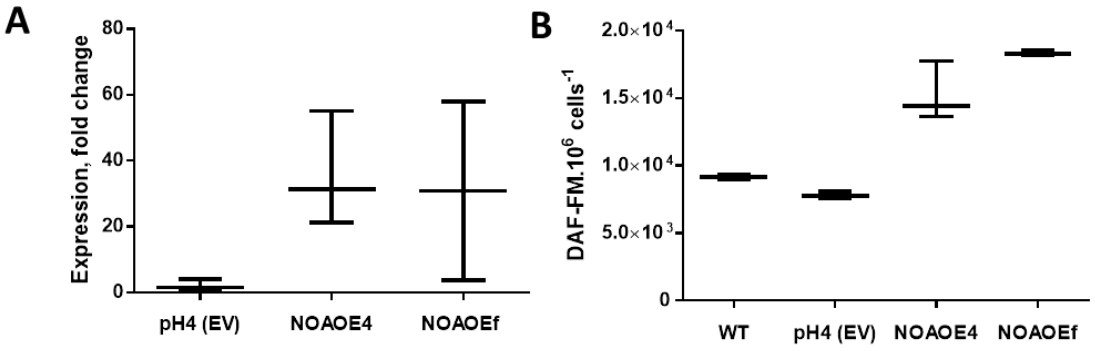

Figure 7. *Phaeodactylum tricornutum* NOA overexpressing lines produce more NO•. A. NOA mRNA level in cells transformed with the empty vector (pH4 (EV)) and the NOA overexpression construct. RNA was extracted from a 10^8 cell pellet and reversely transcribed. Quantitative real time PCR was conducted on 20 ng cDNA using oligonucleotides binding *TUB* and *RPS* as internal controls and *NOA*. **B. NO• production in NOA overexpressing lines measured via fluorescence of DAF-FM.** Cultures of the respective lines were inoculated at 2.10^6 cells.mL^{-1}. DAF-FM (100% DMSO, Sigma) was added at a concentration of 10 µM. After dark incubation and washing, cells were collected into 500 µL aliquots and fluorescence was measured after three hours of incubation.

The RNA level of the NOA gene was more than 30-fold induced in the two independent overexpressing lines, NOAOE4 and NOAOEf (Figure 7A) and led to a 4-5-fold elevated NO• production (Figure 7B), which was consistent with previous reports (Vardi et al., 2008). We thus confirmed that NOA played a role in NO• production and used therefore these overexpressing lines as models for the analysis of the physiological role of NO• in *Phaeodactylum*. We obtained similar results with both independent overexpressing lines and present below results obtained with NOAOE4.

Role of NOA and NO• on the transcriptional control of nitrogen-assimilation genes and on the onset of the response of *Phaeodactylum* to nitrogen starvation.

In plants, the precise molecular function of NOA is unresolved, but some reports suggest an interplay with nitrogen assimilation (Yamasaki and Sakihama, 2000; Moreau et al., 2010). NO• production was also correlated with a transcriptional control of nitrogen-

assimilation genes, as described for *Chlamydomonas* (de Montaigu et al., 2010). We sought whether such transcriptional control could exist in *Phaeodactylum*. To that purpose, we analyzed by qRT-PCR the expression level of the genes coding for NR (Phatr2|30060) and the two nitrite reductases, NiR1 and NiR2 (Phatr2|27759 and Phatr|51344, respectively). In nutrient replete conditions (10 x ESAW), the *NR* and *NiR1* genes were significantly induced in NOAOE4, whereas *NiR2* expression did not appear to be significantly changed compared to the respective wild type and cells transformed with the empty vector (Figure 8).

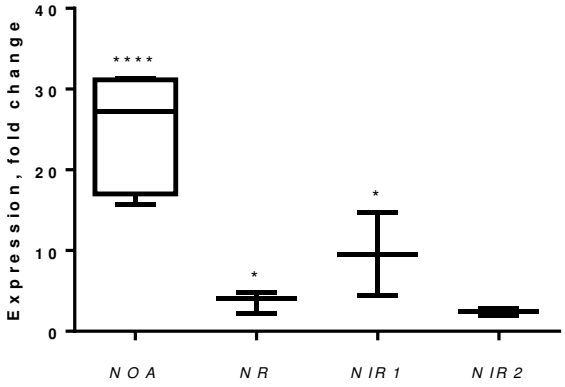

Figure 8: Effect of NOA overexpression on the expression level of nitrogen assimilation genes in nutrient replete condition. RNA was extracted from a 10^8 cell pellet of NOAOE4, WT and pH4 and reversely transcribed. Quantitative real time PCR was conducted on 20 ng cDNA using oligonucleotides binding *TUB* and *RPS* as internal controls and *NOA, NR* and two *NIR* isoforms as genes of interest. Quantification cycles of NOAOE4 derived cDNA were normalized to WT and pH4 values. Significant changes were observed on the level of NOA (p-value < 0.0001), NR (p-value 0.0125) and Nir1 (p-value 0.023).

The expression analyses indicate that the putative ribosome stabilizing GTPase protein NOA (Gas et al., 2009) is involved in the regulation of nitrogen metabolism proteins that are responsible for $NO^{\bullet}$ production. *Phaeodactylum* increases NR levels when nitrogen

is limited (Levitan et al., 2015; Yang et al., 2016). We investigated if NOA was also responsive to nitrogen. In the 3-day time course of cells shifted to nitrogen depleted conditions, the typical nitrogen starvation responses occurred, *i.e*. reduction of *Fv*/*Fm*, chlorophyll fluorescence and cell growth and induction of neutral lipids as measured after Nile red treatment (Figure 9A). We confirmed a rapid and strong early induction of *NR* and *NIR1* in response to nitrogen starvation (Figure 9B). *NIR2* and *NOA* responded to nutrient deprivation, following a late induction pattern, reaching a maximal 4-6-fold induction after three days of cultivation (Figure 9B). Thus, in a nutrient-replete culture the overexpression of *NOA* correlates with higher *NR* and *NIR* levels, but expression patterns under nitrogen starvation are not synchronized downstream an increase of *NOA* mRNA. A regulatory function of NOA during nitrogen depletion, inducing *NR* and *NIR*, cannot be excluded since the *Arabidopsis* NOA protein was shown to be regulated post-translationally (Mandal et al., 2012).

Following nitrogen starvation, there was no difference between the induction of *NIR1* and *NIR2* in the WT or NOAOE lines (Supplementary Figure 5). Altogether, these results are consistent with a transient role of NOA and $NO^{\bullet}$ in the onset of the response to nitrogen starvation, but not on the intensity of this response, including the activation of the nitrogen assimilation systems. Interestingly, in *Chlamydomonas*, $NO^{\bullet}$ produced upon nitrogen shortage was generated from nitrite (Miller et al., 2010; Wei et al., 2014), as shown here in *Phaeodactylum*.

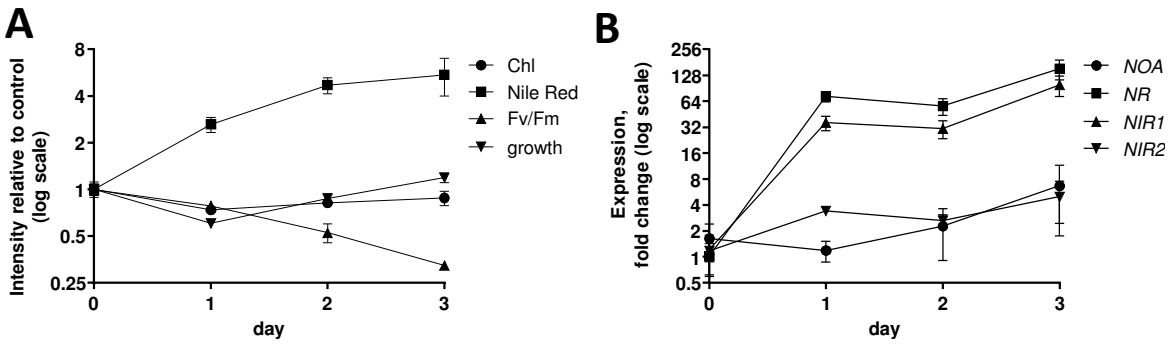

Figure 9: Expression of *NOA*, *NR*, *NIR1* and *NIR2* in the course of nitrogen starvation. Cells were harvested and resuspended in nitrogen-free media in 100 mL cultures a concentration of 10^6 cells.mL^{-1}. Each day, a 20 mL culture aliquot was harvested for RNA extraction and a 300 µL culture aliquot was used for physiological measurements. **A. Physiological parameters.** Chlorophyll (Chl) was measured by the absorption at 680 nm at room temperature, Nile red fluorescence was quantified to indicate neutral lipid contents, *Fv*/*Fm* was measured using fast chlorophyll fluorescence kinetics and cell concentrations were estimated via the absorption at 750 nm. **B. *NOA*, *NR*, *NIR1* and *NIR2* gene expression.** RNA was extracted from a cell pellet and reversely transcribed. Quantitative real time PCR was conducted on 20 ng cDNA using oligonucleotides binding *TUB* and *RPS* as internal controls and *NOA, NR* and two *NIR* isoforms as genes of interest. Data are normalized with value measured with cells harvested before the shift. Data are the results of three independent biological replicates.

The higher expression of *NR* and *NIR*, known to be responsive to nitrogen depletion, together with the elevated TAG level following the treatment of *Phaeodactylum* cells with exogenous $NO^{\bullet}$ (Figure 5) motivated a refined lipid profiling of the NOAOE lines. We could observe that in nutrient replete conditions, the level of TAG per cell estimated by Nile Red staining was higher in NOAOE lines, consistent with a larger number of intracellular lipid droplets as also observed for SNAP treated cells (Supplementary Figure 6).

Consistent with the Nile red measurements, the total fatty acid profile of NOAOE lines compared to the WT indicated significantly higher 16:0 and 18:0 levels and a 2.3 increase in TAG productivity (Figure 10, A and C). By contrast, very long chain polyunsaturated fatty acids (VLC-PUFAs) displayed trends of reductions and accordingly the greatest sink for VLC-PUFAs, *i.e.* chloroplast monogalactosyldiacylglycerol (MGDG), was significantly reduced in the overexpression

lines (Figure 10, B). The distribution of fatty acids in the different lipid classes was reported previously (Abida et al., 2015) and was similar in the present study. The fatty acid profiles of TAG and MGDG were unaltered (Supplementary Figure 7)

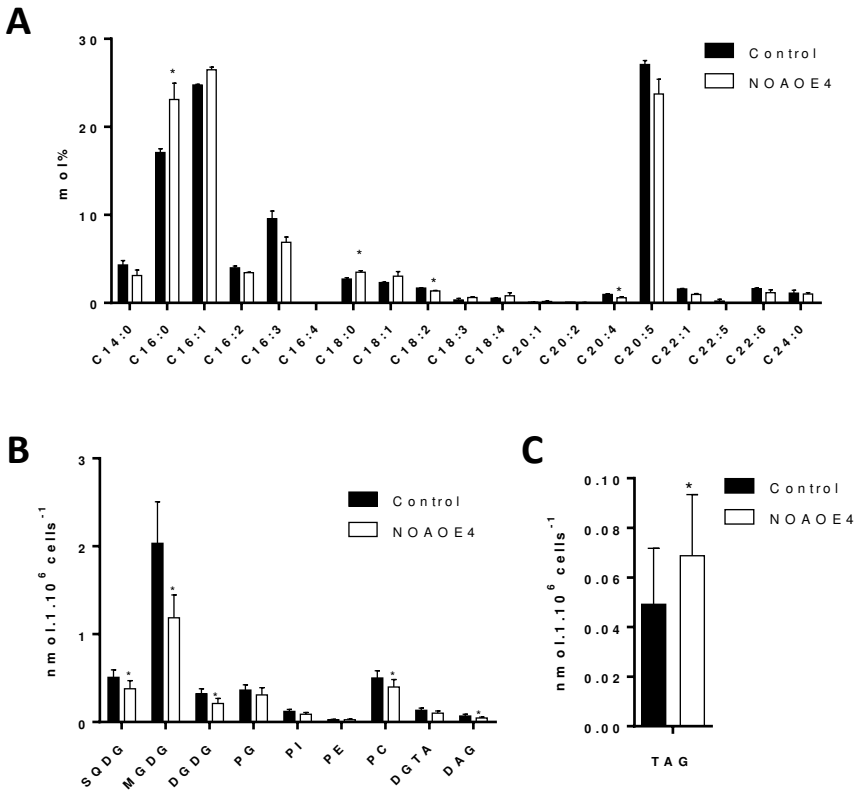

Figure 10: Effect of NOA overexpression on total fatty acid and glycerolipid profiles in *Phaeodactylum* cells grown in nutrient replete conditions. Three day old 50 mL cultures inoculated at 10^6 cells.ml^{-1} were harvested and lipids extracted. **A. Total fatty acid distributions.** The fatty acid distribution in total lipid extracts was based on GC-FID analyses of fatty acid methyl esters. **B. Membrane glycerolipid profiles. C. Triacylglycerol content.** Glycerolipid class abundances per million cells were assessed based on HPLC-MS/MS analyses, as described previously (Abida et al., 2015). DAG, diacylglycerol; DGDG, digalactosyldiacylglycerol; DGTA, diacylglyceryl hydroxymethyltrimethyl-β-alanine, MGDG, monogalactosyldiacylglycerol; PC, phosphatidylcholine; PE, phosphatidylethanolamine; PG, phosphatidylglycerol; PI, phosphatidylinositide; SQDG, sulfoquinovosyldiacylglycerol; TAG, triacylglycerol. Stars indicate significant changes with p-values < 0.05.

The TAG increase in NOA-overexpressing lines, even moderate, could have a biotechnological interest for oil production in diatoms grown in nutrient replete conditions. We evaluated this increase in a pilot experiment, with a supply of air or 1.5% CO_2 and in two growth media, using a multicutivator system consisting of air-lift photobioreactors run in parallel. This comparison was performed between WT and NOAOE4 grown in 50 ml of medium ESAW or medium F for 8 days (late exponential growth phase). Illumination was set to 60 µE for the first three days of cultivation and then increased to 120 µE at day 4 until samples were collected at day 8. Lipids were analyzed from collected cells by LC-MSMS. The supply of CO_2 and the modification of media had no impact on the phenotype due to NOA overexpression, with WT *Phaeodactylum* accumulating 21-45 µg TAG per 10^6 cells (50-101 $\mu g.mL^{-1}$) and NOAOE4 accumulating 101-119 µg TAG per 10^6 cells (105-145 $\mu g.mL^{-1}$). Altogether, our comparisons show that NOA overexpression leads to a doubling in TAG content in *Phaeodactylum*.

Direct effect of $NO^{\bullet}$ on the activity of *Phaeodactylum* MGDG synthase

According to the lipid profiles, only the abundances of MGDG and TAG were affected in NOAOE lines compared to the WT. We sought whether the decrease in galactolipids could occur by a direct effect of $NO^{\bullet}$ on the activity of biosynthetic enzymes. The *Phaeodactylum* genome encodes three putative MGDG synthase isoforms (Phatr_14125, Phatr_54168, and Phatr_9619). We used the enzymatic assay developed for plant MGDG synthase, providing radioactive UDP-galactose to *Phaeodactylum* protein extracts, and measured the incorporation of the radioactivity in galactolipids extracted by solvents, following incubation with increasing concentrations of SNAP (Figure 11). MGDG synthase activity was altered, with a 50% decrease following incubation with 0.5 mM SNAP. This result suggests that $NO^{\bullet}$ can affect MGDG synthases, likely by S-nitrosylation of the thiol groups known to be essential for the activity of this enzyme (Marechal et al., 1994; Marechal et al., 1995), which could be responsible for a decrease of plastid glycerolipid biosynthesis, and for a partial redirection of glycerolipid flux toward TAG.

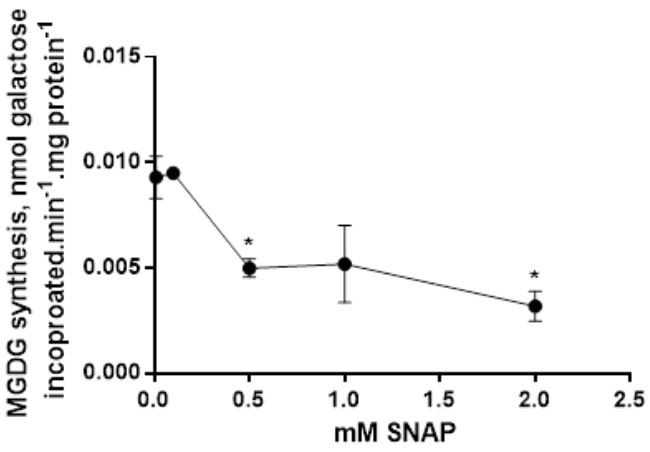

Figure 11: Effect of NO• on the MGDG synthase activity in *Phaeodactylum* membrane extracts. Activity was assayed based on the incorporation of galactose in MGDG, following incubation with radiolabeled UDP-[^{14}C]galactose. Data are the results of three technical replicates. Stars indicate significant changes with p-values < 0.05.

Whole genome transcriptome analysis of *Phaeodactylum* in response to NO•

We analyzed the effects of increasing doses of NO• on the whole transcriptome of *Phaeodactylum*. To that purpose, we supplied NO• as a gas so as to provide reference values for NO• concentrations, *i.e.* 0, 30 and 60 µM.

Comment: *Bioinformatic analyses of transcriptomic studies are ongoing in the laboratory and will complete the present article in preparation, prior submission.*

Conclusion.

This study was motivated by evaluating the possible impact of environmental variations of the NO• level in oceans on phytoplankton, and more particularly diatoms. NO• was

previously reported to be emitted by diatoms in response to high concentrations of PUAs and then to act in cell-to-cell communication, triggering PCD and allowing diatom population size control (Vardi et al., 2006; Vardi, 2008; Vardi et al., 2008; Bidle, 2015). However, using *Phaeodactylum* as a model, we could not confirm the physiological response to DD applied at 3.3 µM or 10 µM, supposed to trigger a specific production of $NO^{\bullet}$ by this diatom. In our experimental design, DD appeared highly cytotoxic, as well as the cPTIO scavenger of $NO^{\bullet}$, previously reported to act as an antidote of the DD effect. Likewise, we could not confirm the previously reported production of $NO^{\bullet}$ by a NOS-like activity using arginine as a substrate, and could not inhibit the $NO^{\bullet}$ production by a NOS inhibitor (Vardi et al., 2006; Vardi et al., 2008). Rather, our work shows that in *Phaeodactylum* wild type cells, $NO^{\bullet}$ is produced *via* a nitrate-dependent pathway, by a side activity of the NR. Exogenous supply of $NO^{\bullet}$ inhibiting growth, we sought whether a role in stress signaling could be detected. We confirmed that the overexpression of *NOA* was correlated with an increase in endogenous $NO^{\bullet}$ (Vardi et al., 2008), but could not provide any evidence on the way NOA controls this level. Our analyses are consistent with a role of $NO^{\bullet}$ on the activation of the transcription of nitrogen assimilation genes and on the remodeling of glycerolipids redirecting the flux toward the production of TAG. These responses are also observed early after nitrogen deprivation (Abida et al., 2015; Alipanah et al., 2015). Our results suggest therefore a role of $NO^{\bullet}$ during the onset of the low-nitrogen response.

The triggering of TAG accumulation by $NO^{\bullet}$ is also interesting for biotechnological applications aiming at using diatoms for producing oil as a feedstock. We observed the phenotype of NOA-overexpressing lines, with a doubling of TAG content per cell and an increase in overall productivity in both flasks and photobioreactor systems, supplied with different growth media and with or without CO_2 supply.

Eventually, an increase of $NO^{\bullet}$ in the environment could therefore perturb the physiological status of diatoms and act as an important stressor at the ecosystem level. Future works include therefore the characterization of the interplay between nitrate, nitrite and nitric oxide in diatoms, involving *NR*, *NIR* and *NOA*, the functional

characterization of these genes and the evaluation of a possible role of $NO^{\bullet}$ in the response to other nutrient variations and other abiotic or biotic stresses.

Acknowledgements

This work was supported by grants from Agence Nationale de la Recherche (ANR DiaDomOil), CEA (Irtelis PhD grant program), the CEA-Total partnership, Programme Investissement d'Avenir (Océanomics).

References

Abida H, Dolch LJ, Mei C, Villanova V, Conte M, Block MA, Finazzi G, Bastien O, Tirichine L, Bowler C, Rebeille F, Petroutsos D, Jouhet J, Marechal E (2015) Membrane glycerolipid remodeling triggered by nitrogen and phosphorus starvation in Phaeodactylum tricornutum. Plant Physiol **167:** 118-136

Alipanah L, Rohloff J, Winge P, Bones AM, Brembu T (2015) Whole-cell response to nitrogen deprivation in the diatom Phaeodactylum tricornutum. J Exp Bot **66:** 6281-6296

Allorent G, Courtois F, Chevalier F, Lerbs-Mache S (2013) Plastid gene expression during chloroplast differentiation and dedifferentiation into non-photosynthetic plastids during seed formation. Plant Mol Biol **82:** 59-70

Anandarajah K, Mahendraperumal G, Sommerfeld M, Hu Q (2012) Characterization of microalga Nannochloropsis sp mutants for improved production of biofuels. Applied Energy **96:** 371-377

Benvenuti G, Bosma R, Cuaresma M, Janssen M, Barbosa MJ, Wijffels RH (2015) Selecting microalgae with high lipid productivity and photosynthetic activity under nitrogen starvation. Journal of Applied Phycology **27:** 1425-1431

Bidle KD (2015) The molecular ecophysiology of programmed cell death in marine phytoplankton. Ann Rev Mar Sci **7:** 341-375

Bligh GE, Dyer WJ (1959) A rapid method of total lipid extraction and purification. Can. J. Biochem. Physiol. **37:** 911-917

Casotti R, Mazza S, Brunet C, Vantrepotte V, Ianora A, Miralto A (2005) Growth inhibition and toxicity of the diatom aldehyde 2-trans, 4-trans-decadienal on Thalassiosira weissflogii (Bacillariophyceae). Journal of Phycology **41:** 7-20

Chomczynski P, Sacchi N (1987) Single-step method of RNA isolation by acid guanidinium thiocyanate-phenol-chloroform extraction. Anal Biochem **162:** 156-159

Chow F, Pedersen M, Oliveira MC (2013) Modulation of nitrate reductase activity by photosynthetic electron transport chain and nitric oxide balance in the red macroalga Gracilaria chilensis (Gracilariales, Rhodophyta). Journal of Applied Phycology **25:** 1847-1853

Cooksey KE, Guckert B, Williams SA, Callis PR (1987) Fluorometric determination of the neutral lipid content of microalgal cells using Nile Red. J. Microbiol. Meth. **6:** 333-345

de Montaigu A, Sanz-Luque E, Galvan A, Fernandez E (2010) A soluble guanylate cyclase mediates negative signaling by ammonium on expression of nitrate reductase in Chlamydomonas. Plant Cell **22:** 1532-1548

De Riso V, Raniello R, Maumus F, Rogato A, Bowler C, Falciatore A (2009) Gene silencing in the marine diatom Phaeodactylum tricornutum. Nucleic Acids Res **37:** e96

Di Dato V, Musacchia F, Petrosino G, Patil S, Montresor M, Sanges R, Ferrante MI (2015) Transcriptome sequencing of three Pseudo-nitzschia species reveals comparable gene sets and the presence of Nitric Oxide Synthase genes in diatoms. Sci Rep **5:** 12329

Dobin A, Davis CA, Schlesinger F, Drenkow J, Zaleski C, Jha S, Batut P, Chaisson M, Gingeras TR (2013) STAR: ultrafast universal RNA-seq aligner. Bioinformatics **29:** 15-21

Engstrom PG, Steijger T, Sipos B, Grant GR, Kahles A, Ratsch G, Goldman N, Hubbard TJ, Harrow J, Guigo R, Bertone P, Consortium R (2013) Systematic evaluation of spliced alignment programs for RNA-seq data. Nat Methods **10:** 1185-1191

Eroglu E, Gottschalk B, Charoensin S, Blass S, Bischof H, Rost R, Madreiter-Sokolowski CT, Pelzmann B, Bernhart E, Sattler W, Hallstrom S, Malinski T, Waldeck-Weiermair M, Graier WF, Malli R (2016) Development of novel FP-based probes for live-cell imaging of nitric oxide dynamics. Nat Commun **7:** 10623

Falciatore A, Casotti R, Leblanc C, Abrescia C, Bowler C (1999) Transformation of Nonselectable Reporter Genes in Marine Diatoms. Mar Biotechnol (NY) **1:** 239-251

Falciatore A, d'Alcala MR, Croot P, Bowler C (2000) Perception of environmental signals by a marine diatom. Science **288:** 2363-2366

Fowler D, Coyle M, Skiba U, Sutton MA, Cape JN, Reis S, Sheppard LJ, Jenkins A, Grizzetti B, Galloway JN, Vitousek P, Leach A, Bouwman AF, Butterbach-Bahl K, Dentener F, Stevenson D, Amann M, Voss M (2013) The global nitrogen cycle in the twenty-first century. Philos Trans R Soc Lond B Biol Sci **368:** 20130164

Gallardo L, Rhodes H (1997) Oxidized nitrogen in the remote pacific: the role of electrical discharges over the oceans. J. Atmos. Chem. **26:** 147-168

Gas E, Flores-Perez U, Sauret-Gueto S, Rodriguez-Concepcion M (2009) Hunting for plant nitric oxide synthase provides new evidence of a central role for plastids in nitric oxide metabolism. Plant Cell **21:** 18-23

Gerrard W (1980) Gas solubilities widespread applications. ,

Holloway JM, Dahlgren RA (2002) Nitrogen in rock: Occurrences and biogeochemical implications. Global Biogechem. Cyc. **16:** 65-61–65-17.

Ianora A, Miralto A (2010) Toxigenic effects of diatoms on grazers, phytoplankton and other microbes: a review. Ecotoxicology **19:** 493-511

IPCC (2014) Climate Change 2014: Synthesis Report. Contribution of Working Groups I, II and III to the Fifth Assessment Report of the Intergovernmental Panel on Climate Change. IPCC, Geneva, Switzerland

Jin CW, Du ST, Zhang YS, Lin XY, Tang CX (2009) Differential regulatory role of nitric oxide in mediating nitrate reductase activity in roots of tomato (Solanum lycocarpum). Ann Bot **104:** 9-17

Jouhet J, Marechal E, Bligny R, Joyard J, Block MA (2003) Transient increase of phosphatidylcholine in plant cells in response to phosphate deprivation. FEBS Lett **544:** 63-68

Kampschreur MJ, Temmink H, Kleerebezem R, Jetten MSM, van Loosdrecht MCM (2009) Nitrous oxide emission during wastewater treatment. Water Research **43:** 4093-4103

Keszler A, Zhang Y, Hogg N (2010) Reaction between nitric oxide, glutathione, and oxygen in the presence and absence of protein: How are S-nitrosothiols formed? Free Radic Biol Med **48:** 55-64

Kikkert JR (1993) The Biolistic(R) Pds-1000 He Device. Plant Cell Tissue and Organ Culture **33:** 221-226

Kumar A, Castellano I, Patti FP, Palumbo A, Buia MC (2015) Nitric oxide in marine photosynthetic organisms. Nitric Oxide **47:** 34-39

Lauritano C, Borra M, Carotenuto Y, Biffali E, Miralto A, Procaccini G, Ianora A (2011) Molecular evidence of the toxic effects of diatom diets on gene expression patterns in copepods. PLoS One **6:** e26850

Lauritano C, Carotenuto Y, Miralto A, Procaccini G, Ianora A (2012) Copepod population-specific response to a toxic diatom diet. PLoS One **7:** e47262

Levitan O, Dinamarca J, Hochman G, Falkowski PG (2014) Diatoms: a fossil fuel of the future. Trends Biotechnol **32:** 117-124

Levitan O, Dinamarca J, Zelzion E, Gorbunov MY, Falkowski PG (2015) An RNA interference knock-down of nitrate reductase enhances lipid biosynthesis in the diatom Phaeodactylum tricornutum. Plant J **84:** 963-973

Lowry OH, Rosebrough NJ, Farr AL, Randall RJ (1951) Protein Measurement with the Folin Phenol Reagent. Journal of Biological Chemistry **193:** 265-275

Mandal MK, Chandra-Shekara AC, Jeong RD, Yu K, Zhu S, Chanda B, Navarre D, Kachroo A, Kachroo P (2012) Oleic acid-dependent modulation of NITRIC OXIDE ASSOCIATED1 protein levels regulates nitric oxide-mediated defense signaling in Arabidopsis. Plant Cell **24:** 1654-1674

Marechal E, Block MA, Joyard J, Douce R (1994) Comparison of the kinetic properties of MGDG synthase in mixed micelles and in envelope membranes from spinach chloroplast. FEBS Lett **352:** 307-310

Marechal E, Block MA, Joyard J, Douce R (1994) Kinetic properties of monogalactosyldiacylglycerol synthase from spinach chloroplast envelope membranes. J Biol Chem **269:** 5788-5798

Marechal E, Miege C, Block MA, Douce R, Joyard J (1995) The catalytic site of monogalactosyldiacylglycerol synthase from spinach chloroplast envelope membranes. Biochemical analysis of the structure and of the metal content. J Biol Chem **270:** 5714-5722

Martens-Habbena W, Qin W, Horak RE, Urakawa H, Schauer AJ, Moffett JW, Armbrust EV, Ingalls AE, Devol AH, Stahl DA (2015) The production of nitric oxide by marine ammonia-oxidizing archaea and inhibition of archaeal ammonia oxidation by a nitric oxide scavenger. Environ Microbiol **17:** 2261-2274

Michalski G, Bhattachary SK, Girsh G (2014) NOx cycle and the tropospheric ozone isotope anomaly: an experimental examination. Atmos. Chem. Phys. **14:** 4935-4953

Miller MR, Megson IL (2007) Recent developments in nitric oxide donor drugs. Br J Pharmacol **151:** 305-321

Miller R, Wu G, Deshpande RR, Vieler A, Gartner K, Li X, Moellering ER, Zauner S, Cornish AJ, Liu B, Bullard B, Sears BB, Kuo MH, Hegg EL, Shachar-Hill Y, Shiu SH, Benning C (2010) Changes in transcript abundance in Chlamydomonas reinhardtii following nitrogen deprivation predict diversion of metabolism. Plant Physiol **154:** 1737-1752

Miralto A, Barone G, Romano G, Poulet SA, Ianora A, Russo GL, Buttino I, Mazzarella G, Laabir M, Cabrini M, Giacobbe MG (1999) The insidious effect of diatoms on copepod reproduction. Nature **402:** 173-176

Misra AN, Misra M, Singh R (2012) Chlorophyll fluorescence in plant biology. *In* AN Misra, ed, Biophysics. InTech, pp 171-192

Moreau M, Lee GI, Wang Y, Crane BR, Klessig DF (2008) AtNOS/AtNOA1 is a functional Arabidopsis thaliana cGTPase and not a nitric-oxide synthase. J Biol Chem **283:** 32957-32967

Moreau M, Lindermayr C, Durner J, Klessig DF (2010) NO synthesis and signaling in plants--where do we stand? Physiol Plant **138:** 372-383

Naqvi SWA, Yoshinari T, Jayakumar DA, Altabet MA, Narvekar PV, Devol AH, Brandes JA, Codispoti LA (1998) Budgetary and biogeochemical implications of N2O isotope signatures in the Arabian Sea. Nature **394:** 462-464

Nicholls JC, Davies CA, Trimmer M (2007) High-resolution profiles and nitrogen isotope tracing reveal a dominant source of nitrous oxide and multiple pathways of nitrogen gas formation in the central Arabian sea. Limnol. Oceanogr. **52:** 156-168.

Olasehinde EF, Takeda K, Sakugawa H (2010) Photochemical production and consumption mechanisms of nitric oxide in seawater. Environ. Sci. Technol. **44**

Pan Y, Ni BJ, Lu H, Chandran K, Richardson D, Yuan Z (2015) Evaluating two concepts for the modelling of intermediates accumulation during biological denitrification in wastewater treatment. Water Res **71:** 21-31

Ribalet F, Bastianini M, Vidoudez C, Acri F, Berges J, Ianora A, Miralto A, Pohnert G, Romano G, Wichard T, Casotti R (2014) Phytoplankton cell lysis associated with polyunsaturated aldehyde release in the Northern Adriatic Sea. PLoS One **9:** e85947

Ribalet F, Berges JA, Ianora A, Casotti R (2007) Growth inhibition of cultured marine phytoplankton by toxic algal-derived polyunsaturated aldehydes. Aquat Toxicol **85:** 219-227

Ribalet F, Wichard T, Pohnert G, Ianora A, Miralto A, Casotti R (2007) Age and nutrient limitation enhance polyunsaturated aldehyde production in marine diatoms. Phytochemistry **68:** 2059-2067

Rockel P, Strube F, Rockel A, Wildt J, Kaiser WM (2002) Regulation of nitric oxide (NO) production by plant nitrate reductase in vivo and in vitro. J Exp Bot **53:** 103-110

Sakihama Y, Nakamura S, Yamasaki H (2002) Nitric oxide production mediated by nitrate reductase in the green alga Chlamydomonas reinhardtii: an alternative NO production pathway in photosynthetic organisms. Plant Cell Physiol **43:** 290-297

Sanz-Luque E, Chamizo-Ampudia A, Llamas A, Galvan A, Fernandez E (2015) Understanding nitrate assimilation and its regulation in microalgae. Front Plant Sci **6:** 899

Sanz-Luque E, Ocana-Calahorro F, Llamas A, Galvan A, Fernandez E (2013) Nitric oxide controls nitrate and ammonium assimilation in Chlamydomonas reinhardtii. J Exp Bot **64:** 3373-3383

Siaut M, Heijde M, Mangogna M, Montsant A, Coesel S, Allen A, Manfredonia A, Falciatore A, Bowler C (2007) Molecular toolbox for studying diatom biology in Phaeodactylum tricornutum. Gene **406:** 23-35

Simionato D, Block MA, La Rocca N, Jouhet J, Marechal E, Finazzi G, Morosinotto T (2013) The response of Nannochloropsis gaditana to nitrogen starvation includes de novo biosynthesis of triacylglycerols, a decrease of chloroplast galactolipids, and reorganization of the photosynthetic apparatus. Eukaryot Cell **12:** 665-676

St Laurent CD, Moon TC, Befus AD (2015) Measurement of nitric oxide in mast cells with the fluorescent indicator DAF-FM diacetate. Methods Mol Biol **1220:** 339-345

Stohr C, Strube F, Marx G, Ullrich WR, Rockel P (2001) A plasma membrane-bound enzyme of tobacco roots catalyses the formation of nitric oxide from nitrite. Planta **212:** 835-841

Vardi A (2008) Cell signaling in marine diatoms. Commun Integr Biol **1:** 134-136

Vardi A, Bidle KD, Kwityn C, Hirsh DJ, Thompson SM, Callow JA, Falkowski P, Bowler C (2008) A diatom gene regulating nitric-oxide signaling and susceptibility to diatom-derived aldehydes. Curr Biol **18:** 895-899

Vardi A, Formiggini F, Casotti R, De Martino A, Ribalet F, Miralto A, Bowler C (2006) A stress surveillance system based on calcium and nitric oxide in marine diatoms. PLoS Biol **4:** e60

Varet H, Brillet-Gueguen L, Coppee JY, Dillies MA (2016) SARTools: A DESeq2- and EdgeR-Based R Pipeline for Comprehensive Differential Analysis of RNA-Seq Data. PLoS One **11:** e0157022

Vunjak-Novakovic G, Kim Y, Wu XX, Berzin I, Merchuk JC (2005) Air-lift bioreactors for algal growth on flue gas: Mathematical modeling and pilot-plant studies. Industrial & Engineering Chemistry Research **44:** 6154-6163

Wei L, Derrien B, Gautier A, Houille-Vernes L, Boulouis A, Saint-Marcoux D, Malnoe A, Rappaport F, de Vitry C, Vallon O, Choquet Y, Wollman FA (2014) Nitric oxide-triggered remodeling of chloroplast bioenergetics and thylakoid proteins upon nitrogen starvation in Chlamydomonas reinhardtii. Plant Cell **26:** 353-372

Wendehenne D, Pugin A, Klessig DF, Durner J (2001) Nitric oxide: comparative synthesis and signaling in animal and plant cells. Trends Plant Sci **6:** 177-183

Wilson ID, Neill SJ, Hancock JT (2008) Nitric oxide synthesis and signalling in plants. Plant Cell Environ **31:** 622-631

Yamasaki H, Sakihama Y (2000) Simultaneous production of nitric oxide and peroxynitrite by plant nitrate reductase: in vitro evidence for the NR-dependent formation of active nitrogen species. FEBS Lett **468:** 89-92

Yang J, Pan YF, Bowler C, Zhang LX, Hu HH (2016) Knockdown of phosphoenolpyruvate carboxykinase increases carbon flux to lipid synthesis in Phaeodactylum tricornutum. Algal Research-Biomass Biofuels and Bioproducts **15:** 50-58

Zehr JP, Ward BB (2002) Nitrogen cycling in the ocean: new perspectives on processes and paradigms. Appl Environ Microbiol **68:** 1015-1024

Zhang Z, Xing L, Wu Z, Liu C, Lin C, Liu L (2006) Discovery of nitric oxide in marine ecological system and the chemical characteristics of nitric oxide. Sci. Cina Ser. B Chem. **49:** 475-481

Zhu W, Xiao S, Zhang D, Liu P, Zhou H, Dai W, Liu F, Li H (2015) Highly efficient and stable Au/CeO2-TiO2 photocatalyst for nitric oxide abatement: potential application in flue gas treatment. Langmuir **31:** 10822-10830

4.4.1 *Supplementary figures*

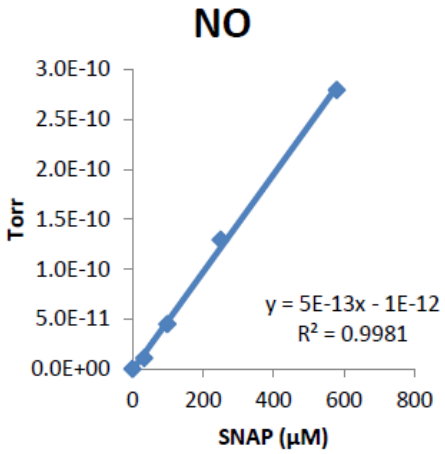

Supplementary Figure 1. MIMS detection of the emission of NO• by SNAP. A solution of S-nitroso-N-acetylpenicillamine (SNAP) was prepared at concentrations from 0 µM to 600 µM. The intensity of the signal corresponding to NO• (m/z = 30) increased linearly with the concentration of dissolved SNAP.

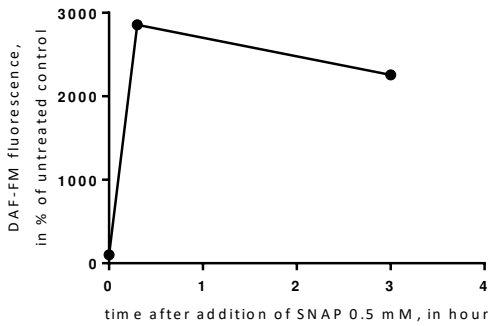

Supplementary Figure 2. Detection of the emission of NO• by SNAP, the NO•-donor used in this study. A concentration of 10 µM DAF-FM (100% DMSO, Sigma) were added to a culture inoculated at 20^6 cells.mL^{-1}. After dark incubation and washing, 500 µL culture aliquots were spread and 0.5 mM S-nitroso-N-acetylpenicillamine (SNAP) (100 mM stock solution in H_2O) was added. DAF-FM fluorescence was measured after 30 minutes and after 3 hours, illustrating the stability of NO• produced by SNAP in this time range.

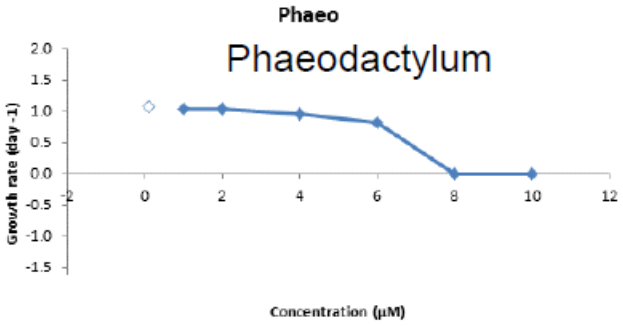

Supplementary Figure 3: Effect of NO• directly supplied as a gas on the growth rate of *Phaeodactylum*.

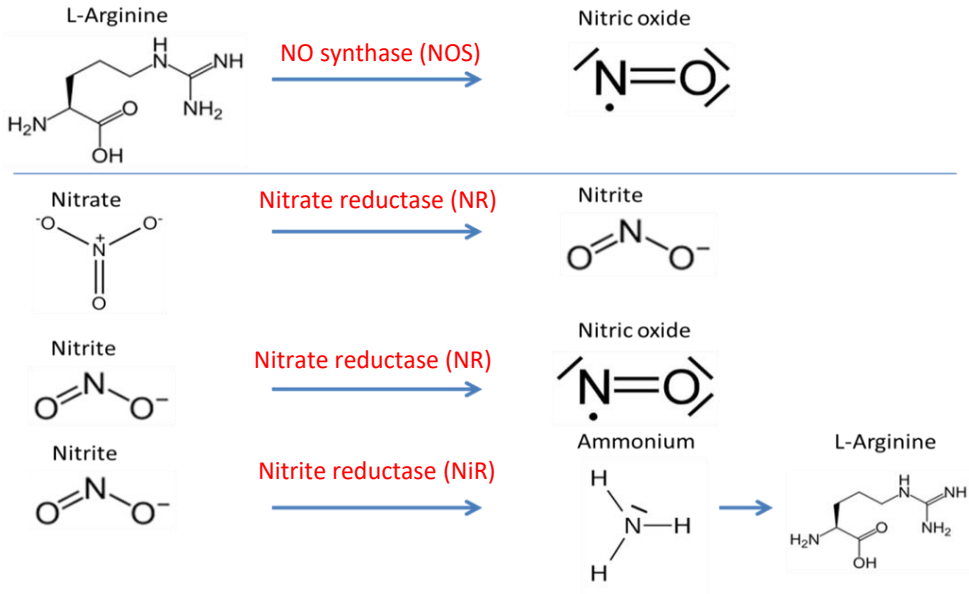

Supplementary Figure 4. Alternative pathways for NO• production in microorganisms.

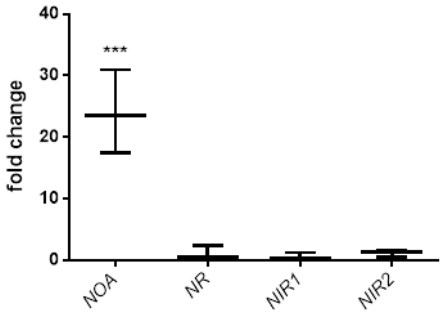

Supplementary Figure 5: Comparison of the expression level of nitrogen assimilation genes in a *NOA* overexpressing line and a WT, after 4 days of nitrogen starvation. RNA was extracted from a 10^8 cell pellet of NOAOE4, WT and pH4 and reversely transcribed. Quantitative real time PCR was conducted on 20 ng cDNA using oligonucleotides binding *TUB* and *RPS* as internal controls and *NOA, NR* and two *NIR* isoforms as genes of interest. Quantification cycles of NOAOE4 derived cDNA were normalized to WT and pH4 values. Data are the results of three independent biological replicates. Stars indicate significant changes (p-value < 0.001).

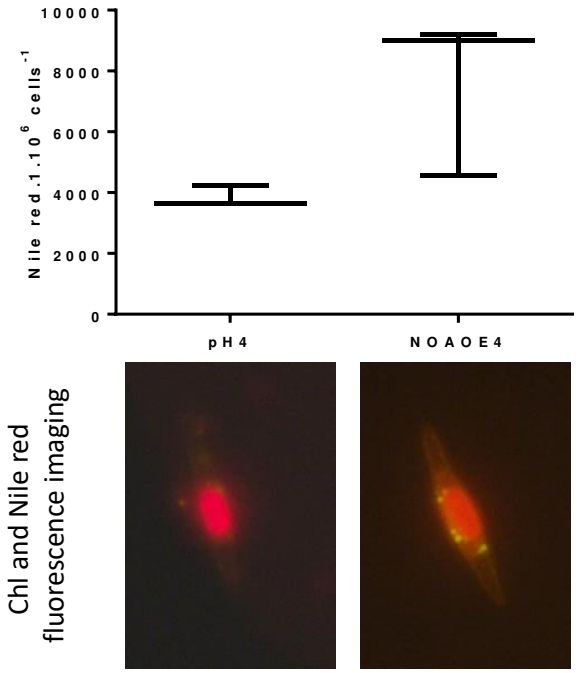

Supplementary Figure 6: Effect of *NOA* overexpression on the level of neutral lipids in *Phaeodactylum* cells. Nile red staining and fluorescence quantification were performed on a 300 µL aliquot of three day old 50 mL-culture inoculated at 10^6 cells.mL^{-1}. Data are the results of three independent biological replicates. A representative cell is shown for each line. These samples were used for complete glycerolipid profiling.

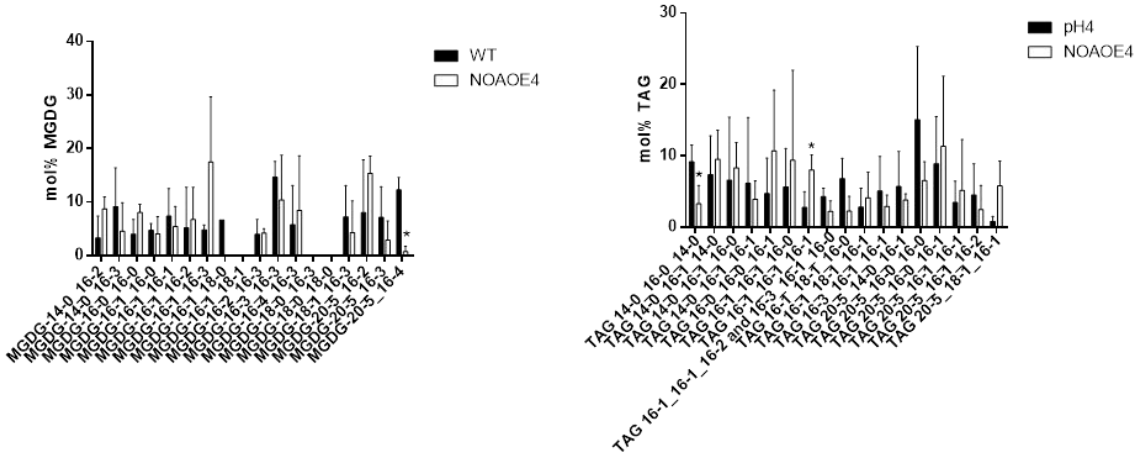

Supplementary Figure 7: Fatty acid distribution in MGDG and TAG in NOAOE4 and WT. Three day old 50 mL cultures inoculated at 10^6 cells.mL^{-1} were harvested and lipids extracted. Glycerolipid fatty acid compositions were revealed by HPLC-MS/MS as described previously (Abida et al., 2015). MGDG, monogalactosyldiacylglycerol; TAG, triacylglycerol.

4.5 The NO• production site is important for its signalling function in *Phaeodactylum tricornutum* neutral lipid metabolism

4.5.1 *The location of NO• production is important for the TAG accumulation function*

During the optimization of the SNAP treatment protocol, we found opposing effects of NO• donation when the chemical was dissolved in the growth media or DMSO, respectively (**figure 4.4**).

Diluted in aqueous solution, SNAP was present in the media and likely to incorporate into membranes (Nedeianu et al. 2004). In this case, the NO• signal came from the outside of the cell as during cell-to-cell communication. If DMSO was used as a vector however, bilayers were destabilized and SNAP was likely to diffuse into the cell. Thus, the NO• signal would have (an additional) intracellular origin. Similarly, DD-induced NO• production was observed in proximity of the nucleus (Vardi et al. 2006) and we could not find evidence for TAG accumulation in response to aldehyde treatment. By contrast, the overexpression of the chloroplast protein NOA increased NO• production as well as neutral lipid synthesis.

NO• is a gaseous signalling molecule that can diffuse within compartments and pass membranes (Missner & Pohl 2009). The spatio-temporal distribution is critical for respective downstream reactions of a ubiquitous second messenger (Batistič & Kudla 2012). Therefore, the finding of a locus-dependent effect was not surprising. NO• was able to trigger oil accumulation only when the signal came from the outside or from the chloroplast. A signal from outside the cell is also perceived in the cell-to-cell signalling function of NO•. This commonly communicates stress conditions, for example in order to induce biofilm formation in single cell organisms (Allen et al. 2006, Brownlee 2008, Kutty et al. 2013, Schreiber et al. 2008, Thompson et al. 2008). Those signals occur in response to stressful life conditions. The chloroplast is highly susceptible to nutrient stress that may alter the redox balance (Allen et al. 2006, Brownlee 2008, Schreiber et al. 2008, Thompson et al. 2008, Lim et al. 2007). For instance, nitrogen stress lowers photoquenching capacities and triggers the production of NO• (Wei et al. 2014).

Furthermore, when quenching capacities are exceeded, oxylipins are produced from peroxidation of thylakoid located PUFAs (Demmig-Adams et al. 2013). Based on these findings we hypothesise NO• signals coming from the chloroplast or from the cells' environment communicate stress conditions and trigger neutral lipid accumulation as a stress response in oleaginous microalgae, whereas NO• signatures from the cytosol may have other functions. To confirm this, we performed feeding assays to investigate a correlation of NR activity on NO_2^- and TAG accumulation.

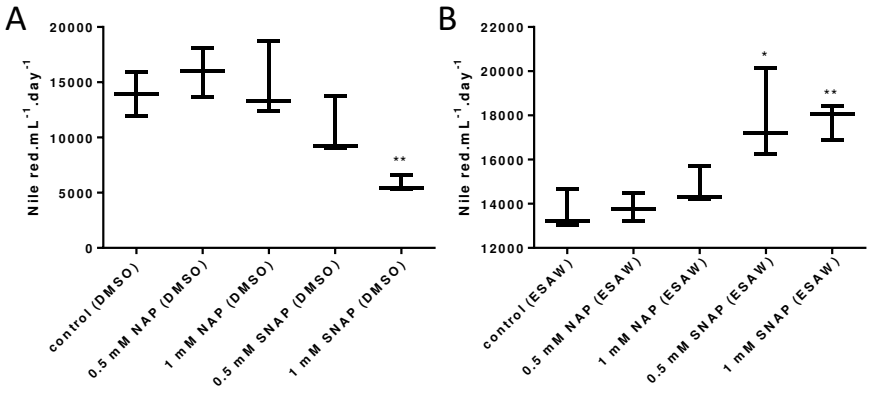

Figure 4.4. Nile red fluorescence quantification of SNAP treated *Phaeodactylum*. A 100 mM SNAP or NAP stock solution was prepared in **100% DMSO (A)** or **ESAW media (B)** and applied to 500 µL cultures inoculated at 1.10^6 cells.mL^{-1}. Relative neutral lipid productivity was measured after two days of incubation using a TECAN plate reader. NAP did not induce significant changes. Dissolved in DMSO, 1 mM SNAP reduced Nile red values (p-value 0.003). When dissolved in ESAW, both 0.5 mM (p-value 0.03) and 1 mM (p-value 0.004) SNAP treatment increased relative neutral lipid productivity.

4.5.2 *Nitrite triggers NO• but not TAG production in Phaeodactylum*

In photosynthetic organisms, most NO• production depends on NR (Moreau et al. 2010). The reductase accepts NO_2^- as a substrate when NO_3^- levels are low thereby producing NO• (Sakihama et al. 2002, Schreiber et al. 2012). Vardi and coworkers fed *Phaeodactylum* with the arginine analogue NG-monomethyl-L-arginine (NMMA) and found lower NO• production. Therefore, they have concluded on a protein possessing NOS activity (Vardi et al. 2006). We conducted feeding experiments to reveal NR

dependent NO• production and NOS activity, and a potential correlation with neutral lipid synthesis (**figure 4.5**). When nitrate in the growth media was entirely or partially replaced by nitrite, a boost in NO• production was indicated by DAF-FM fluorescence measurements in *Phaeodactylum* cultures (**figure 4.5 A**). By contrast, neither feeding the NOS substrate arginine nor the inhibitor Nω-Nitro-L-arginine methyl ester hydrochloride (L-NAME) altered NO• concentrations in the WT. Arginine increased NO• production in NOAOE4 by 61-63% independent on the presence or absence of L-NAME (p-value 0.0002-< 0.0001). Importantly, L-NAME was not able to abolish the signal in neither *Phaeodactylum* WT nor NOAOE4. Furthermore, the arginine caused NO• induction was low compared to the 10-fold increase of NO• synthesis in NOAOE4, when nitrate was replaced by nitrite (p-value 0.001).

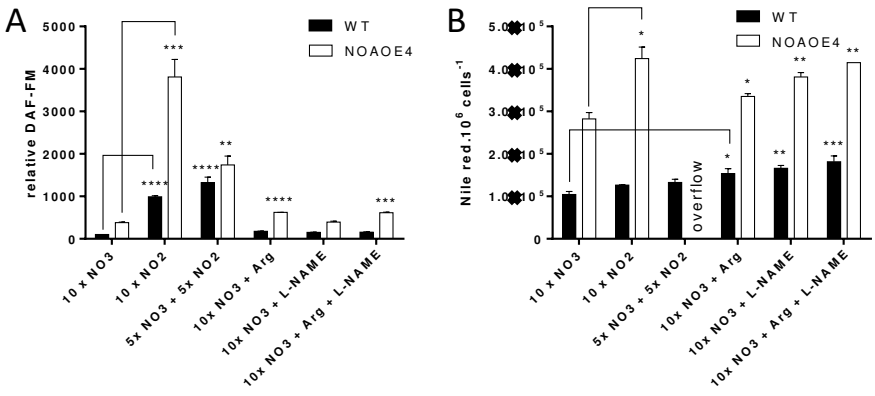

Figure 4.5. NO• production in *Phaeodactylum* WT and NOA overexpressing lines strongly relies on NR activity and is insensitive to NOS inhibitors. Cells from *Phaeodactylum* WT or NOAOE4 cultures were harvested resuspendend in nitrogen depleted media and treated with DAF-FM. After the dye was washed away and cells resuspendend in nitrogen depleted media, aliquots of 500 µL were inoculated at a concentration of 1.10^6 cells.mL^{-1}. Then, the respective N-source was added. A concentration of 466.7 mg.mL^{-1} of NO_3 or NO_2^- is designated as 10 x, and 233.35 mg.mL^{-1} respectively as 5 x, according to the concentrations in 10N10P ESAW media. A. After three hours of incubation, a 160 µL aliquot was collected and DAF-FM fluorescence was measured using a TECAN plate reader. B. After two days of incubation, a 300 µL aliquot was collected for the determination of cell concentrations and out of this volume, 160 µL were taken for Nile red staining and quantification using a TECAN plate reader. All differences between WT and NOAOE4 had a p-value < 0.001.

We can thus conclude that in both lines, NO• production was predominantly caused by NR. Additionally, NOA seemed to be involved in an arginine-dependent NO• production that is however insensitive to the NOS inhibitor L-NAME. This pathway is probably located in the chloroplast (Tewari et al. 2013). These results opposed the earlier observation on *Phaeodactylum* where NO• production was highly sensitive to NMMA (Vardi et al. 2006). Thus, we cannot fully exclude the presence of NOS activity that involves the action of NOA. The effect on nitrite in NOAOE4 could either indicate signal propagation from the chloroplast to the cytosolic NR or indicate that chloroplast NO• production might rely on both arginine and NO_2^-. This would be in line with the finding that mouse eNOS could act as NOS or nitrite reductase (Milsom et al. 2010).

The replacement of nitrate by nitrate in the media did not cause significantly higher Nile red fluorescence after two days of incubation in the WT (**figure 4.5 B**). By contrast, the addition of 1 mM arginine or L-NAME or both led to 47% (p-value 0.024), 59% (p-value 0.003) and 74% (p-value 0.007) higher neutral lipid levels in the WT, respectively. The increase in cellular neutral lipid contents in response to arginine or L-NAME compared to nitrate was WT-like in NOAOE4. This was likely due to a mixotrophy effect since amino acids are readily metabolized by the diatom (Flynn & Syrett 1986). NR is localized in the cytosol (Cookson et al. 2005). Thus, the lack of NO_2^--induced TAG accumulation in the WT was line with our idea that NO• produced in the cytosol does not have a stress signature and is thus unable to trigger neutral lipid production in *Phaeodactylum.* The 3.4-fold induction of TAG contents observed in NOAOE4 when nitrate was replaced by nitrite pointed retrograde signalling from the chloroplast to the cytosol (Chi et al. 2015). Propagation of the chloroplast derived NO• signature could for example serve in the signal transmission to the nucleus to alter stress responsive gene expression (Xiao et al. 2013). Thus, this finding does not contradict the hypothesis that only exterior and chloroplast derived NO• signals cause lipid accumulation. NR activity is highly regulated by NO• levels and both, the addition of an NO• donor molecule as well as scavengers alter its activity (Foresi et al. 2015, Chow et al. 2013).

In *Chlamydomonas*, NO•-dependent inhibition of NR was only functional in living cells and not in cell extracts or on the purified protein. This finding underlines the importance

of compartmentalization for the downstream NO• function (Sanz-Luque et al. 2013). Due to the strong dependence of a second messenger effect not only on its production site but also its concentration, distinct effects of controlled NO• supplies or several NOA overexpression lines should be compared (Batistič & Kudla 2012).We further challenged our hypothesis by the expression of the *N. gaditana NOA* sequence in *Phaeodactylum* that was able to enhance cellular NO• levels but not TAG accumulation.

4.5.3 *Expression of a putative N. gaditana NOA in P. tricornutum triggers NO• but not TAG production*

Using BLAST analyses, we have identified *N. gaditana* protein to be homologous of *P. tricornutum* NOA. The locus Naga_100007g10 (NgNOA) shares 39% sequence identity with PtNOA (**appendix 8.3.1**) and is annotated as ribosome biogenesis GTPase (www.nannochloropsis.org, 01.08.2015). It contains the YqeH domain in the C-terminus. NgNOA contains a long N-terminal tail of 384 bp that is missing in the diatom homolog. When excluding this part, sequence identity between the two NOA proteins was 53% in Clustal2.1 alignment. As typically observed for *N. gaditana* genes, NgNOA was a single copy gene without introns (Vieler et al. 2012). We have codon optimized the full NgNOA cDNA to allow expression in both, *Phaeodactylum* and *Nannochloropsis* (**appendix 8.3.2**). Chloroplast transit peptides are poorly conserved between the species (Patron & Waller 2007). Thus, we did not expect chloroplast localization of NgNOA when expressed in *P. tricornutum* cells. After transformation of the WT and antibiotic selection, 14 colonies were randomly chosen and designated as Pt::OE-NgNOA1-14. They were screened for increased NO• production using the fluorophore DAF-FM (**figure 4.6 A**). Compared to the WT and the empty vector control (pH4), in four lines NO• levels were more than 1.5-fold higher. Pt::OE-NgNOA.4 had 2.2-fold higher DAF-FM fluorescence, Pt::OE-NgNOA.8 1.7, Pt::OE-NgNOA.9 2.0 and Pt::OE-NgNOA.10 3.6.

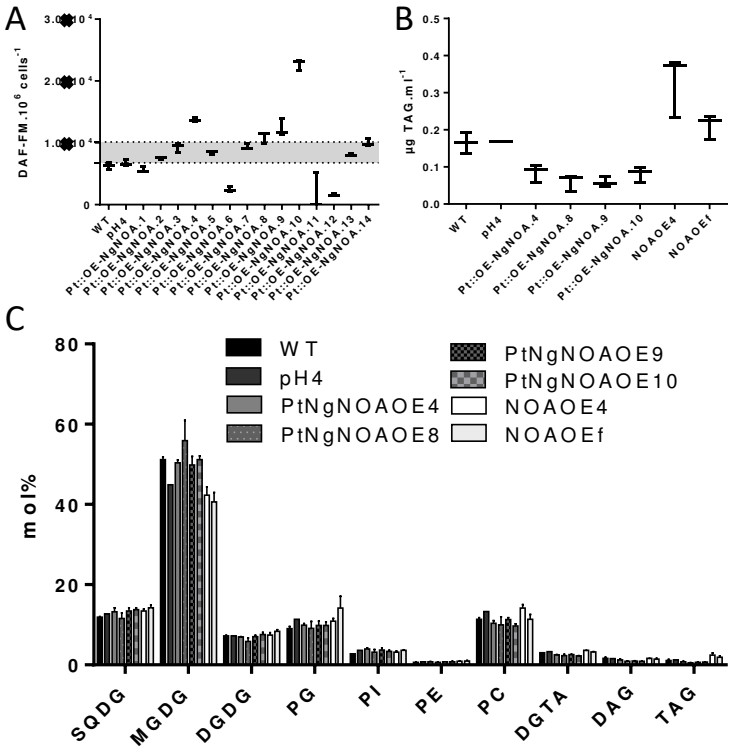

Figure 4.6. Overexpression of NgNOA in *Phaeodactylum* triggers NO• production but does not alter lipid profiles. After transformation, 14 clones were randomly selected. A**. NO• production** was assessed *via* DAF-FM fluorescence. Four lines with higher NO levels were selected for lipid analyses. Lipids were extracted from three day old 50 mL cultures grown in Erlenmeyer flasks and analysed by HPLC-MS/MS. **B. Relative TAG productivity** is increased in NOAOE4 and NOAOEf, but decreased in NgNOA-overexpression lines compared to the wild type (WT) and the empty vector control (pH4). **C. Lipid distributions** are similar in NgNOA-overexpression and control lines whereas relative TAG levels are increased partly on the cost of MGDG in NOAOE4 and NOAOEf.

From those four lines, lipids were extracted and analysed in HPLC-MS/MS. The WT and pH4 as negative controls and the overexpression lines of the endogenous NOA, NOAOE4 and NOAOEf as positive controls were run in parallel (**figure 4.6 B, C**). Unlike NOAOE4 and NOAOEf that had both higher relative productivity (**figure 4.6 B**) and TAG proportions (**figure 4.6 C**) compared to the negative controls, neutral lipid levels were reduced in NgNOA overexpression lines. This could be explained by a different function of NgNOA however the concomitant production of NO• was

conserved. Alternatively, the potential cytosolic localization was likely to alter the NO• effect on lipid accumulation. To confirm this assumption, localization of NgNOA in transformed *Phaeodactylum* cells must be revealed by immunoblotting or GFP-coupling. The result was in line with our hypothesis of locus-dependent NO• signatures for neutral lipid accumulation. With the same NgNOA sequence, *N. gaditana* was transformed to reveal a conservation of the signalling mechanism.

4.5.3.1 NOA dependent TAG accumulation is not conserved in *N. gaditana*

As indicated in the literature review, the control of NO• production and especially the NO• impact on the regulation of NR activity is complicated. We addressed the question if the lipid induction observed in *Phaeodactylum* in response to extracellular or chloroplast derived NO• signals were conserved in *Nannochloropsis*. To this end, we treated the *Eustigmatophyte* with SNAP and measured Nile red fluorescence in 500 µl cultures. While in *Phaeodactylum*, the treatment of medium dissolved SNAP promoted higher TAG productivity (**section 4.4, figure 4.7 A**), relative Nile red fluorescence in *Nannochloropsis* declined in response to the NO• donor. Similarly, 12 independent *N. gaditana* cell lines transformed with the NgNOA overexpression construct (see above) did not have higher neutral lipid contents (**figure 4.7 B**). These data indicate that the regulation of neutral lipid accumulation by NO• is not conserved between *Phaeista* and *Khakista*. We did not further investigate NO• signalling in *Nannochloropsis*.

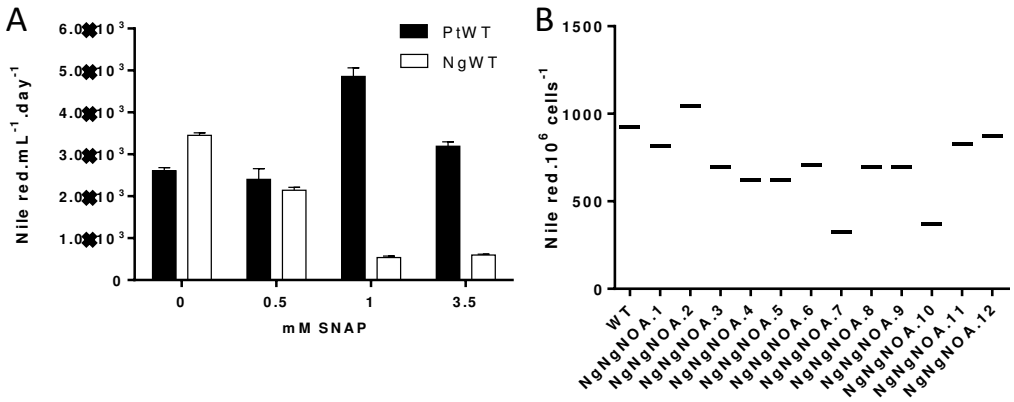

Figure 4.7. ***Nannochloropsis*** **neutral lipid contents are lowered by NO• signals from the environment or the chloroplast. A. SNAP** was added at 0, 0.5, 1 and 3.5 mM per 10^6 cells to 500 µL cultures of *P. tricornutum* WT (PtWT) or *N. gaditana* WT (NgWT) inoculated at a concentration of 2.10^6 cells.mL^{-1}. **B. NgWT was transformed with NgNOA**. From 12 randomly chosen colonies, liquid cultures were inoculated. After two days of incubation of the respective samples, Nile red fluorescence and cell concentrations were measured in 160 µL culture aliquots using a TECAN plate reader.

5 EPA SYNTHESIS AND TRAFFICKING IN *P. TRICORNUTUM* AND *N. GADITANA VIA* THE ELUSIVE "OMEGA PATHWAY"

5.1 Introduction and overview

An intriguing characteristic of *P. tricornutum* and *N. gaditana* lipid profiles is the accumulation of VLC-PUFAs, especially EPA, in the galactolipids MGDG and DGDG,

as well as DGTS/A and PE (Abida et al., 2015; Meksiarun et al., 2015; Simionato et al., 2013). Fatty acids are synthesized in chloroplasts with 14:0, 16:0, 18:0 and 18:1 as major products. They are diversified by elongation in the ER or desaturation processes. (**Section 5.2.1** Dolch & Marechal 2015). Then, produced VLC-PUFAs are trafficked from the ER into the chloroplast via the unknown "omega pathway" (Petroutsos et al. 2014).

The chloroplast phospholipid PG is exclusively produced in the chloroplast of higher plants by the "prokaryotic pathway" (Fritz et al. 2007, Xu et al. 2006). In Heterokonts however, the PG-specific 16:1-*trans* fatty acid pairs frequently with EPA that is produced in the ER (Abida et al. 2015; Meksiarun et al. 2015; Simionato et al. 2013, Domergue et al. 2002, Arao & Yamada 1994). Depending on the species, an "ω-3 pathway", an "ω-6 pathway" or both biosynthesis routes of EPA exist (Schneider et al. 1995, Domergue et al. 2002, Arao and Yamada 1994, Cook & Hildebrand 2015). These findings gave rise to the question how is EPA produced and translocated between the organelles in Heterokonts? Or in other words: What is the "omega pathway" (Petroutsos et al. 2014) (**figure 5.1**)?

While fatty acid elongation is restricted to the ER, acyl-CoA desaturases reside in the ER or chloroplasts and act on lipid-linked or ACP-bound acyl chains. Thus, each EPA molecule must have been translocated twice: after its synthesis by FAS type-II enzymes to the outer ER leaflet and back to the chloroplast for galactolipids and PG assembly (Li et al. 2016b, Petroutsos et al. 2014). In general, EPA could be imported as free fatty acid, CoA/ACP-bound or incorporated into PA or DAG. If the chloroplast import of EPA occurs in a free fatty acid form, free EPA must be activated to acyl-ACP by an acyl-ACP synthetase (AAS) before they are available for lipid assembly. EPA-ACP could then serve as a substrate for the acyl-transferases (ATS) 1 which catalyses the addition of the acyl group to glycerol-3-phosphate forming lyso-PA to which a second fatty acid is added by ATS2 forming PA, both reactions releasing ACP (Fritz et al. 2007, Xu et al. 2006). PAP dephosphorylates PA resulting in the lipid precursor DAG (Nakamura et al. 2007). Alternatively, ER-bound acyl-transferases from the GPAT family produce eukaryotic PA which could be imported. In plants, mathematical

modelling of fluxes denies an important PA import and supports eukaryotic DAG import to allow prokaryotic PG synthesis (Marechal & Bastien 2014). At least in higher plants containing two chloroplast limiting membranes, PC might be the precursor molecule at the outer envelope membrane that is converted to PA or DAG by the action of phospholipase Dζ (Li et al. 2006) (**figure 5.1**).

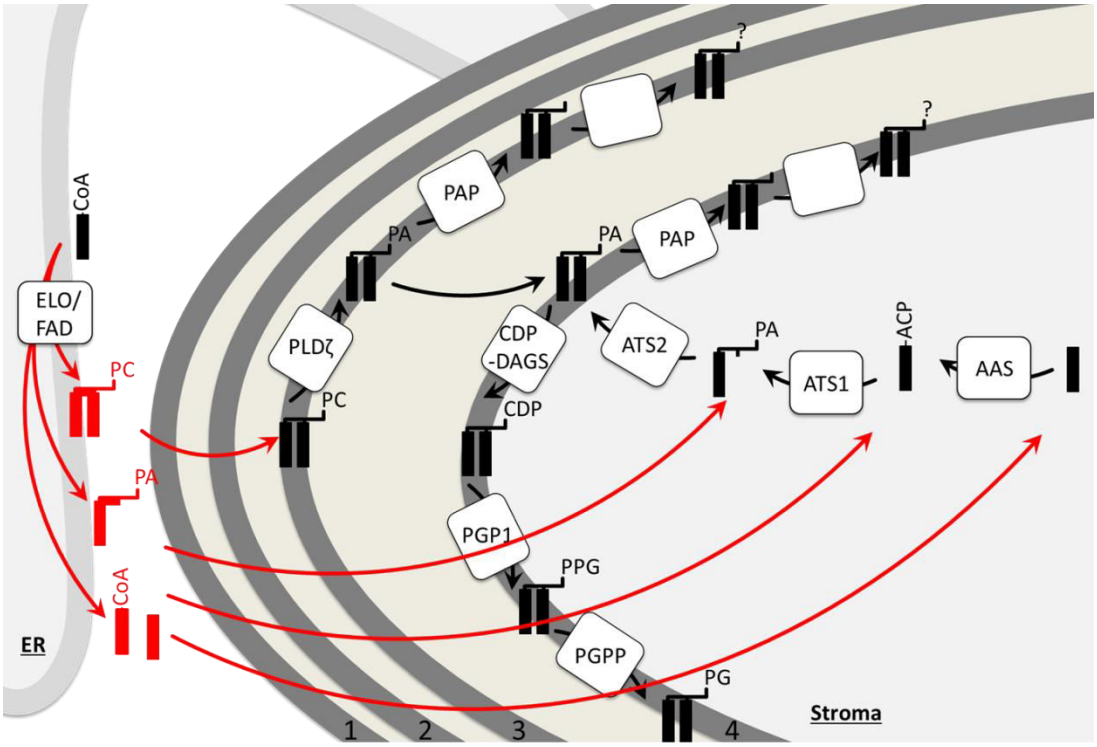

Figure 5.1. Schematic view on the possible EPA import routes from the ER into the chloroplast of Heterokonts. After elongation (ELO) and desaturation (FAD), produced EPA could be incorporated into PC, PA, acyl-CoA or left as a free fatty acid (red bars). In the PC -route, a phospholipase (PLDζ) would generate PA that after PA phosphatase (PAP) activity produces DAG for lipid synthesis in the third membrane. PA could be transported to the fourth membrane. EPA as free fatty acid, acyl-CoA or lyso-PA would somehow translocate over the four membranes. Free EPA would be the substrate for acyl-ACP synthase (AAS). From thioester-bond EPA, acyl-transferase (ATS) 1 could produce lyso-PA which serves as substrate for ATS2 for the synthesis of PA in the fourth membrane. This is the intermediate for inner chloroplast membrane lipid synthesis.

Briefly, four routes for EPA-import from the ER: as PC, as PA, as lyso-PA as acyl-CoA or free fatty acids. In dependence of the precursor molecule imported, different enzymes

would be required for the implementation of EPA into chloroplast lipid synthesis, namely PLD, AAS, ATS1 or ATS2 (**figure 5.1**). In order to elucidate the lipid moiety importing EPA into the chloroplast we constructed antisense lines of those four proteins in *Phaeodactylum* and investigated their lipid profiles with a focus on EPA and PG.

The elusive "omega pathway" might involve not only the proteins involved in the actual VLC-PUFA trafficking but also comprise the elongases and desaturase required for their production. We have addressed the subset of desaturases and elongases in both *Phaeodactylum* (**section 5.2.1**) and *Nannochloropsis* (**section 5.2.3**). Both Heterokonts are equipped with all required genes for the production of EPA from the assumed 18:1 precursor (Arao & Yamada 1994, Domergue et al. 2002). We confirmed Δ-6 elongase activity of one *Phaeodactylum* gene candidate by heterologous expression in yeast. Importantly, we have found a novel group of elongases, acting on saturated fatty acids. According to a nomenclature used for elongases and saturases in which the Δ-position of the double bond was name giving, we called this putative saturated fatty acid elongase family Δ0-elongases (Δ0-ELO). Sequences of Δ0-ELO were enriched in the *N. gaditana* genome and we thus speculated on an important function. We therefore characterized the isoform having the highest expression level (Δ0-ELO1) *in vivo via* targeted gene knock out as well as in the heterologous yeast system. We found Δ0-ELO1 to be involved in the elongation of palmitic acid and to control plastidial MGDG abundances. The knock out mutants had lower MGDG levels, a phenotype correlated with disturbed thylakoid membrane structures. This was accompanied by increased high light susceptibility as indicated by lower photochemistry but induced photoprotection (**section 5.2.3**).

VLC-PUFAs are involved in homeoviscous adaptation that requires membrane fluidization, while MGDG is supposed to rigidify bilayers by triggering the incorporation of proteins (Garab et al. 2000, 2016). Nonetheless, MGDG is the greatest sink for EPA in *Nannochloropsis* (Simionato et al. 2013, **section 5.2.3**). We therefore asked the question of EPA-rich MGDG regulation during cold stress adaptation. Suitable organisms for studying the regulation of fatty acid desaturation and MGDG levels would be among Heterokonts. High cellular content of VLC-PUFAs and betaine lipids together with a natural marine habitat raise the possibility that these organisms would be pre-

equipped for survival in cold environments. This idea is supported by a study of Ma and coworkers that found *N. oculata* cell growth to be optimal at 25°C but inhibited at 30°C, whereas growth was less affected at 10°C. Surprisingly, the most abundant VLC-PUFA, 20:5, was reduced at temperatures below 20°C, whereas less desaturated C20 fatty acid species increased (Ma et al.2011). The *Nannochloropsis* study does not provide fatty acid profiles of the different lipid classes. The role of a linkage between membrane fluidizing fatty acids with putatively rigidifying MGDG was thus addressed in the present study by the comparison of *N. gaditana* NgWT and the *Δ0-ELO1* mutant lines that displayed lower MGDG quantities but unaltered quality. We found a faster induction of cold-stress induced fatty acid remodelling in the mutant compared to the NgWT.

5.2 EPA biosynthesis

5.2.1 *The desaturase equipment of P. tricornutum* (**published article**)

Mar. Drugs **2015**, *13*, 1-x manuscripts; doi:10.3390/md130x000x

OPEN ACCESS

marine drugs

ISSN 1660-3397

www.mdpi.com/journal/marinedrugs

Article

Inventory of Fatty Acid Desaturases in the Pennate Diatom *Phaeodactylum tricornutum*

Lina-Juana Dolch and Eric Maréchal *

Laboratory of Plant and Cell Physiology/Laboratoire de Physiologie Cellulaire et Végétale, Unité mixte de recherche 5168 CNRS-CEA-Université Grenoble Alpes, Institut de Recherche en Sciences et Technologies pour le Vivant, CEA Grenoble, 17 rue des Martyrs, 38054 Grenoble Cedex 9, France; E-Mail: lina-juana.dolch@cea.fr

* Author to whom correspondence should be addressed; E-Mail: eric.marechal@cea.fr; Tel.: +33-438-784-985; Fax: +33-438-785-091.

Academic Editor: Véronique Martin-Jézéquel

Received: 17 December 2014 / Accepted: 28 February 2015 / Published:

Abstract: The diatom *Phaeodactylum* is rich in very long chain polyunsaturated fatty acids (PUFAs). Fatty acid (FA) synthesis, elongation, and desaturation have been studied in depth in plants including *Arabidopsis*, but for secondary endosymbionts the full picture remains unclear. FAs are synthesized up to a chain length of 18 carbons inside chloroplasts, where they can be incorporated into glycerolipids. They are also exported to the ER for phospho- and betaine lipid syntheses. Elongation of FAs up to 22 carbons occurs in the ER. PUFAs can be reimported into plastids to serve as precursors for glycerolipids. In both organelles, FA desaturases are present, introducing double bonds between carbon atoms and giving rise to a variety of molecular species. In addition to the four desaturases characterized in *Phaeodactylum* (FAD2, FAD6, PtD5, PtD6), we identified eight putative desaturase genes. Combining subcellular localization predictions and comparisons with desaturases from other organisms like *Arabidopsis*, we propose a scheme at the whole cell level, including features that are likely specific to secondary endosymbionts.

Keywords: *Arabidopsis*; phaeodactylum; diatoms; fatty acid; desaturase; lipid; EPA; front-end desaturase; polyunsaturated fatty acids

---

1. Introduction

Diatoms are one of the most important groups of unicellular photosynthetic protists living in oceans and fresh water, with an estimated >100,000 different species [1]. They are believed to be responsible for up to one fourth of the primary productivity [2]. The organic carbon generated by diatom photosynthesis in oceans is equivalent to that of all the terrestrial rainforests combined; however, due to the position of diatoms at the base of marine food webs, this organic matter is rapidly consumed [1].

Among the organic molecules produced by diatoms, fatty acids (FAs, see general structure in Figure 1a) are essential in the nutrition of benthic and pelagic animals. FAs are precursors for three complex lipid groups, *i.e.*, glycerolipids, sphingolipids, and acylated-sterols. The most abundant acyl-lipids are glycerolipids, classified as *membrane polar glycerolipids* when one or two FAs are esterified on the glycerol backbone or *storage glycerolipids* when three fatty acids are esterified to glycerol, thus forming triacylglycerol (TAG) also known as "oil" (for review, [3]) (Figure 1b). The simplest glycerolipids synthesized *de novo* are phosphatidic acid (PA) and its dephosphorylated form diacylglycerol (DAG). PA and DAG are the precursors for all of the more complex membrane and storage glycerolipids (Figure 1b). *Non-lipid linked FAs* can serve as substrates for the production of oxygenated molecules acting as signals, called oxylipins [4]. Feeding on phytoplankton, marine arthropods and vertebrates incorporate diatom FAs into their own glycerolipids, including TAG, and thus become an important source of these FAs in human nutrition [5]. Some of the unique phytoplanktonic FAs that humans find in fish oil, including very long chain polyunsaturated fatty acids (VLC-PUFAs), cannot be provided in sufficient amounts by other food sources [5]. The specific production of VLC-PUFAs by phytoplankton has therefore attracted significant attention, and has been studied in different diatom species, in various environmental and physiological contexts.

This scheme has been dissected in model organisms containing a primary chloroplast surrounded by two membranes, like the plant model *Arabidopsis thaliana* (Figure 2a) or the green alga *Chlamydomonas reinhardtii* (for review, [3,6]). The primary chloroplast derives from the engulfment of an ancestral cyanobacterium by a eukaryotic host following so-called primary endosymbiosis. The scheme is more complex in diatoms due to the presence of a chloroplast limited by four membranes, which originates from a secondary endosymbiosis [7,8]. In particular, a continuum between the ER and the outermost membrane of the plastid occurs [9] (dotted line in Figure 2b). It is not known if this connection is permanent or transient, or if lipids could transversally migrate from the ER to the outermost membrane of the chloroplast, or *vice versa*. Glycerolipid composition of each of the four membranes that surround the plastid is simply unknown. It is therefore difficult to speculate on the precise location of glycerolipid synthesis machineries and FA desaturation systems, or on the subcellular transfer of FAs within the cell. In the current state of membrane fractionation techniques, only global analyses could be performed. A reference for the glycerolipidome of *P. tricornutum* was recently detailed [10].

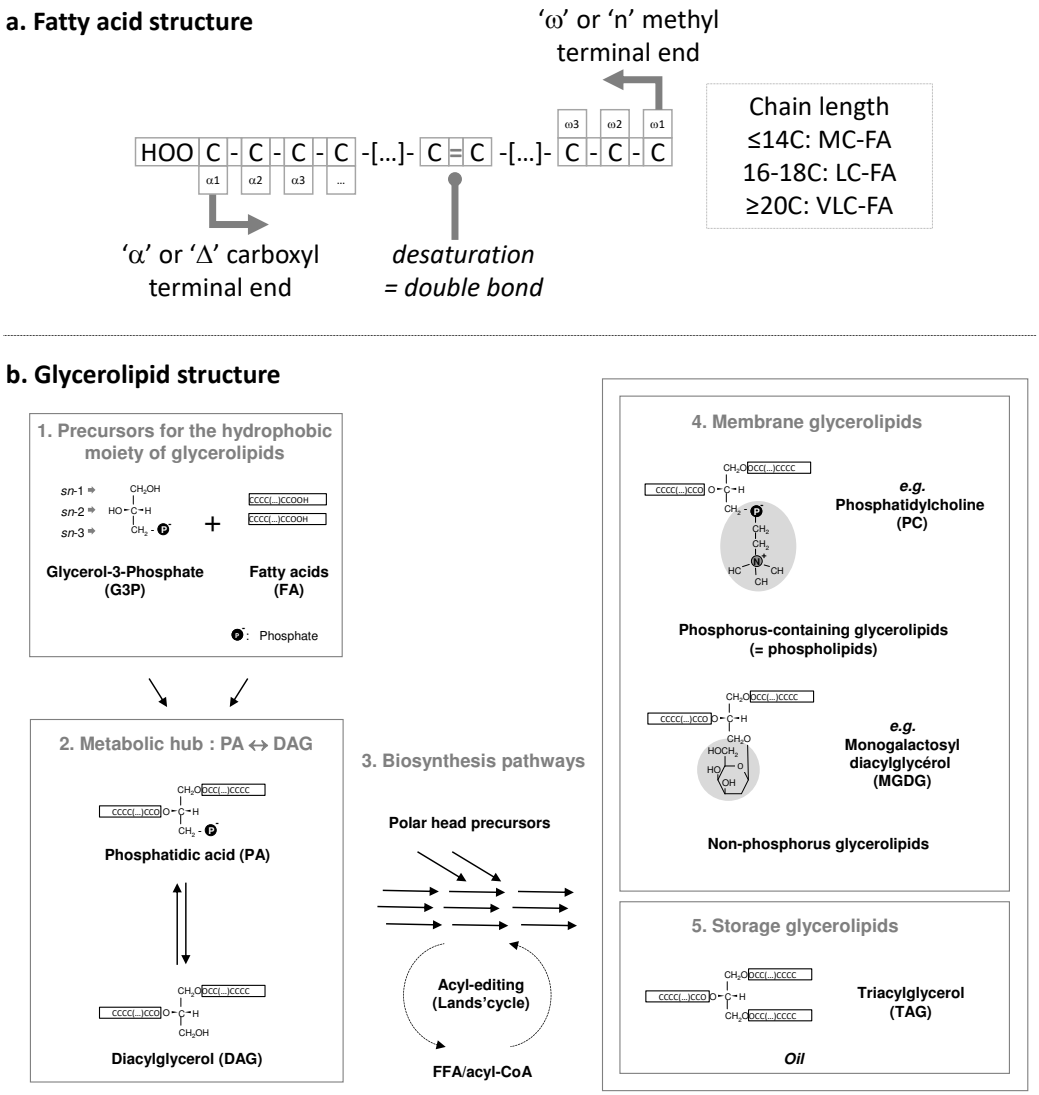

Figure 1. (**a**) Schematic structure of a fatty acid. Carbons are numbered either starting from the carboxyl terminal end ("α" or "Δ" nomenclature) or from the methyl terminal end ("ω" or "n" nomenclature). The chain length can vary. MC, medium chain; LC, long chain; VLC, very long chain; FA, fatty acid; (**b**) Incorporation of fatty acids in glycerolipids. Initial precursors (1), *i.e.*, glycerol-3-phosphate (G3P) and fatty acids (FA) are used to produce phosphatidic acid (PA) and its dephosphorylated form diacylglycerol (DAG), which are at the origin of all glycerolipids. Glycerolipid biosynthesis pathways (3) comprise multiple reactions leading to the production of membrane polar glycerolipids (4), or storage triacylglycerol (5). The *sn*-1, *sn*-2, and *sn*-3 numbering of the glycerol backbone is shown. This scheme gives an example of a phospholipid, phosphatidylcholine (PC), synthesized in the endoplasmic reticulum, and an example of a non-phosphorus glycolipid, monogalactosyldiacylglycerol (MGDG), synthesized in the chloroplast. It is important to note that exchanges of FAs can occur in some lipids, like PC, via a process known as acyl-editing. A PC molecule can be hydrolyzed into Lyso-PC, releasing a FA, and re-acylated using another acyl-CoA. The complete de-acylation/re-acylation process is called the Lands cycle and does not imply any net production of glycerolipid. Neo-synthesized FAs can be massively incorporated into glycerolipids at this step.

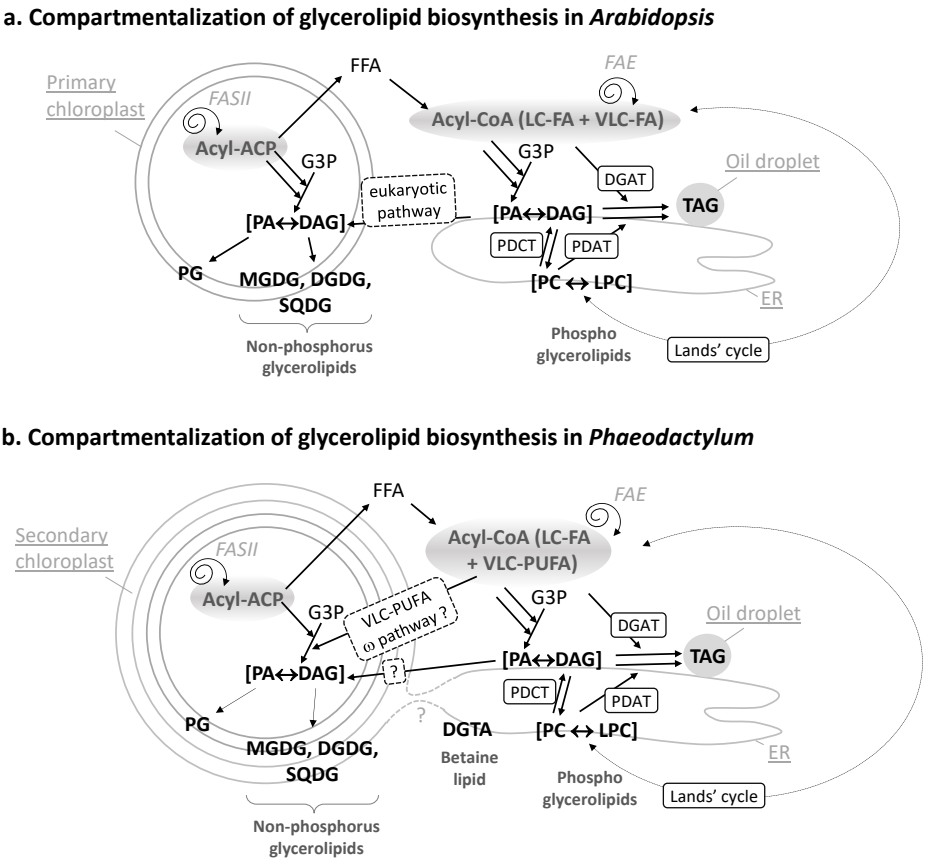

Figure 2. (**a**) Compartmentalization of glycerolipid biosynthesis in *Arabidopsis*. The FA synthase of type II (FASII) is located inside chloroplasts. Neo-synthesized acyl-ACP can be converted into free FAs (FFA), exported and thio-esterified to coenzyme A. Cytosolic acyl-CoA can serve for the esterification of glycerol-3-phosphate (G3P) into phosphatidic acid (PA) and its dephosphorylated form diacylglycerol (DAG). In the ER, PA, and DAG are precursors for phospholipids like phosphatidylcholine (PC). PC can undergo an acyl-editing cycle (Lands cycle), by the hydrolysis of a FA at position *sn*-2 followed by a re-acylation with an FA obtained from the acyl-CoA pool (dashed lines). In *Arabidopsis*, this process is known to incorporate more neo-synthesized fatty acids into ER glycerolipids than the stepwise acylation of G3P. Polar head exchanges can occur by the action of a PC-DAG phosphocholine transferase (PDCT), leading to the coexistence of *de novo*-synthesized or PC-derived DAG molecules with distinct FA molecular species. A third acyl can be added to DAG to form TAG, either obtained from the acyl-CoA pool by a DAG acyltransferase (DGAT) activity or by transfer from a PC molecule by a PC-DAG acyltransferase (PDAT) activity. Overall, this pathway in the ER is called the eukaryotic pathway. In chloroplasts, the prokaryotic pathway generates PA and DAG and lipids like mono and digalactosyldiacylglycerol (MGDG, DGDG), sulfoquinovosyldiacylglycerol (SQDG), or phosphatidylglycerol (PG). Some eukaryotic precursors are imported to the chloroplast. (**b**) Compartmentalization of glycerolipid biosynthesis in *Phaeodactylum*. Similar pathways are predicted to occur. Some specific features, like the import of very-long chain polyunsaturated fatty acids (VLC-PUFA) in plastid, via the omega pathway, are highlighted.

The inventory and subcellular localization of diatom enzymes involved in FA synthesis and modification are critical questions for advancing knowledge of this important group of oceanic biodiversity. It is also a prerequisite for the selection, domestication, or genetic engineering of diatom species. The distribution of PUFAs in glycerolipids has been studied in a few diatoms, including *Fistulifera solaris* [11], *Thalassiosira pseudonana* [12], and *Phaeodactylum tricornutum* [10]. The overall proportion of PUFAs in diatoms is tuned in response to environmental factors (for review, [13]), but their synthesis and precise biological roles are poorly understood. The analysis of FA synthesis and desaturation in diatoms is not a trivial question, mainly because it is difficult to transfer our knowledge from simple eukaryotic models, like the plant model *Arabidopsis thaliana*, to secondary endosymbionts.

When discussing FAs in photosynthetic organisms, it is usually considered that:

- medium chain FAs (MC-FAs, ≤14 carbons) and long chain FAs (LC-FAs, 16–18 carbons) are neo-synthesized in the stroma of chloroplasts;
- VLC-FAs (≥20 carbons) are generated in the ER/cytosol by secondary elongations;
- MC-FAs, LC-FAs, and VLC-FAs are incorporated in phospholipids in the endoplasmic reticulum (ER);
- MC-FAs, LC-FAs, and VLC-FAs are incorporated in non-phosphorus glycolipids in the membranes surrounding the chloroplast;
- specific FA desaturations can occur after each one of these steps.

2. Results and Discussion

2.1. Origin of Molecular Diversity of Fatty Acids: General Principles

As mentioned in the introduction, specific FA desaturations can occur after each important step in the "life" of an FA—after its *de novo* synthesis in the stroma of chloroplasts, its elongation in the cytosol, or its esterification to a glycerolipid in the ER or the chloroplast. Before listing the different desaturases of *Phaedoactylum* and their localizations, we detail therefore the general metabolic context in which they act.

FAs are carboxylic acids with an aliphatic chain of carbons, mainly even numbered, which can vary in length from 4 to >22 carbons (Figure 1a). Carbons are either numbered following the "Δ nomenclature", starting from the α-carbon at the terminal carboxyl group (e.g., the 9th carbon following Cα = Δ9) or following the "ω nomenclature", starting from the ω-carbon at the terminal methyl group (e.g., the 3rd carbon starting from Cω = ω3) (Figure 1a). FAs are synthesized *de novo* from acetyl-CoA and malonyl-CoA precursors through the action of enzymes called fatty acid synthases (FAS), being either a dissociated system ("FAS of type II" or FAS II) in prokaryotes and in the chloroplast, or a multi-enzymatic protein ("FAS of type I" or FAS I) in the cytosol of heterotrophic eukaryotes and some plastid-containing Chromalveolata. During the iterative process of FA synthesis, four enzymatic reactions lead to the addition of 2 carbons per cycle (for review [6]). FAs having 16 or 18 carbons are usually released by specific thioesterases (for review [6]). Some thioesterases can also release short or medium chain FAs having ≤14 carbons. Plants and diatoms both contain a FAS II system localized in the stroma of their chloroplasts (Figure 2b). VLC-FAs having ≥20 carbons are not produced by FAS, but, following a secondary addition of 2-carbon units to an acyl-CoA substrate, are

catalyzed in the ER/cytosol by multi-enzymatic complexes called FA elongases (FAE). The scheme shown in Figure 2b indicates the most likely location of the different systems producing and elongating FAs in a diatom cell.

Once produced, FAs can be used as building blocks for membrane lipids, including mainly glycerolipids, but also waxes and sphingolipids, which are not discussed here. Fatty acids are then esterified to positions *sn*-1 and *sn*-2 of glycerol-3-phosphate (G3P), generating PA. PA and DAG are precursors for membrane and storage glycerolipids (Figure 1b). Based on our knowledge of *Arabidopsis* (Figure 2a), two important sites of glycerolipid production are the ER for phospholipids, mainly phosphatidylethanolamine (PE) and phosphatidylcholine (PC), and the chloroplast envelope for non-phosphorous glycoglycerolipids, *i.e.*, the sulfolipid (sulfoquinovosyldiacylglycerol, SQDG) and the galactolipids (monogalactosyldiacylglycerol, MGDG and digalactosyldiacylglycerol, DGDG) (Figure 2a). One phospholipid can be synthesized in both the ER and plastid, *i.e.*, phosphatidylglycerol (PG). When translating this scheme to diatoms, the presence of four membranes surrounding the chloroplast and the presence of a connection between the outermost membrane of the plastid and the ER, makes the localization of the phospholipid synthesis route difficult (dotted line in Figure 2a). Likewise, the precise localization of SQDG, MGDG, DGDG, and PG in the plastid cannot be predicted amongst the four membranes surrounding this organelle. One could speculate that a physical coupling of ER and chloroplast pathways might occur at the outermost plastid membrane, but this has to be demonstrated. In addition, diatoms synthesize a class of glycerolipids not found in *Arabidopsis* but synthesized in the ER of *Chlamydomonas*, a betaine lipid (BL). By contrast with *Chlamydomonas* synthesizing diacylglyceryltrimethylhomoserine (DGTS), only diacylglyceryl hydroxymethyltrimethyl-β-alanine (DGTA) could be unambiguously detected in *Phaeodactylum* [10]. Localization of lipid synthesis machineries shown in Figure 2b should therefore be confirmed experimentally and for the present article, we did not exclude any alternative possibilities.

The production of TAG was shown to be particularly complex in plants. TAG is built in the ER by addition of a FA to position *sn*-3 of a DAG, but two kinds of DAG can be used as substrate and the FA donor can be obtained from two major sources.

Concerning the origin of DAG, as mentioned above, a net incorporation of FAs into glycerolipids occurs by the stepwise esterification of G3P, generating PA and its dephosphorylated form DAG (Kennedy pathway). The acyl-CoA pool used for the stepwise acylation of G3P can either derive from plastid freshly synthesized FAs (16:0, 16:1, 18:1 molecular species) or from the de-acylation of complex lipids like PC (e.g., 18:2, 18:3 molecular species) [14] (Figure 2a, Lands cycle). A major alternative entry point of plastid neo-synthesized FAs occurs therefore by re-acylation of Lyso-PC to form PC [15–18]. Polar head exchanges can also occur by the action of a PC-DAG phosphocholine transferase (PDCT), leading to the coexistence of *de novo*-synthesized DAG or PC-derived DAG molecules with distinct FA molecular species at position *sn*-1 and *sn*-2 [19] (Figure 2a). Reverse genetics and metabolic labeling experiments have shown that acyl editing and headgroup exchange were the major mechanisms that directed polyunsaturated fatty acid flux into TAG in *Arabidopsis* [20].

The acyl added at position *sn*-3 of DAG to form TAG can be obtained from the acyl-CoA pool by a DAG acyltransferase (DGAT) activity or by transfer from a PC molecule by a PC-DAG acyltransferase (PDAT) activity [19] (Figure 2a).

In plants, the relative importance of *de novo* DAG *vs.* PC-derived DAG to form TAG differs between species, ranging from just a simple Kennedy pathway to a pathway where >90% of the FAs within the seed fluxes through PC before incorporation into TAG [19,21]. All corresponding genes have been identified in diatoms [22] and are proposed to act in TAG biosynthesis in *Phaedoactylum* (Figure 2b). In *Phaeodactylum* cells grown in a nutrient-rich medium, TAG contains mostly neo-synthesized FA molecular species, *i.e.*, 14:0/16:1/16:1 (6.5%), 14:0/16:1/16:0 (9.3%), 16:1/16:1/16:1 (11%), 16:1/16:1/16:0 (23.5%), 16:1/16:0/16:0 (16%), and 16:1/16:0/20:5 (5%), a composition that is distinct from that of PC containing high proportions of MC-PUFAs and VLC-PUFAs [10]. In low-phosphate or low-nitrogen conditions, TAG remains 16:0 and 16:1-rich [10], indicating that in *Phaeodactylum*, the production of TAG most likely relied on a DAG substrate synthesized via the Kennedy pathway and on the combined activity of a DGAT and a PDAT adding a third acyl-group at position *sn*-3.

In summary, the first source of molecular diversity of FAs lies therefore in their chain length (from 8 to 22 carbons), with:

- two distinct FA pools, an acyl-ACP pool in the stroma of the chloroplast, and one or multiple acyl-CoA pool(s) in the cytosol (possibly a LC-FA-CoA pool used for the bulk of TAG synthesis and a VLC-FA-CoA pool used for membrane phospholipids);
- two distinct FA elongation systems, a FAS II in the chloroplast, and a FAE in the ER/cytosol;
- two distinct sites of glycerolipid synthesis, phospholipid (PE, PC, *etc.*), betaine lipid (BL), and TAG pathways in the ER and a non-phosphorous glycerolipid (SQDG, MGDG, DGDG) and PG pathway in the chloroplast, with some possible connections at the level of the outermost chloroplast membrane.

2.2. Classification of Fatty Acid Desaturases: General Principles

The positions of unsaturations are numbered either following the "Δ" or "ω" nomenclature (Figure 1a). Desaturations are introduced by enzymes called FA desaturases. Desaturation does not occur on all possible FA substrates: desaturases operate when FAs are presented in an appropriate form, either linked to ACP, CoA, or when FAs are esterified at positions *sn*-1, *sn*-2, or *sn*-3 of the glycerol backbone in glycerolipids (Figure 1a). Double bonds are not introduced randomly but at very specific positions of FAs. All FA desaturases use a diiron cluster for catalysis [23–26]. Two main classes of FA desaturases have been identified:

- The first class corresponds to *soluble enzymes*, adding a double bond to an acyl-ACP substrate [25,26]. They exist only in the stroma of chloroplasts and their phylogenetic origin is puzzling as cyanobacteria do not have such a system [26]. They use Ferredoxin (Fd) as an electron acceptor [27].
- The second class corresponds to *transmembrane enzymes*, adding a double bond on acyl-glycerolipids, and in some cases, on Acyl-CoA substrates. Three electron acceptor systems have been characterized: Fd, for most chloroplast desaturases [27], Cytochrome b5 (Cytb5) for most ER desaturases [28], or a Cytb5-domain fused to the desaturase itself (Cytb5 fusion), in some enzymes located either in the ER [29] or in the plastid [30].

Previously characterized desaturases of *Phaeodactylum* were named either based on *Arabidopsis* homologues (like FAD2 and FAD6, [31]) or with names that do not clearly refer to a broadly accepted classification of desaturases (like PtD5 and PtD6, [32]). *Arabidopsis* being considered as a well-known reference, we proposed whenever possible some names related to this model.

2.3. The Arabidopsis thaliana Reference

Taking *A. thaliana* as a reference, the action of desaturases is dictated by the localization of the enzyme within the cell, the availability of the specific structure of the FA, whether it is linked to ACP, CoA or a class of glycerolipid, whether it has the appropriate number of carbons, and whether some desaturations are already present on the FA. Desaturations are therefore sequentially introduced, from saturated FAs (SAFAs) to monounsaturated FAs (MUFAs) and the various types of PUFAs. Table 1 summarizes the localization and substrate specificity of the major FA desaturases in *Arabidopsis*. A first observation is that similar acyl desaturations can occur in various cell compartments, catalyzed by distinct enzymes acting on different acyl lipid substrates. Both the soluble stearoyl-ACP desaturase (SAD) of the *chloroplast stroma* [25] and the membrane bound ADS1 of the *cytosol* [33,34] can generate oleic acid ($18:1^{\Delta 9}$). Likewise, the *chloroplastic* FAD6 and the *cytosolic* FAD2 can produce linoleic acid ($18:2^{\Delta 9,12}$), whereas the *chloroplastic* FAD7 and FAD8 and the *cytosolic* FAD3 can catalyze the production of α-linolenic acid (ALA, $18:3^{\Delta 9,12,15}$) (for review, [6]). By contrast, some desaturations can be catalyzed by a unique enzyme, like the introduction of a *cis* double bond in palmitoyl-*sn*2-MGDG by the chloroplastic FAD5 ($16:1^{\Delta 7}$) [35] or the introduction of a *trans*-double bond in palmitoyl-PG by the chloroplastic FAD4 (16:*trans*-$1^{\Delta 3}$) [36]. As a consequence, when we extract lipids and analyze the acyl profile of a biological sample, some acyl molecular species can be considered as signatures, like $16:3^{\Delta 7,10,13}$ for chloroplast galactolipids at position *sn*-2 or 16:*trans*-$1^{\Delta 7}$ for chloroplast PG. As a corollary, if a galactolipid contains a 16:0, this acyl is at position *sn*-1, which cannot be desaturated by FAD5. Since in *Arabidopsis* MGDG is $16:3^{\Delta 7,10,13}$-rich, whereas DGDG that derives from MGDG is 16:0-rich, we can easily deduce that $16:3^{\Delta 7,10,13}$-*sn*2-MGDG is not used as a substrate for the synthesis of DGDG. As a consequence, FAD5, the committing enzyme at the origin of $16:1^{\Delta 7}$-*sn*2-MGDG, $16:2^{\Delta 7,10}$-*sn*2-MGDG and $16:3^{\Delta 7,10,13}$-*sn*2-MGDG, "locks" MGDG, preventing its conversion into DGDG [3,8]. In *Chlamydomonas*, it seems that a distinct desaturase that adds a fourth double bond on C16-MGDG also locks MGDG [30]. This Δ4-desaturase (Cr Δ4FAD) generates $16:4^{\Delta 4,7,10,13}$-*sn*2-MGDG, which cannot be used for the production of DGDG: The overexpression of Cr Δ4FAD therefore triggers the specific accumulation of MGDG [30]. In addition to SAD, ADS1, FAD2, FAD3, FAD4, FAD5, FAD6, FAD7, and FAD8 (see Table 1 and Figure 3a), *Arabidopsis* contains a set of desaturases acting on VLC-FAs, *i.e.*, ADS1, ADS2, ADS4, and probably other members of the ADS family, which are still uncharacterized [34]. The subcellular localization of *Arabidopsis* desaturases is shown in Figure 3a. Gene IDs listed in Table 1 have been used as queries to mine the *Phaedoactylum* genome (see Methods).

2.4. Census of Phaeodactylum Desaturases

2.4.1. A Soluble Palmitoyl-ACP Δ9-Desaturase in the Stroma of Chloroplasts (16:0 → $16:1^{\Delta 9}$)

Mining the *P. tricornutum* genome, only one homologue of the *Arabidopsis* SAD gene can be found having a complete sequence and a predicted signal peptide + chloroplastic-like transit peptide (Sp + Ctp) addressing the protein to the stroma of the chloroplast: Phatr_32224. The presence of the *N*-terminal chloroplast bipartite targeting peptide was further confirmed by the detection of the Heterokont-specific ASAFAP motif using ASAFind [37] and HECTAR [38] tools (sequences shown in Supplementary data). Since the C18 molecular species in chloroplast lipids is mainly 18:0, and the monounsaturated form of C16 is $16:1^{\Delta 9}$, and not $16:1^{\Delta 7}$ like in *Arabidopsis*, it has been proposed that the *P. tricornutum* acyl-ACP desaturase mainly acts on 16:0 and far less on 18:0, *i.e.*, acting as a palmitoyl-ACP desaturase, *i.e.*, a PAD, rather than as a stearoyl-ACP desaturase [10,31] (Table 2, Figure 3b). This soluble enzyme is likely to use Fd as its electron acceptor.

Table 1. Main fatty acid desaturases of *Arabidopsis thaliana*—Localization and substrate specificity.

Name	Gene ID	Subcellular Localization	Main Substrate				Main Product		
			Acyl Linked to:	Carbon Number	Presence of Double Bonds	Position and Configuration of the Introduced Double Bond	Overall Structure	Overall Structure	Name of Unsaturated FA
SAD	At2g43710 At5g16240 At3g02610 At5g16230 At5g16230 At3g02630 At1g43800	Chloroplast stroma	ACP	18	0	Δ9/*cis*	18:0-ACP	$18:1^{\Delta9}$-ACP	Oleic acid
ADS1	At1g06080	Endomembrane system	CoA	≥18	0	Δ9/*cis*	18:0-CoA	$18:1^{\Delta9}$-CoA	Oleic acid
FAD2	At3g12120	ER	Phospholipid	18	1	Δ12 (or ω6)/*cis*	$18:1^{\Delta9}$-PL	$18:2^{\Delta9,12}$-PL	Linoleic acid
FAD3	At2g29980	ER	Phospholipid	18	2	Δ15 (or ω3)/*cis*	$18:2^{\Delta9,12}$-PL	$18:3^{\Delta9,12,15}$-PL	α-Linolenic acid (ALA)
FAD5 (ADS3)	At3g15850	Chloroplast membranes	*sn*2-MGDG	16	0	Δ7 (or ω9)/*cis*	16:0-*sn*2-MGDG	$16:1^{\Delta7}$-*sn*2-MGDG	Palmitoleic acid
FAD6	At4g30950	Chloroplast membranes	*sn*1/*sn*2-MGDG/DGDG + SQDG	16 or 18	1	ω6/*cis*	$16:1^{\Delta7}$-*sn*2-MGDG $18:1^{\Delta9}$-*sn*1/*sn*2-MGDG/DGDG	$16:2^{\Delta7,10}$-*sn*2-MGDG; $18:2^{\Delta9,12}$-*sn*1/*sn*2-MGDG/DGDG	7,10-Hexadecadienoic acid; Linoleic acid
FAD7/ FAD8	At3g11170 At5g05580	Chloroplast membranes	*sn*1/*sn*2-MGDG/DGDG + SQDG	16 or 18	2	ω3/*cis*	$16:2^{\Delta7,10}$-*sn*2-MGDG $18:2^{\Delta9,12}$-*sn*1/*sn*2-MGDG	$16:3^{\Delta7,10,13}$-*sn*2-MGDG; $18:2^{\Delta9,12,15}$-*sn*1/*sn*2-MGDG	7,10,13-Hexadecatrienoic acid; α-Linolenic acid (ALA)
FAD4	At4g27030	Chloroplast membranes	*sn*2-PG	16	0	Δ3/*trans*	16:0-*sn*2-PG	$16:1^{\Delta3trans}$-*sn*2-PG	Δ3-*trans* Hexadecanoic acid
ADS2 ADS4 + ADS family	At2g31360 At1g06350	Endomembrane system	CoA	≥18	-	Δ9, ω6, ω7, ω9/*cis*	VLC-FA	VLC-MUFA/PUFAs	-

Table 2. Fatty acid desaturases of *Phaeodactylum tricornutum*—Characterized or predicted localization and substrate specificity. (*) functionally characterized; (?) based on predictions.

Name	Gene ID	Subcellular Localization	Main Substrate				Main Product	
			Acyl Linked to:	Carbon Number	Presence of Double Bonds	Position and Configuration of the Introduced Double Bond	Overall Structure	Overall Structure
PAD/SAD	Phatraft_9316	Chloroplast stroma	ACP	16 and 18	0	Δ9/*cis*	16:0-ACP	$16:1^{\Delta 9}$-ACP
ADS	Phatr_28797	Endomembrane system	CoA	18?	0	Δ9/*cis*?	18:0-CoA?	$18:1^{\Delta 9}$-CoA?
FAD2 (*)	Phatr_25769	ER	Phospholipid/ Betaine lipid?	18	1	Δ12 (or ω6)/*cis*	$18:1^{\Delta 9}$-PL (-BL?)	$18:2^{\Delta 9,12}$-PL (-BL?)
ERΔ6FAD (*)	Phatr_2948	ER	Phospholipid/ Betaine lipid?	18	2	Δ6/*cis*	$18:2^{\Delta 9,12}$-PL (-BL?)	$18:3^{\Delta 6,9,12}$-PL (-BL?)
ERω3FAD (?)	?	ER	Phospholipid/ Betaine lipid?	18	3	Δ15 (or ω3)/*cis*	$18:3^{\Delta 6,9,12}$-PL (-BL?)	$18:4^{\Delta 6,9,12,15}$-PL (-BL?)
ERΔ5FAD.1 (*) ERΔ5FAD.2 (?)	Phatr_46830 Phatr_22459	ER	Phospholipid/ Betaine lipid?	20	4	Δ5/*cis*	$20:4^{\Delta 8,11,14,17}$-PL (-BL?)	$20:5^{\Delta 5,8,11,14,17}$-PL (-BL?)
ERΔ4FAD	Phatr_22510?	ER	Phospholipid/ Betaine lipid?	22	5	Δ4/*cis*	$22:5^{\Delta 7,10,13,16,19}$-PL (-BL?)	$22:6^{\Delta 4,7,10,13,16,19}$-PL (-BL?)
FAD6 (*)	Phatr_48423	Chloroplast membranes	*sn*1/*sn*2-MGDG/DGDG + SQDG	16	1	Δ12/*cis*	$16:1^{\Delta 9}$-*sn*2-MGDG/DGDG/SQDG	$16:2^{\Delta 9,12}$-*sn*1/*sn*2-MGDG/DGDG/SQDG
PlastidΔ6FAD (?)	Phatr_50443	Chloroplast membranes	*sn*2-MGDG	16	2	Δ6/*cis*	$16:2^{\Delta 9,12}$-*sn*2-MGDG	$16:3^{\Delta 6,9,12}$-*sn*2-MGDG
Plastidω3FAD/ FAD7 (?)	Phatr_41570	Chloroplast membranes	*sn*2-MGDG?	16	3	ω3/*cis*	$16:3^{\Delta 6,9,12}$-*sn*2-MGDG	$16:4^{\Delta 6,9,12,15}$-*sn*2-MGDG
FAD4	Phatr_41301	Chloroplast membranes	*sn*2-PG	16	0	Δ3/*trans*	16:0-*sn*2-PG	$16:1^{\Delta 3trans}$-*sn*2-PG

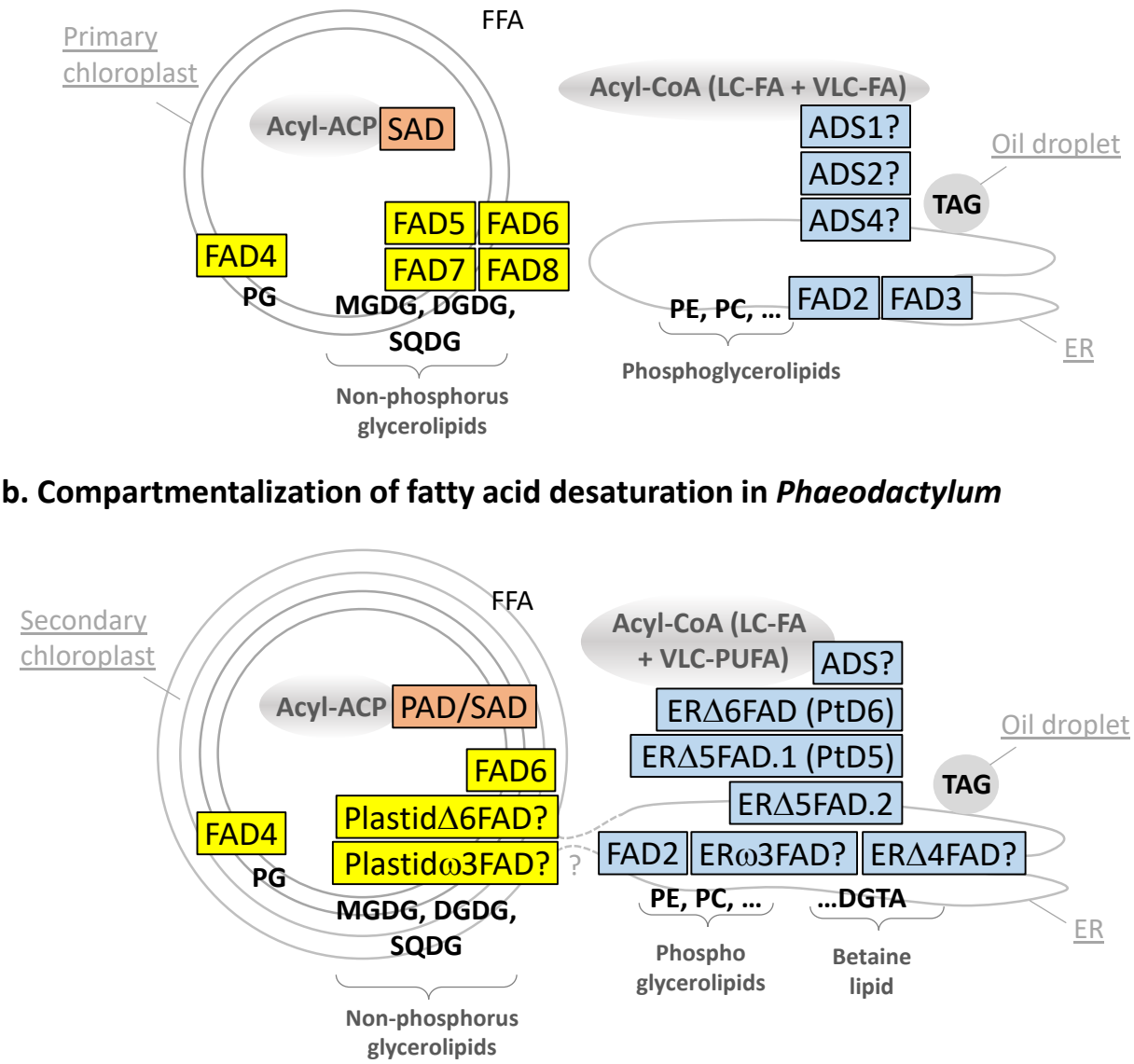

Figure 3. (**a**) Compartmentalization of fatty acid desaturation in *Arabidopsis*; (**b**) compartmentalization of fatty acid desaturation in *Phaeodactylum*. Enzymes in the stroma of chloroplast are shown in pink; enzymes in chloroplast membranes are shown in yellow; enzymes in endosystem membranes are shown in light blue.

2.4.2. Ordered Addition of Double Bonds from 16:1 to 16:2, 16:3, and 16:4

The order of addition of double bonds on the C16 backbone can simply be evaluated based on the structure of 16:1, 16:2, 16:3, and 16:4 in *Phaeodactylum* lipids. A decade ago, Domergue *et al.* showed that the FA distribution in *Phaeodactylum* was characterized by the higher abundance of $16:1^{\Delta 9}$ (25.9% of total FA), $16:2^{\Delta 9,12}$ (3.1%), and $16:3^{\Delta 6,9,12}$ (10.4%), over $16:2^{\Delta 6,9}$ (<1%) [31]. The order of the second desaturation is difficult to assess since both $16:2^{\Delta 9,12}$ and $16:2^{\Delta 6,9}$ are minor. Most unsaturated C16 FAs were detected in chloroplast lipids [10], supporting the idea that the main desaturation route is within this organelle, although some $16:1^{\Delta 9}$ desaturation into $16:2^{\Delta 9,12}$ could be partly attributed to

the activity of the endosomal FAD2 enzyme, which is more specific to $18:1^{\Delta 9}$ (see below). Concerning the major chloroplast desaturation of C16 species, it might be argued on the one hand that the favorite 16:2 *substrate* for the last desaturation, generating $16:3^{\Delta 6,9,12}$, could also be the most rapidly consumed intermediate: in that case $16:2^{\Delta 6,9}$. On the other hand, one might argue that the right chloroplast 16:2 intermediate should simply be the molecular species we detect in the highest proportion: in that case $16:2^{\Delta 9,12}$. In their study of the *Phaeodactylum* chloroplast desaturase introducing a double bond at the Δ12 position, Domergue *et al.* showed that this desaturase had its highest affinity for $16:1^{\Delta 9}$ [31]. In the absence of a similar study of the desaturase introducing a double bond at the Δ6 position of C16, we thus followed the scheme proposed by these authors [31]. We also add the possible production of a $16:4^{\Delta 6,9,12,15}$ based on its detection in very low levels in MGDG [10]:

$$16:1^{\Delta 9} \rightarrow 16:2^{\Delta 9,12} \rightarrow 16:3^{\Delta 6,9,12} \rightarrow 16:4^{\Delta 6,9,12,15}.$$

2.4.3. Absence of FAD5 Homologues and ($16:1^{\Delta 9} \rightarrow 16:2^{\Delta 9,12}$)-Desaturation by FAD6 in Chloroplasts

The presence of $16:1^{\Delta 9}$, and not $16:1^{\Delta 7}$, suggests that no homologue of *Arabidopsis* FAD5 would occur in *Phaeodactylum* chloroplasts. Indeed, we could not identify any putative FAD5 in the complete genome.

In chloroplast glycerolipids, $C16:1^{\Delta 9}$ is the substrate for the addition of a second double bond by the action of a FAD6 homologue (corresponding to Phatr_48423), which has been characterized experimentally [31]. This enzyme was shown to act as a Δ12 desaturase, assayed after heterologous expression in the cyanobacteria *Synechococcus* [31]. The protein sequence contains a predicted Sp + Ctp *N*-terminus, containing an ASAFAP motif (Supplementary data), consistent with its subcellular localization inside chloroplasts. The N-terminal Sp + Ctp of FAD6 was sufficient to target a GFP fluorescent protein into the plastid of *Phaeodactylum* [31]. FAD6 therefore produces $16:2^{\Delta 9,12}$ esterified to plastid lipids (Table 2, Figure 3B). This membrane desaturase is likely to use Fd as its electron acceptor, based on a functional study performed in a yeast heterologous system [31].

2.4.4. The Question of ($16:2^{\Delta 9,12} \rightarrow 16:3^{\Delta 6,9,12}$)-Desaturation in Chloroplasts by the Action of a Cytb5-Containing PlastidΔ6FAD

The addition of a third double bond to $16:2^{\Delta 9,12}$, generating $16:2^{\Delta 6,9,12}$, cannot be deduced from the *Arabidopsis* set of desaturases, which do not harbor such activity inside chloroplasts. We identified a Cytb5-containing putative desaturase (Phatr_50443), with a Sp + Ctp *N*-terminal sequence, containing an ASAFAP motif (Supplementary data), supporting its targeting to the chloroplast (Table 2, Figure 3b). This sequence is homologous to the Endosomal delta-6 desaturase (PtD6 or ERΔ6FAD) functionally characterized in *P. tricornutum* [32] (see 2.4.10) and could therefore act as a PlastidΔ6FAD enzyme. Such front-end desaturase activity has been described for a Cytb5-containing desaturase in *Chlamydomonas*, but with a Δ4 specificity [30]. Together, bioinformatic analysis of the Phatr_50443 sequence, similarity with the ERΔ6FAD enzyme of *P. tricornutum*, and analogy with *Chlamydomonas* Cytb5-containing front-end desaturase in the chloroplast support the annotation as a putative PlastidΔ6FAD (Table 2, Figure 3b, Supplementary data). Its role in the desaturation of $16:2^{\Delta 9,12}$ into $16:2^{\Delta 6,9,12}$ should nevertheless be confirmed by

functional genomic studies. This Cytb5-fusion desaturase is likely to use its own Cytb5 domain as electron acceptor.

2.4.5. The Question of (16:3$^{\Delta6,9,12}$ → 16:4$^{\Delta6,9,12,15}$)-Desaturation in Chloroplasts by the Action of a Plastidω3FAD (or FAD7 Homologue)

A very low level of 16:4$^{\Delta6,9,12,15}$ could be detected in *Phaeodactylum* MGDG [10]. By mining the genome of *Phaeodactylum* we could only identify one FAD3/7/8-like sequence, which could act as a ω3 desaturase, encoded by Phatr_41570, with a predicted subcellular localization in the chloroplast, including the conserved ASAFAP motif (Supplementary data). We called this enzyme a putative Plastidω3FAD (Table 2, Figure 3b). Future studies should be undergone to assess the precise substrate for this desaturase and whether it could act for other ω3 desaturations (see below). This membrane enzyme is likely to use Fd as an electron acceptor.

2.4.6. The Specific (16:0 → 16:*trans*-1$^{\Delta3}$)-Desaturation at the *sn*-2 Position of Chloroplast Phosphatidylglycerol by FAD4

As detailed above, chloroplast phosphatidylglycerol (PG) is characterized by a 16:*trans*-1$^{\Delta3}$ at its *sn*-2, which is critical for structural and functional interactions with components of the photosynthetic machinery (for review, [39]). By mining the *Phaeodactylum* genome, a FAD4 (Table 2, Figure 3b) homologue was identified (Phatr_41301). This membrane desaturase is predicted to be localized in the chloroplast based on the prediction of a Sp + Ctp *N*-terminal sequence, containing the ASAFAP motif (Supplementary data) and is likely to use Fd as an electron acceptor.

2.4.7. The Question of Oleoyl Δ9-Desaturation in the Chloroplast and/or the Cytosol (18:0 → 18:1$^{\Delta9}$)

Small proportions of 18:1$^{\Delta9}$ FA could be detected in chloroplast lipids [10], supporting a possible production by the SAD/PAD in the stroma. Based on *Arabidopsis*, the production of 18:1$^{\Delta9}$ might be obtained via the action of the chloroplast PAD, therefore indicating some SAD activity. However, the 18:1$^{\Delta9}$-ACP thus generated in the stroma of chloroplasts should then be massively exported to the cytosol to form 18:1$^{\Delta9}$-CoA. The addition of a double bond to 18:0, forming 18:1$^{\Delta9}$, might also occur in another localization in the diatom cell, at the origin of 18:2$^{\Delta9,12}$, 18:3$^{\Delta6,9,12}$, and 18:4$^{\Delta6,9,12,15}$ [31], the substrate for VLC-FAs. Alternatively, 18:1$^{\Delta9}$-CoA might therefore be produced in the cytosol by a homologue of *Arabidopsis* ADS1 acting on 18:0-CoA. We found only one such sequence, Phatr_28797, with an *N*-terminal sequence consistent with a cytosolic localization (Table 2, Figure 3b, Supplementary data). The role of this ADS enzyme as a putative Δ9-oleyl desaturase should be experimentally determined. This membrane desaturase is likely to use Cytb5 as its electron acceptor.

2.4.8. Ordered Addition of Double Bonds from 18:1 to 18:2, 18:3, and 18:4

The main C18 unsaturated structures determined in *Phaeodactylum* were 18:1$^{\Delta9}$ (2.4% of total FA), 18:2$^{\Delta9,12}$ (2%), and very low proportions of 18:3$^{\Delta6,9,12}$ (<1%) and 18:3$^{\Delta9,12,15}$ (<1%) [31]. This indicates that the introduction of the second double bond is at position Δ12. For the following desaturations, a 3-h metabolic labeling with (^{14}C) 18:0 led to the accumulation of 45.6% 18:0, 15% 18:1$^{\Delta9}$, 21% 18:2$^{\Delta9,12}$,

2.8% $18:3^{\Delta9,12,15}$, 2.5% $18:3^{\Delta6,9,12}$, and 0.5% $18:4^{\Delta6,9,12,15}$ [40]. Following $18:2^{\Delta9,12}$, it seems therefore that desaturases can operate without order, ending up with the production of 18:3 and 18:4 molecular species that do not accumulate, simply because they are elongated into C20 molecular species. These C20 species are very rapidly desaturated into eicopentaenoic acid (EPA): $20:5^{\Delta5,8,11,14,17}$. Amongst all combinations, a most active route was then proposed based on metabolic labeling experiments [41,42]:

$$18:0 \rightarrow 18:1^{\Delta9} \rightarrow 18:2^{\Delta9,12} \rightarrow 18:3^{\Delta6,9,12} \rightarrow 18:4^{\Delta6,9,12,15}.$$

Based on the substrate specificity of desaturases, an alternative route is also nearly as important [32,41]:

$$18:0 \rightarrow 18:1^{\Delta9} \rightarrow 18:2^{\Delta9,12} \rightarrow 18:3^{\Delta9,12,15} \rightarrow 18:4^{\Delta6,9,12,15}.$$

In the next sections, we describe desaturases following the first route.

2.4.9. The ($18:1^{\Delta9} \rightarrow 18:2^{\Delta9,12}$)-Desaturation by FAD2 in the ER

The ER FAD2 (corresponding to Phatr_25769) of *Phaeodactylum* has been finely characterized functionally in yeast heterologous system [31]. *In vitro*, this enzyme was shown to accept various substrates, like $16:1^{\Delta9}$, $17:1^{\Delta9}$, $18:1^{\Delta9}$, or $20:1^{\Delta11}$, and in all cases it added a second double bond at the level of the third carbon counted from the methyl end, generating $16:1^{\Delta9,12}$, $17:1^{\Delta9,12}$, $18:1^{\Delta9,12}$, or $20:1^{\Delta11,14}$, respectively [31]. It is not therefore a strict Δ12 or ω6 desaturase, although it is labeled as such in Table 2. The fusion of the *N*-terminal sequence of *Phaedoactylum* FAD2 to GFP led to cytoplasmic fluorescence [31] (Table 2, Figure 3b). The localization of this membrane desaturase is not completely characterized; however, it is most likely located at the level of the ER, although other membrane compartments of the endomembrane system or even the outermost membrane of the chloroplast cannot be excluded. Functional analyses in heterologous systems have shown that Cytb5 was the electron acceptor [31].

2.4.10. The ($18:2^{\Delta9,12} \rightarrow 18:3^{\Delta6,9,12}$ and $18:3^{\Delta6,9,12,15} \rightarrow 18:3^{\Delta6,9,12,15} \rightarrow 18:4^{\Delta6,9,12,15}$)-Desaturation by a Δ6 Front-End Desaturase, ERΔ6FAD (PtD6)

The addition of a double bond between the pre-existing ones and the carboxyl end of polyunsaturated FA is not a common process. It is catalyzed by so called front-end desaturases, which share multiple structural features, including a Cytb5 domain fused to their terminal end. The identification of the enzyme catalyzing the desaturation of $18:2^{\Delta9,12}$ into $18:3^{\Delta6,9,12}$ could not be deduced based on homology searches with an *Arabidopsis* template sequence. By analyzing *Phaeodactylum* genomic sequences that could encode desaturases, and by comparison with Δ6 desaturase sequences of other organisms, only one Δ6 front-end Cytb5 fusion desaturase could be identified (Phatr_2948), called here ERΔ6FAD. This desaturase corresponds to PtD6 previously characterized by Domergue *et al.* [32]. This enzyme is most likely associated to the ER or a compartment of the endomembrane system (Table 2, Figure 3b). It uses its Cytb5 domain as an electron acceptor. ERΔ6FAD was characterized functionally in heterologous systems and was shown to act equally on $18:2^{\Delta9,12}$ and $18:3^{\Delta9,12,15}$, generating $18:3^{\Delta6,9,12}$ and $18:4^{\Delta6,9,12,15}$, respectively [32].

2.4.11. The Question of the ($18:2^{\Delta9,12} \rightarrow 18:3^{\Delta9,12,15}$ and $18:3^{\Delta6,9,12} \rightarrow 18:4^{\Delta6,9,12,15}$)-Desaturation by a ERω3FAD

To our knowledge, no gene candidate has been previously identified to code for an enzyme catalyzing the addition of a double bond at position Δ15/ω3 of C18 in the ER of *Phaeodactylum*, tentatively called ERω3FAD in this article. It has been shown in plants that FAD3 enzymes are ω3 desaturases capable of adding double bonds on a variety of C18 or C20 substrates [43]. As mentioned above, we could only identify one FAD3/7/8-like sequence (Phatr_41570) that could act as a ω3 desaturase, *i.e.*, a putative Plastidω3FAD (Table 2, Figure 3b). Functional genomic studies and enzymatic assays should therefore be performed to assess whether this enzyme could act in 18:4 synthesis in *Phaeodactylum*. There might be a dual targeting of the ω3FAD gene leading to a localization of a cytosolic ERω3FAD acting on C18 substrates and a Plastidω3FAD acting on C16 substrates, and this hypothesis should be evaluated. It is also unclear whether an ω3FAD could act on both $18:2^{\Delta9,12}$ and $18:3^{\Delta6,9,12}$ with similar affinities, producing $18:2^{\Delta9,12,15}$ and $18:4^{\Delta6,9,12,15}$, respectively. The actual enzyme and its localization should be unraveled.

Regardless of the order, the actions of ERΔ6FAD and ω3FAD appear to lead to the production of an 18:4 intermediate, which does not accumulate since it is extremely rapidly elongated by a Δ6 elongase, into a C20-FA. This latter fatty acid is found in a very low proportion (<1%) [31], due to it being instantly converted into eicopentaenoic acid.

2.4.12. The ($20:4^{\Delta8,11,14,17} \rightarrow 20:5^{\Delta5,8,11,14,17}$)-Desaturation by a Δ5 Front-End Desaturase, ERΔ5FAD.1 (PtD5) and ERΔ5FAD.2

Among the possible routes producing $20:5^{\Delta5,8,11,14,17}$ in *Phaeodactylum*, pulse chase experiments with (^{14}C)$18:1^{\Delta9}$ and (^{14}C)$18:2^{\Delta9,12}$ suggested the most active one involved the elongation of $20:4^{\Delta8,11,14,17}$ [42]. A Δ5 front-end desaturase, called here ERΔ5FAD.1 (previously described as PtD5, corresponding to Phatr_46830) was identified together with the ERΔ6FAD (PtD6) described above [32]. By testing a subset of possible 20-carbon substrates, ERΔ5FAD.1 was shown to act on $20:1^{\Delta11}$, $20:2^{\Delta11,14}$, $20:3^{\Delta11,14,17}$, or $20:3^{\Delta8,11,14}$ [32]. In these experiments, $20:3^{\Delta8,11,14}$ was the favorite substrate, indicating that this enzyme was versatile enough to accommodate various substrates, with a very high efficiency toward the production of EPA [32]. This membrane desaturase is localized in the ER or another compartment of the endomembrane system. Like ERΔ6FAD, it uses its Cytb5 domain as an electron acceptor. It is also likely to be closely associated with components of the elongase that generates 20:4 from 18:4 [32]. By mining the genome of *Phaeodactylum*, we identified a close homologue, called here ERΔ5FAD.2 (Phatr_22459), which might act as a Δ5 desaturase as well, either as a redundant enzyme or for a specific purpose (Table 2, Figure 3b). The presence of two enzymes might explain the very efficient production of EPA in *Phaeodactylum*.

The lipids bearing the FAs that serve as substrates for ERΔ6FAD, ω3FAD, and ERΔ5FAD are currently debated. Analyses have been performed in another Chromalveolate, *Monodus subterraneus*, which is not a diatom but a eustigmatophyte containing a secondary plastid. In this model, $18:1^{\Delta9}$-precursors are mainly linked to the *sn*-2 position of PC, where it serves as a substrate for FAD2 and ERΔ6FAD. The $18:3^{\Delta6,9,12}$ is then released, elongated into $20:3^{\Delta8,11,15}$, and incorporated into PE, where it serves as a substrate for ω3FAD and ERΔ5FAD [44]. The lipids presenting the FA to the

front-end desaturases are yet to be determined in *Phaedoactylum*, but possibly involve PC, PE, and DGTA. Indeed, all these lipids were shown to contain intermediate unsaturated FA, upstream EPA [10]. In Table 2, DGTA was therefore listed as a possible substrate for FA desaturation, although this hypothesis should be demonstrated experimentally.

Regardless of its synthesis route, EPA is then massively transferred to plastid glycerolipids, with EPA detected in 20%–50% of MGDG or DGDG molecular species, and >50% of acyl-SQDG [10]. Some Chromalveolata like *Chromera velia* accumulate ~80% EPA in MGDG and DGDG [45]. The mechanism transferring EPA to galactolipids, called the "omega pathway" by Petroutsos *et al.* [8], is currently uncharacterized.

2.4.13. The ($22:5^{\Delta7,10,13,16,19} \rightarrow 22:6^{\Delta4,10,13,16,19}$)-desaturation by a Δ4 Front-End desaturase, ERΔ4FAD

In *Phaedoactylum*, low amounts of docosahexaenoic acid (DHA), $22:6^{\Delta4,10,13,16,19}$, can be synthesized, and can be found in such lipids as PE or DGTA [10,46]. DHA is generated following EPA elongation into $22:5^{\Delta7,10,13,16,19}$ catalyzed by a Δ5-elongase, and its subsequent desaturation by a Δ4FAD. Using a Δ4FAD enzyme from *Thalassiosira* as a template, we mined the *Phaeodactylum* genome and found a putative Δ4FAD (Phatr_22510) that might be responsible for desaturation of $22:5^{\Delta7,10,13,16,19}$ into $22:6^{\Delta4,10,13,16,19}$. By heterologous expression of an additional Δ5-elongase from *Ostreococcus* in *Phaeodactylum*, it was shown that the production of DHA could be strikingly increased, thus showing that the endogenous Δ5-elongase was limiting, whereas that of the Δ4FAD was not [46]. Like for EPA synthesis, the lipid harboring the substrate for the desaturation by the Δ4FAD enzyme has to be determined. DHA is a minor FA in *Phaeodactylum* and might reflect a different role compared to EPA.

2.5. Brief Overview of the Roles of Desaturases in Phaeodactylum Tricornutum

Figure 4 summarizes the origin of double bonds in *Arabidopsis* and *Phaeodactylum* PUFAs, also showing the relative order of action of each enzyme (numbered 1, 2, *etc.*). FAs are not randomly desaturated. A very high level of control is exerted, highlighting even further that unsaturated FAs are likely to play specific functions.

The role of desaturases in a given organism is a difficult question. The general variations of the levels of PUFA and more specifically of EPA in *Phaeodactylum* have been reviewed recently [13]. Some physiological functions can be attributed based on physicochemical properties. It is thus commonly considered that adding double bonds to a FA improves the lateral fluidity of the harboring lipid within the membranes, and therefore the tolerance to temperature changes. The optimum temperature for the growth of *Phaeodactylum* is ~20 °C. EPAs and PUFAs increase significantly in *Phaeodactylum* grown at 10 °C [47]. The physicochemical properties of VLC-PUFAs were recently shown to be critical for the flexibility and curvature of membranes [48]. Such a role in *Phaeodactylum* or any photosynthetic organism has not, to our knowledge, been investigated yet.

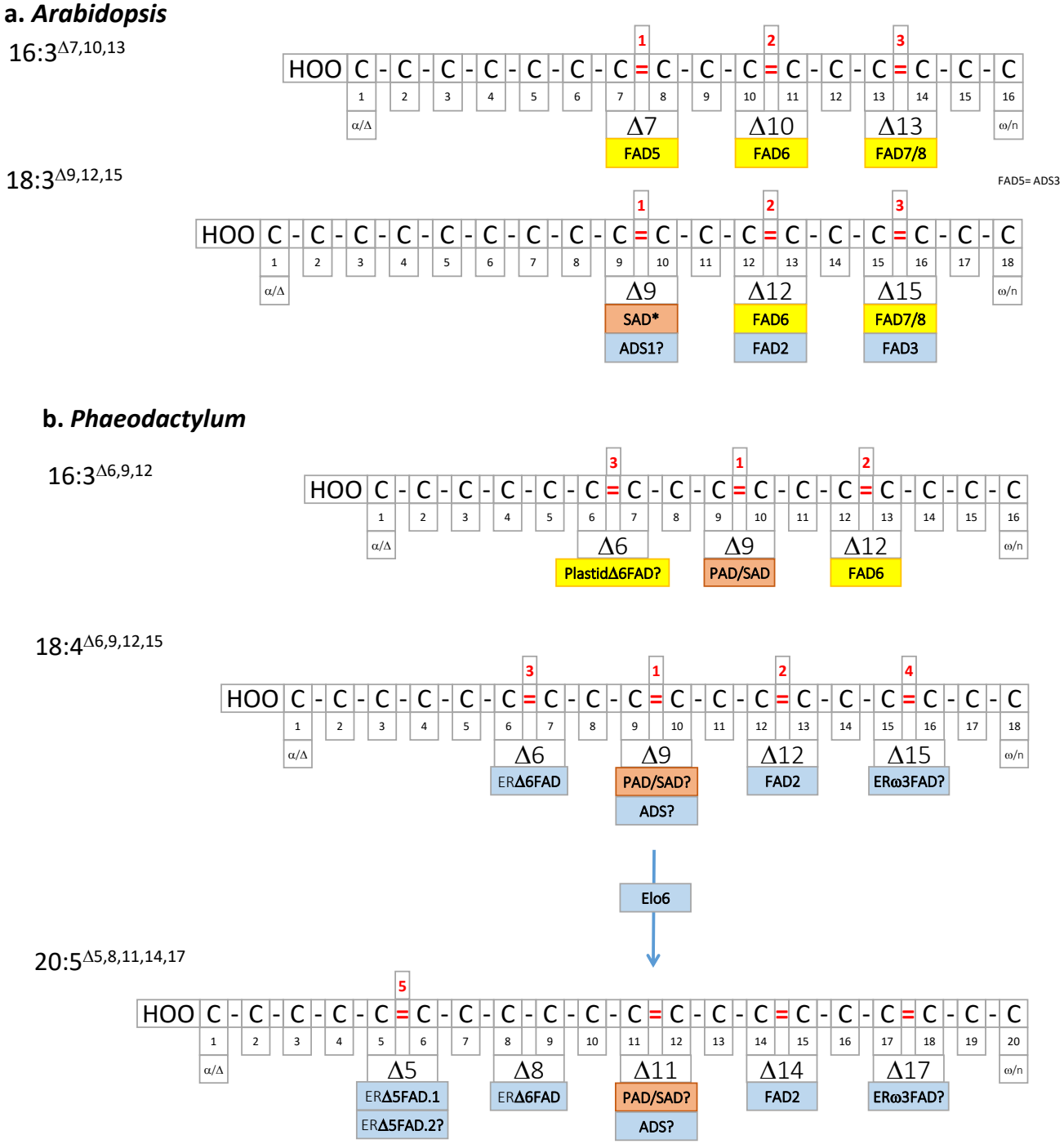

Figure 4. (**a**) *Arabidopsis* PUFAs; (**b**) *Phaeodactylum* PUFAs. Double bonds are localized based on the Δ nomenclature. Desaturases catalyzing the introduction of the corresponding double bond are shown in pink (stroma of chloroplast enzyme), yellow (chloroplast membrane enzymes), or light blue (ER membrane enzymes). Elo6, elongase.

Light also impacts on the level of desaturated FA, as shown by the effect of high light triggering a decrease of EPA in *Phaeodactylum* [13]. This might be consistent with the higher sensitivity of PUFAs to oxidation. Again, the presence of VLC-PUFAs in chloroplast lipids, at the most critical location for oxidative stresses in a photosynthetic cell, is puzzling. The specific roles of EPA in *Phaeodactylum* galactolipids and acyl-SQDG should therefore be analyzed in depth.

Chemical composition was shown to possibly impact on the proportion of PUFAs in *Phaeodactylum*, like an increase of silicate apparently triggering a decrease of EPA [49]. However, this response to the availability of some elements should be taken with caution when analyzing FA total content, firstly because the opposite trend was observed in other diatoms exposed to various silica levels [13], and secondly because total FAs also comprise FAs esterified to the triacylglycerol molecules that accumulate upon a nutrient stress, which contain lower levels of EPA [10]. Effects of environmental changes should therefore take into consideration the level of EPA in each lipid class, rather than the proportion of EPA in the total FA profile.

Other possible roles known for PUFAs include more refined metabolic functions, like their utilization as precursors for oxygenated forms called oxylipins, including diatom specific polyunsaturated aldehydes [50]. *Phaeodactylum* does not contain any lipoxygenase and it is still debated whether this species could produce some oxylipins from its PUFAs, acting as cell-to-cell signaling compounds. The specific toxicity of EPA produced by *Phaeodactylum* against bacteria has also been described [51], but the ecological importance of this phenomenon should be evaluated.

No specific functional characterization has currently been made to attempt to assign more specific roles to each desaturase in *Phaeodactylum*. For instance, FAD4 has been shown in other photosynthetic organisms to add a *trans*-double bond onto 16:0 esterified at position *sn*-2 of PG, generating a 16:*trans*-1$^{\Delta 3}$-PG form that binds to photosystems. It is reasonable to speculate that FAD4 plays the same role in *Phaeodactylum*. As mentioned above, *Arabidopsis* FAD5 or *Chlamydomonas* CrΔ4FAD desaturases can add a double bond on a FA of MGDG, which prevents its subsequent conversion into DGDG. Therefore, these desaturases have a function in the very fine tuning of the MGDG/DGDG balance within the photosynthetic membranes. Could FAD6 and the Plastidω3FAD play a similar role in *Phaeodactylum*? Eventually the remarkably high level of EPA in galactolipids might be related to a specific molecular or biophysical property of this VLC-PUFA: a clear challenge is then to comprehend the function of EPA in MGDG, DGDG, and acyl-SQDG.

3. Experimental Section

3.1. Retrieval of Desaturase Candidate Gene Sequences

All sequences listed in this work have been retrieved from the Joint Genome Institute [52] and gene IDs were given as Phatdraft accessions, according to the ongoing structural annotation of genes models of *Phaeodactylum tricornutum* Pt1 8.6 [53]. When characterized in previous works, Phatdraft accessions of corresponding genes were simply obtained and provided in this article for consistency. For partly annotated or unannotated genes, sequences were retrieved based on BLASTP searches [54] using *Arabidopsis*, *Chlamydomonas*, or *Thalassiosira* desaturase gene models, as described in the text. Retrieved open reading frame sequences were then examined manually to discard fragments and determine full length sequences, based on the presence of an initial methionine, a STOP codon, an alignment with known ESTs, and consistency of multiple alignments [55] with gene homologues from other photosynthetic eukaryotes. The presence of consensus regions and domains characterizing soluble or membrane desaturases, as well as the detection cytochrome b5 fusions, was checked using Pfam hidden Markov models [56] annotated in InterPro [57] and checked manually.

3.2. Prediction of Subcellular Localization

There is no tool specifically developed for the prediction of the subcellular localization of protein sequences in *Phaeodactylum*, and most notably for the 4-membrane chloroplast. The presence of a motif frequently detected in bipartite plastid transit peptides of heterokonts, called ASAFAP, can be detected by scanning the N-terminal sequence with a logo profile [37,38]. In *Phaeodactylum* sequences, the core alanine-phenylalanine dipeptide (AF) was therefore detected using ASAFind [37, 58] and HECTAR [38, 59] online tools, as well as serine residues upstream and downstream of the AF dipeptide. The prediction of the localization in plastids was consolidated by the combined presence of a signal peptide (Sp), supporting the notion that protein precursors might reach the outermost membrane of the chloroplast connected to the ER, and a chloroplast-like transit peptide (Ctp), supporting the idea that protein precursors might go across the innermost membranes of the chloroplast. These features at the terminal end of protein sequences were predicted using generic tools developed for eukaryotes, *i.e.*, SignalP and ChloroP [60,61].

4. Conclusions

In this work, we mined the complete genome of *Phaeodactylum* with gene templates from *Arabidopsis*, *Chlamydomonas*, *Thalassiosira*, and other photosynthetic organisms in an attempt to list the most complete census of fatty acid desaturases. Putative and characterized *Phaeodactylum* desaturase sequences are provided as a supplementary file (Supplementary data), and were used to predict subcellular localization in broad terms, *i.e.*, chloroplastic *vs.* cytosolic (Figures 2 and 4). Substrate specificity was tentatively assessed and provided in Table 2. One important desaturase seems to be missing, *i.e.*, the ERω3FAD involved in the EPA pathway. The possible involvement of the Plastidω3FAD/FAD7 or of a cytosolic isoform of this protein should be investigated. Besides FAD2, FAD6, ERΔ6FAD, and ERΔ5FAD, which have been investigated *in vitro*, in heterologous systems, and by genetic engineering in transformed *Phaeodactylum* cells, future works must now target the characterization of other enzymes and associated proteins. In particular, an important challenge lies in the comprehension of the coordination of desaturases and elongases in the very efficient production of EPA, and the entry of this VLC-PUFA into the omega pathway that leads to its striking accumulation in chloroplast glycerolipids.

Acknowledgments

This work was supported by a grant from Agence Nationale de la Recherche (ANR-12-BIME-0005, DiaDomOil), a bioenergy grant from CEA Life Science Division (EliciTAG), the IRTELIS program (PhD grand of LJD), the OCEANOMICS program from the French Ministry of Research, and the Institut Carnot LISA (Lipides pour la santé et l'industrie). The authors wish to thank Melissa Conte for copyediting.

Author Contributions

LMD and EM have conceived and performed analyses. Both authors have contributed to the writing of the manuscript.

Conflicts of Interest

The authors declare no conflict of interest.

References

1. Armbrust, E.V. The life of diatoms in the world's oceans. *Nature* **2009**, *459*, 185–192.
2. Scala, S.; Bowler, C. Molecular insights into the novel aspects of diatom biology. *Cell. Mol. Life Sci.* **2001**, *58*, 1666–1673.
3. Boudière, L.; Botte, C.; Saidani, N.; Lajoie, M.; Marion, J.; Bréhélin, L.; Yamaryo-Botté, Y.; Satiat-Jeunemaître, B.; Breton, C.; Girard-Egrot, A.; *et al.* Galvestine-1, a novel chemical probe for the study of the glycerolipid homeostasis system in plant cells. *Mol. BioSyst.* **2012**, *287*, 22367–22376.
4. Mosblech, A.; Feussner, I.; Heilmann, I. Oxylipins: Structurally diverse metabolites from fatty acid oxidation. *Plant Physiol. Biochem.* **2009**, *47*, 511–517.
5. Damude, H.G.; Kinney, A.J. Engineering oilseed plants for a sustainable, land-based source of long chain polyunsaturated fatty acids. *Lipids* **2007**, *42*, 179–185.
6. Li-Beisson, Y.; Shorrosh, B.; Beisson, F.; Andersson, M.X.; Arondel, V.; Bates, P.D.; Baud, S.; Bird, D.; Debono, A.; Durrett, T.P.; *et al.* Acyl-lipid metabolism. *Arabidopsis Book* **2010**, *8*, e0133.
7. Dorrell, R.G.; Smith, A.G. Do red and green make brown?: Perspectives on plastid acquisitions within chromalveolates. *Eukaryot. Cell* **2011**, *10*, 856–868.
8. Petroutsos, D.; Amiar, S.; Abida, H.; Dolch, L.J.; Bastien, O.; Rebeille, F.; Jouhet, J.; Falconet, D.; Block, M.A.; McFadden, G.I.; *et al.* Evolution of galactoglycerolipid biosynthetic pathways—From cyanobacteria to primary plastids and from primary to secondary plastids. *Prog. Lipid Res.* **2014**, *54*, 68–85.
9. Kroth, P.G.; Chiovitti, A.; Gruber, A.; Martin-Jezequel, V.; Mock, T.; Parker, M.S.; Stanley, M.S.; Kaplan, A.; Caron, L.; Weber, T.; *et al.* A model for carbohydrate metabolism in the diatom phaeodactylum tricornutum deduced from comparative whole genome analysis. *PLoS One* **2008**, *3*, e1426.
10. Abida, H.; Dolch, L.J.; Mei, C.; Villanova, V.; Conte, M.; Block, M.A.; Finazzi, G.; Bastien, O.; Tirichine, L.; Bowler, C.; *et al.* Membrane glycerolipid remodeling triggered by nitrogen and phosphorus starvation in phaeodactylum tricornutum. *Plant Physiol.* **2015**, *167*, 118–136.
11. Liang, Y.; Maeda, Y.; Yoshino, T.; Matsumoto, M.; Tanaka, T. Profiling of polar lipids in marine oleaginous diatom fistulifera solaris jpcc da0580: Prediction of the potential mechanism for eicosapentaenoic acid-incorporation into triacylglycerol. *Mar. Drugs* **2014**, *12*, 3218–3230.
12. Tonon, T.; Harvey, D.; Larson, T.R.; Graham, I.A. Long chain polyunsaturated fatty acid production and partitioning to triacylglycerols in four microalgae. *Phytochemistry* **2002**, *61*, 15–24.
13. Li, H.Y.; Lu, Y.; Zheng, J.W.; Yang, W.D.; Liu, J.S. Biochemical and genetic engineering of diatoms for polyunsaturated fatty acid biosynthesis. *Mar. Drugs* **2014**, *12*, 153–166.
14. Bates, P.D.; Durrett, T.P.; Ohlrogge, J.B.; Pollard, M. Analysis of acyl fluxes through multiple pathways of triacylglycerol synthesis in developing soybean embryos. *Plant Physiol.* **2009**, *150*, 55–72.

15. Lands, W.E. Metabolism of glycerolipides; a comparison of lecithin and triglyceride synthesis. *J. Biol. Chem.* **1958**, *231*, 883–888.
16. Lands, W.E. Metabolism of glycerolipids. 2. The enzymatic acylation of lysolecithin. *J. Biol. Chem.* **1960**, *235*, 2233–2237.
17. Lands, W.E. Lipid metabolism. *Annu. Rev. Biochem.* **1965**, *34*, 313–346.
18. Bates, P.D.; Ohlrogge, J.B.; Pollard, M. Incorporation of newly synthesized fatty acids into cytosolic glycerolipids in pea leaves occurs via acyl editing. *J. Biol. Chem.* **2007**, *282*, 31206–31216.
19. Bates, P.D.; Browse, J. The significance of different diacylgycerol synthesis pathways on plant oil composition and bioengineering. *Front. Plant Sci.* **2012**, *3*, 147.
20. Bates, P.D.; Fatihi, A.; Snapp, A.R.; Carlsson, A.S.; Browse, J.; Lu, C. Acyl editing and headgroup exchange are the major mechanisms that direct polyunsaturated fatty acid flux into triacylglycerols. *Plant Physiol.* **2012**, *160*, 1530–1539.
21. Bates, P.D.; Stymne, S.; Ohlrogge, J. Biochemical pathways in seed oil synthesis. *Curr. Opin. Plant Biol.* **2013**, *16*, 358–364.
22. Tanaka, T.; Maeda, Y.; Veluchamy, A.; Tanaka, M.; Abida, H.; Marechal, E.; Bowler, C.; Muto, M.; Sunaga, Y.; Tanaka, M.; *et al.* Oil accumulation by the oleaginous diatom fistulifera solaris as revealed by the genome and transcriptome. *Plant Cell* **2015**, *27*, 162–176.
23. Shanklin, J.; Cahoon, E.B. Desaturation and related modifications of fatty acids. *Annu. Rev. Plant Physiol. Plant Mol. Biol.* **1998**, *49*, 611–641.
24. Lopez Alonso, D.; Garcia-Maroto, F.; Rodriguez-Ruiz, J.; Garrido, J.A.; Vilches, M.A. Evolutiuon of membrane-bound fatty acid desaturases. *Biochem. Syst. Ecol.* **2003**, *31*, 1111–1124.
25. Shanklin, J.; Guy, J.E.; Mishra, G.; Lindqvist, Y. Desaturases: Emerging models for understanding functional diversification of diiron-containing enzymes. *J. Biol. Chem.* **2009**, *284*, 18559–18563.
26. Sperling, P.; Ternes, P.; Zank, T.K.; Heinz, E. The evolution of desaturases. *Prostaglandins Leukot. Essent. Fatty Acids* **2003**, *68*, 73–95.
27. Hanke, G.; Mulo, P. Plant type ferredoxins and ferredoxin-dependent metabolism. *Plant Cell Environ.* **2013**, *36*, 1071–1084.
28. Kumar, R.; Tran, L.S.; Neelakandan, A.K.; Nguyen, H.T. Higher plant cytochrome b5 polypeptides modulate fatty acid desaturation. *PLoS One* **2012**, *7*, e31370.
29. Napier, J.A.; Michaelson, L.V.; Sayanova, O. The role of cytochrome b5 fusion desaturases in the synthesis of polyunsaturated fatty acids. *Prostaglandins Leukot. Essent. Fatty Acids* **2003**, *68*, 135–143.
30. Zauner, S.; Jochum, W.; Bigorowski, T.; Benning, C. A cytochrome b5-containing plastid-located fatty acid desaturase from chlamydomonas reinhardtii. *Eukaryot. Cell* **2012**, *11*, 856–863.
31. Domergue, F.; Spiekermann, P.; Lerchl, J.; Beckmann, C.; Kilian, O.; Kroth, P.G.; Boland, W.; Zahringer, U.; Heinz, E. New insight into phaeodactylum tricornutum fatty acid metabolism. Cloning and functional characterization of plastidial and microsomal delta12-fatty acid desaturases. *Plant Physiol.* **2003**, *131*, 1648–1660.
32. Domergue, F.; Lerchl, J.; Zahringer, U.; Heinz, E. Cloning and functional characterization of phaeodactylum tricornutum front-end desaturases involved in eicosapentaenoic acid biosynthesis. *Eur. J. Biochem.* **2002**, *269*, 4105–4113.

33. Fukuchi-Mizutani, M.; Tasaka, Y.; Tanaka, Y.; Ashikari, T.; Kusumi, T.; Murata, N. Characterization of delta 9 acyl-lipid desaturase homologues from arabidopsis thaliana. *Plant Cell Physiol.* **1998**, *39*, 247–253.
34. Smith, M.A.; Dauk, M.; Ramadan, H.; Yang, H.; Seamons, L.E.; Haslam, R.P.; Beaudoin, F.; Ramirez-Erosa, I.; Forseille, L. Involvement of arabidopsis acyl-coenzyme a desaturase-like2 (at2g31360) in the biosynthesis of the very-long-chain monounsaturated fatty acid components of membrane lipids. *Plant Physiol.* **2013**, *161*, 81–96.
35. Heilmann, I.; Mekhedov, S.; King, B.; Browse, J.; Shanklin, J. Identification of the arabidopsis palmitoyl-monogalactosyldiacylglycerol δ7-desaturase gene fad5, and effects of plastidial retargeting of arabidopsis desaturases on the fad5 mutant phenotype. *Plant Physiol.* **2004**, *136*, 4237–4245.
36. Gao, J.; Ajjawi, I.; Manoli, A.; Sawin, A.; Xu, C.; Froehlich, J.E.; Last, R.L.; Benning, C. Fatty acid desaturase4 of *Arabidopsis* encodes a protein distinct from characterized fatty acid desaturases. *Plant J.* **2009**, *60*, 832–839.
37. Gruber, A.; Rocap, G.; Kroth, P.G.; Armbrust, E.V.; Mock, T. Plastid proteome prediction for diatoms and other algae with secondary plastids of the red lineage. *Plant J.* **2015**, *81*, 519–528.
38. Gschloessl, B.; Guermeur, Y.; Cock, J.M. Hectar: A method to predict subcellular targeting in heterokonts. *BMC Bioinform.* **2008**, *9*, 393.
39. Boudiere, L.; Michaud, M.; Petroutsos, D.; Rebeille, F.; Falconet, D.; Bastien, O.; Roy, S.; Finazzi, G.; Rolland, N.; Jouhet, J.; *et al.* Glycerolipids in photosynthesis: Composition, synthesis and trafficking. *Biochim. Biophys. Acta* **2014**, *1837*, 470–480.
40. Moreno, V.J.; Demoreno, J.E.A.; Brenner, R.R. Biosynthesis of unsaturated fatty-acids in the diatom phaeodactylum tricornutum. *Lipids* **1979**, *14*, 15–19.
41. Arao, T.; Sakaki, T.; Yamada, M. Biosynthesis of polyunsaturated lipids in the diatom phaeodactylum tricornutum. *Phytochemistry* **1994**, *36*, 629–635.
42. Arao, T.; Yamada, M. Biosynthesis of polyunsaturated fatty acids in the marine diatom *Phaeodactylum tricornutum*. *Phytochemistry* **1994**, *35*, 1177–1181.
43. Reed, D.W.; Schafer, U.A.; Covello, P.S. Characterization of the brassica napus extraplastidial linoleate desaturase by expression in *Saccharomyces cerevisiae*. *Plant Physiol.* **2000**, *122*, 715–720.
44. Khozin-Goldberg, I.; Didi-Cohen, S.; Shayakhmetova, I.; Cohen, Z. Biosynthesis of eicosapentaenoic acid (epa) in the freshwater eustigmatophyte monodus subterraneus (Eustigmatophyceae). *J. Phycol.* **2002**, *38*, 745–756.
45. Botte, C.Y.; Yamaryo-Botte, Y.; Janouskovec, J.; Rupasinghe, T.; Keeling, P.J.; Crellin, P.; Coppel, R.L.; Marechal, E.; McConville, M.J.; McFadden, G.I. Identification of plant-like galactolipids in chromera velia, a photosynthetic relative of malaria parasites. *J. Biol. Chem.* **2011**, *286*, 29893–29903.
46. Hamilton, M.L.; Haslam, R.P.; Napier, J.A.; Sayanova, O. Metabolic engineering of phaeodactylum tricornutum for the enhanced accumulation of omega-3 long chain polyunsaturated fatty acids. *Metab. Eng.* **2014**, *22*, 3–9.
47. Jiang, H.M.; Gao, K.S. Effects of lowering temperature during culture on the production of polyunsaturated fatty acids in the marine diatom *Phaeodactylum tricornutum* (Bacillariophyceae). *J. Phycol.* **2004**, *40*, 651–654.

48. Pinot, M.; Vanni, S.; Pagnotta, S.; Lacas-Gervais, S.; Payet, L.A.; Ferreira, T.; Gautier, R.; Goud, B.; Antonny, B.; Barelli, H. Lipid cell biology. Polyunsaturated phospholipids facilitate membrane deformation and fission by endocytic proteins. *Science* **2014**, *345*, 693–697.
49. Meiser, A.; Schmid-Staiger, U.; Trosch, W. Optimization of eicosapentaenoic acid production by phaeodactylum tricornutum in the flat panel airlift (fpa) reactor. *J. Appl. Phycol.* **2004**, *16*, 215–225.
50. Leflaive, J.; Ten-Hage, L. Chemical interactions in diatoms: Role of polyunsaturated aldehydes and precursors. *New Phytol.* **2009**, *184*, 794–805.
51. Desbois, A.P.; Smith, V.J. Antibacterial free fatty acids: Activities, mechanisms of action and biotechnological potential. *Appl. Microbiol. Biotechnol.* **2010**, *85*, 1629–1642.
52. Joint Genome Institute, http://genome.jgi-psf.org/Phatr2/Phatr2.home.html, accessed on 15 December 2014
53. Bowler, C.; Allen, A.E.; Badger, J.H.; Grimwood, J.; Jabbari, K.; Kuo, A.; Maheswari, U.; Martens, C.; Maumus, F.; Otillar, R.P.; *et al.* The phaeodactylum genome reveals the evolutionary history of diatom genomes. *Nature* **2008**, *456*, 239–244.
54. Altschul, S.F.; Gish, W.; Miller, W.; Myers, E.W.; Lipman, D.J. Basic local alignment search tool. *J. Mol. Biol.* **1990**, *215*, 403–410.
55. Multalin, http://multalin.toulouse.inra.fr/multalin/, accessed on 15 December 2014
56. Terrapon, N.; Gascuel, O.; Marechal, E.; Breehelin, L. Detection of new protein domains using co-occurrence: Application to plasmodium falciparum. *Bioinformatics* **2009**, *25*, 3077–3083.
57. Interpro, http://www.ebi.ac.uk/interpro/, accessed on 15 December 2014
58. Asafind, http://rocaplab.ocean.washington.edu/tools/asafind, accessed on 15 January 2015
59. Hectar, http://www.sb-roscoff.fr/hectar/, accessed on 15 December 2014
60. Emanuelsson, O.; Brunak, S.; von Heijne, G.; Nielsen, H. Locating proteins in the cell using targetp, signalp and related tools. *Nat. Protoc.* **2007**, *2*, 953–971.
61. Petersen, T.N.; Brunak, S.; von Heijne, G.; Nielsen, H. Signalp 4.0: Discriminating signal peptides from transmembrane regions. *Nat. Methods* **2011**, *8*, 785–786.

5.2.2 *Functional analysis of a P. tricornutum Δ-6 elongase in yeast heterologous system*

EPA is the most abundant VLC-PUFA in *P. tricornutum*. Given that fatty acid synthesis reaches chain length of maximal 18 carbon atoms, one elongase is playing in the production of EPA. In a variety of species, the fatty acid Δ-6 elongase (Elo6) is described to accept Δ-6 desaturated C18 PUFAs, with a preference for 18:4 thereby catalysing the production of 20:4, the direct substrate for the Δ-5 desaturase producing EPA in the ω-3 pathway (Jeennor et al. 2014, Meyer et al. 2004). However, in *Physcomitrella* and *Thalassiosira*, Elo6 was also observed to accept Δ-9 PUFAs (Eiamsa-Ard et al. 2013, Jeennor et al. 2014). In *P. tricornutum*, the "ω-3" and "ω-6" pathways coexist (Arao & Yamada. 1994) but it is unknown whether different Elo6 isoforms would have different substrate specificities or if the same enzyme is accepting both, 18:3 and 18:4 as a template with a higher affinity for the one or the other. We have identified two Elo6 isoforms in *P. tricornutum*, ELO6b_1 (Phatr2_22274) and ELO6b_2 (Phatr2_20508) that share 89% sequence identity and 93% similarity when the N-terminal tail of ELO6b_2 was neglected (**figure 5.2**).

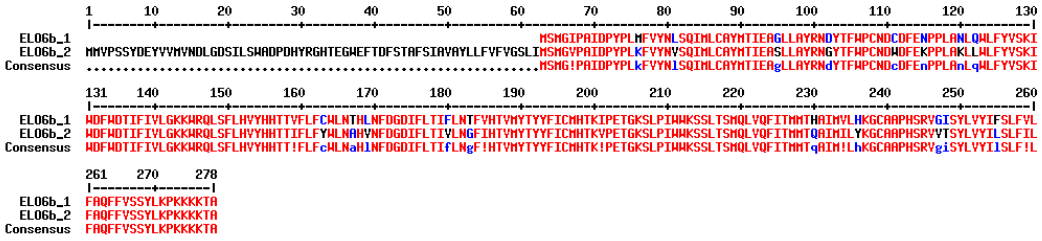

Figure 5.2. Amino acid sequence alignment of *Phaeodactylum* Δ6-elongases ELO6b_1 (Phatr2_22274) and ELO6b_2 (Phatr2_20508).

We cloned the endogenous ELO6b_2 sequence in pYES2 and expressed the gene in *S. cerevisae* WT for substrate feeding experiments. The expression of ELO6b_2 in transformed yeast was induced by the exchange of glucose by galactose in the growth media and cells were fed with different fatty acid species, namely 18:1, 18:2, 18:3 n-6, 18:4 n-3, 20:3 n-6, 20:4 n-3, 20:5 n-3. Elongation activity was followed via GC-FID.

Chromatographs of yeast cells transformed with the empty vector control were WT-like, except for the peaks of the fed FA species. The same was true for ELO6b_2 overexpressing lines fed with most fatty acids. Only 18:3 n-6 and 18:4 n-3 were accepted as a substrate by the transgene (**figure 5.3**). A small proportion of these two fatty acids were elongated to 20:3 n-6 and 20:4 n-3, respectively. This confirmed ELO6b_2 Δ-6-elongase activity with specificity for C18 substrates *in vitro*. In line with the pulse chase experiments performed by Arao and coworkers, the preferred substrate was 18:4 with 7.8% conversion to 20:4 over 18:3 n-6 with 1.7% conversion when fed alone and 9.8% over 0.4% when fed in parallel (**figure 5.3**).

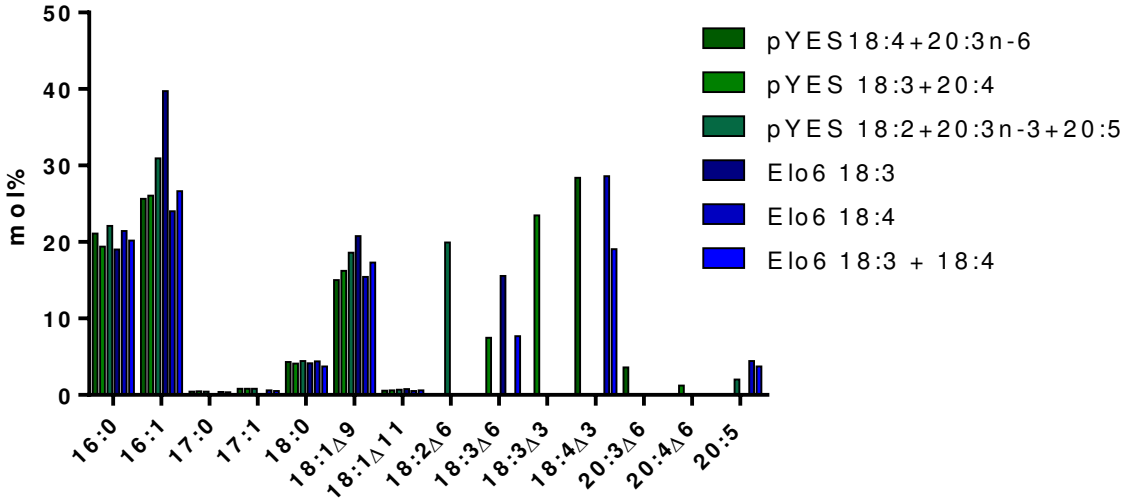

Figure 5.3. Functional analysis of *Phaeodactylum* ELO6b_2 in yeast. Fatty acid profile of a yeast WT line expressing ELO6b_2 (Elo6) (blue bars) compared to cells transformed with an empty pYES vector (green bars) grown on a medium complemented with fatty acid species indicated. No elongation of very long chain polyunsaturated fatty acids was observed for the control but 18:3n-6 and 18:4n-3 was elongated when the Elo6 transgene was expressed.

Low *in vitro* elongation activity of ELO6b_2 was puzzling as higher conversion efficiencies were achieved in similar experiments using desaturase gene sequences with *Phaeodactylum* codon usage (Petrie et al. 2010, Vaezi et al. 2013). We did not rule out if low elongation rates observed in the heterologous system reflected low activity *in vivo*

or if it was a methodological artefact caused by wrong sequences or inadequate conditions for activity. A false annotation of an intron in the CDSs was possible (personal communication F. Beaudoin). It cannot be excluded, that for optimal efficiency *in vivo*, co-factors are required that were missing in the heterologous system. Despite these restrictions we were still able to provide functional evidence of Δ-6-elongase activity for ELO6b_2 in *P. tricornutum*.

5.2.3 *A palmitic acid elongase controls eicosapentaenoic acid and plastid MGDG levels in Nannochloropsis (**submitted article**)*

An ER palmitic acid elongase is involved in eicosapentaenoic acid biosynthesis and controls plastid MGDG level in *Nannochloropsis*

Lina-Juana Dolch[1], Camille Rak[1], Guillaume Tourcier[1], Richard Broughton[2], Marina Leterrier[3], Tomas Morosinoto[4], Frédérique Tellier[5], Jean-Denis Faure[5], Denis Falconet[1], Juliette Jouhet[1], Olga Sayanova[2], Frédéric Beaudoin[2], Eric Maréchal[1,*]

[1]Laboratoire de Physiologie Cellulaire et Végétale, Unité mixte de recherche 5168 CNRS – CEA – Université Grenoble 1, Institut de Recherche en Sciences et Technologies pour le Vivant, CEA Grenoble, 17 rue des Martyrs, 38054, Grenoble Cedex 9, France. [2]Biological Chemistry and Crop Protection Department, Rothamsted Research, Harpenden, Hertfordshire, AL5 2JQ, United Kingdom. [3]Fermentalg, 4 Rue Rivière, 33500, Libourne, France. [4]Padua Algae Research Laboratory, Department of Biology, University of Padova, Via U. Bassi 58/B, 35121 Padova, Italy. [5]Institut Jean-Pierre Bourgin, INRA, AgroParisTech, CNRS, Université Paris-Saclay, 78000, Versailles, France

Submitted to Proceedings of the National Academy of Sciences of the United States of America

Nannochloropsis **species belong to the heterokont phylum and contain a plastid limited by four membranes, deriving from a secondary endosymbiosis. *Nannochloropsis* plastid lipids, including monogalactosyldiacylglycerol (MGDG), are particularly enriched in eicosapentaenoic acid (EPA). Although fatty acids are *de novo* synthesized in the stroma, they are elongated and desaturated into EPA at the ER. The assembly of plastid lipids relies therefore on an EPA supply from the ER, following an unknown process. We identified eight elongases and six desaturases possibly involved in EPA production in *N. gaditana*. Among six heterokont-specific saturated fatty acid elongases, which could act in the most upstream part of this pathway, we characterized the highly expressed isoform $^{\triangle}$*0-ELO1 via* targeted gene knock-out (KO). The $^{\triangle}$0-elo1 mutants exhibited a reduced EPA level and a specific decrease in MGDG. Ng$^{\triangle}$0-elo1 knock out (KO) lines displayed aberrant thylakoid membrane morphologies and a functionally impaired photosynthesis, consistent with a role of MGDG in non-photochemical quenching control. Concomitantly with MGDG decrease, the level of triacylglycerol (TAG) containing medium chain fatty acids increased. In *Nannochloropsis*, part of EPA used for MGDG production is therefore biosynthesized by a channeled process initiated at the first elongation step of palmitic acid by $^{\triangle}$0-ELO1, thus acting as a committing enzyme for galactolipid production. Based on the MGDG/TAG balance controlled by $^{\triangle}$0-ELO1, this study gives insights on the regulation of lipid synthesis in heterokonts and also provides novel prospects for the engineering of these algae for biotechnological applications.**

Nannochloropsis | heterokont | omega pathway | fatty acid elongase | eicosapentaenoic acid.

Introduction.

Heterokonts have emerged from a secondary endosymbiosis event, during which a red alga was engulfed by a eukaryotic host cell. The reduction of the red algal endosymbiont has led to the formation of a photosynthetic organelle surrounded by four membranes, called a complex or secondary plastid (1). The lipid composition of membranes constituting this organelle has not been characterized yet. Four glycerolipids are conserved in the photosynthetic membranes from cyanobacteria to primary plastids, *i.e.* monogalactosyldiacylglycerol (MGDG), digalactosyldiacylglycerol (DGDG), sufoquinovosyldiacylglycerol (SQDG), and only one phospholipid, phosphatidylglycerol (PG) (1). Based on their detection in whole cell extracts of secondary endosymbionts (2-4), these four lipids have been postulated to reside in the thylakoids of secondary plastids as well. A striking feature of heterokonts analyzed to date lies in their high content in very long chain polyunsaturated fatty acids (VLC-PUFAs), especially eicosapentaenoic acid (EPA, 20:5 ^{D5,8,11,14,17}) and docosahexaenoic acid (DHA, 22:6$^{\triangle 4,7,10,13,16,19}$) (2, 4, 5). In *Nannochloropsis*, VLC-PUFAs are overrepresented in MGDG, DGDG, PG, phosphatidylethanolamine (PE) and diacylglyceryltrimethylhomoserine (DGTS) (4, 6). The biological function of VLC-PUFAs in a redox poise environment like photosynthetic membranes is intriguing, especially since unsaturated FAs are more susceptible to oxidation (7).

FAs are initially synthesized in the stroma of plastids by the dissociated fatty acid synthase of type II (FASII) releasing medium chain fatty acids (MC-FAs), up to a chain length of 16 or 18 carbons. *De novo* synthesized MC-FAs are either saturated (16:0-ACP, 18:0-ACP) or mono-unsaturated by a stromal acyl-ACP $^{\triangle}$9-desaturase (16:1$^{\Delta 9}$-ACP, 18:1$^{\Delta 9}$-ACP). MC-FAs are exported to the cytosol, where they are converted into acyl-CoA (16:0-CoA, 16:1$^{\Delta 9}$-CoA, 18:0-CoA, 18:1$^{\Delta 9}$-CoA). The generation of VLC-PUFAs then occurs at the ER by multiple hetero-tetrameric elongase complexes, catalyzing stepwise reactions adding 2 carbons to an acyl-CoA substrate. (8-10). The term elongase (ELO) refers to the first enzyme, β-ketoactyl-CoA synthase (KCS), of which there are two structural different

Significance

Heterokonts are a major lineage of eukaryotic phytoplankton. Their cells contain a photosynthetic plastid limited by four membranes and containing thylakoids. In *Nannochloropsis*, the thylakoid lipids mono- and digalactosyldiacylglycerol (MGDG and DGDG) contain very high levels of eicosapentaenoic acid (EPA, 20:5). EPA is synthesized at the endoplasmic reticulum and is therefore imported to the plastid via an unknown process. We show that EPA biosynthesis pathway starts by the action of heterokont-specific elongases, using palmitic acid (16:0) as substrate. Genetic knock out of the most expressed isoform, $^{\triangle}$*0-ELO1*, leads to a reduced EPA level and a specific MGDG decrease, showing the existence of a channeled process from palmitic acid elongation to MGDG assembly, and highlighting a role of EPA-rich-MGDG on photosynthesis.

Reserved for Publication Footnotes

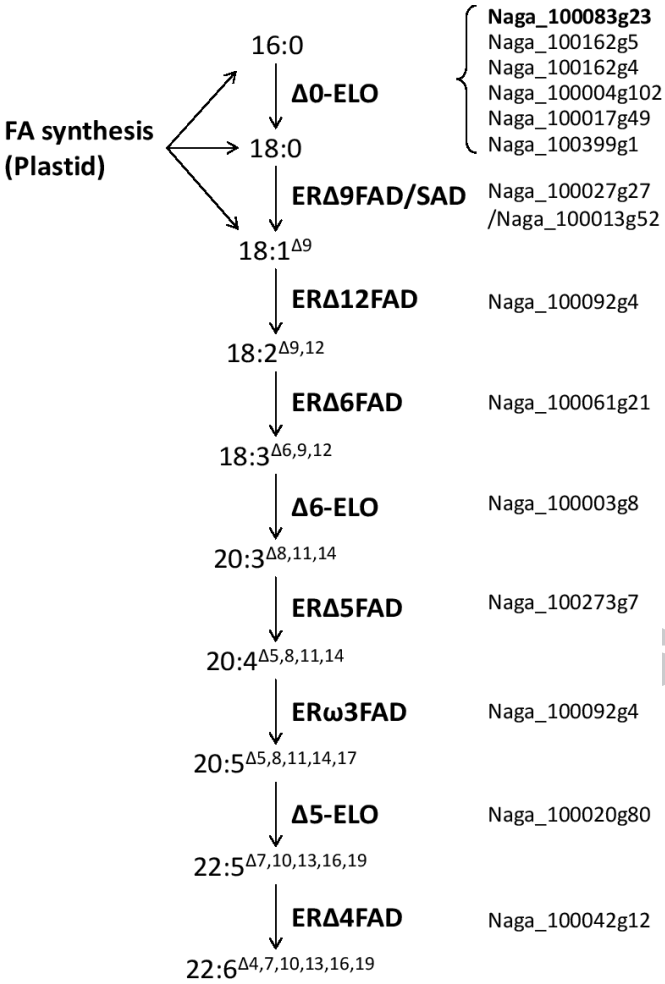

Fig. 1. Reconstructed pathway of very-long chain polyunsaturated fatty acid synthesis in *Nannochloropsis gaditana*. The *de novo* synthesis of fatty acids in the chloroplast stroma can generate 16:0, 18:0 and 18:1 precursors, which can be exported to the cytosol. Desaturation of 18:0 into 18:1 can either occur *via* the action of a stroma stearoyl-ACP ▵9-desaturase (SAD) or an ER fatty acid desaturase (ER▵9FAD). Eight candidate genes coding for elongases and six genes coding for desaturases were retrieved from the *N. gaditana* genome. Elongases were predicted to act either on a saturated substrate (▵0-ELO) or on a polyunsaturated substrate having a double bond at position ▵6 (▵6-ELO) or ▵5 (▵5-ELO).

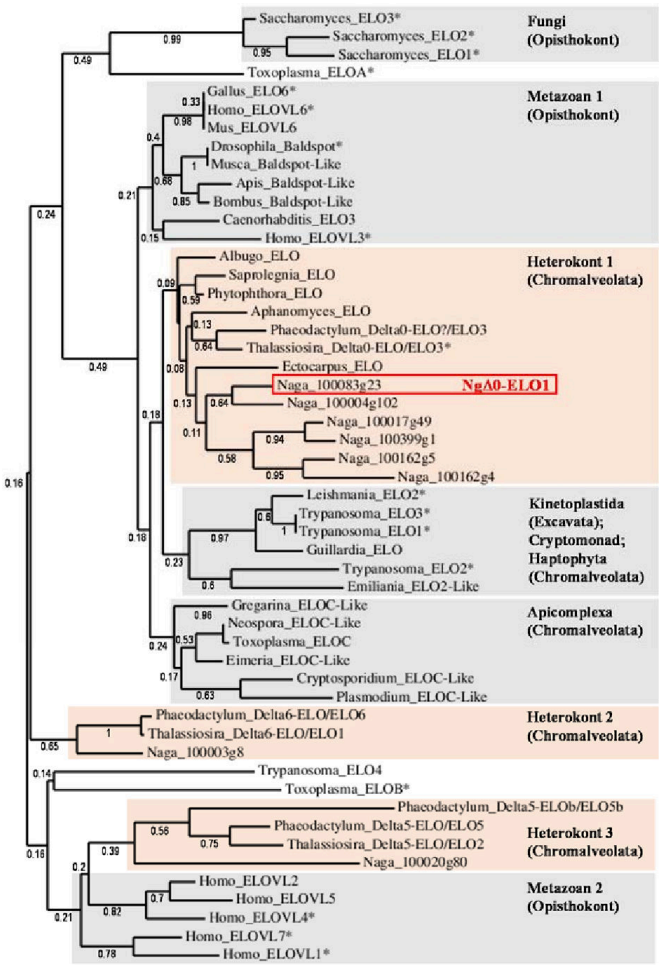

Fig. 2. Unrooted phylogenetic tree of fatty acid elongases. Selected sequences cover the biodiversity of eukaryotes including Opisthokonts, e.g. Fungi (*Saccharomyces*) and Metazoa (*Drosophila*, *Musca*, *Apis*, *Bombus*, *Caenorhabditis*, *Homo*,*Mus*, *Gallus*), Heterokonts (*Phaeodactylum*, *Thalassiosira*, *Ectocarpus*, *Phytophthora*, *Albugo*, *Saprolegnia*, *Aphanomyces*), Apicomplexa (*Toxoplasma*, *Neospora*, *Eimeria*, *Cryptosporidium*, *Plasmodium*, *Gregarina*), Haptophytes (Emiliania), Cryptomonads (Guillardia) and Kinetoplastida (*Trypanosoma*, *Leishmania*). A star indicate sequences with a characterized (or proposed) activity of elongation of saturated fatty acids in previous reports (1-6). The elongase characterized in the present work is shown in red.

enzyme classes: Elo-like (ELO) KCS are present in every phylum whereas fatty acid elongase 1 (FAE1)-type KCS are found only in plants. Organisms are usually equipped with a subset of KCS proteins that display a range of substrate specificities and expression pattern (11).

The biochemical steps of the elongation and desaturation pathway from $18{:}1^{\Delta 9}$ to EPA was studied in the diatom *Phaeodactylum* using pulse chase experiments (12). This study revealed the presence of two interacting routes, the "ω-6" and "ω-3" pathways, that share $18{:}2^{\Delta 9,12}$ as precursor (10). In the ω-6 pathway, $18{:}2^{\Delta 9,12}$ is desaturated into $18{:}3^{\Delta 6,9,12}$ (18:3ω-6) by an ER-localized ▵6-fatty acid desaturase (ERΔ6FAD), while in the ω-3 pathway the substrate is desaturated twice, first by an ERω3FAD into $18{:}3^{\Delta 9,12,15}$ (18:3ω-3) and then by an ERΔ6FAD into $18{:}4^{\Delta 6,9,12,15}$ (18:4ω-3). The predominant route in *Phaeodactylum* was a mix of both pathways in which 18:3ω-6 is desaturated into 18:4ω-3 by an ERω3FAD (12). Both, 18:3ω-6 and 18:4ω-3 serve as substrates for a Δ6-ELO generating $20{:}3^{\Delta 8,11,14}$ (20:3ω-6) in the ω-6 pathway and respectively $20{:}4^{\Delta 8,11,14,17}$ (20:4ω-3 or eicosatetraenoic acid, ETA) in the ω-3 pathway. Both products are substrates for ERΔ5FAD giving rise to $20{:}4^{\Delta 5,8,11,14}$ (20:4ω-6 or arachidonic acid, ARA) and $20{:}5^{\Delta 5,8,11,14,17}$ (20:5ω-3, EPA). In addition to this Δ5-desaturation of ETA, EPA can be obtained by desaturation of ARA by an ERω3FAD (12). EPA can serve as the substrate for a Δ5-ELO producing $22{:}5^{\Delta 7,10,13,16,19}$ (22:5ω-3), which is then Δ4-desaturated into $22{:}6^{\Delta 4,7,10,13,16,19}$ (22:6ω-3, DHA) (13, 14). The parallel existence of the cross-interacting ω-3 and ω-6 routes is not conserved among heterokonts since the *Thalassiosira pseudonana* genomic data allowed the reconstruction only of an ω-3 pathway involving 20:4ω-3 (13). In *Nannochloropsis*, only the presence of 20:4ω-6 was reported (15). Once generated in the ER, it is necessary that VLC-PUFAs are reimported into the plastid for the assembly of MGDG, DGDG, SQDG and PG according to a yet to be characterized process, called the "omega pathway" (1).

In previous studies, VLC-PUFA biosynthesis is considered to start from oleic acid ($18{:}1^{\Delta 9}$). However, the proportions of 16:0, 18:0 and 18:1 that are produced by FASII and exported from sec-

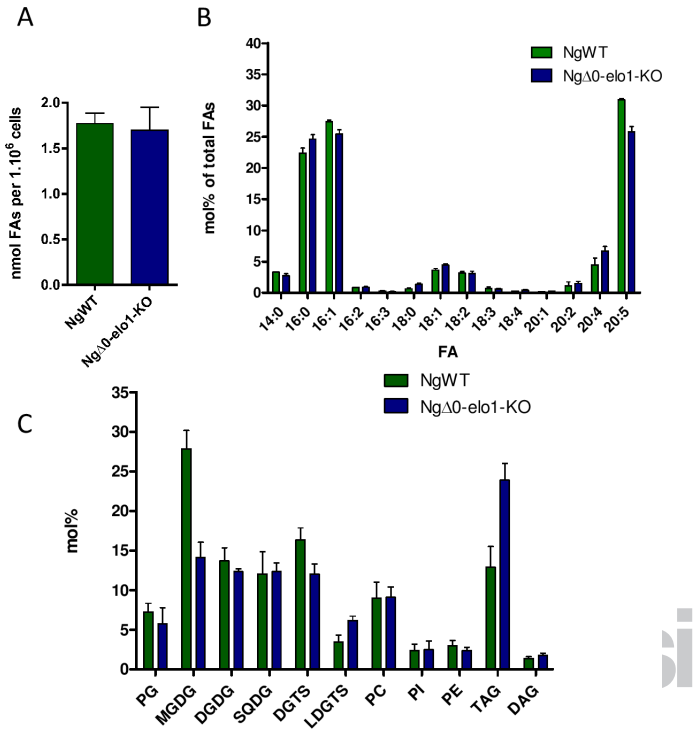

Fig. 3. Comparison of fatty acids and glycerolipids from *Nannochloropsis gaditana* WT and NgΔ0-elo1 knocked out lines. (A) Total amount of fatty acids. FA content is expressed in nmol per 1.10^6 cells. **(B) Fatty acid profiles.** The proportion of each FA is indicated, based on the carbon chain-length and number of desaturations. Statistical significant alterations were an 8% reduction of EPA (p-value 0.0072) and a 0.2% increase of 18:1 (p-value 0.0031) (two-tailed t-test). Error bars correspond to standard error of the mean (SEM, n = 3-9). **(C) Glycerolipid classes.** Glycerolipids from NgWT and NgΔ0-elo1 KO lines were extracted and separated by two-dimensional thin layer chromatography (2D-TLC) for membrane polar lipids and 1D-TLC for neutral lipids. Fatty acids from each glycerolipid class were analysed and quantified. Plastid membrane glycerolipids correspond to phosphatidylglycerol (PG), monogalactosyldiacylglycerol (MGDG), digalactosyldiacylglycerol (DGDG), sulfoquinovosyldiacylglycerol (SQDG). ER-synthesized membrane glycerolipids correspond to diacylglyceryltrimethylhomoserine (DGTS), lyso-DGTS (LDGTS), (PC), phosphatidylinositol (PI), phosphatidylethanolamine (PE), triacylglycerol (TAG) and diacylglycerol (DAG). Significant alterations inNgΔ0-elo1-KO compared to NgWT were observed at the levels of MGDG (p-value 0.0132) and TAG (p-value 0.0216) with a 43.8% reduction and a 71% increase, respectively. Other changes were not significant in two-tailed t-test. NgWT FA analyses are shown in green; NgΔ0-elo1-KO FA analyses are shown in blue. Error bars correspond to standard error of the mean (SEM, n = 3-5).

ondary plastids are unknown, so these three FAs should be equally considered as possible precursors. Here, we chose *N. gaditana* CCMP526 as a model to study the effects of an impairment of VLC-PUFA biosynthesis upstream $18:2^{\Delta 9,12}$, the branching point for the ω-3 and ω-6 pathways. We knocked out the gene coding for the major initial ER-retained elongase, and analyzed the impact on glycerolipid and sphingolipid metabolism, revealing an unexpected function in EPA synthesis that was specifically used for MGDG production. With the disturbance of the secondary plastid lipid balance, photosynthesis parameters and thylakoid membrane structure were altered. This work indicates that the omega pathway relies on channeling processes starting very early in FA elongation and that this process can be considered as a committing step in galactolipid synthesis.

Results.

Bioinformatic and phylogenetic analysis of *Nannochloropsis gaditana* elongases.

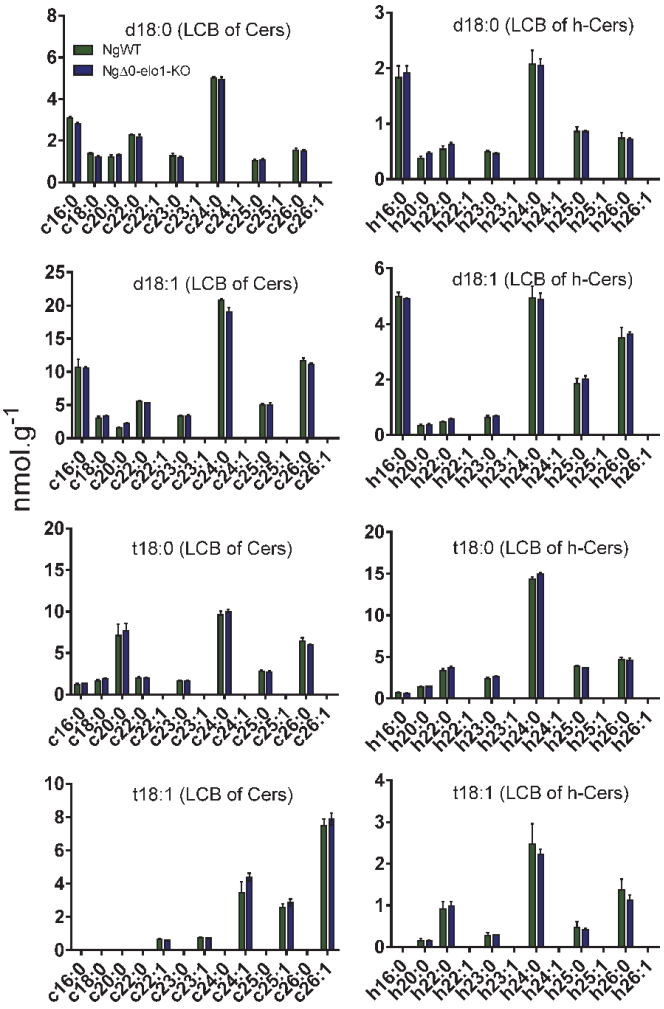

Fig. 4. Fatty acid profile of sphingolipid precursors from *Nannochloropsis gaditana* WT and NgΔ0-elo1 knocked out lines. A targeted analysis of sphingolipids was performed, focusing on long chain bases (LCB) with dihydroxylated (d) and trihydroxylated (t) 18-carbon species, linked to ceramides (Cers) or hydroxyl-ceramides (h-Cers), and with different chain lengths (16-26 carbonyl residues) of saturated or monounsaturated fatty acids. NgWT sphingolipid analyses are shown in green, NgΔ0-elo1-KO in blue. No significant differences were detected.

Based on the genome sequence of *N. gaditana* (30, 31) and on the bioinformatic detection of target peptides targeting proteins to the stroma, FA synthesis up to a chain length of 16 to 18 carbons is predicted to take place in the secondary plastid. The 16:0- and 18:0-ACP, generated by FASII can be $^{\Delta}$9-desaturated by a plastid acyl-ACP desaturase (*SAD*, Naga_100013g52). Theoretically, all FAs produced in the chloroplast can either be used for the synthesis of thylakoid lipids or exported to the cytosol. Upon reaching the ER, 16- and 18-carbon FAs serve as substrates for elongases and desaturases for the biosynthesis of VLC-PUFAs (1, 32). We identified 8 putative elongases in *N. gaditana*, encoded by Naga_100083g23, Naga_100162g4, Naga_100004g102, Naga_100017g49, Naga_100399g1, Naga_100162g5, Naga_100003g8 and Naga_100020g80. Elongases are ER-located transmembrane proteins with a 3-ketoacyl-CoA synthase domain (33) and we could verify these features in all protein sequences, except for those encoded by Naga_100399g1 and Naga_100020g80 that had no lysine-rich C-terminus and were predicted to be possibly located in mitochondria. Amino acid sequences of the putative elongases were compared to homologs having annotated function. We then positioned the

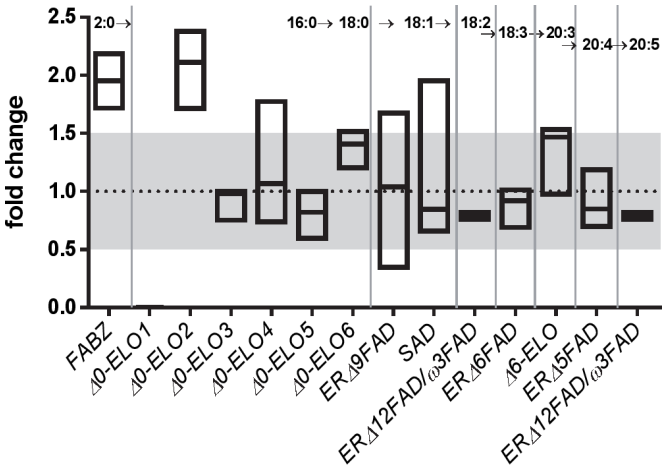

Fig. 5. Relative mRNA levels of elongases and desaturases in Ng△0-elo1 mutants compared to the NgWT. RNA was extracted from NgWT and Ng△0-elo1-KO cells and reversely transcribed. Quantitative real time PCR was performed and curves were evaluated using the△△Cq method provided with the BioRad CFX software. Ng△0-elo1-KO relative gene expression levels were normalized to the mRNA level in the NgWT, both corrected to the Cq of the housekeeping genes *PsbA* and *TUB*. Data is shown as boxplots with the line at the median, representing the fold change of gene expression in three biological replicates of both, Ng△0-elo1-KO and NgWT. A confidence threshold was set at a minimal fold change of 0.5 (grey shade). Significantly upregulated in Ng△0-elo1-KO compared to NgWT were the fatty acid synthase protein *FABZ* (1.95 fold ± 0.2338, p-value 0.0306 in t-test) and △*0-ELO2* (2.1 fold (± 0.1923, (p-value 0.031 in t-test). Genes analyzed correspond to those presented in Figure 1.

N. gaditana gene candidates on a reconstructed FA elongation pathway in *N. gaditana* (Fig. 1). Since elongation of 18:0 or $18{:}1^{\triangle 9}$ was not observed in heterokonts, we hypothesized that most upstream elongases were active on 16:0 (2, 4, 12, 13, 34).

There is no consensus for a nomenclature of elongases. We propose here a simple rule where the desaturation site of the substrate would determine the name. Thus, elongases putatively acting on a saturated fatty acid like 16:0 were labeled as △0-ELO (Naga_100083g23, Naga_100162g4, Naga_100004g102, Naga_100017g49, Naga_100399g1 and Naga_100162g5), '△0' corresponding to the absence of any desaturation in the palmitic acid substrate. Elongases acting on a polyunsaturated substrate were labeled as △6-ELO (Naga_100003g8), when the substrate harbors a double bond at position △6, and respectively △5-ELO (Naga_100020g80) when the substrate harbors a double bond at position △5. Consistently, the △0-ELO sequences are similar to *T. pseudonana* TpElo3, predicted to elongate 16:0 into 18:0 (13). No putative Δ9- or Δ7-elongases could be found. Figure 1 also shows desaturase genes acting in VLC-PUFA biosynthesis.

Fig. 1

The phylogeny of *Nannochloropsis* sequences was reconstructed based on alignments with elongases selected in representative clades of eukaryotes' biodiversity. In the opisthokonts, we selected the elongases of *S. cerevisiae* (ELO1, 2 and 3) (35), *Homo sapiens* (ELOVL1 to ELOVL7) (36), Baldspot-like elongases of *Drosophila melanogaster* (37) and an elongase sequence from *Caenorhabditis*. In kinetoplastida, a group of excavata, we selected the functionally characterized elongases of *Trypanosoma brucei* (ELO1, 2, 3 and 4) (38) and related sequences from *Leishmania*. In apicomplexa, we selected the characterized elongases of *Toxoplasma gondii* (ELOA, B and C) (39) and added related sequences from *Neospora*, *Eimeria*, *Plasmodium*, *Cryptosporidium* and *Gregarina*. We added putative elongase sequences from *Guillardia theta* and *Emiliana huxleyi* to cover the cryptomonad and haptophyta. To get a broader range of the diversity of heterokonts, we retrieved a putative sequence from *Ectocarpus siliculosus*, the elongases identified in *T. pseudonana* (TpELO1, 2 and 3) (13), elongases from *P. tricornutum*, which includes a biochemically characterized △5-ELO/ELO5 (40), as well as elongases from non-photosynthetic heterokonts of the oomycete phylum, *e.g. Phytophtora*, *Albugo*, *Saprolegnia* and *Aphanomyces*. All sequences were aligned using MUSCLE (17) and an unrooted phylogenetic tree was constructed using the Neighbor-Joining method (18) with bootstrapped confidence intervals based on 1,000 replications (Fig. 2). The elongases known to use saturated FAs as a possible substrate are labeled with a star.

Fig. 2

The six putative △0-ELO sequences from *N. gaditana* group into a cluster containing only heterokont sequences, including TpELO3 from *Thalassiosira*, proposed to act in the elongation of 16:0 into 18:0 (13). The Naga_100003g8 sequence belongs to a second heterokont cluster including △6-ELOs from diatoms. The Naga_10002080 sequence belongs to a third heterokont cluster with △5-ELOs from diatoms (Fig. 2). The heterokont cluster containing △0-ELOs is close to a group of elongase sequences from other chromalveolata (cryptomonad and haptophyta) and excavata (kinetoplastida) and to a cluster of apicomplexa elongases of the ELOC-type. The cluster containing human saturated/monounsaturated elongases, *i.e.* ELOVL3 and ELOVL6, the latter being responsible for the elongation of 16:0 and shorter (36), is close to the heterokont △0-ELO cluster. The obtained tree shows a dichotomy between saturated/monounsaturated and polyunsaturated FA elongases and is consistent with the position of *N. gaditana* sequences in the VLC-PUFA biosynthetic pathway shown in Fig. 1.

The conservation of △0-ELO homologs within a heterokont-cluster and the presence of several isoenzymes within *N. gaditana* indicate an important function of this family of elongases. No heterokont Δ0-ELO has been functionally studied to that date. We aimed to verify the proposed scheme of EPA synthesis in *N. gaditana* experimentally, and addressed the question of Δ0-ELO functional redundancy or specificity. To that purpose, we first compared the gene expression profiles of the △*0-ELO* genes.

Sequence analysis of the protein encoded by the Naga_100083g23 gene (△*0-ELO1*)

We retrieved gene expression data from *N. gaditana* cultivated under both nitrogen repletion and deficiency (31). Naga_100083g23 (△*0-ELO1*) had the highest expression level and we therefore investigated its gene product in more detail. △0-ELO1 amino acid sequence possesses an elongase domain (Fig. S1) comprising seven predicted transmembrane domains (TM1-TM7). The C-terminus part is lysine (K) rich indicating an ER retention. The "HXXH" motif essential in yeast elongases for 3-ketoacyl-CoA synthase activity (33) is conserved in the △0-ELO1 sequence, (highlighted in green in Fig. S1). The same motif is present in yeast SFA/MUFA (saturated/monounsaturated FA) elongation protein family, and is not an absolute signature for the substrate specificity (41). A "LYF" motif (highlighted in purple) is also detected, conserved in yeast Fen1p proteins that elongate fatty acids of a chain lengths between C16 and C24 (33). We then addressed the function of Ng△0-ELO1 by heterologous expression in yeast.

Functional characterization of Naga_100083g23 gene product by heterologous expression in yeast.

We cloned the codon optimized sequence of *Ng△0-ELO1* in the pYES expression vector and tested the activity of the pYES2-Ng△0-ELO1 construct on PUFAs. WT yeast clones containing the algal elongase or the empty vector as a control were grown in liquid cultures in the presence or in the absence of exogenously added long chain (C18) and very long chain (C20 and C22) PUFA substrates. No elongation product was detected for any of the PUFA substrate tested, but we could notice a systematic decrease

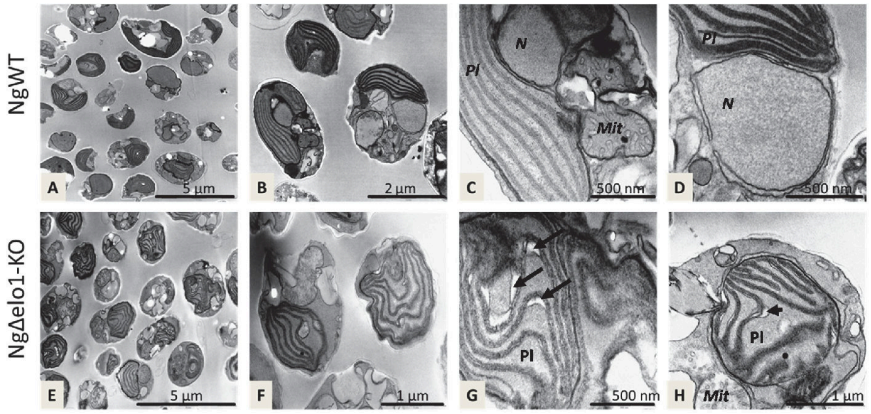

Fig. 6. Transmission electron micrographs of NgWT (A-D) and NgΔ0-elo1-KO (E-H) reveal bent thylakoid structures and lumen expansions in the mutant. Different magnifications of NgWT (A-D) and NgΔ0-elo1-KO (E-H) sections are shown. (A) Wild type *N. gaditana* cells are heterogeneous in size, shape and organelle proportions, partially caused by different cutting planes. (B) WT thylakoid membranes are devoid of grana stacks. Lamellae derive from two to three chloroplast poles. (C) WT chloroplasts consist of five to seven thylakoid lamellae, each consisting of a stack of three membrane bilayers. (D) WT plastid outer-limiting membrane is in continuum with nucleus. (E) NgΔ0-elo1-KO cells display higher thylakoid membrane curvature and two or more thylakoid membrane poles. (F-H) Inter-lamellar space (lumen) appears more expanded (black arrows) and less parallelism between membranes is observed; NgΔ0-elo1-KO thylakoids develop a more pronounced curvature. (H) NgΔ0-elo1-KO polar growth of thylakoid lamellae appears partially aborted in some cells. *N*, nucleus; *Mit*, mitochondria; *Pl*, plastid.

of C16:0 in the presence of Ng△0-ELO1 (data not shown). We then investigated a possible elongation activity of Ng△0-ELO1 on C16:0 and, to eliminate potentially competing endogenous fatty acid synthase activity, we transformed the pYES2-Ng△0-ELO1 vector in a fas2 knock-out (fas2-KO) yeast strain. In yeast the cytosolic fatty acid synthase complex (scFAS) produces 16 and 18 carbons fatty acids while the yeast *scELO1* gene is involved in microsomal elongation of C14:0 to C16:0 (22). Expressing Ng△0-ELO1 in the fas2-KO strain resulted in a decrease in 16:0, as previously observed in WT, and in a small but statistically significant increase in C18:0 suggesting that Ng△0-ELO1 does elongate 16:0 in yeast (Fig. S2A). Since the increase in 18:0 did not match the decrease in 16:0, we suspected that 18:0 might be further elongated, either by Ng△0-ELO or by the yeast endogenous scELO2/scELO3 elongase complex. To verify this hypothesis, we repeated the experiment expressing Ng△0-ELO1 in WT and in the fas2-KO strain. After extraction, FAMEs were this time analyzed on a less polar column more suitable for long-chain hydrocarbons and allowing detection of C26:0 and 2-hydroxy-C26:0 the two majors VLCFAs present in *S. cerevisiae*. Surprisingly, in WT and fas2-KO cells all VLCFAs over 20 carbons and up to C30:0 accumulated at a higher level in the presence of the algal Ng△0-ELO1 protein (Fig. S2B), suggesting an enhancement of endogenous elongation activity and explaining the limited increase in C18:0 observed in the FAS free background (Fig. S2A). This enhanced fatty acid elongase activity was not detected in yeast-elo1-KO strains suggesting that the endogenous scELO1 is required for Ng△0-ELO1 activity in yeast (data not shown). In the complemented yeast, the presence of C28 and C30 fatty acids is surprising as these compounds are normally not synthesized in *S. cerevisiae* with only trace amounts of 28:0 detectable in the fas2-KO/pYES2 control. To verify whether these VLCFAs were the products of Ng△0-ELO1 itself or of the yeast endogenous elongase, we expressed it in a yeast-elo3-KO strain, which is unable to produce C26:0 (42). This confirmed that the enhanced production of VLCFAs observed in the presence of Ng△0-ELO1 in yeast requires a functional endogenous elongase and that the C28 and C30 fatty acids are likely produced by the yeast scELO2/scELO3 complex (data not shown). Altogether, these experiments are consistent with the fact that the *N. gaditana* △0-ELO1 protein uses palmitic acid as a substrate and that it may be involved in determining the fate of the VLCFAs produced downstream.

Cloning and transformation of *Nannochloropsis gaditana* with a Naga_100083g23 knock out (Ng△0-elo1 KO) cassette

For the targeted gene KO *via* homologous recombination, we cloned a Naga_100083g23 disruption cassette and transformed *N. gaditana* wild type (WT) (43). The presence of the KO cassette was tested in 31 colonies, out of which 29 had both flanking sites inserted. Homologous recombination was verified by PCR in 3 out of 15 colonies. In the absence of a *Nannochloropsis* system for gene recovery after KO, we needed to make sure that obtained lines contained only one insert and that independent mutant lines had identical phenotypes. In the 3 selected clones, the presence of a single gene insertion event was confirmed by qPCR performed on genomic DNA (gDNA), based on the similar quantification cycle threshold of the inserted zeocin DNA with a single copy gene reference (*PAP*, Naga_100038g41). Consistently, *△0-ELO1* transcript could not be amplified in qPCR performed on cDNA from the 3 mutant lines. We thus obtained 3 independent Naga_100083g23 KO lines (KO5, KO13 and KO15) that showed similar total fatty acid profiles (Fig. S3) and phenotypes in all assays performed. Data from the KO lines could therefore be pooled and are designated below as Ng△0-elo1-KO.

Analysis of fatty acids and glycerolipids from Ng△0-elo1-KO lines highlights a reduction of EPA and a specific alteration of the MGDG/TAG balance

We investigated whether FA and lipid profiles could be altered in Ng△0-elo1-KO mutants compared to the *Nannochloropsis* wild type (NgWT). TLC-separated lipid classes were introduced by direct infusion into a trap type mass spectrometer to assess all lipid structures and particularly the regioselective localization of acyl groups at the *sn*-1 and *sn*-2 positions of membrane glycerolipids and *sn*-1, *sn*-2 and *sn*-3 positions of TAG (Table S1). FA, polar and neutral lipids were then quantified by GC-FID. Ng△0-elo1-KO and NgWT had same total FA contents per cell, with an average of 1.72 (± 0.19 *SEM*) nmol FA per million cells, when harvested after four days of cultivation (Fig. 3A). The FA profile of Ng△0-elo1-KO was different from that of the WT (Fig. 3B): the proportion of EPA (20:5, Fig. 3B) was significantly lower (*p-value* 0.0072) with a 7.97% (± 0.002 *SEM*) decrease in Ng△0-elo1-KO compared to NgWT. The only significant increase was at the level of 18:1 (*p-value* 0.0031) (Fig. 3B).

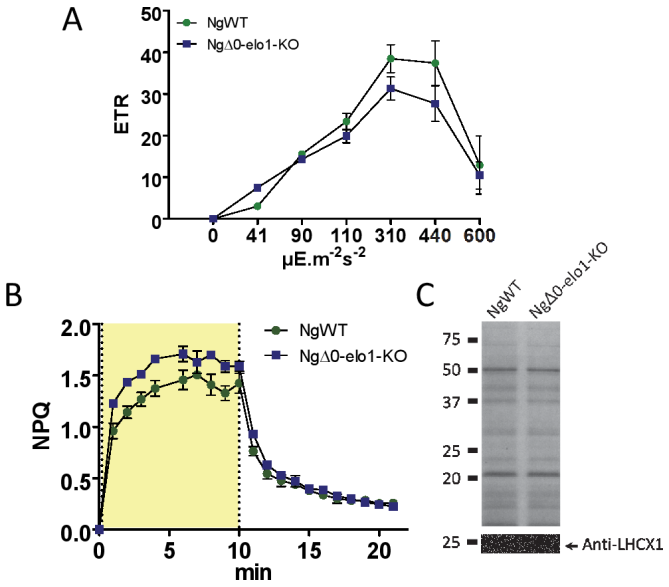

Fig. 7. Impact of Δ0-ELO1 on photosynthesis. (A) Lower photosynthetic electron transport rate (ETR), calculated *via* the quantum yield of photosystem II (YII), in NgΔ0-elo1-KO compared to NgWT. From three three-day old 2 mL cultures per cell line, a 160 µl aliquot was used for ETR estimates. YII was measured *via* room temperature chlorophyll fluorescence kinetics with different photosynthetic active radiations between 41 µE.m^{-2}s^{-2} and 600 µE.m^{-2}s^{-2}, and the ETR was calculated accordingly. ETR was impaired in mutant lines and the differences between the strains as well as between the different light intensities and their interactions were significant based on a 2-way ANOVA (*p-value* < 0.0001). **(B) Increased non-photochemical quenching (NPQ) in NgΔ0-elo1-KO compared to NgWT.** Room temperature chlorophyll fluorescence kinetics were measured to calculate NPQ with constant photosynthetic active radiation of 600 µE.m^{-2}s^{-2}. The yellow shade indicates the irradiation time frame. Representative data from a 160 µl aliquot of three seven-day old 50 mL cultures per strain are shown. Differences between mutant and NgWT were significant based on a 2-way ANOVA (*p-value* < 0.0001). **(C) Increased protein level of LHCX1 in NgΔ0-elo1-KO compared to NgWT.** The same cultures were harvested for protein extraction and 30 µg total extract were separated *via* SDS-PAGE. Gels were stained withCoomassie Brillant Blue as loading control or transferred to a membrane for LHCX1 antibody detection after Western blotting (arrow). Antibody-labeled bands were visualized and intensities determined and normalized to the intensities of the respective loading control lanes. Corrected LHCX1 signal was 18% (± 1.5 SEM) stronger in NgΔ0-elo1-KO than in NgWT (*p-value* = 0.0072 in two-tailed t-test).

In *Nannochloropsis*, EPA is enriched in three chloroplast lipids (MGDG, DGDG and PG) and two ER-synthesized lipids (PE and DGTS) (Table S1). To test if specific glycerolipid classes were reduced in abundance or altered in their fatty acid composition, membrane polar lipids were separated by 2D-TLC, neutral glycerolipids (DAG, TAG and free FA) were separated by 1D-TLC, and all TLC-resolved lipids were quantified by GC-FID (Fig. 3C). MGDG was the predominant lipid class in NgWT, representing 27.8 mol% (± 2.3 *SEM*) of total glycerolipids. Plastid DGDG and SQDG and the endomembrane lipid DGTS and PC ranged from 9 to 19 mol%. PG, which can occur in both plastid and non-plastid membranes, represented 7.25 mol% (± 1.1 *SEM*) of total glycerolipids. The endomembrane lipid classes PE, carboxymethyl-PE (CMPE) and phosphatidylinositol (PI) were below 5 mol%. Neutral lipids, *i.e.* TAG and DAG made 12.9 mol% (± 2.6 *SEM*) and 1.4 mol% (± 0.2 *SEM*) of total glycerolipids, respectively.

Compared to NgWT, the knock out of the *Δ0-ELO1* gene led to a 43.8% reduction of MGDG (*p-value* 0.0132) and a 71% increase of TAG (*p-value* 0.0216), whereas differences between KO and WT proportions of other glycerolipid classes were not significant in two-tailed t-test (Fig. 3C). When analyzing the FA profiles within each lipid class, we could not detect any statistically relevant alterations (Fig. S4).

Taken together, the analyses of glycerolipid profiles show a relationship between the KO of the *Δ0-ELO1* gene, a decrease of the synthesis of EPA, a specific reduction of the EPA-rich lipid class MGDG, and a concomitant increase of EPA-poor TAG. Other lipid classes also rely on FA synthesis, most importantly sphingolipids. We examined whether the KO of the *Δ0-ELO1* gene could also alter sphingolipids, the other major group of acyl-lipids synthesized in eukaryotes.

Targeted analysis of sphingolipid precursors did not show any alteration in NgΔ0-elo1-KO lines

No exhaustive sphingolipid profile of a unicellular alga has been reported, yet. Sphingolipids consist of a long chain base (LCB), a FA linked by an amide bond and a polar head. In plants, LCBs comprise dihydroxylated and trihydroxylated C18-species (d18 and t18) with or without unsaturation. These C18-LCB could theoretically arise from the action of a Δ0-ELO operating on a 16-carbon substrate. We focused therefore our analysis on this category of LCB. When LCBs are N-acylated by a LC-FA (labeled c16 or c18) or a VLC-FA (<c20), a ceramide (Cer) structure is formed. Hydroxylation of the FA (labelled h16, h18 and >h20) generates hydroxyl-ceramides (h-Cers) (44). A variety of possible head groups gives rise to a diversity of sphingolipid classes deriving from Cers and h-Cers, so we focused our analysis on these common procursors (45). Using a targeted mass spectrometry approach, the d18:0, d18:1, t18:0 and t18:1 forms were identified in *N. gaditana*. In this targeted analysis, acyl-profiles in Cers and h-Cers in NgΔ0-elo1-KO and NgWT were similar (Fig. 4), providing no evidence for another effect of NgΔ0-elo1 KO besides the lowering of EPA production and the alteration of the MGDG versus TAG balance.

Loss of *Δ0-ELO1* could be partially compensated by overexpression of *Δ0-ELO2* in NgΔ0-elo1-KO lines

We analyzed the expression of genes that could theoretically compensate a loss of *Δ0-ELO1*, *i.e.* (i) the five other *Δ0-ELO* genes, (ii) genes involved in EPA-biosynthesis and (iii) genes involved in the synthesis of MGDG and TAG, and normalized the expression in NgΔ0-elo1-KO to the NgWT levels of the respective gene (Fig. 5). Due to biological variations in algae cultures, we set an empirical threshold of a minimal 0.5/1.5 fold change to be considered as relevant (Fig. 5, grey shade).

As expected, *Δ0-ELO1* was not detected in qPCR in NgΔ0-elo1-KO lines. The FASII subunit *FABZ* was 1.95 fold ± 0.2338 upregulated, but as mentioned above, this did not affect the total FA content per cell. Among the other putative *Δ0-ELO* isoforms, only *Δ0-ELO2* was upregulated above the 1.5-fold change ratio, with an induction of 2.1 fold (± 0.1923, *p-value* 0.031) and we can speculate that this isoform might have a partly overlapping role with *Δ0-ELO1*. According to available RNAseq data, *Δ0-ELO2* expression is two to four times lower than *Δ0-ELO1* expression in three or six day old cultures, respectively (31).

In *N. gaditana* the galactolipid synthases are encoded by single copy genes, *i.e.* Naga_100092g5 (*MGD*) and Naga_100010g107 (*DGD*). Expression levels of *MGD*, *DGD* and chloroplastic phosphatidic acid phosphatase (*PAP*), which could provide the DAG backbone for MGDG and DGDG assembly were similar in NgΔ0-elo1-KO and NgWT, with tendencies of upregulation for *MGD* and *PAP* (Fig. S5A). The observed decrease of MGDG in the KO line was therefore not attributable to a decrease of *MGD* gene expression.

TAG can be produced in two general ways, by *de novo* synthesis or lipid remodeling. On the one hand, the ER located lysophosphatidate acyltransferases, Naga_100002g46 (LPAAT) and of the acyl-CoA:DAG acyltransferases, Naga_100343g1 (annotated DGAT2) are indicators of a *de novo* TAG synthesis *via*

the Kennedy pathway. On the other hand, a putative phospholipid:DAG acyltransferase, Naga_100065g17 (PDAT) that could also operate on galactolipids and display lipase activities would indicate remodeling (46). A lipase called PSD1 has been reported to be involved in MGDG breakdown to feed TAG pools in *Chlamydomonas*, and an homologous gene was reported in *N. oceanica* (47). We did not detect any *PSD1* homolog in *N. gaditana*. In qPCR analysis, the mRNA levels of *DGAT2* and *LPAAT* in Ng$^{\triangle}$0-elo1-KO normalized to NgWT levels were at 1, whereas *PDAT* was upregulated by 1.4 fold (Fig. S5A). None of the genes tested in qPCR had a fold change higher than 1.5 in Ng$^{\triangle}$0-elo1-KO compared to NgWT, so we were unable to provide evidence for a possible increase of TAG level by a gene expression control.

Taking lipid and qPCR analyses together, the KO of the *$^{\triangle}$0-ELO1* gene was not fully compensated by the overexpression of *$^{\triangle}$0-ELO2* and the MGDG decrease accompanied by TAG increase could not be explained by changes in the expression of galactolipid or TAG synthesis genes. Given the very important role of galactolipids on plastid ultrastructure and function (1, 48, 49), we sought whether this specific alteration of MGDG level could have an impact on the biogenesis and function of the secondary plastid in *N. gaditana* $^{\triangle}$0-elo1 KO lines.

Altered ultrastructure of thylakoid membranes in Ng$^{\triangle}$0-elo1-KO mutants

We conducted transmission electron microscopy (TEM) imaging on mid-log phase grown Ng$^{\triangle}$0-elo1-KO and NgWT cells (Fig. 6). *N. gaditana* WT cells were spherical or sub-spherical cells of 3-5 µm in average, as reported earlier (50, 51) (Fig. 6A). Most of the cell volume was occupied by a single plastid containing in general (95%) six thylakoid lamellae, each consisting of three to four membrane stacks (Fig. 6B and C). The outermost secondary plastid membrane formed a continuum with the outer nuclear envelope membrane (Fig. 6D). Based on the connection between the ER and the nuclear envelope (52), *Nannochloropsis* plastid is structurally associated with the endomembrane system and could therefore represent a platform to exchange VLC-PUFAs synthesized in the ER. In NgWT, thylakoid lamellae are quite uniform and parallel, and extend between two, sometimes three poles where they are associated with the plastid limiting membrane system (Fig. 6A-D). In Ng$^{\triangle}$0-elo1-KO lines, the cell surface was less regular (Fig. 6E and F). Chloroplast cross sections exhibited similar surfaces and number of thylakoid lamellae, but the shape of the stacks displayed a high membrane curvature (Fig. 6E-H) and some lamellae did not span the whole chloroplast but were shorter (Fig. 6H). Most strikingly, Ng$^{\triangle}$0-elo1-KO lamellae displayed frequent expansions with enlarged thylakoid lumen (Fig. 6E-H). These structures correspond to the expansion of one membrane of a lamellae stack, which is no more cohesive, as seen by the reduced lamella width (Fig. 6H).

We sought whether such alterations of chloroplast ultrastructure might have an impact on the function of the photosynthetic machinery.

Fast-fluorescence kinetics indicated impaired photosynthesis in Ng$^{\triangle}$0-elo1-KO mutants

Physiological studies were conducted on the NgWT and Ng$^{\triangle}$0-elo1-KO mutants in different culture volumes and light conditions. Surprisingly, we could not detect any growth or biomass production phenotype in Ng$^{\triangle}$0-elo1-KO in any of the cultivation regimes (Fig. S6). We investigated photosynthesis parameters in more details and measured chlorophyll content, *Fv*/*Fm*, electron transfer rate and quantum yield of PSII ETR/Y(II) and non-photochemical quenching (NPQ). Relative chlorophyll fluorescence per million cells was similar, based on a t-test, in NgWT (mean 5904 RU ± 206 *SEM*) and Ng$^{\triangle}$0-elo1-KO mutants (mean 5758 RU ± 190 *SEM*). The quantum yield of PSII measured by *Fv*/*Fm* was 5% reduced in Ng$^{\triangle}$0-elo1-KO compared to the NgWT (Fig. S7).

The transfer of electrons generated by PSII to PSI is dependent on the light energy and was tested with different photosynthetically active radiation (PAR) levels (Fig. 7A). Maximum ETR was observed at 310 µE/m^{2}s in both NgWT and Ng$^{\triangle}$0-elo1-KO, but transfer was lower in the mutant with a 4.1% reduction at 41 µE.m^{-2}s^{-2}, 7.9% at 90 µE.m^{-2}s^{-2}, 14.8% at 110 µE.m^{-2}s^{-2}, 18.6% at 310 µE.m^{-2}s^{-2}, 26% at 440 µE.m^{-2}s^{-2} and 19.3% at 600 µE.m^{-2}s^{-2}. These data indicated that with increasing PAR values, Ng$^{\triangle}$0-elo1-KO became more light-sensitive than NgWT prior to inhibition of the ETR at 600 µE.m^{-2}s^{-2}. As a consequence, Ng$^{\triangle}$0-elo1-KO mutant lines induced NPQ, possibly preventing the distorted thylakoid membranes from photo-oxidative damage.

We measured NPQ under permanent irradiation with 600 µE.m^{-2}s^{-1} actinic light on dark-adapted cells that were grown for seven days at 30 µE.m^{-2}s^{-1} white fluorescence light (Fig. 7B). In NPQ measurements, the fluorescence in response to the initial saturating light pulse (*F0* to *Fm* transition) was similar in NgWT and Ng$^{\triangle}$0-elo1-KO but the ongoing light pulses on the light-adapted cells (*Fm'*) induced higher NPQ levels in the mutant than in the control. After five minutes of prolonged irradiation, a steady level of fluorescence was reached, which was about 20% higher in Ng$^{\triangle}$0-elo1-KO lines compared to the NgWT. The light measurement represented the qE parameter of NPQ dependent on thermal energy dissipation, by PSII-associated heat emitting pigments, zeaxanthin (Zx) and antheraxanthin (53). Afterwards, light pulses are turned off and fluorescence decreases with kinetics proportional to the release from photoinhibition of PSII, reflecting the qI parameter of NPQ (54). During the relaxation phase, fluorescence rapidly decreased in Ng$^{\triangle}$0-elo1-KO and NgWT and curves superimposed. This indicated a qE but not a qI phenotype in Ng$^{\triangle}$0-elo1-KO. When cells were grown under continuous irradiation at the same light intensity (30 µE.m^{-2}s^{-1} white light), cell growth and maximal NPQ levels were two-fold higher compared to 12/12 h light/dark cycle grown samples after seven days of cultivation in 50 ml. In all these experiments performed at different light regimes, the 20% NPQ difference between the NgWT and Ng$^{\triangle}$0-elo1-KO level were maintained.

In *Nannochloropsis*, the LHCSR-like protein LHCX1 acts in the photoprotective mechanism for excess excitation energy (55), involving the activation of the violaxanthin (Vx) de-epoxidase (VDE) whose activity determines qE. Zx epoxidase (ZEP) reverts VDE reaction. Vx-chlorophyll *a* binding protein (VCP) is the predominant light harvesting protein binding chlorophyll and carotenoids (most likely Vx) (56). We addressed the mRNA level of *VDE*, *ZEP*, *VCP* and *LHCX1* by qRT-PCR, using *TUB* and *PSBA* as reference genes, and plotted the gene expression in Ng$^{\triangle}$0-elo1-KO normalized with that measured in NgWT (Fig. S5B). None of the tested genes displayed any significant change. LHCSR proteins have been previously reported to be mainly translationally regulated (57). A Western blot analysis revealed an 18% increase of the LHCX1 protein level, paralleling with the 20% increase of NPQ values (Fig. 7C) in Ng$^{\triangle}$0-elo1-KO compared to NgWT, consistently with the qE phenotype we observed.

Taking lipid data and physiological measurements together, it is likely that in the Ng$^{\triangle}$0-elo1 KO mutant, the decreased production of MGDG caused thylakoid lamellae disorganization and that this altered ultrastructure led to perturbations in the transport of electrons from PSII to PSI (as indicated by lower ETR) as well as the coupled vertical membrane transfer of protons that could induce the LHCX1-dependend Vx/Zx cycle to induce qE.

Discussion.

We identified sequences in the *N. gaditana* genome involved in VLC-PUFA biosynthesis pathway starting from a 16:0 substrate.

We confirmed the existence of a unique ω-6 pathway based on the presence of 20:4ω-6 and absence of 20-4ω-3 (15). While most of the lipid related enzymes in *N. gaditana* appear to be encoded by single-copy genes (*e.g.* desaturases, elongases, galactolipid synthases), we found six putative Δ0-elongases that grouped in a heterokont cluster and none of them seemed to be a pseudo-gene since we could confirm their expression. We considered the most plausible substrate of these elongases to be 16:0, since elongation of 16:1 would generate 18:1Δ7 and elongation of 18:0 would generate 20:0, two FA that were not detected in glycerolipids.

The specificity of the most expressed isoform, Δ0-ELO1, was assayed in yeast heterologous system and showed an activity on palmitic acid (16:0) but not myristic acid (14:0). The presence of multiple Δ0-ELO sequences appeared initially surprising, since elongation of 16:0 into 18:0 in the ER would be theoretically redundant with the fatty acids produced by FAS II in the plastid (58). This raised our interest in these genes to investigate aspects of FAs' fate determination. If so many putative Δ0-ELO isoforms are involved in upstream reactions, could the branch point defining how a FAs are processed and in which glycerolipids they end up already lay here?

This work and the recent study on ERΔ12FAD in *N. oceanica* (59) pioneer in this question and point out that the EPA fate is determined during its synthesis by elongases and desaturases. In the logic of the EPA synthesis scheme, Δ0-ELOs and ERΔ12FAD operate in the same pathway and in case 18:0 or $18:1^{\Delta 9}$ could be provided by the plastid, one would expect little impact of a genetic modification of a *Δ0-ELO* gene. However, the phenotypes of NgΔ0-elo1-KO compared with ERΔ12FAD overexpression in *N. oceanica* (59) are not consistent with this hypothesis. On one hand, the overexpression of ERΔ12FAD led to an overall reduction of 18:1 and an increase of 18:2, consistent with an increased Δ12-desaturation. A specific modification of PC profile was also observed along with a moderate redirection of EPA and ARA from chloroplast lipids into TAG, whose abundance was marginally elevated (59). On the other hand, following *Δ0-ELO1* KO, the overall FA profile showed a slight increase of 16:0, consistent with the KO of a palmitic acid elongase, and a significant decrease in 20:5, the end product of EPA biosynthesis. The different lipid classes were little affected except for a specific disturbance of EPA and a downregulation of MGDG. This study shows therefore that a *N. gaditana* Δ0-ELO protein plays a role in defining the fate of palmitic acid for the production of EPA required for a specific lipid class (here MGDG) at the very early step of elongation/desaturation. Other Δ0-ELO isoforms could have overlapping function, as suggested in the NgΔ0-elo1-KO by the two-fold upregulation of *Δ0-ELO2*. Available expression data (31) indicated that in NgWT, the expression level of *Δ0-ELO2* was two-fold lower than that of *Δ0-ELO1* in young cultures. Therefore, it is likely that we could not reveal the full Δ0-ELO1 function due to partial compensation by Δ0-ELO2.

The import of EPA and other ω3 VLC-PUFAs from the ER to secondary plastids is unknown and has been called the "omega pathway" (1). Based on radiolabeling experiments it is considered that in the primary plastid of plants, ER-located PC serves as a precursor molecule for MGDG (60), in the so-called "eukaryotic pathway" of galactolipid synthesis (61). The nature of the precursor imported in primary plastids is not clearly identified although it is known to derive from a diacyl-glycerolipid, should it be PC itself (62) and /or lyso-PC (63, 64) and/or PC-derived PA (65) and/or PC-derived DAG (66, 67). We were unable to identify orthologs of any of the known components of the plant chloroplast lipid transporters TGD, *i.e.* TGD1-5 (68). *N. gaditana* PC is poor in EPA and enriched in C18 FA species, which does not comply with a conservation of FA-precursor import in the secondary endosymbiont following the same machinery as that known in primary plastids. One could assume that a high turnover from PC to MGDG would prevent the accumulation of similar FA profiles but our data on NgΔ0-elo1-KO revealed that MGDG reduction did not affect PC content or quality. Similarly, in *N. oceanica* ERΔ12FAD overexpression lines, the altered FA composition in PC did not induce comparable changes in the MGDG profile. It is thus unlikely that PC has a similar precursor role for galactolipids in *Nannochloropsis*.

As an alternative, EPA could be imported as a non-esterified fatty acid. We could not identify any ortholog sequence corresponding to the *Arabidopsis* FA importing system, FAX1 (69). Likewise, the homologous sequences of LACS9, a long chain acyl-CoA synthetase acting in fatty acid trafficking between plastid and cytosol in *Arabidopsis* (70) shared only 30% amino acid similarity, suggesting that the primary plastid components were not conserved in heterokonts. Unlike *Arabidopsis* and other primary endosymbionts, where chloroplasts membranes are disconnected from the ER and rely on specific chloroplast-ER binding sites for material exchanges (71), the outermost membrane of *Nannochloropsis* plastid is in continuum with the outer membrane of the nuclear envelope and the ER, what could possibly allow a transport of FA (72, 73). The present work shows that if EPA is imported *via* the "omega pathway" as a non-esterified FA, at least part of EPA directed to MGDG involves elongation/desaturation components stemming from palmitic acid elongation. NgΔ0-ELO1 would therefore be a committing entry point into the omega pathway of MGDG synthesis.

MGDG lower level in NgΔ0-elo1-KO strongly altered the thylakoid membrane morphology. In *Arabidopsis*, abnormal thylakoids are also observed when MGDG or DGDG synthesis are genetically or chemically reduced (74-76). Membrane curvature is stabilized by unequal distribution of lipids in both leaflets (77). A defined MGDG/DGDG ratio is therefore likely required to stabilize proper membrane morphology and stacking, most likely due to the physical properties of MGDG as a hexagonal II phase building (HII) lipid *versus* DGDG as a lamellar forming (L_α) lipid (49, 77, 78). Thus, the lowered MGDG/DGDG ratio in NgΔ0-elo1-KO could lead the distorted thylakoid architecture we observed.

The membrane structural phenotype in NgΔ0-elo1-KO correlated with an impairment of photosynthesis. During oxidative photosynthesis, light energy is harvested by antenna complexes containing light harvesting proteins, called VCPs in *Nannochloropsis* (56, 79). Briefly, in VCPs light is converted into excitation energy, transferred to a chlorophyll *a* dimer in PSII reaction center. A valent electron is released, accepted by plastoquinone, donated to the electron transport chain and finally to PSI, in which the reaction center receives new light energy captured by PSI antenna. Electrons are transported through the PSI complex from the luminal to the stromal side, where they are accepted by ferredoxin (Fd). Fd-$NADP^+$-oxidoreductase mediates the reduction of $NADP^+$ with electrons donated by Fd. The electron transport promotes translocation of protons, building up the proton motif force driving the ATP synthetase. NADPH and ATP are then injected in the Calvin cycle (80). While chlorophyll contents remained stable in NgΔ0-elo1-KO and energy conversion at PSII was only marginally affected, cells were affected in electron transport and more sensitive to high PAR intensity, reflected by lower energy proportions used for photochemistry and stronger induction of NPQ. When absorbed, light energy is too high to be photochemically quenched, NPQ is induced within seconds. In this photo-acclimation mechanism, photo-energy is emitted as heat and fluorescence (qE) and photo-damaged PSII reaction center protein D1 is substituted by a new translated protein in a relatively slow mechanism, during which PSII is disassembled and thus inactive (qI, photoinhibition) (81). The qE fluorescence is the major part of NPQ and involves the luminal LHCX1 in heterokonts for the activation of VDE (82).

In *Nannochloropsis*, VDE activity converts light harvesting Vx by 76% into heat emitting antheraxanthin and 24% further into Zx (53).

Our study shows that in Ng△0-elo1-KO, both LHCX1 protein level and qE dependent fluorescence were increased, whereas qI was not affected. Together with the lower ETR in the Ng△0-elo1-KO mutant, this further underlined disturbed thylakoid structures and dynamics. Notably, in contrast to higher plants, there is no anti-proportional correlation between NPQ and ETR in heterokonts (83). A similar phenotype of the ETR/NPQ couple in Ng△0-elo1-KO was observed in *Phaeodactylum* during iron starvation, a condition where PSI levels are more impaired than PSII and in which chlorophyll was degraded (84). Here, chlorophyll *a* content was stable so future studies include the assessment of the stoichiometry of PSI *versus* PSII and the contents of accessory pigments.

MGDG was found *in vitro* and *in vivo* to be beneficial for VDE action due to its HII property, solubilizing Vx and allowing VDE integration into the lipid phase (85-88). Upon qE induction, LHCs form aggregates and Vx is released, a process thought to trigger the formation of MGDG HII-phase within the bilayer, acting as a platform for VDE activity (87). Vx disassembly from LHCII complexes and diffusion into the HII phase is believed to be the rate limiting step in Vx de-epoxidation (89). Maximum conversion was observed in LHCII extractions at a MGDG/Vx ratio of 3.5-5; a higher ratio led to a decreased activity (88, 90). Interestingly, the exposure of *N. gaditana* to high light, known to induce NPQ, is also marked by a decrease of the MGDG content (6). Thus, the reduction of MGDG could be the trigger for enforced NPQ in both Ng△0-elo1-KO and high light. The molecular mechanism could lie in the physicochemical properties of MGDG: the decreased MGDG level during high light or in Ng△0-elo1-KO might increase the lipid:protein ratio, thereby limiting Zx solubilization (77). Additionally, MGDG could stabilize the antenna-PSII connection. In *Phaeodactylum*, the quenching of chlorophyll *a* by Zx in LHCs requires Zx-dependent antenna protein aggregation (91, 92). In *N. gaditana*, PSII-VCP bonds are very weak compared to other species (79). Thus, if MGDG was having a stabilizing function, a reduction could facilitate PSII-VCP disconnection, promoting the building up of the NPQ platform in aggregated antenna proteins and thereby lowering the ETR. Similar chlorophyll levels in NgΔ0-elo1-KO and NgWT is consistent with this hypothesis, since in heterokonts unlike plants, PSII antenna sizes are not responsive to light intensities (93).

Eventually, although MGDG levels are reduced at high light, gene expression of MGD is induced (6). This observation suggests that the turnover of EPA-rich MGDG is higher under NPQ inducing conditions. Evidence support a role of VLC-PUFAs as antioxidants, rather than pro-oxidants (94) and a recent study suggests that PUFA-MGDG might act as supramolecular antioxidants capturing oxygen species, limiting damages to proteins (95). It is therefore possible that MGDG molecules in the vicinity of PSII scavenge electrons, generated when the capacity of the ETR is exceeded. This process could be correlated with an increased turnover of MGDG. Thus, released free VLC-PUFAs or VLC-PUFA-MGDG might be involved in a redox stress sensing system, as part of a photoprotection mechanism during high light.

This study leads to some interesting biotechnological developments. EPA is known to be beneficial for health (96, 97). High biomass producing *Nannochloropsis* is a candidate for EPA and TAG production, but productivity has not yet reached industrial feasibility, in spite of efforts put into strain selection and culture optimization (98-104) and first metabolic engineering trials (on *N. oculata* or *salina*) (30, 105-107). The branching point at the level of palmitic acid elongation, directing the fate of the EPA end product for specific lipid classes like MGDG, should be taken into account. The function of EPA-rich MGDG in photosynthesis control should also be considered in future strain optimization strategies. This study should now be expanded to other △0-ELO isoforms.

Methods.

Sequence analyses. The nucleotide and amino acid sequences of putative elongases from *N. gaditana* were retrieved from the *Nannochloropsis* Genome Portal (http://www.nannochloropsis.org), combining ontology searches and comparisons with known elongase sequences from other organisms. Homologous sequences of representative groups of eukaryotes' biodiversity were collected from the NCBI nr databases (SI Appendix). The amino acid sequences were aligned using the MUSCLE program (17). An unrooted phylogenetic tree was constructed based on the alignment results, using the Neighbor-Joining method (18) implemented in the phylogeny.fr platform (19), with gamma correction and bootstrapped confidence intervals based on 1000 replications.

***Nannochloropsis gaditana* strains and cell culture conditions.** *N. gaditana* CCMP526 wild type (NgWT) and mutant lines were maintained in F/2 medium (20) containing modified sea salts (NaCl, 21.194 $g.L^{-1}$; Na_2SO_4, 3.55 $g.L^{-1}$; KCl, 0.599 $g.L^{-1}$; $NaHCO_3$, 0.174 $g.L^{-1}$; KBr, 0.0863 $g.L^{-1}$; H_3BO_3, 0.023 $g.L^{-1}$; NaF, 0.0028 $g.L^{-1}$; $MgCl_2.6H_2O$, 9.592 $g.L^{-1}$; $CaCl_2.2H_2O$, 1.344 $g.L^{-1}$; and $SrCl_2.6H_2O$, 0.0218 $g.L^{-1}$; $NaNO_3$, 46.67 $mg.L^{-1}$ and NaH_2PO_4, 3.094 $mg.L^{-1}$), with a light regime of either 12/12 h dark/night cycle or continuous irradiation (photon flux of 30 µmol $m^{-2}s^{-1}$ white light). All experiments were performed with at least three biological replicates, each representing an individual culture of a given strain.

Cloning of a Naga_100083g23 (△0-ELO1) into a yeast expression vector and functional characterisation in Saccharomyces cerevisiae. The codon optimized ORF encoding Naga_100083g23 (△0-ELO1) was synthesized by Life-Technologies services, France and cloned into the pYES2 vector to generate the pYES2-Ng△0ELO1 construct. The pYES2-Ng△0ELO1 vector was transformed in S. cerevisiae WT (21) and fas2 knock-out strain (22). Yeast transformation, transgene expression and analysis of fatty acid are detailed in SI Appendix.

Cloning of a Naga_100083g23 (△*0-ELO1*) knock out cassette and transformation of *N. gaditana* CCMP526. The transformation vector UEP-p35S-loxP BSD FL1-FL2 526 comprises a p35S-loxP cassette, a zeocin resistance gene (*ZEO*, CDS 3078..3448) under the control of the ubiquitin promotor and the *Phaeodactylum tricornutum* FcpA terminator. Construction of the vector, cell transformation, knock out selection and genotyping are detailed in SI Appendix.

RNA extraction and qPCR expression quantification. A 10^8-cell pellet was frozen in liquid nitrogen and stored at -80 °C until RNA extraction was performed. RNA extraction was performed using TriReagent (SIGMA) as detailed in SI Appendix. Oligonucleotides used to amplify the sequences of △*0-ELO1-6*, Δ*6-ELO*, Δ*5-ELO*, Δ*4FAD*, Δ*5FAD*, Δ*6FAD*, Δ*9FAD*, Δ*12/ω3FAD*, *DGAT2*, *LPAAT*, *MGD*, *PAP*, *PSBA*, *SAD*, *TUB, VCP*, *VDE* and *ZEP* are given in SI Appendix. *PSBA* and *TUB* served as internal loading controls and mutant quantitative cycle (Cq) values were normalized to the NgWT mRNA levels.

Glycerolipid extraction, thin layer chromatography, structural analysis by ion trap spectrometry and quantification by gas chromatography coupled to ion flame detection. Glycerolipids were extracted from 5.10^9 cells harvested from 100 mL-cultures after four days or 50 mL-cultures after seven days of growth, frozen in liquid nitrogen and lyophilized. Extraction, separation and analyses were adapted from previously described method (4, 23) and are detailed in SI Appendix. All experiments were made in triplicate.

Sphingolipid extraction and liquid chromatography coupled to tandem mass spectrometry analyses. *N. gaditana* WT and mutant cultures were harvested upon centrifugation after 7 days of cultivation (12/12 h light/dark cycle) and freeze-dried. Sphingolipids were extracted from 5 mg dry weight cells (three biological replicates per condition) according to previously described method (24) and analyses were performed as previously described (25). The detailed procedure is provided in SI Appendix.

Transmission electron microscopy. For transmission electron microscopy, cells were pelleted (4000 rpm, 15 min, 4°C), frozen in liquid nitrogen and stored at -80 °C until use. Sample fixation in reduced osmium tetroxide was adapted from previously described method (26) (SI Appendix).

Chlorophyll fluorescence kinetics measurements. To determine photosynthesis parameters in cell cultures, room temperature (RT) fast chlorophyll fluorescence kinetics were measured using a Speedzen MX fluorescence imaging system (JBeamBio) with settings previously described (27). Calculation of maximum efficiency of energy conversion at photosystem II (*Fv/Fm*), photochemical quenching capacity (Y(II)), non-photochemical quenching (NPQ) and electron transport rate (ETR) (28, 29) are detailed in SI Appendix.

Protein biochemistry. A 50 mL *N. gaditana* culture was harvested in the mid-log phase (3,500 rpm, 10 min, 4 °C), frozen in liquid nitrogen and thawed on ice to facilitate cell rupture. Protein analyses by SDS PAGE and Western blot analyses are detailed in SI Appendix.

Acknowledgements..

This work was supported by grants from Agence Nationale de la Recherche (ANR DiaDomOil), CEA (Irtelis PhD grant program), the CEA-

Fermentalg partnership, Programme Investissement d'Avenir (Océanomics) and Bpifrance (programme structurant de poles de compétitivité Trans'Alg). Authors wish to thank Olivier Clerc, Grégoire Denay, Gyozo Garab, Giovanni Finazzi, Dimitris Petroutsos, Fabrice Rébeillé and Sylvaine Roy for technical help and fruitful discussions.

1. Petroutsos D, Amiar S, Abida H, Dolch LJ, Bastien O, Rebeille F, Jouhet J, Falconet D, Block MA, McFadden GI, *et al.* (2014) *Prog Lipid Res.* **54,** 68-85.
2. Abida H, Dolch LJ, Mei C, Villanova V, Conte M, Block MA, Finazzi G, Bastien O, Tirichine L, Bowler C, *et al.* (2015) *Plant Physiol* **167,** 118-136.
3. Botte CY, Yamaryo-Botte Y, Janouskovec J, Rupasinghe T, Keeling PJ, Crellin P, Coppel RL, Marechal E, McConville MJ, & McFadden GI (2011) *J Biol Chem* **286,** 29893-29903.
4. Simionato D, Block MA, La Rocca N, Jouhet J, Marechal E, Finazzi G, & Morosinotto T (2013) *Eukaryot Cell* **12,** 665-676.
5. Meksiarun P, Spegazzini N, Matsui H, Nakajima K, Matsuda Y, & Sato H (2015) *Appl Spectrosc* **69,** 45-51.
6. Alboresi A, Perin G, Vitulo N, Diretto G, Block MA, Jouhet J, Meneghesso A, Valle G, Giuliano G, Marechal E, *et al.* (2016) *Plant Physiol*. In press
7. Bielski BH, Arudi RL, & Sutherland MW (1983) *J Biol Chem* **258,** 4759-4761.
8. Leonard AE, Pereira SL, Sprecher H, & Huang YS (2004) *Prog Lipid Res* **43,** 36-54.
9. Hamilton ML, Haslam RP, Napier JA, & Sayanova O (2014) *Metab Eng* **22,** 3-9.
10. Sayanova OV & Napier JA (2004) *Phytochem* **65,** 147-158.
11. Haslam TM & Kunst L (2013) *Plant Sci* **210,** 93-107.
12. Arao T, Sakaki T, & Yamada M (1994) *Phytochem* **36,** 629-635.
13. Cook O & Hildebrand M (2015) *J Appl Phycol* 1-9.
14. Sprecher H & Chen Q (1999) *Prostaglandins, leukotrienes, and essential fatty acids* **60,** 317-321.
15. Schneider JC, Livne A, Sukenik A, & Roessler PG (1995) *Phytochem* **40,** 807-814.
16. Altschul SF, Gish W, Miller W, Myers EW, & Lipman DJ (1990) *J Mol Biol* **215,** 403-410.
17. Edgar RC (2004) *Nucleic Acids Res* **32,** 1792-1797.
18. Saitou N & Nei M (1987) *Mol Biol Evol* **4,** 406-425.
19. Dereeper A, Guignon V, Blanc G, Audic S, Buffet S, Chevenet F, Dufayard JF, Guindon S, Lefort V, Lescot M, *et al.* (2008) *Nucleic Acids Res* **36,** W465-469.
20. Guillard RR & Ryther JH (1962) *Can J Microbiol* **8,** 229-239.
21. Thomas BJ & Rothstein R (1989) *Cell* **56,** 619-630.
22. Toke DA & Martin CE (1996) *J Biol Chem* **271,** 18413-18422.
23. Abbadi A, Domergue F, Bauer J, Napier JA, Welti R, Zahringer U, Cirpus P, & Heinz E (2004) *Plant Cell* **16,** 2734-2748.
24. Markham JE & Jaworski JG (2007) *Rapid Commun Mass Spectrom* **21,** 1304-1314.
25. Tellier F, Maia-Grondard A, Schmitz-Afonso I, & Faure JD (2014) *Phytochem* **103,** 50-58.
26. Deerinck TJ, Bushong EA, Thor A, & Ellisman MH (2010) *Microscop. Microanal.*, 1138-1139.
27. Allorent G, Courtois F, Chevalier F, & Lerbs-Mache S (2013) *Plant Mol Biol* **82,** 59-70.
28. Misra AN, Misra M, & Singh R (2012) in *Biophysics*, ed. Misra AN (InTech), pp. 171-192.
29. Schreiber U (2004) in *Chlorophyll a fluorescence: a signature of photosynthesis*, eds. Papageorgiou GC & Govindjee R (Springer, Dordrecht), pp. 279-319.
30. Radakovits R, Jinkerson RE, Fuerstenberg SI, Tae H, Settlage RE, Boore JL, & Posewitz MC (2012) *Nat Commun* **3,** 686.
31. Corteggiani Carpinelli E, Telatin A, Vitulo N, Forcato C, D'Angelo M, Schiavon R, Vezzi A, Giacometti GM, Morosinotto T, & Valle G (2014) *Mol Plant* **7,** 323-335.
32. Dolch LJ & Marechal E (2015) *Mar Drugs* **13,** 1317-1339.
33. Denic V & Weissman JS (2007) *Cell* **130,** 663-677.
34. Arao T & Yamada M (1994) *Phytochem.*, 1177-1181.
35. Tehlivets O, Scheuringer K, & Kohlwein SD (2007) *Biochim Biophys Acta* **1771,** 255-270.
36. Kihara A (2012) *J Biochem* **152,** 387-395.
37. Jung A, Hollmann M, & Schafer MA (2007) *J Cell Sci* **120,** 2924-2934.
38. Lee SH, Stephens JL, Paul KS, & Englund PT (2006) *Cell* **126,** 691-699.
39. Ramakrishnan S, Docampo MD, Macrae JI, Pujol FM, Brooks CF, van Dooren GG, Hiltunen JK, Kastaniotis AJ, McConville MJ, & Striepen B (2012) *J Biol Chem* **287,** 4957-4971.
40. Jiang M, Guo B, Wan X, Gong Y, Zhang Y, & Hu C (2014) *Mar Drugs* **12,** 1317-1334.
41. Hashimoto K, Yoshizawa AC, Okuda S, Kuma K, Goto S, & Kanehisa M (2008) *J Lipid Res* **49,** 183-191.
42. Oh CS, Toke DA, Mandala S, & Martin CE (1997) *J Biol Chem* **272,** 17376-17384.
43. Kilian O, Benemann CS, Niyogi KK, & Vick B (2011) *Proc Natl Acad Sci U S A* **108,** 21265-21269.
44. Markham JE (2013) *Methods Mol Biol* **1009,** 93-101.
45. Sperling P & Heinz E (2003) *Biochim Biophys Acta* **1632,** 1-15.
46. Li HY, Lu Y, Zheng JW, Yang WD, & Liu JS (2014) *Marine drugs* **12,** 153-166.
47. Li X, Moellering ER, Liu B, Johnny C, Fedewa M, Sears BB, Kuo MH, & Benning C (2012) *Plant Cell* **24,** 4670-4686.
48. Boudiere L, Michaud M, Petroutsos D, Rebeille F, Falconet D, Bastien O, Roy S, Finazzi G, Rolland N, Jouhet J, *et al.* (2014) *Biochim Biophys Acta* **1837,** 470-480.
49. Deme B, Cataye C, Block MA, Marechal E, & Jouhet J (2014) *FASEB J* **28,** 3373-3383.
50. Hibberd DJ & Leedale GF (1970) *Nature* **225,** 758-&.
51. Hibberd DJ (1981) *Bot J Linn Soc* **82,** 93-119.
52. Schwarz DS & Blower MD (2016) *Cell Mol Life Sci* **73,** 79-94.
53. Gentile MP & Blanch HW (2001) *Biotechnol Bioeng* **75,** 1-12.
54. Eberhard S, Finazzi G, & Wollman FA (2008) *Annu Rev Genet* **42,** 463-515.
55. Bailleul B, Rogato A, de Martino A, Coesel S, Cardol P, Bowler C, Falciatore A, & Finazzi G (2010) *Proc Natl Acad Sci U S A* **107,** 18214-18219.
56. Carbonera D, Agostini A, Di Valentin M, Gerotto C, Basso S, Giacometti GM, & Morosinotto T (2014) *Biochim Biophys Acta* **1837,** 1235-1246.
57. Li Z, Wakao S, Fischer BB, & Niyogi KK (2009) *Annu Rev Plant Biol* **60,** 239-260.
58. Li-Beisson Y, Shorrosh B, Beisson F, Andersson MX, Arondel V, Bates PD, Baud S, Bird D, Debono A, Durrett TP, *et al.* (2010) in *The Arabidopsis Book*, p. e0133.
59. Kaye Y, Grundman O, Leu S, Zarka A, Zorin B, Didi-Cohen S, Khozin-Goldberg I, & Boussiba S (2015) *Algal Res* **11,** 387-398.
60. Roughan PG, Holland R, & Slack CR (1980) *Biochem J* **188,** 17-24.
61. Heinz E (1977) in *Lipids and Lipid polymers*, eds. Tevini M & Lichtenthaler HK (Springer-Verlag, Berlin), pp. 102-120.
62. Miquel M, Block MA, Joyard J, Dorne AJ, Dubacq JP, Kader JC, & Douce R (1988) *Biochim Biophys Acta* **937,** 219-228.
63. Mongrand S, Cassagne C, & Bessoule JJ (2000) *Plant Physiol* **122,** 845-852.
64. Botella C, Sautron E, Boudiere L, Michaud M, Dubots E, Yamaryo-Botte Y, Albrieux C, Marechal E, Block MA, & Jouhet J (2016) *Plant Physiol* **170,** 1300-1314.
65. Benning C (2009) *Annu Rev Cell Dev Biol* **25,** 71-91.
66. Nakamura Y, Koizumi R, Shui G, Shimojima M, Wenk MR, Ito T, & Ohta H (2009) *Proc Natl Acad Sci U S A* **106,** 20978-20983.
67. Marechal E & Bastien O (2014) *J Theor Biol* **361,** 1-13.
68. Fan J, Zhai Z, Yan C, & Xu C (2015) *Plant Cell* **27,** 2941-2955.
69. Li N, Gugel IL, Giavalisco P, Zeisler V, Schreiber L, Soll J, & Philippar K (2015) *PLoS Biol* **13,** e1002053.
70. Jessen D, Roth C, Wiermer M, & Fulda M (2015) *Plant Physiol* **167,** 351-366.
71. Block MA & Jouhet J (2015) *Curr Opin Cell Biol* **35,** 21-29.
72. Watson ML (1955) *J Biophys Biochem Cytol* **1,** 257-270.
73. Falciatore A & Bowler C (2002) *Annu Rev Plant Biol* **53,** 109-130.
74. Kobayashi K, Kondo M, Fukuda H, Nishimura M, & Ohta H (2007) *Proc Natl Acad Sci U S A* **104,** 17216-17221.
75. Botte CY, Deligny M, Roccia A, Bonneau AL, Saidani N, Hardre H, Aci S, Yamaryo-Botte Y, Jouhet J, Dubots E, *et al.* (2011) *Nat Chem Biol* **7,** 834-842.
76. Dormann P, Hoffmannbenning S, Balbo I, & Benning C (1995) *Plant Cell* **7,** 1801-1810.
77. Garab G, Lohner K, Laggner P, & Farkas T (2000) *Trends Plant Sci* **5,** 489-494.
78. Jouhet J (2013) *Front Plant Sci* **4,** 494.
79. Basso S, Simionato D, Gerotto C, Segalla A, Giacometti GM, & Morosinotto T (2014) *Biochim Biophys Acta* **1837,** 306-314.
80. Lemeille S & Rochaix JD (2010) *Photosynth Res* **106,** 33-46.
81. Kanervo E, Suorsa M, & Aro EM (2005) *Photochem Photobiol Sci* **4,** 1072-1080.
82. Lepetit B, Sturm S, Rogato A, Gruber A, Sachse M, Falciatore A, Kroth PG, & Lavaud J (2013) *Plant Physiol* **161,** 853-865.
83. Nymark M, Valle KC, Brembu T, Hancke K, Winge P, Andresen K, Johnsen G, & Bones AM (2009) *PLoS One* **4,** e7743.
84. Allen AE, Laroche J, Maheswari U, Lommer M, Schauer N, Lopez PJ, Finazzi G, Fernie AR, & Bowler C (2008) *Proc Natl Acad Sci U S A* **105,** 10438-10443.
85. Goss R, Lohr M, Latowski D, Grzyb J, Vieler A, Wilhelm C, & Strzalka K (2005) *Biochem* **44,** 4028-4036.
86. Goss R & Jakob T (2010) *Photosynth Res* **106,** 103-122.
87. Jahns P, Latowski D, & Strzalka K (2009) *Biochim Biophys Acta* **1787,** 3-14.
88. Schaller S, Latowski D, Jemiola-Rzeminska M, Wilhelm C, Strzalka K, & Goss R (2010) *Biochim Biophys Acta* **1797,** 414-424.
89. Latowski D, Burda K, & Strzalka K (2000) *J Theor Biol* **206,** 507-514.
90. Schaller S, Latowski D, Jemiola-Rzeminska M, Dawood A, Wilhelm C, Strzalka K, & Goss R (2011) *Biochim Biophys Acta* **1807,** 326-335.
91. Lepetit B, Goss R, Jakob T, & Wilhelm C (2012) *Photosynth Res* **111,** 245-257.
92. Valle KC, Nymark M, Aamot I, Hancke K, Winge P, Andresen K, Johnsen G, Brembu T, & Bones AM (2014) *PLoS One* **9,** e114211.
93. Simionato D, Sforza E, Corteggiani Carpinelli E, Bertucco A, Giacometti GM, & Morosinotto T (2011) *Bioresour Technol* **102,** 6026-6032.
94. Richard D, Kefi K, Barbe U, Bausero P, & Visioli F (2008) *Pharmacol Res* **57,** 451-455.
95. Schmid-Siegert E, Stepushenko O, Glauser G, & Farmer EE (2016) *J Biol Chem* **291,** 13005-13013.
96. Wen ZY & Chen F (2003) *Biotechnol Adv* **21,** 273-294.
97. Ji XJ, Ren LJ, & Huang H (2015) *Front Bioeng Biotechnol* **3,** 158.
98. Meng Y, Jiang J, Wang H, Cao X, Xue S, Yang Q, & Wang W (2015) *Bioresour Technol* **179,** 483-489.
99. Camacho-Rodriguez J, Ceron-Garcia MC, Fernandez-Sevilla JM, & Molina-Grima E (2015) *Bioresour Technol* **177,** 102-109.
100. Camacho-Rodriguez J, Ceron-Garcia MC, Gonzalez-Lopez CV, Fernandez-Sevilla JM, Contreras-Gomez A, & Molina-Grima E (2013) *Bioresour Technol* **144,** 57-66.
101. Camacho-Rodriguez J, Gonzalez-Cespedes AM, Ceron-Garcia MC, Fernandez-Sevilla JM, Acien-Fernandez FG, & Molina-Grima E (2014) *Appl Microbiol Biotechnol* **98,** 2429-2440.
102. Ma Y, Wang Z, Yu C, Yin Y, & Zhou G (2014) *Bioresour Technol* **167,** 503-509.
103. Chen CY, Chen YC, Huang HC, Huang CC, Lee WL, & Chang JS (2013) *Bioresour Technol* **147,** 160-167.
104. Van Vooren G, Le Grand F, Legrand J, Cuine S, Peltier G, & Pruvost J (2012) *Bioresour Technol* **124,** 421-432.
105. Iwai M, Hori K, Sasaki-Sekimoto Y, Shimojima M, & Ohta H (2015) *Front Microbiol* **6,** 912.
106. Kang NK, Jeon S, Kwon S, Koh HG, Shin SE, Lee B, Choi GG, Yang JW, Jeong BR, & Chang YK (2015) *Biotechnol Biofuels* **8,** 200.
107. Vieler A, Wu G, Tsai CH, Bullard B, Cornish AJ, Harvey C, Reca IB, Thornburg C, Achawanantakun R, Buehl CJ, *et al.* (2012) *PLoS Genet* **8,** e1003064.

Please review all the figures in this paginated PDF and check if the figure size is appropriate to allow reading of the text in the figure.

If readability needs to be improved then resize the figure again in 'Figure sizing' interface of Article Sizing Tool.

Supplementary Methods.

Sequence analyses.

Homologous sequences of representative groups were collected from the NCBI nr database. Selected sequences cover the biodiversity of eukaryotes including Opisthokonts, e.g. Fungi (*Saccharomyces* ELO1, NP_012339; ELO2, NP_009963; ELO3, NP_013476) and Metazoa (*Drosophila* Baldspot, XP_005187861; *Musca* Baldspot-Like, XP_005187861; *Apis* Baldspot-Like, XP_003251850; *Bombus* Baldspot-Like, XP_003401825; *Caenorhabditis* ELO3, NP_001255291; *Homo* ELOVL1, XP_002040; ELOVL2, NP_060240; ELOVL3, NP_689523; ELOVL4, NP_073563; ELOVL5, NP_068586; ELOVL6, NP_569717; ELOVL7, NP_079206; *Mus* ELOVL6, NP_569717; *Gallus* ELO6; NP_001026710), Heterokonts (*Phaeodactylum* putative Δ0-ELO/ELO3, XP_002184740; Δ6-ELO/ELO6, XP_002180428; Δ5-ELO/ELO5, XP_002176686; Δ5b-ELO/ELO5b, XP_002179048; *Thalassiosira* Δ0-ELO/ELO3; XP_002293395; Δ6-ELO/ELO1, XP_002288481; Δ5-ELO/ELO2, XP_002291938; *Ectocarpus* ELO, CBN78890; *Phytophthora* ELO, ETM45813; *Albugo* ELO, CCI42963; *Saprolegnia* ELO, XP_008620377; *Aphanomyces* ELO, XP_008865117), Apicomplexa (*Toxoplasma* ELOA, TGME49_053880; ELOB TGME49_242380; ELOC TGME49_205350; *Neospora* ELOC-Like, XP_003882280; *Eimeria* ELOC-Like, CDJ36988; *Cryptosporidium* ELOC-Like, AAO34582; *Plasmodium* ELOC-Like, XP_001351023; *Gregarina*, ELOC-Like XP_011131654), Haptophytes (Emiliania ELO2-Like, XP_005769239), Cryptomonads (Guillardia ELO, XP_005838572) and Kinetoplastida (*Trypanosoma* ELO1, Tb927.7.4180; ELO2, Tb927.7.4170; ELO3, Tb927.7.4160; ELO4, Tb927.5.4530; *Leishmania* ELO2, LbrM.14.0670). The amino

acid sequences were aligned using the MUSCLE program (1). An unrooted phylogenetic tree was constructed based on the alignment results, using the Neighbor-Joining method (2) implemented in the phylogeny.fr platform (3), with gamma correction and bootstrapped confidence intervals based on 1000 replications.

***Nannochloropsis gaditana* strains and cell culture conditions.**

N. gaditana CCMP526 wild type (NgWT) and mutant lines were maintained in F/2 medium (4) containing modified sea salts (NaCl, 21.194 $g.L^{-1}$; Na_2SO_4, 3.55 $g.L^{-1}$; KCl, 0.599 $g.L^{-1}$; $NaHCO_3$, 0.174 $g.L^{-1}$; KBr, 0.0863 $g.L^{-1}$; H_3BO_3, 0.023 $g.L^{-1}$; NaF, 0.0028 $g.L^{-1}$; $MgCl_2.6H_2O$, 9.592 $g.L^{-1}$; $CaCl_2.2H_2O$, 1.344 $g.L^{-1}$; and $SrCl_2.6H_2O$, 0.0218 $g.L^{-1}$; $NaNO_3$, 46.67 $mg.L^{-1}$ and NaH_2PO_4, 3.094 $mg.L^{-1}$), under gentle agitation (Infors incubator, 100 rpm) at 20 °C, and with a light regime of either 12/12 h dark/night cycle or continuous irradiation (photon flux of 30 µmol $m^{-2}s^{-1}$ white light). Cultures of 50-100 mL were grown in 250 mL Erlenmeyer flasks, and 2 mL cultures on 24-well culture plates (Thermo Fisher), inoculated with a cell density of 20^6 $cells.mL^{-1}$. For long time storage at -80 °C, 10^7 cells were frozen stepwise (30 min at 4 °C, 60 min at -20 °C) in 15% dimethyl sulfoxide (DMSO, SIGMA). Cell densities were measured by the absorbance at 730 nm of a 300 µL culture aliquot in a transparent 96 well plate (Thermo Fisher), using a TECAN infinite M1000Pro plate reader. All experiments were performed with at least three biological replicates, each representing an individual culture of a given strain.

Cloning of a Naga_100083g23 (Δ0-ELO1) into a yeast expression vector and functional characterisation in *S. cerevisiae*.

The ORF encoding Naga_100083g23 (Δ0-ELO1) was codon optimized and synthesized by Life-Technologies services, France. With the help of the added restriction sites *EcoR*I and *Xba*I, the yeast optimized sequence was cloned into cut pYES2 vector to generate the pYES2-NgΔ0ELO1 construct. The pYES2-NgΔ0ELO1 vector was transformed in *Saccharomyces cerevisiae* WT (W303-1A: MATα, ade2-1, his3-11,15, leu2-3,112, trp1-1, ura3-1 and can1-100) (5) and fas2Δ knock-out strain (DTY-10a2: MATα, fas2Δ::LEU2, can1-100, ura3-1, ade2-1 and his3-11,his3-15) (6) using a lithium acetate based method (7) and transformed clones selected on SD-URA (MP Biochemicals). Expression of the transgene was induced in liquid cultured by addition of 2% (w/v) galactose in the presence or in the absence of exogenously supplied fatty acid substrates as described previously (8). Total fatty acids extracted from yeast cultures were analysed by gas chromatography of methyl ester derivatives. Lipids were extracted and trans-methylated with methanolic HCl and the resulting fatty acid methyl esters (FAMEs) were separated using either a DB-23 (15 m, 0.25 mm, 0.25 μm; Agilent J&W) or a HP-1MS (HP-1MS Ultra Inert 30 m, 0.32 mm, 0.25 μm; Agilent) columns coupled to either a flame ionisation detector or a mass spectrometer.

Cloning of a Naga_100083g23 (*Δ0-ELO1*) knock out cassette and transformation of *N. gaditana* CCMP526

The transformation vector UEP-p35S-loxP BSD FL1-FL2 526 comprises a p35S-loxP cassette, a zeocin resistance gene (*ZEO*, CDS 3078..3448) under the control of the ubiquitin promotor and the *Phaeodactylum tricornutum* FcpA terminator. The two

flanking regions up- and downstream of the zeocin resistance gene were substituted by homologous sequences of *N. gaditana* genomic DNA (gDNA), surrounding the coding sequence of Naga_100083g23 (*Δ0-ELO1*) to induce homologous recombination after nuclear transformation (9). Respective gDNA fragments were amplified by PCR using the oligonucleotide pair 5'-gttgggaataatgcgggacc-3' and 5'-ccgctttggtttcacagtca-3' for the terminal flank, and 5'-acgatgggtatgttgcttgc-3' and 5'-tgtacagggcggatttcact-3' for the upstream flank. Flanks were inserted into the PCR BLUNT vector (Invitrogen) and subcloned into the UEP-P35S-loxP vector using the restriction enzyme activity of *BamH*I/*Sac*I for the downstream flank and *Kpn*I/*EcoR*I (NEB) for the upstream flank. Nuclear transformation was performed as described earlier (9) with the following modifications: 10^8 NgWT cells were harvested during exponential growth at a concentration of 3.10^6 cells.mL^{-1}, washed two times with 375 mM D-sorbitol and resuspended in 100 µL final volume. The recombination cassette was digested from the vector (*Sac*I/*Kpn*I) and 1 µg of the digestion product was applied to the cell suspension and mixed gently. After 15 min of incubation on ice, cells were single-pulse electroporated at 500 Ω and 50 µF capacitance (NEPA21 Type II, Sonidel Limited) with 2400 V, (MicroPulser, BioRad). The transformation mix was transferred to 5 mL fresh F/2 medium in a 50 mL Falcon tube and incubated for 16 hours under continuous light irradiation. Cells were then plated on 1.5% F/2 agar plates containing 7 µg.mL^{-1} zeocin and colonies were obtained after 3-4 weeks of incubation with continuous irradiation.

Genotyping of Naga_100083g23 knock out mutants

PCR-genotyping was carried out on a part of transformed *N. gaditana* colonies re-suspended in 10 µL distilled water transferred to a tube with 90 µL water. Cells were

thermo-lysed (95°C, 5 min) and 1 µL was used in PCR analyses. Knock out (KO) lines were assessed based on the presence of the flanking sequences (primers detailed above) and the zeocin resistance gene (oligonucleotide pair binding in promotor: 5'-gaggaatgtgtgtggttggg-3', and terminator: 5'-gccgtattgttggagtggac-3'), and on the absence of the Naga_100083g23 (*Δ0-ELO1*) sequence, (5'-gacacttctctgcctttgcc-3' and 5'-atggtggtaccagtggagga-3'). The number of cassettes inserted into the *N. gaditana* genome in three independent clones was verified by qPCR on gDNA extracted from thermo-mechanically broken pellets of 10^8 cells using the chloroform-phenol method (Pacific Biosciences of California, Inc, 2012). Genomic DNA (gDNA, 25 ng per reaction) was mixed in SYBR Green qPCR (Agilent) reagent, with 1.2 nM oligonucleotides annealing with tubulin alpha (*TUB*) (10) as loading control, *PAP* (Naga_100038g41) as a single copy gene control, and *ZEO* and *Δ0-ELO1* as genes of interest. After 10 min of initial denaturation, 40 thermo-cycles were performed at 95 °C, then 55°C and 72 °C, each temperature being held for 30 seconds. We sought strains in which *Δ0-ELO1* was not amplified and in which the detection value of *ZEO* equaled that of the single *PAP* gene, corrected to the primer efficiencies, thus revealing a single gene insertion. Primer efficiencies were calculated from the linear regression of a dilution series of the same DNA sample. The qPCR primers were the following, given in the 5'-3' orientation (F, forward; R, reverse): Naga_100083g23F, gtgggcaccaaggttatgga; Naga_100083g23R, gaaggaggtgtggtacggtg; *PAP*F, aagtggtacctttgctccgt; *PAP*R, aaggtagccgagtagccaaa; *TUB*F, ttgagcataccgacgtgact, *TUB*R, gcgatgagcctgttcagatt; *ZEO*F, tgtgccaaaatcatacagcagg; *ZEO*R, cgaagtcgtcctccacgaag.

RNA extraction and qPCR expression quantification.

A 10^8-cell pellet was frozen in liquid nitrogen and stored at -80 °C until RNA extraction was performed. A volume of 1 mL TriReagent (SIGMA) was added to the frozen pellet, transferred to a 1.5 mL tube and mixed vigorously for 30 sec (vortex). Then, 200 µL chloroform (SIGMA) was added and the tube inverted several times during an incubation of 15 min at room temperature. Samples were centrifuged (15 min at full speed at 4°C) and the upper phase transferred to a new tube. RNA was precipitated using 1 mL 100% isopropanol (SIGMA) after 10 min incubation at room temperature and collected by a 30 min-centrifugation (full speed, 4°C). The pellet was washed with 75% ice-cold ethanol and dried in a heat block at 60°C. RNA was suspended in 30 µL diethylpyrocarbonate-treated water (Roth), precipitated *via* the addition of 1 volume of NH_4^+-acetate, 5 M and 3 volumes of 100% ethanol and collected by centrifugation (15 min at full speed at 4°C). Washing, drying and resuspension were repeated following the same procedure and RNA quantity was estimated by the absorbance at 280 nm, 260 nm and 230 nm using a NanoDrop reader. RNA integrity was verified on a 2% agarose ethidium bromide gel. Complementary DNA (cDNA) was generated from 1 µg RNA using the QuantiTect Reverse transcription kit (QIAGEN) and 15-20 ng/reaction were used for qPCR to test differential gene expression using the following oligonucleotides, given in the 5'-3' orientation (F, forward; R, reverse): *DGAT2*F, tggtggtgatcctctccctt; *DGAT2*R, attgcaaaacgcgtcccatc; Δ*0-ELO2*F (Naga_100162g5), ggcccaataggaggcatgtt; Δ*0-ELO2*R (Naga_100162g5), cacaccacacctctccactc; Δ*0-ELO3*F (Naga_100162g4), gcacagccccctactacatc; Δ*0-ELO3*R (Naga_100162g4), ggcctacgtcccttcaaaca; Δ*0-ELO4*F (Naga_100004g102), tgtcgtcccccaccttatct; Δ*0-ELO4*R (Naga_100004g102), gcgagcttggagaggatgaa; Δ*0-ELO5*F (Naga_100017g49), gcaagtattcgcgtcggttc; Δ*0-ELO5*R

(Naga_100017g49), tggaatcaacggtacgcctc; Δ*0-ELO6*F (Naga_100399g1), cctcttcacgcacaaggact; Δ*0-ELO6*R (Naga_100399g1), caggaccaggattaccgtgt; Δ*6-ELO*F (Naga_100003g8), tttttgacgatgaacgcgca; Δ*6-ELO*R (Naga_100003g8), agaggacgagaagcgagaga; Δ*5-ELO*F (Naga_100020g80), agagagcttgcatatcgccc; Δ*5-ELO*R (Naga_100020g80), ccgcacgtaagaacgaggta; Δ*4FAD*F (Naga_100042g12), aggtcccaccgtacttctca; Δ*4FAD*R (Naga_100042g12), gccaaaatgtcgggcgatac; Δ*5FAD*F (Naga_100273g7), cttggcctctttcgtggtct; Δ*5FAD*R (Naga_100273g7), tgcatgacgtgcaacaaagg; Δ*6FAD*F (Naga_100061g21), catctttgcagccttccacc; Δ*6FAD*R (Naga_100061g21), caagtctcgatacgctcgct; Δ*9FAD*F (Naga_100027g27), gtactcggagacagatgcgg; Δ*9FAD*R (Naga_100027g27), aaatccaactgtttgccgcc, Δ*12/ω3FAD*F (Naga_100092g4), gccccatatggcgacattct; Δ*12/ω3FAD*R (Naga_100092g4), aggtggaagaaggaggtggt; *LPAAT*F, ccttcggagcatggcttctt; *LPAAT*R, catccagtctagccgtgtcc; *MGD*F, ccggacaggaagaagggaac; *MGD*R, ctcatcttctcccgcacctc; *PSBA*F, acccaatcggacaaggtagc; *PSBA*R, ccaaacacaccagcaacacc; *SAD*F, cttgaacagagacccggagg; *SAD*R, aagtgctcgaacaggtctgg, *VCP*F, catgcttgccatgctccac; *VCP*R, cggaggtgatggcgttgat; *VDE*F ,agggcaagtggtacatcagc; *VDE*R, gatgcgccagttcagctttc; *ZEP*F, gccagatgcattcggagagt; *ZEP*R, agaccttgtaggccacctct. Quantitative real time PCR was performed using 20 ng cDNA in a BioRad CFX96 qPCR machine and relative expression levels were calculated using the ΔΔCq method provided with the BioRad CFX software. *PSBA* and *TUB* served as internal loading controls and mutant quantitative cycle (Cq) values were normalized to the NgWT mRNA levels.

Glycerolipid extraction, thin layer chromatography separation, structural analysis by ion trap spectrometry and quantification by gas chromatography coupled to ion flame detection

Glycerolipids were extracted from 5.10^9 cells harvested from 100 mL-cultures after four days or 50 mL-cultures after seven days of growth, frozen in liquid nitrogen and lyophilized. Extraction, separation and analyses were adapted from previously described method (11). Cell pellets were suspended in 4 mL of boiling ethanol for 5 min, during which they were mechanically broken. Then, 2 mL methanol and 8 mL chloroform were added at room temperature, saturated with argon, and the mix was incubated for one hour. Cell debris were removed by filtrating the mixture through glass wool and the filter was rinsed with 3 mL chloroform/methanol 2:1, v/v. A volume of 5 mL NaCl 1% was added to the filtrate to induce separation of the organic and the solvent phase. The later was recovered and dried under argon for storage purposes and suspended in chloroform to take aliquots. A 1/100 aliquot of the lipid extract was taken for fatty acid quantification by gas chromatography coupled to ion flame detection (GC-FID). To this end, a known quantity of 15:0 FAs was added to each sample and lipids were methanolyzed into fatty acid methyl esters (FAMEs) for one hour in 3 mL H_2SO_4 2.5% in pure methanol, at 100°C. The reaction was stopped by addition of 3 mL water, and phase separation was induced with 3 mL hexane. The hexane phase was collected and concentrated upon drying prior injection into the GC-FID system (Perkin Elmer). FAMEs were separated on a BPX70 (SGE) GC column and their peaks identified by comparison of their retention times with those of standards (Sigma). Quantifications were based on the elution peak of the 15:0 reference by normalization of the peak areas

and correction to respective molecular masses. Separation of lipid classes was performed using 300 µg of total lipid extracts. For polar and neutral glycerolipids two distinct resolving systems of thin layer chromatography (TLC) on glass-backed silica gel plates (Merck) were used, adapted from (11). For the resolution of neutral lipids and free fatty acids (FFA) one dimensional TLC is sufficient using hexane:diethylether:acetic acid (70:30:1, v/v) as solvent. Adequate separation of polar lipids was achieved by two-dimensional TLC with chloroform:methanol:water (65:25:4, v/v) as first solvent and (chloroform:acetone:methanol:acetic acid:water at 50:20:10:20:5, vol/vol) as second solvent. Lipid spots were sprayed with 2% 8-anilino-1-naphthalenesulfonic acid in methanol for UV visualization, and silica containing the different lipids were scraped off the plate for FAME production or GC-FID analyses of the different lipid classes or for structural analysis by mass spectrometry (MS). For MS analyses, purified lipid classes were dissolved in 10 mM ammonium acetate in pure methanol. They were introduced by direct infusion (ESI-MS) into a trap type mass spectrometer (LTQ-XL, Thermo Scientific) and identified by comparison with standards as described previously (12). In these conditions, the produced ions were mainly present as H^-, H^+, $NH4^+$ or Na^+ adducts. Lipids were identified by MS/MS analysis with their precursor ion or by neutral loss analyses as described previously (12). All experiments were made in triplicate.

Sphingolipid extraction and liquid chromatography coupled to tandem mass spectrometry (UPLC-ESI-MS/MS) analyses

N. gaditana WT and mutant cultures were harvested upon centrifugation after 7 days of cultivation (12/12 h light/dark cycle) and freeze-dried. Sphingolipids were extracted from 5 mg dry weight cells (three biological replicates per condition) according to

previously described method (13). A volume of 500 µL isopropanol-hexane-water (55:20:25) and 10 µL (0.01 nmol) of internal standard [C12-Cer: N-(dodecanoyl)-sphing-4-enine (d18:1-12:0)] were added to freeze-dried material and grinded using a Polytron homogenizer. The plunger was rinsed with 500 µL of extraction solvent and the sample incubated at 60°C for 15 min. After centrifugation at 4,000 rpm for 5 min at room temperature, the supernatant was recovered and the pellet extracted once more with 1 mL of solvent. Supernatants were combined and dried using a speed Vac (Eppendorf) system. Then, the samples were incubated at 50°C for 1 h with 500 µL of 33% methylamine solution in ethanol-water (7:3). Samples were dried under nitrogen and resuspended by sonication in 100 µL of THF-methanol-water (2:1:2) containing 0.1 % formic acid and filtrated prior to analysis. UPLC-ESI-MS/MS analyses were carried out on a Waters Acquity UPLC system coupled to a Waters Xevo tandem quadrupole mass spectrometer (Manchester, UK) equipped with an electro spray ionization (ESI) source. Chromatographic conditions, mass spectrometric parameters and MRM methods were defined as described previously (14).

Transmission electron microscopy.

Cells were pelleted (4000 rpm, 15 min, 4°C), frozen in liquid nitrogen and stored at -80 °C until use. Cell pellets were resuspendend in 0.1 M phosphate buffer (pH 7.4), 2.5% glutaraldehyde and incubated overnight at 4°C in inverted tubes. Cells were then pelleted and washed five times in 0.1 M phosphate buffer. Cells were fixed by a 1-hour incubation on ice in 500 µl 0.1 M phosphate buffer containing 1% osmium and 1.5% ferricyanide potassium red before they were pelleted and washed five times with 0.1 M phosphate buffer. Pellets were resuspended in 0.1 M phosphate buffer containing 0.1%

tannic acid and incubated for 30 min in the dark at room temperature prior to centrifugation at 10 000 x g for 10 min at 30 °C. Again, cells were pelleted and washed five times with 0.1 M phosphate buffer. The samples were dehydrated in ascending sequences of ethanol and infiltrated with ethanol/Epon resin mixture. Finally the algal strains were embedded in Epon. Ultrathin sections (50-70 nm) were prepared with a diamond knife on a UC6 Leica ultramicrotome (Leica, Solms, Germany) and collected on 200 µm nickel grids. Ultrathin sections were examined on a Philips CM120 transmission electron microscope operating at 80 kV.

Chlorophyll fluorescence kinetics measurements

Fast chlorophyll fluorescence kinetics were measured using a Speedzen MX fluorescence imaging system (JBeamBio) (15). To this end, a 140 µL or 300 µL volume of *N. gaditana* culture was transferred to a transparent 96 well-plate and dark-incubated for 20-30 min before measurements. Excitation was performed in the blue range (λ = 450 nm, *F0*) and actinic light pulses were given with a photosynthetic active wavelength of 520 nm. *F0* is the steady state fluorescence in dark-adapted cultures, *F* in light-adapted cultures; *Fm* is the maximal fluorescence after a saturating light pulse of dark-adapted cultures, *Fm'* the same in light adapted cultures, *Fv* is the difference between *F0* and *Fm*. With these parameters, the maximum efficiency of energy conversion at photosystem II (PSII) can be calculated as *Fv/Fm*, photochemical quenching capacity indicated by the quantum yield of PSII as Y(II) = (*Fm'-F*)*/Fm'* and non-photochemical quenching (NPQ) as *Fm-Fm'/Fm'* (16). Based on Y(II), the electron transport rate (ETR) was calculated as ETR = 0.5 x Y(II) x (photon flux density, µE) x 0.84, the latter

term being a constant optimized for *Arabidopsis* that might differ for *Nannochloropsis* (17).

Protein biochemistry

A 50 mL *N. gaditana* culture was harvested in the mid-log phase (3,500 rpm, 10 min, 4 °C), frozen in liquid nitrogen and thawed on ice to facilitate cell rupture. Proteins were extracted from the cell pellet by adjusting the medium to a final concentration of 6 mM CHAPS, 1 mM DTT, 50 mM MOPS pH 7.8 KOH and incubation for 20 min on ice. Protein concentrations were determined (18) and protein samples (30 µg) were analyzed by SDS PAGE (19). Protein bands were visualized by staining with Coomassie Brilliant Blue (Roth). Alternatively, proteins were transferred to a nitrocellulose membrane (Protran BA83, GE Healthcare) *via* Western blotting. The nitrocellulose membrane was blocked with 5% skimmed dry milk in a Tris buffer (10 $mmol.L^{-1}$ Tris, 100 $mmol.L^{-1}$ NaCl, pH 7.5) containing 0.05% Tween-20, overnight at 4°C under gentle agitation. A 1:80,000 dilution of an anti-LHCX1 antibody was added to buffered milk and the nitrocellulose membrane was incubated overnight as described above. Subsequently, the membrane was washed three times with a fresh buffered milk medium prior to the addition of an anti-rabbit antibody (1:10,000; Peroxidase-conjugated AffiniPure Goat Anti-Rabbit IgH, Jackson Immunoresearch). After a 2-hour incubation at room temperature, antibody-labeled protein bands were visualized using a BioRad Chemidoc MP system. Intensities were quantified relatively to the Coomassie-stained loading control, in the non-saturated range, using the Adobe Photoshop software.

References for Supplementary Methods

1. Edgar RC (2004) *Nucleic Acids Res* **32,** 1792-1797.
2. Saitou N & Nei M (1987) *Mol Biol Evol* **4,** 406-425.

3. Dereeper A, Guignon V, Blanc G, Audic S, Buffet S, Chevenet F, Dufayard JF, Guindon S, Lefort V, Lescot M*, et al.* (2008) *Nucleic Acids Res* **36,** W465-469.
4. Guillard RR & Ryther JH (1962) *Canadian journal of microbiology* **8,** 229-239.
5. Thomas BJ & Rothstein R (1989) *Cell* **56,** 619-630.
6. Toke DA & Martin CE (1996) *J Biol Chem* **271,** 18413-18422.
7. Elble R (1992) *Biotechniques* **13,** 18-20.
8. Beaudoin F, Michaelson LV, Hey SJ, Lewis MJ, Shewry PR, Sayanova O, & Napier JA (2000) *Proc Natl Acad Sci U S A* **97,** 6421-6426.
9. Kilian O, Benemann CS, Niyogi KK, & Vick B (2011) *Proc Natl Acad Sci U S A* **108,** 21265-21269.
10. Cao S, Zhang X, Ye N, Fan X, Mou S, Xu D, Liang C, Wang Y, & Wang W (2012) *Biochem Biophys Res Commun* **424,** 118-123.
11. Simionato D, Block MA, La Rocca N, Jouhet J, Marechal E, Finazzi G, & Morosinotto T (2013) *Eukaryot Cell* **12,** 665-676.
12. Abida H, Dolch LJ, Mei C, Villanova V, Conte M, Block MA, Finazzi G, Bastien O, Tirichine L, Bowler C*, et al.* (2015) *Plant Physiol* **167,** 118-136.
13. Markham JE & Jaworski JG (2007) *Rapid Commun Mass Spectrom* **21,** 1304-1314.
14. Tellier F, Maia-Grondard A, Schmitz-Afonso I, & Faure JD (2014) *Phytochemistry* **103,** 50-58.
15. Allorent G, Courtois F, Chevalier F, & Lerbs-Mache S (2013) *Plant Mol Biol* **82,** 59-70.
16. Misra AN, Misra M, & Singh R (2012) in *Biophysics*, ed. Misra AN (InTech), pp. 171-192.
17. Schreiber U (2004) in *Chlorophyll a fluorescence: a signature of photosynthesis*, eds. Papageorgiou GC & Govindjee R (Springer, Dordrecht), pp. 279-319.
18. Lowry OH, Rosebrough NJ, Farr AL, & Randall RJ (1951) *J Biol Chem* **193,** 265-275.
19. Laemmli UK (1970) *Nature* **227,** 680-685.

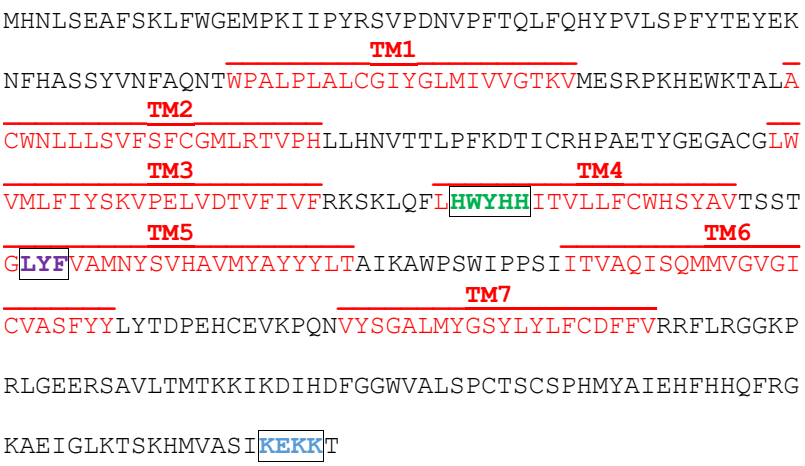

Figure S1: Amino acid sequence motifs in the elongase NgΔ0-ELO1 (Naga_100083g23). Sequence features characteristic for elongase enzymes were identified manually according to (1) and (2). A HxxH motif in a R- and K- rich environment is essential for yeast 3-ketoacyl-CoA synthase activity and is conserved in NgΔ0-ELO1 (boxed, green letters, (1)). More precisely, HxxHH indicates elongation of saturated or monounsaturated fatty acids. Accordingly, the LYF motif (boxed, violet letters) is present in the yeast Fen1p superfamily of elongases accepting saturated or monounsaturated fatty acids with an acyl chain of 18-24 carbon atoms as substrate (2). An ER retention of the protein is likely due to an enrichment of K in the C-terminus (3). Seven transmembrane domains (TM, red) were predicted using the TMHMM Server v. 2.0 (www.cbs.dtu.dk/services/TMHMM). Reference: (1) Denic V & Weissman JS (2007) *Cell* **130,** 663-677; (2) Hashimoto K, Yoshizawa AC, Okuda S, Kuma K, Goto S, & Kanehisa M (2008) *J Lipid Res* **49,** 183-191. (3) Jackson MR, Nilsson T, & Peterson PA (1990) *EMBO J* **9,** 3153-3162.

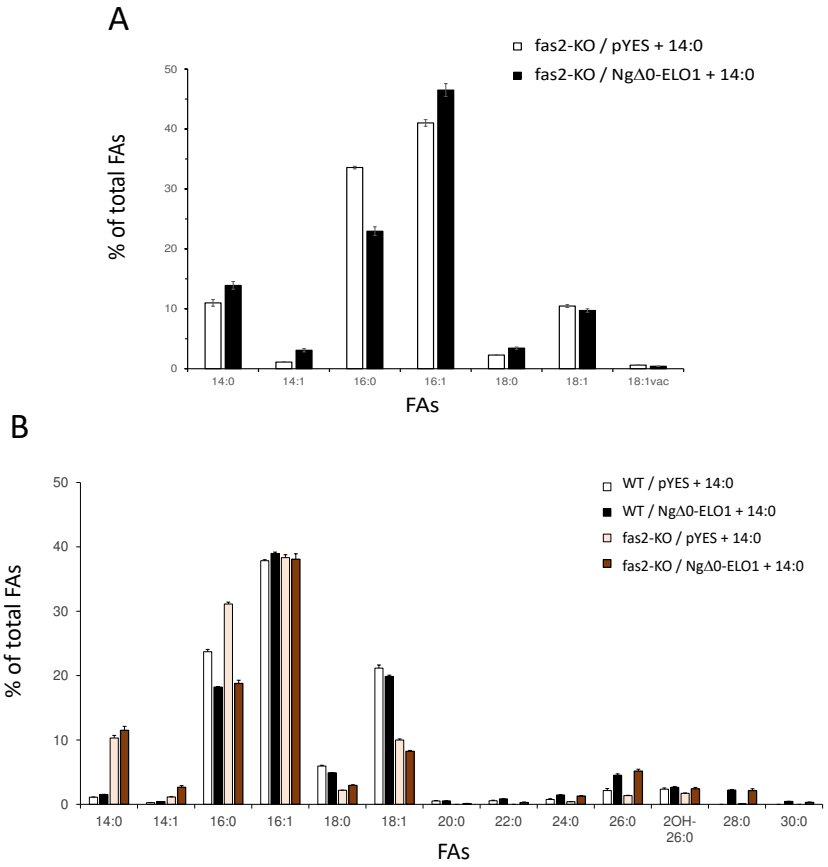

Figure S2: Functional analysis of Δ0-NgELO1 in yeast. (A) Medium chain fatty acid profile of a yeast fas2-KO line expressing NgΔ0-ELO1 (n=5). A yeast fas2 mutant (fas2-KO) was transformed with either an empty pYES vector (white bars) or a vector allowing the expression of NgΔ0-ELO1 (black bars) and was grown on a medium complemented with radiolabeled myristic acid (14:0). We observed a 31% decrease in 16:0 and a statistically relevant 51% increase in 18:0 in the presence of NgΔ0-ELO1 (*p-value* 0.002; two-tailed t-test with a 95% confidence). FAs, fatty acids; 18:1vac, vaccenic acid. Data are the result of 5 biological replicates. **(B) Very long chain fatty acid profile of wild type and fas2Δ yeast expressing Δ0-NgΔELO1 (n=3).** A wild type (WT) yeast and a fas2 yeast mutant (fas2-KO) were transformed with either an empty pYES vector (white and pink bars) or a vector allowing the expression of NgΔ0-ELO1 (black and brown bars). Because of the lack of fatty acid synthesis in the fas2-KO line, cells were grown on a medium complemented with radiolabeled myristic acid (14:0). Very long chain fatty acids (VLC-FAs) were analyzed using a HP1-MS column (Agilent), as described in Methods. A significant increase in all VLC-FAs with chain lengths ≥ 22 carbons and up to 30:0 was observed in both the WT and the fas2-KO backgrounds. FAs, fatty acids. Data are the result of 3 biological replicates.

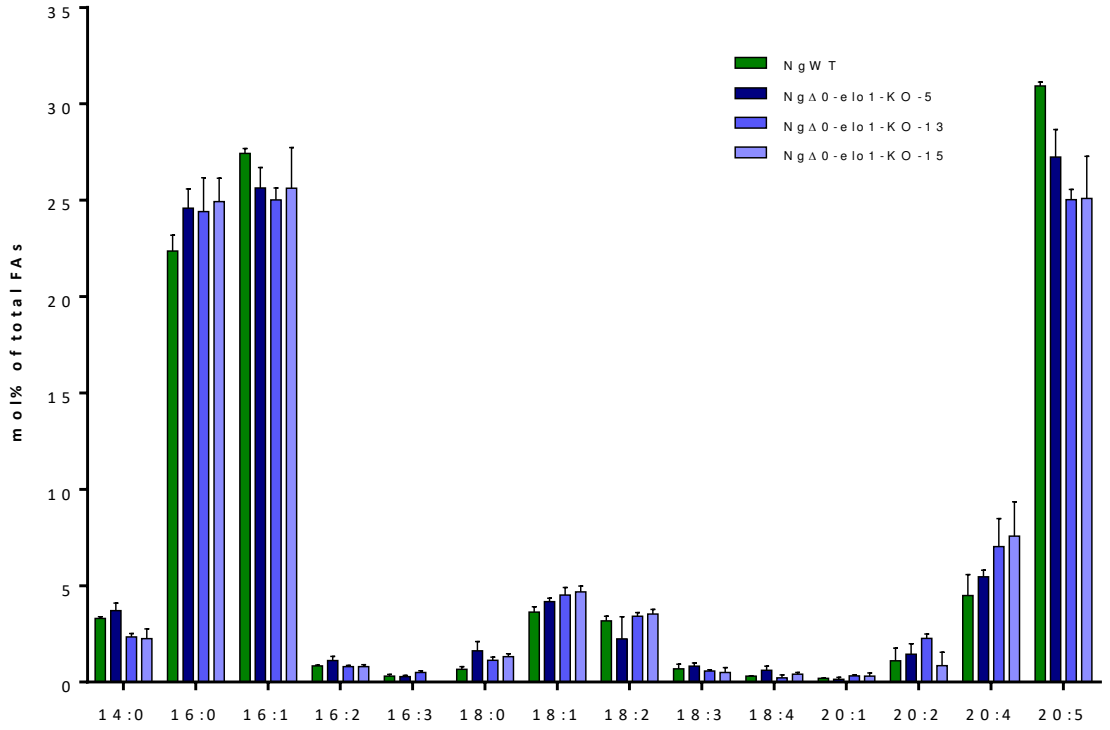

Figure S3: Comparison of the total fatty acid profiles of three independent mutant lines of *Nannochloropsis gaditana* obtained by knocking out the Naga_100083g23/ NgΔ0-elo1 gene. Three independent lines containing single copies of the KO cassette, inserted at the level of the Naga_100083g23/ NgΔ0-elo1 target gene, were obtained (KO5, KO13 and KO15). Glycerolipids were extracted and total fatty acids (FAs) were analysed, based on fatty acid methyl ester separation by gas chromatography coupled to ion flame detection, as described in the Method section. The proportion of each FA is indicated, based on the carbon chain-length and number of desaturations.For each KO line, three independent analyses were performed (bars indicate standard error of the mean). The FA profiles of the three independent KO lines were not statistically different. By contrast, significant changes could be detected between the wild type (NgWT) profile and that of each KO line, i.e. a 8% reduction of EPA (p-value 0.0072) and a 0.2% increase of 18:1 (p-value 0.0031) (two-tailed t-test). NgWT profile is shown in green. KO line profiles are shown in different scales of blue.

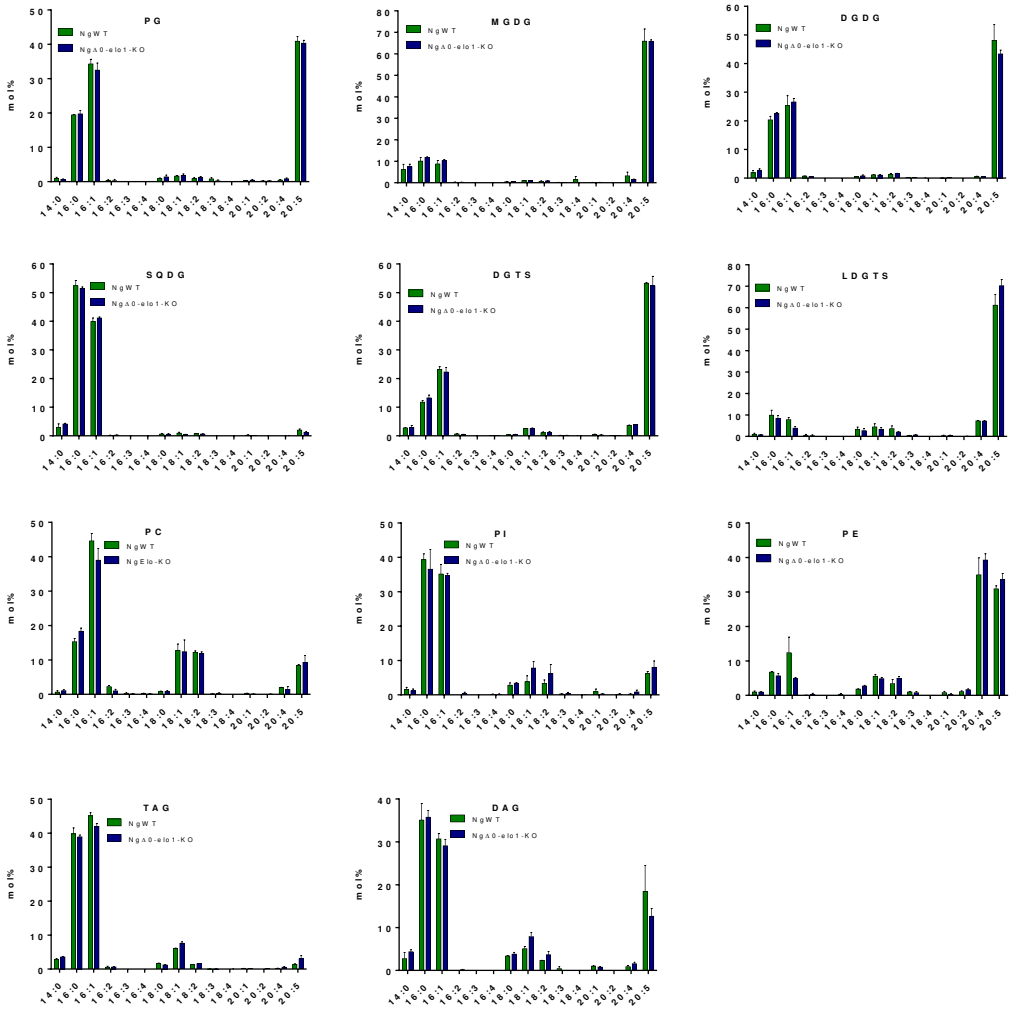

Figure S4: Fatty acid profile of membrane glycerolipid classes from *Nannochloropsis gaditana* WT and NgΔ0-elo1 knocked out lines. Glycerolipids from NgWT and NgΔ0-elo1 KO lines were extracted and separated by two-dimensional thin layer chromatography (2D-TLC). Fatty acids from each glycerolipid class were analysed and quantified, based on fatty acid methyl ester separation by gas chromatography coupled to ion flame detection, as described in the Method section. Plastid membrane glycerolipids correspond to phosphatidylglycerol (PG), monogalactosyldiacylglycerol (MGDG), digalactosyldiacylglycerol (DGDG), sulfoquinovosyldiacylglycerol (SQDG). ER-synthesized membrane glycerolipids correspond to diacylglyceryltrimethylhomoserine (DGTS), lyso-DGTS (LDGTS), phosphatidylcholine (PC), phosphatidylinositol (PI), phosphatidylethanolamine (PE), and neutral lipids triacylglycerol (TAG) and diacylglycerol (DAG). NgWT FA analyses are shown in green; NgΔ0-elo1-KO FA analyses are shown in blue. Analyses were performed in three biological replicates. Bars correspond to standard error of the mean.

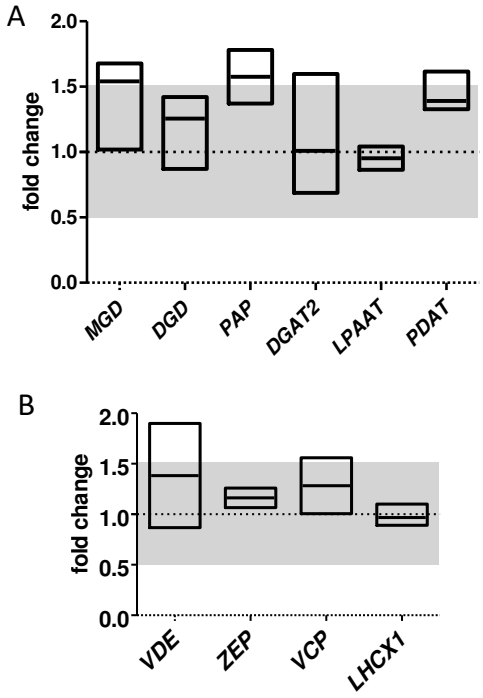

Figure S5: Gene expression analysis. RNA was extracted from NgWT and NgΔ0-elo1-KO cells and reversely transcribed. Quantitative real time PCR was performed and curves were evaluated using theΔΔCq method provided with the BioRad CFX software. NgΔ0-elo1-KO relative gene expression levels were normalized to the mRNA level in the NgWT, both corrected to the Cq of the housekeeping genes *PSBA* and *TUB*. Data is shown as boxplots with the line at the median, representing the fold change of gene expression in three biological replicates of both, NgΔ0-elo1-KO and NgWT. **(A) Non-significant change of the expression of genes involved in galactolipid and triacylglycerol biosynthesis, possibly operating in the alteration of the MGDG *versus* TAG balance, in NgΔ0-elo1 mutants compared to NgWT.** Monogalactosyldiacylglycerol sysnthase (*MGD*), digalactosyldiacylglycerol synthase (*DGD*), chloroplastic phosphatidic acid phosphatase (*PAP*), acyl-CoA:1,2-diacyl-sn-glycerol O-acyltransferase (*DGAT2*), lysophosphatidic acid acyltransferase (*LPAAT*), and plastid galactolipid/phospholipid:1,2-diacyl-sn-glycerol O-acyltransferase (*PDAT*). An empirical confidence threshold was set at a minimal fold change of 0.5 (grey shade) and changes within this region were considered as not important. Concomitantly, none of the changes were significant in paired t-test. **(B) Similar expression of genes involved in non-photochemical quenching in NgΔ0-elo1 mutant and NgWT.** Violaxanthin de-epoxidase (*VDE*), zeaxanthin epoxidase (*ZEP*), violaxanthin-chlorophyll a binding protein (*VCP*), light harvesting complex-like protein 1 (*LHCX1*). An empirical confidence threshold was set at a minimal fold change of 0.5 (grey shade) and changes within this region were considered as not important. Concomitantly, none of the changes were significant in paired t-test.

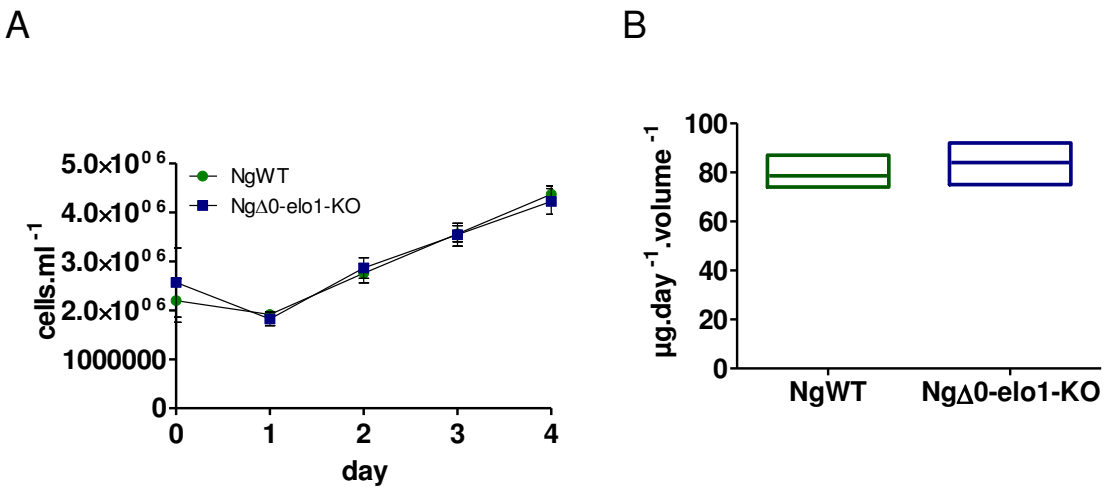

Figure S6: Similar growth (A) and biomass (B) production of NgWT and NgΔ0-elo1 KO. Independent of the culture conditions, neither cell concentration nor biomass productivity were altered in NgΔ0-elo1 mutants. Representatively, small scale (2 mL) cell concentrations (A), and relative biomass productivity (B) are shown. Cell concentrations were calculated based on the absorbance at 750 nm measured with a TECAN plate reader. Biomass productivity was calculated as dry weight of the algal pellet after 7 days of growth in a 50 mL culture. Experiments were carried out in at least three repetitions. Differences between mutant and NgWT were not statistically relevant (2-way ANOVA and two-tailed t-test, respectively).

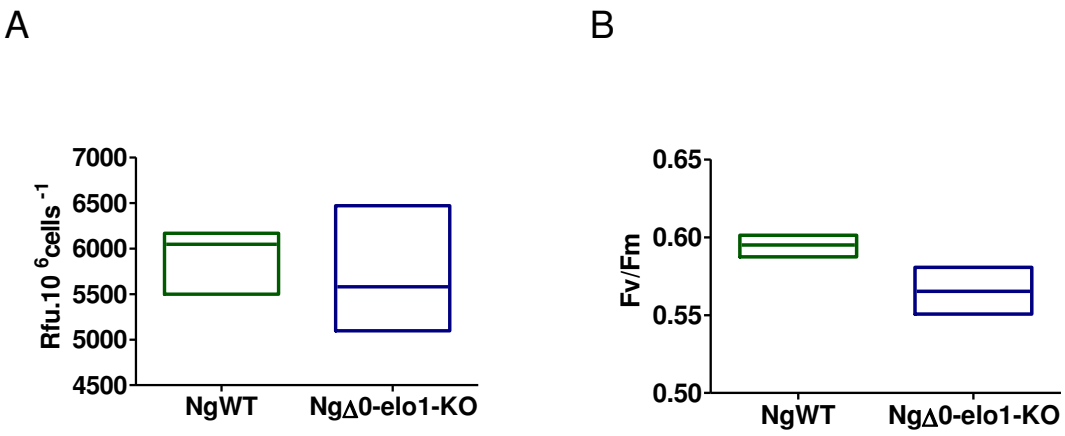

Figure S7: Moderate reduction of PSII efficiency in NgΔ0-elo1-KO compared to NgWT, based on chlorophyll fluorescence (A) and *Fv/Fm* measures (B). From three three-day old 2 mL cultures per cell line, a 160 µl aliquot was taken. Total chlorophyll fluorescence at 680 nm was measured using a TECAN plate reader (A) and normalized to the cell concentration. *Fv/Fm* was measured *via* room temperature chlorophyll fluorescence kinetics using a Speedzen MX fluorescence imaging system (B). Data is presented as boxplots with the line at the median. Chlorophyll levels were similar in NgΔ0-elo1-KO and NgWT. Fv/Fm was at 0.5874 for NgWT and 0.5507 for NgΔ0-elo1-KO (p-value 0.0005 in two-tailed t-test).

5.3 The "omega pathway" addressed by reverse genetics of PLDζ, AAS, ATS1 and ATS2 (Preliminary data)

5.3.1 *Identification of knock down lines*

In order to elucidate the lipid carrying EPA for its import into the chloroplast, knock down lines of those proteins that would use the respective precursors were generated. To this end, the *Phaeodactylum* WT was transformed with the empty vector (pH4) or antisense constructs against PLD, AAS, ATS1 and ATS2. The expression level of the respective gene that we attempted to silence was verified in qPCR and the two lines with the strongest downregulation were selected for phenotyping (**figure 5.4**). We obtained a fold change of 0.82 for PLDas2 (p-value 0.042), 0.41 for PLDas3 (p-value 0.020), 0.64 for AASas2 (p-value 0.146), 0.61 for AASas3 (p-value 0.041), 0.92 for ATS1as2 (p-value 0.318), 0.73 for ATS1as3 (0.040), 0.14 for ATS2as1 (p-value < 0.0001) and 0.6 for ATS2as3 (p-value 0.0023). Downregulations in AASas2 and ATS1as were thus not significant in t-test. With the high residual expression levels in some of these knock down lines, the clones obtained here are less efficient compared to earlier reports in *Phaeodactylum* (De Riso et al. 2009).

With the aim to reveal a function in the "omega pathway" the fatty acid and lipid profiles were investigated. We focused on the profiles of MGDG as the greatest EPA sink as well as PG whose plastidial form should not involve a PC precursor and 16:1-*trans* pairs often with 20:5 (**section 3.3.2**). Lipids were extracted from three day old cultures and the total fatty acid profile was recorded using GC-FID. Then, lipid classes and respective qualities were analysed in HPLC-MS/MS. In most obtained lines, the downregulation of the target gene was weak. To obtain an idea if the altered gene expression would have a consequence for the culture, we investigated the cells fitness by measuring growth and the photosynthesis health indicator *Fv/Fm*.

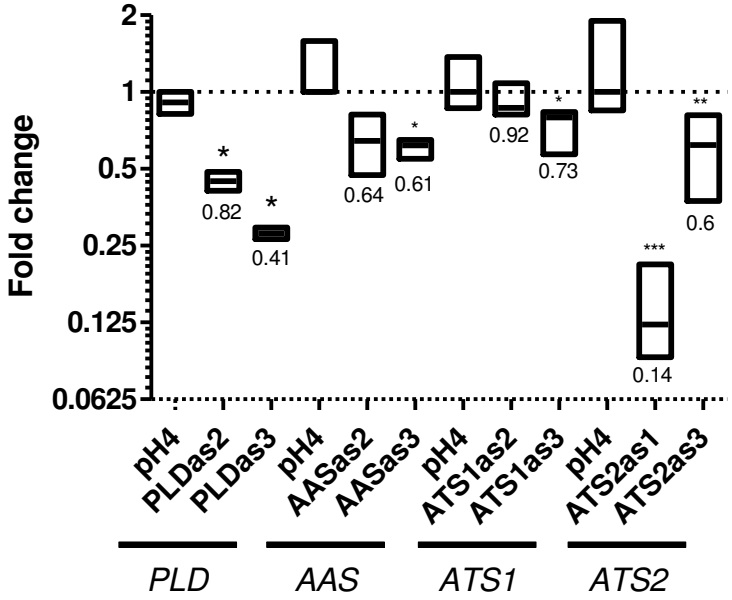

Figure 5.4. Relative mRNA levels of the targeted genes *PLD*, *AAS*, *ATS1* and *ATS2* in respective knock down lines. RNA was extracted from cell pellets and reversely transcribed. Quantitative real time PCR was performed and curves were evaluated using the ΔΔCq method provided with the BioRad CFX software. Relative gene expression levels were normalized to the mRNA level in the empty vector control (pH4), both corrected to the Cq of the housekeeping genes *RPS* and *TUB*. Data is shown as boxplots with the line at the median, representing the fold change of gene expression in three biological replicates. To indicate natural variance of expression, mRNA quantities in pH4 are also plotted.

5.3.2 *Characterization of PLDas lines*

Fatty acid contents in the *Phaeodactylum* WT and the two PLDζ knock down lines were similar with 4.56 nmol ± 0.02 per 10^6 cells (**figure 5.5 A**). Both knock down lines displayed similar total fatty acid profiles with a stronger phenotype of PLDas3 compared to PLDas2 as expected from the lower residual expression of 41% compared to 82% (**figure 5.5 B**). Compared to the WT, trends of 16:1 and 24:0 increases and a 20:5 decrease were observed in PLDas. The 35% EPA reduction in PLDas3 thus seems to be compensated by an induction of 16:1 that, based on the fatty acid distributions in the different *Phaeodactylum* lipid classes (**section 3.3.2**), might indicate a shift from

chloroplast to neural lipids. This shall be revealed in future experiments including MS analyses of the glycerolipid classes.

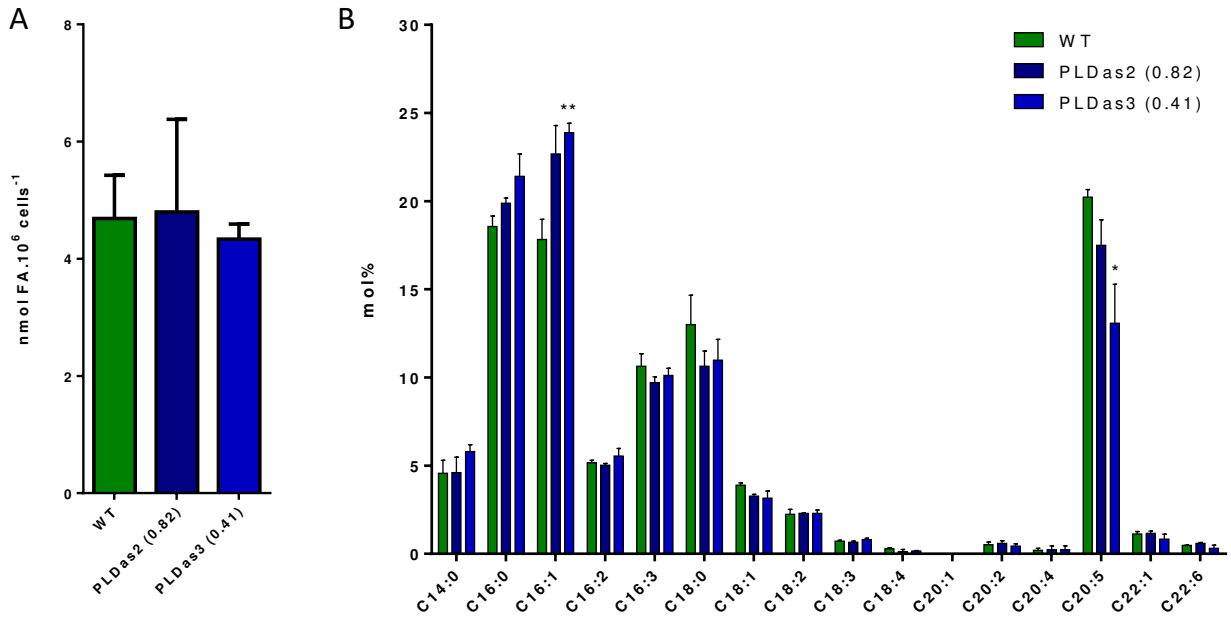

Figure 5.5. Analysis of fatty acids from *Phaeodactylum* wild type (WT) and PLDas lines. Glycerolipids were extracted and total fatty acids (FAs) were analysed, based on fatty acid methyl ester separation by gas chromatography coupled to ion flame detection, as described in the Method section. **A. Comparison of the total cellular FA amount**, expressed in µg per 10^6 cells. No statistical difference could be detected. **B. Comparison of the FA profiles** of the WT and PLDas lines. The proportion of each FA is indicated, based on the carbon chain-length and number of desaturations. Error bars correspond to standard error of the mean (SEM, n = 3-9). Only in PLDas3 being the stronger knock down line with 0.41 compared to 0.82 expression fold change, a 34% increase of 16:1 (p-value 0.009) and a 35% decrease of 20:5 (p-value 0.034) was significant in t-test.

WT cultures had a *Fv/Fm* of 0.556 ± 0.002 and a relative growth rate of 0.621 ± 0.032 when calculated up from day 1 to exclude the lag phase. Culture fitness was slightly impaired in PLDas lines compared to the WT. The maximum photosynthetic quantum yield and the growth rate were 16% and respectively 9% lower in PLDas2. In PLDas3, *Fv/Fm* and growth were reduced by 9% and 1%, although both the knock down level and the fatty acid alterations were more pronounced in PLDas3 than in PLDas2. This

could indicate that gene insertion could have occurred in an important gene in PLDas2 that is concomitantly disrupted. Although 95% of the *Phaeodactylum* genome is non-coding (Vardi et al. 2008b), number and positions of transgene genome insertions are variable and therefore increase the chances of being inserted in a coding region. Furthermore, given the instability of silencing efficiencies we cannot exclude that the *PLDζ* gene expression level had changed during the experiments. The use of targeted gene knock out would overcome these disadvantages.

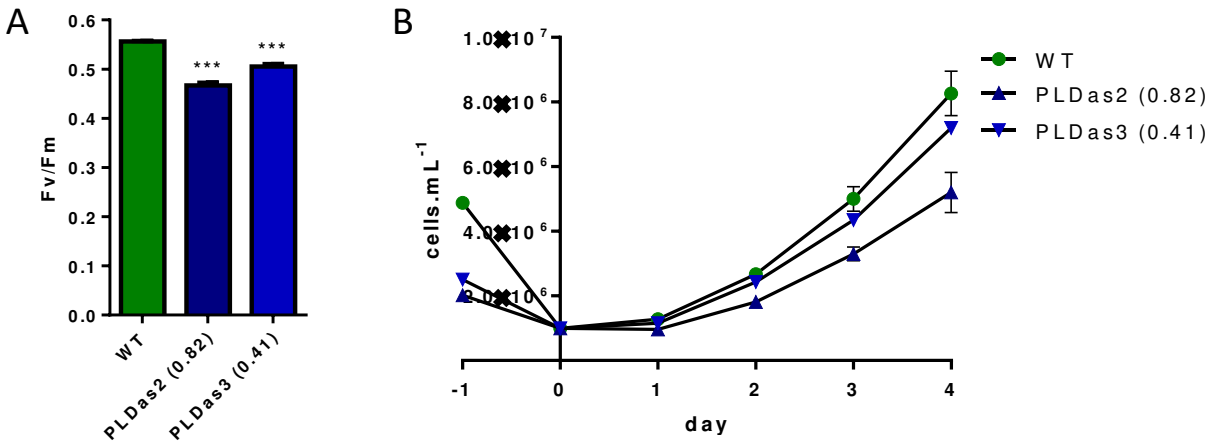

Figure 5.6. Fitness parameters of *Phaeodactylum* wild type (WT) and PLDas lines. From triplicates of 2 mL cultures, 300 µL were collected for analyses. **A. Maximum quantum efficiency of photosystem II** (*Fv/Fm*) was measured *via* room temperature chlorophyll fluorescence kinetics using a Speedzen MX fluorescence imaging system and revealed 16% (p-value 0.0001) and 9% (p-value 0.0006) lower yields in PLDas2 and PLDas3, respectively. **B. Cell concentrations** were calculated based on the absorbance at 750 nm measured with a TECAN plate reader. Growth rates were lower in PLDas compared to WT (p-value < 0.0001 in 2-way ANOVA). Error bars indicate the standard error of the mean.

5.3.3 *Characterization of AASas lines*

In the antisense lines and the control lines, total fatty acid contents were similar with an average of 4.94 ± 0.73 nmol.10^6cells^{-1} (**figure 5.7 A**). Although residual *AAS* expression with about 60% was similar in both lines, significant differences in the total fatty acid profile occurred only in AASas3 but were however small (**figure 5.7 B**).

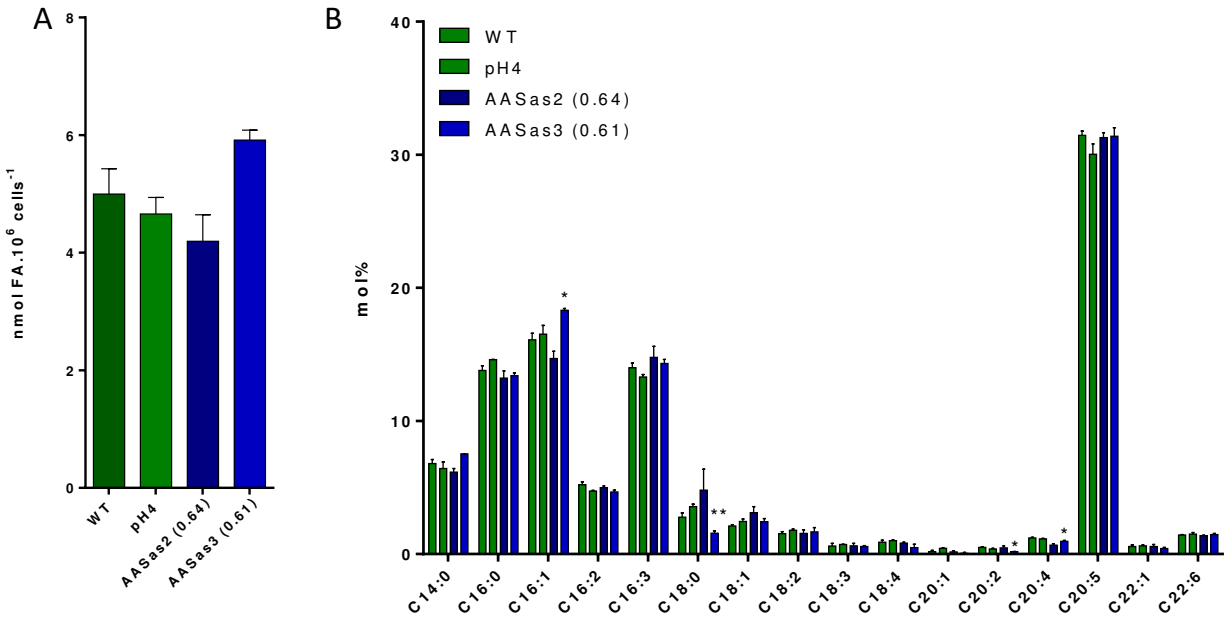

Figure 5.7. Analysis of fatty acids from *Phaeodactylum* wild type (WT), empty vector control (pH4) and AASas lines. Glycerolipids were extracted and total fatty acids (FAs) were analysed, based on fatty acid methyl ester separation by gas chromatography coupled to ion flame detection, as described in the Method section. **A. Comparison of the total cellular FA amount**, expressed in µg per 10^6 cells. No statistical difference could be detected. **B. Comparison of the FA profiles** of the WT and AASas lines. The proportion of each FA is indicated, based on the carbon chain-length and number of desaturations. Error bars correspond to standard error of the mean (SEM, n = 3). Only AASas3 fatty acid profiles were significantly changed with an 14% increase in 16:1 (p-value 0.013), a 43%, 64% and 22% reduction of 18:1 (p-value 0.031) and 20:2 (p-value 0.009) and 20:4 (p-value 0.037), respectively.

In AAS antisense lines, photosynthetic efficiency indicated by the *Fv/Fm* was not affected (**figure 5.8 A**) but growth was strongly impaired in both mutants (**figure 5.8 B**). Notably, the time course was performed while cultures for lipid analyses were growing and thus it is possible, that the phenotype was lost during the culturing time. Given the strong fitness impairment, those cells that silenced the antisense construct would be able to overgrow those with reduced *AAS* expression. This is a common problem with the RNAas approach. The experiment should be repeated with shorter culture times in order to avoid loosening the phenotype.

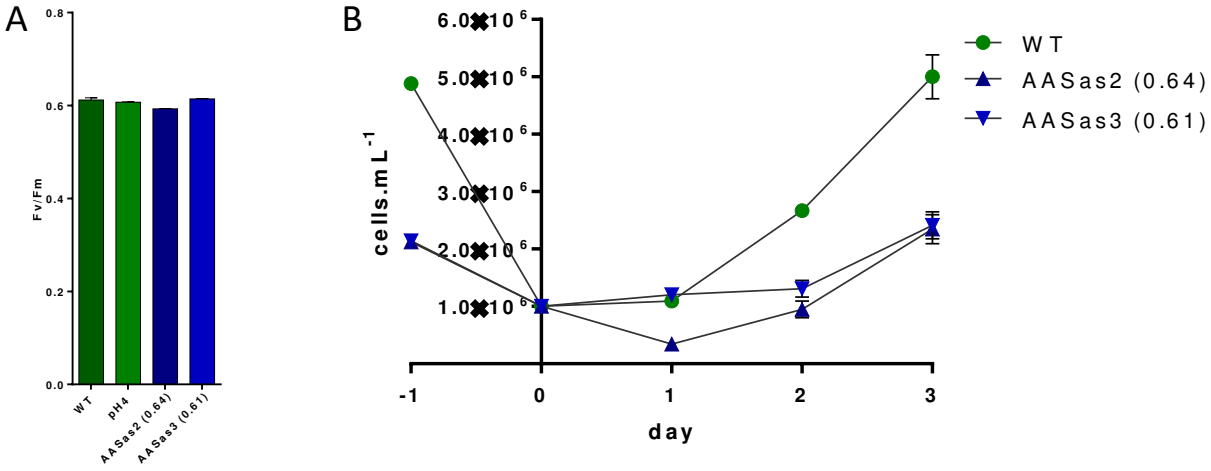

Figure 5.8 Fitness parameters of *Phaeodactylum* wild type (WT), empty vector control (pH4) and AASas lines. From triplicates of 2 mL cultures, 300 µL were collected for analyses. **A. Maximum quantum efficiency of photosystem** II (*Fv/Fm*) measured via room temperature chlorophyll fluorescence kinetics using a Speedzen MX fluorescence imaging system was similar in all lines. **B. Cell concentrations** were calculated based on the absorbance at 750 nm measured with a TECAN plate reader. Growth rates were lower in AAS compared to WT (p-value < 0.0001 in 2-way ANOVA). Error bars indicate the standard error of the mean.

5.3.4 *Characterization of ATS1as lines*

The expression level of *ATS1* was barely affected in ATS1as2 and accordingly, total fatty acid profiles were not significantly altered when compared to the WT. The differences in cellular fatty acid quantities were not significant in t-test giving a mean concentration of 4.93 ± 1.26 nmol.10^6 cells^{-1} (**figure 5.9 A**). The 27% reduction of the transferase in ATS1as3 did however lead to strong changes in the fatty acid distributions (**figure 5.9 B**). Significantly lower were the 28-38% reductions of unsaturated C16 species (p-values 0.007-0.04) as well as 12% lower 20:5 (p-value 0.003). By contrast, relative abundances of C18 fatty acids were increased in ATS1as3 compared to the WT with 2.86-fold (p-value 0.013) induction of 18:0 and 3.11-fold (p-value 0.014) 18:1. The strongest relative increase was observed for the minor fatty acid species 20:1 with a 3.98 induction (p-value 0.020) and 22:1 with a 3.15 induction (p-value 0.05). The Decrease of PUFAs and concomitant increase of 16:0, 18:0 and 18:1 indicated a shift from membrane lipids to neutral lipids, and confirmation via MS analyses is awaited.

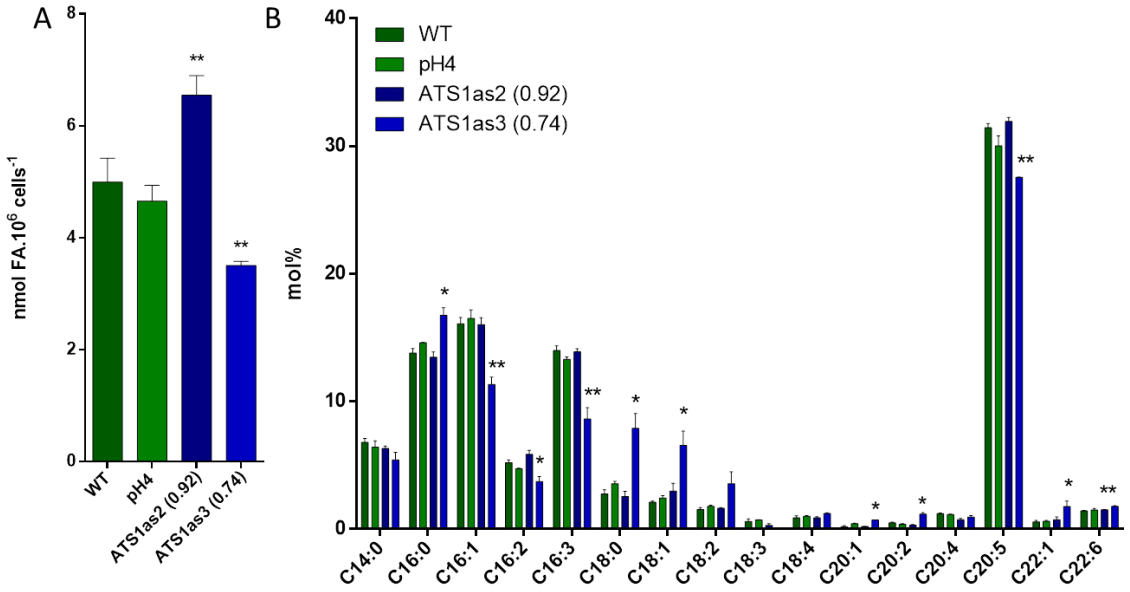

Figure 5.9. Analysis of fatty acids from Phaeodactylum wild type (WT), empty vector control (pH4) and ATS1as lines. Glycerolipids were extracted and total fatty acids (FAs) were analysed, based on fatty acid methyl ester separation by gas chromatography coupled to ion flame detection, as described in the Method section. **A. Comparison of the total cellular FA amount**, expressed in µg per 10^6 cells. Total FA contents were 36% higher in ATS1as2 (p-value 0.008) and 27% lower in ATS1as3 (0.009). **B. Comparison of the FA profiles** of the WT and ATS1as lines. The proportion of each FA is indicated, based on the carbon chain-length and number of desaturations. Error bars correspond to standard error of the mean (SEM, n = 3). Only ATS1as3 FA profiles were significantly changed with increased levels of 16:0 (22%, p-value 0.019), 18:0 (186%, p-value 0.013), 18:1 (311% p-value 0.014), 20:1 (398% p-value 0.02), 20:2 (237% p-value 0.011), 22:1 (315% p-value 0.045), 22:6 (126%, p-value 0.012); and decreased levels of 16:0 (22%, p-value 0.019), 16:1 (30% p-value 0.008), 16:2 (28% 0.037), 16:3 (38%, p-value 0.007), 20:5 (12%, p-value 0.003), 22:6 (26%, p-value 0.012).

Although the glycerolipid profile indicated an alteration in chloroplast lipid composition in ATS1as3, the *Fv/Fm* was unaffected in either mutant line (**Figure 5.10 A**). Nonetheless, cell growth was strongly arrested in both ATS1 antisense lines (**Figure 5.10 B**). Lipid profiles and physiological fitness in two ATS1 lines was thus inconsistent and the experiments shall be repeated with new clones.

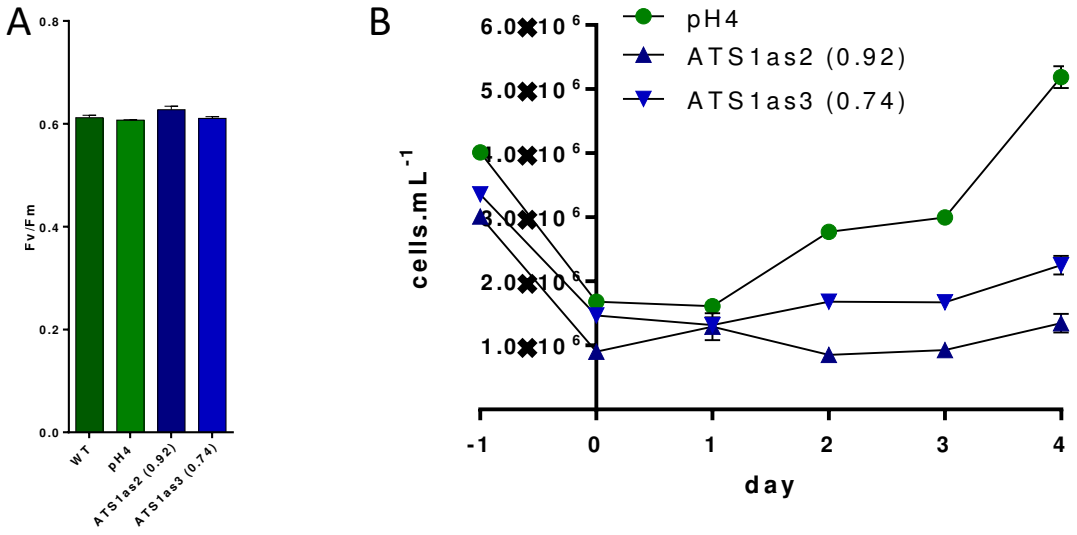

Figure 5.10 Fitness parameters of *Phaeodactylum* wild type (WT), empty vector control (pH4) and ATS1 lines. From triplicates of 2 mL cultures, 300 µL were collected for analyses. **A. Maximum quantum efficiency of photosystem II** (*Fv/Fm*) measured via room temperature chlorophyll fluorescence kinetics using a Speedzen MX fluorescence imaging system was similar in all lines. **B. Cell concentrations** were calculated based on the absorbance at 750 nm measured with a TECAN plate reader. Growth rates were lower in ATS1as compared to WT (p-value < 0.0001 in 2-way ANOVA). Error bars indicate the standard error of the mean.

5.3.5 *Characterization of ATS2as lines*

The total fatty acid content was 1.5-fold (p-value 0.034) and 2-fold (p-value 0.023) elevated in ATS2as1 and ATS2as3, respectively, when compared to the WT (**figure 5.11 A**). Fatty acid distribution was however unaltered in these antisense lines compared to the controls (**figure 5.11 B**).

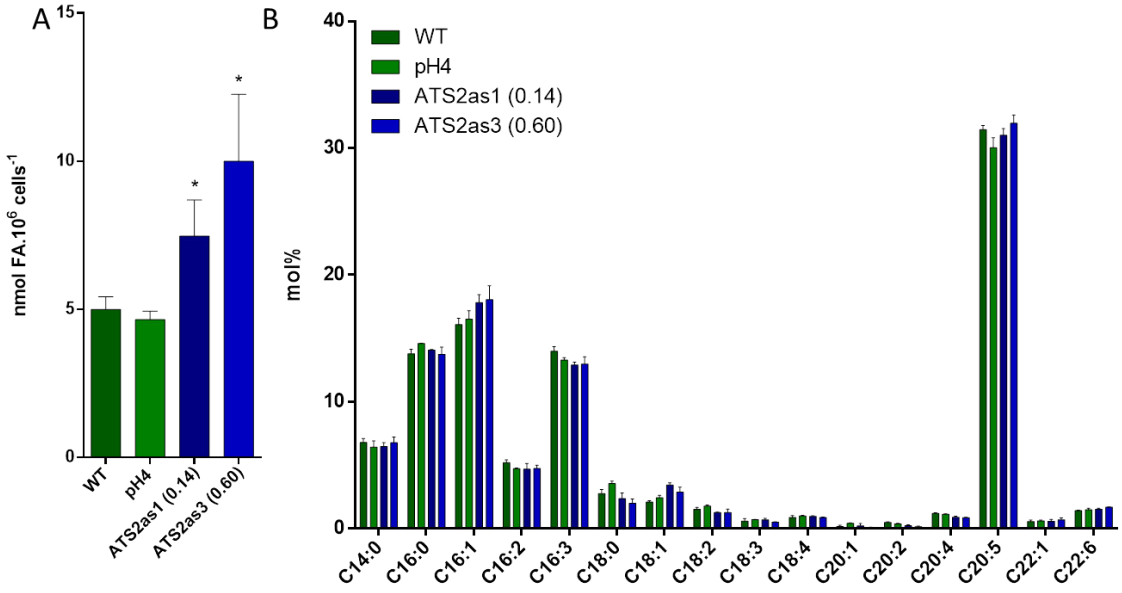

Figure 5.11. Analysis of fatty acids from *Phaeodactylum* wild type (WT), empty vector control (pH4) and ATS2as lines. Glycerolipids were extracted and total fatty acids (FAs) were analysed, based on fatty acid methyl ester separation by gas chromatography coupled to ion flame detection, as described in the Method section. A**. Comparison of the total cellular FA amount**, expressed in µg per 10^6 cells. Total FA contents were 1.5 and 2-fold higher in ATS2as1 (p-value 0.034) ATS2as3, respectively (p-value 0.023). **B. Comparison of the FA profiles** of the WT and ATS1as lines. The proportion of each FA is indicated, based on the carbon chain-length and number of desaturations. Error bars correspond to standard error of the mean (SEM, n = 3). FA was not significantly altered.

Maximal energy conversion at PSII was unaltered in ATS2as (**figure 5.12 A**) lines but nonetheless, a fitness phenotype was observed in the stronger knock down line, with a 30-40% reduced cell concentration after two and three days, respectively (**figure 5.12 B**).

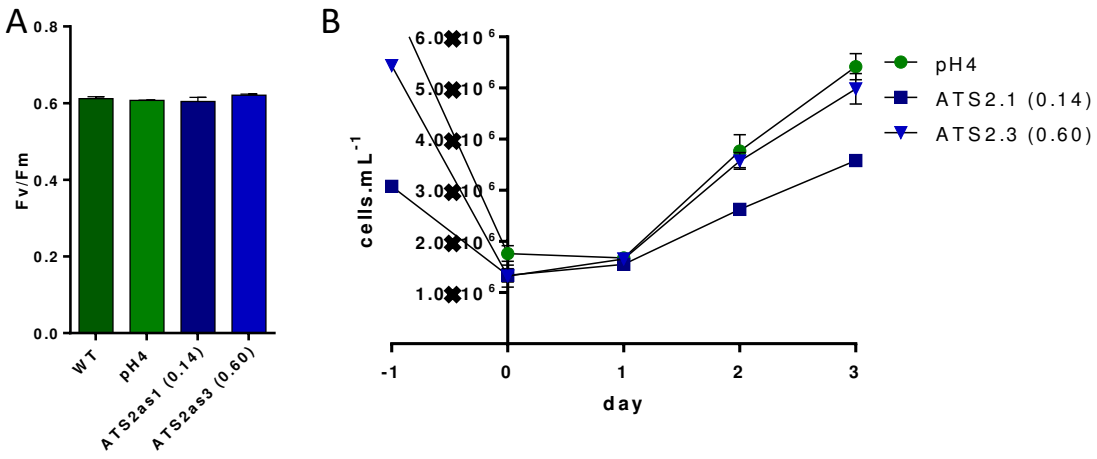

Figure 5.12. Fitness parameters of *Phaeodactylum* wild type (WT), empty vector control (pH4) and ATS2as lines. From triplicates of 2 mL cultures, 300 µL were collected for analyses. **A. Maximum quantum efficiency of photosystem II** (Fv/Fm) measured via room temperature chlorophyll fluorescence kinetics using a Speedzen MX fluorescence imaging system was similar in all lines. **B. Cell concentrations** were calculated based on the absorbance at 750 nm measured with a TECAN plate reader. Growth rates in ATSas3 and pH4 were similar but lower in ATS2as1 (p-value < 0.0001 in 2-way ANOVA). Error bars indicate the standard error of the mean.

These data are obviously preliminary. All these constructs will serve in the future for in-depth lipodomic and physiological analyses, so as to evaluate the possible roles of the corresponding proteins in the “omega pathway”.

5.4 The role of EPA-rich MGDG in homeoviscous adaptation in *Nannochloropsis gaditana*

Nannochloropsis gaditana is rich in EPA and *Eustigmatophytes* might therefore be assumed to be pre-equipped for cold environments. This VLC-PUFA mostly allocates to MGDG (Simionato et al. 2013, section 5.2.3). The role of MGDG in cold-acclimation processes is ambiguous. The hexagonal-II phase (HII) building property is assumed to promote irreversible membrane damage upon cold stress (Steponkus et al., 1993). Furthermore, a high proportion of MGDG allows higher protein packing in the membrane which is negatively correlated to lateral membrane fluidity. Thus, a relative reduction of MGDG in respect to bilayer forming chloroplast lipids as DGDG is induced upon cold stress (Garab et al. 2000). Accordingly, the MGDG/DGDG ratio is reduced in cold acclimated *Arabidopsis* (Welti et al. 2002), and the HII lipid PE level decreases under cold stress in the heterotroph *Tetrahymena* (Nozawa 2011). But not all data support a relative MGDG reduction as cold-response. In *Synechococcus* sp. PCC 7002, a temperature shift from 38°C to 22°C induced the ω3-FAD and overall desaturation levels but led to a decrease of SQDG and DGDG whereas MGDG remained unchanged (Sakamoto et al. 1997). The question of the role of a VLC-PUFA–rich HII lipid is therefore intriguing and we decided to dissect the functions by comparing the cold-stress response of *N. gaditana* wild type and a knock out mutant of the most expressed Δ0-elongase (NgΔ0-elo1-KO) that has significantly lower MGDG contents and might therefore have more fluid thylakoid membranes compared to the NgWT.

5.4.1 *Choice of culture conditions*

In the previous study, *N. gaditana* cells were grown under standard conditions, *i. e*. a 12/12 hour light/dark cycle at 20°C. On the lipid level, the remarkable difference between NgΔ0-elo1-KO and NgWT was the strong reduction of MGDG alongside with increased TAG abundances, whereas the fatty acid profiles of the different lipid classes remained unchanged. We attempted to investigate the response of both cell lines to cold stress. In order to suppress influences of diurnal changes, we have changed from a

dark/light regime to continuous irradiation. The new condition altered the glycerolipid profiles of both NgWT and NgΔ0-elo1-KO (**figure 5.13**).

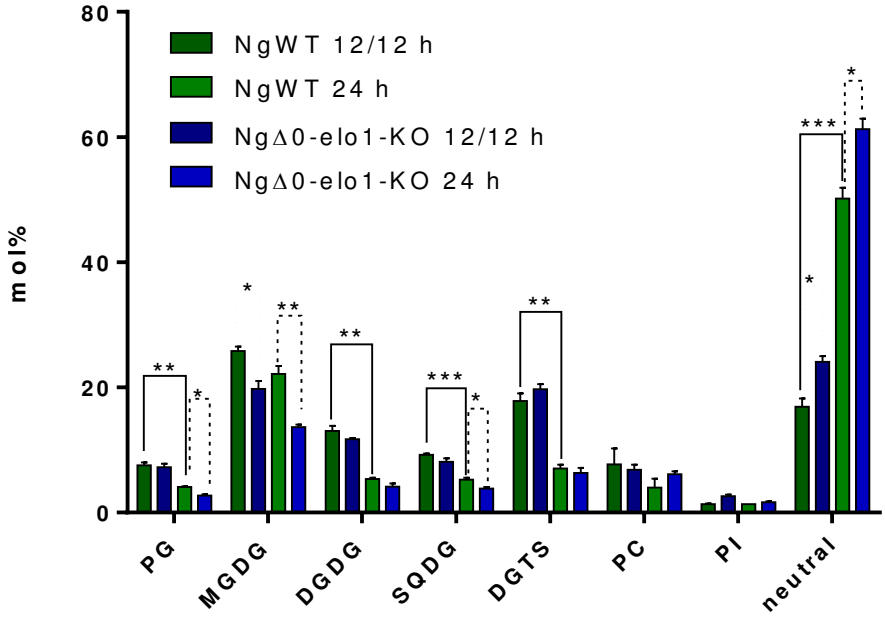

Figure 5.13. Analysis of glycerolipid classes from *Nannochloropsis* wild type (NgWT) and Δ0-ELO1 knock out lines (Ng Δ0-elo1-KO). Glycerolipids were extracted, and their cellular total amount determined based on gas chromatography coupled to ion flame detection after fatty acid methyl ester separation. Lipid classes were analysed using high performance liquid chromatography coupled to tandem mass spectrometry, as described in the Method section. The proportion of each lipid class is indicated. Error bars correspond to standard error of the mean (SEM, n = 3). NgWT grown in a 12/12 hour light/dark cycle (NgWT 12/12) were compared to continuous light grown NgWT cultures (NgWT 24 h) (solid lines). Significant variations (fold change) in NgWT 24 h were observed for PG (0.54, p-value 0.009), DGDG (0.41 p-value 0.005), SQDG (0.57, p-value 0.001), DGTS (0.4 p-value 0.007) and neutral lipids (2.97 p-value < 0.001). Light/dark cycle grown NgΔ0-elo1-KO compared to NgWT was significantly regulated (dotted lines) at the levels of MGDG (0.76, p-value 0.014) and neutral lipids (1.42, p-value 0.011). Continuous light grown NgΔ0-elo1-KO compared to NgWT were significantly regulated (dashed lines) at the level of PG (0.66, p-value 0.021), MGDG (0.61, p-value 0.004), SQDG (0.73, p-value 0.042) and neutral lipids (1.22, p-value 0.022).

As for the light dark regime, TAG and MGDG were strongly altered in NgΔ0-elo1-KO compared to NgWT. MGDG and DGDG levels were about 25% and 60% reduced under the new condition and thus the MGDG/DGDG ratio was 4.15 in NgWT and 3.28 in

NgΔ0-elo1-KO. This ratio was two times higher compared to cells were grown under a 12/12 h light/dark regime with 1.98 in NgWT and 1.68 in NgΔ0-elo1-KO (**figure 5.13**). With the reduction of chloroplast lipids, TAG levels were 3-fold higher during permanent irradiation. This indicated that when cells were not deprived from light energy during night-phases, additional fixed CO_2 allowed higher growth rates and was furthermore directed into TAGs. In total, relative abundance of membrane lipids was reduced by 40-60 % except PI that was unaltered and MGDG that was more stable. This indicated that at the constant light regime, the role of MGDG became more important and we therefore chose continuous irradiation at low light intensities for cold stress experiments (Kaniuga et al. 2010).

5.4.2 *The role of qI in NPQ relaxation in N. gaditana under cold stress conditions*

The NPQ measurement consists of three phases: a dark incubation phase, an irradiation phase during which light flashes with saturating intensities are applied, and a recovery period during which PAR is turned off and fluorescence progressively declines. Fluorescence values during irradiation mainly represent qE (Eberhard et al. 2008). In plants, the NPQ recovery period relies mostly on the release from photoinhibition, qI. In other words, PSII inactivation by long term energy quenching and D1 damage becomes reverted (Ruban et al. 2012). For PSII repair, D1 is *de novo* synthesized and transported through the thylakoid membranes (Järvi et al. 2015). In contrast to plants, diatom qI was indicated to be less important, and the fast NPQ offset to depend on ZEP/DEP activity (Domingues et al. 2012, Lavaud et al. 2012). This could indicate a higher contribution of the prolonged energy quenching at PSII to qI. The role of qI in *Nannochloropsis* NPQ is unknown. We investigated the D1 repair proportion of NPQ relaxation kinetics by treating cells with the chloroplast protein translation inhibitor chloramphenicol (CAP).

A suitable CAP concentration had to be chosen for the treatment. *Nannochloropsis* is characterized by a high resistance to a variety of antibiotics including CAP. *N. oceanica* was reported to tolerate 100 $\mu g.mL^{-1}$ CAP (Vieler et al. 2012). Similarly, CAP concentrations ranging from 10 to 100 $\mu g.mL^{-1}$ had no effect on qI curves in *N. gaditana*

(not shown). Cells grown at 15°C were sensitive to higher concentrations indicated by reduced *Fv/Fm* (**figure 5.14**). The antibiotic reduced the maximal PSII efficiency by more than 50% when concentrations between 400 and 1000 µg.mL^{-1} CAP were used. PSII inactivation was similar in NgWT and Ng Δ0-elo1-KO. CAP induction of qI measured by NPQ relaxation curves was not as drastic as *Fv/Fm* reduction. At a concentration of 600 µg.mL^{-1} CAP, qI levels were the highest in NgΔ0-elo1-KO with a 22% induction compared to control concentrations. This concentration was used for further experiments performed on cultures grown at 10°C.

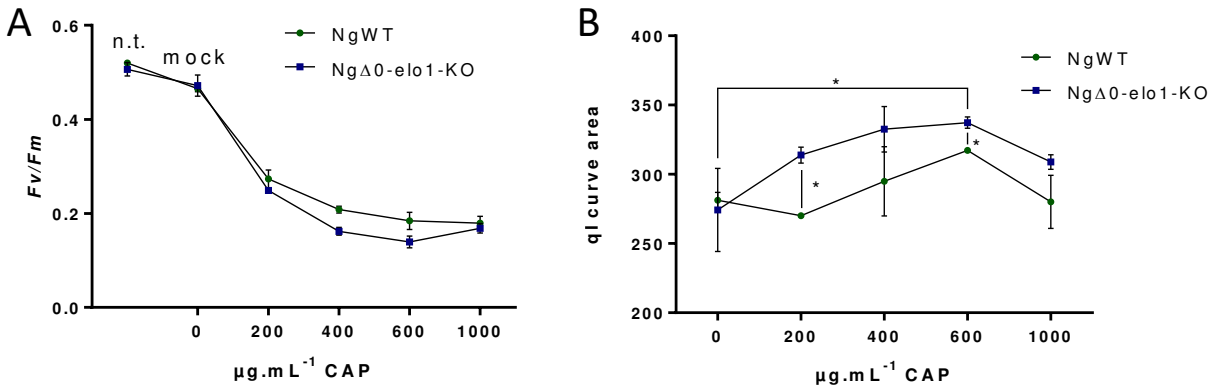

Figure 5.14 Inactivation of PSII in response to chloramphenicol (CAP) in *Nannochloropsis* wild type (NgWT) and *Δ0-ELO1* knock out lines (NgΔ0-elo1-KO) grown at 15°C. Cells were inoculated with different concentrations of CAP (in 100% ethanol) or respective volumes of ethanol (mock), or not treated (n. t). After 24 h of incubation, 160 µL were taken from triplicates of 2 mL cultures for analyses *via* room temperature chlorophyll fluorescence kinetics using a Speedzen MX fluorescence imaging system. Error bars correspond to standard error of the mean (SEM, n = 2). **A. The *Fv/Fm*** declined with increasing CAP concentrations. Compared to the mock, changes caused by CAP were significant in t-test (p-value < 0.0001). **B. The photoinhibition** (qI) component of NPQ was estimated by superimposition of the last values of the light irradiation phase. Then, the area under the curve was calculated and plotted relative to the CAP concentration. The qI increased gradually with CAP concentrations between 200 and 600 µg.mL^{-1}. The 22% qI increase in NgΔ0-elo1-KO incubated with 600 µg.mL^{-1} CAP compared to control conditions (p-value 0.036), and the 16% and 6% relative higher increase in NgΔ0-elo1-KO compared to NgWT at 200 and 600 µg.mL^{-1} CAP, respectively (p-value 0.018 and 0.041) were statistically relevant.

We attempted to confirm the qI phenotype by Westernblot assays using the D1 antibody. To this end, proteins were extracted from triplicates of NgWT and NgΔ0-elo1-KO cultures grown at 10°C for 3 hours. A 10 µg protein aliquot was loaded on a SDS-PAGE, proteins separated and transferred on a nitrocellulose membrane. Treatment with the D1 antibody led to diffuse protein double bands in all samples. The experiment was repeated with new cultured cells and a fresh aliquot of the D1 antibody to exclude protein degradation or other handling errors, but resulted in the same band pattern (**figure 5.15**). Primary and secondary antibodies were removed from the anti-D1 treated membrane using a detergent buffer, and membranes incubated with a VCP antibody. VCP bands appeared at expected position (**figure 5.15**). We were thus unable to confirm the chlorophyll kinetics measurements by protein blots because of an inadequate D1 antibody. As additional control, the same antibody was tested to be functional on *Phaeodactylum* protein extracts (not shown).

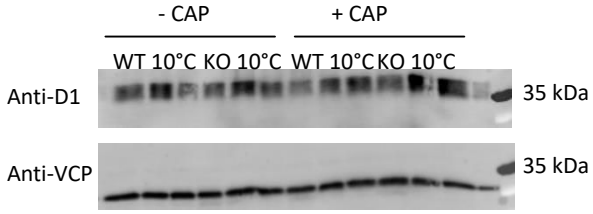

Figure 5.15 Protein blot of *Nannochloropsis* wild type (WT) and *Δ0-ELO1* knock out lines (KO) grown at 10°C in the presence or absence of 600 µg.mL^{-1} chloramphenicol (CAP). Cells were inoculated with CAP (in 100% ethanol) (+ CAP) or respective volumes of ethanol (- CAP) and incubated for 3 hours at 10°C. Proteins were extracted, quantities determined by the Lowry method, 10 µg per sample were loaded on a SDS-PAGE, and transferred to a nitrocellulose membrane. Antibody treatment was performed as described in the method section. First, the D1 antibody was used (upper panel) (expected size 30 kDa). Then, antibodies were removed (Biorad ReadyStrip™) and the membrane treated with anti-VCP (lower panel) (expected size 22 kDa) to control the sample quality.

Having only the chlorophyll fluorescence kinetics method in hands, qI was measured in CAP or ethanol control treated cells grown for three hours at 10°C. With the beginning of the dark phase, NPQ fluorescence values dropped by more than 50% in the first minute. This rapid decline was independent of CAP. Then, the slope of NPQ relaxation

curves was smaller for CAP treated samples (**figure 5.16**). The area under the curves was calculated for each sample and values were compared. The addition of 600 µg.mL^{-1} CAP led to a 57% bigger integral compared to control samples. No significant differences were observed between the two genotypes. Taken together, we could indicate that at least part of the NPQ relaxation curve relied on protein *de novo* synthesis in *N. gaditana,* being most likely accounted to the D1 repair cycle. For a reliable quantification, the Westernblot analyses shall be optimized.

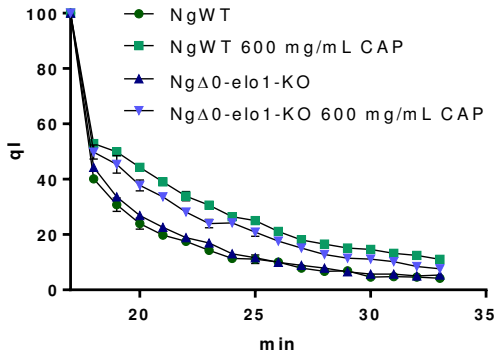

Figure 5.16 Non-photochemical quenching (NPQ) in *Nannochloropsis* wild type (NgWT) and *Δ0-ELO1* knock out lines (NgΔ0-elo1-KO) grown at 10°C in the presence or absence of 600 µg.mL^{-1} CAP. Cells were inoculated with CAP (in 100% ethanol) (+ CAP) or respective volumes of ethanol (- CAP) and incubated for 3 hours at 10°C. From triplicates of 50 mL cultures, 160 µL were collected for chlorophyll fluorescence kinetics measurements using a Speedzen MX fluorescence imaging system, after three hours of incubation at 10°C. NPQ was measured after dark incubation with light pulses of 600 µmol.m^{-2}.s^{-1} PAR for 17 minutes (qE) and a subsequent 17 min dark relaxation phase. Error bars correspond to standard error of the mean (SEM, n = 3). The photoinhibition (qI) component of NPQ was estimated by superimposition of the last values of the light irradiation phase. The area under the curve is about 57% bigger in + CAP samples.

5.4.3 *NPQ in the cold-stress response of N. gaditana grown at 10°C*

Changes in physiological parameters were followed 1, 3, 6, 24, 48 after the shift from 20°C to 10°C in NgWT and NgΔ0-elo1-KO. During this time, cell growth was completely inhibited in cold stressed but not in control cultures (not shown). Energy conversion efficiency of photosystem II was addressed by measuring the *Fv/Fm* and *Y(II)* during the time course in 10°C, and was similar to control conditions in both genotypes (**figure 5.17**).

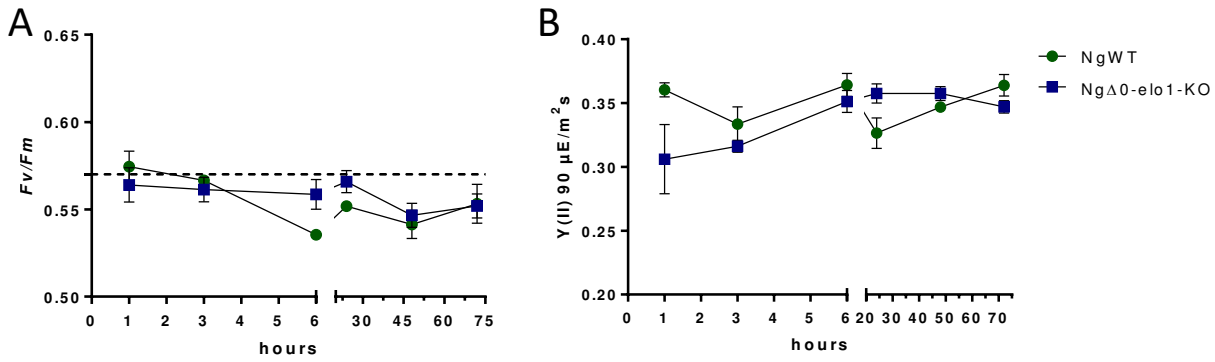

Figure 5.17. Maximum quantum efficiency of photosystem II (*Fv/Fm*) in *Nannochloropsis* wild type (NgWT) and *Δ0-ELO1* knock out lines (NgΔ0-elo1-KO) grown at 10°C. From triplicates of 2 mL cultures, 160 µL were collected after the shift from 20°C to 10°C at indicated time points. Room temperature chlorophyll fluorescence kinetics measurements were performed using a Speedzen MX fluorescence imaging system. Error bars correspond to standard error of the mean (SEM, n = 3-6).A. The *Fv/Fm* describes the maximum PSII quantum yield. **B. Yield of PSII in light-adapted status** (*Y(II)*) during irradiation with 90 µmol photons.$m^{-2}s^{-1}$.

Similarly to our results, the *Fv/Fm* was not affected in cold-sensitive tomato leaves exposed to 10°C for a few days. However, long term exposure to cold temperatures reduces energy conversion efficiencies in overwintering plants (Míguez et al. 2015). In cold resistant plants such as evergreen *Pinus* species, chlorophyll kinetics measurements

indicate a more than 4-fold decrease of the *Fv/Fm* at temperatures below 0°C compared to ambient temperatures (Zhang et al. 2016). We cannot exclude a differential *Fv/Fm* regulation in *Nannochloropsis* during long-term exposure to cold temperatures as might occur during seasonal changes, or to very low temperatures.

Short-term cold stress reduces electron transfer and CO_2 fixation capacities in plants that can partially recover during prolonged exposure (Sage & Kubien 2007, Savitch et al. 2001). The reduced energy sink leads to ROS generation and induces alternative energy quenching including NPQ (Crosatti et al. 2013, Wise 1995). We have therefore addressed NPQ in cold-stressed *Nannochloropsis* lines (**figure 5.18**).

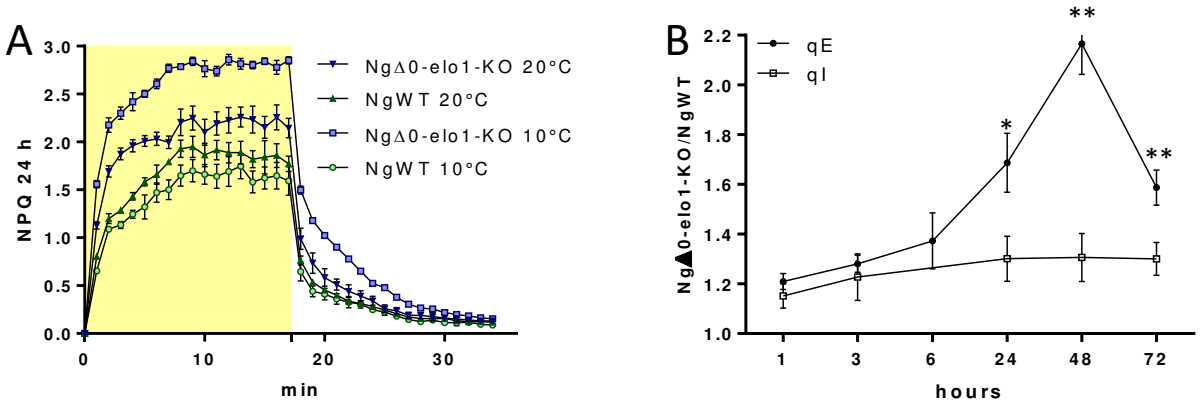

Figure 5.18 Non-photochemical quenching (NPQ) in *Nannochloropsis* wild type (NgWT) and *Δ0-ELO1* knock out lines (NgΔ0-elo1-KO) grown at 10°C. From triplicates of 2 mL cultures, 160 µL were collected for chlorophyll fluorescence kinetics measurements using a Speedzen MX fluorescence imaging system after the shift from 20°C to 10°C at indicated time points. NPQ was measured after dark incubation with light pulses of 600 µmol.m^{-2}.s^{-1} PAR for 17 minutes (qE) and a subsequent 17 min dark relaxation phase. Error bars correspond to standard error of the mean (SEM, n = 3). A. Full NPQ spectra of NgWT and NgΔ0-elo1-KO grown at 10°C and 20°C. B. Time course of qE and qI in 10°C grown samples. The NgΔ0-elo1-KO:NgWT ratio of average qE (fluorescence values between 10-17 min) is plotted. A relative increase in the qE ratio with 30%, 66% and 22% after 24, 48 and 72 hours of incubation at 10°C, respectively, was significant in t-test (p-value 0.018, 0.002 and 0.008, respectively). Photoinhibition (qI) component of NPQ was estimated by superimposition of the last values of the light irradiation phase (yellow shade in A.). The ratio of the area under the curve in NgΔ0-elo1-KO over NgWT is plotted and not significantly changed.

In our earlier study, qE levels were 20% higher in NgΔ0-elo1-KO compared to NgWT, while qI was unaffected (**section 5.2.3**). When cells were grown under continuous irradiation at control temperatures, the 20% increase observed in cells grown in a light/dark cycle was preserved (**Figure 5.18 A**). The qE parameter increased progressively in NgΔ0-elo1-KO, with a maximum difference of 66% after 24 hours of incubation at 10°C and subsequent relaxation (**figure 5.18 B**). This final decrease of the qE ratio was interpreted by advanced temperature acclimation, as also observed in plants (Sage & Kubien 2007, Savitch et al. 2001).

We indirectly measured qI by superimposing light-relaxation curves in NPQ measurements. In order to compare relative photoinhibition recovery efficiencies over the time in cold stress, the peak areas under these qI relaxation curves were calculated, and the ratio of NgΔ0-elo1-KO/NgWT was plotted (**figure 5.18 B**). Relative qI was not significantly regulated over the experimental time. Photoinhibition is a common cold stress feature, but the accumulation of PUFAs was observed and proposed to facilitate D1 repair (Gombos et al. 1994). The D1 repair cycle depends on the thylakoid membrane viscosity (Tietz et al. 2015). According to a study performed on an *Arabidopsis fad5* mutant in which parts of the thylakoid membrane are in crystalline structure, the higher ordered membrane state complicates lateral motion of big proteins and thus qI increases. By contrast, ordered lipids are proposed to form a tunnel-like structure that would facilitate translocation of smaller molecules as PQ and there by allow a higher ETR under cold stress conditions (Tietz et al. 2015). The lack of cold-induced PSII inhibition in *Nannochloropsis* indicated high tolerance towards low temperatures, and that photosynthesis is protected probably due to the high abundances of VLC-PUFAs in galactolipids and PG.

Increasing membrane viscosity is a key element in cold adaptation (Los & Murata 2004). Besides, lateral membrane fluidity is discussed to be controlled by the levels of HII lipids, *i. e.* ratio of MGDG and DGDG in thylakoids. MGDG is supposed to have a rigidifying function by allowing higher protein incorporation into the thylakoid membrane (Garab et al. 2000, 2016). In order to reveal if an MGDG phenotype could

facilitate homeoviscous adaptation in NgΔ0-elo1-KO, we analysed glycerolipid profiles in short-term cold stress experiments.

5.4.4 *Glycerolipid profiles in N. gaditana cultures grown at 10°C*

A variety of studies throughout the phyla indicate higher desaturation levels as a marker of cold stress adaptation. By contrast, no consensus response for the different glycerolipid classes is published. To our knowledge, no comprehensive study on the regulation of different glycerolipid species in a secondary endosymbiont was performed. We therefore addressed the low temperature induced changes in glycerolipid profiles in *N. gaditana* WT and the NgΔ0-elo1-KO lines which have 40% lower MGDG levels when grown at 20°C (**section 5.2.3**).

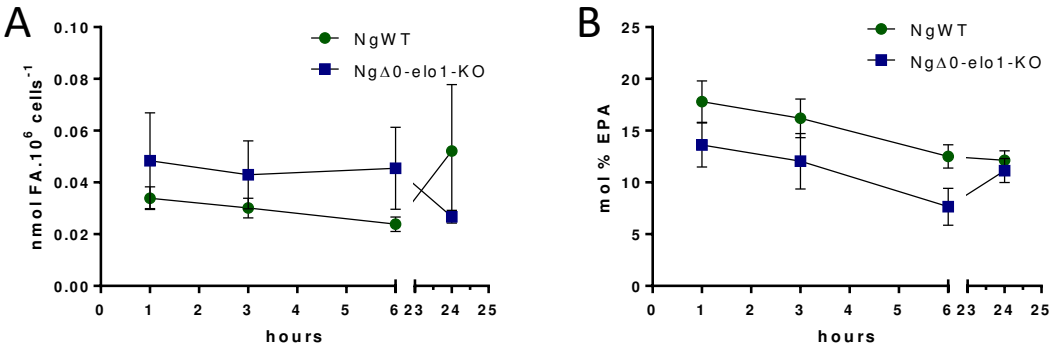

Figure 5.19. Analysis of fatty acid contents from *Nannochloropsis* wild type (NgWT) and *Δ0-ELO1* knock out lines (NgΔ0-elo1-KO) grown at 10°C. Glycerolipids were extracted at time points indicated. Total fatty acids (FAs) were analysed, after fatty acid methyl ester separation by gas chromatography coupled to ion flame detection, as described in the Method section. Error bars correspond to standard error of the mean (SEM, n = 3). **A. Comparison of the total cellular FA amount**, expressed in nmol per 10^6 cells. Changes over time and between the genotypes were not significant. **B. Relative proportion of eicosapentaenoic acid (EPA)**. Trends of reduced levels over the time were not significant.

To reveal whether short-term cold-acclimation in the MGDG mutant differed from NgWT, 50 mL batch cultures of both genotypes were transferred to 10°C and harvested for glycerolipid profiling at time points indicated. No significant changes in total fatty acid contents per cell were observed in the two genotypes over the time (**figure 5.19 A**) and therefore, the more robust mol% demonstration was used for further analyses. The most abundant PUFA, EPA, was not significantly altered during short-term cold stress in the *N. gaditana* cells lines (**figure 5.19 B**).

Lower EPA levels are a fingerprint for chloroplast lipid reduction in *N. gaditana*. We investigated the glycerolipid classes by HPLC-MS/MS in control samples grown at 20°C under continuous light irradiation and 1, 3, 6 and 24 hours after the shift to 10°C. Graphic representation is given in **figure 5.20**, statistical analyses of the responses to the shift in **table 5.1**. We found the NgWT and NgΔ0-elo1-KO to have different homeoviscous adaptation velocities but to reach similar phenotypes after 24 hours of incubation. The early phase of adaptation, namely after 1, 3 and 6 hours of cold stress exposure, was characterized by glycerolipid remodelling. This involved a progressive decrease of the chloroplast quartet where the decline of MGDG and SQDG was initiated already after 1 hour of cold incubation, whereas that of DGDG and PG occurred after 6 hours. PC levels were not significantly altered. TAGs were significantly regulated in the late phase, and levels were 1.1-1.3-fold higher after 24 hours compared to control conditions. DGTS was significantly regulated at each time point of the stress and displayed an initial increase, followed by a decrease that in NgWT started after 1 hour but in NgΔ0-elo1-KO 6 hours after the temperature shift. Changes in the DGTS profiles correlated to changes in both MGDG and TAG (**figure 5.20, table 5.1**). Trends of up- or downregulation of glycerolipid classes was not conserved between *Nannochloropsis* and *Arabidopsis*. In the vascular plant, the shift from 20°C to 4°C led to a 44% induction of PG but we observed similar levels or reductions in *N. gaditana* upon the shift from 20°C to 10°C (Degenkolbe et al. 2012). Another important difference was the 11% reduction of MGDG and a change towards higher proportions of saturated fatty acids in *Arabidopsis*. Furthermore, neutral lipid accumulation was drastically induced in the cold

stressed plant and higher proportions of LC-PUFAs allocated into TAGs (Degenkolbe et al. 2012).

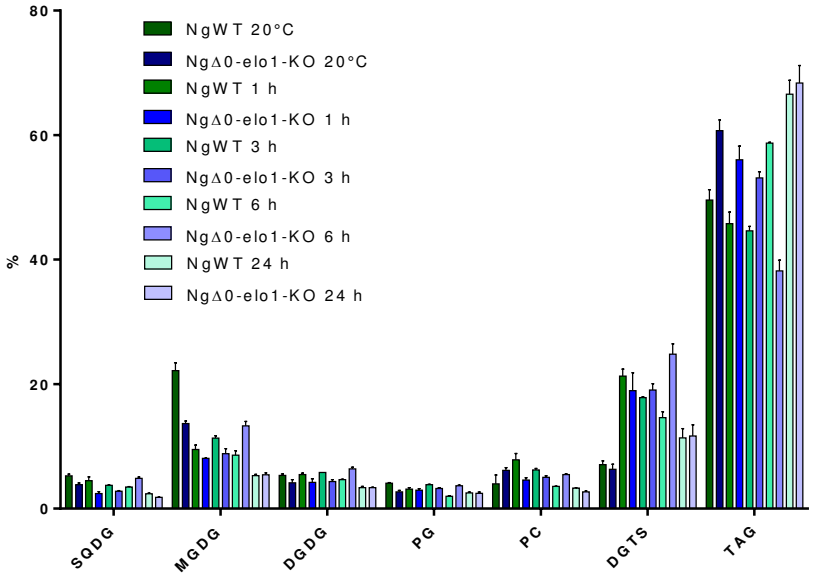

Figure 5.20. Analysis of glycerolipid classes from *Nannochloropsis* wild type (NgWT) and *Δ0-ELO1* knock out lines (NgΔ0-elo1-KO) grown at 10°C. Glycerolipids were extracted, and their cellular contents determined based on gas chromatography coupled to ion flame detection after fatty acid methyl ester separation. Lipid classes were analysed using high performance liquid chromatography coupled to tandem mass spectrometry (HPLC-MS/MS), as described in the Method section. The proportion of each lipid class is indicated. Error bars correspond to standard error of the mean (SEM, n = 3). NgWT is presented in shades of green, NgΔ0-elo1-KO in shades of blue. When grown at 20°C, significant changes in the KO compared to NgWT were at the level of PG (0.66, p-value 0.021), MGDG (0.61, p-value 0.004), SQDG (0.73, p-value 0.042) and neutral lipids (1.22, p-value 0.022) as described above (figure 5.13). For changes within a genotype during the experimental time see table 5.1.

Table 5.1. Statistical analyses of data presented in Figure 5.20. *Nannochloropsis* wild type (NgWT) and *Δ0-ELO1* knock out lines (NgΔ0-elo1-KO) grown at control conditions (20°C) or for 1, 3, 6 or 24 hours at 10°C. The glycerolipid class abundances were compared in NgWT and NgΔ0-elo1-KO grown at 20°C to the time points at 10°C, and differences between NgWT and NgΔ0-elo1-KO during cold stress were calculated. Significant changes are highlighted in yellow.

	NgWT 20°C /1 h 10°C				NgΔ0-elo1-KO 20°C /1 h 10°C				NgΔ0-elo1-KO/NgWT 1 h 10°C			
	20°C /1 h 10°C	p-value	Mean1	Mean2	20°C /1 h 10°C	p-value	Mean1	Mean2	20°C /1 h 10°C	p-value	Mean1	Mean2
SQDG	0.853	0.417	5.256	4.482	0.634	0.045	3.839	2.432	0.543	0.089	4.482	2.432
MGDG	0.428	0.002	22.163	9.486	0.591	0.002	13.658	8.076	0.851	0.226	9.486	8.076
DGDG	1.026	0.709	5.344	5.484	1.009	0.965	4.164	04. Feb	0.766	0.092	5.484	04. Feb
PG	0.765	0.063	4.086	3.126	1.098	0.496	2.699	2.964	0.948	0.686	3.126	2.964
PC	1.968	0.109	3.979	7.829	0.747	0.092	6.152	4.595	0.587	0.099	7.829	4.595
DGTS	3.021	0.003	7.045	21.285	2.996	0.014	6.321	18.934	0.89	0.433	21.285	18.934
TAG	0.923	0.258	49.575	45.772	0.923	0.191	60.7	56.049	1.225	0.039	45.772	56.049

	NgWT 20°C /3 h 10°C				NgΔ0-elo1-KO 20°C /3 h 10°C				NgΔ0-elo1-KO/NgWT 3 h 10°C			
	20°C /3 h 10°C	p-value	Mean1	Mean2	20°C /3 h 10°C	p-value	Mean1	Mean2	20°C /3 h 10°C	p-value	Mean1	Mean2
SQDG	0.714	0.038	5.256	3.753	0.73	0.023	3.839	2.804	0.747	0.005	3.753	2.804
MGDG	0.51	0.014	22.163	11.313	0.645	0.006	13.658	8.812	0.779	0.112	11.313	8.812
DGDG	1.086	0.187	5.344	5.803	1.048	0.741	4.164	4.365	0.752	0.036	5.803	4.365
PG	0.938	0.22	4.086	3.832	01. Feb	0.111	2.699	3.238	0.845	0.042	3.832	3.238
PC	1.563	0.258	3.979	6.22	0.82	0.089	6.152	5.042	0.811	0.038	Jun 22	5.042
DGTS	2.531	0.003	7.045	17.834	3.014	0.001	6.321	19.049	1.068	0.431	17.834	19.049
TAG	0.9	0.111	49.575	44.616	0.875	0.019	60.7	53.135	1.191	0.008	44.616	53.135

	NgWT 20°C /6 h 10°C				NgΔ0-elo1-KO 20°C /6 h 10°C				NgΔ0-elo1-KO/NgWT 6 h 10°C			
	20°C /6 h 10°C	p-value	Mean1	Mean2	20°C /6 h 10°C	p-value	Mean1	Mean2	20°C /6 h 10°C	p-value	Mean1	Mean2
SQDG	0.663	0.004	5.256	3.483	1.265	0.044	3.839	4.857	1.395	0.004	3.483	4.857
MGDG	0.387	0.002	22.163	8.583	0.972	0.676	13.658	13.28	1.547	0.01	8.583	13.28
DGDG	0.869	0.042	5.344	4.642	1.535	0.015	4.164	6.392	1.377	0.003	4.642	6.392
PG	0.487	0.001	4.086	1.989	1.361	0.02	2.699	3.672	1.847	0	1.989	3.672
PC	0.895	0.719	3.979	3.56	0.887	0.206	6.152	5.459	1.533	0	Mrz 56	5.459
DGTS	2.075	0.01	7.045	14.618	3.923	0.001	6.321	24.798	1.696	0.006	14.618	24.798
TAG	1.184	0.005	49.575	58.718	0.629	0.001	60.7	38.179	0.65	0	58.718	38.179

	NgWT 20°C /24 h 10°C				NgΔ0-elo1-KO 20°C /24 h 10°C				NgΔ0-elo1-KO/NgWT 24 h 10°C			
	20°C /24 h 10°C	p-value	Mean1	Mean2	20°C /24 h 10°C	p-value	Mean1	Mean2	20°C /24 h 10°C	p-value	Mean1	Mean2
SQDG	0.452	0.002	5.256	2.373	0.476	0.001	3.839	1.828	0.77	0.014	2.373	1.828
MGDG	0.24	0	22.163	Mai 31	0.398	0	13.658	5.439	1.024	0.734	Mai 31	5.439
DGDG	0.633	0.008	5.344	3.383	0.809	0.002	4.164	3.367	0.995	0.946	3.383	3.367
PG	0.615	0.003	4.086	2.514	0.913	0.011	2.699	2.464	0.98	0.85	2.514	2.464
PC	0.828	0.564	3.979	3.297	0.44	0.318	6.152	2.705	0.82	0.014	3.297	2.705
DGTS	1.611	0.119	7.045	11.35	1.844	0.147	6.321	11.653	1.027	0.903	Nov 35	11.653
TAG	1.343	0.012	49.575	66.569	1.126	0.016	60.7	68.369	1.027	0.641	66.569	68.369

5.4.4.1 The potential role of the "omega pathway" in *Nannochloropsis* homeoviscous adaptation

A rapid 40-60% drop of MGDG was observed one hour after the cold shift. DGTS levels increased concomitantly (**figure 5.20**). While in control samples and after 1 hour of cold stress DGTS abundances were similar in both genotypes, the betaine lipid increased stronger in NgΔ0-elo1-KO. The DGTS level peaked after 3 and 6 hours of incubation at 10°C in NgWT and NgΔ0-elo1-KO, respectively. At the 6 hour time point, DGTS levels were 1.7-fold (p-value 0.006) higher in the mutant compared to NgWT. This peak did not correlate with the lowest MGDG levels that were reached after 24 hours of cold incubation. By contrast, TAG was the lowest at six hours in NgΔ0-elo1-KO. The initial shift from MGDG to DGTS underlined the above-made assumption (**section 5.2.3**) that in *Nannochloropsis*, the betaine lipid could serve as a precursor for chloroplast lipid synthesis, similar to the role proposed for PC in higher plants (Roughan et al. 1980). In the early response to the cold stress TAG levels were reduced. After 24 hours, they are increased with similar levels in both genotypes. We speculate that reduced fatty acid allocation into TAGs contributes to the production of VLC-PUFAs that accumulate in DGTS and subsequently in all membrane lipids.

Based on these lipid profiles we assume that the pathway from DGTS to MGDG would be a rapid mechanism that could be readily controlled in response to stress triggers including low temperatures. Then, the sudden changes in the DGTS/MGDG balance would be attenuated by other processes*, e. g.* the relocation of fatty acids form TAGs to membrane lipids, or involving differential gene expression, especially desaturases. Thus, we propose that the betaine lipid plays a key role in the control of fatty acid flux into TAGs or chloroplast lipids, or in other words, to function in the "omega pathway" (**figure 5.1**). Such a role should be considered in future studies. Biosynthesis of the *Nannochloropsis* betaine lipid is currently investigated in the laboratory of Hiroyuki Ohta (personal communication Hiroki Murakami).

5.4.4.2 The possible roles of MGDG and VLC-PUFAs in the modulation of membrane viscosity

The specific reduction of MGDG in response to cold stress would be in agreement with the hypothesis that this HII lipid rigidifies membranes (Garab et al. 2000, 2016). As a consequence, MGDG would be reduced during homeoviscous adaptation in order to counteract cold-induced slowdown of lateral membrane fluidity. Since *N. gaditana* lacks C16- and C18-PUFAs, the introduction of more than two double bounds is restricted to C20 fatty acid species. Therefore, cold stress induced VLC-PUFA allocation into chloroplast lipids relies on the "omega pathway", with MGDG being the greatest sink (**figure 5.1**). PUFAs are beneficial for membrane viscosity and were found to be enriched during cold stress in other species (Inaba et al. 2003, Los et al. 1997, Panpoom et al. 1998). We therefore analysed the fatty acid profiles of the major glycerolipid classes after the shift from 20°C to 10°C (**figure 5.21**).

The sum of the masses of the two fatty acids esterified to glycero-polar heads is presented, except for TAGs, where the levels of the precise species are given. With the help of positional distributions estimated by trap-MS (**section 5.2.3**), the masses could be converted into actual fatty acid species, for easier understanding. C30 species found in SQGD and DGTS represent 16:x/14:0 couples. C32 species are combinations of 16:0 and 16:1. In glycolipids lipids, only 16:1/16:0 occurs, in PG 16:0/16:1 (where in the chloroplast form it is most likely 16:1-*trans* as observed in higher plants), in PC, DAG and DGTS 16:0/16:1 dominate over 16:1/16:1. C34 in MGDG and DGDG represents 20:5/14:0, while 16:x/18:x couples were found in PC. The high desaturation degree in DGTS C34 species together with the high abundances of VLC-PUFAs in GC-FID profiles (**section 5.2.3**) led us to the conclusion that also these C34 mass represents a 20:x/14:0 couple, but trap MS analyses for these minor species have to be confirmed. Since 18:x/18:x couples are absent from *N. gaditana* glycerolipids, all C36 species reflect a 20:5/16:x-couple and are found in chloroplast lipids and DGTS. C38 was absent from the *Eustigmatophyte*. Higher mass containing fatty acid couples were found in DGTS and MGDG and represented 20:5/20:5 and 20:5/20:4.

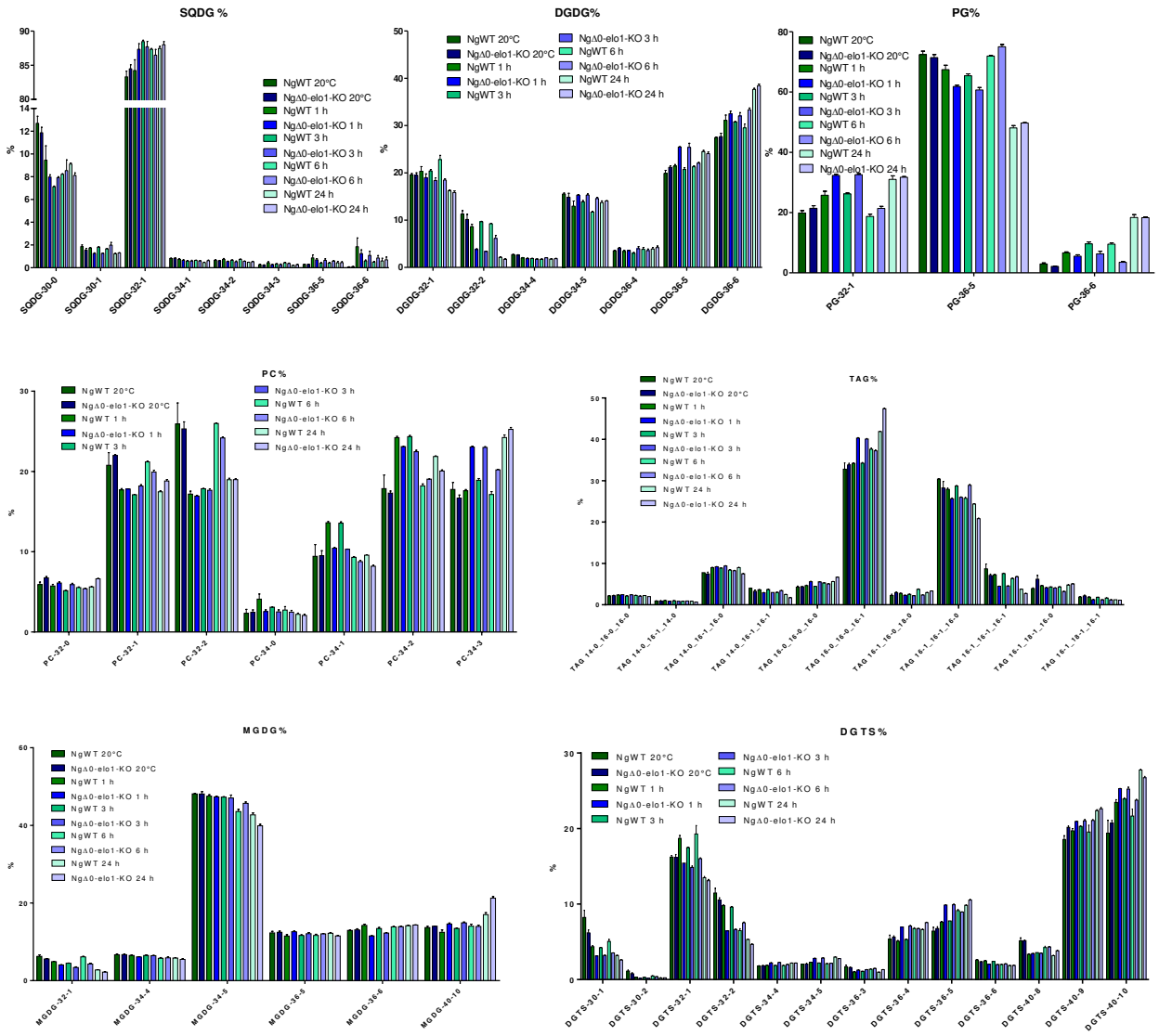

Figure 5.21. Analysis of glycerolipid fatty acid profiles from *Nannochloropsis* wild type (NgWT) and *Δ0-ELO1* knock out lines (NgΔ0-elo1-KO) grown at 10°C. Glycerolipids were extracted, and their cellular contents determined based on gas chromatography coupled to ion flame detection after fatty acid methyl ester separation. Lipid classes were analysed using high performance liquid chromatography coupled to tandem mass spectrometry (HPLC-MS/MS), as described in the Method section. The proportion of each lipid class is indicated. Error bars correspond to standard error of the mean (SEM, n = 3). NgWT is presented in shades of green, NgΔ0-elo1-KO in shades of blue. Significant changes see text.

Reduction of chloroplast lipids in response to the cold shift together with the subsequent increase of VLC-PUFA proportions in the different lipid classes maintained stable EPA levels during the time of cold acclimation in *N. gaditana*. Thus we have not observed a decrease in EPA contents in *N. gaditana* as it was reported for *N. oculata* (Ma et al.2011). Since the earlier study had not addressed glycerolipid class abundances, we would speculate that this reduction was also caused by a decline of MGDG and other chloroplast lipids.

Increased desaturations were observed in other photoautotroph species studied. The modified fatty acyl-chains differ in higher plants, cyanobacteria and *Chlamydomonas*, species that lack VLC-PUFAs. In vascular plants, the C16/C18 ratio increases in response to chilling temperatures and desaturation occurs mainly on C16 acyl chains (Li et al. 2015c). By contrast, cyanobacteria modify preferentially C18 acyl chains, with strong elevations of 18:3 (Chintalapati et al. 2007, Deshnium et al. 2000, Hongsthong et al. 2003). The eukaryotic green algae *Chlamydomonas* increases the abundances of unsaturated C16 and C18, but accumulate dienoic species instead of trienoic (Valledor et al. 2013). Trienoic fatty acids and all C18 species accumulate in very low quantities or are even absent from *N. gaditana*. C34 fatty acid species appeared to be more conserved than C32 species which were reduced proportional to an increase in C36 or C40 species. Thus fatty acid desaturation during cold acclimation in the Eustigmatophyte relies predominantly on the production of EPA. It would be interesting to investigate the cold stress response of *Phaeodactylum*, another Heterokont species. Similar to *Nannochloropsis*, the diatom accumulates high levels of EPA that allocates to chloroplast lipids (**section 3.3.2**). By contrast, *Phaeodactylum* MGDG is also enriched in 16:3 and 16:4, and these fatty acids are absent from other lipid classes. Except for a small proportion of MGDG-16:1-18:1, C18 species are restricted to endomembrane lipids in the diatom (**section 3.3.2**). Given this complicated lipid profile with high abundances of LC-PUFAs, we assume that the refined mechanisms of cold stress responses are not conserved among Heterokonts.

Stable VLC-PUFA levels during homeoviscous adaptation could indicate that from the fatty acid perspective, *Nannochloropsis* was already well equipped for cold habitats.

Indeed, water temperatures at the surface of oceans may be as cold as -2°C (http://sciencelearn.org.nz/Contexts/The-Ocean-in-Action/Science-Ideas-and-Concepts/Ocean-temperature, 18.08.2016). Gene modified yeast producing 18:2 were less sensitive to freezing damage but cell division rates were lower when grown at 15°C or 10°C, although membrane fluidity measured by 1,6-diphenyl-hexa-1,3,5-triene (DPH) fluorescence was higher compared to the WT (Rodríguez-Vargas et al. 2007). Considering that study, the increase of PUFAs during cold-acclimation could function as a preparation for freezing. Consistently, alga communities populating frozen surfaces are enriched in diatoms (Falk-Peterson et al. 1998). The increased PUFA proportions in cold-stressed *N. gaditana* could then be interpreted to compensate the loss of EPA caused by the reduction of MGDG and other membrane lipid classes. Albeit the rapid decline of MGDG in response to the shift to 10°C, fatty acid profiles appeared to be the most stable in the HII lipid. Only up from six hours, MGDG-32-1 and 34-5 declined with a concomitant increase in 40-10. These data on VLC-PUFA-rich *Nannochloropsis* supports the hypothesis that MGDG abundances play a key role in controlling membrane fluidity as proposed before (Garab et al. 2000, 2016). In order to further elucidate the specific role of MGDG in homeoviscous adaptation, we compared the responses of each glycerolipid class in detail in both NgWT and the MGDG-mutant NgΔ0-elo1-KO. Although with the drop of MGDG in response to the cold shock the differences in the glycerolipid profiles were less pronounced when compared to optimal conditions, we found the mutant to have accelerated modifications.

5.4.4.3 Accelerated cold stress induction in NgΔ0-elo1-KO compared to NgWT

At control conditions, the MGDG/DGDG ratio was 4.1 in NgWT and 3.3 in NgΔ0-elo1-KO. After cold stress, MGDG levels and the MGDG/DGDG ratio were similar in both genotypes. This was due to a 4.2-fold and 2.5-fold MGDG reduction in NgWT and NgΔ0-elo1-KO, respectively, together with 18% lower DGDG levels. Already up from the sudden drop after the cold shift, MGDG levels were similar in both genotypes. Nonetheless, detailed changes in glycerolipid profiles during short term cold acclimation

could indicate that the initial difference in the MGDG abundance accelerated homeoviscous adaptation in NgΔ0-elo1-KO.

5.4.5 *Glycerolipid profiles in N. gaditana cultures grown at 15°C*

Lipodomic analyses of *Nannochloropsis* cultures grown at 10°C revealed an earlier induction of cold-stress responses in NgΔ0-elo1-KO compared to NgWT. However, differences were small and lipid profiles were indistinguishable after 24 hours of incubation. We attempted to better point out the head start of the MGDG-mutant for homeoviscous adaptation by exposing cell cultures to mild temperature. To this end, we repeated the lipid profiling described above on cultures grown at 15°C.

In contrast to our expectations, physiological parameters as growth, *Fv/Fm* or qI were similar in both genotypes. After the shift from 20°C to 15°C, *N. gaditana* cells divided once more before the onset of a stationary phase at a concentration of 8.29×10^6 cells.mL^{-1} ± 0.98 (**figure 5.22 A**). At the same time under control conditions, inoculated cells experienced a lag phase but were still in exponential phase after 72 hours with 2-times higher concentrations compared to 15°C grown cells (**figure 5.22 A**).

Similarly to the observation of the response to 10°C, qE was further increased in NgΔ0-elo1-KO (**figure 5.22 B**). Mutant qE was about 1.2-fold higher under both cold stress conditions, compared to growth at 20°C. Despite this stronger NPQ, the cells were not importantly affected by the mild temperature stress.

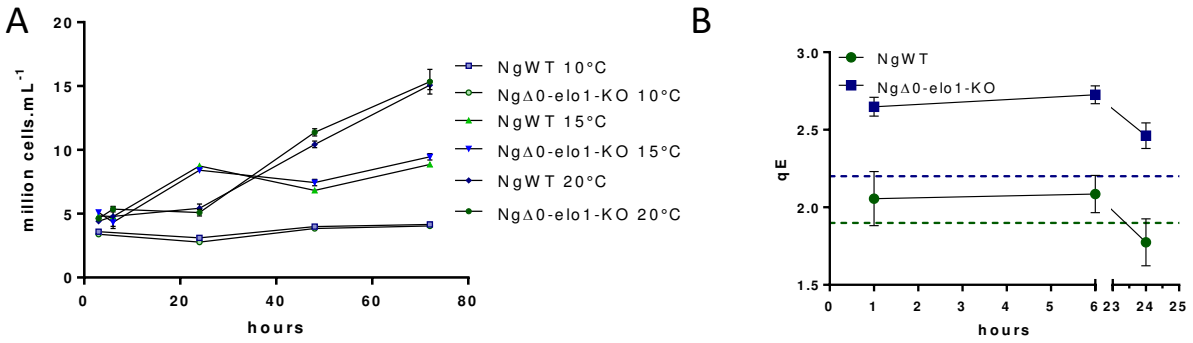

Figure 5.22 Cell growth and energy-dependent non-photochemical quenching (qE) in *Nannochloropsis* wild type (NgWT) and *Δ0-ELO1* knock out lines (NgΔ0-elo1-KO) grown at different temperatures. From triplicates of 2 mL cultures, 300 µL were taken for analyses after the shift from 20°C to 15°C at time points indicated. **A. Cell concentrations** were estimated *via* the absorption at 730 nm using a TECAN plate reader. **B. Chlorophyll fluorescence** kinetics was measured using a Speedzen MX fluorescence imaging system. NPQ was measured after dark incubation with light pulses of 600 µmol.m^{-2}.s^{-1} PAR for 17 minutes (qE). Mean fluorescence values were plotted over the time. Control qE is indicated in dashed lines in green for NgWT and blue for NgΔ0-elo1-KO. Error bars correspond to standard error of the mean (SEM, n = 3-9).

Lipids were extracted from *N. gaditana* WT and NgΔ0-elo1-KO after the shift from 20°C to 15°C, as performed in the cold stress study described in the above chapter. Compared to 10°C, growth at 15°C marginally impaired the distribution of glycerolipid classes (**figure 5.23**). The profiles in NgWT compared to NgΔ0-elo1-KO were not significantly altered. Also, within a genotype, glycerolipid remodelling during cold adaptation was only marginally affected, the only statistically difference being a progressive induction of DGTS in NgWT. Again, MGDG, DGTS and TAGs displayed the biggest differences, while SQDG, DGDG, PG and PC were conserved during incubation at 15°C. The mild temperature drop did not indicate a cold-stress phenotype in the MGDG mutant. The dominant increase of DGTS observed at both cold stress temperatures again underlines an important function of the betaine lipid in fatty acid remodelling. Besides the proposed role of DGTS in the "omega pathway", the head group of this endomembrane lipid might serve in cryoprotection since higher betaine

contents are associated with thermo-tolerant plant species (Kaniuga 2008). This hypothesis should be evaluated by measuring the cytosolic betaine concentration.

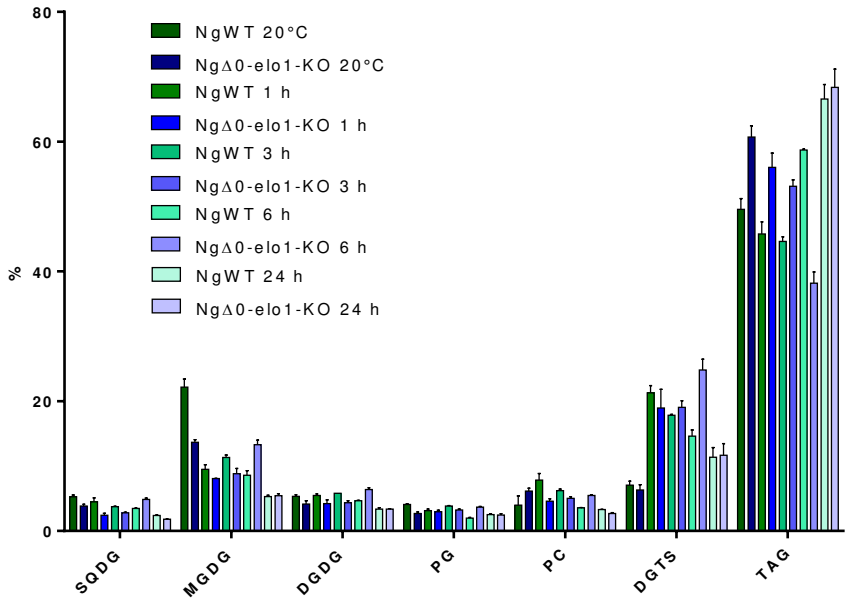

Figure 5.23 Analysis of glycerolipid classes from *Nannochloropsis* wild type (NgWT) and *Δ0-ELO1* knock out lines (NgΔ0-elo1-KO) grown at 15°C. Glycerolipids were extracted, and their cellular contents determined based on gas chromatography coupled to ion flame detection after fatty acid methyl ester separation. Lipid classes were analysed using high performance liquid chromatography coupled to tandem mass spectrometry (HPLC-MS/MS), as described in the Method section. The proportion of each lipid class is indicated. Error bars correspond to standard error of the mean (SEM, n = 3). NgWT is presented in shades of green, NgΔ0-elo1-KO in shades of blue. When grown at 20°C, significant changes in the KO compared to NgWT were observed at the level of PG (0.66, p-value 0.021), MGDG (0.61, p-value 0.004), SQDG (0.73, p-value 0.042) and neutral lipids (1.22, p-value 0.022) as described above (figure 5.13). In NgWT grown at 15°C compared to 20°C a 2.6 (p-value 0.004), 3.2 (p-value 0.011) and 3.7-fold (p-value 0.004) increase in DGTS was observed after 3 h, 6 h and 24 h, respectively. DGDG was 1.5 and PC 1.8-fold increased after 24 h. In NgΔ0-elo1-KO a 0.8-fold decrease in MGDG after 24 h was significant in t-test.

We analysed the fatty acid profiles of the different lipid classes in order to confirm higher desaturation degrees as observed for 10°C grown samples (**figure 5.24**). As

observed during incubation at 10°C, 15°C promoted the accumulation of PUFAs in all lipid classes when compared to the cultivation at 20°C. Again, MGDG appeared to have the most conserved fatty acid profile. When comparing the two genotypes, the higher desaturated C36 and C34 forms of MGDG, DGDG, SQDG, PG, PC, and DGTS were more abundant in NgΔ0-elo1-KO than in NgWT, with a concomitant decrease in the shorter chained, more saturated precursor molecules. This indicated that the induction of the cold-stress response was stronger in the MGDG-mutant compared to the NgWT. However, DGTS-40-9 and DGTS-40-10 as well as MGDG-40-10 levels were lower in the mutant after 3, 6 and 24 hours of incubation at 15°C. This deviation from the trend of temperature-dependent VLC-PUFA levels was not observed in 10°C grown samples. One possible explanation would be that at 15°C the Δ0-ELO1 would function in providing EPA to the chloroplast *via* the DGTS-dependent "omega pathway". To test this, qPCR analyses are indispensable and will be involved in future experiments.

Taken together, these results confirm the trend of increased PUFA-proportions in the different glycerolipid classes, as observed as a common cold stress response in poikilotherm organisms (Los & Murata 2004, Mikami & Murata 2003). However, the total cellular EPA contents were not increased in cold-stressed *N. oculata* (Ma et al. 2011) or *N. gaditana*. In our study, EPA levels remained stable over the time at cold incubation due to a relative increase in the different membrane lipid classes but a strong reduction in the major EPA-sink, MGDG. We therefore assume the Eustigmatophyte to be pre-equipped for cold environments by their fatty acid profile, and agree with the speculation on a negative role of MGDG in the regulation of membrane fluidity (Garab et al. 2000, 2016). We conclude that reduced MGDG levels in NgΔ0-elo1-KO accelerated the cold-stress response when compared to NgWT.

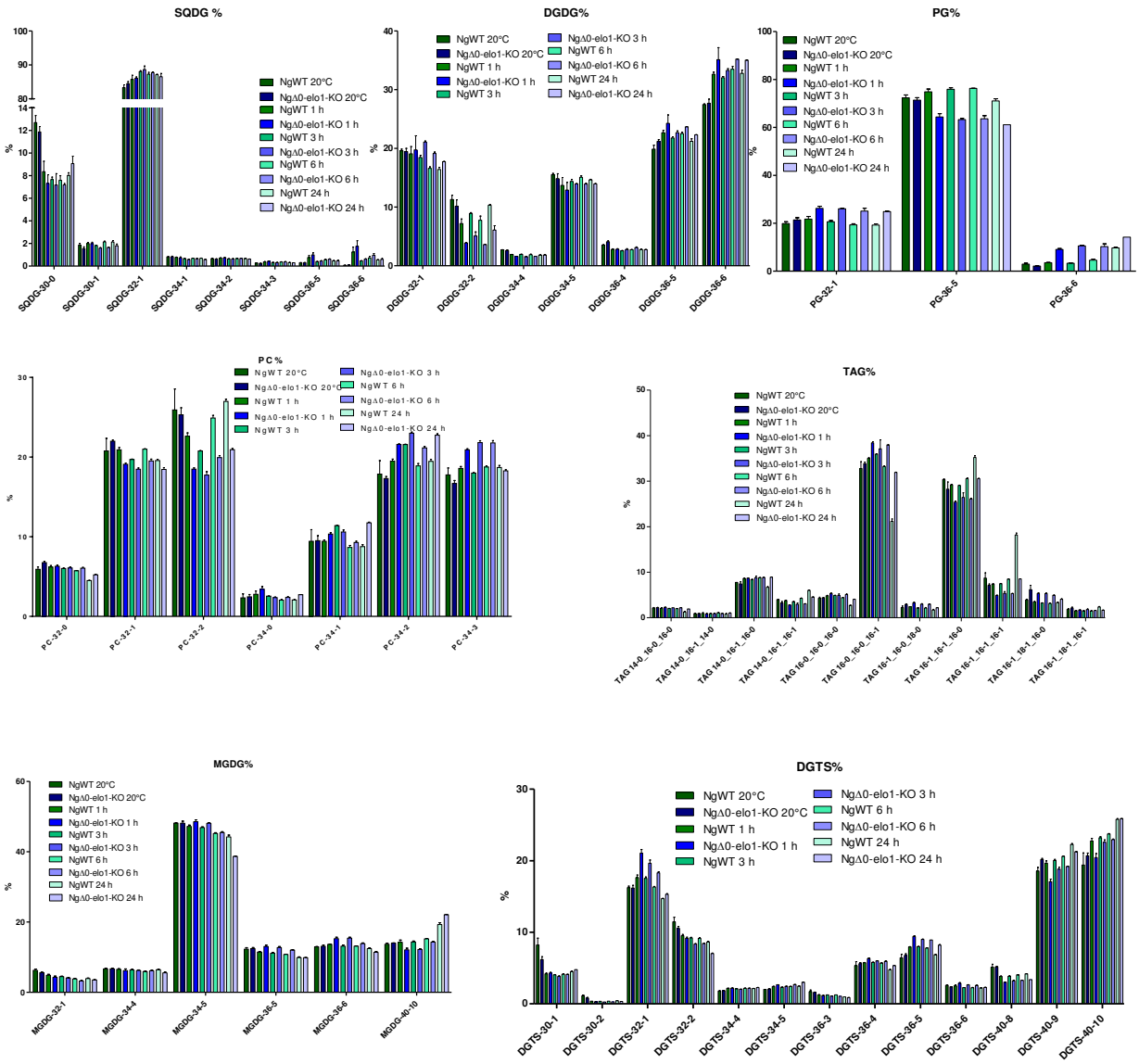

Figure 5.24. Analysis of glycerolipid fatty acid profiles from *Nannochloropsis* wild type (NgWT), and Δ0-ELO1 knock out lines (NgΔ0-elo1-KO) grown at 15°C. Glycerolipids were extracted, cellular contents determined based on gas chromatography coupled to ion flame detection after fatty acid methyl ester separation by, and lipid classes were analysed using high performance liquid chromatography coupled to tandem mass spectrometry (HPLC-MS/MS), as described in the Method section. The proportion of each lipid class is indicated. Error bars correspond to standard error of the mean (SEM, n = 3). NgWT is presented in shades of green, NgΔ0-elo1-KO in shades of blue.

6 DISCUSSION AND CONCLUSION

Lipid remodelling in Phaeodactylum *and* Nannochloropsis

Phaeodactylum and *Nannochloropsis* are model species for glycerolipid research. Most of the studies have focused on increasing the level of neutral lipids or VLC-PUFA for biofuel or pharmaceutical application. Although much effort has been put, only recently an engineered *Phaeodactylum* strain was evaluated to meet the demands for commercialization (Hamilton et al. 2016). The present study aimed to give insights into biological functions associated with changes in glycerolipid profiles in the two Heterokont species. We have addressed changes in *P. tricornutum* glycerolipid profiles induced by phosphate or nitrogen starvation (**section 3.3.2**), and built the base to study enzymes involved in membrane lipid synthesis *via* the characterization of antisense lines (**section 3.3.3** and **7.2.2**).

In our referential analysis of the effects of nutrient availability in the environment, we have observed a quicker response to limitation in nitrogen than to phosphate, in accordance with the finding that phytoplankton species were able to reduce cellular phosphate contents by 50% without suffering from fitness reduction (Feng et al. 2015). Interestingly, while phospholipids were recycled during phosphate depletion, nitrogen-containing lipids such as PC, PE and DGTA were conserved during nitrogen starvation (**section 3.3**). Phosphate deprivation led to an increase in the *Phaeodactylum* betaine lipid DGTA proportional to the decrease in PC, while DGDG increased proportionally to the decline of PG. This tempted to speculate that the galactolipid replaced the chloroplast phospholipid (Jouhet et al. 2004, Kelly & Dörmann 2002, Kelly et al. 2003) and the betaine lipid endomembrane phospholipids (Sato & Murata 1991). From comparisons of the fatty acid couples bond to PC, DGTA, MGDG, DGDG and TAG we propose that C18-rich DGTA would replace phospholipids in the endomembrane system (**section 3.3.3.3**). Since the increase in DGTA was observed earlier than the rebalance of DGDG and PG we assume a higher conservation of chloroplast lipids probably to maintain primary production. Then, DGDG is induced most likely due to the increased activity of the third DGD isoform, DGD3.

We characterized antisense lines of the three DGD synthase isoforms encoded in the *Phaeodactylum* genome. All three seem to be involved in DGDG synthesis but the reduced enzyme levels appeared to be rescued by increased substrate availability. Hence, DGDG levels were unaltered in mutant lines but MGDG accumulated (**section 3.3.3.3**). Important morphological alterations were observed when cells were grown under nutrient repleted conditions but odd-shaped cells were outsourced when an additional selection pressure was applied by phosphate deprivation. Due to the inconveniences coming with the antisense method (**section 2.1.3.3**), the question of lipid remodelling in response to phosphate starvation should be addressed via targeted gene knock out or alternatively in *N. gaditana* since it allows homologous recombination and encodes only one DGD.

We found that a stress condition inducing lipid accumulation could involve the second messenger NO• for cell-to-cell signalling (the signal coming from outside the cell,

applied as SNAP) and retrograde signalling from the chloroplast (overexpression of NOA), the organelle that is commonly sensitive to stresses that change the redox state of the cell (Sewelam et al. 2016). The genetic approach compared to the chemical treatment had the advantage that cell division was maintained. Indeed, while in chemical engineering approaches including nutrient limitations TAG accumulation is usually accompanied by growth arrest, this might be overcome by genetic engineering. Eventually, deciphering the regulatory network controlling the connection of the cell cycle and storage lipid production, could allow uncoupling of the two processes. To our knowledge, the role of ubiquitous second messenger such as calcium, ROS or reactive nitrogen species have not yet been addressed in Heterokonts.

The NO• signatures triggering TAG synthesis in *P. tricornutum* were however ineffective or even having a negative effect on neutral lipid levels in *N. gaditana* (**section 4.5.3**). It is therefore likely that different regulatory processes are involved in the control of fatty acid fluxes. Similarly, while for the *Eustigmatophyte* nitrogen starvation was reported to involve an important fraction of lipid remodelling (Simionato et al. 2013), the vast majority of *Phaeodactylum* TAGs derived from *de novo* synthesis (**section 3.3.2**). Another significant difference between the two Heterokont species is the number of galactolipid synthase isoforms. While the diatom encodes three putative isoforms of each, MGD and DGD, these are single copy genes in *N. gaditana*.

The "omega cycle"

In all experiments performed on *Nannochloropsis* WT, proportions of MGDG and DGTS on the one hand and MGDG and TAG on the other hand appeared in a tight balance. In 21 independent NgWT cultures gown under continuous light under different temperature regimes, the average sum of MGDG and DGTS was 60.1 % ± 5.9 (**section 5.4.4**). Similarly, DGTA and MGDG were balanced in in *Phaeodactylum* WT and DGDas lines together representing 72.8% ± 7.0 of all membrane lipids when grown in full media and 74.7% ± 7.3 of all membrane lipids under when grown under phosphate starvation (**section 3.3.3.3**). Similarly, in a study comparing *N. gaditana* grown at low

light, medium light and high light, DGTS plus MGDG made 40-50% of all glycerolipid classes while the proportions of MGDG were reduced with increasing light intensity. Moreover, during high light, the relative abundance of 20:5 was upregulated in MGDG and by the same extent reduced in DGTS (Alboresi et al. 2016). We therefore suspect DGTS to be involved in the elusive "omega pathway". Notably, the balance may be disturbed by genetic engineering such as the overexpression of NOA (**section 4.4**), knock down of DGDG synthases (**section 3.3**) or knock out of a Δ0-elongase (**section 5.2.3** and **section 5.4**).

The term "omega pathway" was introduced by our group to describe those chloroplast lipid species where at least one fatty acid must have undergone ER modifications and hence do not fit in the "prokaryotic" or "eukaryotic" discrimination applied for plants (Petroutsos et al. 2014). Importantly, desaturases but not elongases are present in the chloroplast (**section 5.2.1**). The fatty acid profile of the most common MGDG species comprised a potentially "prokaryotic" fatty acid at *sn*-2 and an "omega pathway" derived VLC-PUFA at *sn*-1 (Domergue et al. 2002, **section 2.7**). Based on different results obtained in the present study, we broadened our view on Heterokont fatty acid trafficking and speculate on an existence of an "omega cycle" (**figure 6.1**).

We propose that the fate of the fatty acid that is trafficked from the chloroplast to the ER is determined at the earliest level. Either, it is incorporated into neutral lipids, or it enters acyl-editing reaction chains taking the "omega route". This assumption is based on the predominance of 14:0, 16:0 and 16:1 species in TAGs in both *Phaeodactylum* (**section 3.3.2**) and *Nannochloropsis* (**section 5.2.2** and **5.4.4**). Notably, C18 species might probably not be exported from the chloroplast of species derived from the red lineage (personal communication Naoki Sato). Moreover, knock out of a Δ0-elongase isoform in *N. gaditana* specifically affected TAG and MGDG levels (**section 5.2.3**). When expressed in yeast, NgΔ0-ELO1 was able to induce elongation of even and odd chain saturated fatty acids with a minimal length of 15 carbon atoms. Interestingly, the transgene controlled a switch from fatty acyl-precursors used for sphingolipid synthesis in the ScWT towards the accumulation of saturated fatty acids up to 31:0 (**section 5.2.3**). Hence, the *N. gaditana* Δ0-elongase has the potential to redirect fatty acid fluxes.

The activity of a Δ0-elongase would be the first ER protein in the "omega cycle" (**figure 6.1 A**). Its catalytic product could then serve as a substrate for VLC-PUFA production being part of the "omega cycle". The elongation and desaturation chain for the production of EPA (or DHA) might have several "exits" allowing the synthesis of endomembrane lipids. Indeed, in contrast to plants where acyl-editing occurs on lipid-linked substrates, microalgae may modify FFAs or thioester-bound acyl chains (Domergue et al. 2005, Hoffmann et al. 2008, Sayanova et al. 2012, Vaezi et al. 2013). At the end of the VLC-PUFA production route we propose the betaine lipid to play a central role in *N. gaditana* and in *Phaeodactylum*. This is because the fatty acid profile of DGTS in *Nannochloropsis* resemble those found in MGDG and DGDG, whereas C36 and C40-couples are absent from PC (**section 5**). This is not the case of *Phaeodactylum* DGTA when the fatty acid profiles observed under optimal growth conditions were compared (**section 3.3.2**). However, the distinct regulation observed under phosphate starvation point that the betaine lipid would serve as an EPA-donor for galactolipid synthesis (**section 3.3.3**). From PC or DGTS, a VLC-PUFA-rich lipid precursor or a FFA would be imported back into the chloroplast *via* the "omega pathway" (**figure 6.1 A**).

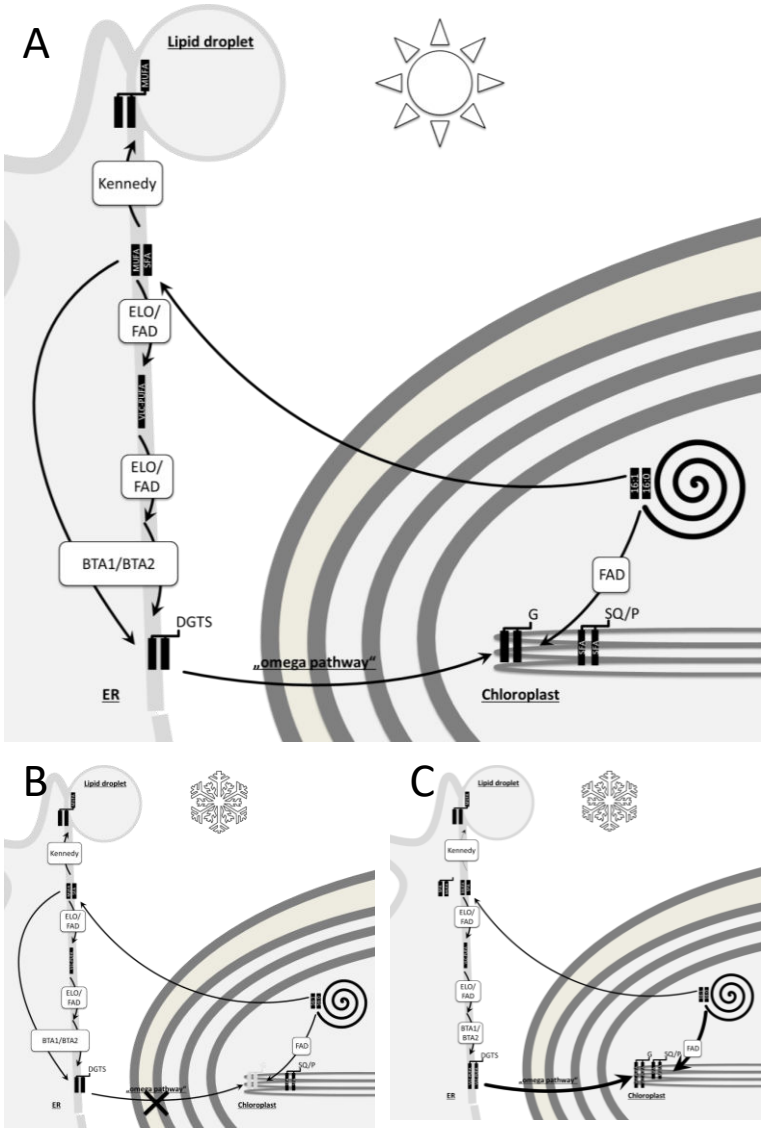

Figure 6.1 Hypothetical model of the role of DGTS in an "omega cycle" (A) and remodelling upon cold shock (B), and during homeoviscous adaptation (C) in *Nannochloropsis gaditana*. Fatty acid (FA) synthesis in the stroma generates saturated (SFA) or monounsaturated (MUFA) C16 species. These are exported for ER editing or retained in the chloroplast for the "prokaryotic pathway". Exported C16 are used for the production of TAGs *via* the Kennedy pathway, possibly involving PC or DGTS intermediates. Alternatively, FAs enter the "omega cycle". They are elongated and desaturated (ELO/FAD) to very long chain polyunsaturated FAs (VLC-PUFAs). Betaine lipid synthases (BTA1/BTA2) produce DGTS. Based on comparisons of the FA profiles, DGTS could be at the base for FA trafficking from the ER membrane into the chloroplast *via* the elusive "omega pathway". This route is probably temperature-regulated in order to maintain membrane fluidity in a process called homeoviscous adaptation. **A. Under optimal temperatures**, the bulk part of *N. gaditana* galactolipids (G) comprise one prokaryotic fatty acid (FA) edited by chloroplast located desaturases (FAD), and one FA derived from the "omega pathway". Most SQDG (SQ) and PG (P) contain SFAs. **B. The first response to cold stress** is the drop of MGDG and an increase in DGTS. Possibly, a step in the DGTS to MGDG FA trafficking is readily inhibited. **C. During the early acclimation phase**, fewer FAs are channelled into TAGs but provided for ELO/FAD. Produced VLC-PUFAs are found in DGTS and G. Hence, in G, the "prokaryotic"/"omega" FA ratio is reduced. The MUFA/SFA ratio increases in SQ and P, possibly involving chloroplast FADs. Higher desaturation levels increase membrane fluidity to counteract cold-induced rigidification.

We have challenged this working model of the "omega cycle" in studies on the cold stress response in *N. gaditana* (**section 5.4**). After cold shock, a drop in MGDG and an accumulation of DGTS was observed (**figure 6.1 B**). This could involve a regulatory switch inhibiting the DGTS-to-MGDG transfer. During homeoviscous adaptation caused by prolonged low temperature cultivation, changes in the protein equipment would reinforce the "omega cycle" in order to increase the proportions of VLC-PUFAs in chloroplast lipids (**figure 6.1 C**). The proposed model is based on changes in MGDG and DGTS abundances and all membrane lipid fatty acid profiles observed during incubation at 10°C of 15°C (**section 5.4.4**).

When we compared the induction of unsaturations in the time courses at 10°C or 15°C, we found a stronger response in the MGDG mutant Δ0-elo1-KO compared to NgWT. During growth at 10°C, changes in the fatty acid couples were induced earlier in NgΔ0-elo1-KO but resulted in similar levels after 6 or 24 hours of incubation. Growth at 15°C revealed stronger induction of desaturases and elongases in the MGDG-mutant except for a noticeable lack of EPA increase probably attributed to increased Δ0-ELO1 function. In response to the lower temperature, other elongases might have compensated the loss of Δ0-ELO1 in NgΔ0-elo1-KO. Analyses of desaturase and elongase protein abundances are indispensable for better understanding of the differential regulations in the two genotypes. Nonetheless, the lipid profiles already demonstrated a head start of NgΔ0-elo1-KO in homeoviscous adaptation and thus point an important regulatory function of MGDG in this stress response. Therefore we propose MGDG signals to be involved in the regulation of the "omega cycle".

The role of MGDG in thylakoid membranes

MGDG profiles were not affected by nutrient deprivation or in DGDas lines in *Phaeodactylum* (Abida et al. 2015, **section 3**), nor by a mutation in a 16:0-elongase (**section 5.2.3**) or temperature stress (**section 5.4.4**) in *N. gaditana*. One may hence rule out a specific conservation of the hexagonal-II phase lipid. Since the properties of maintaining MGDG in the bilayer phase of membranes also depends on their fatty acid

profiles (Baczynski et al. 2015) we assume that a tightly control of MGDG is required to maintain membrane integrity.

VLC-PUFA-rich MGDG located in the thylakoids is likely to be prone to oxidative damage, *e.g.* by PSII derived electrons that are not quenched *via* photochemistry or photoprotection. When cells were grown at high light, MGDG levels were reduced in *N. gaditana* but the expression of MGD was induced (Alboresi et al. 2016). This would indicate a higher turnover of this galactolipid. The high light response reflects insufficient electron sinks, and under prolonged irradiation induces metabolic changes (Eberhard et al. 2008). Sudden nutrient deprivations causing cell cycle arrest also reduce cellular energy sinks and then redirect fluxes into storage lipid production (**section 3.3.2**). One could therefore speculate that MGDG could act as a sensor for the electron transfer capacity and that liberated oxidized fatty acids could serve in redox stress signalling. Although no lipoxygenase protein was found in Heterokonts, those phytoplankton species are sensitive to oxylipin signalling (**section 4.3**). MGDG oxidation would furthermore serve in alternative energy quenching.

Indeed, the role of MGDG for NPQ described in the literature must be reconsidered. On the one hand, in *in vitro* analyses a certain amount of MGDG was required for the onset of NPQ, and plant MGDG mutants were affected in this photoprotection pathway (**section 2.3** and **5.2.3**). On the other hand, at least in microalgae from the red and the green lineage, MGDG levels were reduced (or the turnover was higher) at NPQ-triggering conditions (Lepetit et al. 2012, **section 5.2.3, 5.4.3**, personal communication Christian Pfaff). In diatoms, an MGDG "shield" was observed to surround FCP complexes (**figure 2.11**) (Goss & Lepetit 2015). In these pigment containing proteins, light harvesting but also energy quenching takes place and involves protein aggregation (Horton 2012). MGDG could therefore function in stabilizing a low aggregation state of PSII antenna proteins. Reduction of the HII lipid could alter the membrane homeostasis towards facilitated aggregation possibly involving higher membrane fluidity for facilitated protein motility (Garab et al. 2000, 2016).

Towards the aim of boosting neutral lipid contents for biofuel, or redirecting VLC-PUFAs into TAGs for pharmaceutical applications, we believe that a fundamental understanding of the underlying processes is indispensable. The present study points a complicated interplay of the pathways determining a fatty acids' fate, involving NO• and probably redox signals that possibly involve MGDG. We propose the presence of an "omega cycle" that controls fluxes of fatty acids that were trafficked from the chloroplast into the ER into neutral lipids via the Kennedy pathway or the "omega route" of VLC-PUFA production, part of which are reimported into the chloroplast.

7 MATERIAL AND METHODS

7.1 *Phaeodactylum* and *Nannochloropsis* strains and culture conditions

7.1.1 *Strains*

Phaeodactylum tricornutum wild type (WT) strain Pt_1 (CCAP 1055/3) was obtained from the Culture Collection of Algae and Protozoa (CCAP). *Nannochloropsis gaditana* wild type CCMP526 (NgWT) was obtained from Pravosali-Guillard National Center for Culture of Marine Phytoplankton (CCMP). Cultures were handled sterile at all times.

7.1.2 *Culture conditions*

7.1.2.1 Culture media (ESAW and F/2)

P. tricornutum strains were cultured in Enriched Seawater, Artificial Seawater (ESAW) based on containing modified sea salts (NaCl, 21.194 $g.L^{-1}$; Na_2SO_4, 3.55 $g.L^{-1}$; KCl, 0.599 $g.L^{-1}$; $NaHCO_3$, 0.174 $g.L^{-1}$; KBr, 0.0863 $g.L^{-1}$; H_3BO_3, 0.023 $g.L^{-1}$; NaF, 0.0028 $g.L^{-1}$; $MgCl_2.6H_2O$, 9.592 $g.L^{-1}$; $CaCl_2.2H_2O$, 1.344 $g.L^{-1}$; and $SrCl_2.6H_2O$, 0.0218 $g.L^{-1}$; $NaNO_3$, 46.67 $mg.L^{-1}$ and NaH_2PO_4, 3.094 $mg.L^{-1}$), vitamins (vitamin H, 1 $mg.L^{-1}$; vitamin B12, 1 $mg.L^{-1}$; 0.2 $g.L^{-1}$), trace metals ($Na_2EDTA•2H_2O$, 3.09 $mg.L^{-1}$; $ZnSO_4•7H_2O$, 73 $\mu g.L^{-1}$; $CoCl_2•6H_2O$, 16 $\mu g.L^{-1}$; $MnCI_2•4H_2O$, 540 $\mu g.L^{-1}$; $Na_2MoO_4•2H_2O$, 1,48 $\mu g.\ L^{-1}$; Na_2SeO_3, 0.173 $\mu g.\ L^{-1}$; $NiCI_2•6H_2O$, 1.49 $\mu g.\ L^{-1}$; $CuSO_4•5H_2O$, 9,8 $\mu g.L^{-1}$ and Fe-EDTA, 3 $mg.L^{-1}$) (Berges et al. 2001) or enriched ESAW containing 10 times more nitrate and phosphate resources, namely 466.7 $mg.L^{-1}$ $NaNO_3$ (10N) and respectively 30.94 $mg.L^{-1}$ NaH_2PO_4 (10P). Full, enriched ESAW media was thus designated as 10N10P, nitrogen depleted media 0N10P and phosphate depleted media 10N0P. *N. gaditana* was cultured in 10N10P ESAW or with the substitution of F/2 trace metals ($Na_2EDTA•2H_2O$, 4,36 $mg.L^{-1}$; $ZnSO_4•7H_2O$, 22 $\mu g.L^{-1}$; $CoCl_2•6H_2O$, 10 $\mu g.L^{-1}$; $MnCI_2•4H_2O$, 180 $\mu g.L^{-1}$; $Na_2MoO_4•2H_2O$, 6,3 $\mu g.\ L^{-1}$; $CuSO_4•5H_2O$, 10 $\mu g.L^{-1}$ and FeCl3•$6H_2O$, 3.15 $mg.L^{-1}$) (Guillard & Ryther 1962). For solid media, 1.5% agar (ROTH) was added. Antibiotic selection of transformants was achieved by adding 100 $\mu g.mL^{-1}$ and 7 $\mu g.mL^{-1}$ zeocin (Promega) into the media for *P. tricornutum* and *N. gaditana*, respectively.

7.1.2.2 Culture conditions for batch and solid cultures

Depending on the experiment, microalgae cells were cultivated in different scales from 500 µL cultures on 48 well plates (Thermo Fisher), 1 mL or 2 mL cultures on 24 well plates (Thermo Fisher) containing a glass bead (ROTH) to facilitate aeration, 10 mL cultures in 25 mL Erlenmeyer flasks and 20-100 mL cultures in 250 mL Erlenmeyer flasks. Liquid cultures were incubated at 20°C (if not indicated otherwise) under gentle

agitation (Infors incubator, 100 rpm) and with a light regime of either 12/12 h dark/night cycle (*P. tricornutum* and *N. gaditana*) or continuous irradiation (*N. gaditana*), with a photon flux of 30 µmol.$m^{-2}s^{-1}$ white light (Neon bulbs). For batch culture maintenance, a part of the pre-existing culture was transferred to fresh medium twice per week with an inoculum size of 10^6 cells.mL^{-1} for *P. tricornutum* and 2-4.10^6 cells.mL^{-1} for *N. gaditana*, respectively. Cells on solid ESAW10N10P media were incubated under constant dim light irradiation with monthly subculturing.

7.1.2.3 Cryopreservation

For long time storage at -80°C, 10^7 cells were stepwise frozen (30 min at 4°C, 60 min at -20°C) in 15% dimethyl sulfoxide (DMSO, SIGMA) diluted in ESAW or ESAW10N10P. To start a new culture from a stock, 200 µL of room temperature ESAW10N10P was added to the frozen suspension and quickly 1000 µL were transferred into 20 ml ESAW10N10P media. The Erlenleyer flask was incubated for about three weeks before cells recovered from the stress and started growing again. While only one out of two *P. tricornutum* cultures recovered from freeze-thawing, a 100% recovery rate was observed for *N. gaditana* samples.

7.2 Molecular biology

7.2.1 *Genomic DNA extraction from microalgae*

For cloning purposes, genomic DNA (gDNA) was extracted from *P. tricornutum* and *N. gaditana* according to Edwards et al 1991 (Edwards et al. 1991). A 100 mL wild type culture was harvested (5,000 rpm, 7 min, 4°C), transferred to a 1.5 mL Eppendorf tube and remaining supernatant was removed by centrifugation. The cell pellet was grinded in 200 µL extraction buffer (200 mM Tris-HCl, pH 7; 250 mM NaCl; 25 mM ethylenediaminetetraacetic acid (EDTA); 0.5% sodium dodecyl sulphate (SDS)) using a hand-potter. Another 200 µL of buffer were added and cell debris removed upon

centrifugation (full speed, 5 min, RT). DNA was precipitated in 1 volume of isopropanol (full speed, 30 min, 4°C), the pellet washed with 75% ethanol (full speed, 5 min, 4°C) and air dried prior to resuspension in water. Concentrations were measured using a NanoDrop 2000c (Thermo Fisher).

To perform quantitative real time PCR (qPCR) on *N. gaditana* gDNA, clean extracts were obtained by using the chloroform-phenol method (Pacific Biosciences of California, Inc, 2012). Cells were harvested upon centrifugation (full speed, 5 min, RT) and the supernatant discarded. Cells were grinded using a hand potter. An equal volume of phenol/chloroform/isoamyl alcohol (25:24:1) solution was added and thoroughly mixed with a vortex for one minute. Phases were then separated by centrifugation (full speed, 5 min, RT). The supernatant was transferred into a new tube and an equal volume of chloroform/isoamyl alcohol (24:1) was added, phases separated and the aqueous phase collected, as above. DNA was precipitated, washed and quantified as described in the above protocol.

7.2.2 *Generation of constructs for transformation of P. tricornutum and N. gaditana*

7.2.2.1 Cloning methods

All molecular biological constructions realized in this study relied on classic cloning strategies, if not stated otherwise. From a genomic DNA template, the gene of interest was amplified using the proof reading Phusion® High-Fidelity DNA Polymerase (NEB). Colony-PCRs were performed with EuroTaq DNA Polymerase (BioCat). All oligonucleotides (Eurofins Genomics) for cloning purposes were designed in order to have a melting temperature of 59°C and were used in a 10-cycle touch-down polymerase chain reaction (PCR) from 65°C to 55°C prior to 23-cycles with an elongation temperature of 55°C. DNA concentrations and purity were determined photometrically using a NanoDrop 2000c (Thermo Fisher). Vectors or amplified and gel-purified (NucleoSpin ® Extract II Kit, Macherey-Nagel) DNA were digested with restriction enzymes (NEB) estimating an efficiency of 1 µg per hour at 37°C. Vector and insert

DNAs were ligated overnight by leaving the samples on melting ice using a vector/insert ratio of 1:3 with maximal 120 fmol of total nucleotide quantity. BL21 *Escherichia coli* cells were transformed with the ligation mix *via* heat shock, and clones containing the vector-mediated resistance were selected on antibiotic plates. After an overnight incubation, positive clones were verified by colony-PCR. Plasmids were isolated from 4 mL overnight cultures of positive clones (NucleoSpin ® Plasmid Quick Pure, Macherey-Nagel) and validated by sequencing (Eurofins Genomics).

7.2.2.2 Gene expression in *P. tricornutum* using the pH4-GUS-AS vector

Genetic constructs to transform *P. tricornutum* were based on the pH4-GUS-AS (pH4) vector (De Riso et al. 2009). Vector map and sequence are given in **appendix 8.4.1**. It should be noted that the *Xho*I restriction site is mutated in the vector we have obtained from Angela Falciatore, Paris, France. Thus, all inserts for this vector were cloned using *Xba*I on the 5'-end and *EcoR*I on the 3'-end, thereby removing the GUS-AS sequence. Transformed *P. tricornutum* will express a fusion protein consisting of the zeocin-resistance gene and the inserted DNA sequence from the vector, which is supposed to improve silencing efficiencies in antisense lines.

In this work, antisense constructs of putative *P. tricornutum* genes involved in glycerolipid metabolism were generated, namely against: AAS, ATS1, ATS2, DGD1, DGD2, DGD3, MGD1, MGD2, MGD3, PLDζ, SFR2, SQD1, SQD2 and SQD2-like (**table 7.1**). The endogenous *P. tricornutum* NOA sequence as well as codon-optimized *N. gaditana* NOA (see below) was cloned into pH4 for overexpression. Oligonucleotides used for amplification from *P. tricornutum* gDNA fragments that were inserted into pH4 are listed below with indications of the Protein ID and manual annotation (**table 7.1**). All constructs were verified by sequencing. Vector specific oligonucleotides used in colony-PCR or sequencing were hybridizing with the promotor (5'-TATCCCAGGAAACCTACGGC-3') and terminator (5'-CTCACTGAAAGTGTCCCAGC-3') region of the sense strand in forward and reverse orientation, respectively.

Table 7.1. Oligonucleotide couples used for *P. tricornutum* constructs

Protein ID	Protein annotation	*EcoR*I primer (promotor end) in 5'- to -3' orientation	*Xba*I primer (terminator end) in 5'- to -3' orientation
Phatr_12420	AAS	TTTGAATTCTGGCTTATGGACTGACGGAA	TTTTCTAGAGGTTTCGGCCACATCTTTGT
Phatr_3262	ATS1	AAAGAATTCGCTCGTCCATCGGATCCTTA	TCTAGAAAAGCCGTCATGTACTCGTTGAC
Phatr_43099	ATS2	TTTGAATTCGCTGTTTCCGTCTTTACGGG	TTTCTCGAGGCTGTTTCCGTCTTTACGGG
Phatr_12884	DGD1	AAAGAATTCACACGGATCGTTGGGAAGC	AAACTCGAGGCTCAAACCTGCCGTCATC
Phatr_11390	DGD2	TTTGAATTCGTGTCGTGCACACTGTCATC	TCTAGATTTAGCGACCCTAATCCTTTTGAC
Phatr_43116	DGD3	TTTGAATTCCAGCTCCACACAAACTACGG	TCTAGATTTAGTTTCGGACTTTCGTTGGG
Phatr_14125	MDG1	TTTGAATTCGTCTGGGTGTTGCTTTAGGC	TCTAGATTTGCATGCAAGGTAGTCCACAG
Phatr_54168	MGD2	AAAGAATTCACGTACCCATGAAAAGCGTC	TCTAGAAAAAGTGAACAGCAAAGTCGTGG
Phatr_9619	MDG3	AAAGAATTCCGGCTGGTTTAGAAATGGCG	AAATCTAGAGTGCCGAAAGGTGCTTGTAT
Phatr2 56150	NOA	TTTAGAATTCCTAATTACGCCCTACACCTTTTCTTC	TTTATCTAGAATGGTCCCCACTGGTTGTATG
Phatr_12431	PLDζ	TTTGAATTCATGAGCTTTCGTGCCAACG	TCTAGATTTCGTAGGGGTCGCTAACATTG
Phatr_16856	SFR2	TTTGAATTCTCTCGAGAGGTCAGCAATGG	TTTCTAGAGTTTCAGGAAAGCGGACTGG
Phatr_21201	SQD1	AAAGAATTCGATGCCAACATTCTGCACC	TCTAGATTTGGCTTGCATCAAGAAACGGT
Phatr_50356	SQD2	AAAGAATTCAGTCCGCAAATGCAGGAAG	AAATCTAGATAATCTCGCGTTGGGCATTC
Phatr_42467	SQD2-like	TTTGAATTCTTGCACGTCATTCAGTACGC	TCTAGATTACGACCCCATACTTGGAGTG

7.2.2.3 Gene synthesis of codon optimized *N. gaditana* NOA sequence

In order to express the NgNOA sequence in both *N. gaditana* and *P. tricornutum* the sequence was codon optimized to allow efficient expression using a tool designed by Séverine Collin, TOTAL, with the protein sequence as a template (**appendix 8.3.1**). Codon usage tables of *P. tricornutum* and *N. gaditana* are given in **appendix 8.5.1**. *Xba*I and *EcoR*I restriction sites were added to the sequence for cloning into pH4 for expression in *P. tricornutum*. Additionally, *BamH*I and *Nde*I were added at the 5'-end and 3'-end, respectively, for insertion into the pCT2 vector (sequence confidential, property of TOTAL) for expression in *N. gaditana*. The sequence was synthesized by Invitrogen (construct ID 15ACCZJP, see appendix **8.3.2**) and subcloned into the respective vectors for microalgae transformation.

7.2.2.4 Targeted gene knock out of Naga_100083g23 in *N. gaditana* using the UEP-p35S-loxP BSD FL1-FL2 526 vector

N. gaditana has homologous recombination activity that allows targeted gene knock out. (Kilian et al. 2011). The transformation vector UEP-p35S-loxP BSD FL1-FL2 526 was obtained from Tomas Morosinotto, Padova, Italy. It comprises a p35S-loxP cassette, a zeocin resistance gene (CDS 3078..3448) under the control of the ubiquitin promotor and the *P. tricornutum* FcpA terminator (**appendix 8.4.2**). The two flanks up- and downstream of the zeocin resistance gene are homologous to *N. gaditana* genomic DNA (gDNA) sequences surrounding the coding sequence of Naga_100083g23 (NgΔ0-elo1) to induce homologous recombination after nuclear transformation (Kilian et al. 2011). Respective gDNA fragments were amplified by PCR using the oligonucleotide pair 5'-GTTGGGAATAATGCGGGACC-3' and 5'-CCGCTTTGGTTTCACAGTCA-3' for the terminal flank, and 5'-ACGATGGGTATGTTGCTTGC-3' and 5'-TGTACAGGGCGGATTTCACT-3' for the upstream flank. Flanks were inserted into the PCR BLUNT vector (Invitrogen) and subcloned into the UEP-P35S-loxP vector using the restriction enzyme activity of *BamH*I/*Sac*I for the downstream flank and *Kpn*I/*EcoR*I (NEB) for the upstream flank. The cassette comprising both gene flanks and the antibiotic resistance gene was digested from the vector prior to transformation.

7.2.2.5 Gene synthesis of codon optimized *N. gaditana* NgΔ0-ELO1 sequence

For substrate feeding assays, NgΔ0-ELO1 (Naga_100083g23) was expressed in *Saccharomyces cerevisae*. The coding sequence was optimized for yeast expression using the services of GenScript. *EcoR*I and *Xba*I restriction sites were added (**appendix 8.3.3**) for expression in pYES2 (**appendix 8.4.3**). The vector was obtained from Frédéric Beaudoin, Rothamsted Research, United Kingdom. Codon usage of *S. cerevisae* is given in (**appendix 8.5.2**). The sequence was synthesized by Invitrogen (construct ID 15ABNLYP).

7.2.3 *Relative gene expression quantification by quantitative real time PCR*

7.2.3.1 RNA extraction and reverse transcription

From an exponential phase grown cell culture, 10^8 cells were harvested (4000 rpm, 7 min, 4°C), frozen in liquid nitrogen and stored at -80°C until RNA extraction was performed. A volume of 1 mL TriReagent (SIGMA) was added to the frozen pellet, transferred to a 1.5 mL tube and mixed vigorously for 30 sec using a vortex. Then, 200 µL chloroform (SIGMA) was added and the tube inverted several times during an incubation of 15 min at room temperature. Samples were centrifuged (15 min at full speed, 4°C) and the upper phase transferred to a new tube. RNA was precipitated using 1 mL 100% isopropanol (SIGMA). After 10 min incubation at room temperature, samples were centrifuged (30 min at full speed, 4°C). The pellet was washed with 75% ice-cold ethanol and dried in a heat block at 60°C. RNA was resuspended in 30 µL diethylpyrocarbonate-treated water (ROTH), precipitated *via* the addition of 1 volume of 5 M NH_4^+-acetate, and 3 volumes of 100% ethanol, and collected by centrifugation (15 min at full speed, 4°C). Washing, drying and resuspension were repeated following the same procedure. RNA quantity was estimated using a NanoDrop 2000c reader (Thermo Fisher) and integrity was verified on a 2% agarose gel in gel electrophoresis. For reverse transcription, the QuantiTect Reverse transcription kit (QIAGEN) was used according to manufacturer instructions. Complementary DNA (cDNA) was diluted to a concentration of 10 ng/µL (estimating 100% RNA to cDNA conversion efficiency) and tested in classic PCR for the amplification of housekeeping genes prior to usage in qPCR.

7.2.3.2 Quantitative real time PCR (qPCR) using the BioRad CFX96™

Determination of gene expression was realized by qPCR using the BioRad CFX96™ thermo cycler. A cDNA concentration of 15-20 ng per reaction was found to result in the optimal quantitation cycle (Cq) after testing a cDNA dilution series with several housekeeping genes and genes of interest. The Cqs ranged between 20 and 30 cycles for

both *P. tricornutum* and *N. gaditana* samples. Oligonucleotides were designed to amplify cDNA fragments of 110-130 bp of the genes of interest with a melting temperature of 60-63°C and if possible, one intron-spanning sequence to avoid amplification from gDNA contaminations. A list of oligonucleotides used for qPCR in *P. tricornutum* and *N. gaditana* is given below (**table 7.2** and **7.3**).

Table 7.1. Oligonucleotide couples used for q PCR on *P. tricornutum* cDNA.

Annotation	*Forward* 5'- to -3' orientation	*Reverse* 5'- to -3' orientation
Housekeeping genes		
RPS	CGAAGTCAACCAGGAAACCAA	GTGCAAGAGACCGGACATACC
TUB	CTGGGAGCTTTACTGCTTGGA	ATGGCTCGAGATCGACGTAAA
Antisense lines controls		
AAS	CCAAAACTGGGATTTGTTCG	GGTTGGGTGAGGAGCTTACA
ATS1	GCAGCTTGCCGATGGTGAGA	GCGGCCAAGTCTCCGTATCC
ATS2	CGGATTTGGCCTTTGGTGCG	GATTCGGATCCCAGTCGGCG
DGD1	GTGCGCACTACTCGGGACTG	GGCGCGTATGTTTGCAGAGC
DGD2	CATGGTCAACGGGGCCATGA	TGCAGAAGAGAGTGCCGACC
DGD3	CAAGTGCGAAGAGGAGGAACA	CCTAAGAAAGAAGCAGACGTGG
MGD1	AGGCGTCTCGTAAGGCGTTG	ACTGCCGCTATCGAAACCGATG
MGD2	GCAGCTTCGGCAATGCTTCC	GTCAACGCGAGAGCCACAGT
MGD3	TGCCCGGTCAAGAGGAAGGA	AACTTGGCTGGGTCGTGCAA
PLD-zeta	CAGCTTTGATCCAGAATTCGTCT	CTGCGAATGTGATACACCATAGC
SFR2	TGGGGATGTTGCTTGCGACC	CTCCCCCTGTTCCATTGGGC
SQD1	ATCTCAGCCGACGCAACATT	TCCAAGTTGACGAAGCGGAT
SQD2	TCAAATTCATGGCCAAAGCC	CCCTGTGTGTGCTTGATGGA
SQD2-like	GTACGGCCTTGCACGTCATT	TGTGCTTGAGCCAGGAAAGG
Nitrogen metabolism genes		
Nir1	GCAAATCTTCCGTATCTCGCAG	GTTTGCCTGTACGTTCATCG
Nir2	CTTGTCCGACGAAGAAATCATG	CCACACCTGATACGATTTGGC
NR	GGATCAACTTAGTCTCCTCGACA	GCGAGCTTCGTTACGAGAAT
NOA	CCTGAAAAGTTCGCTACGCA	CGGATCCTTTTTGCCCTGAG

Sequences were selected according to lowest self-complementary values using the NCBI primer design tool (http://www.ncbi.nlm.nih.gov/tools/primer-blast). The absence of secondary primer structures was verified in PCR followed by gel electrophoresis. Housekeeping gene sequences for *P. tricornutum* were selected from (Siaut et al. 2007), and for *N. gaditana* reference genes were those mentioned in (Cao et al. 2012).

Table 7.3. Oligonucleotide couples used for qPCR on *N. gaditana* DNA.

Annotation	*Forward* 5'- to -3' orientation	*Reverse* 5'- to -3' orientation
Housekeeping genes and targeted gene knock out control genes		
18S	AGGGGACCGTACTATTGTTGG	AATGTATTCAGGGCCTAAGC
ACT1	GGATACTCCTTCACTACCACG	CCAAGCTGGAAGACTCCTCC
PsbA	ACCCAATCGGACAAGGTAGC	CCAAACACACCAGCAACACC
TUA	TGACCTGCTGCCTCATGTACC	TTGATGCCGCACTTGAAGC
TUB	TTGAGCATACCGACGTGACT	GCGATGAGCCTGTTCAGATT
PAP	AAGTGGTACCTTTGCTCCGT	AAGGTAGCCGAGTAGCCAAA
ZEO	TGTGCCAAAATCATACAGCAGG	CGAAGTCGTCCTCCACGAAG
Genes of interest, elongases and desaturases		
Δ0-ELO1	GTGGGCACCAAGGTTATGGA	GAAGGAGGTGTGGTACGGTG
Δ0-ELO2	GGCCCAATAGGAGGCATGTT	CACACCACACCTCTCCACTC
Δ0-ELO3	GCACAGCCCCCTACTACATC	GGCCTACGTCCCTTCAAACA
Δ0-ELO4	TGTCGTCCCCCACCTTATCT	GCGAGCTTGGAGAGGATGAA
Δ0-ELO5	GCAAGTATTCGCGTCGGTTC	TGGAATCAACGGTACGCCTC
Δ0-ELO6	CCTCTTCACGCACAAGGACT	CAGGACCAGGATTACCGTGT
Δ5-ELO	AGAGAGCTTGCATATCGCCC	CCGCACGTAAGAACGAGGTA
Δ6-ELO	TTTTTGACGATGAACGCGCA	AGAGGACGAGAAGCGAGAGA
Δ4-FAD	AGGTCCCACCGTACTTCTCA	GCCAAAATGTCGGGCGATAC
Δ5-FAD	CTTGGCCTCTTTCGTGGTCT	TGCATGACGTGCAACAAAGG
Δ9-FAD	GTACTCGGAGACAGATGCGG	AAATCCAACTGTTTGCCGCC
Δ12/Ꞷ3-FAD	GCCCCATATGGCGACATTCT	AGGTGGAAGAAGGAGGTGGT
ERΔ6FAD	CATCTTTGCAGCCTTCCACC	CAAGTCTCGATACGCTCGCT
FAD4	CTCCACCAGGTTTCTGCGAT	ATACACAGCTTGCGTCGTCA
SAD	CTTGAACAGAGACCCGGAGG	AAGTGCTCGAACAGGTCTGG
Genes of interest, lipid synthesis		
DGAT2	TGGTGGTGATCCTCTCCCTT	ATTGCAAAACGCGTCCCATC
DGD	ACGAGGAGGAAATCAAGCGG	TCGGAGATGGAGGGGTTGAT
LPAAT	CCTTCGGAGCATGGCTTCTT	CATCCAGTCTAGCCGTGTCC
MGD	CCGGACAGGAAGAAGGGAAC	CTCATCTTCTCCCGCACCTC
PDAT	TTTTCATGCCCGGCTTTTGG	CCATGTCGTGCAGAGAGAGG
Genes of interest, photosynthesis		
LHCX1	CTGCCTTCGTCAAGCCCA	GGAAAGGAGAGGTCTTGCCC
VCP	CATGCTTGCCATGCTCCAC	CGGAGGTGATGGCGTTGAT
VDE	AGGGCAAGTGGTACATCAGC	GATGCGCCAGTTCAGCTTTC
VEP	GCTGCCACCCTTTTTACGTG	CCCAGGCAAGACGAAAATTGA
ZEP	GCCAGATGCATTCGGAGAGT	AGACCTTGTAGGCCACCTCT

One qPCR reaction comprised 15-20 ng template DNA, 1.2 µM oligonucleotides and the 2 x SSoAdvance™ Universal SYBR® Green Supermix (BioRad) in a final volume of 10 µL. For each biological replicate, three technical replicates were carried out on the same green 96 well reaction plate (BioRad). Plates were sealed with sticky tape (BioRad), spun down and inserted into the CFX96™ Real-Time PCR Detection System. After an initial denaturation for 3 min at 98°C, a two-step thermocycling protocol was used in 39 cycles consisting of 10 sec denaturation at 98°C and 15 sec elongation at 59°C. After the cycling, a DNA melting curve from 65-95°C was recorded (0.5°C/0.05 s) to verify the presence of only one amplicon *per* oligonucleotide pair. Analysis of expression was performed using the CFX-manager tool according to the ΔΔCq method. With this method, dilution errors are suppressed by normalizing Cq values of genes of interests with those of housekeeping genes. Then, expression fold change in one sample compared to another is calculated. Each experiment comprised two or three housekeeping genes. Cell lines were used in biological triplicates so that the deviation in expression levels between the three control lines gives insights into the biological variance of gene abundance. Based on such values, an empirical range of a fold change of 0.5-1.5 was considered as not biologically relevant for *N. gaditana*. Since antisense lines seldom have a stronger down regulation, this rule was not applied to *P. tricornutum* but the gene expression in a given strain was always compared to the three biological reference values in statistical analyses.

7.3 Cell transformation of *Phaeodactylum* and *Nannochloropsis*

7.3.1 *Biolistic transformation of Phaeodactylum tricornutum*

P. tricornutum WT cells were transformed using the PDS-1000/He Particle Delivery System (BioRad) with transformation vector DNA being coated on tungsten particles (BioRad). The protocol was adapted from the Gene Shooting Protocol provided by the University of Cambridge (http://hibberdlab.com/assets/ParticleBombardment.pdf). The biolistic transformation system relies on rupture disks that break upon a defined pressure applied *via* helium in a low-pressure system (**figure 7.1**). The sudden pressure release

upon rupture disk breakage shoots the tungsten-DNA particles held on the microcarrier onto the agar plate exposing the cells. By chance, a cell is penetrated by one or several tungsten-DNA particles and might or might not recover from the stress and express the transgene.

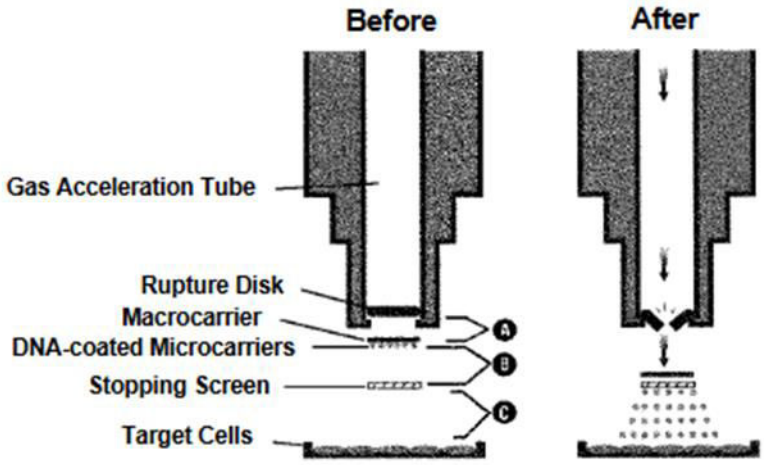

Figure 7.1. Scheme of the biolistic bombardment process using the PDS-1000/He Particle Delivery System (BioRad). Helium is applied through the gas acceleration tube and breaks the rupture disk at a defined pressure. Under the rupture disk, a macrocarrier is located on which bottom side tungsten-bound vector-DNA is fixed. The pressure release together with the partial vacuum accelerates the particles towards the target cells exposed on solid media, whereas the plastic carriers and disks are held back by the stopping screen grid. Image taken from http://www.bio-rad.com/webroot/web/pdf/lsr/literature/M1652249.pdf

For biolistic transformation, tungsten particles (M17, Biorad) were homogenized, washed, sterilized and stored at –80°C until usage. To this end, 60 mg tungsten M17 particles were boiled in 1 mL 100% ethanol for one hour. Afterwards, particles were mixed thoroughly for 1 min in 100% ethanol, centrifuged (600 x g, 20 sec, RT), and the supernatant removed. The ethanol washing procedure was repeated three times. Then, particles were washed twice with 1 mL sterile ddH_2O and finally resuspended in 1 mL sterile ddH_2O. Of this suspension, aliquots of 50 µL (for two constructs) were prepared and stored at –80°C for long terms or -20°C for short periods.

For the coating, 25 µL of tungsten were added to a 1.5 mL Eppendorf tube under constant mixing using a vortex. Respecting the order, precooled 3 µg of vector DNA, 25 µL of sterile-filtered 2.5 M $CaCl_2$ and 10 µL of 0.1 M spermidin (SIGMA) were rapidly added. The sample was mixed for another three minutes to allow homogenous DNA-tungsten binding. Particles were spun down (600 x g, 20 sec, RT) and the pellet washed twice with 250 µL ice-cold 100% ethanol. Finally, particles were resuspended in 40 µL ice-cold 100% ethanol and left on ice for maximal two hours before usage.

A log-phase grown *P. tricornutum* culture was concentrated upon centrifugation (700 x g, 10 min, RT) and 4.10^7 cells were spread on solid ESAW10N10P media and the residual liquid media was evaporated under a sterile bench.

All parts of the PDS-1000/He Particle Delivery System were cleaned with 70% ethanol prior to utilization and after each sample. The setup of the machine was as described in the manufacturers' protocol (http://www.bio-rad.com/webroot/web/pdf/lsr/literature/M1652249.pdf) using 1550 psi rupture disks (**figure 7.1**). Macrocarriers and stopping screens were dipped into 100% ethanol, 1550 psi rupture disks were not. *Per* shoot, 10 µL of the tungsten-DNA particle mix was applied on a macrocarrier and dried. This was assembled in the metal holder and inserted into the macrocarrier cover lid. The lid was fixed on the adjustable nest using the retaining spring. This macrocarrier assembly was inserted in the particle gun (**figure 7.1**). A rupture disk was applied into the retaining cap and screwed in the end of the gas acceleration tube. The open agar-plate containing the cells was inserted in the second top shelf of the dish holder. The cabinet door was closed and vacuum was generated in the accelerator until the needle reached 25 on the manometer. Helium was inserted by constantly pushing the "fire" button until the breakage of the rupture disk at 1550 psi. After disk rupture, helium pressure dropped immediately to zero. Vacuum was released, the petri dish recovered and the device cleaned for the next sample. Agar-plates were sealed with parafilm and incubated for two to three days under constant light irradiation. Afterwards, cells were washed from the plate using ESAW10N10P and a spatula. This cell suspension was transferred to a fresh ESAW10N10P plate containing 100 µg/mL zeocin for the selection of positive transformants. Plates were incubated under constant

light irradiation at 10-20 µmol.m^{-2}.s^{-1} at 20°C. Colonies appeared two to six weeks after transformation and were subcultured to another antibiotic-containing plate for one week before 2 mL liquid cultures were started from colony material.

7.3.2 *Electropulse transformation of Nannochloropsis gaditana*

Nuclear transformation of *N. gaditana* was performed as described earlier (Kilian et al. 2011) with several modifications. During exponential growth, 10^8 NgWT cells were harvested (4000 rpm, 10 min, RT), washed two times with 375 mM D-sorbitol and resuspended in 100 µL final volume. The recombination cassette was digested from the vector (*Sac*I/*Kpn*I) and 1 µg of the digestion product was added to the cell suspension and mixed gently. After 15 min of incubation on ice, cells were single-pulse electroporated at 500 Ω and 50 µF capacitance (NEPA21 Type II, Sonidel Limited), with 2400 V (MicroPulser BioRad). The transformation mix was transferred to 5 mL fresh F/2 medium in a 50 mL polycarbonate (Falcon) tube and incubated for 16 hours under continuous light irradiation. Cells were plated on 1.5% F/2 agar plates containing 7 µg.mL^{-1} zeocin. Colonies were obtained after three to four weeks of incubation with continuous irradiation and were subcultured onto another antibiotic-containing plate for one week before 2 mL liquid cultures were started from colony material.

7.4 Physiological analyses of microalgae cultures

7.4.1 *Determination of cell concentration*

Traditionally, cell concentrations in a culture were determined using counting chambers such as Malassez-chambers (Marienfeld Superior) into which a given volume is suspended onto a grid with defined geometrical parameters. This allows calculating the cell concentration per mL in respect to the cell number counted by eye. We have found a linear correlation of this determination method with the light absorption at 730 nm of a 300 µL culture aliquot in a transparent 96 well plate (Thermo Fisher) using a TECAN Infinite M1000 plate reader, by comparing both values in a variety of starved and repleated cultures of *P. tricornutum* and *N. gaditana*. This formula can be applied to

cultures diluted to absorb in the linear range between an OD730 of 0.05 and 0.15. For *P. tricornutum*, the conducted formula is:

$$\frac{\text{P. tricornutum } cells}{ml} = \frac{(OD730 - 0.03758)}{1{,}834.\,10^{-8}}$$

And for *N. gaditana*:

$$\frac{\text{N. gaditana } cells}{ml} = \frac{(OD730 - 0.03919)}{6.604.\,10^{-9}}$$

7.4.2 *Detection of neutral lipids using Nile red staining*

A fast and easy method to determine relative lipid quantities in cells is the staining with Nile red (SIGMA). When dissolved in DMSO, this fluorophore interacts with lipids and can be detected by the fluorescence emitted at 580 nm following excitation at 530 nm. Fluorescence can be quantified using a TECAN Infinite M1000 Pro plate reader or qualified by confocal laser-scanning microscopy or epifluorescence microscopy using the FITC filter. To this end, a 160 µL culture aliquot with a cell concentration between 1.10^6 and 5.10^6 cells.mL^{-1} for *P. tricornutum* and 2.10^6 and 2.10^7 cells.mL^{-1} for *N. gaditana* was transferred into a black 96 well plate (Thermo Fisher). 40 µL of a 2.5 µg.mL^{-1} Nile red (100% DMSO) solution was added, resuspended and dark-incubated for 20 min prior to fluorescence quantification or imaging. Nile Red fluorescence values were normalized to the cell concentration and expressed as relative fluorescence units (Rfu) per million cells. Alternatively, relative productivity was calculated as Rfu *per* culture volume *per* day.

7.4.3 *Relative chlorophyll fluorescence determination*

Relative Chlorophyll fluorescence was detected by measuring the fluorescence of a 160 µL culture aliquot with a cell concentration between 1.10^6 and 5.10^6 cells.mL^{-1} for *P. tricornutum,* and 2.10^6 and 2.10^7 cells.mL^{-1} for *N. gaditana*. Such an aliquot was transferred into a black 96 well plate (Greiner/Thermo Fisher) using a TECAN Infinite

M1000 Pro plate reader with an excitation wavelength of 440 nm and emission at 680 nm. This quick method may give a hint on a potential fitness phenotype.

7.4.4 *Chlorophyll a fluorescence spectroscopy at room temperature*

Emission spectroscopy relies on the spontaneous decay of molecules that have been excited to a higher energy state by a given wavelength whereby they emit radiation. At room temperature, most measured chlorophyll fluorescence derives from Chl *a* located photosystem II so that the maximum energy conversion efficiency of PSII (*Fv/Fm*), the energy proportion used for photochemistry (*Y(II)*), and NPQ can be measured (Misra et al. 2012) using a Speedzen MX fluorescence imaging system (JBeamBio) with settings described in (Allorent et al. 2013).

Fast chlorophyll kinetics were measured in 140 µL or 300 µL volumes of microalgae cell culture in a transparent 96 well-plate after 10-30 min dark incubation. Excitation was performed in the blue range (λ = 450 nm, F0) and actinic light pulses were given with a photosynthetic active wavelength of 520 nm. Photosynthetic active radiance (PAR) pulses are indicated in presented measurements and ranged from 90-600 $\mu E.m^{-2}s^{-1}$. *F0* is the steady state fluorescence in dark-adapted cultures, *F* in light-adapted cultures; *Fm* is the maximal fluorescence after a saturating light pulse on dark-adapted cultures, *Fm'* the same in light adapted cultures, *Fv* is the difference between *F0* and *Fm*. These parameters allow the calculation of the maximum quantum efficiency of PSII:

$$\frac{Fv}{Fm} = \frac{(Fm - F0)}{Fm}$$

that was always measured at 170 PAR; the maximum quantum yield in light adapted cells:

$$Y(II) = \frac{(Fm' - F)}{Fm'}$$

and concomitantly the electron transport rate from PSII to PSI as:

$$ETR = 0.5 \cdot Y(II) \cdot \mu E.m^{-2}s^{-1} \cdot 0.84$$

where 0.84 is a constant optimized for *Arabidopsis* (Schreiber 2004), and NPQ measured at 440 PAR for *P. tricornutum* and 600 PAR for *N. gaditana* as:

$$NPQ = \frac{(Fm - Fm')}{Fm'}$$

7.4.5 *Detection of nitric oxide using 4-amino-5-methylamino-2',7'-difluororescein diacetate (DAF-FM)*

The fluorophore 4-amino-5-methylamino-2',7'-difluororescein diacetate (DAF-FM) allows the sensitive detection of low levels of peroxynitrite ($ONOO^-$) ,which is in equilibrium with NO• and thus indicates NO• levels (St Laurent et al. 2015). This fluorophore was previously used to detect NO• levels in *P. tricornutum* cells (Vardi et al., 2008a). Once entered the cell, endogenous esterase activity turns DAF-FM into a low fluorescent molecule. Upon reaction with $ONOO^-$, fluorescence is induced proportionally to the amount of NO present in the cell.

Cultures were diluted to obtain 10^6 cells.mL^{-1} in 10 mL and cells were incubated under gentle shaking with 20 µL of a 5 mM DAF-FM solution (in 100% DMSO) for 1.5 hours, at room temperature and in the dark. During this time, DAF-FM could enter the cells. Then, cells were washed (1000 rpm, 10 min, RT) and resuspended in 10 mL of fresh ESAW10N10P medium in order to remove residual fluorophore. Aliquot fractions of 500 µL were transferred to a 48 well culture plate. Fluorescence was measured in 150 µL aliquots of the culture transferred into a black 96 well plate (Thermo Fisher) with a TECAN infinite M1000Pro plate reader (excitation wavelength at 488 nm, emission at 529 nm). The following incubation was performed under standard culture conditions. The measurement time point was optimized since DAF-FM fluorescence depends not only on the presence of NO• but also on the spontaneous decay of the molecule upon light irradiation. Three hours of incubation were defined as standard

incubation for DAF-FM measurements. Additionally, right after the inoculation of 500 µL cultures, a first measurement was performed and used as blank.

In order to measure NO• production in response to different concentrations of the NO• donor molecule S-Nitroso-N-acetyl-DL-penicillamine (SNAP, Molecular Probes N-7927) or the inactive structural analog N-acetylpenicillamine (NAP, Sigma), a given concentration of a 100 mM stock solution (dissolved in ESAW or DMSO as indicated) was added to the 500 µL cultures. Alternatively, NO production was measured in different cell lines without any additional treatment.

7.5 Imaging

7.5.1 *Confocal laser scanning microscopy (CLSM)*

For confocal laser scanning microscopy (CLSM) imaging, a straight TCS SP2 (Leica) microscope was used. Captured images were analysed using the LAS AF-software. All studies were performed using the 63 x water objective (HCX APO L U-V-I 63.0x0.90W). The argon laser power was set to 25 %. One image integrates eight recorded lines in a size of 512 x 512 or 1024 x 1024 pixels. Comparative studies of Nile red fluorescence were carried out with equal gains of the respective channels with an excitation wavelength of 543 nm and an emission window of 556-606 nm. Chlorophyll autofluorescence was visualized in a range of 654-734 nm with excitation at 405 nm and 488 nm.

7.5.2 *Transmission electron microscopy (TEM)*

For transmission electron microscopy, cells were pelleted (4,000 rpm, 15 min, 4°C), frozen in liquid nitrogen and stored at -80°C until usage. Sample fixation in reduced osmium tetroxide was adapted from Deerinck et al. (Deerinck et al. 2010). To this end, cell pellets were resuspendend in 0.1 M phosphate buffer (pH 7.4) containing 2.5% glutaraldehyde and incubated overnight at 4°C on a turning wheel. Afterwards, cells were pelleted and washed five times in 0.1 M phosphate buffer. Cells were fixed by a

one-hour incubation on ice in 500 µL 0.1 M phosphate buffer containing 1% osmium and 1.5% ferricyanide potassium red, before they were pelleted and washed five times with 0.1 M phosphate buffer. Pellets were resuspended in 0.1 M phosphate buffer containing 0.1% tannic acid and incubated for 30 min in the dark at room temperature prior to centrifugation (10 min, 10 000 x g, 30°C). Again, cells were pelleted and washed five times with 0.1 M phosphate buffer. The samples were dehydrated in ascending sequences of ethanol and infiltrated with ethanol/Epon resin mixture. To this end, cells were resuspended in 70%, 95% and two times 100% ethanol, respectively, incubated for 20 min, centrifuged (5,000 x g, 1 min, RT) and the supernatant discarded. Then, cells were resuspended two times in 100%:ethanol:Epon (2:1 v/v) and allowed to sediment for one hour. Finally the microalgal strains were embedded in pure Epon. Ultrathin sections (50-70 nm) were prepared with a diamond knife on a UC6 Leica ultramicrotome (Leica) and collected on 200 µm nickel grids. Ultrathin sections were examined on a Philips CM120 transmission electron microscope operating at 80 kV.

7.6 Lipodomic analyses

7.6.1 *Glycerolipid extraction*

Glycerolipids were extracted from three or four day old 50-100 mL *P. tricornutum* or *N. gaditana* cultures, if not stated otherwise. Cultures were harvested (5000 x rpm, 7 min, 4°C), and pellets frozen in liquid nitrogen and stored at -80°C until lyophilisation. Glycerolipid extraction, separation and analyses were adapted from previously described methods (Simionato et al. 2013, Blyer & Dyer 1959). Lyophilized cell pellets were resuspended in 4 mL of boiling ethanol for 5 min, during which they were mechanically broken. Then, 2 mL methanol and 8 mL chloroform were added at room temperature, saturated with argon, and the mix was incubated for one hour. Cell debris was removed by filtrating the mixture through glass wool. The filter was rinsed with 3 mL chloroform/methanol 2:1, v/v. A volume of 5 mL NaCl 1% was added to the filtrate to induce separation of the organic and the solvent phases. The later was recovered and dried under argon for storage purposes and resuspended in chloroform to take aliquots.

7.6.2 *Gas chromatography-ion flame detection (GC-FID) of fatty acid methyl esters (FAMEs)*

A 1/100 or 1/50 aliquot of the lipid extract was taken for fatty acid quantification by gas chromatography coupled to ion flame detection (GC-FID). A known quantity of 15:0 FAs was added to each sample and lipids were methanolyzed into fatty acid methyl esters (FAMEs) for one hour in 3 mL 2.5% H_2SO_4 (100% methanol) at 100°C. The reaction was stopped by the addition of 3 mL water, and phase separation was induced with 3 mL hexane. The hexane phase was collected and concentrated upon drying prior injection into the GC-FID system (Perkin Elmer). FAMEs were separated on a BPX70 (SGE) GC column and their peaks identified by comparison of their retention times with those of standards (Sigma). Quantifications were based on the elution peak of the 15:0 reference by normalization of the peak areas and correction to respective molecular masses.

7.6.3 *Thin layer chromatography (TLC)*

Separation of lipid classes was performed using 300 µg of total lipid extracts. For polar and neutral glycerolipids two distinct resolving systems of thin layer chromatography (TLC) on glass-backed silica gel plates (Merck) were used. For the resolution of neutral lipids and free fatty acids (FFA) one dimensional TLC was sufficient using hexane:diethylether:acetic acid (70:30:1, v/v) as solvent. Adequate separation of polar lipids was achieved by two-dimensional TLC with chloroform:methanol:water (65:25:4, v/v) as first solvent and (chloroform:acetone:methanol:acetic acid:water at 50:20:10:20:5, v/v) as second solvent. Lipid spots were sprayed with 2% 8-anilino-1-naphthalenesulfonic acid in methanol for UV visualization, and silici containing the different lipids were scraped off the plate for FAME production and GC-FID analyses of the different lipid classes (Abida et al. 2015).

7.6.4 *Mass Spectrometric (MS) analyses*

7.6.4.1 Structural analyses using an ion-trap spectrometer (LTQ)

For mass spectrometric (MS) analyses, purified lipid classes were dissolved in 10 mM ammonium acetate in pure methanol. They were introduced by direct infusion into a trap type mass spectrometer (LTQ-XL, Thermo Scientific) and identified by comparison with standards. In these conditions, the produced ions were mainly present as H^-, H^+, NH_4^+ or Na^+ adducts. Lipids were identified by MS/MS analysis with their precursor ion or by neutral loss (Abida et al. 2015). The position of fatty acid molecular species esterified to the glycerol backbone of the various glycerolipids was determined based on tandem MS (MS/MS) analyses. Depending on the nature of the glycerolipid and the type of adduct the substituents at *sn*-1 (or *sn*-3) and *sn*-2 positions were differently cleaved when submitted to low energy collision-induced dissociation. This is reflected in MS/MS analyses by the preferential loss of one of the two fatty acids, leading to a dissymmetrical abundance of the collision fragments. The patterns of MS2 fragments for all glycerolipids are described in Abida et al. (Abida et al. 2015).

7.6.4.2 Glycerolipid profiling by liquid chromatography coupled to tandem mass spectrometry

Total lipid extracts were separated and identified *via* high performance liquid chromatography (HPLC) coupled to quadrupole mass spectrometry (MS/MS). The method was adapted from (Michaud et al. 2016). A 25 nmol aliquot of lipid extracts was resuspended in 100 µL of chloroform/methanol 2:1 (v/v) containing 500 pmol of each internal standard. Internal standards used were PE 18:0-18:0 and DAG 18:0-22:6 from Avanti Polar Lipid and SQDG 16:0-18:0 extracted from spinach thylakoid (Demé et al., 2014) and hydrogenated as described in Buseman et al;2006. Lipids were then separated by HPLC and quantified by MS/MS.

HPLC separation method was adapted from (Rainteau et al. 2012). Glycerolipid classes were separated successively according to their polar head group using an Agilent 1200 HPLC system with a 150 mm×3 mm (length × internal diameter) 5 µm diol column (Macherey-Nagel), at 40°C. The mobile phases consisted of isopropanol/water/ammonium acetate 1 M, pH 5.3 [850/150/1, (v/v/v)] (A) and hexane/isopropanol/water/ammonium acetate 1 M, pH 5.3 [625/350/24/1, (v/v/v/v)] (B) with a flow rate of 200 µL.min^{-1}. When the column was equilibrated in solvent B, 20 µL of sample were injected. After 5 min, the percentage of A was increased linearly from 0% to 100% in 30 min and maintained at 100% for 15 min. This elution period was followed by a 20 min re-equilibration with 100% B prior to the insertion of the next sample.

Glycerolipid species were identified using a 6460 triple quadrupole mass spectrometer (Agilent) with a jet stream electrospray ion source under following settings: drying gas heater: 260°C, drying gas flow 13 L/min, sheath gas heater: 300°C, sheath gas flow: 11 L/min, nebulizer pressure: 25 psi, capillary voltage: ± 5000 V, nozzle voltage ± 1000 V. Nitrogen was used as collision gas. The quadrupoles Q1 and Q3 were operated at widest and unit resolution respectively.

PC and DGTS analysis were carried out in positive ion mode by scanning for precursors of m/z 184 and 236 respectively at collision energy (CE) of 34 and 52 eV. SQDG analysis was carried out in negative ion mode by scanning for precursors of m/z -225 at a CE of -56eV. PE, PI, PG, MGDG and DGDG measurements were performed in positive ion mode by scanning for neutral losses of 141 Da, 277 Da, 189 Da, 179 Da and 341 Da at CEs of 20 eV, 12 eV, 16 eV, 8 eV and 8 eV, respectively. Quantification was done by multiple reaction monitoring (MRM) with 50 ms dwell time. DAG and TAG species were identified and quantified by MRM as singly charged ions [M+NH4]+ at a CE of 16 and 22 eV respectively with 50 ms dwell time. Mass spectra were processed by MassHunter Workstation software (Agilent) for identification and quantification of lipids. Lipid amounts (pmol) were corrected for response differences between internal standards and endogenous lipids and by comparison with a quality control (QC). QC

extract correspond to a known Nannochloropsis lipid extract qualified and quantified by TLC and GC-FID as described by (Abida et al. 2015).

7.6.4.3 Sphingolipid extraction and liquid chromatography coupled to tandem mass spectrometry (UPLC-ESI-MS/MS) analyses

These experiments were carried out by Frédérique Tellier in Saclay, France. *N. gaditana* WT and mutant cultures were harvested upon centrifugation after 7 days of cultivation (12/12 h light/dark cycle) and freeze-dried. Sphingolipids were extracted from 5 mg dry weight cells (three biological replicates per condition) according to previously described method (Markham & Jaworski 2007). A volume of 500 µL isopropanol-hexane-water (55:20:25) and 10 µL (0.01 nmol) of internal standard [C12-Cer: N-(dodecanoyl)-sphing-4-enine (d18:1-12:0)] were added to freeze-dried material and grinded using a Polytron homogenizer. The plunger was rinsed with 500 µL of extraction solvent and the sample incubated at 60°C for 15 min. After centrifugation at 4,000 rpm for 5 min at room temperature, the supernatant was recovered and the pellet extracted once more with 1 mL of solvent, as previously. Supernatants were combined and dried using a speed Vac (Eppendorf) system. Then, the samples were incubated at 50°C for 1 h with 500 µL of 33% methylamine solution in ethanol-water (7:3). Samples were dried under nitrogen and resuspended by sonication in 100 µL of THF-methanol-water (2:1:2) containing 0.1% formic acid and filtrated prior to analysis. UPLC-ESI-MS/MS analyses were carried out on a Waters Acquity UPLC system coupled to a Waters Xevo tandem quadrupole mass spectrometer (Manchester, UK) equipped with an electro spray ionization (ESI) source. Chromatographic conditions, mass spectrometric parameters and MRM methods were defined as described previously (Tellier et al. 2014)

7.6.5 *Yeast transformation and substrate feeding experiments*

These experiments were performed at Rothamsted Research, Harpenden, UK during a short term visit in March 2015 under the supervision of Frédéric Beaudoin and Olga Sayanova.

7.6.5.1 *Saccharomyces cerevisae* transformation

The *Saccharomyces cerevisae* strain W303-1A Mat alpha ade-ura-leu-his-trp strain (W303) was transformed with a pYES2_URA4 vector construct that compensates uracil auxotrophy. The pYES2 vector possesses a GAL1 or a GAL10 (for bidirectional transcription induction) promotor being activated by galactose but silenced by glucose with a high sensitivity. Yeast transformation was performed as described by Randolph Elble, 1992 (Elble 1992). Cells of W303 were inoculated into 10 ml YPD media (Yeast extract, 10 $g.L^{-1}$; peptone, 20 $g.L^{-1}$; URA, 0.1 $g.L^{-1}$; adenine, 0.1 $g.L^{-1}$) containing 2% glucose and grown over night at 30°C. When an OD600 of 3-6 was reached, 0.5-1 mL of the culture was harvested (30 sec, full speed, RT) and 1 µg carrier DNA (sonicated herring or salmon DNA) and 2 µg transformation vector were added. The suspension was mixed with 500 µl PLATE buffer (0.1 M LiAc in 40.5% PEG 4000; 1% Tris HCl pH 7.5; 0.1% EDTA) and incubated over night at RT. The destabilized cells were pelleted for a few seconds at 1000 x g, the supernatant was removed using vacuum. The pellet was resuspended in 200 µl ddH_2O before being plated on selective YPD media lacking URA. Colonies appeared after 3-5 days. A single colony was transferred to a new selective plate from which all future cultures were started.

7.6.5.2 Yeast fatty acid substrate feeding

In order to reveal elongation activity *S. cerevisae* transformed with codon optimized microalgae elongase sequences (**section 7.2.2**), cell cultures were fed with fatty acids and their fate was followed after FAME generation using GC-FID. To this end, a 10 mL overnight culture was inoculated in SD media (Yeast Nitrogen Base including Ammonium (SIGMA), 6.7 $g.L^{-1}$; amino acids (LEU, HIS, TRP, LYS, MET; URA if required), 0.02 $g.L^{-1}$; adenine, 0.1 $g.L^{-1}$) containing 2% raffinose. From this preculture, 20 mL SD cultures containing 2% raffinose and 1% tergitiol were inoculated with an OD600 of 1 in 250 mL Erlenmeyer flasks. Growth was allowed over night until an OD600 of 1/mL was reached. The culture was split to allow substrate feeding

experiment on an equal cell basis. Fatty acids (0.25-0.5 M stocks in 100% EtOH, except 18:1 in 5% tergitol) were added to a final concentration of 0.5 mM and cultures supplemented with either 2% galactose for gene expression induction or 1% glucose for negative controls. Cultures were grown for two days at 22°C to prevent from protein degradation. Cells were harvested (5 min, full speed, RT) and washed three times with 1% and 0.5% tergitol and ddH_2O, respectively. For the production of FAMEs, cells were resuspended in residual supernatant and dried under a nitrogen stream. To each sample, 10% HCl dissolved in MeOH supplemented with 5% 2,2-dimethoxypropane was added and fatty acid methylation was allowed for one hour at 85-100°C. The reaction was inhibited by the addition of 1% NaCl and phase separation was induced by adding 0.5 mL hexane for 5 min. The upper phase was collected and 30 µL were transferred into a GC-FID vial. Using a 7890A GC System (Agilent), 1 µL of the FAMEs were injected and separated according to their hydrophobicity.

7.7 Biochemistry

7.7.1 *Protein extraction and quantification using Lowry reagent*

Microalgae cultures were harvested in the mid log phase (10 min, 5000 rpm, 4°C), frozen in liquid nitrogen and thawed on ice to facilitate cell rupture. Proteins were extracted from the cell pellet with 6 mM final concentration 3-[(3-Cholamidopropyl)dimethylammonio]-1-propanesulfonate (CHAPS), 0.5 mM final concentration dithiothreitol (DTT) in 25 mM final concentration 3-(N-morpholino)propanesulfonic acid (MOPS) pH 7.8 KOH, for 20 min on ice. Protein concentrations were determined photospectometrically using the Lowry method (Lowry et al. 1951). To this end, a dilution series of bovine serum albumin (BSA) (0-50 µg) as well as 10 µL of total protein extracts were transferred to Eppendorf tubes and volumes adjusted to 200 µL with water. A fresh 50:1 mixture of Lowry reagent A (2% CO_3Na_2 in 0.1 M NaOH) and Lowry reagent B (0.5% $CuSO_4$ x 5 H_2O in 1% sodium tartrate) was prepared and 1 mL added. After a 10 min incubation at RT, 100 µL 1 M Folin-Ciocalteu

reagent was added, samples were mixed vigorously using a vortex, and incubated for 30 min prior to the measurement of absorption at 750 nm. Based on the BSA ODs, the protein concentration in the samples was calculated.

7.7.2 *Sodium dodecyl sulphate polyacrylamide gel electrophoresis (SDS-PAGE) and Western Blot analyses*

The discontinuous gel-system of Laemmli was used for the separation of proteins according to their mass (kDa) (Laemmli 1970). Protein samples were diluted in loading buffer (250 mM Tris-HCl, pH 6.8; 4% glycerol; 0.8% SDS; 0.5% b-mercapto-ethanol, 0.004% bromophenol blue) on an equal concentration-basis (15-30 µg protein), incubated at 100°C for 5 min and subsequently separated by polyacryl amide gel electrophoresis (PAGE). Protein bands were visualized with Coomassie Brilliant Blue (ROTH). Alternatively, proteins were transferred to a nitrocellulose membrane (Protran BA83, GE Healthcare) using SDS-free Laemmli buffer. Nitrocellulose membranes were blocked with 5% skimmed dry milk in a Tris buffer (10 mmol.L^{-1} Tris, 100 mmol.L^{-1} NaCl, pH 7.5) overnight at 4°C under gentle agitation or for 45 min at RT. A dilution of the protein-specific antibody was added to 15 mL of buffered milk and incubated as described for the blocking step. Antibodies were used at the following dilutions: anti-VCP 1:80,000, anti-LHCX1 1:80,000 (obtained from Tomas Morosinotto, Padova, Italy) and anti-D1 (Agrisera) 1:10,000. After incubation, the membrane was washed three times with fresh milk-Tris buffer prior to the addition of an anti-rabbit antibody (1:10,000). After incubation for 1-2 h at room temperature, antibody-labelled protein bands were visualized using a BioRad Chemidoc MP system. Intensities were quantified relatively to the Coomassie-stained loading control using Adobe Photoshop.

7.7.3 *Galactolipid synthase assay*

With [^{14}C-Gal] as their soluble substrate, galactolipid synthases transfer the radiolabelled sugar head onto their lipid substrates. Consequentially, radioactivity is detected in the lipid fraction as described in (Maréchal et al. 1995). For the enzymatic assay of galactolipid synthase activity in *P. tricornutum*, 100 µg DAG and/or 200 µg PG dissolved in chloroform were combined in a glass tube as indicated and dried under

argon. A volume corresponding to 10 µg protein extract solubilized in the CHAPS buffer was added to the lipids and mixed with 11 µL of DET buffer (85 mM CHAPS, 0.7 M MOPS pH7.8 KOH and 14 mM of DTT) and 30 µL 1 M KH_2PO_4 pH7.8 (KOH). The reaction volume was adjusted to 282 µL with water and incubated for one hour at room temperature. The reaction was started by the addition of 18 µL radiolabeled UDP-[^{14}C]-galactose (37 Bq.µmol^{-1}). Reaction was stopped at indicated time points by the addition of solvents required for lipid extraction.

For the extraction of the lipid phase, 1.5 mL $CHCl_3$/MeOH 1:2 v/v, 500 µL $CHCl_3$ and 600 µL H_2O were added stepwise. Tubes were sealed with a cap and samples mixed vigorously using a vortex. Phases were separated upon centrifugation (10 min, 1,000 rpm, RT). The lower phase was collected, transferred into scintillation vials completed with 10 mL scintillation liquid (ready Safe, Beckman Coulter) and radioactivity was measured using a β-counter (TRI-CARB 2900, Perkin Elmer). Galactose transfer was measured based on disintegrations per minute. Specific galactolipid synthase activity was expressed in nmol galactose *per* min *per* mg protein.

7.8 In silico analyses

7.8.1 *Retrieval of Phaeodactylum and Nannochloropsis Gene Sequences*

Phaeodactylum sequences have been retrieved from the Joint Genome Institute (http://genome.jgi-psf.org/Phatr2/Phatr2.home.html) and gene IDs were given as Phatdraft 2 accessions, according to the on-going structural annotation of genes models of *Phaeodactylum tricornutum* Pt1 8.6 (Bowler et al. 2008). For partly annotated or unannotated genes, sequences were retrieved based on BLASTP searches (Altschul et al. 1990) using *Arabidopsis, Chlamydomonas*, or *Thalassiosira* gene models as queries. For comparison to *Arabidopsis* genes, respective gene sequences were retrieved from the TAIR (www.arabidopsis.org). Retrieved open reading frame sequences were then examined manually to discard fragments and determine full length sequences, based on

the presence of an initial methionine, a stop codon, an alignment with known estimated sequence tags (ESTs), and consistency of multiple alignments (Multalin, http://multalin.toulouse.inra.fr/multalin/, or t-Coffee, http://www.ebi.ac.uk/Tools/msa/tcoffee/) with gene homologues from other photosynthetic eukaryotes.

The nucleotide and amino acid sequences of putative proteins from *Nannochloropsis gaditana* were retrieved from the *Nannochloropsis* Genome Portal developed by the Interdepartmental Biotechnology Centre of the University of Padua (CRIBI) (http://www.nannochloropsis.org/), combining an ontology search in *N. gaditana* gene annotations and comparisons with known elongase sequences retrieved from the National Center for Biotechnology Information (NCBI) non-redundant (nr) database, using the Blastp alignment search tool (Altschul et al. 1990).

7.8.2 *Sequence analyses and phylogenetic reconstruction*

The presence of consensus regions and domains in algae proteins was checked using Pfam hidden Markov models (HMM) (Terrapon et al. 2009) annotated in InterPro (Interpro, http://www.ebi.ac.uk/interpro/) or using the SMART tool (http://smart.embl-heidelberg.de/) that combines information from Pfam, HMM, protein data bank (PDB) BLAST for outlier homolog identification, signal peptides and internal repeats.

For the reconstruction of a phylogenetic tree of *N. gaditana* elongases, the amino acid sequences were aligned using the MUSCLE program (Edgar 2004). An unrooted phylogenetic tree was constructed based on the alignment results, using the Neighbour-Joining method (Saitou & Nei 1987) implemented in the phylogeny.fr platform (Dereeper et al. 2008), with gamma correction and bootstrapped confidence intervals based on 1000 replications.

7.8.3 *Prediction of Subcellular Localization*

There is no tool specifically developed for the prediction of the subcellular localization of protein sequences in *Phaeodactylum*, and most notably for the 4-membrane chloroplast. The presence of a motif frequently detected in bipartite plastid transit

peptides of Heterokonts, called ASAFAP, can be detected by scanning the N-terminal sequence with a logo profile (Gruber et al. 2014). In *Phaeodactylum* sequences, the core alanine-phenylalanine dipeptide (AF) was therefore detected using ASAFind (Gruber et al. 2010), (http://rocaplab.ocean.washington.edu/tools/asafind) and HECTAR (Gschloessl et al. 2008) (http://www.sb-roscoff.fr/hectar) online tools, as well as serine residues upstream and downstream of the AF dipeptide. The prediction of the localization in plastids was consolidated by the combined presence of a signal peptide (Sp), supporting the notion that protein precursors might reach the outermost membrane of the chloroplast connected to the ER, and a chloroplast-like transit peptide (Ctp), supporting the idea that protein precursors might go across the innermost membranes of the chloroplast. These features were predicted using generic tools developed for eukaryotes, SignalP and ChloroP (Emanuelsson et al. 2007), that are combined on the TargetP server (http://www.cbs.dtu.dk/services/TargetP). TargetP analysis was also used for *N. gaditana* sequences.

8 APPENDIX

8.1 Additional publication

Progress in Lipid Research 54 (2014) 68–85

Contents lists available at ScienceDirect

Progress in Lipid Research

journal homepage: www.elsevier.com/locate/plipres

Review

Evolution of galactoglycerolipid biosynthetic pathways – From cyanobacteria to primary plastids and from primary to secondary plastids

Dimitris Petroutsos [a], Souad Amiar [b], Heni Abida [c], Lina-Juana Dolch [a], Olivier Bastien [a], Fabrice Rébeillé [a], Juliette Jouhet [a], Denis Falconet [a], Maryse A. Block [a], Geoffrey I. McFadden [d], Chris Bowler [c], Cyrille Botté [b], Eric Maréchal [a,*]

[a] Laboratoire de Physiologie Cellulaire et Végétale, CNRS, CEA, INRA, Univ. Grenoble Alpes, UMR 5168, Institut de Recherches en Sciences et Technologies pour le Vivant, CEA Grenoble, F-38054 Grenoble, France
[b] ApicoLipid Group, Laboratoire Adapation et Pathogenie des Microorganismes, CNRS, Univ. Grenoble Alpes, UMR 5163, Institut Jean Roget, F-38042 Grenoble, France
[c] Environmental and Evolutionary Genomics Section, Institut de Biologie de l'École Normale Supérieure, CNRS UMR 8197, INSERM U1024, 46 rue d'Ulm, 75005 Paris, France
[d] Plant Cell Biology Research Centre, School of Botany, University of Melbourne, Victoria 3010, Australia

ARTICLE INFO

Article history:
Received 24 October 2013
Received in revised form 19 February 2014
Accepted 20 February 2014
Available online 2 March 2014

Keywords:
Galactolipids
Monogalactosyldiacylglycerol
Digalactosyldiacylglycerol
Secondary endosymbiosis
Plastid
Chloroplast

ABSTRACT

Photosynthetic membranes have a unique lipid composition that has been remarkably well conserved from cyanobacteria to chloroplasts. These membranes are characterized by a very high content in galactoglycerolipids, i.e., mono- and digalactosyldiacylglycerol (MGDG and DGDG, respectively). Galactoglycerolipids make up the bulk of the lipid matrix in which photosynthetic complexes are embedded. They are also known to fulfill specific functions, such as stabilizing photosystems, being a source of polyunsaturated fatty acids for various purposes and, in some eukaryotes, being exported to other subcellular compartments. The conservation of MGDG and DGDG suggests that selection pressures might have conserved the enzymes involved in their biosynthesis, but this does not appear to be the case. Important evolutionary transitions comprise primary endosymbiosis (from a symbiotic cyanobacterium to a primary chloroplast) and secondary endosymbiosis (from a symbiotic unicellular algal eukaryote to a secondary plastid). In this review, we compare biosynthetic pathways based on available molecular and biochemical data, highlighting enzymatic reactions that have been conserved and others that have diverged or been lost, as well as the emergence of parallel and alternative biosynthetic systems originating from other metabolic pathways. Questions for future research are highlighted.

Contents

* Corresponding author. Tel.: +33 438784985.
E-mail address: eric.marechal@cea.fr (E. Maréchal).

http://dx.doi.org/10.1016/j.plipres.2014.02.001
0163-7827/

1. Introduction

1.1. Galactoglycerolipids are a landmark of oxygen-evolving photosynthetic organisms

Photosynthetic eukaryotes (algae, plants and some protists) are characterized by the presence of a chlorophyll-containing organelle, the chloroplast, whose origin dates back to a primary endosymbiotic event, when an ancestral cyanobacterium was engulfed within or invaded a primary eukaryotic host (for review, [1–8]). The membrane architecture of cyanobacteria and primary chloroplasts are similar: both are delimited by a two-membrane envelope and contain flattened membrane sacs, or thylakoids, in which the photosynthetic complexes are embedded. These membranes have a lipid composition, which has been remarkably well conserved through evolution. In particular, they are characterized by a very high content in galactoglycerolipids, i.e., mono- and digalactosyldiacylglycerol (MGDG and DGDG, respectively). The anomery of the terminal galactosyl groups differs in these two lipids: in MGDG, the galactose is in β conformation, forming the 1,2-diacyl-3-O-(β-D-galactopyranosyl)-*sn*-glycerol structure, whereas in DGDG, the second galactose is in α conformation, forming 1,2-diacyl-3-O-(α-D-galactopyranosyl-(1→6)-O-β-D-galactopyranosyl)-*sn*-glycerol [9,10] (Fig. 1). In this review, we shall refer to these structures as β−MGDG and αβ−DGDG. The transfer of galactose from one galactolipid to another, which occurs in Angiosperms during certain environmental stresses including exposure to ozone or cold, and leading to the production of ββ−DGDG, βββ−triGDG and ββββ−tetraGDG [11,12] shall not be discussed here.

MGDG and DGDG were first isolated from the benzene extract of wheat flour (*Triticum aestivum*) by Carter et al. in 1956 [9]. The systematic inventory of lipids in photosynthetic organisms was initiated a decade later, taking advantage of the thin-layer chromatography separation methods developed by Nichols in 1963 [13] and Allen et al. in 1966 [14]. The ubiquity of galactolipids in all photosynthetic organisms emerged as they were discovered successively in cyanobacteria, e.g., *Anacystis nidulans* and *Anabaena variabilis* [15], various green algae, firstly *Chlorella vulgaris* [16,17] and then *Chlamydomonas reinhardtii* [18,19], various embryophyta (plants), e.g., the moss *Hypnum cupressiforme* [20], the fern *Adiantum capillus-veneris* [21], the gymnosperm *Pinus sylvestris* [22] and the angiosperm *Spinacia oleracea* [23], and eventually to various photosynthetic protists deriving from green algae, such as *Euglena gracilis* [24] or deriving from red algae, such as the diatom *Phaeodactylum tricornutum* [25]. The presence of MGDG and DGDG was recognized as a hallmark of all oxygen-evolving photosynthetic organisms [10], and consequently as the most abundant lipid classes on Earth [26]. Analytical technologies (mass spectrometry, NMR) have increased in sensitivity and throughput the last 15 years. Lipidomic

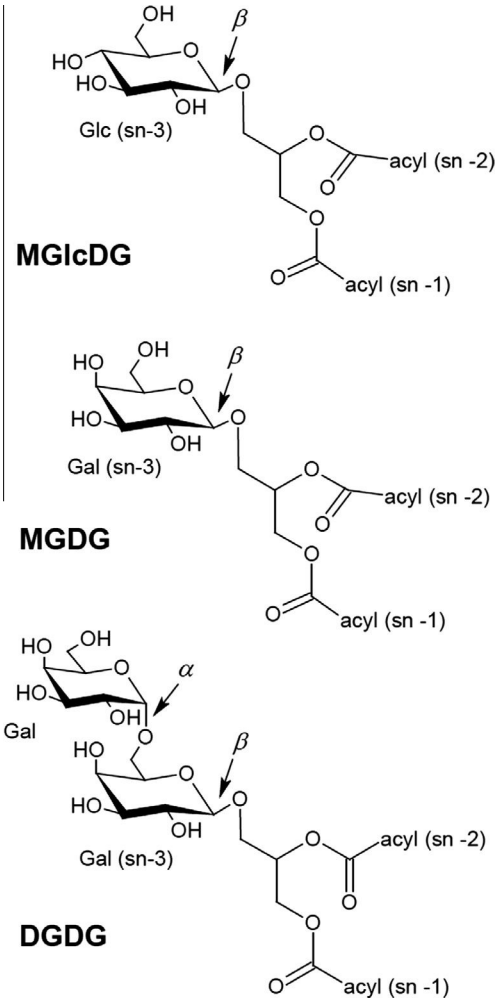

Fig. 1. Galactoglycerolipids conserved in photosynthetic membranes from cyanobacteria to primary chloroplasts of algae and plants. Positions *sn*-1 and *sn*-2 of the glycerol backbone are esterified to fatty acids and position *sn*-3 harbors the polar head. The α and β anomery are indicated. The precursor of galactolipids in cyanobacteria, MGlcDG, is also shown. MGlcDG, monoglucosyldiacylglycerol; MGDG, monogalactosyldiacylglycerol; DGDG, diagalactosyldiacylglycerol.

characterization of numerous photosynthetic microorganisms in a large variety of genetic backgrounds, growth conditions and stresses have been made available [27] and provide precious information to start reconstructing the evolution of glycerolipid metabolism.

Together with phosphatidylglycerol (PG) and sulfoquinovosyldiacylglycerol (SQDG), MGDG and DGDG make up the lipid matrix hosting the photosystems [29]. Besides their role as a membrane component, galactoglycerolipids are also known to fulfill specific molecular functions. They stabilize photosystem subunits [29,30], bind to the plastid protein import machinery [31], are a source of polyunsaturated fatty acids for various purposes and, in some eukaryotes like plants, DGDG was furthermore shown to be exported to extra-plastidial membrane compartments [32–34], where it could substitute for phosphoglycerolipids [32,35–37]. These roles shall not be detailed here and the reader is invited to refer to some recent reviews [12,28,29].

Considering the ubiquity of MGDG and DGDG, one might expect that the enzymes involved in their biosynthesis have been conserved through evolution. Surprisingly, this is not the case: the biosynthetic machinery producing MGDG and DGDG in eukaryotes has strongly diverged from that found in extant cyanobacteria.

Here, we summarize the evolution of galactolipid metabolism beginning with the cyanobacteria, although this was not the first system to be elucidated. Indeed, genes coding for galactolipid synthesis enzymes were initially characterized in angiosperms by Shimojima et al. in 1997 [38] and Dörman et al. in 1999 [39]. Subsequently, other organisms were explored based on sequence similarity. Frustratingly, bioinformatic searches for galactolipid orthologs of plant genes in cyanobacteria provided no candidates, and their identification was eventually achieved by Awai et al. in 2006 [40] and 2007 [41] and by Sakurai et al. in 2007 [42] through more classical means. We shall therefore describe the evolution of these pathways, regardless of the timeline of scientific discovery.

1.2. How has galactoglycerolipid metabolism evolved in photosynthetic organisms, following primary and secondary endosymbioses?

The question of the evolution of galactoglycerolipid metabolism has to be formulated in the context of photosynthetic eukaryote evolution, which is characterized by dramatic transitions in subcellular architecture. Important evolutionary transitions comprise primary and secondary endosymbiotic events, from an ancestral cyanobacterium to a primary chloroplast (Fig. 2A), and then from a symbiotic unicellular alga to a secondary plastid (Fig. 2B), respectively (for reviews, [1–7]).

If we first consider the simplest situation observed in plants and algae (the Archaeplastida kingdom, Fig. 2A), cells contain "simple plastids" and molecular evidence supports the view that all these plastids trace back to a single event of endosymbiosis [1]. An envelope comprising two membranes (the inner envelope membrane, IEM, and the outer envelope membrane, OEM) delineates the chloroplasts and derives from the two limiting membranes of the Gram-negative cyanobacterial ancestor. Based on photosynthetic pigments, storage material and cell walls, three lineages of these primary plastid bearing eukaryotes have diverged: a blue lineage (Glaucophyta), a red lineage (Rhodophyta), and a green lineage (green algae and plants) (Fig. 2A). In the "blue lineage", in which chlorophyll *a* is associated to phycocyanin and allophycocyanin, there is a small group of unicellular organisms (Glaucophyta), including *Cyanophora paradoxa*, in which the chloroplast still contains a peptidoglycan cell wall between the inner and outer envelopes. The "red lineage", in which chlorophyll *a* is energetically coupled to phycobilin, includes the red algae or Rhodophyta, such as *Cyanidioschyzon merolae*. Lastly, the "green lineage", in which chlorophyll *a* is associated to chlorophyll *b*, contains green algae or Chlorophyta, such as *C. reinhardtii*, and plants, or Streptophyta, such as *Arabidopsis thaliana*.

Recently it has emerged that the primary endosymbiotic creation of plastids was not a unique event. Reduced endosymbiotic cyanobacteria within cells of the amoeba Paulinellia (in the Rhizaria taxon) are now recognized as a second, independent origin of plastids [43]. This organelle, also called the chromatophore, is therefore derived from a cyanobacterium, but is not ontogenetically related to chloroplasts found in all other species examined to date.

It is more difficult to understand how unicellular organisms may contain plastids limited by more than two membranes. Fig. 2B gives some examples of reasonable scenarios (adapted from [1]). Protists originating from a secondary endosymbiosis belong to at least three lineages: two independent green lineages (Chlorarachniophytes and Euglenids), and a red lineage (Chromalveolates). The Chlorarachniophytes, such as *Bigelowiella natans*, have a plastid surrounded by four membranes. They have retained a relic of the endosymbiont algal nucleus, called a nucleomorph, between the two innermost and the two outermost membranes of their plastid [44] (Fig. 2B). On the other hand, some Euglenozoa such as *E. gracilis* contain a plastid limited by three membranes, and they lack a nucleomorph. Parasites of the Trypanosomatidae phylum, such as *Trypanosoma bruceii*, belong to Euglenozoa, but have no plastid.

The "red lineage", in which a red alga is believed to have been engulfed by another eukaryote, is thought to account for all the other plastid-bearing protists. Significant biodiversity is represented in this lineage, including Cryptomonads, such as *Guillardia theta*, which have conserved a nucleomorph, Haptophytes, such as *Nannochloropsis gaditana*, Heterokonts, such as the diatoms *P. tricornutum* and *Thalassiosira pseudonana*, Chromerida, such as *Chromera velia*, and the closely related phylum of Apicomplexa, comprising human parasites such as *Toxoplasma gondii* and *Plasmodium falciparum*. Cavalier-Smith has proposed that most secondary endosymbionts of the red lineage can be grouped as Chromalveolata [45], a super-group which might not be monophyletic [46,47]. They were also shown to have been subjected to large transfers of genes from a green algal origin, proposed to be from a secondary endosymbiosis involving a green alga prior to the red algal endosymbiosis that is believed to be common to all Chromalveolates [48]. The nuclear genomes of Chromalveolata are therefore chimeric, a feature we shall consider further later on. Alveolata, including Apicomplexa and Chromerida, and Heterokontophyta, including Diatoms and Eustigmatophytes discussed here, seem to be monophyletic within the Chromalveolata.

With respect to lipid metabolism it is well known that cyanobacteria, primary and secondary plastids all contain a machinery to generate fatty acids in their stroma, the dissociated fatty acid synthase of type II (FASII) [49]. These fatty acids are used as building blocks for glycerolipids, including the galactoglycerolipids discussed here. Fatty acids are successively esterified to the *sn*-1 and *sn*-2 positions of glycerol-3-phopshate to generate phosphatidic acid (PA), which is then dephosphorylated to form diacylglycerol (DAG), the universal precursor for galactoglycerolipids (for review, [50,51]). In green algae and in plants, the assembly of galactolipids has progressively evolved from a utilization of PA/DAG precursors synthesized de novo within the plastid, like in cyanobacteria (the so called "prokaryotic" pathway), to the utilization of diacyl-moieties imported from the endoplasmic reticulum (the "eukaryotic" pathway) [52–54]. We shall therefore focus on the evolution of the synthesizing enzymes *per se*, which is of relevance for the first transition (cyanobacteria to primary chloroplasts), and also on the evolution of the upstream pathways, which generate the substrates for galactoglycerolipids.

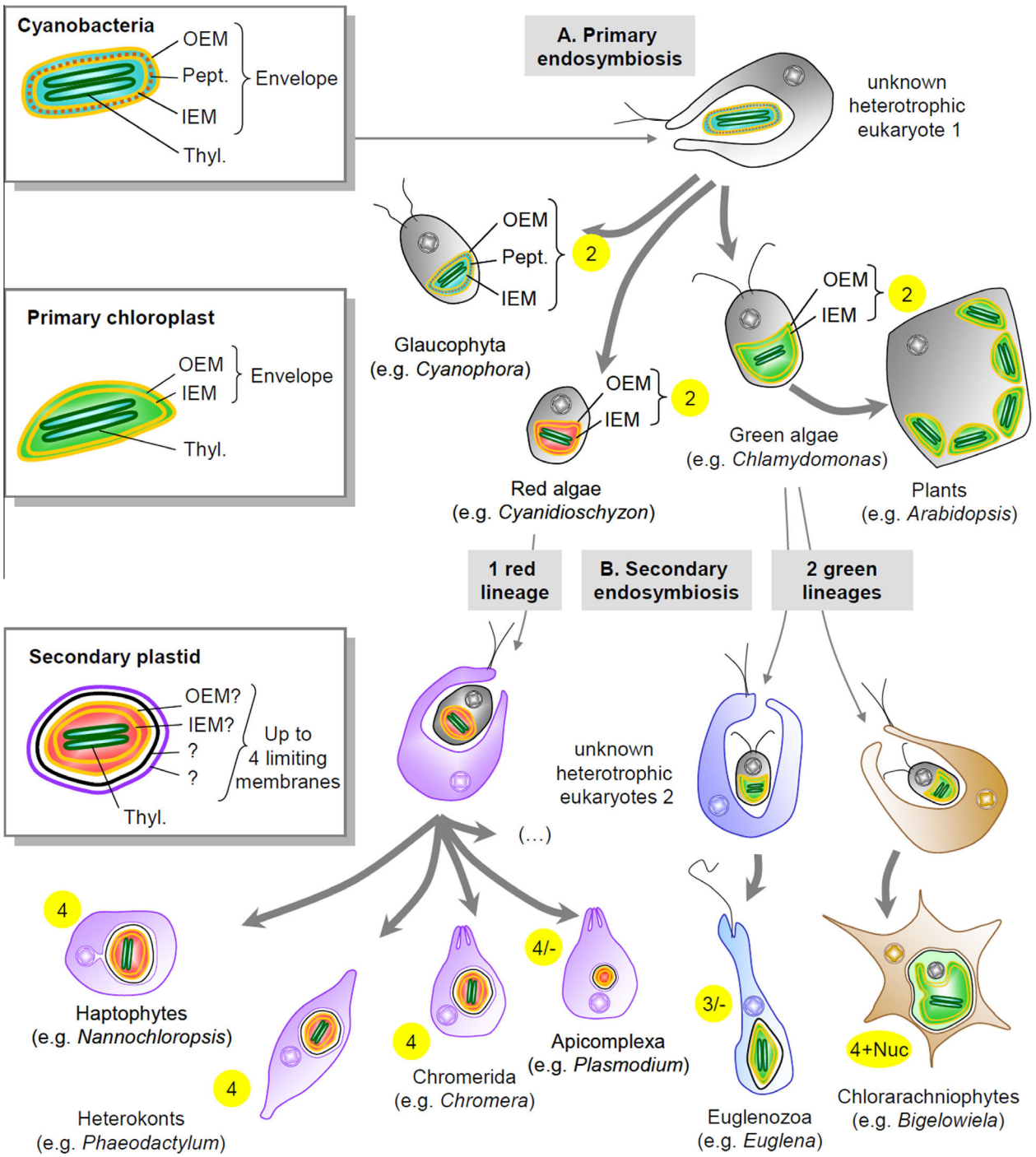

Fig. 2. Schematic representation of plastid evolution. (A) Primary endosymbiosis. In the upper panel, a single primary endosymbiosis between an unknown heterotrophic eukaryote and a Gram-negative cyanobacterium led to the three primary-plastid-bearing lineages, i.e., the "blue" lineage (glaucocystophytes), the "red" lineage (red algae) and the green lineage (green algae and plants, forming together the Viridiplantae clade). The primary plastid is always surrounded by an envelope containing two membranes, vertically inherited from the two membranes limiting the cyanobacterium (see schemes in figures on the left side). An independent endosymbiosis has led to the emergence of Paulinella, not shown in this figure. (B) Secondary endosymbiosis. Two types of secondary endosymbioses involving two different green algae and unrelated unknown heterotrophic eukaryotes led to Euglenozoa and Chlorarachniophytes. A single endosymbiosis between a red alga and a heterotrophic eukaryote probably led to all remaining plastid-bearing protists. Loss of photosynthesis is pervasive in several lineages. The number of membranes limiting primary and secondary plastids is highlighted in yellow: (2), (3) or (4). Phyla that include species that have lost their plastids are indicated: (3/−) and (4/−). Phyla in which the primary nucleus has been conserved as a nucleomorph are indicated: (4+Nuc). To maintain simplicity, the proposed origin of diatoms and other Chromalveolates from serial secondary endosymbioses involving both a green and a red alga [48] in (4) are not shown.

Concerning the second transition (primary to secondary plastids), information is scarce and the field of research is still open for a range of fundamental investigations. Little is known regarding the localization of galactoglycerolipids in the secondary plastid membranes, or about their biosynthetic machinery and their integration into the general scheme of cellular metabolism. We have thus compared pathways based on available molecular and biochemical data, highlighting enzymatic reactions that

appear to be conserved and some that may have diverged or been lost.

2. Biosynthesis of galactoglycerolipids in cyanobacteria

Cyanobacteria have been primarily classified as Gram-negative bacteria [55]. Their cell envelope is composed of an outer and a plasma membrane, separated by a peptidoglycan layer [56]. In addition to MGDG, DGDG, PG and SQDG, cyanobacteria were shown to also contain a very low proportion of a monoglucosyldiacylglycerol, or MGlcDG [55]. The glucosyl group is in β conformation, forming 1,2-diacyl-3-O-(β-D-glucopyranosyl)-*sn*-glycerol, or β−MGlcDG (see Fig. 1). This lipid has been detected in major phyla of cyanobacteria, including strains of the Pasteur Culture Collection of Cyanobacteria (PCC), a library initiated by Stanier in the late 1960s (see Supplementary Table 1 and Fig. 3). Although MGlcDG seems to be absent in some cyanobacteria (see Supplementary Table 1), suggesting that MGDG could be synthesized directly without this intermediate (see below), its occurrence, even at very low levels, has been assumed based on MGlcDG detection in other strains of the same taxonomic clusters. In *Gloeothece*, a group now called *Gloeobacter*, all tested strains seem to lack MGlcDG (see Supplementary Table 1 and Fig. 3). On average, cyanobacteria thus contain ~52% MGDG, ~15% DGDG, ~22% PG, ~9% SQDG and ~0–1% MGlcDG.

Because a unique primary endosymbiosis is at the source of all plastids (with the exception of the *Paulinella* example discussed above), the question of the uniqueness of a biosynthetic pathway to generate all galactoglycerolipids in cyanobacteria is critical. The biosynthetic scheme was first analyzed by biochemical approaches. Enzymatic activities responsible for the production of phosphatidic acid (PA), i.e., glycerol-3-phosphate acyltransferase and lyso-PA acyltransferase activities, were first characterized in *A. variabilis* [57–59]. These enzymes use fatty acids thio-esterified to the acyl carrier protein generated by the activity of FASII.

The production of MGlcDG synthesis was then measured in *A. variabilis* [60–62]. Labeling experiments using [^{14}C]-bicarbonate showed that the synthesis of MGlcDG preceded that of MGDG suggesting that MGlcDG served as a precursor for the synthesis of galactolipids. Conversion of MGlcDG into MGDG by an epimerase was indeed characterized in both *A. variabilis* [60–62] and *A. nidulans* [63], i.e., by stereochemical isomerization of the carbon-4 of the glucosyl group, and not by a replacement of glucose by galactose. DGDG synthesis was then shown to occur by transfer of a galactosyl group (and not a repetition of a glucosyl transfer followed by an isomerization) to MGDG [60–62]. The complete biosynthetic pathway can therefore be summarized as in Fig. 4, at least as initially characterized biochemically in *Anabaena*, *Anacystis* and eventually in the best studied model *Synechocystis*.

Interestingly, one of the most ancient cyanobacterial lineages also contains enzymes that were shown to be related to eukaryotic MGDG synthases (called "MGDs"), capable of synthesizing MGDG in one step, from DAG and UDP-Gal, just like in eukaryotic algae and plants. For example, in *Gloeobacter violaceus* Yuzawa et al. reported the presence of a sequence forming a clade with different MGD homologues from green non-sulfur bacteria, *Chloroflexus aurantiacus* and *Chloroflexus aggregans* [64]. Supposing that chloroplasts derive from an ancient cyanobacterium, it could be hypothesized that a cyanobacterial MGD may be at the origin of algal and plant MGDs; this cyanobacterial MGD might be lost in modern cyanobacteria besides a few species such as *Gloeobacter*. But in contradiction with this hypothesis, rigorous phylogenetic analyses [64] rather support that the *Gloeobacter* MGD may find its origin in a more recent *Chloroflexi* → *Gloeobacter* horizontal gene transfer [64]. Nevertheless, one cannot exclude that such horizontal transfer might have occurred with the primal cyanobacteria, the mother of all plastids.

2.1. Enzymes synthesizing MGlcDG

Amongst prokaryotes, MGlcDG, with β-anomeric configuration of the glucose, is not unique to cyanobacteria. In particular, it has been found in *Bacillus subtilis*, where it accounts for 10% of the lipids [65]. Furthermore, in the cell-wall less bacterium *Acholeplasma laidlawii*, a MGlcDG in an α-anomeric configuration of glucose represents the most abundant lipid, accounting for about half of the lipids in these membranes [66]. Genes coding for the corresponding β-MGlcDG and α-MGlcDG synthases in these bacterial models have been cloned and characterized [67,68] but no ortholog has been identified in available complete cyanobacteria genomes. Awai et al. in 2006 [40] resolved the question with an elegant strategy. They first considered that the gene for MGlcDG synthase should be conserved between two sequenced cyanobacteria, the unicellular *Synechocystis* sp. PCC 6803 strain and the filamentous *Anabaena* sp. PCC 7120. They then assumed two characteristics of the enzyme, namely that its sequence should harbor a glycosyltransferase motif, and that its annotation should fall into the category of

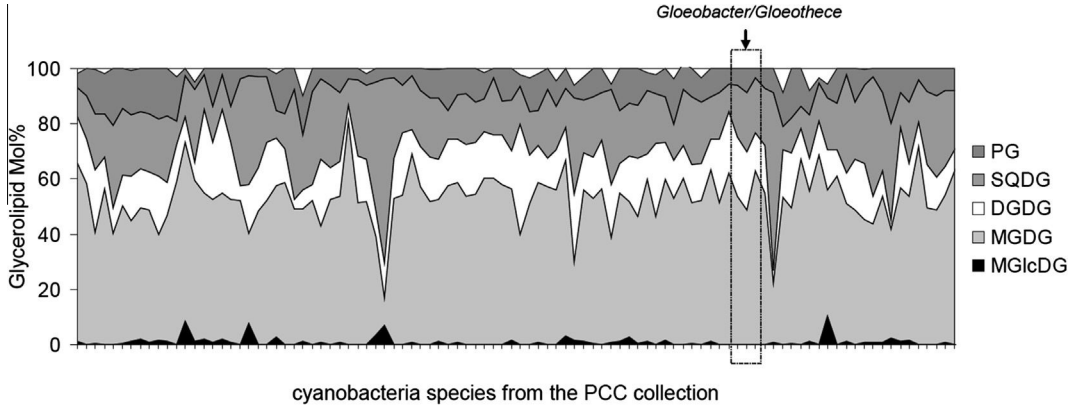

Fig. 3. Systematic analysis of the glycerolipid profiles of cyanobacteria from the PCC collection. MGDG, DGDG, SQDG, PG and MGlcDG have been analyzed in 98 strains of the Pasteur Culture Collection of Cyanobacteria, covering at least 2 representative groups of the following spiecies: *Anabaena*, *Arthrospira*, *Calothrix*, *Chamaesiphon*, *Chroococcus*, *Cyanothece*, *Cylindrospermum*, *Geitlerinema*, *Gloeocapsa*, *Gloeothece/Gloeobacter*, *Leptolyngbya*, *Microcystis*, *Nodularia*, *Nostoc*, *Oscillatoria*, *Pseudanabaena*, *Scytonema*, *Synechococcus* and *Synechocystis*. Doted frame highlight *Gloeothece/Gloeobacter* strains apparently missing MGlcDG. Graph was built with values reported in Supplementary Table 1, based on analyses kindly provided by A.J. Dorne.

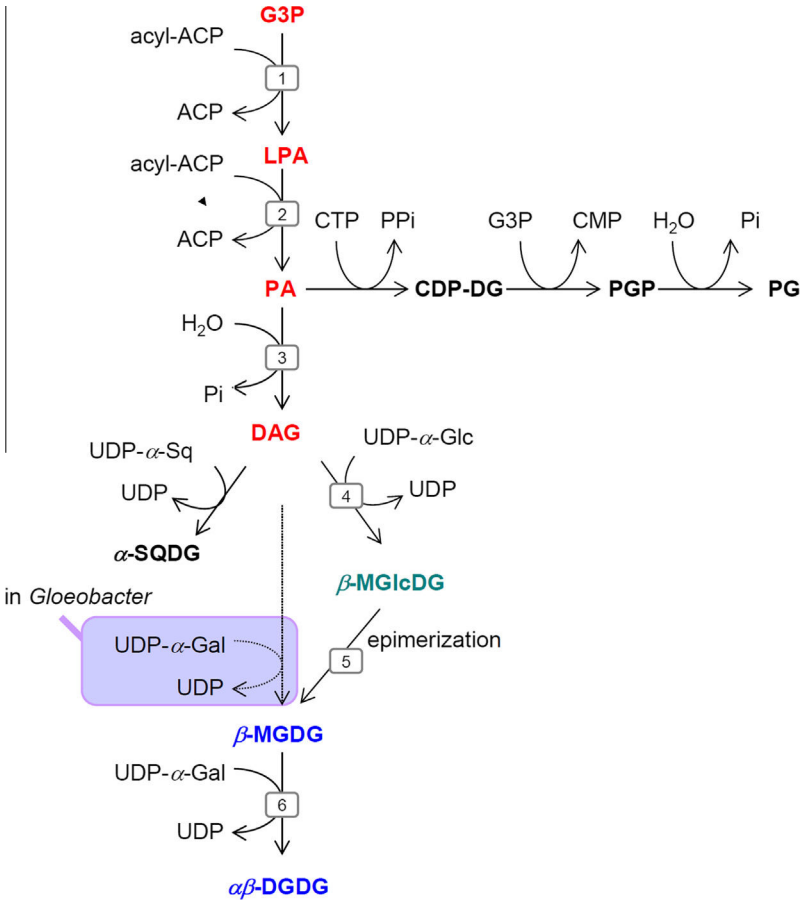

Fig. 4. Biosynthesis of galactoglycerolipids in cyanobacteria. (1) *sn*-glycerol-3-phosphate acyltransferase or ATS1, (2) 1-acylglycerol-phosphate acyltransferase or ATS2, (3) phosphatidate phosphatase, (4) MGlcDG synthase; (5) epimerase, (6) dgdA-type DGDG synthase. The SQDG synthase, CTP: phosphatidate cytosine transferase, glycerol-3-phosphate:CDP-diacylglycerol phosphatidyltransferase, phosphatidylglycerol synthase are also shown. In cyanobacteria, a major difference occurs in the synthesis of galactolipids, by a two-step process involving a synthesis of MGlcDG followed by an epimerization of the glucose polar head into galactose, thus forming MGDG (see text). In *Gloeobacter*, a MGD-like enzyme, catalyzing the direct synthesis of MGDG using UDP-Gal, has been acquired by a recent horizontal transfer.

genes with unknown function. Out of the four gene candidates identified based on these criteria in *Synechocystis*, only one, sll1377, led to the synthesis of β-MGlcDG when expressed in *Escherichia coli*. One ortholog was found in *Anabaena*, all3944. MGlcDG synthase was shown to use UDP-Glc and DAG as substrates [40]. A systematic survey of available cyanobacteria genomes subsequently showed the presence of an ortholog in all species, with >40% identity in amino acids.

MGlcDG synthase sequences show putative membrane spanning domains in the N- and C-terminal regions of the protein. MGlcDG synthases also contain two motifs (D...DXD and QXXRW) found in the GT2 family of glycosyltransferases classified in the CAZy database (carbohydrate-active enzymes database; http://www.cazy.org/) [69]. The GT2 family contains inverting glycosyltransferases such as cellulose synthases or chitin synthases. The activity of the MGlcDG synthase linking glucose in a β configuration is thus consistent with this classification. Glycosyltransferases containing D...DXD and QXXRW motifs also occur in the GT21 family. Glycosyltransferases containing such a sequence motif in the CAZy database include processive enzymes. In addition, like other GT2 proteins, MGlcDG synthase was shown to require divalent cations, in particular magnesium [40]. Interestingly, plant and algal MGDG synthases, which are also inverting enzymes, do not belong to either the GT2 or GT21 family (see below).

We found a putative ortholog of the MGlcDG synthase in *Paulinella chromatophora*, (RefSeq YP_002049084) with 43% identity and a Blast E-value of 5×10^{-97}, supporting the hypothesis that in the chromatophore of Rhizaria, MGlcDG is synthesized like in cyanobacteria. The *P. chromatophora* sequence is presently annotated as a glycosyltransferase of the GT2 family. Functional analysis is now required to confirm this activity in chromatophore organelles.

Concerning chloroplasts, no ortholog of MGlcDG synthases has been found in any algal or plant genome [40]. Based on comparative genomic surveys, MGlcDG synthases appear therefore restricted to cyanobacteria and possibly to the chromatophore of Rhizaria.

The localization of the cyanobacterial MGlcDG synthases has not been unambiguously assessed yet, although the presence of membrane spanning domains indicates a tight association with membranes. Based on membrane fractionation and enzymatic measurements, MGlcDG synthase activity was detected in both thylakoid and plasma membranes of *A. nidulans* [63].

2.2. Epimerases converting MGlcDG into MGDG

The search for the epimerase acting on the conversion of β-MGlcDG into β-MGDG is still open for investigation and is one of the last challenges to fully understand galactoglycerolipid synthesis in cyanobacteria. No epimerase candidate genes have been found associated with any MGlcDG synthase operon [40], and of the nine epimerases currently listed in the annotation of *Synechocystis* PCC6803 (according to the reference database Cyanobase, http://genome.microbedb.jp/cyanobase/Synechocystis), none appear to act on a glucolipid substrate.

2.3. Enzymes synthesizing DGDG

As for MGlcDG synthase, the identification of the cyanobacterial gene coding for a DGDG synthase, called dgdA, was determined based on comparative genomic studies. In 2007, Awai et al. [41] and Sakurai et al. [42] simultaneously reported the discovery of the same *dgdA* gene in both *Synechocystis*, slr1508, and in *Anabaena*, alr4178. The first group had previously reported the identification of MGlcDG synthase amongst 4 genes of *Synechocystis* containing glycosyltransferase motifs and being functionally uncharacterized. They added a third criterion, specifically, the presence of a similar sequence in the genomes of Cyanidophytina, a red alga living in very acidic environments that lack the eukaryotic DGD gene, e.g., *C. merolae*, *Cyanidium caldarium* and *Galdieria sulphuraria*. They thus identified a unique candidate gene in *Synechocystis* and *Anabaena* and assessed function based on the lack of DGDG in knockout lines of cyanobacteria, and on synthesis of DGDG after heterologous expression in *E. coli* [41]. The second group had a similar approach, using a supervised phylogenetic profiling to identify putative glycosyltransferase genes shared by cyanobacteria and *Cyanidioschyzon*, and not present in green plants. They based the functional characterization on single gene knockout analyses [42]. The dgdA protein belongs to the GT4 family of the CAZy classification [69], just like the unrelated DGD proteins catalyzing the synthesis of DGDG in all algae and plants, with the notable exception of some red algae.

When *E. coli* expresses the *Synechocystis dgdA* gene, the synthesis of αβ-DGDG can only be detected if a plant β-MGDG synthase is coexpressed and UDP-Gal provided [41]. By contrast, when dgdA is coexpressed with a β-MGlcDG synthase, no diglycosyl-lipid is synthesized, showing that MGlcDG is not a substrate for dgdA. This specificity is, on the one hand, consistent with previous analyses showing that α-MGlcDG and α-MGDG produced in *Synechococcus* following genetic engineering are not used for the synthesis of α-Gal-α-GlcDG or αα-DGDG [70]. On the other hand, this result confirms the biosynthetic scheme shown in Fig. 4. In the absence of a reliable assay to measure the activity of dgdA, the subcellular localization has not been documented by enzymatic detection in subcellular fractions and should therefore be obtained by proteomic analyses of membrane fractions.

As for the conservation of a cyanobacterial gene synthesizing DGDG in eukaryotes, we could only identify a sequence in the genome of *P. chromatophora* (RefSeq YP_002049341) coding for a *dgdA* ortholog. This again supports the inheritance of biosynthetic pathways from modern cyanobacteria in the chromatophore of Rhizaria, with an evolutionary story that is distinct from that of chloroplast-containing eukaryotes.

Interestingly, whereas MGlcDG synthase, and possibly the associated epimerase, have been totally lost in chloroplasts, being replaced by a simple MGDG synthase, dgdA has been retained in some red algae even though it has been lost in the vast majority of algae and all plants. Thus, the loss of the enzymes of the cyanobacterial pathway has not occurred in a single step during the early evolution of primary plastids.

3. From cyanobacteria to primary plastids: emergence of a new galactolipid synthetic pathway

The galactolipid biosynthetic pathway in primary chloroplasts has been mainly characterized enzymatically in angiosperms and in a few green algal models. Once MGDG synthase (MGD) and DGDG synthase (DGD) genes had been identified in angiosperms [38,39], it was rapidly evident that this pathway did not derive from the ubiquitous cyanobacterial system, and that this innovation was shared by all eukaryotic plastids, from Archaeplastida (Glaucophyta, Red algae, Green algae, plants) to secondary endosymbionts. In all cases, the biosynthesis of MGDG and DGDG was reported to occur in the outer envelope of chloroplasts. We start the description of the evolution of this pathway with the source of the diacyl-precursors that are utilized because cooperation between the plastid and other compartments of the cell, most notably the endoplasmic reticulum, is an important innovation that has occurred here.

3.1. Diacyl-precursors for MGDG and DGDG synthesis

3.1.1. Neosynthesis of C18/C16 phosphatidic acid and diacylglycerol in the stroma of chloroplasts (prokaryotic pathway)

Some of the lipid biosynthetic machineries have been remarkably well conserved in the cyanobacteria → primary chloroplast transition, e.g. the biosynthesis of fatty acids, thio-esterified to the acyl carrier protein (in angiosperms: 16:0-ACP and C18:0-ACP), is carried out by the same enzymatic system found in prokaryotes, i.e., an acetyl-CoA carboxylase complex and a fatty acid synthase of type II (FASII) (see above and [49]). Furthermore, some fatty acids generated inside the chloroplast harbor features that make them useful as *signatures* allowing their detection when esterified to glycerolipids, such as the length (in general C16 or C18), the number of double bonds (like the desaturation of C16:0 to C16:3 or C16:4 in numerous algae and plants), as well as specific transfers to positions *sn*-1 and *sn*-2 of glycerol-3-phosphate (G3P). Desaturation of chloroplast fatty acids can be initiated by a stromal delta-9 acyl/stearoyl-ACP desaturase (FAB2) that catalyzes the synthesis of 18:1-ACP from 18:0-ACP [71]. In some tissues or in certain organisms the desaturation of 16:0-ACP into 16:1-ACP can also be catalyzed [72]. De novo fatty acids can then be used either in chloroplasts or exported to the cytosol where they feed the cytosolic pool of acyl-CoAs [35,49,73–75].

The synthesis of G3P, the other important building block of glycerolipids, can occur in the stroma [75]. Using acyl-ACP and G3P, the envelope is known to be the site of biosynthesis of PA and DAG, by the stepwise action of *sn*-glycerol-3-phosphate acyltransferase (ATS1) in the stroma, a 1-acylglycerol-phosphate acyltransferase (ATS2) in the IEM, and a phosphatidic acid phosphatase (PAP) in the IEM [76] (Fig. 5). In the case of angiosperms, the specificity of ATS1 and ATS2 leads to the production of PA and DAG with 18:1 and 16:0 at positions *sn*-1 and *sn*-2, respectively. The glycerolipids assembled in the plastid, with 16-carbon fatty acids at the *sn*-2 position, harbor a diacyl-structure similar to that observed in cyanobacterial glycerolipids, named therefore a 'prokaryotic' structure [35,37,75,77].

3.1.2. Import of extraplastidial C18/C18 and C16/C18 diacyl-precursors (eukaryotic pathway)

In the endoplasmic reticulum of angiosperm cells, acyl-CoAs and G3P are used for the stepwise synthesis of PA and DAG within the ER, with 16:0, 18:0 or 18:1 at *sn*-1 and 18:0 or 18:1 at *sn*-2 positions. Membrane glycerolipids assembled in the ER, with 18-carbon acyls at *sn*-2 position, have a diacyl structure defined as 'eukaryotic' [35,37,75,77]. Import of precursors from the ER to the chloroplast is reflected by the high proportion of this eukaryotic signature in galactoglycerolipids. This import system was first described by Ohlrogge and Browse in 1995 [78]: the plastid pathway is known as the prokaryotic pathway, whereas the endoplasmic route is known as the eukaryotic pathway.

An important issue concerns the *dual origin of PA/DAG substrates* in all primary plastids, and the presence of a *eukaryotic pathway* in all these organisms. In green algae, this has been particularly well studied in *Chlorella kessleri*, thanks to a careful analysis of fatty acids at the *sn*-1 and *sn*-2 positions of glycerolipids [79]. In this study, galactolipids contained almost exclusively C18 acyls at the

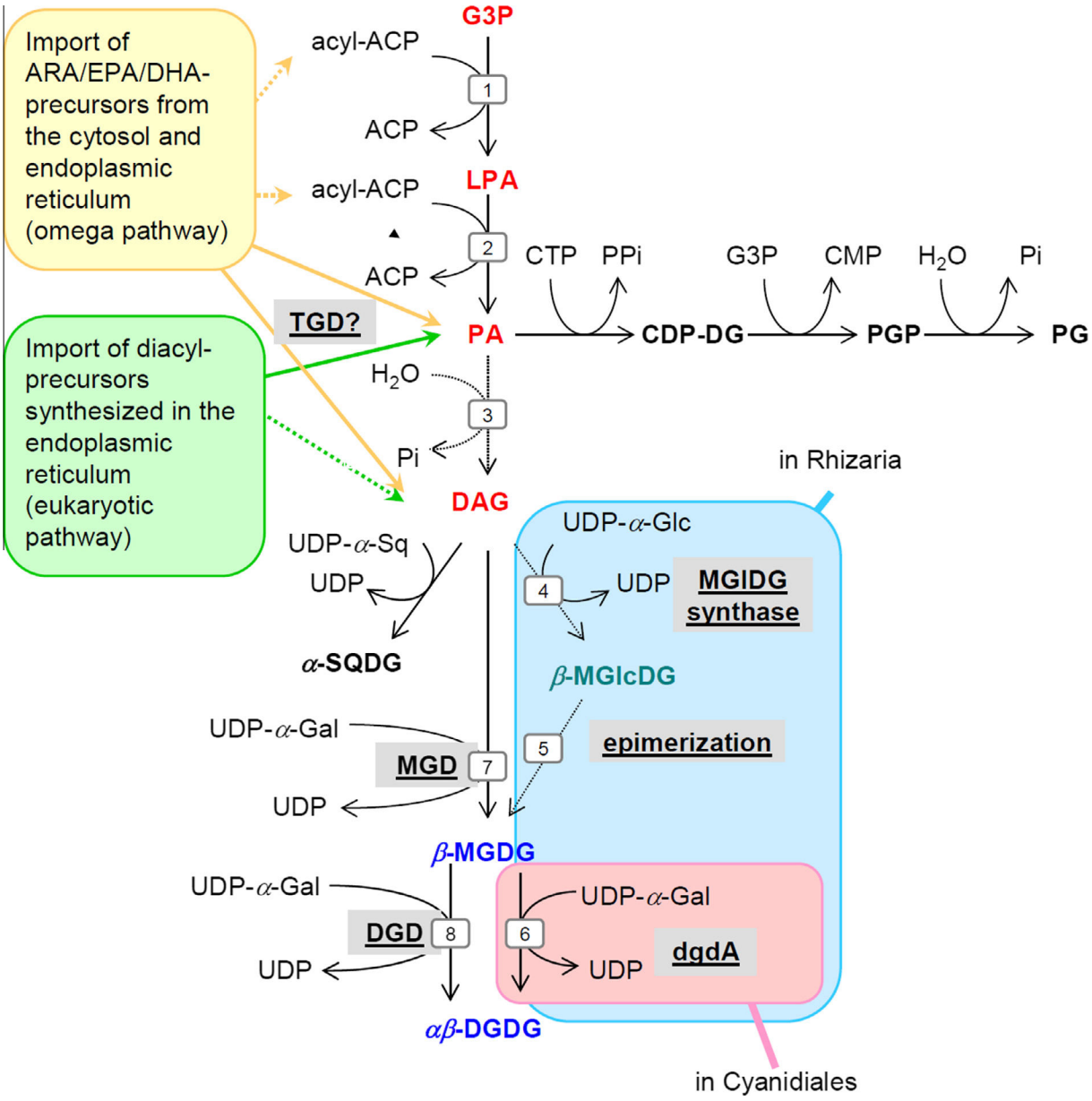

Fig. 5. Biosynthesis of thylakoid lipids in the chloroplast envelope of angiosperms. (1) *sn*-glycerol-3-phosphate acyltransferase or ATS1, (2) 1-acylglycerol-phosphate acyltransferase or ATS2, (3) phosphatidate phosphatase, (4) MGlcDG synthase; (5) epimerase, (6) dgdA-type DGDG synthase, (7) MGDG synthase or MGD, (8) DGDG synthase or DGD. The synthesis of PG and SQDG are also shown. The catalysis of DGDG via a cyanobacterial dgdA-type enzyme is unique to Cyanidiales, a sub-group of red algae. The genome of the chromatophore of Paulinella encodes the cyanobacterial enzymes. Dotted lines indicate hypothetical precursor transfers that still need to be demonstrated.

sn-1 position whereas the *sn*-2 position contained both C16 and C18 acyls. Based on the structural definition given above, MGDG was found to contain 65% of prokaryotic molecular species and 35% of eukaryotic ones. By contrast, and with a similar trend to that observed in higher plants, DGDG contained 68% of eukaryotic structures. Pulse-chase experiments using [^{14}C] acetate showed that MGDG and DGDG were primarily labeled as C18/C16 (prokaryotic) molecular species, and subsequently as C18/C18 (eukaryotic) molecular species, with a concomitant decrease of C18/C18 labeling in extraplastidial phosphatidylcholine [79]. This study supports the existence of a eukaryotic pathway in green algae functionally related to that described in Angiosperms, with a route of lipid intermediates coming from PC and feeding the chloroplast with precursors for the synthesis of galactolipids. Today, besides the TGD machinery that is conserved in green algae, components of the machinery that specifically divert PC to feed galactolipid synthesis are unknown and it is therefore difficult to speculate on the evolution of this system.

3.1.3. Import of extraplastidial ω3/ω6 very-long chain polyunsaturated acyl precursors (omega pathway)

In addition to the ER → chloroplast route that has been studied in great detail in Chlorophyta and Embryophyta, the elaboration of fatty acids with more than 20 carbons, containing multiple double bounds and forming the so called very long chain poly-unsaturated fatty acids (VL-PUFAs), requires elongase and desaturase activities that are associated with the cytosol and the endoplasmic reticulum [27]. The presence of such fatty acids like all-*cis*-$\Delta^{5,8,11,14}$ 20:4 (C20:4 ω-3, arachidonic acid, or ARA), all-*cis*-$\Delta^{5,8,11,14,17}$ 20:5 (C20:5 ω-3, eicosapentaenoic acid, or EPA) and all-*cis*-$\Delta^{4,7,10,13,16,19}$ 22:6 (C22:6 ω-3, docosahexaenoic acid, or DHA) in galactolipids is a clear evidence of an ER/cytosol → chloroplast

import (Fig. 5). These fatty acids have been identified in primary plastids in the green lineage (e.g., *Chlorella minutissima* [80]) as well as the red lineage (e.g., *Porphyridium purpureum*, previously known as *P. cruentum* [81]). The biosynthesis of ω3/ω6-VL-PUFAs in the cytosol of *P. purpureum* has been exquisitely dissected using externally supplied fatty acids and precursors [82,83], and the identified activities serve as a reference to better understand the conservation of this pathway in the cytosol of other organisms. Interestingly, based on a specific inhibitor response, it was shown that part of the synthesis of ω3/ω6-VL-PUFAs requires FAs to be linked to PC, for the C18:1 → C18:2ω6 desaturation catalyzed by a Δ12-desaturase. Following desaturation of C20, FAs would then occur on various phospholipid classes (for review, [27]). ARA/EPA-rich-PC could then be a source of ARA/EPA-rich DAG, used as precursor for other lipid classes including MGDG. In the chloroplast, a Δ17-(ω3) desaturase was proposed to convert ARA-MGDG into EPA-MGDG [82]. Regardless of this activity that allows ARA → EPA conversion in chloroplasts, all of the ω3/ω6-VL-PUFAs found in galactolipids are likely to originate from the cytosol.

In the case of the green alga *C. minutissima*, diacylglyceryl-N,N,N-trimethylhomoserine (DGTS) is composed of up to 44% of total lipids, which is accompanied by PC as the major phospholipid. In *C. minutissima*, both positions of DGTS are acylated with EPA (>90% of total). The DGTS level shows a rhythmic fluctuation with time which is inversely correlated with the level of MGDG and it has thus been proposed that EPA in galactolipids might originate from EPA in extraplastidial DGTS [80]. In the case of the red alga *P. purpureum*, pulse-chase labeling with radioactive fatty acid precursors showed incorporation into EPA-rich PC and TAG and, during the chase, a decrease of the labeling of these lipids and an increase of that of MGDG. It was thus concluded that TAG could supply EPA precursors for the biosynthesis of MGDG [81].

Could ω3/ω6-VL-PUFAs found in galactolipids be imported via a similar mechanism as the C18/C18 eukaryotic system? Is there a specific import of free fatty acids for ARA, EPA of DHA? Alternatively, is there a transfer of a diacyl-moiety from extra-plastidial phospholipids to feed MGDG synthesis? This overall import system is called here the omega pathway. Is the TGD machinery involved in this route? To our knowledge, these questions are still unresolved.

3.1.4. Evolution of plastidial and extra-plastidial pathways

The evolution of the integrated prokaryotic/eukaryotic systems has not been investigated extensively in green and red algae. In particular, understanding of the evolution of the ω3/ω6-VL-PUFA import system requires more data. It will be extremely important to address this question in the future since the omega pathway for the synthesis of MGDG and DGDG has been conserved in secondary endosymbionts (see later).

In angiosperms, Mongrand et al. (1998) have provided the most comprehensive analysis, by searching for correlations between the existence of the prokaryotic and eukaryotic pathways and the evolutionary position of different organisms (Fig. 6) [54,84]. By using all-*cis*-$\Delta^{7,10,13}$ C16:3 as a marker for the existence of the plastidial pathway, they studied the overall fatty acid composition of 468 plant species distributed among 141 botanical families. The synthesis of galactoglycerolipids using prokaryotic precursors was found to have been lost during evolution and, in the case of dicots, this loss occurred independently in numerous groups and at different rates [54]. A trend can therefore be noted in the upstream pathway feeding galactolipids, characterized by an increasing dependence on imported precursors from the ER. The importance of this phenomenon has been established in angiosperms, but it remains to be investigated in algae, in particular concerning the analogous import of eukaryotic diacyl-substrates and the specific case of VL-PUFA precursor import.

In conclusion, there has been an intense adaptation of the pathways feeding galactolipids with PA and DAG precursors, with a clear trend towards an import from the cytosol. Indeed, besides plastidial PG, whose synthesis seems to be highly dependent on the conservation of a prokaryotic production of PA [76], it seems that during the course of evolution MGDG and DGDG synthesis relies more and more on extraplastidial substrates. The "long" path for FAs, first synthesized in the stroma, then reaching the endoplasmic reticulum where they are incorporated into phosphoglycerolipids, and then imported back into the chloroplast, appears to be a costly system compared with the local production and utilization of FAs for chloroplast lipids *via* the prokaryotic route. The emergence of a specific import system might therefore provide benefits that could ensure a better fitness. One such benefit could be an improved integration of biosynthetic pathways in the ER and the chloroplast at the whole cell level [51,85]. This has been proposed in the context of the activation of MGDG synthases from angiosperms by extraplastidial PA [51,85]. This feature appears therefore to be important in order to understand the evolution of galactolipid synthesizing enzymes.

3.2. Evolution of galactoglycerolipid synthesis in primary endosymbionts

3.2.1. MGDs

As detailed above, in cyanobacteria MGDG is not synthesized by a homolog of MGDG synthase, but by a two-step process. This raises several questions, such as (i) the importance of conserving MGDG in photosynthetic membranes, (ii) the reasons for the loss of the MGlcDG synthase/epimerase system, and (iii) the origin of MGDG synthases in eukaryotes following the primary endosymbiosis. MGD enzymatic activities have been analyzed in great detail in Angiosperm models. MGD proteins belong to the GT28 family of glycosyltransferases classified in the CAZy database [69]. The presence of MGD orthologs in all primary endosymbionts analyzed to date, except Rhizaria, has been reported in numerous comparative phylogenies. In green and red algae, only one *MGD* gene is usually detected [64,86]. In the green alga *C. reinhardtii*, it has thus been annotated as *MGD1*, although no other paralog has yet been detected [87].

Molecular phylogenetic analysis of MGD sequences has been recently published by two teams [64,86] drawing similar conclusions on the origin of contemporary plant MGDs. Both were based on amino acid sequence alignments, maximum likelihood and Bayesian inference. The more thorough analysis [64] included four million iterations, rather than the classical 10–20 thousands to determine phylogenetic trees. These studies support the lateral transfer of a MGDG synthase ancestral gene from a chlorobacterium ancestor of the Chloroflexi type. Based on these phylogenetic reconstructions, the analysis of MGDs from Rhodophyta, Chlorophyta and Embryophyta show a monophyly and a single ancestor. The modern group of Chloroflexi comprises anoxygenic phototrophic bacteria, having diverged before cyanobacteria. The *in vitro* analysis of the substrate specificity and anomeric configuration of the sugar head group for the three prokaryotic genes closely related to eukaryotic *MGDs* in *Roseiflexus castenholzii* showed one member that encoded a MGDG synthase [64]. Other studies have explored the possibility that a Chlorobacculum type gene might have been transferred [88]. When and how this horizontal transfer of a *MGD* gene from a Chloroflexi ancestor to the nuclear genome of an early chloroplast-bearing eukaryote has occurred is unknown. A large-scale phylogenetic analysis has revealed that a considerable amount of non-cyanobacterial genomic material has been acquired prior to red and green lineage divergence [89]. The analysis of the genome of *C. paradoxa* has also highlighted important gene transfers from a *Chlamydia*-like ancestor, also supporting

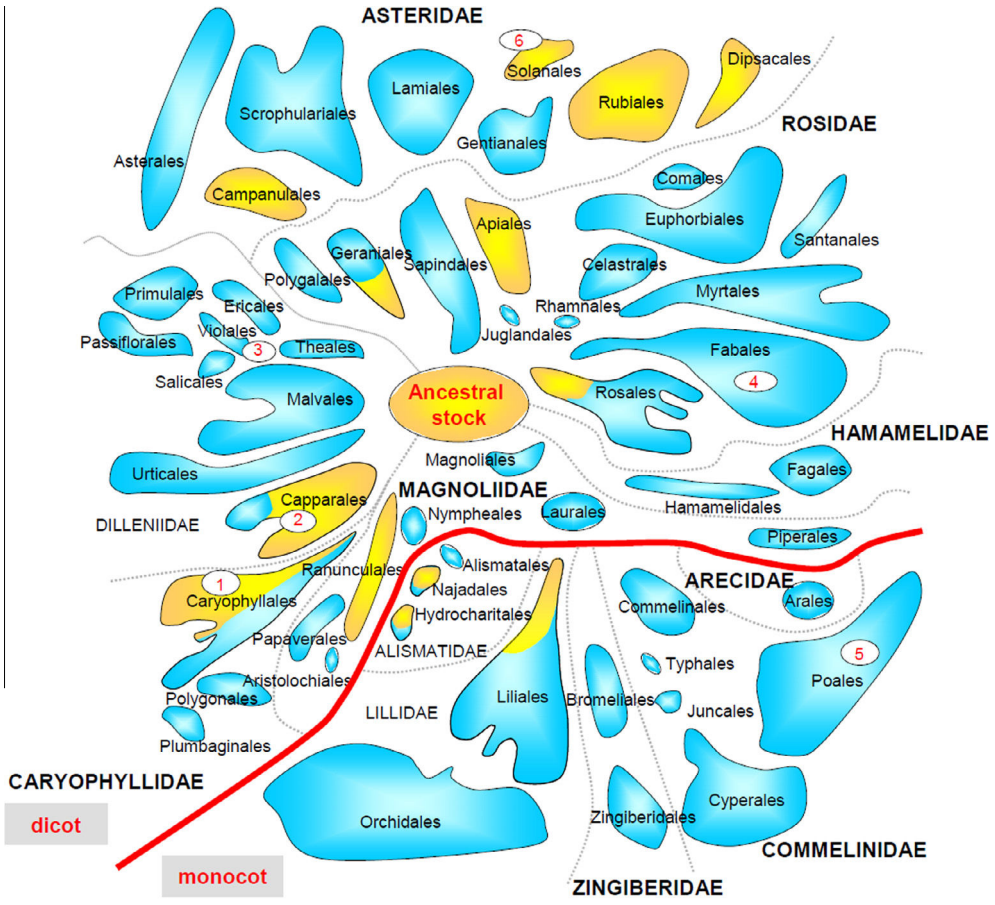

1, *Spinacia*; 2, *Arabidopsis*; 3, *Cucumis*; 4, *Pisum*, *Medicago*, *Lotus*, *Glycine*; 5 *Zea*, *Hordeum*; 6, *Lycopersicon*.

sn-1/*sn*-2	C16:3 plants	C18:3 plants
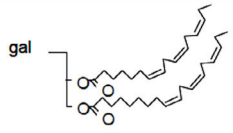	C18:3/C16:3	-
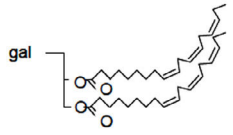	C18:3/C18:3	C18:3/C18:3

Fig. 6. Evolution of the plastidial (prokaryotic) and extra-plastidial (eukaryotic) pathways, generating substrates for galactoglycerolipids in Angiosperms. Two kinds of angiosperms have been distinguished based on their ω3-trienoic fatty acid composition in photosynthetic tissues. The *cis*-9,12,15-octadecatrienoic acid/*cis*-7,10,13-hexadecatrienoic acid (or C18:3/C16:3) balance reflects the pathways that produce diacyl-precursors for galactoglycerolipids: a plastidial or prokaryotic one and an extra-plastidial or eukaryotic one. Mongrand et al. [54,84] have analyzed the correlation between the existence of these pathways and the evolutionary classification of Angiosperms. By using *cis*-7,10,13-hexadecatrienoic acid as a marker for the existence of the plastidial pathway, they studied the fatty acid composition of 468 plant species distributed among 141 botanical families. The lower part illustrates the distribution of major MGDG molecular species in C16:3 and C18:3 plants. The upper part of the figure shows the extrapolated distribution of so called C16:3 plants (in yellow) and C18:3 plants (in blue) in the classification of angiosperms. The blue color thus reflects the loss of the prokaryotic pathway in galactoglycerolipids. Number allows localizing major plants analyzed in the literature, 1, spinach; 2, *Arabidopsis*; 3, cucumber; 4, pea, alfalfa, soybean; 5, corn, wheat; 6, tomato.

that the primary endosymbiosis with a cyanobacteria had been accompanied by some associations with other prokaryotes who provided substantial portions of genetic material [90]. In the absence of any trace of the cyanobacterial system in eukaryotes, we thus propose that acquisition of Chloroflexi-type *MGD* likely occurred very early during the primary endosymbiotic process.

In angiosperms, *MGD* genes have evolved into two main types, denoted A and B, that were first characterized in spinach [91] and *Arabidopsis* [92]. Type A is characterized by a cleavable N-terminal region (about 100 amino acids) allowing targeting to chloroplasts via the translocon protein import system. By contrast, Type B is characterized by a very short non-cleavable N-terminus. In the

case of *Arabidopsis*, type A has only one member, MGD1, whereas type B has two members, MGD2 and MGD3 [92]. Based on *in vitro* enzymatic studies, analyses of subcellular fractions of chloroplast membranes, and GFP-fusion localization by epifluorescence microscopy [91–96], MGD1 was shown to be the most abundant and most active enzyme, localized in the inner envelope membrane, and to be essential for the expansion of thylakoids. This subcellular localization is consistent with the presence of an N-terminal transit peptide. A knockout of *MGD1* [97] is lethal in the absence of an external source of carbon substrate [98]. MGD2 and MGD3 are in the outer envelope membrane and their expression is triggered in some stress conditions, such as a shortage of phosphate [92]. Simple and combined genetic disruptions of *MGD2* and *MGD3* genes have no striking phenotype in normal growth conditions [99], so these enzymes seem likely to act mostly in specific contexts like in response to phosphate starvation or in specific cell types such as elongating pollen tubes [100,101]. Type B seems therefore to be an invention of Angiosperms.

Based on the gene structures in *Arabidopsis*, *MGD2* lacks two introns (Fig. 7), suggesting that the ancestral sequences for *MGD1* and *MGD3* originated from an early divergence marked by a deep modification of the N-terminal region and that *MGD2* originated likely from the duplication of a *MGD3* ancestral sequence [92].

A comprehensive phylogenetic analysis has shown that Bryophytes had only one type of *MGD* and that the divergence between Type A and B preceded that of Gymnosperms and Angiosperms [64]. Based on phylogenetic tree calibrations, the A/B divergence was dated to around 320 million years ago, during the Carboniferous period, and so after the emergence of Spermatophyta. By comparing functional and phylogenetic studies, this recent evolution of *MGD* genes in Spermatophyta suggests an increased specialization of a novel type (Type B), at the periphery of chloroplasts, to respond to environmental changes (e.g., nutrient shortages) in the context of an intense membrane lipid remodeling within plant cells.

3.2.2. Cyanobacterial-type dgdA in Cyanidiales, a subdivision of Rhodophyta

By contrast with the synthesis of MGDG, two systems exist in eukaryotes to synthesize DGDG. A small number of sequenced red algae contain, in their plastid genome, orthologs of the cyanobacterial *dgdA* gene. The presence of *dgdA* is thus clear in the

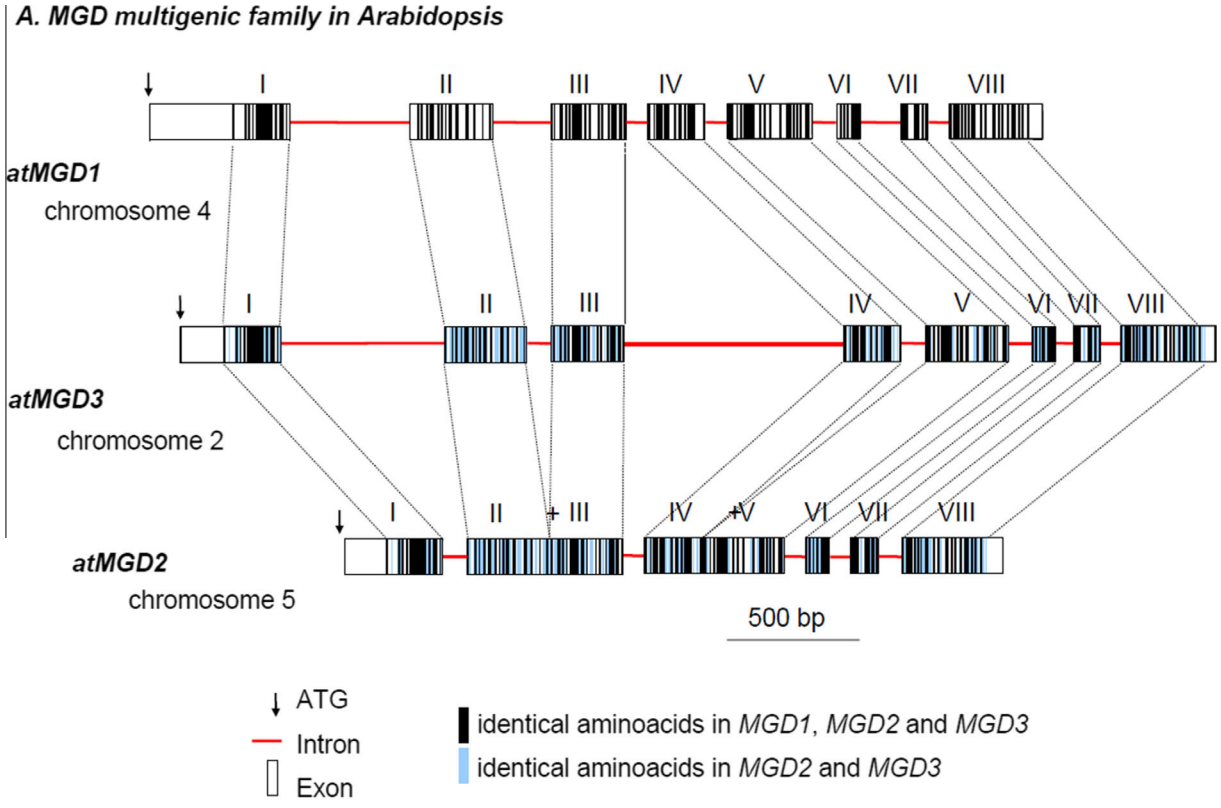

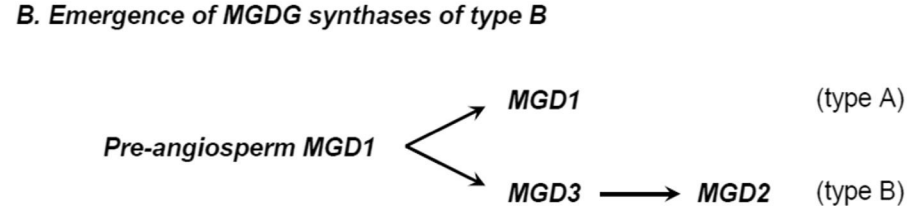

Fig. 7. Type A and Type B *MGD* genes. (A) Genomic organization of *MGD1*, *MGD2* and *MGD3* in *Arabidopsis*. Introns are presented as lines and exons as rectangles. Exons were compared for identical translated amino acids. Black rectangles, identical amino acids among the 3 proteins; blue rectangles, identical amino acids between MGD2 and MGD3 (not observed in MGD1). MGD1 has a longer N-terminal domain corresponding to a chloroplast transit peptide. (B) Model of evolutionary divergence leading to the two types of MGD proteins.

genomes of *C. merolae*, *C. caldarium* and *G. sulphuraria* [41,42]. Interestingly, *C. merolae* contains a typically eukaryotic MGD enzyme that was confirmed to have a MGDG synthase activity by expression in *E. coli* [41]. Cyanidiales contain species living in very acidic environments, which might have been isolated early after the primary endosymbiosis. The conservation of the *dgdA* gene in Cyanidiales supports an early divergence of this group amongst red algae and provides a clue about the loss of cyanobacterial galactolipid biosynthesis genes.

3.2.3. DGDs in all other primary endosymbionts (Rhodophyta, Glaucophyta, Chlorophyta and Plants)

Based on previous reports and on systematic surveys of genomic databases, no *dgdA* ortholog can be detected in the plastid genomes of multicellular red algae, including in *Gracilaria* or *Porphyra*. No *dgdA* gene could be found in the glaucophyta *Cyanophora*, the green alga *Chlamydomonas*, the moss *Physcomitrella*, nor in higher plants [41,87]. By contrast, orthologs of the *DGD* genes identified in Angiosperms [39] have been unambiguously identified in Glaucophyta, Chlorophyta and most Rhodophyta (except Cyanidiales, discussed above) [41,87]. DGD genes have also been found in the genome of the Bryophyte *Physcomitrella patens* [102].

In Angiosperms, two types of *DGD* genes could be identified based on primary sequences. One type, known as *DGD1* in *Arabidopsis*, is a two-domain protein with an N-terminal segment of unknown function, and a C-terminal galactosyltransferase domain [103,104]. The second type, known as DGD2 in *Arabidopsis*, corresponds to a shorter amino acid sequence, consisting only of a galactosyltransferase domain. The DGD1 and DGD2 galactosyltransferase domains belong to the GT4 family defined in the CAZy classification [69].

The expression patterns of *MGD1*, *MGD2*, *MGD3*, *DGD1* and *DGD2* in different tissues of *Arabidopsis* or in response to some stresses, such as phosphate shortage, indicate that MGDs and DGDs act as specific pairs [34,92,100,104–107]. On the one hand, *DGD1* and *MGD1* are expressed in green tissues and the corresponding enzymes act together in the biogenesis of thylakoid lipids. On the other hand, *DGD2* is expressed together with *MGD2* and/or *MGD3* and the corresponding enzymes act together to produce galactolipids in non-green tissues (including in roots and flower organs) and in response to environmental stress. Because MGD1 and DGD1 are localized in different membranes, the inner and outer envelope membranes, respectively, a specific transfer of MGDG from one membrane to the other is necessary. Furthermore, because MGD2/MGD3 and DGD2 are found in the outer envelope membrane, a metabolic channeling is supposedly made easier thanks to the co-localization of enzymes. Since Type B MGDs are unique to Spermatophyta, the emergence of this system might be optimal to respond to signaling processes occurring in the cytosol and at the periphery of the chloroplast.

The DAG → MGDG → DGDG chanelling via the MGD1/DGD1 or the MGD2;MGD3/DGD2 system does not mean that all MGDG is used as substrates for DGDG. Only a fraction of MGDG, that with a eukaryotic structure, is converted into DGDG by the action of DGDG synthase [37]. In angiosperms, the fatty acid compositions of MGDG and DGDG are therefore different, with MGDG being 16:3-rich and DGDG being 16:3-poor. This observation suggests that (i) a desaturase (FAD5) catalyzes the very rapid desaturation of 16:0 into 16:1 at the *sn*-2 position of MGDG, and that (ii) 16:1, 16:2 and 16:3-MGDG species are not utilized by DGD1 and DGD2. This being said, one would expect that a correlation of the evolution of DGDs might have occurred, linking the evolution of MGD1 with DGD1, MGD2/MGD3 with DGD2 and possibly MGD1/DGD1 with FAD5. These hypothetical co-evolutionary processes have not been explored yet.

In the genome of the Bryophyte *P. patens*, the four orthologous sequences (Phypadraft_162919, Phytadraft_137342, Phytadraft_216055 and Phytadraft _218058) have longer N-terminal domains, like the angiosperm DGD1. Similarly, sequences in Chlorophyta, such as the unique DGD protein in *C. reinhardtii* (XP_001693597; Cre13.g583600), harbor longer N-terminal extensions like DGD1. By contrast, some sequences in Rhodophyta, like the unique DGD protein in *Chondrus crispus*, consist only of the GT4 domain, like the angiosperm DGD2. It seems therefore that the evolution of DGD genes is not simple. The conservation level of the GT4 domain seems furthermore to be higher than that of the N-terminal domain. The emergence of DGD2 in Spermatophyta might therefore correlate with the emergence of MGDs of Type B, but this hypothesis still needs confirmation.

4. From primary plastids to secondary plastids

4.1. The puzzling question of the lipidome of secondary plastids

Although the presence of MGDG and DGDG was confirmed decades ago in a range of important phyla including secondary endosymbionts deriving from green algae, e.g., *E. gracilis* [24], or Chromalveolata deriving from red algae, e.g., the non-photosynthetic diatom *Nitzschia alba* [108], the photosynthetic diatom *P. tricornutum* [25] and the eustigmatophyte *Nannochloropsis* [109,110], we still lack clear information about (i) the precise localization of galactoglycerolipids in the three to four membranes that delineate the secondary chloroplasts and (ii) the subcellular mapping of the biosynthetic enzymes. While it is common for secondary endosymbionts to have an intricate association of their chloroplasts and endoplasmic reticulum (often referred to as Chloroplast-ER) [111,112] various representatives of Chromalveolata such as *Ochromonas danica* and *P. tricornutum* also display continuity between the Chloroplast-ER and the nuclear membrane [111]. Other notable examples include Apicomplexans, which are characterized by the conservation of a reduced non-photosynthetic relict plastid, known as the apicoplast [113,114]. Apicomplexa is a phylum of unicellular eukaryotes that mainly comprises obligates intracellular parasites, responsible of major human diseases such as malaria and toxoplasmosis, respectively cause by *Plasmodium* spp. and *T. gondii*. To the exception of *Cryptosporidium* spp. and possibly free living gregarins, all Apicomplexa possess an apicoplast. Very recent analyses have provided evidence that neither MGDG nor DGDG were present in the apicoplast [115], indicating a rare but puzzling loss of the galactoglycerolipid biosynthetic pathway. Following secondary endosymbiosis, many genes were transferred from the endosymbiont to the host cell nucleus, which means that protein targeting mechanisms must have adapted accordingly to allow transport across the newly acquired membrane structure [116,117]. Here, we discuss how the metabolism of galactoglycerolipids has evolved following each of the secondary endosymbiotic events illustrated in Fig. 2.

Based on the variety of evolutionary scenarios, one possibility is that each lineage has had an independent evolution. The metabolic pathways in secondary endosymbionts combine metabolic routes inherited from the ancient cyanobacteria at the origin of chloroplasts, the primary endosymbiont genome, the secondary endosymbiont genome and multiple other organisms via horizontal transfers. Thus, in this part of the review, we do not try to define a unique scheme but rather address questions that in our opinion should be prioritized in future research.

4.2. Multiple possible systems to synthesize fatty acids de novo in the stroma and the cytosol

In most secondary endosymbionts studied so far, the neosynthesis of fatty acids occurs mainly via a FASII system likely to have

been inherited from the cyanobacterial progenitor of the plastid. In some species, e.g., *Nannochloropsis* and *Toxoplasma*, a cytosolic FASI also exists. In the case of a co-occurrence of both FASII and FASI, the most extensive biochemical studies have been performed in *T. gondii*, with apparently contradicting results [118,119] and in a galactolipid-free context. Current consensus is that the apicoplast pathway essential in Apicomplexa parasites as based on molecular disruption of the pathway. However, this essentiality differs depending on the parasite: whilst it is always essential for *T. gondii* [119], it appears to be only essential during *Plasmodium* asymptomatic liver stages or mosquito sporozoite division stages [120–122]. Initial biochemical analyses have suggested that the *T. gondii* FASII was not essential for bulk lipid synthesis but rather for the apicoplast biogenesis and maintenance [118,119,123], possibly due to a chloroplast-analogous necessity for the synthesis of these lipids to be utilized during the growth and division of this organelle. However, more refined metabolic labeling experiments showed that the *T. gondii* FASII was responsible for the majority of the long chain saturated fatty acids [123]. Lipid analyses of the apicoplast of *P. falciparum* confirmed that this organelle was highly enriched in saturated fatty acids (~90% of all fatty acids), mainly in C18:0 [115]. The C18:0-ACP desaturation activity might have been also lost in this organelle. Furthermore, the apicoplast seem to be able to utilize FA to generate PA by stepwise acylations of a G3-P backbone via a glycerol 3-phosphate acyltransferase (ATS1) and a lyso-phosphatidic acid (LPA) acyltransferase (ATS2/LPAAT), both predicted to be present in the apicoplast [51,121,124]. Recently, the disruption of the rodent malaria *P. yoelii* ATS1 gene led to the impairement of the biogenesis of the parasite intracellular compartments, including the apicoplast, during liver stages [125]. Together, these results suggest that the apicoplast might be involved in bulk lipid neosynthesis in Apicomplexa via the generation of FA, LPA and/or PA. The role of this prokaryotic pathway in the absence of galactoglycerolipids remains to be fully understood. The respective roles of FASII in the apicoplast and of FASI and fatty acid elongase in the cytosol of *T. gondii* has been recently analyzed in the context of a parasitic life style of this Apicomplexa [123,126].

The combination of functionally active plastid FASII and cytosolic FASI has been known in *E. gracilis* since the early 1970s [127], indicating that this dual FASII/FASI system exists in photosynthetic secondary endosymbionts of the green lineage. In the red lineage, recent efforts to sequence the genomes of different *Nannochloropsis* species (e.g., *N. oceanica* [128]) have highlighted that, in addition to a plastid FASII, a cytosolic FASI-like protein also exists (e.g., CCMP1779 in *N. oceanica*). FASI enzymes are similar to animal FAS, but also close to polyketide synthases and it is not always straightforward to infer their function from primary structure [129]. To our knowledge, the activity harbored by the *Nannochloropsis* FASI-like enzyme has not yet been fully characterized. It has been speculated that FASI in *Nannochloropsis* catalyzes the production of shorter fatty acids (C14:0) as proposed in *Schizochytrium* [130], a heterotrophic species belonging to the Labyrinthulomycetes, phylogenetically related to the Eustigmatophytes within the Heterokonts.

The origin of the fatty acids used as precursors for glycerolipids can therefore be far more complicated in secondary endosymbionts compared to primary ones. The fate of fatty acids, from their neosynthesis to their incorporation into galactoglycerolipids, is therefore obscure in most of the species that have so far been analyzed. It is difficult to address the question of the import of eukaryotic diacyl-precursors, synthesized outside secondary plastids, for the following reasons: (i) the simple C18/C18 or C18/C16 definition initially stated might not hold true with the set of acyl transferases acting in a given species, and (ii) the presence of 4 membranes around secondary chloroplasts makes the presence of an import system that would be homologous to that in the envelope of primary chloroplasts unlikely. It is therefore very difficult, based solely on the diacyl signature in glycerolipids, to infer the presence or absence of such a pathway. Metabolic labeling should thus be performed in each species of interest to assess the precise origin of precursors for plastid galactoglycerolipids. Nevertheless, regardless of this C16 and C18-based definition of eukaryotic molecular species, the large number of species accumulating ω3/ω6-VL-PUFAs in galactoglycerolipids, with C20 to C22 major molecular species, is striking [27,131,132], indicating that at least the omega pathway has been conserved.

4.3. The conservation of the omega pathway

In numerous secondary endosymbionts, the presence of ω3/ω6-VL-PUFAs (ARA, EPA, DHA) has been observed in galactoglycerolipids in both the green and the red lineages [27]. The highest level of EPA in MGDG and DGDG has been recently reported in the Chromerid *C. velia*, a close photosynthetic relative of Apicomplexa, with 70–80% EPA in MGDG and DGDG [86]. Based on genomic surveys, the synthesis of ω3/ω6-VL-PUFAs seems always to be catalyzed by cytosolic enzymes. The corresponding enzymes have been predicted in the sequenced genomes from the diatoms *T. pseudonana* [133] and *P. tricornutum* [134], and from the eustigmatophyte *Nannochloropsis* sp., e.g., *N. oceanica* [128]. Some of these enzymes have been functionally characterized, in particular in *P. tricornutum* and *T. pseudonana* [135–138]. In the Eustigmatophyte *Monodus subterraneus*, metabolic labeling experiments were performed using radiolabelled acetate or linoleic (C18:2) acid [139]. PC was mostly involved in the desaturation of C18 acyls, whereas PE and DGTS were substrates for further desaturations of C20 acyls, resulting in the accumulation of C20:5 (EPA) in these protists [139]. Metabolic labeling results were consistent with PE and DGTS providing EPA, either as free C20:5 or as C20:5/C20:5-DAG for the synthesis of MGDG in the chloroplast [139]. The route from the cytosolic production of ω3/ω6-VL-PUFAs to their plastidial incorportation in galactoglycerolipids has been further assessed experimentally in *Phaeodactylum* [137] and *Nannochloropsis* [128]. The presence of an omega pathway, supplying the plastid with ω3/ω6-VL-PUFAs for galactoglycerolipids therefore seems to be one of the main features that has been conserved in secondary endosymbionts. As for the eukaryotic pathway in Angiosperms, it appears to have become the major provider of fatty acids for MGDG and DGDG in several species, whereas the prokaryotic route has assumed a minor role. This trend might be related to a better integration of plastid lipid synthases with extra-plastidial biosynthetic pathways. It might also highlight the importance of ω3/ω6-VL-PUFA specific functions.

4.4. Mapping galactolipid-synthesizing enzymes in the multiple membranes that delimit secondary plastids

Available genomic data indicate that secondary endosymbionts contain genes encoding eukaryotic MGDs and DGDs. In our surveys, we did not detect any orthologs of genes encoding cyanobacterial MGlcDG synthase or *dgdA*.

The question of the localization of MGD and DGD within the three to four membranes limiting secondary plastids has not been addressed experimentally, due to the lack of an accurate fractionation method for these organelles. The only secondary plastid that has been isolated to date is the apicoplast of *Plasmodium* [115], which does not contain any galactoglycerolipids (see below). The only secondary plastid in which galactoglycerolipids have been localized using anti-DGDG antibodies is from *Chromera* [86].

If we look more closely at the *P. tricornutum* example, we can predict three *MGD* genes. One of these (Phatr_14125) encodes a

protein harboring an unambiguous bipartite targeting sequence (signal peptide + chloroplast transit peptide) [140] consistent with its likely localization in the innermost membrane of the plastid. A second gene (Phatr_54168) encodes a protein with an N-terminal segment that shares some features of a bipartite targeting sequence. The third gene (Phatr_9619) encodes a protein whose subcellular localization cannot be predicted using available bioinformatic tools. These MGDs might be localized in different plastid membranes or possibly outside. The *P. tricornutum* genome is also predicted to contain three *DGD* genes, all having a longer N-terminal sequence than the angiosperm *DGD2*. One gene (Phatr_12884) encodes a protein with a bipartite targeting sequence, supporting a localization in the innermost membrane of the chloroplast. The two other genes (Phatr_11390 and Phatr_43116) have no known targeting sequences. They might be located in more peripheral membranes or even outside the plastid. Like in angiosperms, a Phatr_14125 (MGD1)/Phatr_12884 (DGD1) system might operate in the innermost membrane for the synthesis of thylakoids, whereas other combinations of enzymes might act in other locations for the expansion of specific membranes or to respond to some physiological or environmental contexts. The precise localization of these enzymes is therefore an important objective for future efforts, as are attempts to discover novel types of diatom targeting sequences [141].

4.5. Origin of MGDs and DGDs in Chromalveolates

The nuclear genomes of Chomalveolata contain genes deriving from the different actors of the secondary endosymbiosis, including the primary eukaryotic red alga and the secondary eukaryotic host. As mentioned above, a phylogenomic analysis of the diatom proteome using complete genome data from *Thalassiosira* and *Phaeodactylum* has allowed the identification of about 2500 genes likely derived from eukaryotic algae [48], with more than 70% of these genes being of green rather than red lineage provenance. These green genes seem to derive from an ancestor organism closely related to present-day Prasinophyta, e.g., *Micromonas* and *Ostreococus*. The green gene contribution constitutes ~16% of the diatom proteome and is also found in various Chromalveolata, including Apicomplexa and Haptophyta [48]. The occurrence of green genes together with genes inherited from the red algal endosymbiont seems to predate the split of Cryptophyta and Haptophyta from other Chromalveolata [48]. These conclusions have been recently reevaluated and the detection of green genes might have been overestimated due to a taxonomic sampling bias [142]. The detection of horizontal transfers of genes deriving from other actors than those strictly involved in the secondary endosymbiosis is reminiscent to the vast proportion of bacterial genes also found in primary endosymbiosis. In primary endosymbionts, *MGD* genes were thus shown to derive from Chloroflexi bacteria and the source of *DGD* genes is unknown.

A similar question can be raised about the red or green origin of *MGD* and *DGD* genes in Chromalveolata. In published phylogenetic analyses, MGD sequences from *Phaeodactylum*, *Thalassiosira* and *Aureococcus* are more closely related to the sequence from the Rhodophyta *Cyanidioschyzon*, than from *Ostreococcus* and *Micromonas*, supporting a red algal origin. Nevertheless, since we could not reproduce the bootstrap values of this study by reiterating the phylogenetic reconstruction, this origin should be re-evaluated. A refined analysis of the DGD sequences should also be undergone to answer this question.

4.6. Loss of galactolipids in the secondary plastid of Apicomplexa

The apicoplast in Apicomplexa is a very specific case amongst secondary plastids, as it contains the smallest known plastid circular DNA, with the most reduced genome [7,113,143–145]. This organelle has lost its photosynthetic capacity and no photosynthetic genes have been detected. Significant efforts have focused on the search for galactoglycerolipids by metabolic labeling with radioactive precursors [146,147], immunostaining strategies [148] or whole parasite lipidomic analyses [148,149].

The search for *MGD* or *DGD* orthologs in Apicomplexa has also been inconclusive, although both *P. falciparum* and *T. gondii* genomes are now available [150,151]. The genome of *P. falciparum* is particularly difficult to mine, due to a strong nucleotidic compositional bias [150,152,153]. Approximately half of the genes have been functionally annotated, due to improved bioinformatics tools [154]. Using the CAZy classification [69], no glycosyltransferase of the GT28 family and only one of the GT4 family, unrelated to DGD, could be identified in *Plasmodium*. In spite of the lack of these enzymes, it could not be excluded that galactoglycerolipids might be synthesized via the action of a non-homologous set of glycosyltransferases in Apicomplexa.

Other groups of secondary endosymbionts also contain non-photosynthetic species. For instance, the non-photosynthetic diatom *N. alba* was shown to contain galactoglycerolipids [108]. Additional evidence for loss of galactoglycerolipids in the apicoplast was therefore required. Very recently, purification of the apicoplast from *P. falciparum* has been achieved [115]. This is actually the first report of the isolation of a secondary plastid. The method, based on immunopurification with magnetic beads, yielded sufficient amounts of purified organelle to perform an in-depth lipidomic analysis. No galactoglycerolipid could be detected, providing the first evidence for the absence of this landmark lipid of green and non-green plastids. Other lipids, such as sphingomyelin, ceramides and cholesterol, were detected and, along with most apicoplast structural lipids, were proposed to be generated and imported from the endomembranes, at least during this life stage [115].As mentioned above, *C. velia*, a close relative of Apicomplexa, has large amounts of MGDG and DGDG [86] and its genome contains orthologs of *MGD* and *DGD* genes [86]. Bioinformatic predictions were confirmed by biochemical measurements and metabolic labeling [86]. Chromerida like *C. velia* and *Vitrella brassicaformis* [155] share a common photosynthetic ancestor with Apicomplexa. Comparative studies might therefore help us understand the evolutionary history of the galactoglycerolipid pathway in Apicomplexa in the context of the disappearance of photosynthesis combined with the dramatic simplification of the parasite's lipid metabolism.

5. Conclusion and perspectives

In conclusion, the evolution of galactoglycerolipid metabolism is marked by important transitions. In cyanobacteria, all species rely on a stepwise synthesis via a glucosyl intermediate, catalyzed by a MGlcDG synthase, incorporating glucose from UDP-Glc, an unknown epimerase converting glucose into galactose, and a dgdA-type DGDG synthase. As an exception to this rule, some cyanobacteria like *Gloeobacter* sp. have acquired a bacterial MGD enzyme by a recent horizontal transfer, enabling them to synthesize MGDG by direct incorporation of galactose.

In the conversion of a cyanobacterial endosymbiont into the primary plastid, the MGlcDG synthase/epimerase system was rapidly lost, and it can no longer be found in any present-day primary endosymbiont. On the other hand, a *MGD* gene from a Chloroflexi-like ancestor has been acquired by horizontal transfer. In some red algae living in acidic environments, the Cyanidiales, a DgdA-type DGDG synthase of cyanobacterial origin has been conserved, whereas in all other eukaryotes the synthesis of this lipid relies on *DGD* genes of unknown origin. The emergence of eukaryotic MGD and DGD enzymes is therefore not synchronous in all

phylogenetic groups. MGD and DGD are thus likely to have evolved by duplication and intense reorganization of N-terminal domains. Type A and B MGDG synthases have emerged in Spermatophyta, with Type A being dedicated to the production of lipids for thylakoids, and Type B operating mostly in non-green tissues and in response to some environmental stresses such as phosphate limitation. Pairs of MGD and DGD isoforms seem to act together, like MGD1/DGD1 and (MGD2;MGD3)/DGD2 in *Arabidopsis*. The evolution of primary endosymbionts seems to reflect an increasing level of integration with the lipid metabolism of the whole cell. In particular precursors for the synthesis of galactoglycerolipids seem to be more and more dependent on import from the cytosol, via the so-called eukaryotic pathway and/or the omega pathway.

With respect to the conversion from primary endosymbionts to secondary plastids, many important questions remain to be elucidated, in particular regarding the subcellular topology of MGD and DGD enzymes in the three to four membranes that bound secondary chloroplasts. Because secondary endosymbionts are not monophyletic, multiple scenarios can be envisaged. MGD and DGD genes seem to be conserved in all cases except Apicomplexa. Based on published phylogenetic studies, Chromalveolata *MGD* genes seem to derive from the red algal endosymbiont rather than from a cryptic Prasinophyta algal source. The origin of *DGD* genes in Chromalveolata remains to be established. The omega pathway feeding galactoglycerolipids with extraplastidial precursors has been conserved in numerous species. The machinery importing ω3/ω6-VL-PUFAs in the secondary chloroplast and the benefits for their high proportion of galactoglycerolipids are still unknown, and MGDG and DGDG have been lost in the apicoplast. How a plastid can be maintained without galactoglycerolipids is a major question for future research, and will require both the evolution of the upstream plastidial biosynthesis of PA and the import of all other membrane components to be addressed. There is no doubt that the analysis of galactoglycerolipid pathways in complex plastids will be a fascinating subject of research in the next decade.

Acknowledgements

The authors were supported by Agence Nationale de la Recherche (ANR-10-BLAN-1524, ReGal; ANR-12-BIME-0005, DiaDomOil; ANR-12-JCJC, ChloroMitoLipid and ApicoLipid), ATIP-Avenir-FINO-VI (C.Y.B.), Région Rhône-Alpes, the Labex GRAL (Grenoble Alliance for Integrated Structural Cell Biology), Investissement d'Avenir OCEANOMICS, the EU-funded Diatomite and MicroB3 projects and the Australian Research Council.

Appendix A. Supplementary data

Supplementary data associated with this article can be found, in the online version, at http://dx.doi.org/10.1016/j.plipres.2014.02.001.

References

[1] Archibald JM, Keeling PJ. Recycled plastids: a 'green movement' in eukaryotic evolution. Trends Genet 2002;18:577–84.
[2] Kutschera U, Niklas KJ. Endosymbiosis, cell evolution, and speciation. Theory Biosci 2005;124:1–24.
[3] Gould SB, Waller RR, McFadden GI. Plastid evolution. Annu Rev Plant Biol 2008;59:491–517.
[4] Ginger ML, McFadden GI, Michels PAM. The evolution of organellar metabolism in unicellular eukaryotes Introduction. Philos Trans R Soc Lond B Biol Sci 2010;365:693–8.
[5] Janouskovec J, Horak A, Obornik M, Lukes J, Keeling PJ. A common red algal origin of the apicomplexan, dinoflagellate, and heterokont plastids. Proc Natl Acad Sci U S A 2010;107:10949–54.
[6] Lim L, McFadden GI. The evolution, metabolism and functions of the apicoplast. Philos Trans R Soc Lond B Biol Sci 2010;365:749–63.
[7] McFadden GI. Endosymbiosis and evolution of the plant cell. Curr Opin Plant Biol 1999;2:513–9.
[8] Falconet D. Origin, evolution and division of plastids. In: Eaton-Rye J, Tripathy B, Sharkey TD, editors. Photosynthesis: plastid biology, energy conversion and carbon assimilation. Springer Verlag; 2012. p. 35–61.
[9] Carter HE, Mccluer RH, Slifer ED. Lipids of wheat flour.1. Characterization of galactosylglycerol components. J Am Chem Soc 1956;78:3735–8.
[10] Allen CF, Hirayama O, Good P. Lipid composition in photosynthetic systems. In: Goodwin TW, editor. Biochemistry of chloroplasts. London: Academic Press; 1966. p. 195–200.
[11] Moellering ER, Muthan B, Benning C. Freezing tolerance in plants requires lipid remodeling at the outer chloroplast membrane. Science 2010;330:226–8.
[12] Moellering ER, Benning C. Galactoglycerolipid metabolism under stress: a time for remodeling. Trends Plant Sci 2011;16:98–107.
[13] Nichols BW. Separation of the lipids of photosynthetic tissues: improvements in analysis by thin-layer chromatography. Biochim Biophys Acta 1963;70:417–22.
[14] Allen CF, Good P, Davis HF, Chisum P, Fowler SD. Methodology for the separation of plant lipids and application to spinach leaf and chloroplast lamellae. J Am Oil Chem Soc 1966;43:223–31.
[15] Nichols BW, Harris RV, James AT. The lipid metabolism of blue-green algae. Biochem Biophys Res Commun 1965;20:256–62.
[16] Nichols BW. Light induced changes in the lipids of *Chlorella vulgaris*. Biochim Biophys Acta 1965;106:274–9.
[17] Safford R, Nichols BW. Positional distribution of fatty acids in monogalactosyl diglyceride fractions from leaves and algae – structural and metabolic studies. Biochim Biophys Acta 1970;210:57–64.
[18] Bloch K, Constantopoulos G, Kenyon C, Nagai J. Lipid metabolism in algae in the light and in the dark. In: Goodwin TW, editor. Biochemistry of chloroplast. New York: Academic Press; 1967. p. 195–211.
[19] Eichenberger W. Lipids of *Chlamydomonas reinhardtii* under different growth conditions. Phytochemistry 1976;15:459–63.
[20] Nichols BW. The lipid of a moss (*Hypnum cupressiforme*) and of the leaves of green holly (*Ilex aquifolium*). Phytochemistry 1965;4:769–72.
[21] Sato N, Furuya M. The composition of lipids and fatty acids determined at various stages of haploid and diploid generations in the fern *Adiantum capillus veneris*. Physiol Plantarum 1984;62:139–47.
[22] Jamieson GR, Reid EH. Leaf lipids of some conifer species. Phytochemistry 1972;11:269–75.
[23] Allen CF, Good P, Davies HF, Foxler SD. Plant and chloroplast lipids. I-Separation and composition of major spinach lipids. Biochem Biophys Res Commun 1964;15:424–30.
[24] Constantopoulos G, Bloch K. Effect of light intensity on lipid composition of *Euglena gracilis*. J Biol Chem 1967;242:3538–42.
[25] Arao T, Kawaguchi A, Yamada M. Positional distribution of fatty-acids in lipids of the marine diatom *Phaeodactylum tricornutum*. Phytochemistry 1987;26:2573–6.
[26] Gounaris K, Barber J. Monogalactosyldiacylglycerol – the most abundant polar lipid in nature. Trends Biochem Sci 1983;8:378–81.
[27] Guschina IA, Harwood JL. Lipids and lipid metabolism in eukaryotic algae. Prog Lipid Res 2006;45:160–86.
[28] Boudière L, Michaud M, Petroutsos D, Rébeillé F, Falconet D, Bastien O, et al. Glycerolipids in photosynthesis: composition, synthesis and trafficking. Biochim Biophys Acta Bioenerg 2014;1837:470–80.
[29] Mizusawa N, Wada H. The role of lipids in photosystem II. Biochim Biophys Acta 2012;1817:194–208.
[30] Loll B, Kern J, Saenger W, Zouni A, Biesiadka J. Lipids in photosystem II: interactions with protein and cofactors. Biochim Biophys Acta 2007;1767:509–19.
[31] Schleiff E, Soll J, Kuchler M, Kuhlbrandt W, Harrer R. Characterization of the translocon of the outer envelope of chloroplasts. J Cell Biol 2003;160:541–51.
[32] Tjellstrom H, Andersson MX, Larsson KE, Sandelius AS. Membrane phospholipids as a phosphate reserve: the dynamic nature of phospholipid-to-digalactosyl diacylglycerol exchange in higher plants. Plant Cell Environ 2008;31:1388–98.
[33] Andersson MX, Larsson KE, Tjellstrom H, Liljenberg C, Sandelius AS. The plasma membrane and the tonoplast as major targets for phospholipid-to-glycolipid replacement and stimulation of phospholipases in the plasma membrane. J Biol Chem 2005;280:27578–86.
[34] Jouhet J, Marechal E, Baldan B, Bligny R, Joyard J, Block MA. Phosphate deprivation induces transfer of DGDG galactolipid from chloroplast to mitochondria. J Cell Biol 2004;167:863–74.
[35] Jouhet J, Marechal E, Block MA. Glycerolipid transfer for the building of membranes in plant cells. Prog Lipid Res 2007;46:37–55.
[36] Benning C. A role for lipid trafficking in chloroplast biogenesis. Prog Lipid Res 2008;47:381–9.
[37] Benning C. Mechanisms of lipid transport involved in organelle biogenesis in plant cells. Annu Rev Cell Dev Biol 2009;25:71–91.
[38] Shimojima M, Ohta H, Iwamatsu A, Masuda T, Shioi Y, Takamiya K. Cloning of the gene for monogalactosyldiacylglycerol synthase and its evolutionary origin. Proc Natl Acad Sci U S A 1997;94:333–7.
[39] Dormann P, Balbo I, Benning C. Arabidopsis galactolipid biosynthesis and lipid trafficking mediated by DGD1. Science 1999;284:2181–4.
[40] Awai K, Kakimoto T, Awai C, Kaneko T, Nakamura Y, Takamiya K, et al. Comparative genomic analysis revealed a gene for

monoglucosyldiacylglycerol synthase, an enzyme for photosynthetic membrane lipid synthesis in cyanobacteria. Plant Physiol 2006;141:1120–7.
[41] Awai K, Watanabe H, Benning C, Nishida I. Digalactosyldiacylglycerol is required for better photosynthetic growth of *Synechocystis* sp. PCC6803 under phosphate limitation. Plant Cell Physiol 2007;48:1517–23.
[42] Sakurai I, Mizusawa N, Wada H, Sato N. Digalactosyldiacylglycerol is required for stabilization of the oxygen-evolving complex in photosystem II. Plant Physiol 2007;145:1361–70.
[43] Parfrey LW, Barbero E, Lasser E, Dunthorn M, Bhattacharya D, Patterson DJ, et al. Evaluating support for the current classification of eukaryotic diversity. PLoS Genet 2006;2:e220.
[44] Curtis BA, Tanifuji G, Burki F, Gruber A, Irimia M, Maruyama S, et al. Algal genomes reveal evolutionary mosaicism and the fate of nucleomorphs. Nature 2012;492:59–65.
[45] Keeling PJ. Chromalveolates and the evolution of plastids by secondary endosymbiosis. J Eukaryot Microbiol 2009;56:1–8.
[46] Burki F, Shalchian-Tabrizi K, Pawlowski J. Phylogenomics reveals a new 'megagroup' including most photosynthetic eukaryotes. Biol Lett 2008;4:366–9.
[47] Kim E, Graham LE. EEF2 analysis challenges the monophyly of *Archaeplastida* and *Chromalveolata*. PLoS One 2008;3:e2621.
[48] Moustafa A, Beszteri B, Maier UG, Bowler C, Valentin K, Bhattacharya D. Genomic footprints of a cryptic plastid endosymbiosis in diatoms. Science 2009;324:1724–6.
[49] Brown AP, Slabas AR, Rafferty JB. Fatty acid biosynthesis in plants — metabolic pathways, structure and organization. In: Wada H, Murata N, editors. Lipids in photosynthesis. Dordrecht: Springer; 2010. p. 11–34.
[50] Miege C, Marechal E. 1,2-sn-Diacylglycerol in plant cells: product, substrate and regulator. Plant Physiol Biochem 1999;37:795–808.
[51] Dubots E, Botté C, Boudière L, Yamaryo-Botté Y, Jouhet J, Maréchal E, et al. Role of phosphatidic acid in plant galactolipid synthesis. Biochimie 2012;94:86–93.
[52] Heinz E. Enzymatic reactions in galactolipid biosynthesis. In: Tevini M, Lichtenthaler HK, editors. Lipids and lipid polymers. Berlin: Springer-Verlag; 1977. p. 102–20.
[53] Browse J, Warwick N, Somerville CR, Slack CR. Fluxes through the prokaryotic and eukaryotic pathways of lipid synthesis in the 16-3 plant *Arabidopsis thaliana*. Biochem J 1986;235:25–31.
[54] Mongrand S, Bessoule JJ, Cabantous F, Cassagne C. The C16:3/C18:3 fatty acid balance in photosynthetic tissues from 468 plant species. Phytochemistry 1998;49:1049–64.
[55] Stanier RY, Cohen-Bazire G. Phototrophic prokaryotes: the cyanobacteria. Annu Rev Microbiol 1977;31:225–74.
[56] Murata N, Omata T. Isolation of cyanobacterial plasma membranes. Methods Enzymol 1988;167:245–51.
[57] Lem NW, Stumpf PK. In vitro fatty acid synthesis and complex lipid metabolism in the cyanobacterium *Anabaena variabilis*: I. Some characteristics of fatty acid synthesis. Plant Physiol 1984;74:134–8.
[58] Stapleton SR, Jaworski JG. Characterization and purification of malonyl-coenzyme A – [Acyl-Carrier-Protein] transacylases from spinach and *Anabaena variabilis*. Biochim Biophys Acta 1984;794:240–8.
[59] Stapleton SR, Jaworski JG. Characterization of fatty acid biosynthesis in the cyanobacterium *Anabaena variabilis*. Biochim Biophys Acta 1984;794:249–55.
[60] Sato N, Murata N. Lipid biosynthesis in the blue-green alga (cyanobacterium), *Anabaena variabilis*. 3. UDP-glucose diacylglycerol glucosyltransferase activity in vitro. Plant Cell Physiol 1982;23:1115–20.
[61] Sato N, Murata N. Lipid biosynthesis in the blue-green alga, *Anabaena variabilis*. 2. Fatty acids and lipid molecular species. Biochim Biophys Acta 1982;710:279–89.
[62] Sato N, Murata N. Lipid biosynthesis in the blue-green alga, *Anabaena variabilis*.1. Lipid classes. Biochim Biophys Acta 1982;710:271–8.
[63] Omata T, Murata N. Glucolipid synthesis activities in cytoplasmic and thylakoid membranes from the cyanobacterium *Anacystis nidulans*. Plant Cell Physiol 1986;27:485–90.
[64] Yuzawa Y, Nishihara H, Haraguchi T, Masuda S, Shimojima M, Shimoyama A, et al. Phylogeny of galactolipid synthase homologs together with their enzymatic analyses revealed a possible origin and divergence time for photosynthetic membrane biogenesis. DNA Res 2012;19:91–102.
[65] Matsumoto K, Okada M, Horikoshi Y, Matsuzaki H, Kishi T, Itaya M, et al. Cloning, sequencing, and disruption of the *Bacillus subtilis* psd gene coding for phosphatidylserine decarboxylase. J Bacteriol 1998;180:100–6.
[66] Foht PJ, Tran QM, Lewis RN, McElhaney RN. Quantitation of the phase preferences of the major lipids of the *Acholeplasma laidlawii* B membrane. Biochemistry 1995;34:13811–7.
[67] Jorasch P, Wolter FP, Zahringer U, Heinz E. A UDP glucosyltransferase from *Bacillus subtilis* successively transfers up to four glucose residues to 1,2-diacylglycerol: expression of ypfP in *Escherichia coli* and structural analysis of its reaction products. Mol Microbiol 1998;29:419–30.
[68] Berg S, Edman M, Li L, Wikstrom M, Wieslander A. Sequence properties of the 1,2-diacylglycerol 3-glucosyltransferase from *Acholeplasma laidlawii* membranes. Recognition of a large group of lipid glycosyltransferases in eubacteria and archaea. J Biol Chem 2001;276:22056–63.
[69] Campbell JA, Davies GJ, Bulone V, Henrissat B. A classification of nucleotide-diphospho-sugar glycosyltransferases based on amino acid sequence similarities. Biochem J 1997;326:929–39.
[70] Holzl G, Zahringer U, Warnecke D, Heinz E. Glycoengineering of cyanobacterial thylakoid membranes for future studies on the role of glycolipids in photosynthesis. Plant Cell Physiol 2005;46:1766–78.
[71] Boudière L, Botte C, Saidani N, Lajoie M, Marion J, Bréhélin L, et al. Galvestine-1, a novel chemical probe for the study of the glycerolipid homeostasis system in plant cells. Mol BioSyst 2012;287:22367–76.
[72] Suh MC, Schultz DJ, Ohlrogge JB. Isoforms of acyl carrier protein involved in seed-specific fatty acid synthesis. Plant J 1999;17:679–88.
[73] Jouhet J, Dubots E, Maréchal E, Block MA. Lipid trafficking in plant photosynthetic cells. In: Wada H, Murata N, editors. Lipids in photosynthesis. Dordrecht: Springer; 2010. p. 349–72.
[74] Li-Beisson Y, Shorrosh B, Beisson F, Andersson MX, Arondel V, Bates PD, et al. Acyl-lipid metabolism. The Arabidopsis book. Washington: The American Society of Plant Biologists; 2010. p. 1–65.
[75] Joyard J, Ferro M, Masselon C, Seigneurin-Berny D, Salvi D, Garin J, et al. Chloroplast proteomics highlights the subcellular compartmentation of lipid metabolism. Prog Lipid Res 2010;49:128–58.
[76] Xu CC, Yu B, Cornish AJ, Froehlich JE, Benning C. Phosphatidylglycerol biosynthesis in chloroplasts of Arabidopsis mutants deficient in acyl-ACP glycerol-3-phosphate acyltransferase. Plant J 2006;47:296–309.
[77] Heinz E, Roughan PG. Similarities and differences in lipid metabolism of chloroplasts isolated from 18:3 and 16:3 plants. Plant Physiol 1983;72:273–9.
[78] Ohlrogge J, Browse J. Lipid biosynthesis. Plant Cell 1995;7:957–70.
[79] Sato N, Tsuzuki M, Kawaguchi A. Glycerolipid synthesis in *Chlorella kessleri* 11h. I. Existence of a eukaryotic pathway. Biochim Biophys Acta 2003;1633:27–34.
[80] Haigh WG, Yoder TF, Ericson L, Pratum T, Winget RR. The characterisation and cyclic production of a highly unsaturated homoserine lipid in *Chlorella minutissima*. Biochim Biophys Acta 1996;1299:183–90.
[81] Khozin-Goldberg I, Yu HZ, Adlerstein D, Didi-Cohen S, Heimer YM, Cohen Z. Triacylglycerols of the red microalga *Porphyridium cruentum* can contribute to the biosynthesis of eukaryotic galactolipids. Lipids 2000;35:881–9.
[82] Khozin I, Adlerstein D, Bigongo C, Heimer YM, Cohen Z. Elucidation of the biosynthesis of eicosapentaenoic acid in the microalga *Porphyridium cruentum* (II. Studies with radiolabeled precursors). Plant Physiol 1997;114:223–30.
[83] Shiran D, Khozin I, Heimer YM, Cohen Z. Biosynthesis of eicosapentaenoic acid in the microalga *Porphyridium cruentum*. I: The use of externally supplied fatty acids. Lipids 1996;31:1277–82.
[84] Mongrand S. De l'origine des lipides chloroplastiques eucaryotes – Distribution dans le règne végétal des lipides procaryotiques plastidiaux. Bordeaux: Université Victor Segalen; 1998.
[85] Dubots E, Audry M, Yamaryo Y, Bastien O, Ohta H, Marechal E, et al. Activation of the chloroplast monogalactosyldiacylglycerol synthase, MGD1, by phosphatidic acid and phosphatidylglycerol. J Biol Chem 2010:6003–11.
[86] Botte CY, Yamaryo-Botte Y, Janouskovec J, Rupasinghe T, Keeling PJ, Crellin P, et al. Identification of plant-like galactolipids in *Chromera velia*, a photosynthetic relative of malaria parasites. J Biol Chem 2011;286:29893–903.
[87] Riekhof WR, Sears BB, Benning C. Annotation of genes involved in glycerolipid biosynthesis in *Chlamydomonas reinhardtii*: discovery of the betaine lipid synthase BTA1(Cr). Eukaryot Cell 2005;4:242–52.
[88] Masuda S, Harada J, Yokono M, Yuzawa Y, Shimojima M, Murofushi K, et al. A monogalactosyldiacylglycerol synthase found in the green sulfur bacterium *Chlorobaculum tepidum* reveals important roles for galactolipids in photosynthesis. Plant Cell 2011;23:2644–58.
[89] Suzuki K, Miyagishima SY. Eukaryotic and eubacterial contributions to the establishment of plastid proteome estimated by large-scale phylogenetic analyses. Mol Biol Evol 2010;27:581–90.
[90] Price DC, Chan CX, Yoon HS, Yang EC, Qiu H, Weber AP, et al. *Cyanophora paradoxa* genome elucidates origin of photosynthesis in algae and plants. Science 2012;335:843–7.
[91] Miege C, Marechal E, Shimojima M, Awai K, Block MA, Ohta H, et al. Biochemical and topological properties of type A MGDG synthase, a spinach chloroplast envelope enzyme catalyzing the synthesis of both prokaryotic and eukaryotic MGDG. Eur J Biochem 1999;265:990–1001.
[92] Awai K, Marechal E, Block MA, Brun D, Masuda T, Shimada H, et al. Two types of MGDG synthase genes, found widely in both 16:3 and 18:3 plants, differentially mediate galactolipid syntheses in photosynthetic and nonphotosynthetic tissues in *Arabidopsis thaliana*. Proc Natl Acad Sci U S A 2001;98:10960–5.
[93] Marechal E, Block MA, Joyard J, Douce R. Purification of Udp-Galactose – 1,2-diacylglycerol galactosyltransferase from spinach chloroplast envelope membranes. C R Acad Sci Paris 1991;313:521–8.
[94] Marechal E, Block MA, Joyard J, Douce R. Comparison of the kinetic properties of MGDG synthase in mixed micelles and in envelope membranes from spinach chloroplast. FEBS Lett 1994;352:307–10.
[95] Marechal E, Block MA, Joyard J, Douce R. Kinetic properties of monogalactosyldiacylglycerol synthase from spinach chloroplast envelope membranes. J Biol Chem 1994;269:5788–98.
[96] Marechal E, Miege C, Block MA, Douce R, Joyard J. The catalytic site of monogalactosyldiacylglycerol synthase from spinach chloroplast envelope membranes. Biochemical analysis of the structure and of the metal content. J Biol Chem 1995;270:5714–22.

[97] Kobayashi K, Kondo M, Fukuda H, Nishimura M, Ohta H. Galactolipid synthesis in chloroplast inner envelope is essential for proper thylakoid biogenesis, photosynthesis, and embryogenesis. Proc Natl Acad Sci U S A 2007;104:17216–21.
[98] Kobayashi K, Fukuda H, Baba S, Kondo M, Nishimura M, Takamiya K, et al. Identification and characterization of a MGD1 knockout mutant in Arabidopsis. Plant Cell Physiol 2006;47. S32–S32.
[99] Kobayashi K, Awai K, Nakamura M, Nagatani A, Masuda T, Ohta H. Type-B monogalactosyldiacylglycerol synthases are involved in phosphate starvation-induced lipid remodeling, and are crucial for low-phosphate adaptation. Plant J 2009;57:322–31.
[100] Kobayashi K, Awai K, Takamiya K, Ohta H. Arabidopsis type B monogalactosyldiacylglycerol synthase genes are expressed during pollen tube growth and induced by phosphate starvation. Plant Physiol 2004;134:640–8.
[101] Botte CY, Deligny M, Roccia A, Bonneau AL, Saidani N, Hardre H, et al. Chemical inhibitors of monogalactosyldiacylglycerol synthases in *Arabidopsis thaliana*. Nat Chem Biol 2011;7:834–42.
[102] Nishiyama T, Fujita T, Shin IT, Seki M, Nishide H, Uchiyama I, et al. Comparative genomics of *Physcomitrella patens* gametophytic transcriptome and *Arabidopsis thaliana*: implication for land plant evolution. Proc Natl Acad Sci U S A 2003;100:8007–12.
[103] Ge C, Georgiev A, Ohman A, Wieslander A, Kelly AA. Tryptophan residues promote membrane association for a plant lipid glycosyltransferase involved in phosphate stress. J Biol Chem 2011;286:6669–84.
[104] Kelly AA, Froehlich JE, Dormann P. Disruption of the two digalactosyldiacylglycerol synthase genes DGD1 and DGD2 in Arabidopsis reveals the existence of an additional enzyme of galactolipid synthesis. Plant Cell 2003;15:2694–706.
[105] Dormann P, Benning C. Galactolipids rule in seed plants. Trends Plant Sci 2002;7:112–8.
[106] Kobayashi K, Nakamura Y, Ohta H. Type A and type B monogalactosyldiacylglycerol synthases are spatially and functionally separated in the plastids of higher plants. Plant Physiol Biochem 2009;47:518–25.
[107] Nakamura Y, Arimitsu H, Yamaryo Y, Awai K, Masuda T, Shimada H, et al. Digalactosyldiacylglycerol is a major glycolipid in floral organs of *Petunia hybrida*. Lipids 2003;38:1107–12.
[108] Anderson R, Livermore BP, Kates M, Volcani BE. The lipid composition of the non-photosynthetic diatom *Nitzschia alba*. Biochim Biophys Acta 1978;528:77–88.
[109] Schneider JC, Livne A, Sukenik A, Roessler PG. A mutant of *Nannochloropsis* deficient in eicosapentaenoic acid production. Phytochemistry 1995;40:807–14.
[110] Schneider JC, Roessler P. Radiolabeling studies of lipids and fatty acids in *Nannochloropsis* (Eustigmatophyceae), an oleaginous marine alga. J Phycol 1994;30:594–8.
[111] Gibbs SP. The chloroplasts of some algal groups may have evolved from endosymbiotic eukaryotic algae. Ann N Y Acad Sci 1981;361:193–208.
[112] Kroth PG, Chiovitti A, Gruber A, Martin-Jezequel V, Mock T, Parker MS, et al. A model for carbohydrate metabolism in the diatom *Phaeodactylum tricornutum* deduced from comparative whole genome analysis. PLoS One 2008;3:e1426.
[113] McFadden GI, Reith ME, Munholland J, Lang-Unnasch N. Plastid in human parasites. Nature 1996;381:482.
[114] Kohler S, Delwiche CF, Denny PW, Tilney LG, Webster P, Wilson RJ, et al. A plastid of probable green algal origin in Apicomplexan parasites. Science 1997;275:1485–9.
[115] Botte CY, Yamaryo-Botte Y, Rupasinghe TW, Mullin KA, MacRae JI, Spurck TP, et al. Atypical lipid composition in the purified relict plastid (apicoplast) of malaria parasites. Proc Natl Acad Sci U S A 2013;110:7506–11.
[116] Cavalier-Smith T. Genomic reduction and evolution of novel genetic membranes and protein-targeting machinery in eukaryote-eukaryote chimaeras (meta-algae). Philos Trans R Soc Lond B Biol Sci 2003;358:109–33 [discussion 33–34].
[117] Lang M, Apt KE, Kroth PG. Protein transport into "complex" diatom plastids utilizes two different targeting signals. J Biol Chem 1998;273:30973–8.
[118] Bisanz C, Bastien O, Grando D, Jouhet J, Marechal E, Cesbron-Delauw MF. *Toxoplasma gondii* acyl-lipid metabolism: de novo synthesis from apicoplast-generated fatty acids versus scavenging of host cell precursors. Biochem J 2006;394:197–205.
[119] Mazumdar J, Wilson EH, Masek K, Christopher AH, Striepen B. Apicoplast fatty acid synthesis is essential for organelle biogenesis and parasite survival in *Toxoplasma gondii*. Proc Natl Acad Sci U S A 2006;103:13192–7.
[120] Vaughan A, Vaughan AM, O'Neill MT, Tarun AS, Camargo N, Phuong TM, et al. Type II fatty acid synthesis is essential only for malaria parasite late liver stage development. Cell Microbiol 2009;14:506–20.
[121] Yu M, Kumar TR, Nkrumah LJ, Coppi A, Retzlaff S, Li CD, et al. The fatty acid biosynthesis enzyme FabI plays a keyrole in the development of liver-stage malarial parasites. Cell Host Microbe 2008;9:567–78.
[122] van Schaijk BC, Kumar TR, Vos MW, Richman A, van Gemert GJ, Li T, et al. Type II fatty acid biosynthesis is essential for *Plasmodium falciparum* sporozoite development in the midgut of Anopheles mosquitoes. Eukaryot Cell (in press).
[123] Ramakrishnan S, Docampo MD, Macrae JI, Pujol FM, Brooks CF, van Dooren GG, et al. Apicoplast and endoplasmic reticulum cooperate in fatty acid biosynthesis in apicomplexan parasite *Toxoplasma gondii*. J Biol Chem 2012;287:4957–71.
[124] Botte CY, Dubar F, McFadden GI, Marechal E, Biot C. *Plasmodium falciparum* apicoplast drugs: targets or off-targets? Chem Rev 2012:1269–83.
[125] Lindner SE, Sartain MJ, Hayes K, Harupa A, Moritz RL, Kappe SH, et al. Enzymes involved in plastid-targeted phosphatidic acid synthesis are essential for *Plasmodium yoelii* liver-stage development. Mol Microbiol 2014;10:1111–21.
[126] Ramakrishnan S, Serricchio M, Striepen B, Butikofer P. Lipid synthesis in protozoan parasites: a comparison between kinetoplastids and apicomplexans. Prog Lipid Res 2013;52:488–512.
[127] Goldberg I, Bloch K. Fatty acid synthetases in *Euglena gracilis*. J Biol Chem 1972;247:7349–57.
[128] Vieler A, Wu G, Tsai CH, Bullard B, Cornish AJ, Harvey C, et al. Genome, functional gene annotation, and nuclear transformation of the heterokont oleaginous alga *Nannochloropsis oceanica* CCMP1779. PLoS Genet 2012;8:e1003064.
[129] Metz JG, Roessler P, Facciotti D, Levering C, Dittrich F, Lassner M, et al. Production of polyunsaturated fatty acids by polyketide synthases in both prokaryotes and eukaryotes. Science 2001;293:290–3.
[130] Hauvermale A, Kuner J, Rosenzweig B, Guerra D, Diltz S, Metz JG. Fatty acid production in *Schizochytrium* sp.: involvement of a polyunsaturated fatty acid synthase and a type I fatty acid synthase. Lipids 2006;41:739–47.
[131] Yongmanitchai W, Ward OP. Growth of and omega-3 fatty acid production by *Phaeodactylum tricornutum* under different culture conditions. Appl Environ Microbiol 1991;57:419–25.
[132] Yongmanitchai W, Ward OP. Positional distribution of fatty acids, and molecular species of polar lipids, in the diatom *Phaeodactylum tricornutum*. J Gen Microbiol 1993;139:465–72.
[133] Armbrust EV, Berges JA, Bowler C, Green BR, Martinez D, Putnam NH, et al. The genome of the diatom *Thalassiosira pseudonana*: ecology, evolution, and metabolism. Science 2004;306:79–86.
[134] Bowler C, Allen AE, Badger JH, Grimwood J, Jabbari K, Kuo A, et al. The *Phaeodactylum* genome reveals the evolutionary history of diatom genomes. Nature 2008;456:239–44.
[135] Domergue F, Abbadi A, Zahringer U, Moreau H, Heinz E. In vivo characterization of the first acyl-CoA Delta6-desaturase from a member of the plant kingdom, the microalga *Ostreococcus tauri*. Biochem J 2005;389:483–90.
[136] Domergue F, Lerchl J, Zahringer U, Heinz E. Cloning and functional characterization of *Phaeodactylum tricornutum* front-end desaturases involved in eicosapentaenoic acid biosynthesis. Eur J Biochem 2002;269:4105–13.
[137] Domergue F, Spiekermann P, Lerchl J, Beckmann C, Kilian O, Kroth PG, et al. New insight into *Phaeodactylum tricornutum* fatty acid metabolism. Cloning and functional characterization of plastidial and microsomal delta12-fatty acid desaturases. Plant Physiol 2003;131:1648–60.
[138] Meyer A, Kirsch H, Domergue F, Abbadi A, Sperling P, Bauer J, et al. Novel fatty acid elongases and their use for the reconstitution of docosahexaenoic acid biosynthesis. J Lipid Res 2004;45:1899–909.
[139] Khozin-Goldberg I, Didi-Cohen S, Shayakhmetova I, Cohen Z. Biosynthesis of eicosapentaenoic acid (EPA) in the freshwater eustigmatophyte *Monodus subterraneus* (Eustigmatophyceae). J Phycol 2002;38:745–56.
[140] Apt KE, Zaslavkaia L, Lippmeier JC, Lang M, Kilian O, Wetherbee R, et al. *In vivo* characterization of diatom multipartite plastid targeting signals. J Cell Sci 2002;115:4061–9.
[141] Kilian O, Kroth PG. Identification and characterization of a new conserved motif within the presequence of proteins targeted into complex diatom plastids. Plant J 2005;41:175–83.
[142] Deschamps P, Moreira D. Reevaluating the green contribution to diatom genomes. Genome Biol Evol 2012;4:683–8.
[143] Marechal E, Cesbron-Delauw MF. The apicoplast: a new member of the plastid family. Trends Plant Sci 2001;6:200–5.
[144] Fichera ME, Roos DS. A plastid organelle as a drug target in apicomplexan parasites. Nature 1997;390:407–9.
[145] Dahl EL, Rosenthal PJ. Apicoplast translation, transcription and genome replication: targets for antimalarial antibiotics. Trends Parasitol 2008;24:279–84.
[146] Marechal E, Azzouz N, de Macedo CS, Block MA, Feagin JE, Schwarz RT, et al. Synthesis of chloroplast galactolipids in apicomplexan parasites. Eukaryot Cell 2002;1:653–6.
[147] Ramasamy R, Field MC. Terminal galactosylation of glycoconjugates in *Plasmodium falciparum* asexual blood stages and *Trypanosoma brucei* bloodstream trypomastigotes. Exp Parasitol 2012;130:314–20.
[148] Botte C, Saidani N, Mondragon R, Mondragon M, Isaac G, Mui E, et al. Subcellular localization and dynamics of a digalactolipid-like epitope in *Toxoplasma gondii*. J Lipid Res 2008;49:746–62.
[149] Welti R, Mui E, Sparks A, Wernimont S, Isaac G, Kirisits M, et al. Lipidomic analysis of *Toxoplasma gondii* reveals unusual polar lipids. Biochemistry 2007;46:13882–90.
[150] Gardner MJ, Hall N, Fung E, White O, Berriman M, Hyman RW, et al. Genome sequence of the human malaria parasite *Plasmodium falciparum*. Nature 2002;419:498–511.
[151] Aurrecoechea C, Barreto A, Brestelli J, Brunk BP, Cade S, Doherty R, et al. EuPathDB: the eukaryotic pathogen database. Nucleic Acids Res 2013;41:D684–91.

[152] Bastien O, Roy S, Marechal E. Construction of non-symmetric substitution matrices derived from proteomes with biased amino acid distributions. CR Biol 2005;328:445–53.
[153] Bastien O, Lespinats S, Roy S, Metayer K, Fertil B, Codani JJ, et al. Analysis of the compositional biases in *Plasmodium falciparum* genome and proteome using *Arabidopsis thaliana* as a reference. Gene 2004;336:163–73.
[154] Florent I, Marechal E, Gascuel O, Brehelin L. Bioinformatic strategies to provide functional clues to the unknown genes in *Plasmodium falciparum* genome. Parasite 2011;17:273–83.
[155] Obornik M, Modry D, Lukes M, Cernotikova-Stribrna E, Cihlar J, Tesarova M, et al. Morphology, ultrastructure and life cycle of *Vitrella brassicaformis* n. sp., n. gen., a novel chromerid from the Great Barrier Reef. Protist 2012;163:306–23.

8.2 Additional results

8.2.1 *DGD isoforms in Arabidopsis and Phaeodactylum*

Table 8.2.1. Amino acid identity matrix of the two *Arabidopsis* DGDG synthase isoforms and gene candidates from *P. tricornutum* created by Clustal2.1 after t-Coffee alignment.

% identity	AtDGD1	AtDGD2	DGD1_Phatr_12884	DGD2_Phatr_11390	DGD3_Phatr_43116
AtDGD1	100.00	53.62	38.03	33.55	34.55
AtDGD2	53.62	100.00	42.57	40.05	36.51
DGD1_Phatr_12884	38.03	42.57	100.00	41.07	41.40
DGD2_Phatr_11390	33.55	40.05	41.07	100.00	38.48
DGD3_Phatr_43116	34.55	36.51	41.40	38.48	100.00

8.3 Insert sequences

8.3.1 *NgNOA (Naga_100007g10)*

Sequence alignment of PtNOA and NgNOA

8.3.2 *Codon optimized NgNOA*

Codon optimized NgNOA (Naga_100007g10) CDS sequence for expression in *N. gaditana* and *P. tricornutum* with addition of restriction sites for cloning into PCT2 and pH4, respectively.

>NgNOAcodon-optimizedCDS

```
GGATCCTCTAGAATGGCTCCCCACCTCTCCGGCCTCAACTTCCACTCCCTCGTCAAGCGCTCCTCCGCTGCTGCTCTCCTCTTCTCCCT
CTTCATCATGAAGCTCCCCTGCGTCGGCGCTTTCCAGGGCGTCGTCCGCGTCTGGTCCTCCGCTGTCGCTCCCTCCCGCGCTGCTGTCC
TCACCTCCTTCATGTCCCCCAAGCGCCACGTCCTCAAGCGCATGCCCATCTCCGCTCTCTGCCGCCGCTCCACCATCATGGCTTCCCGC
AAGGCTGGCGCTGGCCAGGGCGAGCACGAGGCTGAGGGCGAGGGCATCTCCCCCGAGTCCATCTCCTCCACCGGCTCCAACGCTGGCGG
CAAGGGCATCGGCCGCGGCCCCCGCAACCGCCGCAAGATCGCTGTCTCCGCTGAGGAGGAGGAGTTCTCCGCTCTCTCCGACTCCCGCA
CCTCCGTCTCCGAGGAGAAGGACTCCATCCGCCGCCCCCGCGTCATCTCCCGCCCCCCCTCCCGCCCCGTCAAGCGCACCATGACCATC
AACCCCAACTGGCGCGCTCACGGCGGCCCCGAGAACTCCATCAAGGGCCCCGAGGAGGCTGCTTCCTCCTCCTCCGGCACCGCTGGCTC
CGGCAAGGCTCGCGTCGGCAAGAACGGCCCCCGCGGCGCTTCCCCCCTCGGCGCTGAGGTCCCCCGCTACGTCGAGGACGAGGACGAGG
ACGGCATCACCTTCCCCAAGGACATGGTCATCCGCGGCCTCGACTCCCAGTCCTACGAGGAGGCTCGCCGCCAGGCTGTCCTCTCCGAC
GACGAGGGCGAGGAGGAGGAGTGGGCTGACGAGGGCGTCATGGTCGAGGAGGAGGAGGGCGAGGACTTCGACGAGGAGGAGGAGGAGGA
GGACTTCGACGAGGAGGAGGAGGAGGAGGACTTCGACGAGGGCGACGAGGAGGAGGAGGACGGCGCTCACCTCCCCCCCGTCCGCCCCG
TCTCCATGGAGGAGCGCCTCCGCCTCGCTGAGTCCGGCAACATCTTCAACCCCTACGTCGCTCGCATGCACACCCGCGCTGGCACCGGC
GAGGGCCCCTCCGGCGAGGCTGAGGACCCCGGCCCCATGGACGGCGGCGGCCTCCGCTTCCTCGAGGAGGACGTCTCCCCCGGCGAGAA
GCGCGAGGAGGCTCGCCGCGCTCAGGCTCCCTCCCTCCCCGTCAAGTTCCAGTACAAGGTCGTCGTCGGCGCTGGCACCTGCCCCGGCT
GCGGCAACGCTTTCCAGACCAAGAACGAGTCCTCCCCCGGCTTCCTCCCCCCCGACGTCTACGAGCGCCTCCAGGCTCAGATGACCGCT
CTCCGCCCCGGCGCTCCCCGCAAGCCCCGCCCCGACGCTCCCCCCCTCTCCAAGTCCGCTGCTGGCGCTCTCCGCAAGAAGACCGAGAC
CCGCGGCGAGGAGGGCGACCTCTTCCAGGGCCTCTCCGCTGAGGAGGAGGTCGAGATGCTCCTCTCCGGCAAGTCCCGCGAGGAGTTCG
AGATCGAGCGCGCTGCTGGCCGCGGCCGCGAGGCTCAGGGCGGCGAGGTCGACCTCGACCTCGACGAGGAGGGCAAGGAGGAGAAGGAG
GGCGAGGGCCGCGAGGGCGAGGAGGGCGGCGAGGGCGAGGAGGAGGAGGAGTTCCGCGCTGTCATCTGCCAGCGCTGCCACAAGCT
CAAGCACTACGGCGACGTCGAGGACGCTCTCCGCCCCGGCTGGTCCGCTAACGAGCTCCTCACCCCCGAGCGCTTCCGCGAGCTCGTCT
CCGTCGTCCGCCGCAAGCGCTGCGCTGTCGTCTGCCTCGTCGACATCTTCGACTTCCACGGCTCCCTCCTCTACAACCTCCCCCGCATC
GTCGGCTCCAACCCCGTCCTCGTCGCTGTCAACAAGGCTGACCTCCTCCCCGCTGACTTCTCCCAGGACCGCGTCCGCATCTGGGTCAA
GCAGGAGCTCGAGAAGGTCGGCATGACCGACGTCTCCACCCGCGACATCCACCTCATCTCCTGCAAGACCGGCAACAACGTCCGCCCCC
TCCTCCGCTCCATGAAGCAGATGGCTCGCCAGCGCCGCCGCGACCTCTACGTCATCGGCGCTGCTAACGTCGGCAAGTCCACCTTCATC
AACCGCCTCATCGAGCTCGGCCGCTCCGGCGGCGACGCTCAGCGCAAGAAGAAGAAGAAGCAGGGCGAGCAGTCCAAGGGCGGCTCCCT
CGTCACCACCTCCGCTCTCCCCGGCACCACCCTCGACTTCATCGAGGTCGACCTCGGCGACAAGGTCTCCCTCTACGACACCCCCGGCC
TCATCCTCCCCCACCAGATCACCACCCTCCTCAACACCGAGGAGCTCAAGGCTGTCATCCCCCAGAAGCGCATCAACCACGTCACCCTC
CGCCTCAAGGAGGGCAAGTCCGTCCTCCTCGGCGGCCTCGTCCGCCTCGACATGCTCGAGGGCCGCCCCTTCCTCTTCACCTTCTACGT
CTCCAACGAGGTCAAGCTCCACCAGACCGCTACCGACCGCGCTGGCGAGTTCCTCGACTCCCACCTCGGCGAGCTCATCTCCCCCCCCT
TCACCCAGGAGCGCCGCGCTGCTATGGGCCCCTGGGTCCCCCGCGACTTCGAGATCGAGGGCACCGGCTGGAAGACCTCCGCTGTCGAC
ATCGTCATCTCCGGCCTCGGCTGGATCTCCGTCACCGGCGCTCTCGACTGCAAGGTCCGCGTCATGGCTCCCGAGGCTGTCGGCGTCCG
CCTCCGCTCCCCCCTCATGCCCTACGAGACCTGGGCTACCACCGCTAAGTGGACCGGCCTCCGCGCTGTCAAGTCCGACAAGCAGAAGG
GCTCCTCCCGCTAAGAATTCCATATG
```

8.3.3 *Condon optimized Ng*Δ*0-ELO1*

Codon optimized Ng*Δ0-ELO1* sequence for expression in yeast with the addition of restriction enzyme recognition sequences for cloning into pYES2.

> Ng*Δ0-ELO1*-opt

```
GAATTCATGAACAACCTCTCCGAAGCCTTCTCTAAACTCATCTGGGGTGAAATGCCTAAAATCATCCCTTATCGCTCCGTGCCTGACAA
TGTGCCCTTCACGCAGCTCTTTCAACACTACCCTGTTTTGTCCCCATTCTATACCGAGTACGAAAAGAACTTTCATGCCTCCTCTTACG
TGAACTTCGCTCAGAATACCTGGCCAGCCTTGCCCCTCGCTTTGTGCGGCATCTACGGTCTCATGATTGTCGTTGGCACCAAGGTTATG
GAGTCCCGCCCTAAGCACGAATGGAAAACTGCCCTCGCTTGCTGGAACCTCTTGCTCTCCGTCTTCTCTTTTTGTGGTATGCTCCGAAC
CGTGCCACACTTGCTCCAGAATGTCACCACTTTGCCATTTAAGGACACTATCTGCCGTCATCCCGCCGAGACGTATGGCGAAGGTGCTT
GTGGCCTCTGGGTTATGTTGTTCATCTACTCCAAAGTGCCCGAGCTCGTTGATACCGTGTTCATCGTCTTCAGAAAGTCTAAACTCCAA
TTCTTGCACTGGTATCACCATATTACTGTCTTGCTCTTCTGCTGGCATTCCTACGCCGTCACGTCCTCTACCGGCCTCTATTTTGTTGC
TATGAACTACTCTGTTCACGCCGTGATGTACGCTTACTATTACTTGACTGCCATCAAGGCTTGGCCTTCCTGGATTCCCCCTTCTATCA
```

TTACGGTGGCCCAGATCTCCCAAATGATGGTGGGCGTCGGTATTTGCGTCGCCTCTTTCTATTACCTCTACACCGACCCCGAGCATTGT
GAAGTCAAGCCTCAAAATGTTTATTCCGGCGCCCTCATGTACGGTTCTTACCTCTACTTGTTTTGTGATTTCTTTGTCCGCAGATTCTT
GCGAGGCGGTAAACCCCGCCTCGGTGAAGAACGCTCCGCTGTGTTGACGATGACGAAAAAGATTAAGGATATGTAGTCTAGA

8.4 Vector sequences

8.4.1 *pH4-GUS-AS*

pH4-GUS-AS vector sequence. Colour code: SHBLE-H4p-GUS short antisense (*Sac*I, *Kpn*I, *EcoR*I, *BamH*I, *Nco*I, *Stu*I, *Xba*I)

>pH4-GUS-AS

CTAAATTGTAAGCGTTAATATTTTGTTAAAATTCGCGTTAAATTTTTGTTAAATCAGCTCATTTTTTAACCAATA
GGCCGAAATCGGCAAAATCCCTTATAAATCAAAAGAATAGACCGAGATAGGGTTGAGTGTTGTTCCAGTTTGGAA
CAAGAGTCCACTATTAAAGAACGTGGACTCCAACGTCAAAGGGCGAAAAACCGTCTATCAGGGCGATGGCCCACT
ACGTGAACCATCACCCTAATCAAGTTTTTTGGGGTCGAGGTGCCGTAAAGCACTAAATCGGAACCCTAAAGGGAG
CCCCCGATTTAGAGCTTGACGGGGAAAGCCGGCGAACGTGGCGAGAAAGGAAGGGAAGAAAGCGAAAGGAGCGGG
CGCTAGGGCGCTGGCAAGTGTAGCGGTCACGCTGCGCGTAACCACCACACCCGCCGCGCTTAATGCGCCGCTACA
GGGCGCGTCCCATTCGCCATTCAGGCTGCGCAACTGTTGGGAAGGGCGATCGGTGCGGGCCTCTTCGCTATTACG
CCAGCTGGCGAAAGGGGGATGTGCTGCAAGGCGATTAAGTTGGGTAACGCCAGGGTTTTCCCAGTCACGACGTTG
TAAAACGACGGCCAGTGAGCGCGCGTAATACGACTCACTATAGGGCGAATTGGAGCTCGCAATCTCACGCACCAG
GCGCTGGAAGGGCAACTTGCGGATGAGAAGGTCCGTGGACTTCTGGTAACGACGGATCTCACGCAGAGCGACGGT
TCCAGGGCGATAACGGTGGGGCTTCTTGACTCCTCCGGTAGCCGGAGCGGACTTGCGGGCAGCCTTGGTGGCAAG
CTGCTTGCGCGGCGCTTTGCCTCCGGTGGATTTACGGGCGGTTTGCTTGGTTCGGGCCATTTTGACGGTTTTTTT
TACAAGAGAAGAGTTCTTGAAATTTGTGAGGTTAAAGTGTGTGGCTTCCGCCGTAGTCAAGGAGCGTGCGGTTGC
CGATCGCACCGGTACGTTCTGTAGAAATGAACACAGTGTGTTGAATTGAAAGTATGGCGCAGGTATGGTGTGTGA
TAAGTAGCAGCCGCGCCGAGACAAACAAACTTTGGTTTCTACGACAATCTCTGTAGACAAGTACTAGAAACCCGT
TTGAACGAGCATAAATCTGCACCGGCAGGCCACCAGACATCGTTTCAACGTAATATTCTACGTAACCATTTTATC
CCAGGAAACCTACGGCCTGTGAACCACCGAGACGGAGCACTCACAATTCGCTCTCGGCAACAACCGACAATCGTC
TTACTCACAGTCAATACCGAAAACAAACAACAGCCATGGCCAAGTTGACCAGTGCCGTTCCGGTGCTCACCGCGC
GCGACGTCGCCGGAGCGGTCGAGTTCTGGACCGACCGGCTCGGGTTCTCCCGGGACTTCGTGGAGGACGACTTCG
CCGGTGTGGTCCGGGACGACGTGACCCTGTTCATCAGCGCGGTCCAGGACCAGGTGGTGCCGGACAACACCCTGG
CCTGGGTGTGGGTGCGCGGCCTGGACGAGCTGTACGCCGAGTGGTCGGAGGTCGTGTCCACGAACTTCCGGGACG
CCTCCGGGCCGGCCATGACCGAGATCGGCGAGCAGCCGTGGGGGCGGGAGTTCGCCCTGCGCGACCCGGCCGGCA
ACTGCGTGCACTTCGTGGCCGAGGAGCAGGACTGACCGACGCCGACCAACACCGCCGGTCCGACGGCGGCCCACG
GGTCCCAGGCCTTCTAGACGCGGTGATACATATCCAGCCATGCACACTGATACTCTTCACTCCACATGTCGGTGT
ACATTGAGTGCAGCCCGGCTAACGTATCCACGCCGTATTCGGTGATGATAATCGGCTGATGCAGTTTCTCCTGCC
AGGCCAGAAGTTCTTTTTCCAGTACCTTCTCTGCCGTTTCCAAATCGCCGCTTTGGACATACCATCCGTAATAAC
GGTTCAGGCACAGCACATCAAAGAGATCGCTGATGGAATTCtcgagCTACCTCGACTTTGGCTGGGACACTTTCA
GTGAGGACAAGAAGCTTCAGAAGCGTGCTATCGAACTCAACCAGGGACGTGCGGCACAAATGGGCATCCTTGCTC
TCATGGTGCACGAACAGTTGGGAGTCTCTATCCTTCCTTAAAAATTTAATTTTCATTAGTTGCAGTCACTCCGCT
TTGGTTTCACAGTCAGGAATAACACTAGCTCGTCTTCAggtaccCAGCTTTTGTTCCCTTTAGTGAGGGTTAATT
GCGCGCTTGGCGTAATCATGGTCATAGCTGTTTCCTGTGTGAAATTGTTATCCGCTCACAATTCCACACAACATA
CGAGCCGGAAGCATAAAGTGTAAAGCCTGGGGTGCCTAATGAGTGAGCTAACTCACATTAATTGCGTTGCGCTCA
CTGCCCGCTTTCCAGTCGGGAAACCTGTCGTGCCAGCTGCATTAATGAATCGGCCAACGCGCGGGGAGAGGCGGT
TTGCGTATTGGGCGCTCTTCCGCTTCCTCGCTCACTGACTCGCTGCGCTCGGTCGTTCGGCTGCGGCGAGCGGTA
TCAGCTCACTCAAAGGCGGTAATACGGTTATCCACAGAATCAGGGGATAACGCAGGAAAGAACATGTGAGCAAAA
GGCCAGCAAAAGGCCAGGAACCGTAAAAAGGCCGCGTTGCTGGCGTTTTTCCATAGGCTCCGCCCCCCTGACGAG
CATCACAAAAATCGACGCTCAAGTCAGAGGTGGCGAAACCCGACAGGACTATAAAGATACCAGGCGTTTCCCCCT
GGAAGCTCCCTCGTGCGCTCTCCTGTTCCGACCCTGCCGCTTACCGGATACCTGTCCGCCTTTCTCCCTTCGGGA
AGCGTGGCGCTTTCTCATAGCTCACGCTGTAGGTATCTCAGTTCGGTGTAGGTCGTTCGCTCCAAGCTGGGCTGT
GTGCACGAACCCCCCGTTCAGCCCGACCGCTGCGCCTTATCCGGTAACTATCGTCTTGAGTCCAACCCGGTAAGA
CACGACTTATCGCCACTGGCAGCAGCCACTGGTAACAGGATTAGCAGAGCGAGGTATGTAGGCGGTGCTACAGAG
TTCTTGAAGTGGTGGCCTAACTACGGCTACACTAGAAGGACAGTATTTGGTATCTGCGCTCTGCTGAAGCCAGTT
ACCTTCGGAAAAAGAGTTGGTAGCTCTTGATCCGGCAAACAAACCACCGCTGGTAGCGGTGGTTTTTTTGTTTGC
AAGCAGCAGATTACGCGCAGAAAAAAAGGATCTCAAGAAGATCCTTTGATCTTTTCTACGGGGTCTGACGCTCAG
TGGAACGAAAACTCACGTTAAGGGATTTTGGTCATGAGATTATCAAAAAGGATCTTCACCTAGATCCTTTTAAAT
TAAAAATGAAGTTTTAAATCAATCTAAAGTATATATGAGTAAACTTGGTCTGACAGTTACCAATGCTTAATCAGT

GAGGCACCTATCTCAGCGATCTGTCTATTTCGTTCATCCATAGTTGCCTGACTCCCCGTCGTGTAGATAACTACG
ATACGGGAGGGCTTACCATCTGGCCCCAGTGCTGCAATGATACCGCGAGACCCACGCTCACCGGCTCCAGATTTA
TCAGCAATAAACCAGCCAGCCGGAAGGGCCGAGCGCAGAAGTGGTCCTGCAACTTTATCCGCCTCCATCCAGTCT
ATTAATTGTTGCCGGGAAGCTAGAGTAAGTAGTTCGCCAGTTAATAGTTTGCGCAACGTTGTTGCCATTGCTACA
GGCATCGTGGTGTCACGCTCGTCGTTTGGTATGGCTTCATTCAGCTCCGGTTCCCAACGATCAAGGCGAGTTACA
TGATCCCCCATGTTGTGCAAAAAAGCGGTTAGCTCCTTCGGTCCTCCGATCGTTGTCAGAAGTAAGTTGGCCGCA
GTGTTATCACTCATGGTTATGGCAGCACTGCATAATTCTCTTACTGTCATGCCATCCGTAAGATGCTTTTCTGTG
ACTGGTGAGTACTCAACCAAGTCATTCTGAGAATAGTGTATGCGGCGACCGAGTTGCTCTTGCCCGGCGTCAATA
CGGGATAATACCGCGCCACATAGCAGAACTTTAAAAGTGCTCATCATTGGAAAACGTTCTTCGGGGCGAAAACTC
TCAAGGATCTTACCGCTGTTGAGATCCAGTTCGATGTAACCCACTCGTGCACCCAACTGATCTTCAGCATCTTTT
ACTTTCACCAGCGTTTCTGGGTGAGCAAAAACAGGAAGGCAAAATGCCGCAAAAAAGGGAATAAGGGCGACACGG
AAATGTTGAATACTCATACTCTTCCTTTTTCAATATTATTGAAGCATTTATCAGGGTTATTGTCTCATGAGCGGA
TACATATTTGAATGTATTTAGAAAAATAAACAAATAGGGGTTCCGCGCACATTTCCCCGAAAAGTGCCAC

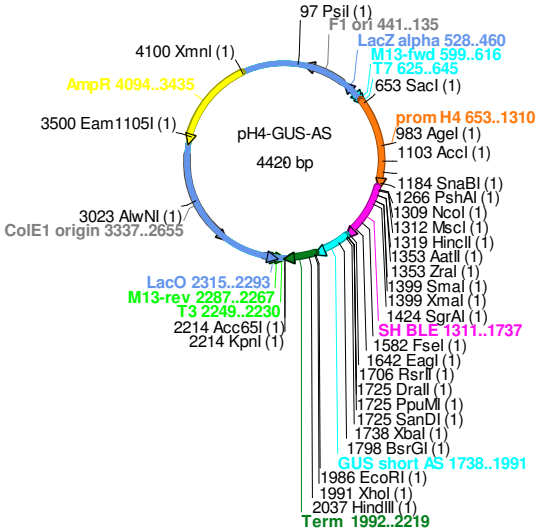

Figure 8.4.1. Vector map of pH4-GUS-AS vector used for gene expression in *P. tricornutum*. The plasmid mediates ampicillin resistance (AmpR) in bacteria and zeocin resistance (SH BLE) in algae. The inserted gene is under the control of the histone 4 promotor (H4) and the fucoxanthin A terminator. Notably, the *Xho*I restriction site appeared to be mutated. The vector was obtained from Angela Falciatore, Paris, France.

8.4.2 *UEP-p35S-loxP BSD FL1-FL2 526*

> UEP-p35S-loxP BSD FL1-FL2 526

```
CTAAATTGTAAGCGTTAATATTTTGTTAAAATTCGCGTTAAATTTTTGTTAAATCAGCTCATTTTTTAACCAATAGGCCGAAATCGGCA
AAATCCCTTATAAATCAAAAGAATAGACCGAGATAGGGTTGAGTGTTGTTCCAGTTTGGAACAAGAGTCCACTATTAAAGAACGTGGAC
TCCAACGTCAAAGGGCGAAAAACCGTCTATCAGGGCGATGGCCCACTACGTGAACCATCACCCTAATCAAGTTTTTTGGGGTCGAGGTG
CCGTAAAGCACTAAATCGGAACCCTAAAGGGAGCCCCCGATTTAGAGCTTGACGGGGAAAGCCGGCGAACGTGGCGAGAAAGGAAGGGA
AGAAAGCGAAAGGAGCGGGCGCTAGGGCGCTGGCAAGTGTAGCGGTCACGCTGCGCGTAACCACCACACCCGCCGCGCTTAATGCGCCG
CTACAGGGCGCGTCCCATTCGCCATTCAGGCTGCGCAACTGTTGGGAAGGGCGATCGGTGCGGGCCTCTTCGCTATTACGCCAGCTGGC
GAAAGGGGGATGTGCTGCAAGGCGATTAAGTTGGGTAACGCCAGGGTTTTCCCAGTCACGACGTTGTAAAACGACGGCCAGTGAGCGCG
CGTAATACGACTCACTATAGGGCGAATTGGGTACCGGGCCCCCCCTCGAGGTCGACGGTATCGATAAGCTTGATATCGAATTCAGCTGC
TGCCCCGACCGTATCTCCAAGTCAGACATGAAATCTTCAGTTGCGTTAAAAACTCTACGATGCTACCAGCGTTAAATAACCTTGCCCAC
GCCTTTAAACGTACCCGATCATTAACATATCGACTGGCTGCCTTGGCTTTGCACCAGCCATCATCAGACTTAACGATGGGTATGTTGCT
TGCCTTTCCTGCTTGAAGGGGGTCCGACTCTCTGCTTTCTCGATCGCGGGTGTGACCTCTGAATTGGAATGTAAAAATGTAAGAAGCGA
CGTGTCCGGTAAAGAAATGCCCAAGCTCCATCAAATCTGCGTTGTCGGCGACCAAACCATGCTGGCTCGTCGACCTGCCCCGGATGCAG
GAGCATGGCACTCGGCGGCATGGCACTTGAGCCTCGCGGGAGGAATGTGTGTGGTTGGGCGCAGGCTGTGGACGGCCCCCCTCCAGCGA
AGCGGTCGCCTCCCTTTCCGACGCTTTGTGCACGTTGTCTGGTGTCCTCTGTCTCACGCACCTCTTCACCGACGTGGTGTCCCTCTTGT
TGCTGGTGAGGGACTTGGAATGTGGTCCTGGTTCTATCCTGGGCGCGTGTGTTCCTTTTTTTCTCTACCGTTATTCTCTCCATTTCTGA
TGTCTCACCACCATCTCCCTCACCCTCCAACCGCGTCGTTGTGCCAAAATCATACAGCAGGATGGCCAAGTTGACCAGTGCCGTTCCGG
TGCTCACCGCGCGCGACGTCGCCGGAGCGGTCGAGTTCTGGACCGACCGGCTCGGGTTCTCCCGGGACTTCGTGGAGGACGACTTCGCC
GGTGTGGTCCGGGACGACGTGACCCTGTTCATCAGCGCGGTCCAGGACCAGGTGGTGCCGGACAACACCCTGGCCTGGGTGTGGGTGCG
CGGCCTGGACGAGCTGTACGCCGAGTGGTCGGAGGTCGTGTCCACGAACTTCCGGGACGCCTCCGGGCCGGCCATGACCGAGATCGGCG
AGCAGCCGTGGGGGCGGGAGTTCGCCCTGCGCGACCCGGCCGGCAACTGCGTGCACTTCGTGGCCGAGGAGCAGGACTGAACCTTCCTT
AAAAATTTAATTTTCATTAGTTGCAGTCACTCCGCTTTGGTTTCACAGTCAGGAATAACACTAGCTCGTCTTCACCATGGATGCCAATC
TCGCCTATTCATGGTGTATAAAAGTTCAACATCCAAAGCTAGAACTTTTGGAAAGAGAAAGAATATCCGAATAGGGCACGGCGTGCCGT
ATTGTTGGAGTGGACTAGCAGAAAGTGAGGAAGGCACAGGATGAGTTTTCTCGAGGCCGGTCTCCCTATAGTGAGTCATATGGATCCTA
GAGCGGCCGCCACCGCGGTGGAGCTCCAGCTTTTGTTCCCTTTAGTGAGGGTTAATTGCGCGCTTGGCGTAATCATGGTCATAGCTGTT
TCCTGTGTGAAATTGTTATCCGCTCACAATTCCACACAACATACGAGCCGGAAGCATAAAGTGTAAAGCCTGGGGTGCCTAATGAGTGA
GCTAACTCACATTAATTGCGTTGCGCTCACTGCCCGCTTTCCAGTCGGGAAACCTGTCGTGCCAGCTGCATTAATGAATCGGCCAACGC
GCGGGGAGAGGCGGTTTGCGTATTGGGCGCTCTTCCGCTTCCTCGCTCACTGACTCGCTGCGCTCGGTCGTTCGGCTGCGGCGAGCGGT
ATCAGCTCACTCAAAGGCGGTAATACGGTTATCCACAGAATCAGGGGATAACGCAGGAAAGAACATGTGAGCAAAAGGCCAGCAAAAGG
CCAGGAACCGTAAAAAGGCCGCGTTGCTGGCGTTTTTCCATAGGCTCCGCCCCCCTGACGAGCATCACAAAAATCGACGCTCAAGTCAG
AGGTGGCGAAACCCGACAGGACTATAAAGATACCAGGCGTTTCCCCCTGGAAGCTCCCTCGTGCGCTCTCCTGTTCCGACCCTGCCGCT
TACCGGATACCTGTCCGCCTTTCTCCCTTCGGGAAGCGTGGCGCTTTCTCATAGCTCACGCTGTAGGTATCTCAGTTCGGTGTAGGTCG
TTCGCTCCAAGCTGGGCTGTGTGCACGAACCCCCCGTTCAGCCCGACCGCTGCGCCTTATCCGGTAACTATCGTCTTGAGTCCAACCCG
GTAAGACACGACTTATCGCCACTGGCAGCAGCCACTGGTAACAGGATTAGCAGAGCGAGGTATGTAGGCGGTGCTACAGAGTTCTTGAA
GTGGTGGCCTAACTACGGCTACACTAGAAGGACAGTATTTGGTATCTGCGCTCTGCTGAAGCCAGTTACCTTCGGAAAAAGAGTTGGTA
GCTCTTGATCCGGCAAACAAACCACCGCTGGTAGCGGTGGTTTTTTTGTTTGCAAGCAGCAGATTACGCGCAGAAAAAAAGGATCTCAA
GAAGATCCTTTGATCTTTTCTACGGGGTCTGACGCTCAGTGGAACGAAAACTCACGTTAAGGGATTTTGGTCATGAGATTATCAAAAAG
GATCTTCACCTAGATCCTTTTAAATTAAAAATGAAGTTTTAAATCAATCTAAAGTATATATGAGTAAACTTGGTCTGACAGTTACCAAT
GCTTAATCAGTGAGGCACCTATCTCAGCGATCTGTCTATTTCGTTCATCCATAGTTGCCTGACTCCCCGTCGTGTAGATAACTACGATA
CGGGAGGGCTTACCATCTGGCCCCAGTGCTGCAATGATACCGCGAGACCCACGCTCACCGGCTCCAGATTTATCAGCAATAAACCAGCC
AGCCGGAAGGGCCGAGCGCAGAAGTGGTCCTGCAACTTTATCCGCCTCCATCCAGTCTATTAATTGTTGCCGGGAAGCTAGAGTAAGTA
GTTCGCCAGTTAATAGTTTGCGCAACGTTGTTGCCATTGCTACAGGCATCGTGGTGTCACGCTCGTCGTTTGGTATGGCTTCATTCAGC
TCCGGTTCCCAACGATCAAGGCGAGTTACATGATCCCCCATGTTGTGCAAAAAAGCGGTTAGCTCCTTCGGTCCTCCGATCGTTGTCAG
AAGTAAGTTGGCCGCAGTGTTATCACTCATGGTTATGGCAGCACTGCATAATTCTCTTACTGTCATGCCATCCGTAAGATGCTTTTCTG
TGACTGGTGAGTACTCAACCAAGTCATTCTGAGAATAGTGTATGCGGCGACCGAGTTGCTCTTGCCCGGCGTCAATACGGGATAATACC
GCGCCACATAGCAGAACTTTAAAAGTGCTCATCATTGGAAAACGTTCTTCGGGGCGAAAACTCTCAAGGATCTTACCGCTGTTGAGATC
CAGTTCGATGTAACCCACTCGTGCACCCAACTGATCTTCAGCATCTTTTACTTTCACCAGCGTTTCTGGGTGAGCAAAAACAGGAAGGC
AAAATGCCGCAAAAAAGGGAATAAGGGCGACACGGAAATGTTGAATACTCATACTCTTCCTTTTTCAATATTATTGAAGCATTTATCAG
GGTTATTGTCTCATGAGCGGATACATATTTGAATGTATTTAGAAAAATAAACAAATAGGGGTTCCGCGCACATTTCCCCGAAAAGTGCC
AC
```

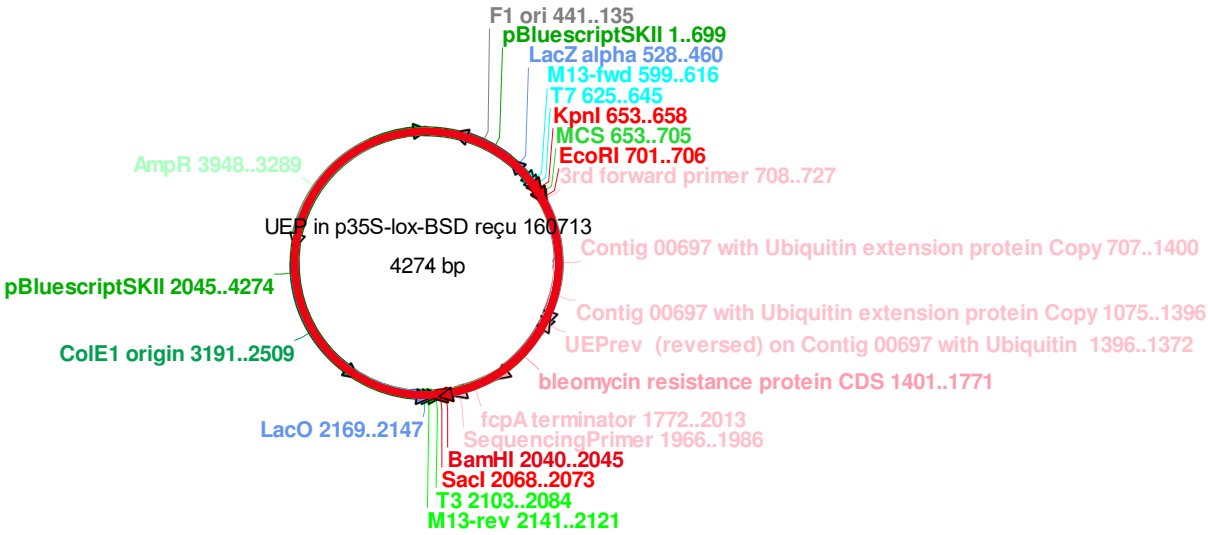

Figure 8.4.2. Vector map of UEP-p35S-loxP BSD FL1-FL2 526 vector used for gene knock out in *N. gaditana*. The plasmid mediates ampicillin resistance (AmpR) in bacteria and zeocin (bleomycin resistance protein CDS 1401..1771) resistance under the control of the Ubiquitin extension protein promotor and the *P. tricornutum* FcpA terminator in algae. The flanking regions of the target gene are inserted up- and downstream of the zeocin resistance and the transformation cassette was digested from the vector backbone using *Kpn*I and *BamH*I. Vector was obtained from Tomas Morosinotto, Padova, Italy.

8.4.3 *pYES*

>pYES2

```
ACGGATTAGAAGCCGCCGAGCGGGTGACAGCCCTCCGAAGGAAGACTCTCCTCCGTGCGTCCTCGTCTTCACCGGTCGCGTTCCTGAAA
CGCAGATGTGCCTCGCGCCGCACTGCTCCGAACAATAAAGATTCTACAATACTAGCTTTTATGGTTATGAAGAGGAAAAATTGGCAGTA
ACCTGGCCCCACAAACCTTCAAATGAACGAATCAAATTAACAACCATAGGATGATAATGCGATTAGTTTTTTAGCCTTATTTCTGGGGT
AATTAATCAGCGAAGCGATGATTTTTGATCTATTAACAGATATATAAATGCAAAAACTGCATAACCACTTTAACTAATACTTTCAACAT
TTTCGGTTTGTATTACTTCTTATTCAAATGTAATAAAAGTATCAACAAAAAATTGTTAATATACCTCTATACTTTAACGTCAAGGAGAA
AAAACCCCGGATCGGACTACTAGCAGCTGTAATACGACTCACTATAGGGAATATTAAGCTTGGTACCGAGCTCGGATCCACTAGTAACG
GCCGCCAGTGTGCTGGAATTCTGCAGATATCCATCACACTGGCGGCCGCTCGAGCATGCATCTAGAGGGCCGCATCATGTAATTAGTTA
TGTCACGCTTACATTCACGCCCTCCCCCCACATCCGCTCTAACCGAAAAGGAAGGAGTTAGACAACCTGAAGTCTAGGTCCCTATTTAT
TTTTTTATAGTTATGTTAGTATTAAGAACGTTATTTATATTTCAAATTTTTCTTTTTTTTCTGTACAGACGCGTGTACGCATGTAACAT
TATACTGAAAACCTTGCTTGAGAAGGTTTTGGGACGCTCGAAGGCTTTAATTTGCGGCCCTGCATTAATGAATCGGCCAACGCGCGGGG
AGAGGCGGTTTGCGTATTGGGCGCTCTTCCGCTTCCTCGCTCACTGACTCGCTGCGCTCGGTCGTTCGGCTGCGGCGAGCGGTATCAGC
TCACTCAAAGGCGGTAATACGGTTATCCACAGAATCAGGGGATAACGCAGGAAAGAACATGTGAGCAAAAGGCCAGCAAAAGCCCAGGA
ACCGTAAAAAGGCCGCGTTGCTGGCGTTTTTCCATAGGCTCCGCCCCCCTGACGAGCATCACAAAAATCGACGCTCAAGTCAGAGGTGG
CGAAACCCGACAGGACTATAAAGATACCAGGCGTTTCCCCCTGGAAGCTCCCTCGTGCGCTCTCCTGTTCCGACCCTGCCGCTTACCGG
ATACCTGTCCGCCTTTCTCCCTTCGGGAAGCGTGGCGCTTTCTCATAGCTCACGCTGTAGGTATCTCAGTTCGGTGTAGGTCGTTCGCT
CCAAGCTGGGCTGTGTGCACGAACCCCCCGTTCAGCCCGACCGCTGCGCCTTATCCGGTAACTATCGTCTTGAGTCCAACCCGGTAAGA
CACGACTTATCGCCACTGGCAGCAGCCACTGGTAACAGGATTAGCAGAGCGAGGTATGTAGGCGGTGCTACAGAGTTCTTGAAGTGGTG
GCCTAACTACGGCTACACTAGAAGGACAGTATTTGGTATCTGCGCTCTGCTGAAGCCAGTTACCTTCGGAAAAAGAGTTGGTAGCTCTT
GATCCGGCAAACAAACCACCGCTGGTAGCGGTGGTTTTTTTGTTTGCAAGCAGCAGATTACGCGCAGAAAAAAAGGATCTCAAGAAGAT
CCTTTGATCTTTTCTACGGGGTCTGACGCTCAGTGGAACGAAAACTCACGTTAAGGGATTTTGGTCATGAGATTATCAAAAAGGATCTT
CACCTAGATCCTTTTAAATTAAAAATGAAGTTTTAAATCAATCTAAAGTATATATGAGTAAACTTGGTCTGACAGTTACCAATGCTTAA
TCAGTGAGGCACCTATCTCAGCGATCTGTCTATTTCGTTCATCCATAGTTGCCTGACTCCCCGTCGTGTAGATAACTACGATACGGGAG
CGCTTACCATCTGGCCCCAGTGCTGCAATGATACCGCGAGACCCACGCTCACCGGCTCCAGATTTATCAGCAATAAACCAGCCAGCCGG
AAGGGCCGAGCGCAGAAGTGGTCCTGCAACTTTATCCGCCTCCATTCAGTCTATTAATTGTTGCCGGGAAGCTAGAGTAAGTAGTTCGC
CAGTTAATAGTTTGCGCAACGTTGTTGGCATTGCTACAGGCATCGTGGTGTCACTCTCGTCGTTTGGTATGGCTTCATTCAGCTCCGGT
TCCCAACGATCAAGGCGAGTTACATGATCCCCCATGTTGTGCAAAAAAGCGGTTAGCTCCTTCGGTCCTCCGATCGTTGTCAGAAGTAA
GTTGGCCGCAGTGTTATCACTCATGGTTATGGCAGCACTGCATAATTCTCTTACTGTCATGCCATCCGTAAGATGCTTTTCTGTGACTG
GTGAGTACTCAACCAAGTCATTCTGAGAATAGTGTATGCGGCGACCGAGTTGCTCTTGCCCGGCGTCAATACGGGATAATAGTGTATCA
CATAGCAGAACTTTAAAAGTGCTCATCATTGGAAAACGTTCTTCGGGGCGAAAACTCTCAAGGATCTTACCGCTGTTGAGATCCAGTTC
GATGTAACCCACTCGTGCACCCAACTGATCTTCAGCATCTTTTACTTTCACCAGCGTTTCTGGGTGAGCAAAAACAGGAAGGCAAAATG
CCGCAAAAAAGGGAATAAGGGCGACACGGAAATGTTGAATACTCATACTCTTCCTTTTTCAATGGGTAATAACTGATATAATTAAATTG
AAGCTCTAATTTGTGAGTTTAGTATACATGCATTTACTTATAATACAGTTTTTTAGTTTTGCTGGCCGCATCTTCTCAAATATGCTTCC
CAGCCTGCTTTTCTGTAACGTTCACCCTCTACCTTAGCATCCCTTCCCTTTGCAAATAGTCCTCTTCCAACAATAATAATGTCAGATCC
TGTAGAGACCACATCATCCACGGTTCTATACTGTTGACCCAATGCGTCTCCCTTGTCATCTAAACCCACACCGGGTGTCATAATCAACC
AATCGTAACCTTCATCTCTTCCACCCATGTCTCTTTGAGCAATAAAGCCGATAACAAAATCTTTGTCGCTCTTCGCAATGTCAACAGTA
CCCTTAGTATATTCTCCAGTAGATAGGGAGCCCTTGCATGACAATTCTGCTAACATCAAAAGGCCTCTAGGTTCCTTTGTTACTTCTTC
TGCCGCCTGCTTCAAACCGCTAACAATACCTGGGCCCACCACACCGTGTGCATTCGTAATGTCTGCCCATTCTGCTATTCTGTATACAC
CCGCAGAGTACTGCAATTTGACTGTATTACCAATGTCAGCAAATTTTCTGTCTTCGAAGAGTAAAAAATTGTACTTGGCGGATAATGCC
TTTAGCGGCTTAACTGTGCCCTCCATGGAAAAATCAGTCAAGATATCCACATGTGTTTTTAGTAAACAAATTTTGGGACCTAATGCTTC
AACTAACTCCAGTAATTCCTTGGTGGTACGAACATCCAATGAAGCACACAAGTTTGTTTGCTTTTCGTGCATGATATTAAATAGCTTGG
CAGCAACAGGACTAGGATGAGTAGCAGCACGTTCCTTATATGTAGCTTTCGACATGATTTATCTTCGTTTCCTGCAGGTTTTTGTTCTG
TGCAGTTGGGTTAAGAATACTGGGCAATTTCATGTTTCTTCAACACTACATATGCGTATATATACCAATCTAAGTCTGTGCTCCTTCCT
TCGTTCTTCCTTCTGTTCGGAGATTACCGAATCAAAAAAATTTCAAAGAAACCGAAATCAAAAAAAAGAATAAAAAAAAAATGATGAAT
TGAATTGAAAAGCTAGCTTATCGATGATAAGCTGTCAAAGATGAGAATTAATTCCACGGACTATAGACTATACTAGATACTCCGTCTAC
TGTACGATACACTTCCGCTCAGGTCCTTGTCCTTTAACGAGGCCTTACCACTCTTTTGTTACTCTATTGATCCAGCTCAGCAAAGGCAG
TGTGATCTAAGATTCTATCTTCGCGATGTAGTAAAACTAGCTAGACCGAGAAAGAGACTAGAAATGCAAAAGGCACTTCTACAATGGCT
GCCATCATTATTATCCGATGTGACGCTGCAGCTTCTCAATGATATTCGAATACGCTTTGAGGAGATACAGCCTAATATCCGACAAACTG
TTTTACAGATTTACGATCGTACTTGTTACCCATCATTGAATTTTGAACATCCGAACCTGGGAGTTTTCCCTGAAACAGATAGTATATTT
GAACCTGTATAATAATATATAGTCTAGCGCTTTACGGAAGACAATGTATGTATTTCGGTTCCTGGAGAAACTATTGCATCTATTGCATA
GGTAATCTTGCACGTCGCATCCCCGGTTCATTTTCTGCGTTTCCATCTTGCACTTCAATAGCATATCTTTGTTAACGAAGCATCTGTGC
TTCATTTTGTAGAACAAAAATGCAACGCGAGAGCGCTAATTTTTCAAACAAAGAATCTGAGCTGCATTTTTACAGAACAGAAATGCAAC
GCGAAAGCGCTATTTTACCAACGAAGAATCTGTGCTTCATTTTTGTAAAACAAAAATGCAACGCGACGAGAGCGCTAATTTTTCAAACA
AAGAATCTGAGCTGCATTTTTACAGAACAGAAATGCAACGCGAGAGCGCTATTTTACCAACAAAGAATCTATACTTCTTTTTTGTTCTA
CAAAAATGCATCCCGAGAGCGCTATTTTTCTAACAAAGCATCTTAGATTACTTTTTTTCTCCTTTGTGCGCTCTATAATGCAGTCTCTT
GATAACTTTTTGCACTGTAGGTCCGTTAAGGTTAGAAGAAGGCTACTTTGGTGTCTATTTTCTCTTCCATAAAAAAAGCCTGACTCCAC
TTCCCGCGTTTACTGATTACTAGCGAAGCTGCGGGTGCATTTTTTCAAGATAAAGGCATCCCCGATTATATTCTATACCGATGTGGATT
GCGCATACTTTGTGAACAGAAAGTGATAGCGTTGATGATTCTTCATTGGTCAGAAAATTATGAACGGTTTCTTCTATTTTGTCTCTATA
TACTACGTATAGGAAATGTTTACATTTTCGTATTGTTTTCGATTCACTCTATGAATAGTTCTTACTACAATTTTTTTGTCTAAAGAGTA
ATACTAGAGATAAACATAAAAAATGTAGAGGTCGAGTTTAGATGCAAGTTCAAGGAGCGAAAGGTGGATGGGTAGGTTATATAGGGATA
TAGCACAGAGATATATAGCAAAGAGATACTTTTGAGCAATGTTTGTGGAAGCGGTATTCGCAATGGGAAGCTCCACCCCGGTTGATAAT
CAGAAAAGCCCCAAAAACAGGAAGATTGTATAAGCAAATATTTAAATTGTAAACGTTAATATTTTGTTAAAATTCGCGTTAAATTTTTG
TTAAATCAGCTCATTTTTTAACGAATAGCCCGAAATCGGCAAAATCCCTTATAAATCAAAAGAATAGACCGAGATAGGGTTGAGTGTTG
TTCCAGTTTCCAACAAGAGTCCACTATTAAAGAACGTGGACTCCAACGTCAAAGGGCGAAAAAGGGTCTATCAGGGCGATGGCCCACTA
CGTGAACCATCACCCTAATCAAGTTTTTTGGGGTCGAGGTGCCGTAAAGCACTAAATCGGAAGGGTAAACGGATGCCCCCATTTAGAGC
```

TTGACGGGGAAAGCCGGCGAACGTGGCGAGAAAGGAAGGGAAGAAAGCGAAAGGAGCGGGGGCTAGGGCGGTGGGAAGTGTAGGGGTCA
CGCTGGGCGTAACCACCACACCCGCCGCGCTTAATGGGGCGCTACAGGGCGCGTGGGGATGATCCACTAGT

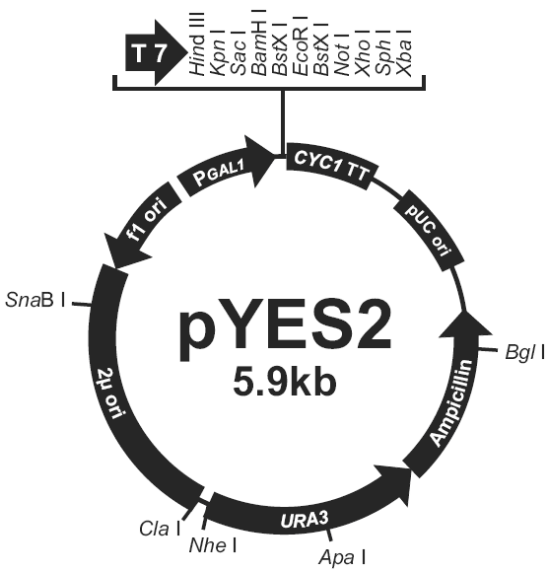

Figure 8.4.3. Vector map of pYES2 vector used for gene expression in *Saccharomyces cerevisae*. The plasmid mediates ampicillin resistance (AmpR) in bacteria and URA3 as auxotrophy marker for selection in yeast. The gene of interest is inserted under the control of the Gal1 promotor that is activated by galactose and repressed by glucose. Vector was obtained from Frédéric Beaudoin, Rothamsted Research, United Kingdom.

8.5 Codon usage tables

8.5.1 *Phaeodactylum tricornutum and Nannochloropsis gaditana*

triplet	amino acid	frequency per thousand		triplet	amino acid	frequency per thousand	
UUU	F	14.1	20.1	CUU	L	13.7	15.1
UUC	F	21.4	26.0	CUC	L	23.1	29.0
UUA	L	4.8	1.7	CUA	L	5.6	4.3
UUG	L	23.5	21.7	CUG	L	27.7	12.4
UCU	S	10.4	9.6	CCU	P	13.9	8.2
UCC	S	19.6	22.7	CCC	P	19.9	16.5
UCA	S	7.1	4.1	CCA	P	8.5	5.0
UCG	S	13.9	12.5	CCG	P	13.9	11.9
UAU	Y	7.0	5.5	CAU	H	9.3	6.6
UAC	Y	16.6	25.4	CAC	H	14.7	16.8
UAA	*	0.6	2.1	CAA	Q	14.9	12.9
UAG	*	0.6	0.3	CAG	Q	22.3	21.2
UGU	C	5.1	5.2	CGU	R	9.0	16.6
UGC	C	9.7	8.0	CGC	R	16.9	12.6
UGA	*	1.0	0.2	CGA	R	10.1	4.9
UGG	W	12.5	14.6	CGG	R	17.5	3.9
AUU	I	11.0	30.4	GUU	V	8.7	16.6
AUC	I	20.2	27.2	GUC	V	22.3	34.5
AUA	I	5.3	1.6	GUA	V	7.3	6.9
AUG	M	23.3	31.0	GUG	V	31.1	16.0
ACU	T	7.6	10.1	GCU	A	16.2	23.5
ACC	T	16.5	24.3	GCC	A	35.5	52.3
ACA	T	9.6	6.8	GCA	A	16.6	10.0
ACG	T	17.5	12.2	GCG	A	27.9	14.7
AAU	N	10.9	11.4	GAU	D	17.3	23.0
AAC	N	15.8	26.2	GAC	D	32.1	32.8
AAA	K	17.6	14.1	GAA	E	23.3	37.9
AAG	K	28.8	42.2	GAG	E	46.3	18.8
AGU	S	7.2	7.7	GGU	G	12.5	23.9
AGC	S	16.4	7.8	GGC	G	27.1	22.2
AGA	R	5.5	1.5	GGA	G	18.0	27.5
AGG	R	9.6	0.7	GGG	G	26.4	6.4

8.5.2 *Saccharomyces cerevisae*

triplet	amino acid	frequency per thousand	triplet	amino acid	frequency per thousand
UUU	F	26.1	CUU	L	12.3
UUC	F	18.4	CUC	L	5.4
UUA	L	26.2	CUA	L	13.4
UUG	L	27.2	CUG	L	10.5
UCU	S	23.5	CCU	P	13.5
UCC	S	14.2	CCC	P	6.8
UCA	S	18.7	CCA	P	18.3
UCG	S	8.6	CCG	P	5.3
UAU	Y	18.8	CAU	H	13.6
UAC	Y	14.8	CAC	H	7.8
UAA	*	1.1	CAA	Q	27.3
UAG	*	0.5	CAG	Q	12.1
UGU	C	8.1	CGU	R	6.4
UGC	C	4.8	CGC	R	2.6
UGA	*	0.7	CGA	R	3.0
UGG	W	10.4	CGG	R	1.7
AUU	I	30.1	GUU	V	22.1
AUC	I	17.2	GUC	V	11.8
AUA	I	17.8	GUA	V	11.8
AUG	M	20.9	GUG	V	10.8
ACU	T	20.3	GCU	A	21.2
ACC	T	12.7	GCC	A	12.6
ACA	T	17.8	GCA	A	16.2
ACG	T	8.0	GCG	A	6.2
AAU	N	35.7	GAU	D	37.6
AAC	N	24.8	GAC	D	20.2
AAA	K	41.9	GAA	E	45.6
AAG	K	30.8	GAG	E	19.2
AGU	S	14.2	GGU	G	23.9
AGC	S	9.8	GGC	G	9.8
AGA	R	21.3	GGA	G	10.9
AGG	R	9.2	GGG	G	6.0

9 ACKNOWLEDGEMENTS

I thank Eric Maréchal for having me given an elefant, a little spoon and a lot of freedom. I acknowledge the scientific network I was able to build thanks to Eric who had sent me on international conferences and for trainings in Paris and Harpenden. I am hence proud to have such an excellent PhD jury and I thank Katrin Philippar, Yonghua Li-Beisson, Olga Sayanova, Giovanni Finazzi and Frédéric Beaudoin for their time they dedicate to my work. I especially thank Fred and Olga whom are not only members of the jury and my thesis committee, but have also welcomed me in their lab for a three week visit and have always been available for helpful advice and discussion. Likewise, I thank Angela Falciatore for having me hosted in her team for three days.

The presented work would not have been possible without the help of some colleagues. First I like to thank Guillaume Tourcier who always provides a helping hand and brain.

Likewise, I warmly thank Melissa Conte, Coline Meï, Camille Rak and Séverine Collin for the pleasant teamwork. I especially thank Séverine for all her support and the loads she constantly took off the TOTAL-teams shoulders. I thank Juliette Jouhet, also called Juliette-knows-everything for her technical and methodological help. I thank these girls as well as Sophie Mistri and Grégoire Denay for having me led through the French jungle of administration.

10 REFERENCES

10.1 Web sources

http://genome.jgi-psf.org/Phatr2/Phatr2.home.html
http://hibberdlab.com/assets/ParticleBombardment.pdf
http://multalin.toulouse.inra.fr/multalin/
http://rocaplab.ocean.washington.edu/tools/asafind
http://sciencelearn.org.nz/Contexts/The-Ocean-in-Action/Science-Ideas-and-Concepts/Ocean-temperature, 18.08.2016
http://smart.embl-heidelberg.de/
http://www.arabidopsis.org
http://www.cbs.dtu.dk/services/TargetP/
http://www.ebi.ac.uk/interpro
http://www.ebi.ac.uk/Tools/msa/tcoffee
http://www.eia.gov/cfapps/ipdbproject/iedindex3.cfm?tid=5&pid=54&aid=2; 18.06.2016
http://www.genome.jp/kegg-bin/show_pathway?map00020+C00122, 30.06.2016
http://www.nannochloropsis.org
http://www.sb-roscoff.fr/hectar/]

10.2 Bibliography

Abbadi A, Brummel M, Spener F. 2000. Knockout of the regulatory site of 3-ketoacyl-ACP synthase III enhances short- and medium-chain acyl-ACP synthesis. Plant J. 24(1):1–9

Abida H, Dolch LJ, Meï C, Villanova V, Conte M, et al. 2015. Membrane glycerolipid remodeling triggered by nitrogen and phosphorus starvation in Phaeodactylum tricornutum. Plant Physiol. 167(1):118–136

Adeyo O, Horn PJ, Lee S, Binns DD, Chandrahas A, et al. 2011. The yeast lipin orthologue Pah1p is important for biogenesis of lipid droplets. J Cell Biol. 192(6):1043–1055

Akimoto S, Teshigahara A, Yokono M, Mimuro M, Nagao R, Tomo T. 2014. Excitation relaxation dynamics and energy transfer in fucoxanthin-chlorophyll a/c-protein complexes, probed by time-resolved fluorescence. Biochim Biophys Acta

Alboresi A, Perin G, Vitulo N, Diretto G, Block M, et al. 2016. Light Remodels Lipid Biosynthesis in Nannochloropsis gaditana by Modulating Carbon Partitioning between Organelles. Plant Physiol. 171(4):2468–2482

Alia A, Buda F, de Groot HJ, Matysik J. 2013. Solid-state NMR of nanomachines involved in photosynthetic energy conversion. Annu Rev Biophys. 42:675–699

Alipanah L, Rohloff J, Winge P, Bones AM, Brembu T. 2015. Whole-cell response to nitrogen deprivation in the diatom Phaeodactylum tricornutum. J Exp Bot. 66(20):6281–6296

Allen AE, Vardi A, Bowler C. 2006. An ecological and evolutionary context for integrated nitrogen metabolism and related signaling pathways in marine diatoms. Curr Opin Plant Biol. 9(3):264–273

Allen JF. 2003. Cyclic, pseudocyclic and noncyclic photophosphorylation: new links in the chain. Trends Plant Sci. 8(1):15–19

Allorent G, Courtois F, Chevalier F, Lerbs-Mache S. 2013. Plastid gene expression during chloroplast differentiation and dedifferentiation into non-photosynthetic plastids during seed formation. Plant Mol Biol. 82(1-2):59–70

Alvarez HM. 2015. Triacylglycerol and wax ester-accumulating machinery in prokaryotes. Biochimie

Altschul, S.F.; Gish, W.; Miller, W.; Myers, E.W.; Lipman, D.J. Basic local alignment search tool. J. Mol. Biol. 1990, 215, 403–410

An Y, Cao Y, Xu Y. 2015. Purification and characterization of the plastid-localized NAD-dependent malate dehydrogenase from Arabidopsis thaliana. Biotechnol Appl Biochem

Andersson MX, Goksör M, Sandelius AS. 2007a. Optical manipulation reveals strong attracting forces at membrane contact sites between endoplasmic reticulum and chloroplasts. J Biol Chem. 282(2):1170–1174

Andersson MX, Goksör M, Sandelius AS. 2007b. Membrane contact sites: physical attachment between chloroplasts and endoplasmic reticulum revealed by optical manipulation. Plant Signal Behav. 2(3):185–187

Arao, T., & Yamada, M. (1994). Biosynthesis of polyunsaturated fatty acids in the marine diatom, Phaeodactylum tricornutum. Phytochemistry, 35(5), 1177-1181.

Arroyo-Caro JM, Chileh T, Kazachkov M, Zou J, Alonso DL, García-Maroto F. 2013. The multigene family of lysophosphatidate acyltransferase (LPAT)-related enzymes in Ricinus communis: cloning and molecular characterization of two LPAT genes that are expressed in castor seeds. Plant Sci. 199-200:29–40

Aslan S, Hofvander P, Dutta P, Sitbon F, Sun C. 2015. Transient silencing of the KASII genes is feasible in Nicotiana benthamiana for metabolic engineering of wax ester composition. Sci Rep. 5:11213

Austin JR, Staehelin LA. 2011. Three-dimensional architecture of grana and stroma thylakoids of higher plants as determined by electron tomography. Plant Physiol. 155(4):1601–1611

Avidan O, Brandis A, Rogachev I, Pick U. 2015. Enhanced acetyl-CoA production is associated with increased triglyceride accumulation in the green alga Chlorella desiccata. J Exp Bot

Awai K, Xu C, Tamot B, Benning C. 2006. A phosphatidic acid-binding protein of the chloroplast inner envelope membrane involved in lipid trafficking. Proc Natl Acad Sci U S A. 103(28):10817–10822

Babior BM. 1978. Oxygen-dependent microbial killing by phagocytes (first of two parts). N Engl J Med. 298(12):659–668

Bach L, Michaelson LV, Haslam R, Bellec Y, Gissot L, et al. 2008. The very-long-chain hydroxy fatty acyl-CoA dehydratase PASTICCINO2 is essential and limiting for plant development. Proc Natl Acad Sci U S A. 105(38):14727–14731

Baczynski K, Markiewicz M, Pasenkiewicz-Gierula M. 2015. A computer model of a polyunsaturated monogalactolipid bilayer. Biochimie

Bajpai P, Bajpai PK. 1993. Eicosapentaenoic acid (EPA) production from microorganisms: a review. J Biotechnol. 30(2):161–183

Basso S, Simionato D, Gerotto C, Segalla A, Giacometti GM, Morosinotto T. 2013. Characterization of the photosynthetic apparatus of the Eustigmatophycean Nannochloropsis gaditana: Evidence of convergent evolution in the supramolecular organization of photosystem I. Biochim Biophys Acta

Banskota, Arjun H., et al. "Monogalactosyldiacylglycerols, potent nitric oxide inhibitors from the marine microalga Tetraselmis chui." Natural product research 27.12 (2013): 1084-1090

Bastien O, Botella C, Chevalier F, Block MA, Jouhet J, et al. 2016. New Insights on Thylakoid Biogenesis in Plant Cells. Int Rev Cell Mol Biol. 323:1–30

Bates PD. 2016. Understanding the control of acyl flux through the lipid metabolic network of plant oil biosynthesis. Biochim Biophys Acta

Batistič O, Kudla J. 2012. Analysis of calcium signaling pathways in plants. Biochim Biophys Acta. 1820(8):1283–1293

Beaudoin F, Gable K, Sayanova O, Dunn T, Napier JA. 2002. A Saccharomyces cerevisiae gene required for heterologous fatty acid elongase activity encodes a microsomal beta-keto-reductase. J Biol Chem. 277(13):11481–11488

Beaudoin F, Wu X, Li F, Haslam RP, Markham JE, et al. 2009. Functional characterization of the Arabidopsis beta-ketoacyl-coenzyme A reductase candidates of the fatty acid elongase. Plant Physiol. 150(3):1174–1191

Bennett MR. 1997. Non-adrenergic non-cholinergic (NANC) transmission to smooth muscle: 35 years on. Prog Neurobiol. 52(3):159–195

Benning C. 2009. Mechanisms of lipid transport involved in organelle biogenesis in plant cells. Annu Rev Cell Dev Biol. 25:71–91

Berges, J. A., Franklin, D. J., & Harrison, P. J. (2001). Evolution of an artificial seawater medium: improvements in enriched seawater, artificial water over the last two decades. Journal of Phycology, 37(6), 1138-1145.

REFERENCES

Bernal-Bayard P, Molina-Heredia FP, Hervas M, Navarro JA. 2013. Photosystem I reduction in diatoms: as complex as the green lineage systems but less efficient. Biochemistry

Bidle KD, Bender SJ. 2008. Iron starvation and culture age activate metacaspases and programmed cell death in the marine diatom Thalassiosira pseudonana. Eukaryotic Cell. 7(2):223–236

Bidle KD, Falkowski PG. 2004. Cell death in planktonic, photosynthetic microorganisms. Nat Rev Microbiol. 2(8):643–655

Bína D, Herbstová M, Gardian Z, Vácha F, Litvín R. 2016. Novel structural aspect of the diatom thylakoid membrane: lateral segregation of photosystem I under red-enhanced illumination. Sci Rep. 6:25583

Bligh EG, Dyer WJ. 1959. A rapid method of total lipid extraction and purification. Can. J. Biochem. Physiol. 37: 911-917.

Block MA, Jouhet J. 2015. Lipid trafficking at endoplasmic reticulum-chloroplast membrane contact sites. Curr Opin Cell Biol. 35:21–29

Bonaventure G, Salas JJ, Pollard MR, Ohlrogge JB. 2003. Disruption of the FATB gene in Arabidopsis demonstrates an essential role of saturated fatty acids in plant growth. Plant Cell. 15(4):1020–1033

Boudière L, Maréchal E. 2014. Screening for inhibitors of chloroplast galactolipid synthesis acting in membrano and in planta. Methods Mol Biol. 1056:79–93

Boudière L, Michaud M, Petroutsos D, Rébeillé F, Falconet D, et al. 2014. Glycerolipids in photosynthesis: composition, synthesis and trafficking. Biochim Biophys Acta. 1837(4):470–480

Bowler C, Allen AE, Badger JH, Grimwood J, Jabbari K, et al. 2008. The Phaeodactylum genome reveals the evolutionary history of diatom genomes. Nature. 456(7219):239–244

Brown JS. 1987. Functional Organization of Chlorophyll a and Carotenoids in the Alga, Nannochloropsis salina. Plant Physiol. 83(2):434–437

Brownlee C. 2008. Diatom signalling: deadly messages. Curr Biol. 18(12):R518–9

Browse J, Warwick N, Somerville CR, Slack CR. 1986. Fluxes through the prokaryotic and eukaryotic pathways of lipid synthesis in the "16:3" plant Arabidopsis thaliana. Biochem J. 235(1):25–31

Brzezowski P, Richter AS, Grimm B. 2015. Regulation and function of tetrapyrrole biosynthesis in plants and algae. Biochim Biophys Acta

Caldwell GS. 2009. The influence of bioactive oxylipins from marine diatoms on invertebrate reproduction and development. Mar Drugs. 7(3):367–400

Camacho-Rodríguez J, González-Céspedes AM, Cerón-García MC, Fernández-Sevilla JM, Acién-Fernández FG, Molina-Grima E. 2014. A quantitative study of eicosapentaenoic acid (EPA) production by Nannochloropsis gaditana for aquaculture as a function of dilution rate, temperature and average irradiance. Appl Microbiol Biotechnol. 98(6):2429–2440

Cao J, Jiang F, Sodmergen, Cui K. 2003. Time-course of programmed cell death during leaf senescence in Eucommia ulmoides. J Plant Res. 116(1):7–12

Cao S, Zhang X, Xu D, Fan X, Mou S, et al. 2013. A transthylakoid proton gradient and inhibitors induce a non-photochemical fluorescence quenching in unicellular algae Nannochloropsis sp. FEBS Lett. 587(9):1310–1315

Cao S, Zhang X, Ye N, Fan X, Mou S, et al. 2012. Evaluation of putative internal reference genes for gene expression normalization in Nannochloropsis sp. by quantitative real-time RT-PCR. Biochem Biophys Res Commun. 424(1):118–123

Carbonera D, Agostini A, Di Valentin M, Gerotto C, Basso S, et al. 2014. Photoprotective sites in the Violaxanthin-Chlorophyll a binding Protein (VCP) from Nannochloropsis gaditana. Biochim Biophys Acta

Cardol P, Forti G, Finazzi G. 2011. Regulation of electron transport in microalgae. Biochim Biophys Acta. 1807(8):912–918

Cavalier-Smith T. 2003. Genomic reduction and evolution of novel genetic membranes and protein-targeting machinery in eukaryote-eukaryote chimaeras (meta-algae). Philos Trans R Soc Lond, B, Biol Sci. 358(1429):109–33; discussion 133

Cerutti H, Ma X, Msanne J, Repas T. 2011. RNA-mediated silencing in Algae: biological roles and tools for analysis of gene function. Eukaryotic Cell. 10(9):1164–1172

Chapman, AD. 2009. Numbers of living species in Australia and the world. Report for the Australian Biological Ressources study. Australian Gouvernment.

Chapman KD, Dyer JM, Mullen RT. 2012. Biogenesis and functions of lipid droplets in plants: Thematic Review Series: Lipid Droplet Synthesis and Metabolism: from Yeast to Man. J Lipid Res. 53(2):215–226

Chapman KD, Ohlrogge JB. 2012. Compartmentation of triacylglycerol accumulation in plants. J Biol Chem. 287(4):2288–2294

Chen CY, Chen YC, Huang HC, Huang CC, Lee WL, Chang JS. 2013. Engineering strategies for enhancing the production of eicosapentaenoic acid (EPA) from an isolated microalga Nannochloropsis oceanica CY2. Bioresour Technol. 147:160–167

Chen JE, Smith AG. 2012. A look at diacylglycerol acyltransferases (DGATs) in algae. J Biotechnol. 162(1):28–39

Chen M, Thelen JJ. 2013. ACYL-LIPID DESATURASE2 is required for chilling and freezing tolerance in Arabidopsis. Plant Cell. 25(4):1430–1444

Chen S, Lei Y, Xu X, Huang J, Jiang H, et al. 2015. The Peanut (Arachis hypogaea L.) Gene AhLPAT2 Increases the Lipid Content of Transgenic Arabidopsis Seeds. PLoS ONE. 10(8):e0136170

Cheng R, Ge Y, Yang B, Zhong X, Lin X, Huang Z. 2013. Cloning and functional analysis of putative malonyl-CoA:acyl-carrier protein transacylase gene from the docosahexaenoic acid-producer Schizochytrium sp. TIO1101. World J Microbiol Biotechnol. 29(6):959–967

Chi W, Feng P, Ma J, Zhang L. 2015. Metabolites and chloroplast retrograde signaling. Curr Opin Plant Biol. 25:32–38

Chintalapati S, Prakash JS, Singh AK, Ohtani S, Suzuki I, et al. 2007. Desaturase genes in a psychrotolerant Nostoc sp. are constitutively expressed at low temperature. Biochem Biophys Res Commun. 362(1):81–87

Chiu SY, Kao CY, Tsai MT, Ong SC, Chen CH, Lin CS. 2009. Lipid accumulation and CO2 utilization of Nannochloropsis oculata in response to CO2 aeration. Bioresour Technol. 100(2):833–838

Choi CJ, Berges JA. 2013. New types of metacaspases in phytoplankton reveal diverse origins of cell death proteases. Cell Death Dis. 4:e490

Chow F, Pedersén M, Oliveira, MC. 2013. Modulation of nitrate reductase activity by photosynthetic electron transport chain and nitric oxide balance in the red macroalga Gracilaria chilensis (Gracilariales, Rhodophyta). Journal of applied phycology 25.6: 1847-1853

Collos, Y. 1986. Time-lag algal growth dynamics: biological constraints on primary production in aquatic environments. Mar. Ecol. Prog. Ser, 33, 193-206.

Conte M, Dolch LJ, Mei C, Barette C, Petroutsos D, Finazzi G, Falconet D, Jouhet J, Rébeillé F, Cintrat JC, Maréchal E. 2015. WO2015111029 A1

Cook, O., & Hildebrand, M. 2016. Enhancing LC-PUFA production in Thalassiosira pseudonana by overexpressing the endogenous fatty acid elongase genes. Journal of Applied Phycology, 28(2), 897-905.

Cookson SJ, Williams LE, Miller AJ. 2005. Light-dark changes in cytosolic nitrate pools depend on nitrate reductase activity in Arabidopsis leaf cells. Plant Physiol. 138(2):1097–1105

Corpas FJ, Barroso JB. 2013. Nitro-oxidative stress vs oxidative or nitrosative stress in higher plants. New Phytol. 199(3):633–635

Corteggiani Carpinelli E, Telatin A, Vitulo N, Forcato C, D'Angelo M, et al. 2014. Chromosome scale genome assembly and transcriptome profiling of Nannochloropsis gaditana in nitrogen depletion. Mol Plant. 7(2):323–335

Courchesne NM, Parisien A, Wang B, Lan CQ. 2009. Enhancement of lipid production using biochemical, genetic and transcription factor engineering approaches. J Biotechnol. 141(1-2):31–41

Crosatti C, Rizza F, Badeck FW, Mazzucotelli E, Cattivelli L. 2013. Harden the chloroplast to protect the plant. Physiol Plant. 147(1):55–63

Curtis BA, Tanifuji G, Burki F, Gruber A, Irimia M, et al. 2012. Algal genomes reveal evolutionary mosaicism and the fate of nucleomorphs. Nature. 492(7427):59–65

Daboussi F, Leduc S, Maréchal A, Dubois G, Guyot V, et al. 2014. Genome engineering empowers the diatom Phaeodactylum tricornutum for biotechnology. Nat Commun. 5:3831

Dahlqvist A, Stahl U, Lenman M, Banas A, Lee M, et al. 2000. Phospholipid:diacylglycerol acyltransferase: an enzyme that catalyzes the acyl-CoA-independent formation of triacylglycerol in yeast and plants. Proc Natl Acad Sci U S A. 97(12):6487–6492

Dailey FE, McGraw JE, Jensen BJ, Bishop SS, Lokken JP, et al. 2015. The Microbiota of Freshwater Fish and Freshwater Niches Contain Omega-3 Producing Shewanella species. Appl Environ Microbiol

DalCorso G, Pesaresi P, Masiero S, Aseeva E, Schünemann D, et al. 2008. A complex containing PGRL1 and PGR5 is involved in the switch between linear and cyclic electron flow in Arabidopsis. Cell. 132(2):273–285

Davidi L, Katz A, Pick U. 2012. Characterization of major lipid droplet proteins from Dunaliella. Planta. 236(1):19–33

Davis MS, Cronan JE. 2001. Inhibition of Escherichia coli acetyl coenzyme A carboxylase by acyl-acyl carrier protein. J Bacteriol. 183(4):1499–1503

De Mendoza D. 2014. Temperature Sensing by Membranes. Annu Rev Microbiol

De Meyer FJ, Rodgers JM, Willems TF, Smit B. 2010. Molecular simulation of the effect of cholesterol on lipid-mediated protein-protein interactions. Biophys J. 99(11):3629–3638

De Riso V, Raniello R, Maumus F, Rogato A, Bowler C, Falciatore A. 2009. Gene silencing in the marine diatom Phaeodactylum tricornutum. Nucleic Acids Res. 37(14):e96

Degenkolbe T, Giavalisco P, Zuther E, Seiwert B, Hincha DK, Willmitzer L. 2012. Differential remodeling of the lipidome during cold acclimation in natural accessions of Arabidopsis thaliana. Plant J. 72(6):972–982

Dehesh K, Tai H, Edwards P, Byrne J, Jaworski JG. 2001. Overexpression of 3-ketoacyl-acyl-carrier protein synthase IIIs in plants reduces the rate of lipid synthesis. Plant Physiol. 125(2):1103–1114

Demé B, Cataye C, Block MA, Maréchal E, Jouhet J. 2014. Contribution of galactoglycerolipids to the 3-dimensional architecture of thylakoids. FASEB J

Demmig-Adams B, Cohu CM, Amiard V, Zadelhoff G, Veldink GA, et al. 2013. Emerging trade-offs - impact of photoprotectants (PsbS, xanthophylls, and vitamin E) on oxylipins as regulators of development and defense. New Phytol. 197(3):720–729

Depauw FA, Rogato A, Ribera d'Alcalá M, Falciatore A. 2012. Exploring the molecular basis of responses to light in marine diatoms. J Exp Bot. 63(4):1575–1591

Dereeper A, Guignon V, Blanc G, Audic S, Buffet S, et al. 2008. Phylogeny.fr: robust phylogenetic analysis for the non-specialist. Nucleic Acids Res. 36(Web Server issue):W465–9

Deerinck, T.J., Bushong, E.A., Thor, A. and Ellisman, M.H. 2010. A new protocol for preparation of biological specimens for serial block face scanning electron microscopy. Microscop. Microanal. 16(sup2): 1138-9.

Derks A, Schaven K, Bruce D. 2015. Diverse mechanisms for photoprotection in photosynthesis. Dynamic regulation of photosystem II excitation in response to rapid environmental change. Biochim Biophys Acta. 1847(4-5):468–485

Deshnium P, Paithoonrangsarid K, Suphatrakul A, Meesapyodsuk D, Tanticharoen M, Cheevadhanarak S. 2000. Temperature-independent and -dependent expression of desaturase genes in filamentous cyanobacterium Spirulina platensis strain C1 (Arthrospira sp. PCC 9438). FEMS Microbiol Lett. 184(2):207–213

Di Dato V, Musacchia F, Petrosino G, Patil S, Montresor M, et al. 2015. Transcriptome sequencing of three Pseudo-nitzschia species reveals comparable gene sets and the presence of Nitric Oxide Synthase genes in diatoms. Sci Rep. 5:12329

Di Mascio P, Devasagayam TP, Kaiser S, Sies H. 1990. Carotenoids, tocopherols and thiols as biological singlet molecular oxygen quenchers. Biochem Soc Trans. 18(6):1054–1056

Dolch LJ, Maréchal E. 2015. Inventory of fatty acid desaturases in the pennate diatom Phaeodactylum tricornutum. Mar Drugs. 13(3):1317–1339

Domergue F, Abbadi A, Zähringer U, Moreau H, Heinz E. 2005. In vivo characterization of the first acyl-CoA Delta6-desaturase from a member of the plant kingdom, the microalga Ostreococcus tauri. Biochem J. 389(Pt 2):483–490

Domergue F, Lerchl J, Zähringer U, Heinz E. 2002. Cloning and functional characterization of Phaeodactylum tricornutum front-end desaturases involved in eicosapentaenoic acid biosynthesis. Eur J Biochem. 269(16):4105–4113

Domingo JL, Bocio A, Falcó G, Llobet JM. 2007. Benefits and risks of fish consumption Part I. A quantitative analysis of the intake of omega-3 fatty acids and chemical contaminants. Toxicology. 230(2-3):219–226

Domingues N, Matos AR, Marques da Silva J, Cartaxana P. 2012. Response of the diatom Phaeodactylum tricornutum to photooxidative stress resulting from high light exposure. PLoS ONE. 7(6):e38162

Doubnerová Hýsková V, Miedzińska L, Dobrá J, Vankova R, Ryšlavá H. 2014. Phosphoenolpyruvate carboxylase, NADP-malic enzyme, and pyruvate, phosphate dikinase are involved in the acclimation of Nicotiana tabacum L. to drought stress. J Plant Physiol. 171(5):19–25

REFERENCES

Doulias PT, Tenopoulou M, Greene JL, Raju K, Ischiropoulos H. 2013. Nitric oxide regulates mitochondrial fatty acid metabolism through reversible protein S-nitrosylation. Sci Signal. 6(256):rs1

Du ZY, Benning C. 2016. Triacylglycerol Accumulation in Photosynthetic Cells in Plants and Algae. Subcell Biochem. 86:179–205

Dubots E, Audry M, Yamaryo Y, Bastien O, Ohta H, et al. 2010. Activation of the chloroplast monogalactosyldiacylglycerol synthase MGD1 by phosphatidic acid and phosphatidylglycerol. J Biol Chem. 285(9):6003–6011

Dubots E, Botté C, Boudière L, Yamaryo-Botté Y, Jouhet J, et al. 2012. Role of phosphatidic acid in plant galactolipid synthesis. Biochimie. 94(1):86–93

Durner J, Klessig DF. 1999. Nitric oxide as a signal in plants. Curr Opin Plant Biol. 2(5):369–374

Durrett TP, Benning C, Ohlrogge J. 2008. Plant triacylglycerols as feedstocks for the production of biofuels. Plant J. 54(4):593–607

Dyhrman ST, Jenkins BD, Rynearson TA, Saito MA, Mercier ML, et al. 2012. The transcriptome and proteome of the diatom Thalassiosira pseudonana reveal a diverse phosphorus stress response. PLoS ONE. 7(3):e33768

Eberhard S, Finazzi G, Wollman FA. 2008. The dynamics of photosynthesis. Annu Rev Genet. 42:463–515

Edgar RC. 2004. MUSCLE: a multiple sequence alignment method with reduced time and space complexity. BMC Bioinformatics. 5:113

Edwards K, Johnstone C, Thompson C. 1991. A simple and rapid method for the preparation of plant genomic DNA for PCR analysis. Nucleic Acids Res. 19(6):1349

Eiamsa-Ard P, Kanjana-Opas A, Cahoon EB, Chodok P, Kaewsuwan S. 2013. Two novel Physcomitrella patens fatty acid elongases (ELOs): identification and functional characterization. Appl Microbiol Biotechnol. 97(8):3485–3497

Elble R. 1992. A simple and efficient procedure for transformation of yeasts. BioTechniques. 13(1):18–20

Emanuelsson O, Brunak S, von Heijne G, Nielsen H. 2007. Locating proteins in the cell using TargetP, SignalP and related tools. Nat Protoc. 2(4):953–971

Falciatore A, Bowler C. 2002. Revealing the molecular secrets of marine diatoms. Annu Rev Plant Biol. 53:109–130

Falk-Petersen S, Sargent JR, Henderson J, Hegseth EN, Hop H, Okolodkov YB. 1998. Lipids and fatty acids in ice algae and phytoplankton from the Marginal Ice Zone in the Barents Sea. Polar Biology, 20(1), 41-47.

Falkowski PG, Barber RT, Smetacek V. 1998. Biogeochemical Controls and Feedbacks on Ocean Primary Production. Science. 281(5374):200–207

Fan J, Zhai Z, Yan C, Xu C. 2015. Arabidopsis TRIGALACTOSYLDIACYLGLYCEROL5 Interacts with TGD1, TGD2, and TGD4 to Facilitate Lipid Transfer from the Endoplasmic Reticulum to Plastids. Plant Cell

Feng TY, Yang ZK, Zheng JW, Xie Y, Li DW, et al. 2015. Examination of metabolic responses to phosphorus limitation via proteomic analyses in the marine diatom Phaeodactylum tricornutum. Sci Rep. 5:10373

Fidalgo JP, Cid A, Torres E, Sukenik A, Herrero C. 1998. Effects of nitrogen source and growth phase on proximate biochemical composition, lipid classes and fatty acid profile of the marine microalga Isochrysis galbana

Flori S, Jouneau PH, Finazzi G, Maréchal E, Falconet D. 2016. Ultrastructure of the Periplastidial Compartment of the Diatom Phaeodactylum tricornutum. Protist. 167(3):254–267

Flynn K.J, Syrett PJ. 1986. Utilization of L-lysine and L-arginine by the diatomPhaeodactylum tricornutum. Marine Biology, 90(2), 159-163.

Fogg GE, Thake B. 1987. Algal cultures and phytoplankton ecology. Univ of Wisconsin Press.

Foresi N, Correa-Aragunde N, Santolini J, Lamattina L. 2016. Analysis of the Expression and Activity of Nitric Oxide Synthase from Marine Photosynthetic Microorganisms. Methods Mol Biol. 1424:149–162

Foresi N, Mayta ML, Lodeyro AF, Scuffi D, Correa-Aragunde N, et al. 2015. Expression of the tetrahydrofolate-dependent nitric oxide synthase from the green alga Ostreococcus tauri increases tolerance to abiotic stresses and influences stomatal development in Arabidopsis. Plant J

Forján E, Garbayo I, Henriques M, Rocha J, Vega JM, Vílchez C. 2011. UV-A mediated modulation of photosynthetic efficiency, xanthophyll cycle and fatty acid production of Nannochloropsis. Mar Biotechnol. 13(3):366–375

Franklin DJ, Brussaard CP., Berges JA. 2006. What is the role and nature of programmed cell death in phytoplankton ecology?. European Journal of Phycology, 41(1), 1-14.

Fritz M, Lokstein H, Hackenberg D, Welti R, Roth M, et al. 2007. Channeling of eukaryotic diacylglycerol into the biosynthesis of plastidial phosphatidylglycerol. J Biol Chem. 282(7):4613–4625

Fujimoto T, Parton RG. 2011. Not just fat: the structure and function of the lipid droplet. Cold Spring Harb Perspect Biol. 3(3):

Funk CD. 2001. Prostaglandins and leukotrienes: advances in eicosanoid biology. Science. 294(5548):1871–1875

Garab G, Lohner K, Laggner P, Farkas T. 2000. Self-regulation of the lipid content of membranes by non-bilayer lipids: a hypothesis. Trends Plant Sci. 5(11):489–494

Garab G, Ughy B, Goss R. 2016. Role of MGDG and Non-bilayer Lipid Phases in the Structure and Dynamics of Chloroplast Thylakoid Membranes. Subcell Biochem. 86:127–157

Garay LA, Boundy-Mills KL, German JB. 2014. Accumulation of high value lipids in single cell microorganisms: A mechanistic approach and future perspectives. J Agric Food Chem

Gardiner SE, Heinz E, Roughan PG. 1984. Rates and products of long-chain Fatty Acid synthesis from [1-C]acetate in chloroplasts isolated from leaves of 16:3 and 18:3 plants. Plant Physiol. 74(4):890–896

Gas E, Flores-Pérez U, Sauret-Güeto S, Rodríguez-Concepción M. 2009. Hunting for plant nitric oxide synthase provides new evidence of a central role for plastids in nitric oxide metabolism. Plant Cell. 21(1):18–23

Ge F, Huang W, Chen Z, Zhang C, Xiong Q, et al. 2014. Methylcrotonyl-CoA Carboxylase Regulates Triacylglycerol Accumulation in the Model Diatom Phaeodactylum tricornutum. Plant Cell. 26(4):1681–1697

Gentile MP, Blanch HW. 2001. Physiology and xanthophyll cycle activity of Nannochloropsis gaditana. Biotechnol Bioeng. 75(1):1–12

Gibbs SP. 1962. Nuclear envelope-chloroplast relationships in algae. J Cell Biol. 14:433–444

Gibson S, Arondel V, Iba K, Somerville C. 1994. Cloning of a temperature-regulated gene encoding a chloroplast omega-3 desaturase from Arabidopsis thaliana. Plant Physiol. 106(4):1615–1621

Gil A, Gil F. 2015. Fish, a Mediterranean source of n-3 PUFA: benefits do not justify limiting consumption. Br J Nutr. 113 Suppl 2:S58–67

Giovagnetti V, Flori S, Tramontano F, Lavaud J, Brunet C. 2014. The velocity of light intensity increase modulates the photoprotective response in coastal diatoms. PLoS ONE. 9(8):e103782

Giroud C, Gerber A, Eichenberger, W. 1988. Lipids of Chlamydomonas reinhardtii. Analysis of molecular species and intracellular site (s) of biosynthesis. Plant and Cell Physiology, 29(4), 587-595.

Gombos Z, Wada H, Murata N. 1994. The recovery of photosynthesis from low-temperature photoinhibition is accelerated by the unsaturation of membrane lipids: a mechanism of chilling tolerance. Proc Natl Acad Sci U S A. 91(19):8787–8791

Gong Y, Guo X, Wan X, Liang Z, Jiang M. 2011. Characterization of a novel thioesterase (PtTE) from Phaeodactylum tricornutum. J Basic Microbiol. 51(6):666–672

Gong Y, Zhang J, Guo X, Wan X, Liang Z, et al. 2013. Identification and characterization of PtDGAT2B, an acyltransferase of the DGAT2 acyl-coenzyme A: diacylglycerol acyltransferase family in the diatom Phaeodactylum tricornutum. FEBS Lett. 587(5):481–487

González-Mellado D, von Wettstein-Knowles P, Garcés R, Martínez-Force E. 2010. The role of beta-ketoacyl-acyl carrier protein synthase III in the condensation steps of fatty acid biosynthesis in sunflower. Planta. 231(6):1277–1289

Goold H, Beisson F, Peltier G, Li-Beisson Y. 2015. Microalgal lipid droplets: composition, diversity, biogenesis and functions. Plant Cell Rep. 34(4):545–555

Goss R, Jakob T. 2010. Regulation and function of xanthophyll cycle-dependent photoprotection in algae. Photosyn Res. 106(1-2):103–122

Goss R, Lepetit B. 2015. Biodiversity of NPQ. J Plant Physiol. 172:13–32

Goss R, Lohr M, Latowski D, Grzyb J, Vieler A, et al. 2005. Role of hexagonal structure-forming lipids in diadinoxanthin and violaxanthin solubilization and de-epoxidation. Biochemistry. 44(10):4028–4036

Gould N, Doulias PT, Tenopoulou M, Raju K, Ischiropoulos H. 2013. Regulation of protein function and signaling by reversible cysteine S-nitrosylation. J Biol Chem

Grosche C, Hempel F, Bolte K, Zauner S, Maier UG. 2014. The periplastidal compartment: a naturally minimized eukaryotic cytoplasm. Curr Opin Microbiol. 22C:88–93

Grouneva I, Gollan PJ, Kangasjärvi S, Suorsa M, Tikkanen M, Aro EM. 2013. Phylogenetic viewpoints on regulation of light harvesting and electron transport in eukaryotic photosynthetic organisms. Planta. 237(2):399–412

Grouneva I, Rokka A, Aro EM. 2011. The thylakoid membrane proteome of two marine diatoms outlines both diatom-specific and species-specific features of the photosynthetic machinery. J Proteome Res. 10(12):5338–5353

Gruber A, Rocap G, Kroth PG, Armbrust EV, Mock T. 2014. Plastid proteome prediction for diatoms and other algae with secondary plastids of the red lineage. Plant J

Gschloessl B, Guermeur Y, Cock JM. 2008. HECTAR: a method to predict subcellular targeting in heterokonts. BMC Bioinformatics. 9:393

Gu H, Jinkerson RE, Davies FK, Sisson LA, Schneider PE, Posewitz MC. 2016. Modulation of Medium-Chain Fatty Acid Synthesis in Synechococcus sp. PCC 7002 by Replacing FabH with a Chaetoceros Ketoacyl-ACP Synthase. Front Plant Sci. 7:690

Gu K, Chiam H, Tian D, Yin Z. 2011. Molecular cloning and expression of heteromeric ACCase subunit genes from Jatropha curcas. Plant Sci. 180(4):642–649

Gueguen V, Macherel D, Jaquinod M, Douce R, Bourguignon J. 2000. Fatty acid and lipoic acid biosynthesis in higher plant mitochondria. J Biol Chem. 275(7):5016–5025

Guihéneuf F, Leu S, Zarka A, Khozin-Goldberg I, Khalilov I, Boussiba S. 2011. Cloning and molecular characterization of a novel acyl-CoA:diacylglycerol acyltransferase 1-like gene (PtDGAT1) from the diatom Phaeodactylum tricornutum. FEBS J. 278(19):3651–3666

Guillard RR, Ryther JH. 1962. Studies of marine planktonic diatoms. I. Cyclotella nana Hustedt, and Detonula confervacea (cleve) Gran. Can J Microbiol. 8:229–239

Gupta A, Barrow CJ, Puri M. 2012a. Omega-3 biotechnology: Thraustochytrids as a novel source of omega-3 oils. Biotechnol Adv. 30(6):1733–1745

Gupta M, DeKelver RC, Palta A, Clifford C, Gopalan S, et al. 2012b. Transcriptional activation of Brassica napus β-ketoacyl-ACP synthase II with an engineered zinc finger protein transcription factor. Plant Biotechnol J. 10(7):783–791

Haimovich-Dayan M, Garfinkel N, Ewe D, Marcus Y, Gruber A, et al. 2013. The role of C4 metabolism in the marine diatom Phaeodactylum tricornutum. New Phytol. 197(1):177–185

Hall CN, Garthwaite J. 2009. What is the real physiological NO concentration in vivo? Nitric Oxide. 21(2):92–103

Hall JM, Parrish CC, Thompson RJ. 2002. Eicosapentaenoic acid regulates scallop (Placopecten magellanicus) membrane fluidity in response to cold. Biol Bull. 202(3):201–203

Hamilton ML, Powers S, Napier JA, Sayanova O. 2016. Heterotrophic Production of Omega-3 Long-Chain Polyunsaturated Fatty Acids by Trophically Converted Marine Diatom Phaeodactylum tricornutum. Mar Drugs. 14(3):

Hamilton ML, Warwick J, Terry A, Allen MJ, Napier JA, Sayanova O. 2015. Towards the Industrial Production of Omega-3 Long Chain Polyunsaturated Fatty Acids from a Genetically Modified Diatom Phaeodactylum tricornutum. PLoS ONE. 10(12):e0144054

Härtel H, Dormann P, Benning C. 2000. DGD1-independent biosynthesis of extraplastidic galactolipids after phosphate deprivation in Arabidopsis. Proc Natl Acad Sci U S A. 97(19):10649–10654

Haslam TM, Kunst L. 2013. Extending the story of very-long-chain fatty acid elongation. Plant Sci. 210:93–107

He L, Han X, Yu Z. 2014. A rare Phaeodactylum tricornutum cruciform morphotype: culture conditions, transformation and unique fatty acid characteristics. PLoS ONE. 9(4):e93922

Hema R, Senthil-Kumar M, Shivakumar S, Chandrasekhara Reddy P, Udayakumar M. 2007. Chlamydomonas reinhardtii, a model system for functional validation of abiotic stress responsive genes. Planta. 226(3):655–670

Herbstová M, Tietz S, Kinzel C, Turkina MV, Kirchhoff H. 2012. Architectural switch in plant photosynthetic membranes induced by light stress. Proc Natl Acad Sci U S A. 109(49):20130–20135

Hertle AP, Blunder T, Wunder T, Pesaresi P, Pribil M, et al. 2013. PGRL1 is the elusive ferredoxin-plastoquinone reductase in photosynthetic cyclic electron flow. Mol Cell. 49(3):511–523

REFERENCES

Hibberd DJ. 1981. Notes on the taxonomy and nomenclature of the algal classes Eustigmatophyceae and Tribophyceae (synonym Xanthophyceae). Botanical journal of the linnean society, 82(2), 93-119.

Hii YS, Soo CL, Chuah TS, Mohd-Azmi A, Abol-Munafi AB. 2011. Interactive effect of ammonia and nitrate on the nitrogen uptake by Nannochloropsis sp. Journal of Sustainability Science and Management 6.1 (2011): 60-68.

Hockin NL, Mock T, Mulholland F, Kopriva S, Malin G. 2012. The response of diatom central carbon metabolism to nitrogen starvation is different from that of green algae and higher plants. Plant Physiol. 158(1):299–312

Hoffmann M, Wagner M, Abbadi A, Fulda M, Feussner I. 2008. Metabolic engineering of omega3-very long chain polyunsaturated fatty acid production by an exclusively acyl-CoA-dependent pathway. J Biol Chem. 283(33):22352–22362

Hongsthong A, Deshnium P, Paithoonrangsarid K, Cheevadhanarak S, Tanticharoen M. 2003. Differential responses of three acyl-lipid desaturases to immediate temperature reduction occurring in two lipid membranes of Spirulina platensis strain C1. J Biosci Bioeng. 96(6):519–524

Hopkinson BM. 2013. A chloroplast pump model for the CO2 concentrating mechanism in the diatom Phaeodactylum tricornutum. Photosyn Res

Horton P. 2012. Optimization of light harvesting and photoprotection: molecular mechanisms and physiological consequences. Philos Trans R Soc Lond, B, Biol Sci. 367(1608):3455–3465

Hsueh HT, Li WJ, Chen HH, Chu H. 2009. Carbon bio-fixation by photosynthesis of Thermosynechococcus sp. CL-1 and Nannochloropsis oculta. J Photochem Photobiol B, Biol. 95(1):33–39

Hu Q, Sommerfeld M, Jarvis E, Ghirardi M, Posewitz M, et al. 2008. Microalgal triacylglycerols as feedstocks for biofuel production: perspectives and advances. Plant J. 54(4):621–639

Hu Q, Xiang W, Dai S, Li T, Yang F, et al. 2015. The influence of cultivation period on growth and biodiesel properties of microalga Nannochloropsis gaditana 1049. Bioresour Technol. 192:157–164

Huang C, Li S. 1999. Calorimetric and molecular mechanics studies of the thermotropic phase behavior of membrane phospholipids. Biochim Biophys Acta. 1422(3):273–307

Huerlimann R, Steinig EJ, Loxton H, Zenger KR, Jerry DR, Heimann K. 2014. The effect of nitrogen limitation on acetyl-CoA carboxylase expression and fatty acid content in Chromera velia and Isochrysis aff. galbana (TISO). Gene

Huerlimann R, Zenger KR, Jerry DR, Heimann K. 2015. Phylogenetic Analysis of Nucleus-Encoded Acetyl-CoA Carboxylases Targeted at the Cytosol and Plastid of Algae. PLoS ONE. 10(7):e0131099

Huertas IE, Espie GS, Colman B, Lubian LM. 2000. Light-dependent bicarbonate uptake and CO2 efflux in the marine microalga Nannochloropsis gaditana. Planta. 211(1):43–49

Hügler M, Sievert SM. 2011. Beyond the Calvin cycle: autotrophic carbon fixation in the ocean. Ann Rev Mar Sci. 3:261–289

Hugly S, Somerville C. 1992. A role for membrane lipid polyunsaturation in chloroplast biogenesis at low temperature. Plant Physiol. 99(1):197–202

Ianora A, Miralto A. 2010. Toxigenic effects of diatoms on grazers, phytoplankton and other microbes: a review. Ecotoxicology. 19(3):493–511

Inaba M, Suzuki I, Szalontai B, Kanesaki Y, Los DA, et al. 2003. Gene-engineered rigidification of membrane lipids enhances the cold inducibility of gene expression in synechocystis. J Biol Chem. 278(14):12191–12198

Iwai M, Takizawa K, Tokutsu R, Okamuro A, Takahashi Y, Minagawa J. 2010. Isolation of the elusive supercomplex that drives cyclic electron flow in photosynthesis. Nature. 464(7292):1210–1213

Jahns P, Latowski D, Strzalka K. 2009. Mechanism and regulation of the violaxanthin cycle: the role of antenna proteins and membrane lipids. Biochim Biophys Acta. 1787(1):3–14

Järvi S, Suorsa M, Aro EM. 2015. Photosystem II repair in plant chloroplasts - Regulation, assisting proteins and shared components with photosystem II biogenesis. Biochimica et Biophysica Acta.

Jeennor S, Cheawchanlertfa P, Suttiwattanakul S, Panchanawaporn S, Chutrakul C, Laoteng K. 2014. Novel elongase of Pythium sp. with high specificity on Δ(6)-18C desaturated fatty acids. Biochem Biophys Res Commun. 450(1):507–512

Jessen D, Roth C, Wiermer M, Fulda M. 2014. Two activities of long-chain acyl-CoA synthetase are involved in lipid trafficking between the endoplasmic reticulum and the plastid in Arabidopsis. Plant Physiol

Ji XJ, Ren LJ, Huang H. 2015. Omega-3 Biotechnology: A Green and Sustainable Process for Omega-3 Fatty Acids Production. Frontiers in bioengineering and biotechnology. 3:158

Jiang Y, Chan CH, Cronan JE. 2006. The soluble acyl-acyl carrier protein synthetase of Vibrio harveyi B392 is a member of the medium chain acyl-CoA synthetase family. Biochemistry. 45(33):10008–10019

Jin CW, Du ST, Zhang YS, Lin XY, Tang CX. 2009. Differential regulatory role of nitric oxide in mediating nitrate reductase activity in roots of tomato (Solanum lycocarpum). Ann Bot. 104(1):9–17

Jinkerson RE, Radakovits R, Posewitz MC. 2013. Genomic insights from the oleaginous model alga Nannochloropsis gaditana. Bioengineered. 4(1):37–43

Johnson GN. 2005. Cyclic electron transport in C3 plants: fact or artefact? J Exp Bot. 56(411):407–416

Lewin JC, Lewin RA, Philpott DE. 1958. Observations on Phaeodactyulm tricornutum. Microbiology 18.2 (1958): 418-426.

Joliot P, Johnson GN. 2011. Regulation of cyclic and linear electron flow in higher plants. Proc Natl Acad Sci U S A. 108(32):13317–13322

Joubès J, Raffaele S, Bourdenx B, Garcia C, Laroche-Traineau J, et al. 2008. The VLCFA elongase gene family in Arabidopsis thaliana: phylogenetic analysis, 3D modelling and expression profiling. Plant Mol Biol. 67(5):547–566

Jouhet J, Maréchal E, Baldan B, Bligny R, Joyard J, Block MA. 2004. Phosphate deprivation induces transfer of DGDG galactolipid from chloroplast to mitochondria. J Cell Biol. 167(5):863–874

Kaczmarzyk D, Hudson EP, Fulda M. 2016. Arabidopsis acyl-acyl carrier protein synthetase AAE15 with medium chain fatty acid specificity is functional in cyanobacteria. AMB Express. 6(1):7

Kajikawa M, Matsui K, Ochiai M, Tanaka Y, Kita Y, et al. 2008. Production of arachidonic and eicosapentaenoic acids in plants using bryophyte fatty acid Delta6-desaturase, Delta6-elongase, and Delta5-desaturase genes. Biosci Biotechnol Biochem. 72(2):435–444

Kanervo E, Suorsa M, Aro EM. 2005. Functional flexibility and acclimation of the thylakoid membrane. Photochem Photobiol Sci. 4(12):1072–1080

Kaniuga Z. 2008. Chilling response of plants: importance of galactolipase, free fatty acids and free radicals. Plant Biol (Stuttg). 10(2):171–184

Ke J, Behal RH, Back SL, Nikolau BJ, Wurtele ES, Oliver DJ. 2000. The role of pyruvate dehydrogenase and acetyl-coenzyme A synthetase in fatty acid synthesis in developing Arabidopsis seeds. Plant Physiol. 123(2):497–508

Keeling PJ. 2010. The endosymbiotic origin, diversification and fate of plastids. Philos Trans R Soc Lond, B, Biol Sci. 365(1541):729–748

Kelly AA, Dörmann P. 2002. DGD2, an arabidopsis gene encoding a UDP-galactose-dependent digalactosyldiacylglycerol synthase is expressed during growth under phosphate-limiting conditions. J Biol Chem. 277(2):1166–1173

Kelly AA, Froehlich JE, Dörmann P. 2003. Disruption of the two digalactosyldiacylglycerol synthase genes DGD1 and DGD2 in Arabidopsis reveals the existence of an additional enzyme of galactolipid synthesis. Plant Cell. 15(11):2694–2706

Kilian O, Benemann CS, Niyogi KK, Vick B. 2011. High-efficiency homologous recombination in the oil-producing alga Nannochloropsis sp. Proc Natl Acad Sci U S A. 108(52):21265–21269

Kim J, Fabris M, Baart G, Kim MK, Goossens A, et al. 2016. Flux balance analysis of primary metabolism in the diatom Phaeodactylum tricornutum. Plant J. 85(1):161–176

Kim S, Yamaoka Y, Ono H, Kim H, Shim D, et al. 2013. AtABCA9 transporter supplies fatty acids for lipid synthesis to the endoplasmic reticulum. Proc Natl Acad Sci U S A. 110(2):773–778

Kirchhoff H. 2013. Architectural switches in plant thylakoid membranes. Photosyn Res. 116(2-3):481–487

Klaus D, Ohlrogge JB, Neuhaus HE, Dörmann P. 2004. Increased fatty acid production in potato by engineering of acetyl-CoA carboxylase. Planta. 219(3):389–396

Koc I, Filiz E, Tombuloglu H. 2015. Comparative analysis of plant lycopene cyclases. Comput Biol Chem. 58:81–92

Kodama H, Hamada T, Horiguchi G, Nishimura M, Iba K. 1994. Genetic Enhancement of Cold Tolerance by Expression of a Gene for Chloroplast [omega]-3 Fatty Acid Desaturase in Transgenic Tobacco. Plant Physiol. 105(2):601–605

Kohlwein SD, Eder S, Oh CS, Martin CE, Gable K, et al. 2001. Tsc13p is required for fatty acid elongation and localizes to a novel structure at the nuclear-vacuolar interface in Saccharomyces cerevisiae. Mol Cell Biol. 21(1):109–125

Koo AJ, Fulda M, Browse J, Ohlrogge JB. 2005. Identification of a plastid acyl-acyl carrier protein synthetase in Arabidopsis and its role in the activation and elongation of exogenous fatty acids. Plant J. 44(4):620–632

Kroth PG, Chiovitti A, Gruber A, Martin-Jezequel V, Mock T, et al. 2008. A model for carbohydrate metabolism in the diatom Phaeodactylum tricornutum deduced from comparative whole genome analysis. PLoS ONE. 3(1):e1426

Krumova SB, Dijkema C, de Waard P, Van As H, Garab G, van Amerongen H. 2008. Phase behavior of phosphatidylglycerol in spinach thylakoid membranes as revealed by 31P-NMR. Biochim Biophys Acta. 1778(4):997–1003

Kuczynska P, Jemiola-Rzeminska M, Strzalka K. 2015. Photosynthetic Pigments in Diatoms. Mar Drugs. 13(9):5847–5881

Kular L, Pakradouni J, Kitabgi P, Laurent M, Martinerie C. 2011. The CCN family: a new class of inflammation modulators? Biochimie. 93(3):377–388

Kumar A, Sharma A, Upadhyaya KC. 2016. Vegetable Oil: Nutritional and Industrial Perspective. Curr Genomics. 17(3):230–240

Kutty SK, Barraud N, Pham A, Iskander G, Rice SA, et al. 2013. Design, Synthesis and Evaluation of Fimbrolide-Nitric Oxide Donor Hybrids as Antimicrobial Agents. J Med Chem

Kuznetsova S, Knaff DB, Hirasawa M, Lagoutte B, Sétif P. 2004. Mechanism of spinach chloroplast ferredoxin-dependent nitrite reductase: spectroscopic evidence for intermediate states. Biochemistry. 43(2):510–517

Laemmli UK. 1970. Cleavage of structural proteins during the assembly of the head of bacteriophage T4. Nature. 227(5259):680–685

Lang I, Hodac L, Friedl T, Feussner I. 2011. Fatty acid profiles and their distribution patterns in microalgae: a comprehensive analysis of more than 2000 strains from the SAG culture collection. BMC Plant Biol. 11:124

Lavaud J, Lepetit B. 2013. An explanation for the inter-species variability of the photoprotective non-photochemical chlorophyll fluorescence quenching in diatoms. Biochim Biophys Acta. 1827(3):294–302

Lavaud J, Materna AC, Sturm S, Vugrinec S, Kroth PG. 2012. Silencing of the violaxanthin de-epoxidase gene in the diatom Phaeodactylum tricornutum reduces diatoxanthin synthesis and non-photochemical quenching. PLoS ONE. 7(5):e36806

Lebeau T, Robert JM. 2003. Diatom cultivation and biotechnologically relevant products. Part I: cultivation at various scales. Appl Microbiol Biotechnol. 60(6):612–623

Lee JM, Lee H, Kang S, Park WJ. 2016. Fatty Acid Desaturases, Polyunsaturated Fatty Acid Regulation, and Biotechnological Advances. Nutrients. 8(1):

Lemeille S, Rochaix JD. 2010. State transitions at the crossroad of thylakoid signalling pathways. Photosyn Res. 106(1-2):33–46

Lemoine Y, Schoefs B. 2010. Secondary ketocarotenoid astaxanthin biosynthesis in algae: a multifunctional response to stress. Photosyn Res. 106(1-2):155–177

Lepetit B, Goss R, Jakob T, Wilhelm C. 2012. Molecular dynamics of the diatom thylakoid membrane under different light conditions. Photosyn Res. 111(1-2):245–257

Leterrier M, Calleja P, Marechal E. 2015. MODIFIED ALGAE STRAIN AND METHOD OF TRIACYLGLYCEROL ACCUMULATION USING SAID STRAIN. WO2015008160 A2

Levitan O, Dinamarca J, Hochman G, Falkowski PG. 2014. Diatoms: a fossil fuel of the future. Trends Biotechnol. 32(3):117–124

Levitan O, Dinamarca J, Zelzion E, Gorbunov MY, Falkowski PG. 2015. An RNAi knock-down of nitrate reductase enhances lipid biosynthesis in the diatom Phaeodactylum tricornutum. Plant J

Lewis TE, Nichols PD, McMeekin TA. 1999. The Biotechnological Potential of Thraustochytrids. Mar Biotechnol. 1(6):580–587

Li-Beisson Y, Shorrosh B, Beisson F, Andersson MX, Arondel V, et al. 2010. Acyl-lipid metabolism. Arabidopsis Book. 8:e0133

Li HY, Lu Y, Zheng JW, Yang WD, Liu JS. 2014. Biochemical and genetic engineering of diatoms for polyunsaturated fatty acid biosynthesis. Mar Drugs. 12(1):153–166

Li J, Han D, Wang D, Ning K, Jia J, et al. 2014b. Choreography of Transcriptomes and Lipidomes of Nannochloropsis Reveals the Mechanisms of Oil Synthesis in Microalgae. Plant Cell

Li J, Xu X. 2016. DNA double-strand break repair: a tale of pathway choices. Acta Biochim Biophys Sin (Shanghai)

Li X, Moellering ER, Liu B, Johnny C, Fedewa M, et al. 2012. A galactoglycerolipid lipase is required for triacylglycerol accumulation and survival following nitrogen deprivation in Chlamydomonas reinhardtii. Plant Cell. 24(11):4670–4686

REFERENCES

Li M, Welti R, Wang X. 2006. Quantitative profiling of Arabidopsis polar glycerolipids in response to phosphorus starvation. Roles of phospholipases D zeta1 and D zeta2 in phosphatidylcholine hydrolysis and digalactosyldiacylglycerol accumulation in phosphorus-starved plants. Plant Physiol. 142(2):750–761

Li N, Gügel IL, Giavalisco P, Zeisler V, Schreiber L, et al. 2015a. FAX1, a novel membrane protein mediating plastid fatty acid export. PLoS Biol. 13(2):e1002053

Li N, Xu C, Li-Beisson Y, Philippar K. 2016b. Fatty Acid and Lipid Transport in Plant Cells. Trends Plant Sci. 21(2):145–158

Li Q, Zheng Q, Shen W, Cram D, Fowler DB, et al. 2015c. Understanding the biochemical basis of temperature-induced lipid pathway adjustments in plants. Plant Cell. 27(1):86–103

Li X, Moellering ER, Liu B, Johnny C, Fedewa M, et al. 2012. A galactoglycerolipid lipase is required for triacylglycerol accumulation and survival following nitrogen deprivation in Chlamydomonas reinhardtii. Plant Cell. 24(11):4670–4686

Li Y, Florova G, Reynolds KA. 2005. Alteration of the fatty acid profile of Streptomyces coelicolor by replacement of the initiation enzyme 3-ketoacyl acyl carrier protein synthase III (FabH). J Bacteriol. 187(11):3795–3799

Li Z, Wakao S, Fischer BB, Niyogi KK. 2009. Sensing and responding to excess light. Annu Rev Plant Biol. 60:239–260

Liang MH, Jiang JG. 2013. Advancing oleaginous microorganisms to produce lipid via metabolic engineering technology. Prog Lipid Res. 52(4):395–408

Lim PO, Kim HJ, Nam HG. 2007. Leaf senescence. Annu Rev Plant Biol. 58:115–136

Litvín R, Bína D, Herbstová M, Gardian Z. 2016. Architecture of the light-harvesting apparatus of the eustigmatophyte alga Nannochloropsis oceanica. Photosyn Res

Liu B, Vieler A, Li C, Jones AD, Benning C. 2013a. Triacylglycerol profiling of microalgae Chlamydomonas reinhardtii and Nannochloropsis oceanica. Bioresour Technol. 146:310–316

Liu T, Huang J. 2016. DNA End Resection: Facts and Mechanisms. Genomics Proteomics Bioinformatics

Liu X, Duan S, Li A, Xu N, Cai Z, Hu Z. 2009. Effects of organic carbon sources on growth, photosynthesis, and respiration of Phaeodactylum tricornutum. Journal of Applied Phycology, 21(2), 239-246.

Liu Y, Feng Y, Wang Y, Li X, Cao X, Xue S. 2015. Structural and biochemical characterization of MCAT from photosynthetic microorganism Synechocystis sp. PCC 6803 reveal its stepwise catalytic mechanism. Biochem Biophys Res Commun

Liu Y, Zhang C, Shen X, Zhang X, Cichello S, et al. 2013b. Microorganism lipid droplets and biofuel development. BMB Rep. 46(12):575–581

Los DA, Murata N. 2004. Membrane fluidity and its roles in the perception of environmental signals. Biochim Biophys Acta. 1666(1-2):142–157

Los DA, Ray MK, Murata N. 1997. Differences in the control of the temperature-dependent expression of four genes for desaturases in Synechocystis sp. PCC 6803. Mol Microbiol. 25(6):1167–1175

Los DA, Zorina A, Sinetova M, Kryazhov S, Mironov K, Zinchenko VV. 2010. Stress sensors and signal transducers in cyanobacteria. Sensors Basel Sensors. 10(3):2386–2415

Losh JL, Young JN, Morel FM. 2013. Rubisco is a small fraction of total protein in marine phytoplankton. New Phytol. 198(1):52–58

Lowry OH, Rosebrough NJ, Farr AL, Randall RJ. 1951. Protein measurement with the Folin phenol reagent. J Biol Chem. 193(1):265–275

Lu B, Benning C. 2009. A 25-amino acid sequence of the Arabidopsis TGD2 protein is sufficient for specific binding of phosphatidic acid. J Biol Chem. 284(26):17420–17427

Ma X, Zhang L, Zhu B, Pan K, Li S, Yang G. 2011. Low-temperature affected LC-PUFA conversion and associated gene transcript level in Nannochloropsis oculata CS-179. Journal of Ocean University of China, 10(3), 270-274.

Ma XN, Chen TP, Yang B, Liu J, Chen F. 2016. Lipid Production from Nannochloropsis. Mar Drugs. 14(4):

Ma YH, Wang X, Niu YF, Yang ZK, Zhang MH, et al. 2014. Antisense knockdown of pyruvate dehydrogenase kinase promotes the neutral lipid accumulation in the diatom Phaeodactylum tricornutum. Microb Cell Fact. 13(1):100

Madden MC. 2016. A paler shade of green? The toxicology of biodiesel emissions: Recent findings from studies with this alternative fuel. Biochim Biophys Acta

Madoka Y, Tomizawa K, Mizoi J, Nishida I, Nagano Y, Sasaki Y. 2002. Chloroplast transformation with modified accD operon increases acetyl-CoA carboxylase and causes extension of leaf longevity and increase in seed yield in tobacco. Plant Cell Physiol. 43(12):1518–1525

Maisonneuve S, Bessoule JJ, Lessire R, Delseny M, Roscoe TJ. 2010. Expression of rapeseed microsomal lysophosphatidic acid acyltransferase isozymes enhances seed oil content in Arabidopsis. Plant Physiol. 152(2):670–684

Mandal MK, Chandra-Shekara AC, Jeong RD, Yu K, Zhu S, et al. 2012. Oleic acid-dependent modulation of NITRIC OXIDE ASSOCIATED1 protein levels regulates nitric oxide-mediated defense signaling in Arabidopsis. Plant Cell. 24(4):1654–1674

Mann JE, Myers J. 1968. Photosynthetic Enhancement in the Diatom Phaeodactylum tricornutum. Plant Physiol. 43(12):1991–1995

Mansfeldt CB, Richter LV, Ahner BA, Cochlan WP, Richardson RE. 2016. Use of De Novo Transcriptome Libraries to Characterize a Novel Oleaginous Marine Chlorella Species during the Accumulation of Triacylglycerols. PLoS ONE. 11(2):e0147527

Maréchal E, Bastien O. 2014. Modeling of regulatory loops controlling galactolipid biosynthesis in the inner envelope membrane of chloroplasts. J Theor Biol

Maréchal E, Miège C, Block MA, Douce R, Joyard J. 1995. The catalytic site of monogalactosyldiacylglycerol synthase from spinach chloroplast envelope membranes. Biochemical analysis of the structure and of the metal content. J Biol Chem. 270(11):5714–5722

Markham JE, Jaworski JG. 2007. Rapid measurement of sphingolipids from Arabidopsis thaliana by reversed-phase high-performance liquid chromatography coupled to electrospray ionization tandem mass spectrometry. Rapid Commun Mass Spectrom. 21(7):1304–1314

Martin P, Van Mooy BA, Heithoff A, Dyhrman ST. 2011. Phosphorus supply drives rapid turnover of membrane phospholipids in the diatom Thalassiosira pseudonana. The ISME journal, 5(6), 1057-1060.

Masoodi M, Kuda O, Rossmeisl M, Flachs P, Kopecky J. 2014. Lipid signaling in adipose tissue: Connecting inflammation & metabolism. Biochim Biophys Acta

Matsuda O, Sakamoto H, Hashimoto T, Iba K. 2005. A temperature-sensitive mechanism that regulates post-translational stability of a plastidial omega-3 fatty acid desaturase (FAD8) in Arabidopsis leaf tissues. J Biol Chem. 280(5):3597–3604

Matsumoto K, Murata T, Nagao R, Nomura CT, Arai S, et al. 2009. Production of short-chain-length/medium-chain-length polyhydroxyalkanoate (PHA) copolymer in the plastid of Arabidopsis thaliana using an engineered 3-ketoacyl-acyl carrier protein synthase III. Biomacromolecules. 10(4):686–690

McFadden GI. 2014. Origin and evolution of plastids and photosynthesis in eukaryotes. Cold Spring Harb Perspect Biol. 6(4):a016105

Medipally SR, Yusoff FM, Banerjee S, Shariff M. 2015. Microalgae as sustainable renewable energy feedstock for biofuel production. BioMed research international. 2015:519513

Meï C, Michaud M, Cussac M, Albrieux C, Gros V, et al. 2015. Levels of polyunsaturated fatty acids correlate with growth rate in plant cell cultures. Sci Rep. 5:15207

*Meksiarun P, Spegazzini N, Matsui H, Nakajima K, Matsuda Y, & Sato H. 2015. Applied spectroscopy **69,** 45-51.M*

Meng Y, Jiang J, Wang H, Cao X, Xue S, et al. 2015. The characteristics of TAG and EPA accumulation in Nannochloropsis oceanica IMET1 under different nitrogen supply regimes. Bioresour Technol. 179:483–489

Merchant SS, Kropat J, Liu B, Shaw J, Warakanont J. 2012. TAG, you're it! Chlamydomonas as a reference organism for understanding algal triacylglycerol accumulation. Curr Opin Biotechnol. 23(3):352–363

Meyer A, Kirsch H, Domergue F, Abbadi A, Sperling P, et al. 2004. Novel fatty acid elongases and their use for the reconstitution of docosahexaenoic acid biosynthesis. J Lipid Res. 45(10):1899–1909

Michaud M, Gros V, Tardif M, Brugière S, Ferro M, et al. 2016. AtMic60 Is Involved in Plant Mitochondria Lipid Trafficking and Is Part of a Large Complex. Curr Biol. 26(5):627–639

Míguez F, Fernández-Marín B, Becerril JM, García-Plazaola JI. 2015. Activation of photoprotective winter photoinhibition in plants from different environments: a literature compilation and meta-analysis. Physiol Plant. 155(4):414–423

Mikami K, Hosokawa M. 2013. Biosynthetic pathway and health benefits of fucoxanthin, an algae-specific xanthophyll in brown seaweeds. Int J Mol Sci. 14(7):13763–13781

Mikami K, Murata N. 2003. Membrane fluidity and the perception of environmental signals in cyanobacteria and plants. Prog Lipid Res. 42(6):527–543

Miller R, Wu G, Deshpande RR, Vieler A, Gärtner K, et al. 2010. Changes in transcript abundance in Chlamydomonas reinhardtii following nitrogen deprivation predict diversion of metabolism. Plant Physiol. 154(4):1737–1752

Milsom AB, Patel NS, Mazzon E, Tripatara P, Storey A, et al. 2010. Role for endothelial nitric oxide synthase in nitrite-induced protection against renal ischemia-reperfusion injury in mice. Nitric Oxide. 22(2):141–148

Minagawa J. 2011. State transitions--the molecular remodeling of photosynthetic supercomplexes that controls energy flow in the chloroplast. Biochim Biophys Acta. 1807(8):897–905

Miquel M, Browse J. 1992. Arabidopsis mutants deficient in polyunsaturated fatty acid synthesis. Biochemical and genetic characterization of a plant oleoyl-phosphatidylcholine desaturase. J Biol Chem. 267(3):1502–1509

Misra AN, Misra M, Singh R. 2012. Chlorophyll fluorescence in plant biology. In AN Misra, ed, Biophysics. InTech, pp 171-192

Misra N, Panda PK, Parida BK. 2014. Genome-wide identification and evolutionary analysis of algal LPAT genes involved in TAG biosynthesis using bioinformatic approaches. Mol Biol Rep. 41(12):8319–8332

Misra N, Patra MC, Panda PK, Sukla LB, Mishra BK. 2013. Homology modeling and docking studies of FabH (β-ketoacyl-ACP synthase III) enzyme involved in type II fatty acid biosynthesis of Chlorella variabilis: a potential algal feedstock for biofuel production. J Biomol Struct Dyn. 31(3):241–257

Missner A, Pohl P. 2009. 110 years of the Meyer-Overton rule: predicting membrane permeability of gases and other small compounds. Chemphyschem. 10(9-10):1405–1414

Misson J, Raghothama KG, Jain A, Jouhet J, Block MA, et al. 2005. A genome-wide transcriptional analysis using Arabidopsis thaliana Affymetrix gene chips determined plant responses to phosphate deprivation. Proc Natl Acad Sci U S A. 102(33):11934–11939

Mittler R. 2002. Oxidative stress, antioxidants and stress tolerance. Trends Plant Sci. 7(9):405–410

Moellering ER, Benning C. 2011. Galactoglycerolipid metabolism under stress: a time for remodeling. Trends Plant Sci. 16(2):98–107

Mokhtari-Zaer A, Khazdair MR, Boskabady MH. 2015. Smooth muscle relaxant activity of Crocus sativus (saffron) and its constituents: possible mechanisms. Avicenna journal of phytomedicine. 5(5):365–375

Mongrand S, Cassagne C, Bessoule JJ. 2000. Import of lyso-phosphatidylcholine into chloroplasts likely at the origin of eukaryotic plastidial lipids. Plant Physiol. 122(3):845–852

Moreau M, Lindermayr C, Durner J, Klessig DF. 2010. NO synthesis and signaling in plants--where do we stand? Physiol Plant. 138(4):372–383

Moreira D, Deschamps P. 2014. What was the real contribution of endosymbionts to the eukaryotic nucleus? Insights from photosynthetic eukaryotes. Cold Spring Harb Perspect Biol. 6(7):a016014

Morton CJ, Campbell ID. 1994. SH3 domains. Molecular "Velcro". Curr Biol. 4(7):615–617

Moustafa A, Beszteri B, Maier UG, Bowler C, Valentin K, Bhattacharya D. 2009. Genomic footprints of a cryptic plastid endosymbiosis in diatoms. Science. 324(5935):1724–1726

Mühlroth A, Li K, Røkke G, Winge P, Olsen Y, et al. 2013. Pathways of lipid metabolism in marine algae, co-expression network, bottlenecks and candidate genes for enhanced production of EPA and DHA in species of Chromista. Mar Drugs. 11(11):4662–4697

Murphy DJ. 2012. The dynamic roles of intracellular lipid droplets: from archaea to mammals. Protoplasma. 249(3):541–585

Mus F, Toussaint JP, Cooksey KE, Fields MW, Gerlach R, et al. 2013. Physiological and molecular analysis of carbon source supplementation and pH stress-induced lipid accumulation in the marine diatom Phaeodactylum tricornutum. Appl Microbiol Biotechnol. 97(8):3625–3642

Nakamura Y, Koizumi R, Shui G, Shimojima M, Wenk MR, et al. 2009. Arabidopsis lipins mediate eukaryotic pathway of lipid metabolism and cope critically with phosphate starvation. Proc Natl Acad Sci U S A. 106(49):20978–20983

Nakamura Y, Teo NZ, Shui G, Chua CH, Cheong WF, et al. 2014. Transcriptomic and lipidomic profiles of glycerolipids during Arabidopsis flower development. New Phytol

REFERENCES

Natarajan S, Kim JK, Jung TK, Doan TT, Ngo HP, et al. 2012. Crystal structure of malonyl CoA-Acyl carrier protein transacylase from Xanthomanous oryzae pv. oryzae and its proposed binding with ACP. Mol Cells. 33(1):19–25

Nedeianu S, Páli T, Marsh D. 2004. Membrane penetration of nitric oxide and its donor S-nitroso-N-acetylpenicillamine: a spin-label electron paramagnetic resonance spectroscopic study. Biochim Biophys Acta. 1661(2):135–143

Nelson N, Ben-Shem A. 2004. The complex architecture of oxygenic photosynthesis. Nat Rev Mol Cell Biol. 5(12):971–982

Nilsson T, Lundin CR, Nordlund G, Ädelroth P, von Ballmoos C, Brzezinski P. 2016. Lipid-mediated Protein-protein Interactions Modulate Respiration-driven ATP Synthesis. Sci Rep. 6:24113

Niu YF, Wang X, Hu DX, Balamurugan S, Li DW, et al. 2016. Molecular characterization of a glycerol-3-phosphate acyltransferase reveals key features essential for triacylglycerol production in Phaeodactylum tricornutum. Biotechnol Biofuels. 9:60

Niu YF, Zhang MH, Li DW, Yang WD, Liu JS, et al. 2013. Improvement of neutral lipid and polyunsaturated fatty acid biosynthesis by overexpressing a type 2 diacylglycerol acyltransferase in marine diatom Phaeodactylum tricornutum. Mar Drugs. 11(11):4558–4569

Nozawa Y. 2011. Adaptive regulation of membrane lipids and fluidity during thermal acclimation in Tetrahymena. Proc Jpn Acad, Ser B, Phys Biol Sci. 87(8):450–462

Nymark M, Sharma AK, Sparstad T, Bones AM, Winge P. 2016. A CRISPR/Cas9 system adapted for gene editing in marine algae. Sci Rep. 6:24951

Nymark M, Valle KC, Brembu T, Hancke K, Winge P, et al. 2009. An integrated analysis of molecular acclimation to high light in the marine diatom Phaeodactylum tricornutum. PLoS ONE. 4(11):e7743

O'Donnell VB, Freeman BA. 2001. Interactions between nitric oxide and lipid oxidation pathways: implications for vascular disease. Circ Res. 88(1):12–21

Okazaki Y, Saito K. 2014. Roles of lipids as signaling molecules and mitigators during stress response in plants. Plant J. 79(4):584–596

Pain D, Kanwar YS, Blobel G. 1988. Identification of a receptor for protein import into chloroplasts and its localization to envelope contact zones. Nature. 331(6153):232–237

Panpoom S, Los DA, Murata N. 1998. Biochemical characterization of a delta12 acyl-lipid desaturase after overexpression of the enzyme in Escherichia coli. Biochim Biophys Acta. 1390(3):323–332

Patil S, Moeys S, von Dassow P, Huysman MJ, Mapleson D, et al. 2015. Identification of the meiotic toolkit in diatoms and exploration of meiosis-specific SPO11 and RAD51 homologs in the sexual species Pseudo-nitzschia multistriata and Seminavis robusta. BMC Genomics. 16(1):930

Patron NJ, Waller RF. 2007. Transit peptide diversity and divergence: A global analysis of plastid targeting signals. Bioessays. 29(10):1048–1058

Paul Abishek M, Patel J, Prem Rajan A. 2014. Algae oil: a sustainable renewable fuel of future. Biotechnology research international. 2014:272814

Peers G, Price NM. 2006. Copper-containing plastocyanin used for electron transport by an oceanic diatom. Nature. 441(7091):341–344

Peleg M, Corradini MG. 2011. Microbial growth curves: what the models tell us and what they cannot. Crit Rev Food Sci Nutr. 51(10):917–945

Pesaresi P, Pribil M, Wunder T, Leister D. 2011. Dynamics of reversible protein phosphorylation in thylakoids of flowering plants: the roles of STN7, STN8 and TAP38. Biochim Biophys Acta. 1807(8):887–896

Petrie JR, Liu Q, Mackenzie AM, Shrestha P, Mansour MP, et al. 2010. Isolation and characterisation of a high-efficiency desaturase and elongases from microalgae for transgenic LC-PUFA production. Mar Biotechnol. 12(4):430–438

Petroutsos D, Amiar S, Abida H, Dolch LJ, Bastien O, et al. 2014. Evolution of galactoglycerolipid biosynthetic pathways--from cyanobacteria to primary plastids and from primary to secondary plastids. Prog Lipid Res. 54:68–85

Pohnert G. 2005. Diatom/copepod interactions in plankton: the indirect chemical defense of unicellular algae. Chembiochem. 6(6):946–959

Pribil M, Labs M, Leister D. 2014. Structure and dynamics of thylakoids in land plants. J Exp Bot

Pribil M, Pesaresi P, Hertle A, Barbato R, Leister D. 2010. Role of plastid protein phosphatase TAP38 in LHCII dephosphorylation and thylakoid electron flow. PLoS Biol. 8(1):e1000288

Qiu H, Yoon HS, Bhattacharya D. 2013. Algal endosymbionts as vectors of horizontal gene transfer in photosynthetic eukaryotes. Front Plant Sci. 4:366

Radakovits R, Jinkerson RE, Fuerstenberg SI, Tae H, Settlage RE, et al. 2012. Draft genome sequence and genetic transformation of the oleaginous alga Nannochloropis gaditana. Nat Commun. 3:686

Rainteau D, Humbert L, Delage E, Vergnolle C, Cantrel C, et al. 2012. Acyl chains of phospholipase D transphosphatidylation products in Arabidopsis cells: a study using multiple reaction monitoring mass spectrometry. PLoS ONE. 7(7):e41985

Rebolloso-Fuentes MM, Navarro-Pérez A, García-Camacho F, Ramos-Miras JJ, Guil-Guerrero JL. 2001. Biomass nutrient profiles of the microalga Nannochloropsis. J Agric Food Chem. 49(6):2966–2972

Reiland S, Finazzi G, Endler A, Willig A, Baerenfaller K, et al. 2011. Comparative phosphoproteome profiling reveals a function of the STN8 kinase in fine-tuning of cyclic electron flow (CEF). Proc Natl Acad Sci U S A. 108(31):12955–12960

Ribalet F, Berges JA, Ianora A, Casotti R. 2007. Growth inhibition of cultured marine phytoplankton by toxic algal-derived polyunsaturated aldehydes. Aquat Toxicol. 85(3):219–227

Riekhof WR, Naik S, Bertrand H, Benning C, Voelker DR. 2014. Phosphate starvation in fungi induces the replacement of phosphatidylcholine with the phosphorus-free betaine lipid diacylglyceryl-N,N,N-trimethylhomoserine. Eukaryotic Cell. 13(6):749–757

Riekhof WR, Sears BB, Benning C. 2005. Annotation of genes involved in glycerolipid biosynthesis in Chlamydomonas reinhardtii: discovery of the betaine lipid synthase BTA1Cr. Eukaryotic Cell. 4(2):242–252

Riisberg I, Orr RJ, Kluge R, Shalchian-Tabrizi K, Bowers HA, et al. 2009. Seven gene phylogeny of heterokonts. Protist. 160(2):191–204

Roach T, Krieger-Liszkay A. 2014. Regulation of photosynthetic electron transport and photoinhibition. Curr Protein Pept Sci. 15(4):351–362

Roberts K, Granum E, Leegood RC, Raven JA. 2007. C3 and C4 pathways of photosynthetic carbon assimilation in marine diatoms are under genetic, not environmental, control. Plant Physiol. 145(1):230–235

Robles Medina A, Molina Grima E, Giménez Giménez A, Ibañez González MJ. 1998. Downstream processing of algal polyunsaturated fatty acids. Biotechnol Adv. 16(3):517–580

Rodolfi L, Zittelli GC, Barsanti L, Rosati G, Tredici MR. 2003. Growth medium recycling in Nannochloropsis sp. mass cultivation. Biomol Eng. 20(4-6):243–248

Rodríguez-Vargas S, Sánchez-García A, Martínez-Rivas JM, Prieto JA, Randez-Gil F. 2007. Fluidization of membrane lipids enhances the tolerance of Saccharomyces cerevisiae to freezing and salt stress. Appl Environ Microbiol. 73(1):110–116

Roháček K, Bertrand M, Moreau B, Jacquette B, Caplat C, et al. 2014. Relaxation of the non-photochemical chlorophyll fluorescence quenching in diatoms: kinetics, components and mechanisms. Philos Trans R Soc Lond, B, Biol Sci. 369(1640):20130241

Rolfe MD, Rice CJ, Lucchini S, Pin C, Thompson A, et al. 2012. Lag phase is a distinct growth phase that prepares bacteria for exponential growth and involves transient metal accumulation. J Bacteriol. 194(3):686–701

Rolland N, Curien G, Finazzi G, Kuntz M, Maréchal E, et al. 2012. The Biosynthetic Capacities of the Plastids and Integration Between Cytoplasmic and Chloroplast Processes. Annu Rev Genet

Romano G, Russo GL, Buttino I, Ianora A, Miralto A. 2003. A marine diatom-derived aldehyde induces apoptosis in copepod and sea urchin embryos. J Exp Biol. 206(Pt 19):3487–3494

Roughan PG, Holland R, Slack CR. 1980. The Role of Chloroplasts and Microsomal Fractions in Polar-Lipid Synthesis from [Acetate-1-C-14 by Cell-Free Preparations from Spinach (Pinacia-Oleracea) Leaves. Biochemical Journal 188: 17-24

Ruban AV, Johnson MP, Duffy CD. 2012. The photoprotective molecular switch in the photosystem II antenna. Biochim Biophys Acta. 1817(1):167–181

Ruiz-Lopez N, Usher S, Sayanova OV, Napier JA, Haslam RP. 2015. Modifying the lipid content and composition of plant seeds: engineering the production of LC-PUFA. Appl Microbiol Biotechnol. 99(1):143–154

Ruocco N, Varrella S, Romano G, Ianora A, Bentley MG, et al. 2016. Diatom-derived oxylipins induce cell death in sea urchin embryos activating caspase-8 and caspase 3/7. Aquat Toxicol. 176:128–140

Ryckebosch E, Bruneel C, Termote-Verhalle R, Lemahieu C, Muylaert K, et al. 2013. Stability of Omega-3 LC-PUFA-rich Photoautotrophic Microalgal Oils Compared to Commercially Available Omega-3 LC-PUFA Oils. J Agric Food Chem

Sage RF, Kubien DS. 2007. The temperature response of C(3) and C(4) photosynthesis. Plant Cell Environ. 30(9):1086–1106

Saitou N, Nei M. 1987. The neighbor-joining method: a new method for reconstructing phylogenetic trees. Mol Biol Evol. 4(4):406–425

Sakamoto T, Higashi S, Wada H, Murata N, Bryant DA. 1997. Low-temperature-induced desaturation of fatty acids and expression of desaturase genes in the cyanobacterium Synechococcus sp. PCC 7002. FEMS Microbiol Lett. 152(2):313–320

Sakihama Y, Nakamura S, Yamasaki H. 2002. Nitric oxide production mediated by nitrate reductase in the green alga Chlamydomonas reinhardtii: an alternative NO production pathway in photosynthetic organisms. Plant Cell Physiol. 43(3):290–297

Salas JJ, Ohlrogge JB. 2002. Characterization of substrate specificity of plant FatA and FatB acyl-ACP thioesterases. Arch Biochem Biophys. 403(1):25–34

Samol I, Shapiguzov A, Ingelsson B, Fucile G, Crèvecoeur M, et al. 2012. Identification of a photosystem II phosphatase involved in light acclimation in Arabidopsis. Plant Cell. 24(6):2596–2609

Sanz-Luque E, Chamizo-Ampudia A, Llamas A, Galvan A, Fernandez E. 2015. Understanding nitrate assimilation and its regulation in microalgae. Front Plant Sci. 6:899

Sanz-Luque E, Ocaña-Calahorro F, Llamas A, Galvan A, Fernandez E. 2013. Nitric oxide controls nitrate and ammonium assimilation in Chlamydomonas reinhardtii. J Exp Bot. 64(11):3373–3383

Sato N. 2004. Roles of the acidic lipids sulfoquinovosyl diacylglycerol and phosphatidylglycerol in photosynthesis: their specificity and evolution. J Plant Res. 117(6):495–505

Savitch LV, Barker-Astrom J, Ivanov AG, Hurry V, Oquist G, et al. 2001. Cold acclimation of Arabidopsis thaliana results in incomplete recovery of photosynthetic capacity, associated with an increased reduction of the chloroplast stroma. Planta. 214(2):295–303

Sayanova O, Ruiz-Lopez N, Haslam RP, Napier JA. 2012. The role of Δ6-desaturase acyl-carrier specificity in the efficient synthesis of long-chain polyunsaturated fatty acids in transgenic plants. Plant Biotechnol J. 10(2):195–206

Sayanova OV, Napier JA. 2004. Eicosapentaenoic acid: biosynthetic routes and the potential for synthesis in transgenic plants. Phytochemistry. 65(2):147–158

Scala S, Carels N, Falciatore A, Chiusano ML, Bowler C. 2002. Genome properties of the diatom Phaeodactylum tricornutum. Plant Physiol. 129(3):993–1002

Schattat M, Barton K, Baudisch B, Klösgen RB, Mathur J. 2011. Plastid stromule branching coincides with contiguous endoplasmic reticulum dynamics. Plant Physiol. 155(4):1667–1677

Schellenberger Costa B, Jungandreas A, Jakob T, Weisheit W, Mittag M, Wilhelm C. 2013. Blue light is essential for high light acclimation and photoprotection in the diatom Phaeodactylum tricornutum. J Exp Bot. 64(2):483–493

*Schneider JC, Livne A, Sukenik A, Roessler PG. 1995 Phytochem **40,** 807-814*

Schnurr JA, Shockey JM, de Boer GJ, Browse JA. 2002. Fatty acid export from the chloroplast. Molecular characterization of a major plastidial acyl-coenzyme A synthetase from Arabidopsis. Plant Physiol. 129(4):1700–1709

Schreiber F, Polerecky L, de Beer D. 2008. Nitric oxide microsensor for high spatial resolution measurements in biofilms and sediments. Anal Chem. 80(4):1152–1158

Schreiber F, Wunderlin P, Udert KM, Wells GF. 2012. Nitric oxide and nitrous oxide turnover in natural and engineered microbial communities: biological pathways, chemical reactions, and novel technologies. Front Microbiol. 3:372

Schreiber U. 2004. Pulse-amplitude-modulation (PAM) fluorometry and saturation pulse method: an overview. In: Papageorgiou GC, Govindjee (eds) Chlorophyll a fluorescence: a signature of photosynthesis, vol 19. Advances in photosynthesis and respiration. Springer, Dordrecht, pp 279–319)

Sedkova N, Tao L, Rouvière PE, Cheng Q. 2005. Diversity of carotenoid synthesis gene clusters from environmental Enterobacteriaceae strains. Appl Environ Microbiol. 71(12):8141–8146

REFERENCES

Serio R, Zizzo MG, Mulè F. 2003. Nitric oxide induces muscular relaxation via cyclic GMP-dependent and -independent mechanisms in the longitudinal muscle of the mouse duodenum. Nitric Oxide. 8(1):48–52

Sewelam N, Kazan K, Schenk PM. 2016. Global Plant Stress Signaling: Reactive Oxygen Species at the Cross-Road. Front Plant Sci. 7:187

Shiratake T, Sato A, Minoda A, Tsuzuki M, Sato N. 2013. Air-drying of cells, the novel conditions for stimulated synthesis of triacylglycerol in a Green Alga, Chlorella kessleri. PLoS ONE. 8(11):e79630

Shockey JM, Fulda MS, Browse J. 2003. Arabidopsis contains a large superfamily of acyl-activating enzymes. Phylogenetic and biochemical analysis reveals a new class of acyl-coenzyme a synthetases. Plant Physiol. 132(2):1065–1076

Siaut M, Heijde M, Mangogna M, Montsant A, Coesel S, et al. 2007. Molecular toolbox for studying diatom biology in Phaeodactylum tricornutum. Gene. 406(1-2):23–35

Simionato D, Block MA, La Rocca N, Jouhet J, Maréchal E, et al. 2013. The response of Nannochloropsis gaditana to nitrogen starvation includes de novo biosynthesis of triacylglycerols, a decrease of chloroplast galactolipids, and reorganization of the photosynthetic apparatus. Eukaryotic Cell. 12(5):665–676

Simionato D, Sforza E, Corteggiani Carpinelli E, Bertucco A, Giacometti GM, Morosinotto T. 2011. Acclimation of Nannochloropsis gaditana to different illumination regimes: effects on lipids accumulation. Bioresour Technol. 102(10):6026–6032

Sims PA, Mann DG, Medlin LK. 2006. Evolution of the diatoms: insights from fossil, biological and molecular data. Phycologia, 45(4), 361-402.

Sinensky M. 1974. Homeoviscous adaptation--a homeostatic process that regulates the viscosity of membrane lipids in Escherichia coli. Proc Natl Acad Sci U S A. 71(2):522–525

Singh D, Carlson R, Fell D, Poolman M. 2015. Modelling metabolism of the diatom Phaeodactylum tricornutum. Biochem Soc Trans. 43(6):1182–1186

Sing S, Bisen PS. 1994. Inhibition of nitrite reductase and urease by arginine and proline in the cyanobacterium Anabaena cycadeae. Journal of Basic Microbiology, 34, 401-401

Smirnova N, Reynolds KA. 2001. Engineered fatty acid biosynthesis in Streptomyces by altered catalytic function of beta-ketoacyl-acyl carrier protein synthase III. J Bacteriol. 183(7):2335–2342

Sobrino C, Neale PJ, Lubián LM. 2005. Interaction of UV radiation and inorganic carbon supply in the inhibition of photosynthesis: spectral and temporal responses of two marine picoplankters. Photochem Photobiol. 81(2):384–393

Somerville C. 1995. Direct tests of the role of membrane lipid composition in low-temperature-induced photoinhibition and chilling sensitivity in plants and cyanobacteria. Proc Natl Acad Sci U S A. 92(14):6215–6218

St Laurent CD, Moon TC, Befus AD. 2015. Measurement of nitric oxide in mast cells with the fluorescent indicator DAF-FM diacetate. Methods Mol Biol. 1220:339-45

Sturm S, Engelken J, Gruber A, Vugrinec S, Kroth PG, et al. 2013. A novel type of light-harvesting antenna protein of red algal origin in algae with secondary plastids. BMC Evol Biol. 13(1):159

Sun Z, Gong J, Wu L, Li P. 2013. Imaging lipid droplet fusion and growth. Methods Cell Biol. 116:253–268

Suzuki M, Shinohara Y, Ohsaki Y, Fujimoto T. 2011. Lipid droplets: size matters. J Electron Microsc (Tokyo). 60 Suppl 1:S101–16

Szabó I, Bergantino E, Giacometti GM. 2005. Light and oxygenic photosynthesis: energy dissipation as a protection mechanism against photo-oxidation. EMBO Rep. 6(7):629–634

Szabó M, Parker K, Guruprasad S, Kuzhiumparambil U, Lilley RM, et al. 2014. Photosynthetic acclimation of Nannochloropsis oculata investigated by multi-wavelength chlorophyll fluorescence analysis. Bioresour Technol. 167:521–529

Takahashi S, Murata N. 2008. How do environmental stresses accelerate photoinhibition? Trends Plant Sci. 13(4):178–182

Takami T, Shibata M, Kobayashi Y, Shikanai T. 2010. De novo biosynthesis of fatty acids plays critical roles in the response of the photosynthetic machinery to low temperature in Arabidopsis. Plant Cell Physiol. 51(8):1265–1275

Tamburic B, Szabó M, Tran NA, Larkum AW, Suggett DJ, Ralph PJ. 2014. Action spectra of oxygen production and chlorophyll a fluorescence in the green microalga Nannochloropsis oculata. Bioresour Technol. 169:320–327

Tarallo R, Sordino P. 2004. Time course of programmed cell death in Ciona intestinalis in relation to mitotic activity and MAPK signaling. Dev Dyn. 230(2):251–262

Teh OK, Ramli US. 2011. Characterization of a KCS-like KASII from Jessenia bataua that elongates saturated and monounsaturated stearic acids in Arabidopsis thaliana. Mol Biotechnol. 48(2):97–108

Tehlivets O, Scheuringer K, Kohlwein SD. 2007. Fatty acid synthesis and elongation in yeast. Biochim Biophys Acta. 1771(3):255–270

Tellier F, Maia-Grondard A, Schmitz-Afonso I, Faure JD. 2014. Comparative plant sphingolipidomic reveals specific lipids in seeds and oil. Phytochemistry. 103:50–58

Teo CL, Idris A, Zain NA, Taisir M. 2014. Synergistic effect of optimizing light-emitting diode illumination quality and intensity to manipulate composition of fatty acid methyl esters from Nannochloropsis sp. Bioresour Technol. 173:284–290

Terrapon N, Gascuel O, Marechal E, Breehelin L. 2009. Detection of new protein domains using co-occurrence: Application to plasmodium falciparum. Bioinformatics, 25, 3077–3083

Tewari RK, Prommer J, Watanabe M. 2013. Endogenous nitric oxide generation in protoplast chloroplasts. Plant Cell Rep. 32(1):31–44

Thompson SE, Taylor AR, Brownlee C, Callow ME, Callow JA. 2008. The role of nitric oxide in diatom adhesion in relation to substratum properties(1). J Phycol. 44(4):967–976

Tian J, Zheng M, Yang G, Zheng L, Chen J, Yang B. 2013. Cloning and stress-responding expression analysis of malonyl CoA-acyl carrier protein transacylase gene of Nannochloropsis gaditana. Gene. 530(1):33–38

Tietz S, Puthiyaveetil S, Enlow HM, Yarbrough R, Wood M, Semchonok DA, Lowry T, Li Z, Jahns P, Boekema EJ, Lenhert S, Niyogi, KK, Kirchhoff H. 2015. Functional Implications of Photosystem II Crystal Formation in Photosynthetic Membranes. The Journal of Biological Chemistry.

Tirichine L, Bowler C. 2011. Decoding algal genomes: tracing back the history of photosynthetic life on Earth. Plant J. 66(1):45–57

Tjellström H, Strawsine M, Silva J, Cahoon EB, Ohlrogge JB. 2013. Disruption of plastid acyl:acyl carrier protein synthetases increases medium chain fatty acid accumulation in seeds of transgenic Arabidopsis. FEBS Lett. 587(7):936–942

Tonon T, Harvey D, Larson TR, Graham IA. 2002. Long chain polyunsaturated fatty acid production and partitioning to triacylglycerols in four microalgae. Phytochemistry. 61(1):15–24

Trentacoste EM, Shrestha RP, Smith SR, Glé C, Hartmann AC, et al. 2013. Metabolic engineering of lipid catabolism increases microalgal lipid accumulation without compromising growth. Proc Natl Acad Sci U S A. 110(49):19748–19753

Tsutakawa SE, Lafrance-Vanasse J, Tainer JA. 2014. The cutting edges in DNA repair, licensing, and fidelity: DNA and RNA repair nucleases sculpt DNA to measure twice, cut once. DNA Repair (Amst). 19:95–107

Turkish AR, Sturley SL. 2009. The genetics of neutral lipid biosynthesis: an evolutionary perspective. Am J Physiol Endocrinol Metab. 297(1):E19–E27

Upchurch RG. 2008. Fatty acid unsaturation, mobilization, and regulation in the response of plants to stress. Biotechnol Lett. 30(6):967–977

Vaezi R, Napier JA, Sayanova O. 2013. Identification and functional characterization of genes encoding omega-3 polyunsaturated fatty acid biosynthetic activities from unicellular microalgae. Mar Drugs. 11(12):5116–5129

Valentine RC, Valentine DL. 2004. Omega-3 fatty acids in cellular membranes: a unified concept. Prog Lipid Res. 43(5):383–402

Valenzuela J, Mazurie A, Carlson RP, Gerlach R, Cooksey KE, et al. 2012. Potential role of multiple carbon fixation pathways during lipid accumulation in Phaeodactylum tricornutum. Biotechnol Biofuels. 5(1):40

Valle KC, Nymark M, Aamot I, Hancke K, Winge P, et al. 2014. System responses to equal doses of photosynthetically usable radiation of blue, green, and red light in the marine diatom Phaeodactylum tricornutum. PLoS ONE. 9(12):e114211

Valledor L, Furuhashi T, Hanak AM, Weckwerth W. 2013. Systemic cold stress adaptation of Chlamydomonas reinhardtii. Mol Cell Proteomics. 12(8):2032–2047

Van Doorn WG, Woltering EJ. 2005. Many ways to exit? Cell death categories in plants. Trends Plant Sci. 10(3):117–122

Van Eerden FJ, de Jong DH, de Vries AH, Wassenaar TA, Marrink SJ. 2015. Characterization of thylakoid lipid membranes from cyanobacteria and higher plants by molecular dynamics simulations. Biochim Biophys Acta. 1848(6):1319–1330

Van Mooy BA, Fredricks HF, Pedler BE, Dyhrman ST, Karl DM, et al. 2009. Phytoplankton in the ocean use non-phosphorus lipids in response to phosphorus scarcity. Nature. 458(7234):69–72

Van Vooren G, Le Grand F, Legrand J, Cuiné S, Peltier G, Pruvost J. 2012. Investigation of fatty acids accumulation in Nannochloropsis oculata for biodiesel application. Bioresour Technol. 124:421–432

Vardi A, Bidle KD, Kwityn C, Hirsh DJ, Thompson SM, et al. 2008a. A diatom gene regulating nitric-oxide signaling and susceptibility to diatom-derived aldehydes. Curr Biol. 18(12):895–899

Vardi A, Formiggini F, Casotti R, De Martino A, Ribalet F, et al. 2006. A stress surveillance system based on calcium and nitric oxide in marine diatoms. PLoS Biol. 4(3):e60

Vardi A, Thamatrakoln K, Bidle KD, Falkowski PG. 2008b. Diatom genomes come of age. Genome Biol. 9(12):245

Verwoert II, van der Linden KH, Walsh MC, Nijkamp HJ, Stuitje AR. 1995. Modification of Brassica napus seed oil by expression of the Escherichia coli fabH gene, encoding 3-ketoacyl-acyl carrier protein synthase III. Plant Mol Biol. 27(5):875–886

Vieler A, Wu G, Tsai CH, Bullard B, Cornish AJ, et al. 2012. Genome, functional gene annotation, and nuclear transformation of the heterokont oleaginous alga Nannochloropsis oceanica CCMP1779. PLoS Genet. 8(11):e1003064

Vigh L, Nakamoto H, Landry J, Gomez-Munoz A, Harwood JL, Horvath I. 2007. Membrane regulation of the stress response from prokaryotic models to mammalian cells. Ann N Y Acad Sci. 1113:40–51

Vinayak V, Manoylov KM, Gateau H, Blanckaert V, Hérault J, et al. 2015. Diatom milking: a review and new approaches. Mar Drugs. 13(5):2629–2665

Wang CW, Miao YH, Chang YS. 2014. A sterol-enriched vacuolar microdomain mediates stationary phase lipophagy in budding yeast. J Cell Biol. 206(3):357–366

Wang J, Xu R, Wang R, Haque ME, Liu A. 2016. Overexpression of ACC gene from oleaginous yeast Lipomyces starkeyi enhanced the lipid accumulation in Saccharomyces cerevisiae with increased levels of glycerol 3-phosphate substrates. Biosci Biotechnol Biochem, pp. 1–9

Wang Y, Chen C, Loake GJ, Chu C. 2010. Nitric oxide: promoter or suppressor of programmed cell death? Protein Cell. 1(2):133–142

Wang Z, Anderson NS, Benning C. 2013. The Phosphatidic Acid Binding Site of the Arabidopsis Trigalactosyldiacylglycerol 4 (TGD4) Protein Required for Lipid Import into Chloroplasts. J Biol Chem. 288(7):4763–4771

Watson ML. 1955. The nuclear envelope; its structure and relation to cytoplasmic membranes. J Biophys Biochem Cytol. 1(3):257–270

Webb AJ, Milsom AB, Rathod KS, Chu WL, Qureshi S, et al. 2008. Mechanisms underlying erythrocyte and endothelial nitrite reduction to nitric oxide in hypoxia: role for xanthine oxidoreductase and endothelial nitric oxide synthase. Circ Res. 103(9):957–964

Weeks DP. 2011. Homologous recombination in Nannochloropsis: a powerful tool in an industrially relevant alga. Proc Natl Acad Sci U S A. 108(52):20859–20860

Wei L, Derrien B, Gautier A, Houille-Vernes L, Boulouis A, et al. 2014. Nitric oxide-triggered remodeling of chloroplast bioenergetics and thylakoid proteins upon nitrogen starvation in Chlamydomonas reinhardtii. Plant Cell. 26(1):353–372

Welti R, Li W, Li M, Sang Y, Biesiada H, et al. 2002. Profiling membrane lipids in plant stress responses. Role of phospholipase D alpha in freezing-induced lipid changes in Arabidopsis. J Biol Chem. 277(35):31994–32002

Wen ZY, Chen F. 2003. Heterotrophic production of eicosapentaenoic acid by microalgae. Biotechnol Adv. 21(4):273–294

Wendehenne D, Pugin A, Klessig DF, Durner J. 2001. Nitric oxide: comparative synthesis and signaling in animal and plant cells. Trends Plant Sci. 6(4):177–183

Wichard T, Poulet SA, Halsband-Lenk C, Albaina A, Harris R, et al. 2005. Survey of the chemical defence potential of diatoms: screening of fifty one species for alpha,beta,gamma,delta-unsaturated aldehydes. J Chem Ecol. 31(4):949–958

Wise RR. 1995. Chilling-enhanced photooxidation: The production, action and study of reactive oxygen species produced during chilling in the light. Photosyn Res. 45(2):79–97

Wong DM, Franz AK. 2013. A comparison of lipid storage in Phaeodactylum tricornutum and Tetraselmis suecica using laser scanning confocal microscopy. J Microbiol Methods. 95(2):122–128

Work VH, D'Adamo S, Radakovits R, Jinkerson RE, Posewitz MC. 2012. Improving photosynthesis and metabolic networks for the competitive production of phototroph-derived biofuels. Curr Opin Biotechnol. 23(3):290–297

Worm B, Barbier EB, Beaumont N, Duffy JE, Folke C, et al. 2006. Impacts of biodiversity loss on ocean ecosystem services. Science. 314(5800):787–790

REFERENCES

Xian M, Zhai L, Zhong N, Ma Y, Xue Y, Ma Y. 2013. [A novel gene (Aa-accA) encoding acetyl-CoA carboxyltransferase alpha-subunit of Alkalimonas amylolytica N10 enhances salt and alkali tolerance of Escherichia coli and tobacco BY-2 cells]. Wei Sheng Wu Xue Bao. 53(8):809–816

Xiao Y, Wang J, Dehesh K. 2013. Review of stress specific organelles-to-nucleus metabolic signal molecules in plants. Plant Sci. 212:102–107

Xu C, Fan J, Cornish AJ, Benning C. 2008. Lipid trafficking between the endoplasmic reticulum and the plastid in Arabidopsis requires the extraplastidic TGD4 protein. Plant Cell. 20(8):2190–2204

Xu C, Fan J, Riekhof W, Froehlich JE, Benning C. 2003. A permease-like protein involved in ER to thylakoid lipid transfer in Arabidopsis. EMBO J. 22(10):2370–2379

Xu C, Härtel H, Wada H, Hagio M, Yu B, et al. 2002. The pgp1 mutant locus of Arabidopsis encodes a phosphatidylglycerolphosphate synthase with impaired activity. Plant Physiol. 129(2):594–604

Xu C, Moellering ER, Muthan B, Fan J, Benning C. 2010. Lipid transport mediated by Arabidopsis TGD proteins is unidirectional from the endoplasmic reticulum to the plastid. Plant Cell Physiol. 51(6):1019–1028

Xu C, Shanklin J. 2016. Triacylglycerol Metabolism, Function, and Accumulation in Plant Vegetative Tissues. Annu Rev Plant Biol. 67:179–206

Xu C, Yu B, Cornish AJ, Froehlich JE, Benning C. 2006. Phosphatidylglycerol biosynthesis in chloroplasts of Arabidopsis mutants deficient in acyl-ACP glycerol-3- phosphate acyltransferase. Plant J. 47(2):296–309

Xu J, Kazachkov M, Jia Y, Zheng Z, Zou J. 2013. Expression of a type 2 diacylglycerol acyltransferase from Thalassiosira pseudonana in yeast leads to incorporation of docosahexaenoic acid β-oxidation intermediates into triacylglycerol. FEBS J. 280(23):6162–6172

Xue J, Niu YF, Huang T, Yang WD, Liu JS, Li HY. 2015. Genetic improvement of the microalga Phaeodactylum tricornutum for boosting neutral lipid accumulation. Metab Eng. 27:1–9

Yamagishi A, Ikeda Y, Komura M, Koike H, Satoh K, et al. 2010. Shallow sink in an antenna pigment system of photosystem I of a marine centric diatom, Chaetoceros gracilis, revealed by ultrafast fluorescence spectroscopy at 17 K. J Phys Chem B. 114(27):9031–9038

Yang J, Pan Y, Bowler C, Zhang L, Hu H. 2016. Knockdown of phosphoenolpyruvate carboxykinase increases carbon flux to lipid synthesis in Phaeodactylum tricornutum. Algal Research, 15, 50-58.

Yang L, Ding Y, Chen Y, Zhang S, Huo C, et al. 2012. The proteomics of lipid droplets: structure, dynamics, and functions of the organelle conserved from bacteria to humans. J Lipid Res. 53(7):1245–1253

Yang ZK, Ma YH, Zheng JW, Yang WD, Liu JS, Li HY. 2014. Proteomics to reveal metabolic network shifts towards lipid accumulation following nitrogen deprivation in the diatom Phaeodactylum tricornutum. J Appl Phycol. 26:73–82

Yazawa K. 1996. Production of eicosapentaenoic acid from marine bacteria. Lipids. 31 Suppl:S297–300

Yoneda K, Yoshida M, Suzuki I, Watanabe MM. 2016. Identification of a Major Lipid Droplet Protein in a Marine Diatom Phaeodactylum tricornutum. Plant Cell Physiol. 57(2):397–406

Yongmanitchai W, Ward OP. 1993. Positional distribution of fatty acids, and molecular species of polar lipids, in the diatom Phaeodactylum tricornutum. J Gen Microbiol. 139(3):465–472

Young JN, Heureux AM, Sharwood RE, Rickaby RE, Morel FM, Whitney SM. 2016. Large variation in the Rubisco kinetics of diatoms reveals diversity among their carbon-concentrating mechanisms. J Exp Bot. 67(11):3445–3456

Zank TK, Zähringer U, Beckmann C, Pohnert G, Boland W, et al. 2002. Cloning and functional characterisation of an enzyme involved in the elongation of Delta6-polyunsaturated fatty acids from the moss Physcomitrella patens. Plant J. 31(3):255–268

Zehr JP, Ward BB. 2002. Nitrogen cycling in the ocean: new perspectives on processes and paradigms. Appl Environ Microbiol. 68(3):1015–1024

Zhang AO, Cui ZH, Yu JL, Hu ZL, Ding R, et al. 2016. Dissipation of excess excitation energy of the needle leaves in Pinus trees during cold winters. Int J Biometeorol

Zhang X, Agrawal A, San KY. 2012. Improving fatty acid production in Escherichia coli through the overexpression of malonyl coA-acyl carrier protein transacylase. Biotechnol Prog. 28(1):60–65

Zhao JF, Shyue SK, Lin SJ, Wei J, Lee TS. 2014. Excess nitric oxide impairs LXR(α)-ABCA1-dependent cholesterol efflux in macrophage foam cells. J Cell Physiol. 229(1):117–125

Zheng H, Rowland O, Kunst L. 2005. Disruptions of the Arabidopsis Enoyl-CoA reductase gene reveal an essential role for very-long-chain fatty acid synthesis in cell expansion during plant morphogenesis. Plant Cell. 17(5):1467–1481

Zhu SQ, Zhao H, Liang JS, Ji BH, Jiao DM. 2008. Relationships between phosphatidylglycerol molecular species of thylakoid membrane lipids and sensitivities to chilling-induced photoinhibition in rice. J Integr Plant Biol. 50(2):194–202